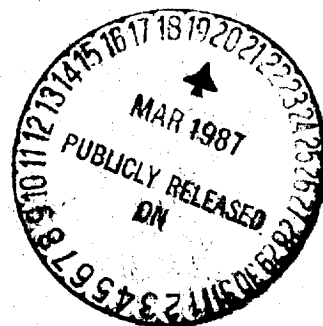$CNT-27$

$P-8\ 21$

$CR-171267$

FINAL REPORT
March, 1984

PRODUCTION OF LARGE-PARTICLE-SIZE
MONODISPERSE LATEXES
NAS8-32591

Prepared for

National Aeronautics and Space Administration

George C. Marshall Space Flight Center

Huntsville, Alabama

Prepared by

Lehigh University

Emulsion Polymers Institute

Sinclair Laboratory, Bldg #7

Date of general release _December, 1986_

FINAL REPORT

March, 1984

PRODUCTION OF LARGE-PARTICLE-SIZE MONODISPERSE LATEXES

NAS8-32951

Prepared for

National Aeronautics and Space Administration

George C. Marshall Space Flight Center

Huntsville, Alabama

Prepared by

Principal Investigator: J.W. Vanderhoff

Co-Investigators: M.S. El-Aasser

F.J. Micale

Research Assistants: E.D. Sudol

C.M. Tseng

A. Silwanowicz

Lehigh University

Emulsion Polymers Institute

Sinclair Laboratory, Bldg. #7

Bethlehem, Pennsylvania 18015

ACKNOWLEDGMENT

FOREWARD

The ground based development and experimental work, as well as the flight experiments, included in this Final Report took place over a five and one-half year period. The objective of this research program is explicitly stated in the title, "Production of Large-Particle-Size Monodisperse Latexes", where at the time at which this program was initiated monodisperse latexes could be prepared only up to $2\mu m$. The research program included in this Final Report have achieved two objectives: (1) it has refined and extended the experimental techniques for preparing monodisperse latexes in quantity on the ground up to a particle diameter of $10\mu m$, and (2) it has demonstrated that a microgravity environment can be used to grow monodisperse latexes to larger sizes, where the limitations in size have yet to be defined.

Two research assistants, E.D. Sudol and C.M. Tseng, have been working on this project from the beginning, and a third research assistant, A. Silwanowicz, has spent two years on this project. All three graduate students have recently graduated, E.D. Sudol with a Ph.D. in Chemical Engineering, C.M. Tseng with a Ph.D. in Polymer Science and Engineering, and A. Silwanowicz with a M.S. Degree in Chemical Engineering, where their theses work represents all the research carried out under this contract. This Final Report consists of the material taken from the three theses of Sudol, Tseng, and Silwanowicz, which are designated Parts A, B, and C, respectively. Although some redundancy is present, it should be noted that in these cases essentially the same material is treated from a different point of view.

Part A treats the experimental development of the monodisperse latex reactor, MLR, and the seeded emulsion polymerizations carried out in the laboratory prototype of the flight hardware, LUMLR, as a function of the operational parameters. The emphasis in this section is directed towards the measurement, interpretation, and

modeling of the kinetics of seeded emulsion polymerization and successive seeded emulsion polymerization. Part B treats the recipe development of seeded emulsion polymerization as a function of particle size. The equilibrium swelling of latex particles with monomers was investigated both theoretically and experimentally. Extensive studies are reported on both the type and concentration of initiators, surfactants, and inhibitors, which eventually led to the development of the flight recipes. Parts A and B both report on the experimental results of the flight experiments. Part C treats the experimental development of inhibition of seeded emulsion polymerization in terms of time of inhibition and the effect of inhibitors on the kinetics of polymerization.

PART A

Kinetics of Successive Seeding

of

Monodisperse Latexes

Based on the Ph.D. Thesis

by

E. David Sudol

ABSTRACT

A stainless steel piston/cylinder prototype dilatometer (volume ~100 cm^3), designed for use in microgravity, was tested and modified for obtaining the polymerization kinetics of monodisperse polystyrene latexes, as well as the latexes themselves. Conversion histories, accurate to within 2%, were obtained after modifications and procedural changes were implemented. A low speed, oscillatory agitation (10 rpm, 30° arc per cycle) and redesigned stirrer paddle were recommended for the low shear requirements of the microgravity experiments.

The kinetics of successive seeding in the region between Smith-Ewart Case 2 ($\bar{n} = 1/2$) and Case 3 ($\bar{n} \gg 1$) were studied using both aqueous and oil phase initiation. A recipe formulation method was developed by which a constant emulsifier (Aerosol-MA) surface coverage was maintained throughout a sequence. Swelling ratios (2/1), final solids (~30%) and the polymerization temperature (69°C) were maintained throughout each sequence, all beginning with a 0.19 μm polystyrene seed.

Monodisperse latexes up to 1 μm in size were prepared using $K_2S_2O_8$ (0.5 mM) and a 4% Aerosol-MA surface coverage. The kinetics were characterized by the autoacceleration of the gel effect with the overall polymerization rate decreasing with increasing particle size. The Case 2 to Case 3 kinetic transition was described by a change in the dependency of the polymerization rate on the particle diameter from d^{-3} to $d^{1/2}$. This was based on results of a simplified kinetic model in which the collision theory of radical absorption was

1

used to obtain reasonable agreement with the experimental results.

Extension of the particle size limit was sought using oil phase initiators (AIBN, AMBN) in combination with aqueous phase inhibitors (hydroquinone, $NaNO_2$, NH_4SCN). This was accomplishing using AMBN (4.0 mM) and hydroquinone (14.5 mM) whereby 2.45 μm monodisperse polystyrene particles were prepared with an emulsifier coverage of 15%. The polymerization kinetics were affected by the nature of the inhibitor. The gel effect again dominated the behavior; however, some cases of retardation were noted. The transition from emulsion $(R_p \alpha d^{-3})$ to bulk $(R_p \neq f(d))$ kinetics was found to occur between 0.3 and 1.2 μm particle size.

Nine seeded polymerizations of large particle-size latexes were carried out in microgravity by which 'monodisperse' latexes from 3.4 to 18 μm were prepared. Particle size distribution broadening was found in ground-based counterparts due to insufficient mixing. Massive flocculation was also experienced for the ground samples of particle size greater than 10 μm. The overall polymerization rates were generally smaller on the ground, again because of thermal gradients caused by poor mixing.

A submicron 'control' recipe (0.19 μm seed) did not survive the four-day delay prior to launch while in a second experiment unexpected retardation of the polymerization was found.

CHAPTER 1

INTRODUCTION AND OBJECTIVES

Polymer latexes, which are used industrially in large quantities, generally have a relatively broad particle size distribution (PSD). This is not usually of much concern in the manufacture of such products as latex paints, paper coatings, adhesives, and others, in that there is no need for a specifically narrow PSD. Monodisperse latexes, having very narrow PSD's however, are used in much smaller quantities and primarily for scientific purposes. These include the calibration of various measuring instruments such as electron microscopes, determination of pore sizes, and applications in medical serological tests. These latexes are also valuable as model colloids for studies of particle-particle stability, latex rheology, the adsorption of surfactants, electrophoresis, etc. The use of monodisperse latexes in seeded emulsion polymerization greatly simplifies analysis in kinetic studies designed to elucidate some of the various mechanisms involved in this complex process.

Monodisperse polystyrene and polyvinyltoluene latexes are marketed in the size range 0.09 - 2.35 µm particle diameter. The smaller sizes are prepared by conventional emulsion polymerization, while the concept of seeding is applied to produce the larger sizes [19 - 22]. The upper limit is reached due to the sensitivity of the preparation to emulsifier concentration and mechanical shear. If the amount of emulsifier exceeds a certain limit a new crop of particles is generated producing a bimodal particle size distribution. Too little emulsifier will fail to maintain the stability of the

3

latex during polymerization resulting in excessive amounts of coag-
ulum. Moreover, with increasing size creaming and settling at low

and high conversions during the polymerization must be offset by in-
creased agitation which often results in the formation of coagulum

due to the increased sensitivity of the latex to mechanical shear.

These effects can be partially alleviated by producing polymers with

densities closer to one, however, this approach can only resolve the

difficulties caused by settling of the particles in the latter stages

of polymerization.

The gravitational effect of creaming and settling could be

eliminated by carrying out the polymerization in a microgravity en-
vironment. In this case, the emulsifier concentration could be kept

at a low enough level to ensure against new particle generation while

maintaining the stability of the latex. Agitation would only be

necessary to prevent significant temperature gradients within the

polymerizing latex. A technical proposal was submitted to,

accepted and funded by the National Aeronautic and Space Administra-
tion (NASA) by which the preparation of large-particle-size monodis-
perse latexes was proposed via the successive seeding method in the

mid-deck of the Orbiters 'Columbia' and 'Challenger'. The objectives

not only included the latex preparation but also the determination

of the kinetics and mechanism of the polymerization as a function of

various recipe parameters. This information is valuable from both

scientific and practical considerations. The effect of microgravity

on such a heterogeneous chemical reaction can be observed and factors

involved in reactor scale-up can be evaluated. The success of these

4

microgravity experiments ultimately depends on the pre-flight preparation and understanding gained of the polymerization process.

The principle objective of this research program is to determine the kinetics of sequentially seeded emulsion polymerization of monodisperse polystyrene latexes in what has been described as the transition region between emulsion and bulk kinetics. Secondary objectives include: 1) the development, testing, and use of a prototype dilatometer, designed for use in microgravity, to obtain these polymerization kinetics; 2) to develop a model capable of simulating the kinetics of successive seeding; and 3) to cooperate in an effort to prepare large-particle size monodisperse latexes in microgravity.

The method of seeding in emulsion polymerization has often been cited as a means of studying the kinetics and mechanism of this somewhat complex process. Successive seeding from small to large particle size has not previously been taken much advantage of, particularly in studies in which $\bar{n}$, the average number of radicals per particle, exceeds 1/2 (known as Smith-Ewart Case 2) but is not so large as to cause the polymerization kinetics to be independent of particle size and number (known as Case 3). This kinetic region is described in Chapter 3 and is characterized by a number of sequences performed using both aqueous and oil phase initiation. A recipe formulation method is also described which was designed to maintain certain variables constant with successive seeding to large-particle-size latexes.

Before presenting the actual kinetic findings, the means of obtaining the data by use of a prototype dilatometer (LUMLR) are des-

5

cribed in Chapter 2. Characterization and modification of the reactor are discussed in view of the requirements set by the preparation of large-particle-size latexes. Agitation and relative mixing efficiencies are evaluated. The problems and solutions involved in obtaining and interpreting kinetic data are discussed.

A simplified model is constructed in Chapter 4 to simulate the data obtained in the successive seeding studies. Current methods are incorporated to account for the changing rate 'constants' caused by the diffusion limitations of the gel effect. Differences between aqueous and oil phase initiation are discussed.

The preparation of large-particle-size monodisperse latexes in microgravity is the subject of Chapter 5. Four sets of experiments aboard the orbiters 'Columbia' and 'Challenger' are described in a chronological fashion. Attention is given to pre-flight preparation and especially, post-flight analysis of the particles and the kinetic data obtained. Differences between the flight and ground-based control experiments are emphasized.

Finally, a summary of the findings and conclusions of the work are given in Chapter 6, together with some suggestions for continued research in areas requiring further clarification and substantiation.

CHAPTER 2

A DILATOMETER AND REACTOR - DESIGN AND DEVELOPMENT

2.1 Introduction

Much can be learned about the kinetics and mechanism of vinyl polymerization through the measurement of polymerization rates and resulting polymer molecular weights. The conversion of monomer to polymer as a function of time can be measured in a number of ways [1]. These include direct weighing, various chemical methods, dilatometry, refractometry, viscometry, gas chromatography, and others. Each of these has its own advantages, disadvantages, and limitations depending on the application. In emulsion polymerization, the direct weighing method is the most common, being simple and requiring no complex or specialized equipment. Dilatometry, which takes advantage of density differences between monomers and polymers, is also commonly used, most often in the form of a glass reaction vessel coupled to a capillary tube. This type of apparatus, which is relatively fragile, is operated by placing it in a constant temperature bath and measuring the capillary height at regular time intervals during the reaction. More sophisticated recording dilatometers have also been described in the literature [2,3,4,5,6]. Most of these apparatuses incorporate a device for automatically following and recording the height of a fluid in the capillary tube of a dilatometer. This type of dilatometer cannot fulfill the more strict requirements of what is termed 'space-flight hardware'.

In order to develop a dilatometer which could be used to monitor the polymerization of large-particle-size latexes in microgravity the scientific and engineering requirements for the reactor were first defined. These requirements were set by the needs and limitations of three interacting parties, Lehigh University (Principal Investigators), General Electric (Hardware Contractor), and NASA. The science requirements were set by the original objectives of the program. A dilatometer was needed which could accurately and reproducibly produce kinetic data and large-particle-size monodisperse latex. The polymerization would be conducted at $70^{\circ}C$ with 'gentle agitation' to a 'high' conversion. To achieve these goals the reactor requirements had to be determined. These included specifications for the reaction temperature and its measurement, reactor volume and volume change and their measurement, agitator design and mode and speed of agitation. The source of heat and the desired heat-up schedule had to be defined. The materials which would contact the reaction fluid would also have to be specified along with power requirements, process timing, vessel configuration, data acquisition, and many others involved in space flight.

2.2 Proposed Possibilities

Three vessel configurations were initially considered as possibilities for this unusual dilatometer: a bellows, a piston/cylinder, and a diaphragm.

2.2.1 Bellows

The bellows-type dilatometer was considered first. Since a bellows by design is able to expand and contract it appeared to fit the

8

requirements of a dilatometer which can accommodate the expansion of a latex as the temperature is increased to the polymerization temperature and the contraction due to the conversion of monomer to polymer with subsequent cooling to room temperature. A crude bellows-type reactor was assembled as depicted in Figure 2.1. It consisted of a stainless steel bellows sealed at each end by rubber gaskets mounted on aluminum endplates and maintained in compression by springs held by 4 bolts. Two fill ports were drilled in the top end plate for filling and draining the vessel. A magnetic stirrer was used for agitation. Several seeded emulsion polymerizations were satisfactorily carried out by placing the vessel in a constant temperature bath $(70^{\circ}C)$. No attempt was made to collect any kinetic data. Experimental details of this experiment are not given here. For use in microgravity it was judged impractical to provide heat externally due to the shape of the vessel. Subsequently tests were conducted to check the feasibility of using an immersion heater placed inside the vessel. It was found that the rate of heating had to be adjusted to what was considered to be an undesirably low level due to the buildup of coagulum on the surface of the heater sheath. The relatively small area for heat transfer from the immersion heater was a definite drawback of this design. Also of major concern was the fact that the bellows fins contained a large amount of fluid volume which would be difficult to mix with the fluid in the open volume of the vessel, especially at the low shear agitation conditions envisioned for these experiments. Interest was then shifted to the more promising piston/cylinder configuration.

9

injection ports

springs

Al endplates

rubber gaskets

0·8 cm.

0·2cm

7·6 cm

13·0 cm.

6·7 cm.

SS bellows

galvanized bolts

5·0 cm

0·1·5 cm.

9·5 cm.
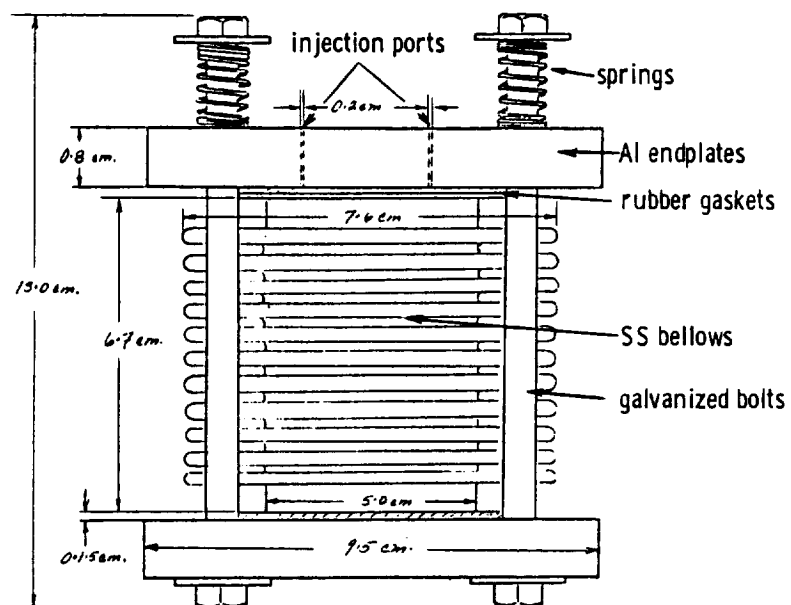
Figure 2.1   Bellows Polymerization Vessel - Side View

2.2.2 Piston/Cylinder

It was believed that the inherent drawbacks in the bellows-type
design, i.e. dead volume and immersion heating, could be remedied by
using the piston/cylinder type configuration. Heating could be pro-
vided externally by a resistance wire over a much larger surface area
thus avoiding the problems of immersion heating. The piston/cylinder
type dilatometer, however, would have other possible disadvantages.
Leak-free and dependable piston movement would have to be provided
by o-ring seals, required to be inert to the chemicals in the system.

In order to test the piston/cylinder concept, GE designed and
manufactured a crude version of this reactor, as illustrated in Fig-
ure 2.2. The three major components were the piston, the cylinder,
and the end cap which could be removed. A Buna o-ring was supplied
with the piston. To test this design, heating and temperature con-
trol, agitation, and a means of measuring the piston displacement had
to be improvised. A bread-board temperature controller was provided
by GE, which made use of thermocouples to measure and control the temp-
erature of the reaction fluid through the 'on-off' condition of a
heating tape wrapped around the lower half of the cylinder (i.e. the
half containing the reaction fluid). Agitation was accomplished using
a magnetic stirring bar modified with a Teflon propellor together with
a relatively slow magnetic drive mechanism. The piston displacement
was monitored using a dial indicator. As in the case of the bellows
vessel, testing was accomplished via seeded emulsion polymerizations.
No experimental details will be given here of the chemistry of the
experiment, except to say that the details of the recipe and its prep-

SS piston

SS cylinder

o-ring

$100 cm^3$ fluid
volume

thermistor

propellar

rubber gasket

removable cap

16 cm
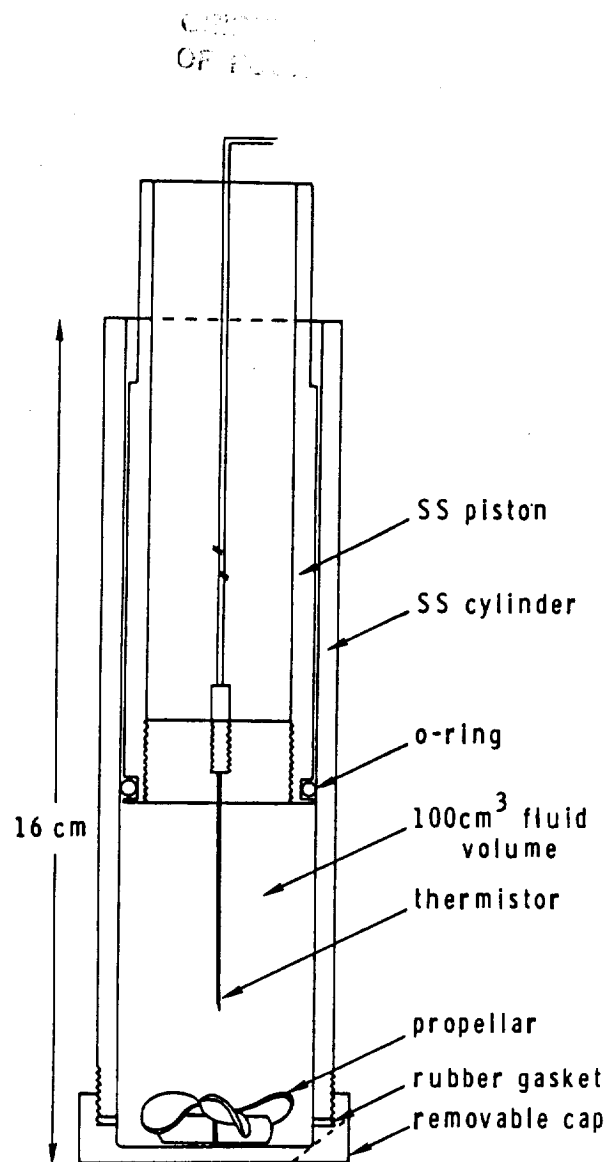
Figure 2.2   'Crude' Piston/Cylinder Dilatometer, Designed by the
General Electric Co.

aration had been worked out previously in this laboratory.

The initial tests of the reactor proved to be most enlightening. The design specifications for the reactor called for a 100 cc reaction fluid volume. In order to fill the reactor to this volume, the required piston position was calculated and pre-set using a Vernier caliper. The test fluid (water or latex) was poured in through the open end of the cylinder and the cap was secured. In this manner it was impossible not to include a significant amount of air in the reactor. The reactor was then inverted, and the rest of the apparatus was assembled. The heating rate was adjusted through a variac connected to the heating tape with a temperature set-point at $\sim 70^{\circ}$C. At a setting of 60 volts, 70°C was reached in approximately 20 minutes. With water as the working fluid, piston movement indicating expansion was observed as expected. A seeded emulsion polymerization was next attempted to check whether reasonable kinetic data could be obtained. After reaching temperature, the movement of the piston ceased as if no polymerization was taking place. From this it was obvious that the presence of air space in the reactor coupled with the resistance of the piston to movement prevented an change in the piston position. A second polymerization was attempted in which a 2.27 kg (5 lb.) lead weight was balanced on top of the piston in order to effect its downward travel. The cylinder end cap was also modified with a port to allow expulsion of the air left in the reactor when sealed. This was accomplished by tilting the reactor at $\sim 45^{\circ}$ with the port at the top, carefully moving the piston until some latex was expelled, and then sealing. With these 'innovations' the first kinetic data were recorded

13

using this 'crude' dilatometer. This set of data is presented in Figure 2.3 along with a second set obtained using a greater amount of monomer in the recipe. Qualitatively these curves represented what was expected for these polymerizations. The piston/cylinder design concept with some modification thus appeared to be a good choice for further development work.

2.3 Prototype Design

The piston/cylinder design became favored over the bellows because the reactor was inherently more rugged, had less dead space and no need for an immersion heater. Initial tests in a crude version of the piston/cylinder encouraged its adoption as the flight design. Subsequently a prototype was designed and constructed at the General Electric Space Sciences Labs (Valley Force, PA). A description of this vessel follows.

A cut-away drawing of the MLR (Monodisperse Latex Reactor) prototype (later designated LUMLR) is shown in Figure 2.4, along with a photograph in Figure 2.5. The mechanical aspects of the MLR apparatus were designed to provide temperature control, fluid containment, and data measurement. The apparatus consists of a stainless steel (SS 303) cylinder with a 4.1 cm ID in which rides a SS piston, sealed by two Viton o-rings. Piston movement is measured by a Linear Voltage Differential Transformer (LVDT) attached to an arm connected to a bolt mounted in the piston and fixed relative to the cylinder, i.e. mounted on the Textolite housing cover. The downward movement of the piston is assisted by a spring exerting approximately 1.01×10^5 Pa
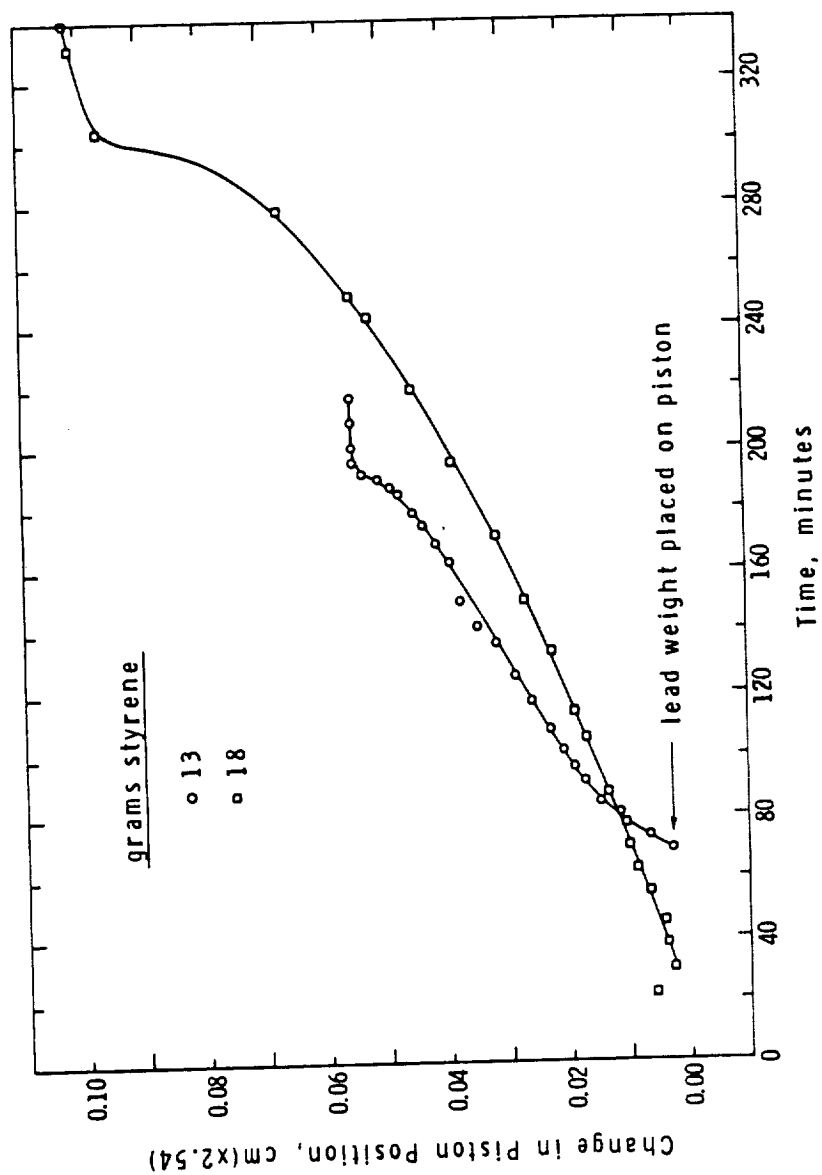
Figure 2.3 Piston Position as a Function of Time for a Seeded Emulsion Polymeriza-
tion Conducted in the 'Crude' Piston/Cylinder Dilatometer

#	Description
1	bolt support
2	support arm
3	piston adjustment nut
4	insulation
5	Viton o-rings
6	housing
7	heater wire leads
8	wall temperature sensor, diode
9	fluid temperature sensor
10	stirrer shaft
11	Viton o-rings
12	insulation plate (textolite)
13	quarter plate
14	base plate
15	stirrer motor
16	LVDT shaft
17	LVDT support
18	washer, special
19	housing cover (textolite)
20	LVDT -DC (Schaevitz)
21	spring
22	piston assembly
23	exit port vent
24	reactor volume (100cm^3)
25	cylinder assembly
26	bearings
27	quick connect fill port

Figure 2.4   Schematic of the Prototype Dilatometer Designed by the General Electric Co.

16

Figure 2.5   Photograph of the LUMLR Dilatometer, from Left to Right,
the Cylinder Assembly, Housing, and Piston Assembly with
a Plexiglas Replica of the Cylinder in Place on the Base
Assembly

17

(1 atm.) pressure. This was a direct result of the experimental success using the lead weight in the tests of the crude piston/cylinder. The cylinder is bolted to a SS base plate, sealed by a Viton o-ring. A SS shaft for mounting a stirrer paddle is inserted through the bottom of the base plate and is held in place by two bearings separated by a spacer. The stirrer paddle will be described in detail in Section 2.4.2. A 24 volt D.C. motor is coupled to the shaft by means of a roll pin which fits into a groove at the bottom of the shaft. The motor is attached to an aluminum adapter plate which in turn is attached to the base plate. The base plate is attached to an aluminum quarter plate with a Textolite insulator plate in between. Protruding from the center of the piston is a SS temperature sensor well for monitoring the fluid temperature. Multi-pellet diodes (KE 1N4157) are used for all temperature measurements. Two apertures are provided into the cylinder. The bottom one, lo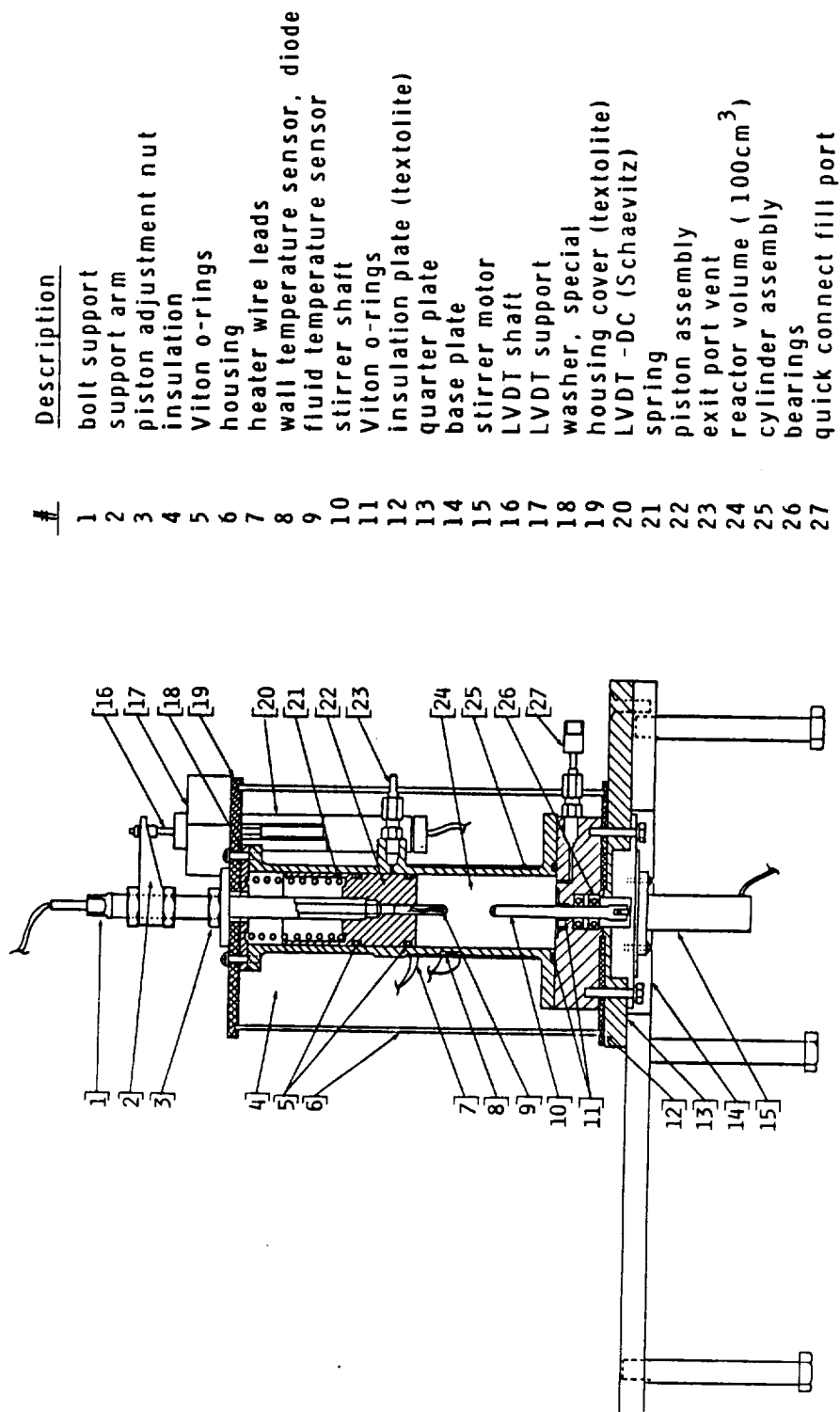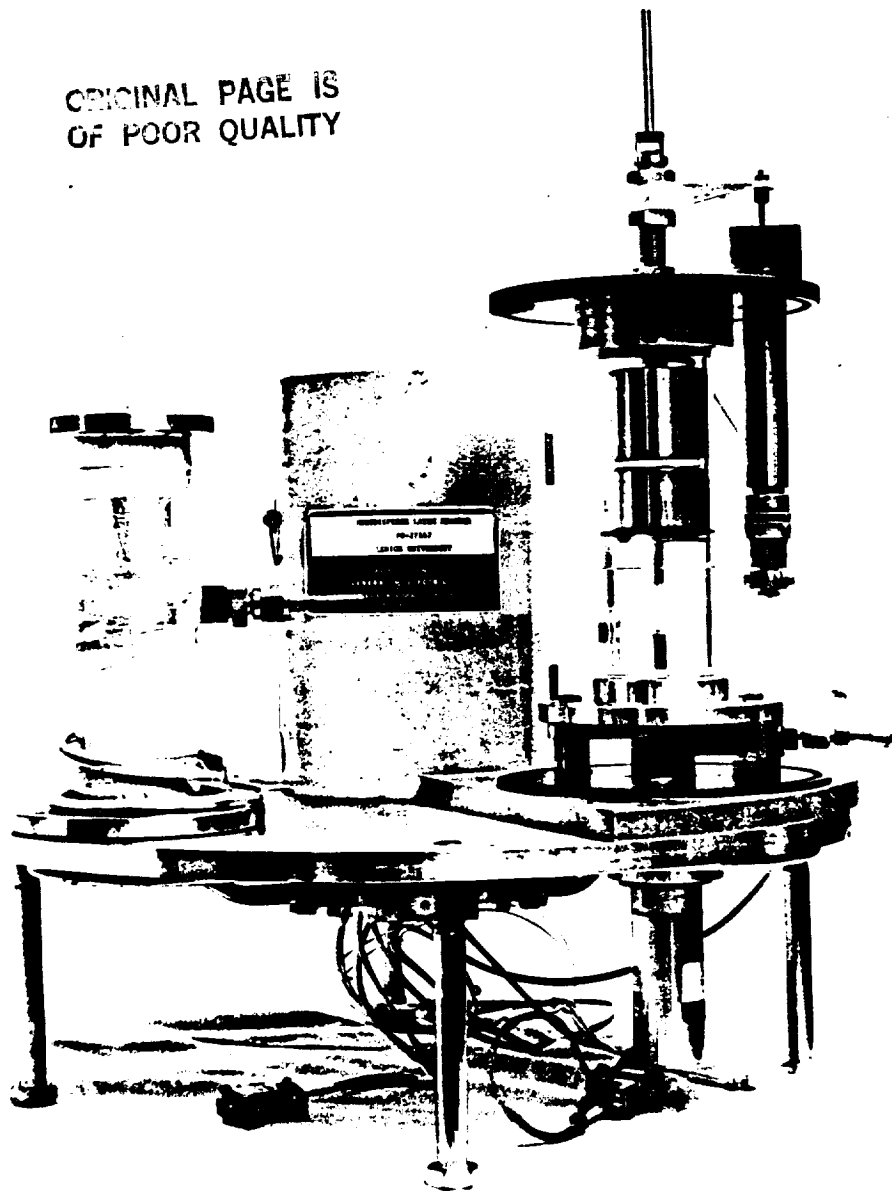cated on the base plate, serves at the inlet port for loading the reactor. A Swagelok Quick Connect serves as the inlet seal. The upper port is used as an outlet port for the loading operation. This serves the same purpose as the vent port on the original crude version of the reactor. It enables the reactor to be loaded with a minimal amount of air inclusion.

The lower half of the cylinder is wrapped with a layer of commercial grade aluminum foil (0.5 mil) and a layer of thermosetting tape (No. 69, 3M Co.). Over the tape is wound a nichrome heater wire (No. 24) with a 0.12 pitch. Another layer of tape is wrapped over the heater wire and over this a layer of aluminum foil. A 3

18

pellet diode (the wall temperature sensor) is mounted in a groove machined into the cylinder below the first layer of aluminum foil. Fiberglass insulation (Owens-Corning) is wrapped around the cylinder and contained by a fiberglass housing.

The electrical wiring, carrying power to the heater wire and stirrer motor and signals from the fluid and wall temperature diodes and the LVDT, runs to a connector mounted on the MLR platform. From this connector wiring runs to the MLR 'Controller'. A photo of the front of the controller is shown in Figure 2.6. This controller pro-vides AC to DC conversion of power for the unit, plus it processes the signals from the diodes and LVDT. Temperature (^{o}C) and LVDT voltage along with heater and stirrer voltage can be monitored on a digital panel meter by use of a multiposition switch. The mode and speed (rpm) of the stirrer can be adjusted using a multiposition switch and a multiturn potentiometer, respectively. Recorder output connectors are provided in the rear of the unit.

2.4 Prototype Testing and Development

Accurate interpretation of dilatometric data can be achieved only after sufficient knowledge and understanding of a reactor's be-havior is gained. This knowledge includes the calibration of the var-ious sensors, studies of the agitation system, and most importantly the expansion (and contraction) behaviors of the reactor and its con-tents. The final test of this knowledge is accomplished by obtaining accurate kinetic data along with the desired product (in this case, monodisperse latex).
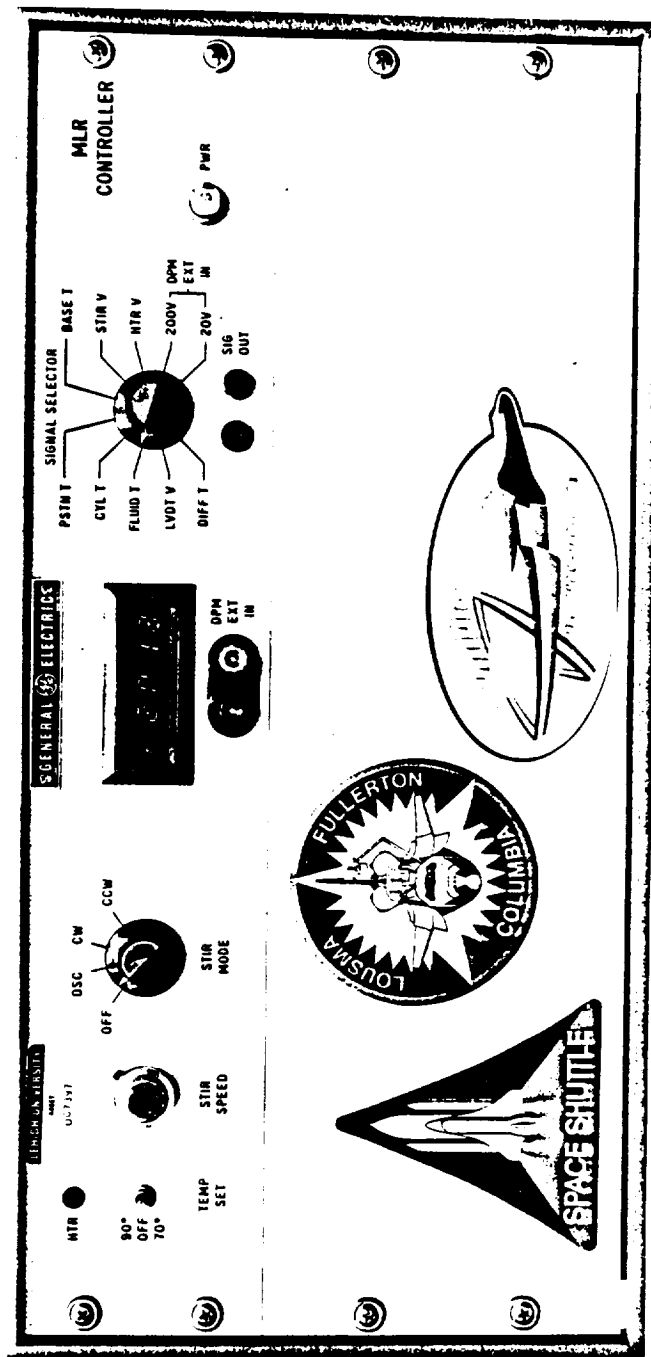
Figure 2.6 Front Panel of MLR Prototype Control Unit

Initial testing of the MLR prototype took place at GE. The first seeded emulsion polymerization conducted in the prototype resulted in a polydisperse product latex. This result was attributed to the presence of relatively large temperature gradients present in the reaction fluid during the experiment which caused particles to polymerize at different rates depending on their location (temperature) in the reactor. It was speculated that these gradients were due to inadequate mixing by the stirrer paddle (Section 2.4.2) rotating at a constant 12 rpm plus a relatively large heat sink provided by the base plate (i.e. the temperature increased from the bottom to the top of the fluid in the reactor). A second polymerization with an identical recipe was run after much of the excess metal was machined from the base plate and the stirrer motion was changed to a stop/start type of motion (4 rpm) to produce better mixing. The product latex showed a much narrower particle size distribution but the stirrer was noted to have stopped some time late in the polymerization. An oscillatory or "washing machine" type motion was introduced in a third polymerization to induce better mixing at a relatively low rpm and reduce the risk of the stirrer shaft freezing during the polymerization. Kinetic data was obtained in subsequent testing at GE and initial attempts at interpretation of these data were made. The problems confronted in this will be described further on. Testing of the prototype at GE came to an end with the design and construction of what was termed the 'Engineering Unit', the model for the Space Flight Reactors. The prototype subsequently came to Lehigh University for more detailed testing and use in seeded emulsion polymerizations. It was henceforth designated

the LUMLR to distinguish it from the MLR flight hardware.

2.4.1 Sensor Calibration

In order to calibrate the temperature sensors they were first removed from the apparatus. The fluid temperature sensor was simply removed from the well, not being fixed in place, while the wall temperature sensor was removed only after carefully removing tape, foil, and heating wire from the cylinder in which it was embedded. These sensors were then calibrated at various temperatures in a Haake constant temperature bath versus a thermometer and a copper-constantin thermocouple. Two readings were recorded for each sensor at a given temperature, the first being the LED panel meter readout from the Controller, which already contained a built in conversion factor for a readout in $^{\circ}C$. The second reading was measured via a Keithley DMM by which the voltage signal, proportional to the temperature, was recorded. (The redundance of the latter data proved quite valuable later when the LED panel meter failed.) Each set of data obtained from the panel meter and the DMM are given in Figures 2.7 and 2.8, respectively. The slopes and intercepts obtained via least squares analysis are given in each figure. The calibrations were linear in the $20 - 70^{\circ}C$ range, i.e. that range over which experiments would be conducted.

The LVDT (Linear Voltage Differential Transformer, type 250 HCD, Schaevetz Engineering) was calibrated in place on the LUMLR unit by recording a voltage from the sensor via the panel meter versus the reading from a dial indicator (Model C81S, Federal Products Corp.) placed atop the piston-LVDT connecting arm. These data were recorded at various piston positions to obtain a calibration curve. The results
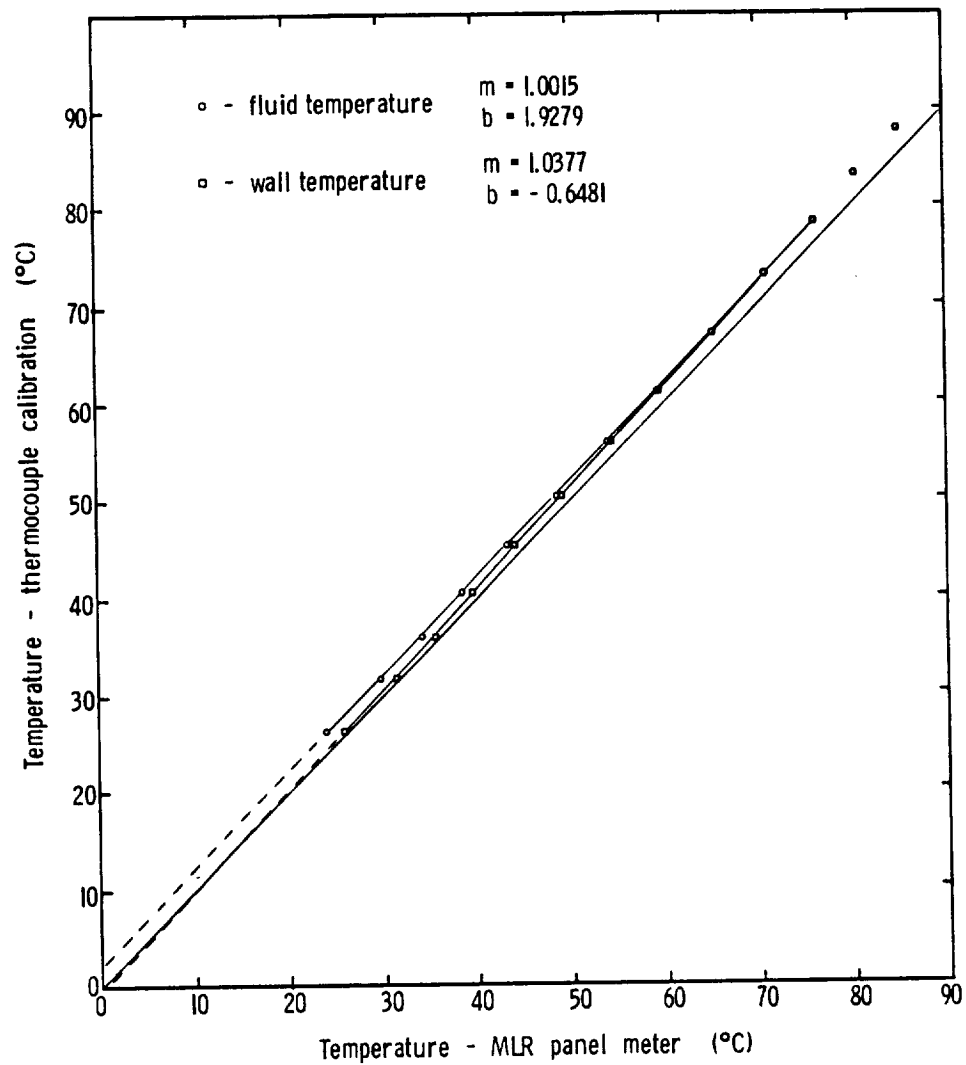
22

Figure 2.7 Calibration of Fluid and Wall Temperature Sensors versus
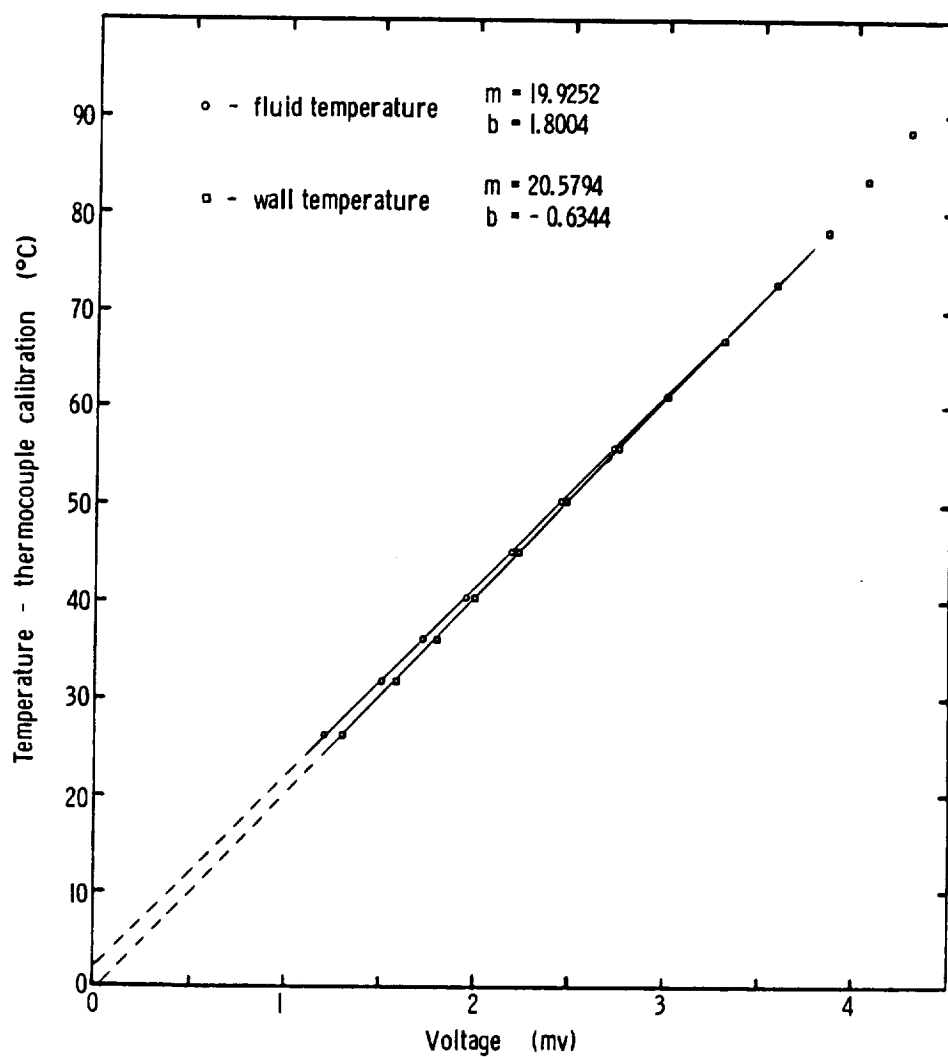a Copper-Constantin Thermocouple using the MLR Panel Meter

23

Figure 2.8 Calibration of Fluid and Wall Temperature Sensors (DMM Voltage) versus a Copper-Constantin Thermocouple

24

are given in Figure 2.9. The slope was -14.7868 volts/cm over the 1.8 to 3.8 volt range (correlation coefficient = -0.99998). This was later verified over the -2.0 to +2.0 volt range. A 1.0 cm^3 volume change would, therefore, register as a 0.0756 cm piston displacement or a 1.118 volt change in the LVDT reading.

2.4.2 Agitation Behavior - Stirrer Paddle Design and Testing

The agitation requirements for the MLR were defined by the limitations imposed by the preparation of large-particle-size monodisperse latexes. As stated in the Introduction, seeded emulsion polymerizations for producing monodisperse latexes above 2 μm diameter must have carefully controlled amounts of emulsifier and degrees of agitation. Shear induced flocculation or severe temperature gradients can both result in the production of polydisperse latexes. Therefore, an optimum agitation rate must be found which can ensure that: 1) particle-particle coalescence does not take place due to creaming prior to (or during) polymerization, 2) particle coagulation does not occur due to high shear rates in the neighborhood of the agitator blade, and 3) particles do not 'grow' or polymerize at different rates due to experiencing different temperature environments in the reactor. The agitation system in the MLR was required to satisfy all of these requirements for each latex system to be polymerized. The ultimate test of the agitator would be in actual polymerization of flight-type recipes and examining the resulting particle size distributions. This would not only involve a great deal of long and laborious work but was impossible early on when no recipes were available for testing. Other tests in the form of measurements of temperature gradients, sedimentation rates, and mixing
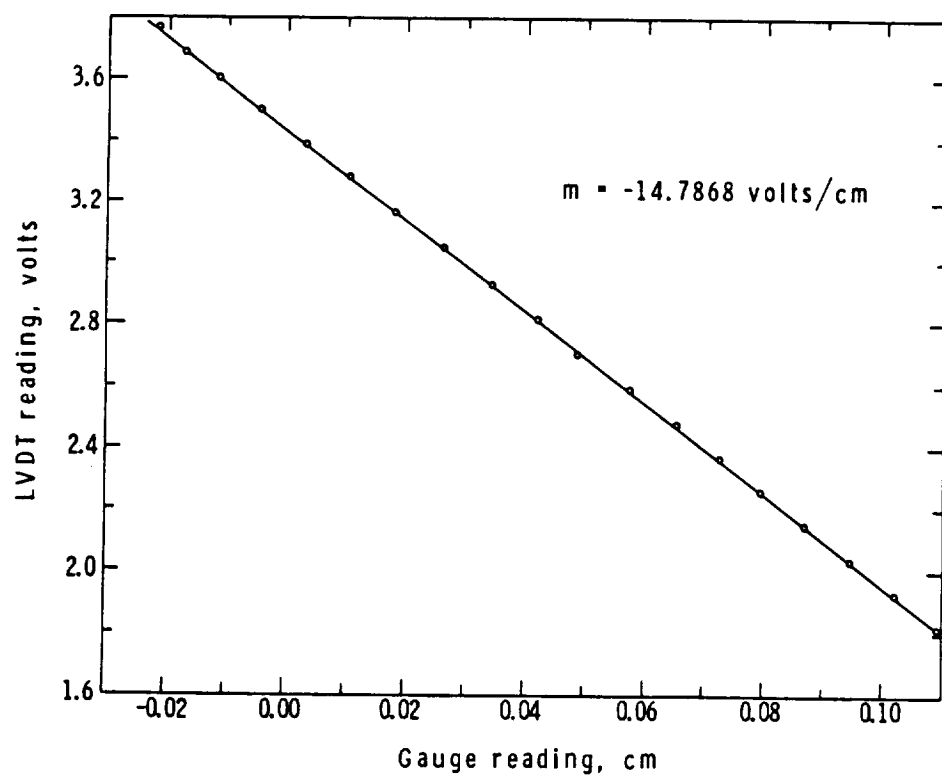
Figure 2.9   LVDT Calibration Data

26

rates were used in the interim to arrive at a satisfactory agitation system.

2.4.2.1 Calibration

The stirrer on the LUMLR has the capability of operating in one of two modes, either continuous rotation (clockwise or counter-clockwise) or oscillatory motion ("washing machine"). The STIR SPEED control on the MLR Controller Panel provides a continuous variation of stirrer rpm in settings from 0 to 10. These settings were calibrated versus rpm as shown in Figure 2.10. A minimum speed of 5 rpm is attained at a setting of 3, below which the stirrer shaft does not move due to resistance from the o-ring seal. The maximum rate is about 26 rpm. Note that the rpm decreases slightly when the heater is turned on due to the limited available power in the system. Figure 2.10 also relates stir speed to stirrer blade tip speed (3.2 cm wide stirrer paddel) and Reynolds number. The oscillatory motion was characterized in terms of the arc traced before reversal of stirrer direction. The arc (degrees) as a function of stir setting is shown in Figure 2.11. The counter-clockwise (viewed from the top) arc was designed to be slightly greater than the clockwise arc so that the net movement of the stirrer paddle was in the counter-clockwise direction. The frequency of reversal was not an adjustable parameter in these tests, being fixed at about 27 cycles/min. A slight reduction in the arc traced was also noted when power was applied to the heater wire.

2.4.2.2 Initial Paddle Designs and Testing

The efficiency of agitation in the LUMRL was not only a function

27

Figure 2.10   Calibration of Stirrer Speed (Tip Speed and N_{Re}) versus
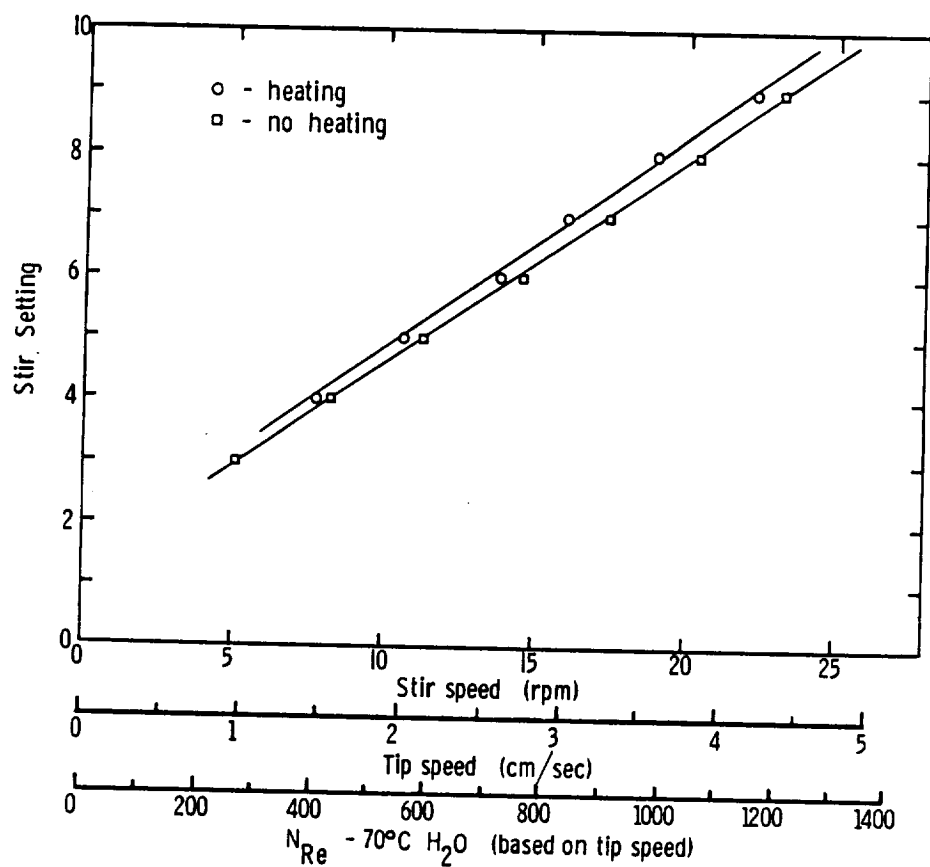Stir Speed Setting under Conditions of No Power ($\square$)
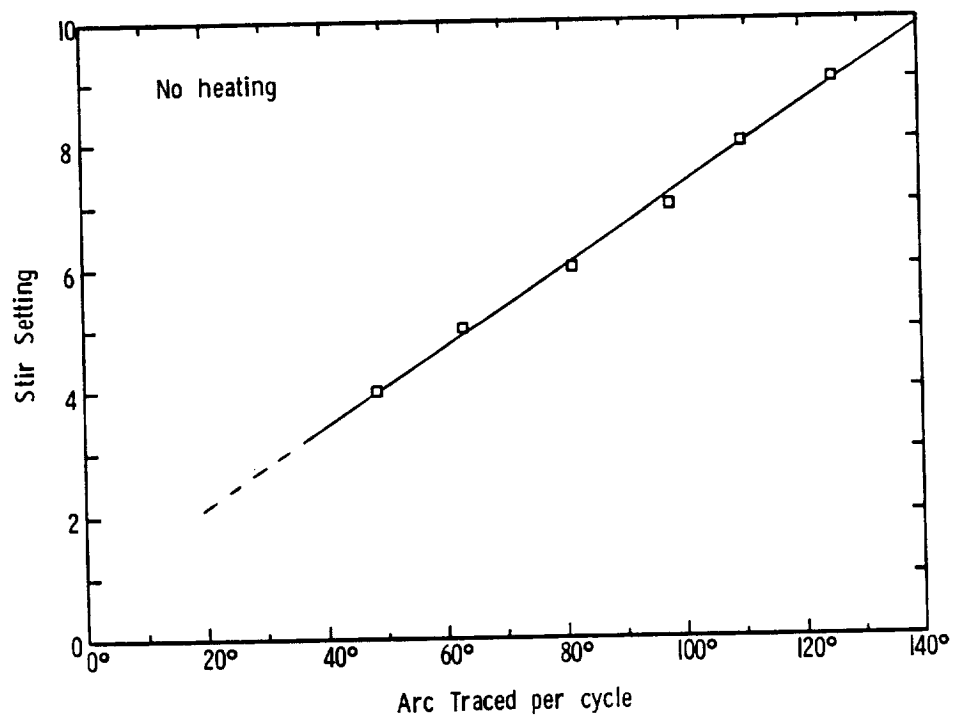and Power ($\bigcirc$) to the Heating Element

Figure 2.11 Calibration of Arc Traced (Counter-Clockwise) Versus
Stir Speed Setting in the Oscillatory Stir Mode

of the mode and speed of stirring but more importantly the size and configuration of the impeller. Originally the impeller was desgined as a flat 2-bladed stainless steel paddle perforated with small holes. The length and width were of the same order as the dimensions of the reactor volume itself. It resembled somewhat a leaf impeller paddle with rows of holes drilled in it [8]. Further modification resulted in the paddle shown in Figure 2.12a. Note that the paddle was oriented at a slight angle from the horizontal to facilitate some axial movement of the fluid. This design was conceived with the idea that gentle but adequate mixing could be achieved if the entire volume of the reactor could be swept by the impeller blade at a low rpm (<25 rpm). This paddle was used during the testing of the prototype at GE. A second paddle was designed and fabricated at GE [9] for testing in the MLR Engineering Unit and was tentatively adopted as the stirrer paddle for the MLR Flight Units. This paddle was modified for mounting on the LUMLR stirrer shaft (Figure 2.12b). It was narrower and shorter than the original paddle and instead of holes, directional fins (as in a pitched blade impellor) were incorporated.

A number of tests were devised and conducted in the LUMLR in order to determine the relative mixing efficiency of the MLR paddle at various stir speeds in the OSC (oscillatory) stir mode. The wall to center temperature gradient was monitored by taping the fluid sensor probe to the inner wall of the reactor, half way into the fluid (H_2O) and recording its temperature versus a thermocouple located opposite to it in the center of the reactor. The piston was not positioned in the cylinder to allow access for the wiring. Data were recorded with

(a)   (b)

Figure 2.12   (a) Original MLR Blade and (b) Production Blade
Designed for Use in all MLR Reactors (Actual Size)

31

time as the fluid was heated up from room temperature. Wall-to-center temperature gradients are plotted in Figure 2.13 at three OSC Stir Speeds (0, 4 and 8) corresponding to 0 rpm - 0° arc, 7.7 rpm - 49.1° arc, and 19.2 rpm - 108.9° arc, respectively. In 18 min. this temperature differential dropped to $2^{\circ}C$ or less for all three agitation conditions. These results pointed to a need to obtain more information on mixing and temperature gradients in more remote areas of the reactor, further removed from the stirrer paddle. A more precise experiment was conducted in which five thermocouples, connected to strip chart recorders, were placed at various locations in the LUMLR. This time the piston was positioned in the cylinder which was again filled with water. The thermocouple wires exited the reactor through the o-ring seal between the cylinder and base plate. The thermocouple voltages, along with the fluid temperature sensor reading, were monitored once again during the heat-up cycle of the fluid. The results of the two extreme cases, i.e. no agitation and agitation at OSC Stir Speed 8.0, are given in Figure 2.14. Fluid temperatures were monitored at the probe (p), top edge (te), center (c), bottom center (bc), and bottom edge (be) of the reactor. The fluid temperature, as monitored through the MLR Controller, was also recorded. Once again temperature gradients were evident but the most severe were found at the bottom of the reactor. The mixing in this region of the reactor was able to counteract natural convection and heat loss to the base place to a certain degree but still left $4 - 5^{\circ}C$ temperature differences between the center and bottom of the reactor. The question remained whether or not a monodisperse latex could be polymerized without significantly broadening the particle
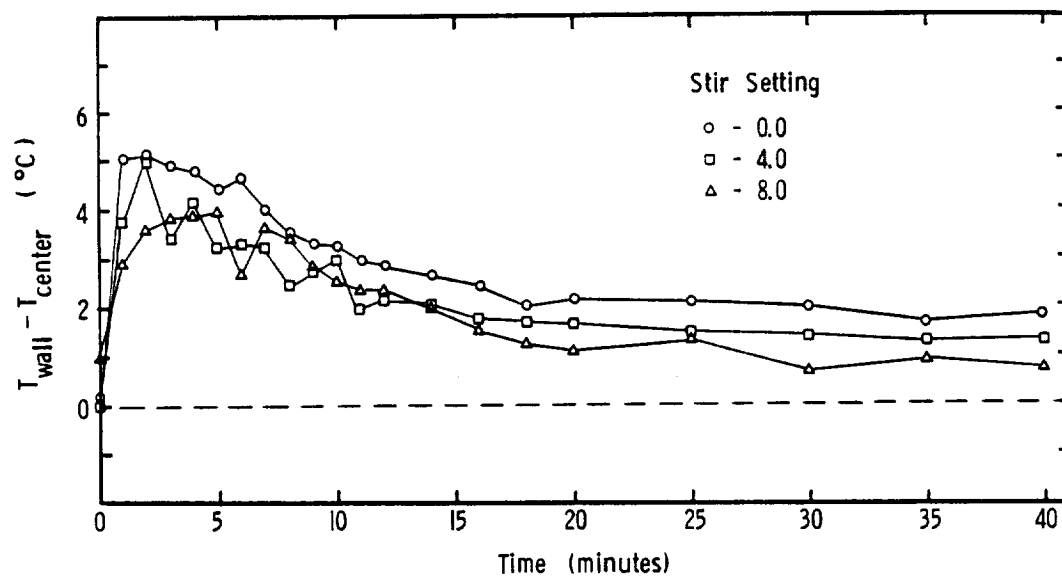
32

Figure 2.13   Temperature Gradients versus Time at Various OSC Stir Speeds
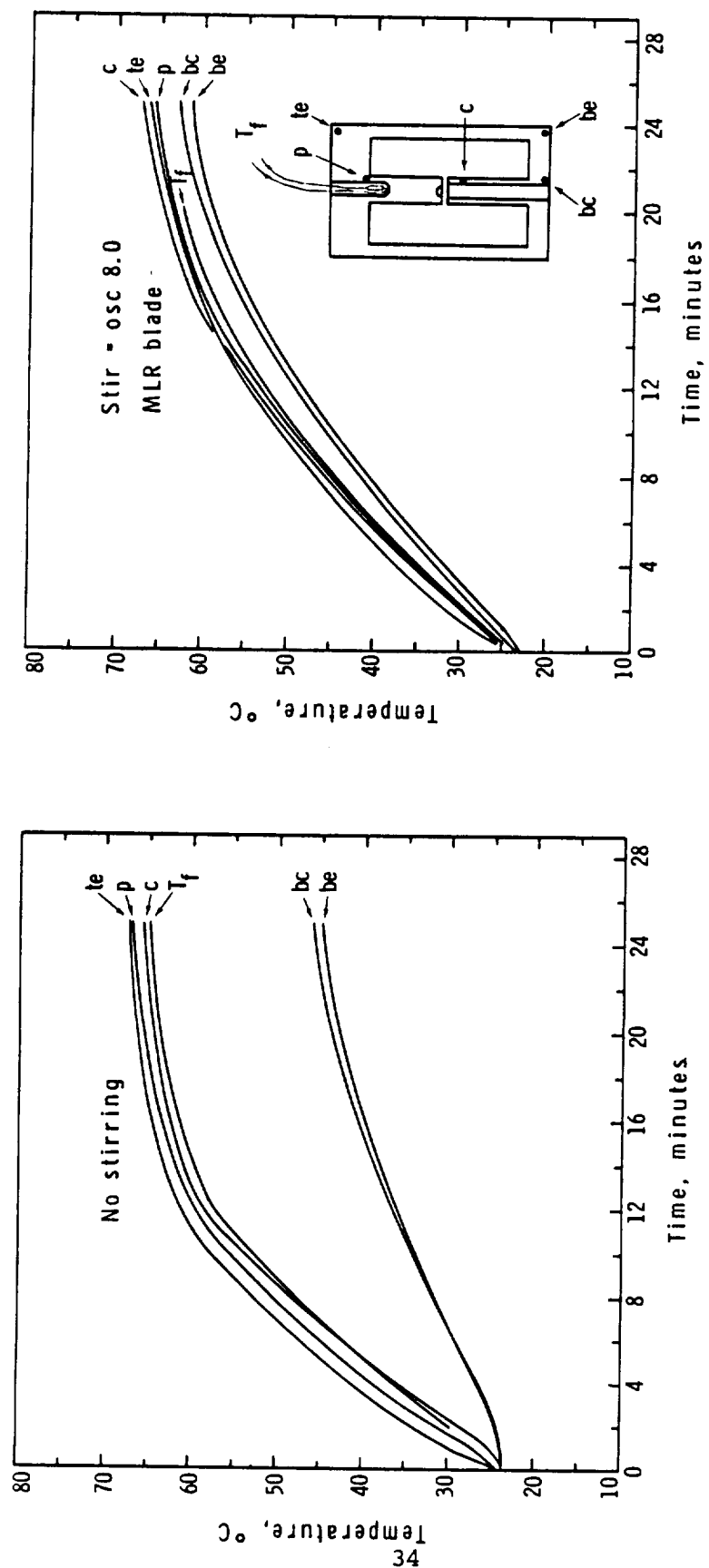
33

Figure 2.14 Temperature vs. Time Recorded at the Probe (p), Top Edge (te), Center (c), Bottom Center (bc), Bottom Edge (be), and Fluid Temperature Probe (T_f) with no Agitation (Left) and at OSC Stir Speed 8.0 with Water as the Medium

size distribution. Three seeded polymerizations with identical re-
cipes were run at OSC Stir Speeds of 0, 5, and 8 to investigate the
effect of agitation not only on the resulting PSD's (Particle Size
Distributions) of the latex but also on the interpretation of the
kinetic data. Three hours were required to reach high conversion
(>95%) for each experiment. TEM (Transmission Electron Microscope)
examination of the resulting particles did not reveal any gross dif-
ferences between those polymerized with no stirring and those with
stirring. However, a PSD analysis revealed a difference in the
breadth of the distribution as indicated by the standard deviation
on the number average diameter. In the case where agitation was pro-
vided at OSC Stir Speed 0.8 the measured standard deviation was 1.9%
while with no agitation the particles produced had a 3.0% standard de-
viation. (Note: The standard deviation of a single particle when mea-
sured 100 times is approximately 1.0%.) The particle size for all
samples was about 0.45 μm. This difference, though small, was signif-
icant and reflected the difference in the conditions of the polymeriza-
tion. Mixing caused by thermal convection was considered to be the
reason for not seeing a larger difference. The polymerization ran at
OSC Stir Speed 5 resulted in a latex similar to that produced at the
higher stirring rate. These results proved only that some agitation
was needed to maintain a 'monodisperse' PSD with a single recipe which
used submicron particles which did not cream or settle to any signifi-
cant extent within the time frame of the experiment. The question
again remained whether or not seed particles greater than 2 μm in size
swollen with monomer could be maintained in a dispersed and stable

35

condition on the ground and then polymerized in a microgravity environment (in the absence of natural convection) without destroying the monodispersity. An attempt was made to address the first of these conditions by performing sedimentation experiments.

The sedimentation of large size latex particles was studied as a function of the degree of agitation (MLR paddle), in an effort to approximate the creaming rates of swollen particles. A poly(styrene-co-divinylbenzene) latex, having a particle size range of 4 - 7 μm, was calculated to sediment at rates roughly equivalent to the creaming rate of 2 μm polystyrene particles swollen with 2.3 to 16 x their volume in styrene monomer. These represented swollen diameters of 3.0 to 5.2 μm which approximated the sizes and swelling ratios intended for the first microgravity experiments. These numbers were calculated based on assumptions of unhindered sedimentation in water, additive densities of monomer and polymer, and the density of the poly(styrene-co-divinylbenzene) being that of polystyrene. A plexiglas replica of the LUMLR was constructed to replace the original cylinder for reasons of visibility and ease of modification, with the addition of sampling ports. A photograph is given in Figure 2.15 of the assembled LUMLR with the replica in place. Mixing efficiency was judged by the relative amount of latex particles found in the bottom of the reactor after agitating an originally well mixed system for a given time interval. Samples (0.5 cc) were removed via a syringe and the solids contents were determined gravimetrically. The results for various OSC Stir Speeds are presented in Figure 2.16. No change in the solids concentration was found for a setting of 7 or higher while settings of 4 and 5 both
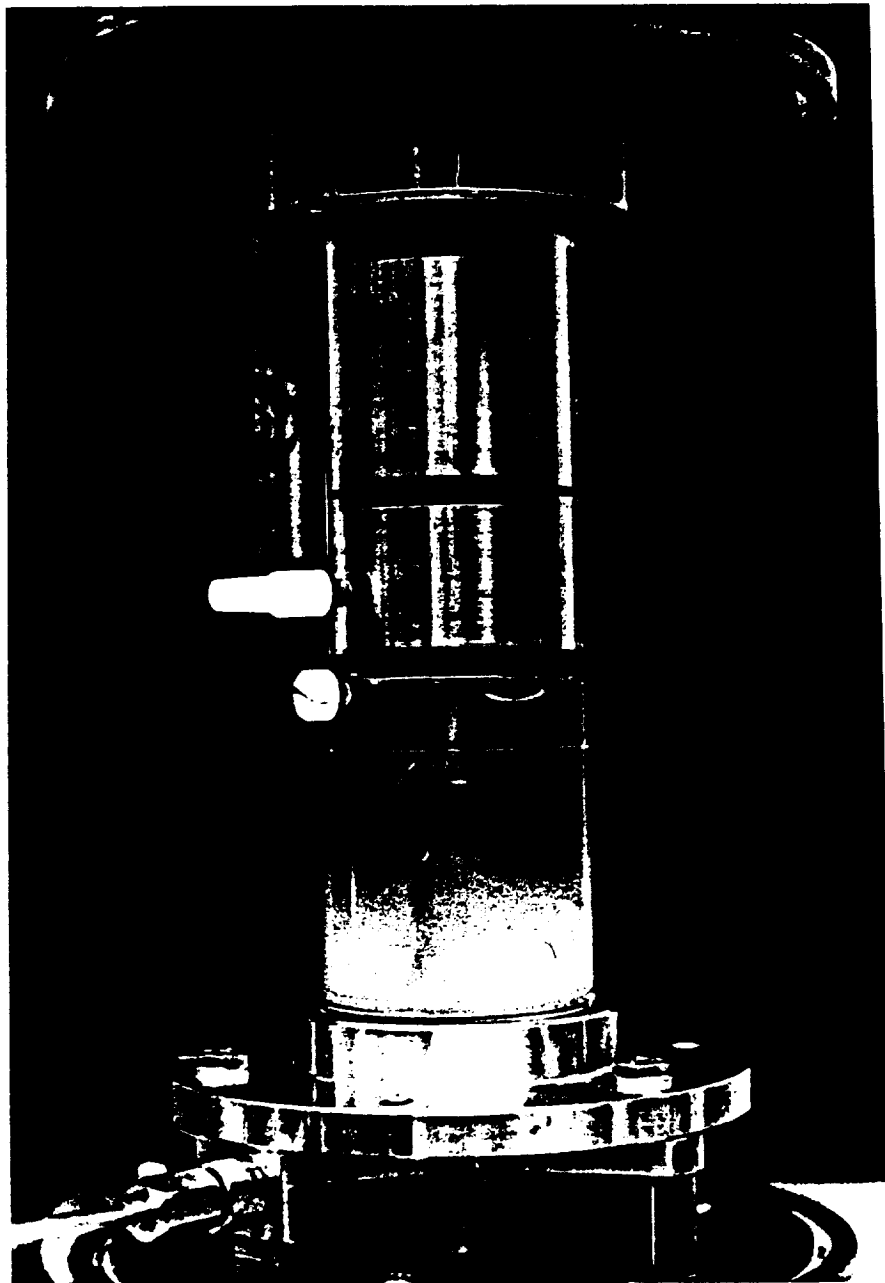
36

Figure 2.15   LUMLR Prototype with Plexiglas Replica of the Cylinder
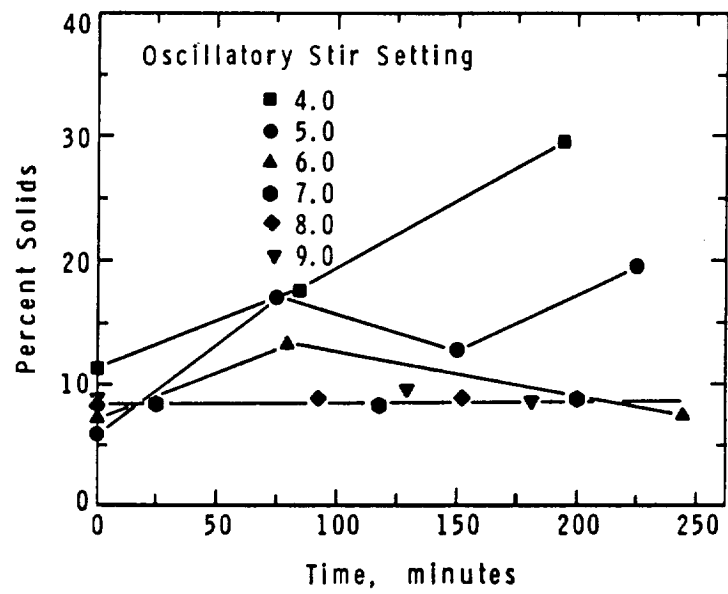in Place.   Sedimenting Latex is Contained in the Vessel

Figure 2.16   Sedimentation of 4 - 7 µm poly(styrene-co-divinylbenzene) Latex Particles as a Function of the Agitation Rate in the LUMLR.

showed increases in the amount of sedimentation with time over a 4 hr. period. This indicated that with the given agitation system an OSC Stir Speed greater than 6 (14 rpm, 79° arc) was needed to maintain a uniform concentration of 4 - 7 µm poly(styrene-co-divinylbenzene) particles or the equivalent swollen particles. The PSD of the sedimented particles was not determined but invariably contained a large fraction of the 7 µm type particles. This would have the effect of weighting the results towards the extreme of a 16/1 swelling ratio. With this in mind, the OSC Stir Speed 6 was defined as the lower limit for agitation of swollen flight latexes.

2.4.2.3 Paddle Redesign and Pulse Testing

During the experiments outlined above, it was found that even under the most rigorous agitation conditions a small sediment layer was found along the bottom edge of the reactor where the cylinder meets the base plate. This did not affect the interpretation of the results but did once again point out, as in the temperature gradient studies, that "dead" or unstirred areas existed in remote regions of the reactor. This was a continuing concern throughout the development of the reactors and led to the decision to design and test alternate stirrer paddles before a final commitment was made. The goal of this redesign was not only to reduce the amount of 'poorly mixed' volume but also to increase the agitation efficiency at lower OSC Stir Speeds.

The approach chosen for redesign was to enlarge the paddle so that it would sweep the largest volume possible (within 1 mm of all surfaces) and to incorporate a greater number of directional fins (to increase axial mixing). Figure 2.17a is a drawing of such a paddle. Six H-shaped

39
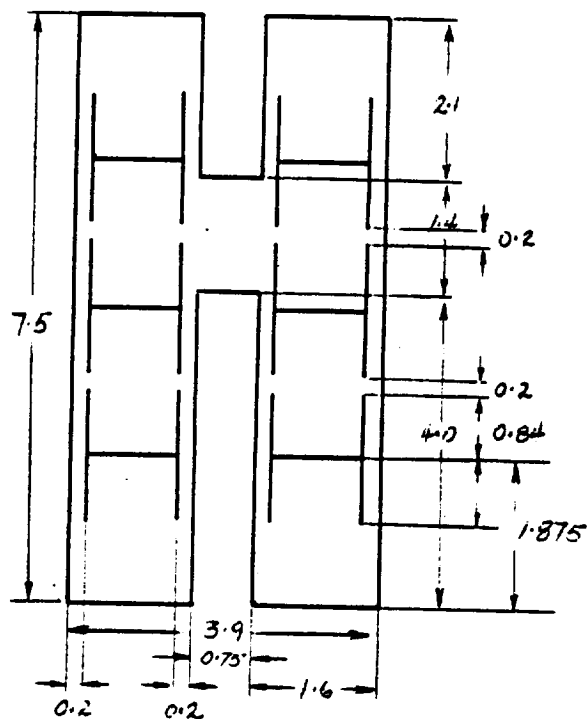
(a)
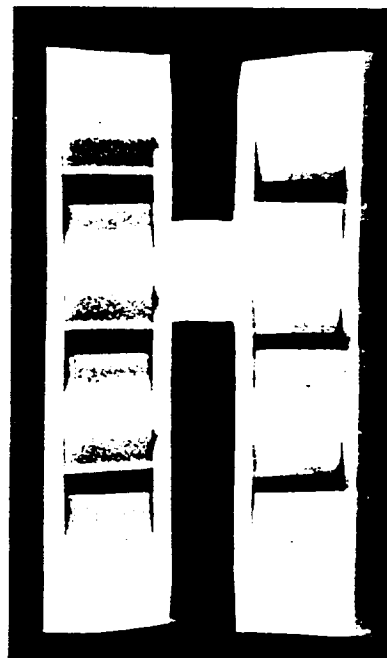
(b)

Figure 2.17   (a) Initial Proposed Redesign of Stirrer Paddle
              (b) Photograph of Actual Teflon Test Paddle (Teflon
              Blade #3)

40

cuts were incorporated to produce additional fins. All test paddles were made from 0.8 mm thick Teflon sheet.

It was evident that the measurement of relative agitation efficiencies by temperature gradients or sedimentation rates would be impractical with the close clearances and the many tests required and, therefore, an alternate approach was adopted. A modified tracer method was developed by which the response to the injection of a tracer was monitored until it approached a constant value. The procedure involved the continuous sampling of fluid (water) from the reactor bottom (fill port) after a tracer pulse (styrene dissolved in water) was injected at the top edge, the relative concentration being continuously recorded via a UV Absorbance Monitor (Model 1840, Instrumentation Specialties Co.) at 245 nm. The flow rate was maintained constant by a syringe pump at 0.733 cm^3/min. A 0.72 cm^3 loop was employed for tracer injection. The output was normalized for comparison of different agitation conditions.

The MLR paddle was the first tested by the tracer or pulse method. The results are given in Figure 2.18 (bottom). As a reference, the OSC Stir Speed conversions to rpm and arc are given in Table 2-1. The

Table 2-1

OSC Stir Speed Conversions

Stir Speed	rpm	Arc^o
3	5.2	34.2
4	8.2	49.1
5	11.3	64.1
6	14.3	79.0
8	20.3	108.9
10	26.4	138.8
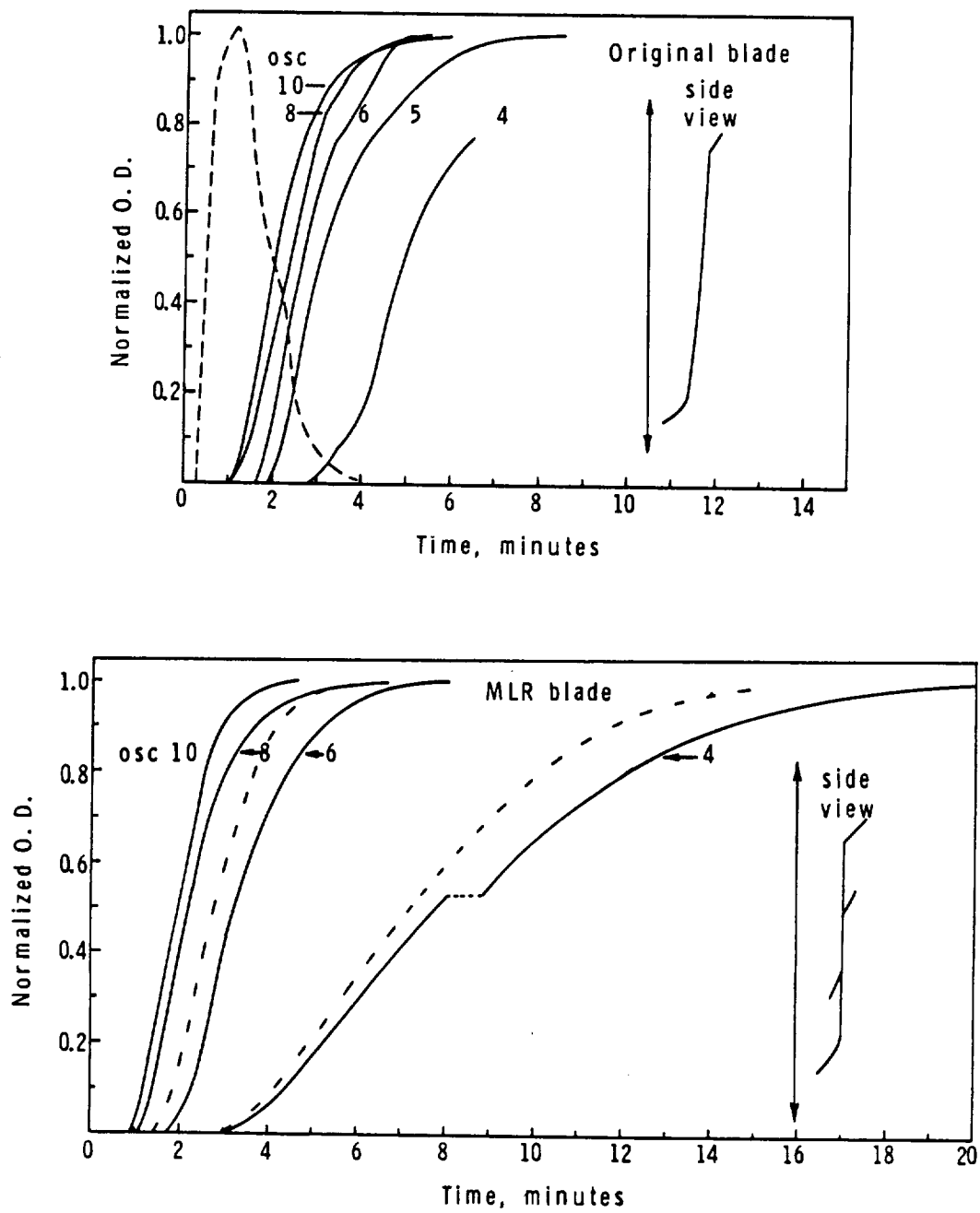
Figure 2.18   Pulse Tests of Original Perforated Stainless Steel
Paddle (Top) and MLR Blade Adapted to LUMLR Stir
Shaft (Bottom)

large vertical arrow on the right side of Figures 2.18 to 2.22 repre-
sents the top to bottom (piston to base plate) distance in the reactor.
To the right of the arrow, the "side view" represents the paddle con-
figuration and orientation relative to the top and bottom of the reac-
tor as seen on edge. The improvement in agitation efficiency with OSC
Stir Speed for the MLR blade was considerable going from 4 to 6 and
continued improvement was noted going to the highest stir speed avail-
able, 10. In the top portion of Figure 2.18 are the results obtained
from pulse tests using the original paddle shown in Figure 2.12a.
This paddle was more efficient in comparison to the MLR paddle at the
lower OSC Stir Speeds 4 - 6 while a close comparison showed it to be
slightly worse at the higher settings of 8 and 10. The dashed line in
the top figure represents the tracer concentration/time profile when
the reactor was by-passed. This gave some idea of how fast the respon-
ses were in the pulse tests. Three variations of a Teflon paddle
(Figure 2.17b) were tested in which the configuration of the direction-
al fins was varied. The results, shown in Figure 2.19, indicated that
the orientation of the directional fins was critical to obtaining good
mixing at low OSC Stir Speeds. The stirrer paddle represented in Fig-
ure 2.19 (bottom) was the best in terms of mixing efficiency, showing
little sensitivity to changes in the stir setting over the tested range.
From this it was obvious that a great improvement in agitation effic-
iency would be gained by substituting the stainless steel equivalent
of Teflon blade #3 for the MLR paddle in the MLR Flight Units.

The increased difficulty involved in the fabrication of stainless
steel paddles which required internal H-shaped cuts stimulated the
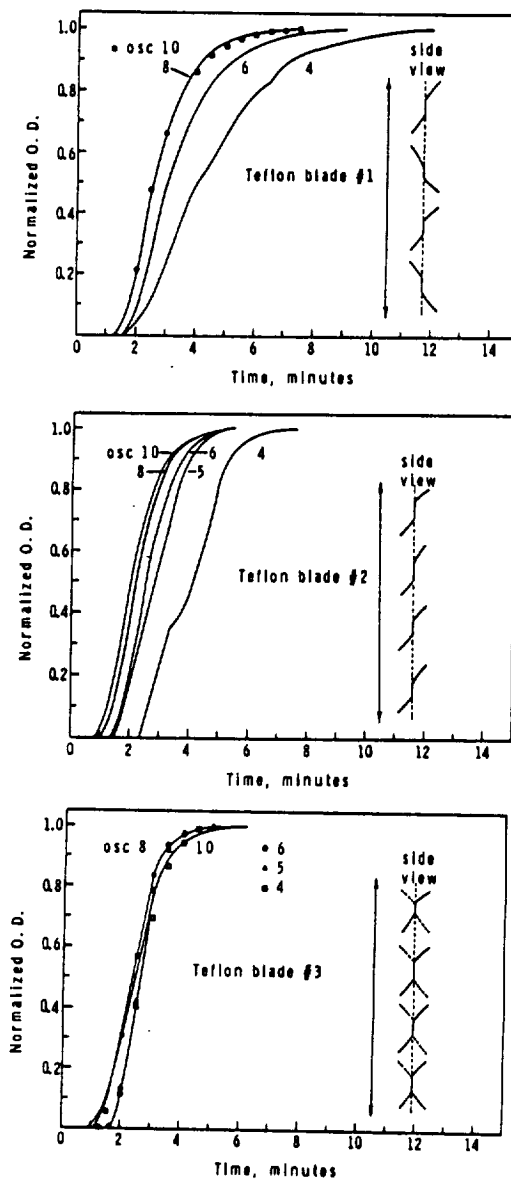
Figure 2.19 Pulse Tests of Teflon Paddles #1 (Top), #2 (Middle) and #3 (Bottom)

44

design and testing of modified forms of the MLR paddle. These alterations involved simply increased dimensions and varied fin configurations. Modified MLR Blade #1 was merely a "blow-up" of the dimensions of the MLR Blade but resulted in much improved agitation efficiencies as given in Figure 2.20 (top). The reduction in "dead" volumes was directly responsible for this improved efficiency. As in the case of Teflon Blade #3, a reversal in the fin orientation on one side of the paddle greatly increased the agitation efficiency as given in Figure 2.20 (bottom). In comparison, the modified MLR Blade #2 resulted in quicker responses in the pulse tests than Teflon Blade #3, indicating improved agitation efficiencies. As seen in Figure 2.20 (bottom), lower OSC Stir Speeds were tested in order to define the lower limits of the efficiency of this stirring paddle. Below a setting of 4, the mixing was shown to become very sensitive to the stir speed. With these results, a modified MLR Blade design was tested which allowed a 0.51 cm (0.2 in) space between the paddle and the piston when set at the 100 cm^3 level, as called for in the MLR blueprints. The results, given in Figure 2.21 (bottom), are quite similar to those in Figure 2.20 (bottom) except that increasing sensitivity to the stir setting began at slightly higher stir rates, being somewhere between 4 and 5. This design gave the best agitation characteristics within the allowed design and time limitations. Subsequently, this design (Figure 2-21, top), modified for mounting in the MLR units, was submitted to and accepted by NASA (MSFC) for the Space Flight experiments.

Even though the stirrer paddle design was finalized, questions still remained as to the arc and speed desired for the Flight experi-

Figure 2.20   Pulse Tests of the MLR Type Blade Modified by Increased
Dimensions (Top) and Altered Fin Configuration (Bottom)

46

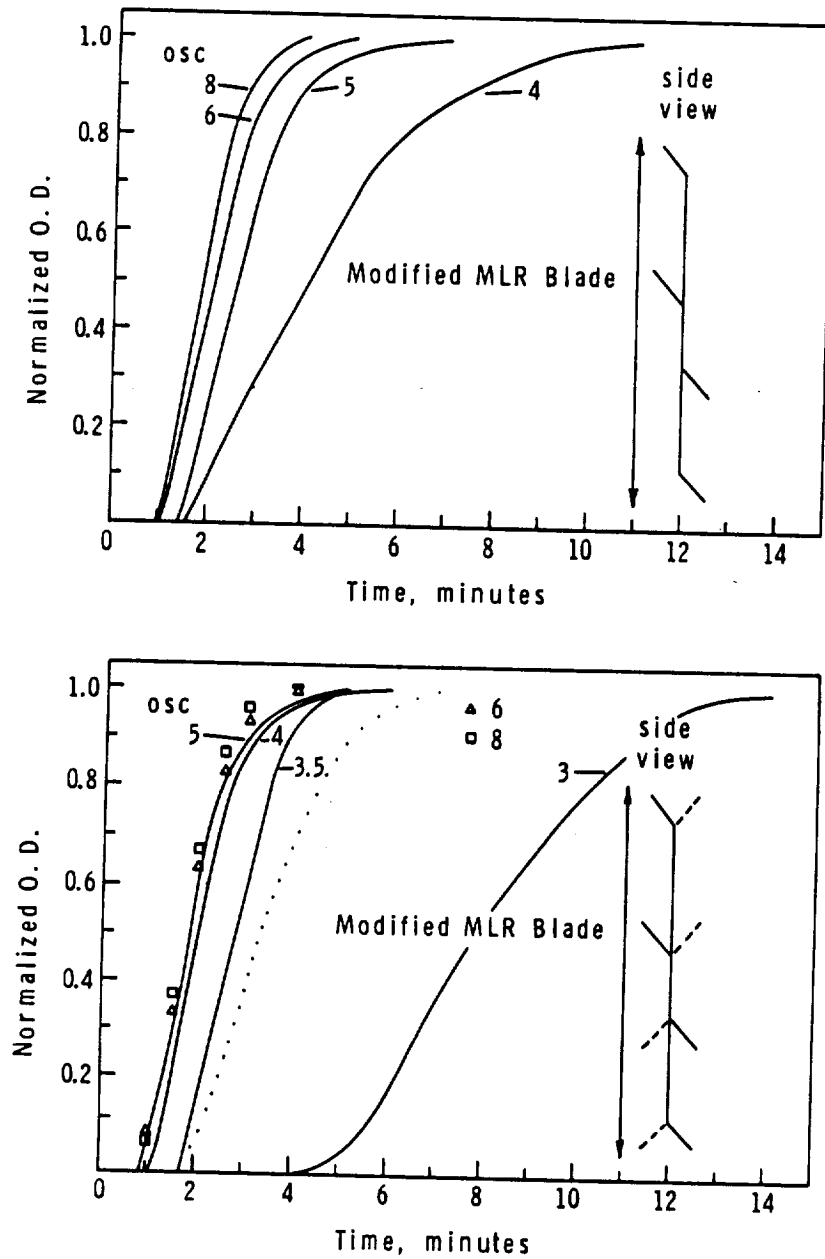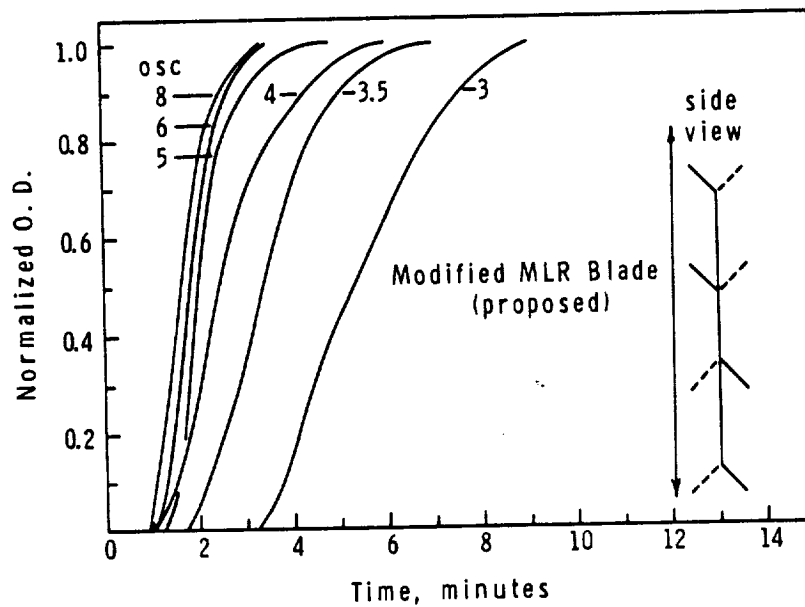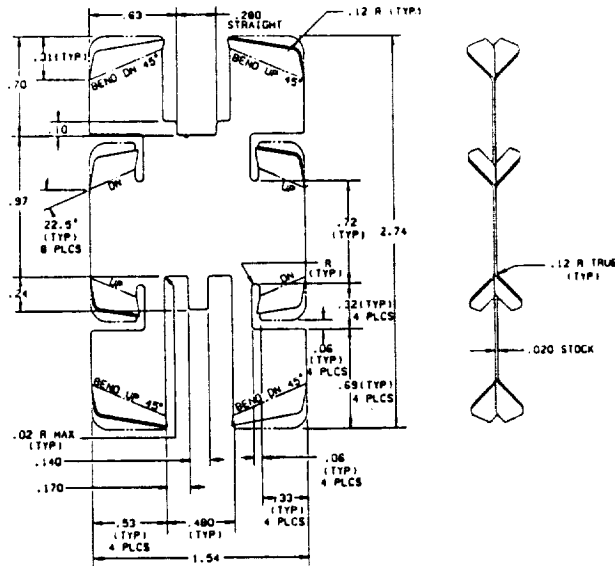Figure 2.21   Proposed MLR Paddle Redesign (Top) with Pulse Tests of
this Design made with a Teflon Blade Adapted to the
LUMLR (Bottom)

47

ments. In the LUMLR the arc was fixed by the rotational speed chosen.
However, the MLR units had a greater flexibility in separating these
two variables. It was initially conjectured that a rotational speed
of 10 - 12 rpm with an arc of 90 - 120° would be sufficient for provid-
ing for the needs of the experiment. The former values were chosen as
a result of these experiments while the arcs were merely based on spec-
ulation. Subsequently, further pulse tests were conducted in which
the arc of rotation was studied (no advancing angle). The clockwise-
counter-clockwise switch on the Stir Mode control was used to reverse
direction based on visual sightings of the stirrer paddle position rel-
ative to arc calibration marks made on the plexiglas cylinder. Using
the modified MLR paddle, pulse tests were run at various Stir Speeds,
two of which are presented in Figure 2.22. At the center of each fig-
ure is a top view schematic indicating the tracer injection location
relative to the oscillating stirrer paddle. From these it was obvious
that the earlier speculation was in error in that the agitation effi-
ciency increased with decreasing arc of rotation from 150° to 30°.
The sensitivity to the magnitude of the arc decreased with increasing
Stir Speed. These results seemed to indicate that the fluid in the
region of the stirrer paddle quickly approached the speed of the paddle
and thus the motion of the paddle was ineffective through much of its
travel. The reversal of direction caused the turbulence required for
mixing and therefore, the sooner the reversal (smaller the arc) the
more efficient the mixing at least up to a 30° arc.

It was apparent from these studies that adequate mixing could
be achieved with as low a Stir Speed as 10 rpm and an arc of rotation

48
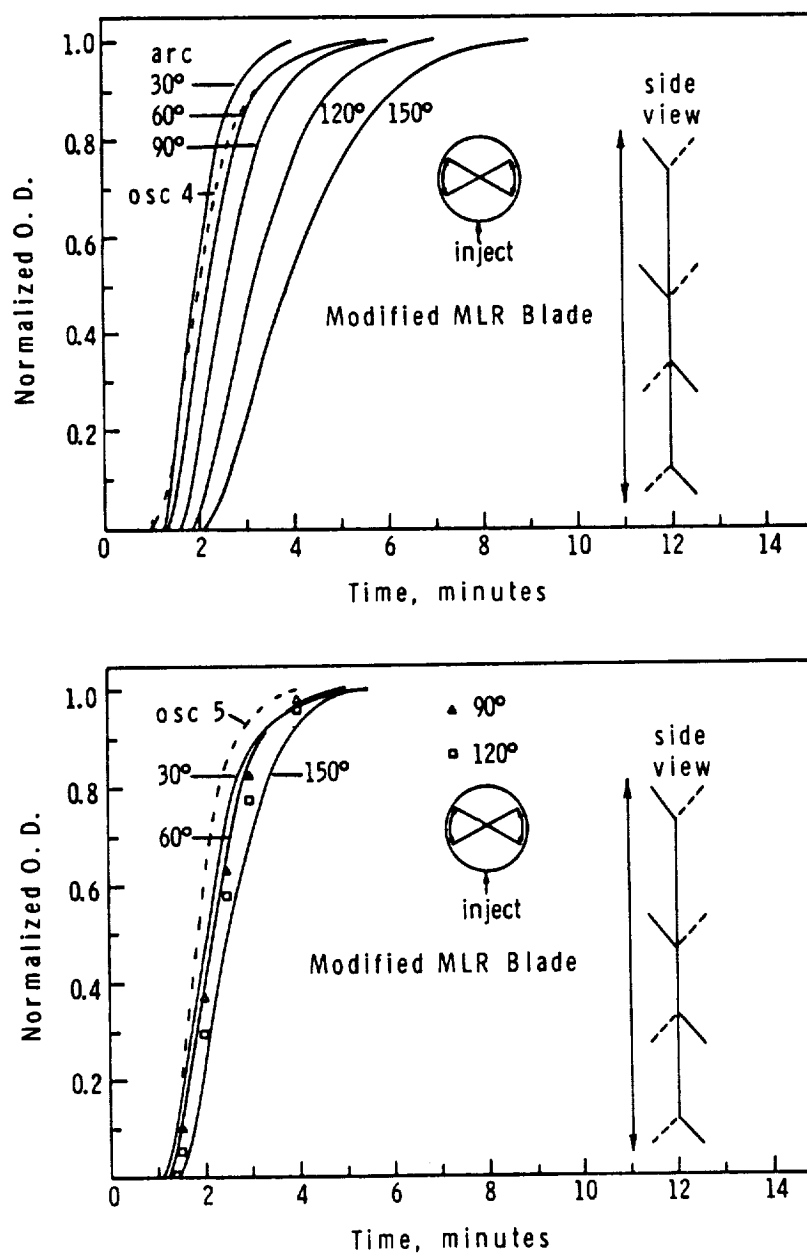
Figure 2.22 Pulse Test Response as a Function of Arc of Rotation
in the Oscillatory Stir Mode; OSC Stir Speeds 4 (Top)
and 5 (Bottom)

of 30° with the improved stirrer paddle design. This applied specif-
ically to the mixing of a molecular species which does not sediment
or cream due to any density differences. This must be kept in mind
when choosing agitation conditions for large-particle-size latexes
swollen with monomer, as proposed for the microgravity experiments.

2.4.3 Volume, Volume Change, and Conversion

The interpretation of kinetic data obtained by dilatometry is
often accomplished by measuring the final conversion by an independent
means, assuming isothermal polymerization conditions, and adjusting
the data end point to match the measured conversion.   This method
would not be applicable to data obtained from microgravity experiments
since during the last hour of polymerization the temperature would be
raised to 90^OC and also several days would pass before recovery of the
latexes. Therefore, data obtained from the reactors should be used to
obtain the conversion histories directly. The LUMLR prototype was
used to define the difficulties and limitations in obtaining accurate
kinetic data from this type dilatometer.

2.4.3.1 Volume Calibration

The LUMLR volume was initially calibrated at GE by loading the
vessel with water and weighing it, recording this value versus the
LVDT voltage reading. This was done several times, obtaining a cali-
bration curve and thereby a means of setting the volume at 100 cm^3.
There were several flaws in this method, however. A means had not
been worked out by which the reactor could be filled without retaining
an undefined and non-reproducible amount of air and therefore, the
LVTD reading would be off by an unknown amount. The amount of fluid

remaining in non-productive regions was included in this (i.e. in fill and exit ports). The LVDT's location and mounting made it extremely sensitive to the handling and disturbances which were routine in the assembly and disassembly of the apparatus. Also, it was necessary to be able to adjust and readjust its position to obtain a desirable voltage range for the piston travel. For these reasons it was necessary to recalibrate the volume and determine a more reliable means of reproducing the 100 cm^3 volume.

The volume of the LUMLR was calibrated by determining the piston position relative to the base plate which gave 100 cm^3 of reactor volume. This 100 cm^3 volume excluded volume contributions from fluid trapped in the o-ring spaces on the piston and below the stirrer shaft cover plate (see Figure 2.5) and in the fill line. It also took into account the volumes of the fluid temperature well, the stirrer shaft and paddles, and the depression of the stirrer shaft cover plate. These contributions were included in the final volume calculations represented in Table 2-2. The 102.12 cm^3 was converted to piston

Table 2-2

Prototype Reactor Volume Computations

	Volume, cm^3
Fluid temperature well[1]	+ 0.33
Stirrer shaft [1]	+ 1.11
Stirrer paddle (original)[2]	+ 0.81
Cover plate depression[1]	− 0.13
Total volume added to 100 cm^3	+ 2.12 = 102.13 cm^3

[1]Determined from measured dimensions

[2]Determined by weight and density

position by simply dividing by the cross-sectional area of the cylinder as determined from the blueprint specification of the cylinder I.D., 4.205 cm. The piston was set at 7.73 cm above the base plate and a permanent marker was scored on the support bolt and nut, thereby creating a reliable method to reproduce the position without relying on an LVDT reading.

2.4.3.2 Volume Change Measurements and Corrections

A polymerization was conducted in the LUMLR by loading the reactor with 100 cm^3 of swollen latex and switching on the heater. The fluid and cylinder temperatures and the LVDT voltages were recorded at regular time intervals until the polymerization was terminated. A detailed description of this procedure can be found in the following section. An example of these data is given in Figure 2.23. During the initial temperature rise, the LVDT voltage decreases, indicating a rise of the piston or an increase in volume followed by an isothermal polymerization in which the LVDT voltage increases corresponding to a decrease in the volume due to polymerization. The objective was then to translate the LVDT voltage data into conversion-time information. In order to accomplish this, the reactor and fluid behavior must be known as a function of temperature. Initial attempts at interpretation of such data often resulted in conversion-time curves such as that given in Figure 2.24, in which the initial portion of the curve did not rise smoothly from zero conversion but instead showed positive and negative deviations from what was expected.

The successful interpretation of kinetic information obtained from the LUMLR requires a knowledge of many factors: 1) the volume of

52
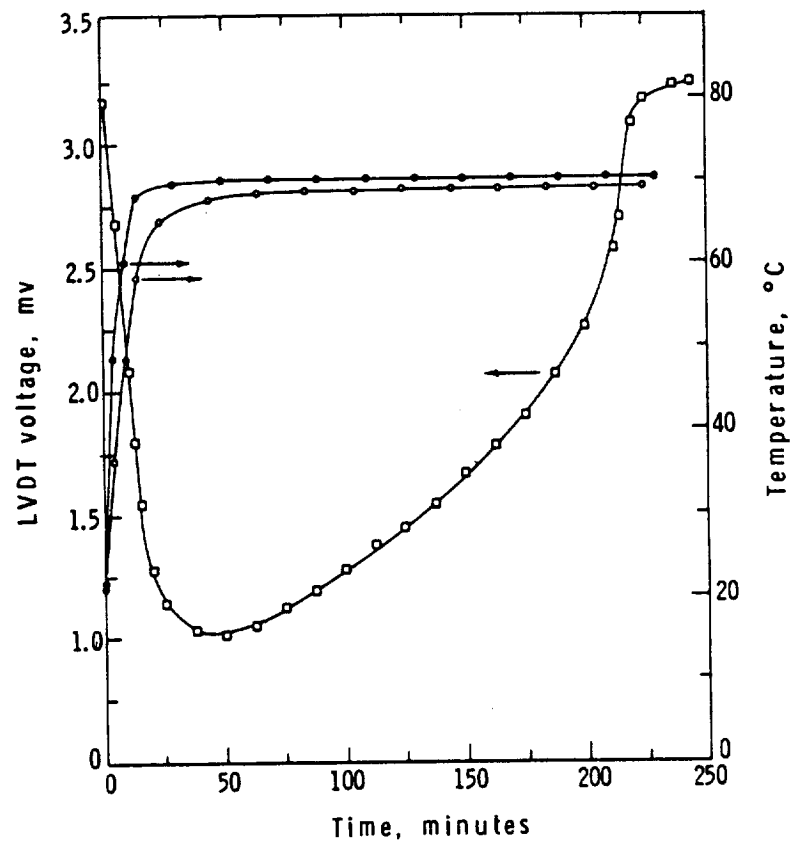
Figure 2.23   LVDT Voltage, Fluid (Open Circles) and Wall
Temperature Data Recorded for a Polymerization
in the LUMLR
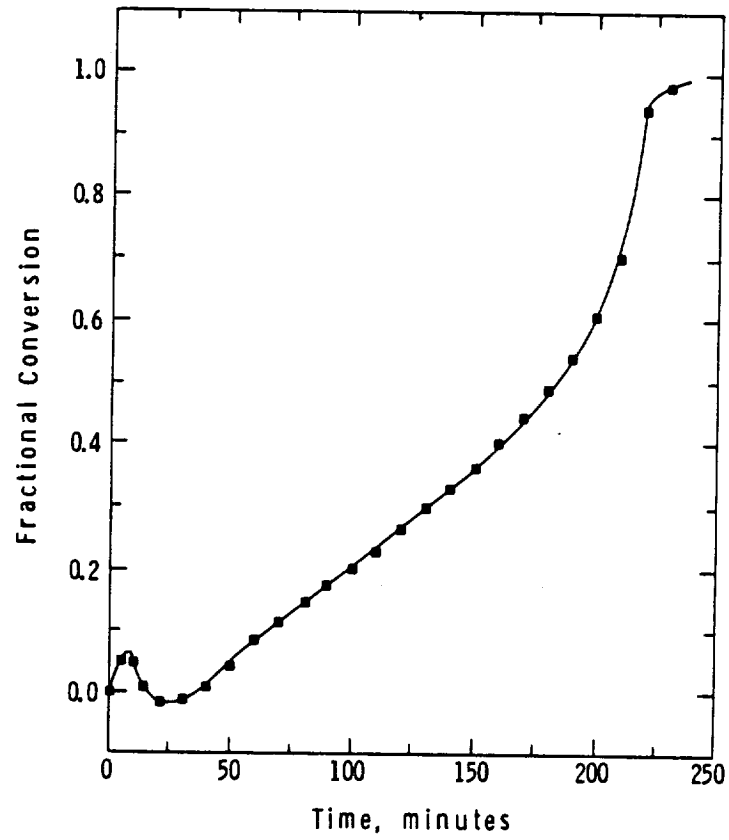
Figure 2.24   Example of an Early Attempt to Obtain Conversion-Time
Information by Interpreting LVDT and Temperature Data

the fluid in the reactor at a given temperature, 2) the average temperature of the fluid at any time, 3) the behavior of the reactor itself (e.g. expansion of metal components and their influence on volume measurements), 4) the composition of the fluid (water, monomer, polymer), and 5) the density/temperature relationship for the fluid at any composition of water, monomer, and polymer. Each of these plays a critical role in the behavior of the system and the interpretation of polymerization data. It was apparent from early attempts at interpretation of kinetic data (Figure 2.24) that not all of these variables or relationships were known with certainty and therefore, a more rigorous understanding was required.

Over an extended period of time numerous experiments were performed in order to better define the behavior of the LUMLR as a dilatometer. Concurrently, polymerizations were run despite the incomplete understanding of this behavior. The evolution of these events will not be described as they took place chronologically but instead will be broken down into a description of the problems found and the eventual solutions which were decided.

2.4.3.2.1 Expansion of Water - Difficulties and Solutions

If the behavior of the LUMLR system (reactor and contents) was well understood it would be possible to predict the movement of the piston during the expansion period in which the temperature is increased to 70°C provided there is no polymerization taking place at the same time. Knowledge of the total contents of the reactor was necessary to be able to predict this movement. As already described,

the volume could be set at 100 cm^3 but this was not easily accomplished due to problems encountered in the loading. The design specifications for the reactor required that it should be filled with a test fluid with a minimal inclusion of air. This was set at 0.1 cm^3. To accomplish this, a fill procedure was outlined by the designers at GE in which the test fluid, contained in a 250 cm^3 separatory funnel, was introduced into the reactor at a slow rate (0.3 - 0.6 m head) through tygon tubing connected to the fill port. The reactor was tilted approximately 30° with the exit port positioned at the upper edge, the piston being just above this position. Once the fluid began flowing from the exit port, a visual check was made for the exit of air bubbles. When no bubbles were detected, the piston was lowered to the 100 cm^3 level, the fill port valve closed, and the tubing disconnected. The LVDT reading was recorded and then the piston was released by loosening the nut holding it in place, thereby allowing the spring to act on the fluid through the piston. The drop of the piston, as recorded by a change in the LVDT reading, was then checked to see if it met the specifications. If not, the piston was once again raised and the procedure repeated until the change in the LVDT reading was within the design criteria. This criteria was established by assuming a pressure of 1 atm. was exerted by the piston via the spring, thereby compressing any bubble present to about half its volume. In reality, this proved to be difficult and non-reproducible. Ten attempts at loading water yielded an average drop of 0.015 cm ($\pm$.003 cm) which was equivalent to a 0.4 cm^3 sized bubble, assuming 1 atm. (gage) was exerted by the piston. However, using a Hg open gage manometer attached to the fill port of the reactor, it was found that the pressure varied from 0.6 to 0.9 atm.

depending upon how well the piston o-rings were lubricated and thus 1 atm. would be an upper limit. (Note that there were two Viton o-rings on the piston, the upper one not contacting the fluid, acting only as a guide.) In order to determine the effect a bubble had on the interpretation of expansion data, experiments were performed by which water was injected into the reactor, previously filled with water, via a microsyringe and the piston position monitored as a function of the amount of water introduced. Two sets of results are given in Figure 2.25 which shows the relationship between the amount of water injected and the amount recorded by converting LVDT voltages into volumes measured. The deviations from ideality, i.e., where injected equals measured, were shown to increase with increasing bubble size (determined by assuming 1 atm. pressure). The compression of the air bubble took place as the amount injected increased until a point was reached in which no further compression took place. After this point the amount injected equaled the amount measured. Fluid was also removed from the cylinder via the microsyringe and compared to the measured volume. The results in Figure 2.25 show that the original relationship obtained by injection was not retraced with removal of water but instead a hysteresis type curve was obtained. Once again, the extent of this hysteresis increased with increasing bubble size, as might be expected. These results were intuitively expected in the case where a bubble's presence was the only problem manifested. In a few cases, however, results were obtained such as given in Figure 2.26, in which a bubble was known to be present and yet the response differed in that the deviation from ideality (volume measured minus

57
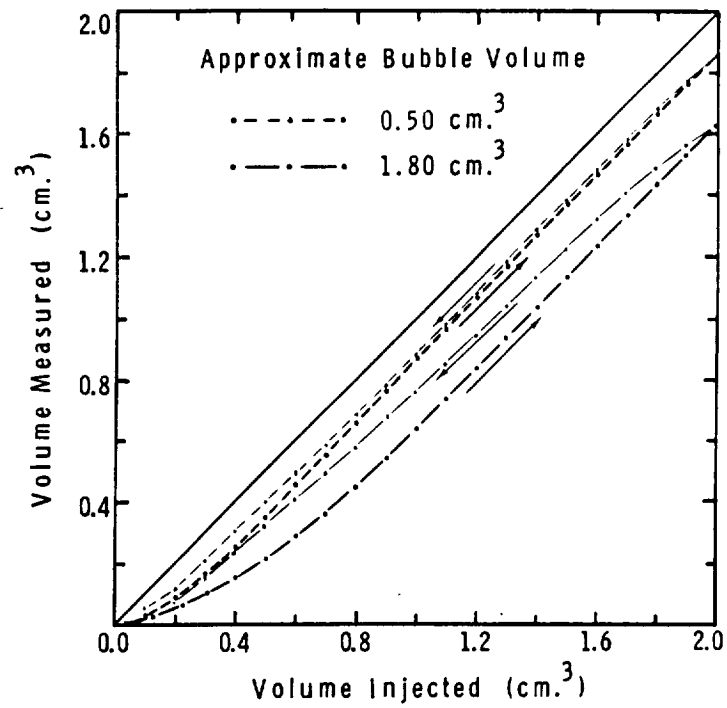
Figure 2.25   Relationships between Volume of Water Injected and
Volume Measured for Two Different Bubble Sizes
Initially Entrapped in the LUMLR
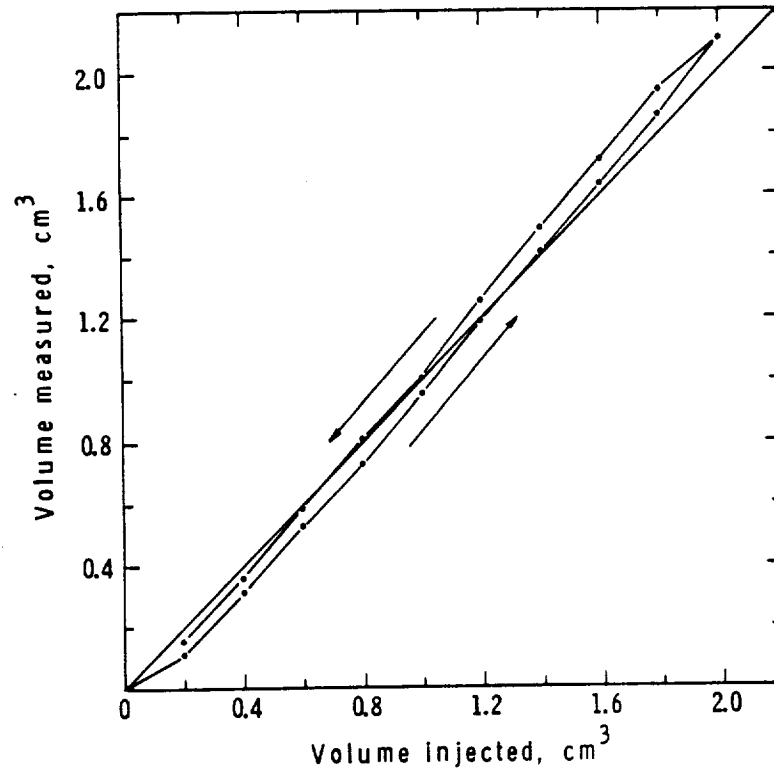
Figure 2.26 Combined Effect of Bubble and o-Ring Roll in the
Comparison of Measured and Injected Volumes

volume injected) was at first negative as expected from the air bubble but then went positive with increasing amounts of water injected. This phenomenon was attributed to the roll of the lower piston o-ring in its groove as it moved upward, displacing water into the main volume of the reactor and offsetting the LVDT reading. The extent of this effect depended on the original position of the o-ring at the start of an experiment (i.e. if it were at the bottom of its groove there was no effect and if it were at the top the effect would be maximum such as in Figure 2.26).

The situation was further complicated through running expansion experiments by simply heating up the water in the reactor, monitoring the LVDT voltage and fluid and wall temperatures. In this case, the prediction of the piston movement was done by computing the volume of the fluid as it increased with increasing temperature and again comparing it to the LVDT converted volume. An attempt at doing this is illustrated in Figure 2.27. First note the curve labelled "No Compensation". This represents a first try at matching the two results. It was obvious that a bubble present in the reactor was at least partially responsible for the deviation of the results from the ideal. As alluded to earlier, it was suspected that the expansion of the reactor itself (i.e. components such as the cylinder, stirrer shaft assembly, temperature well, support bolt) may have to be corrected for, to account for some deviations in the expected results. The most critical of these was found to be the expansion of the cylinder itself. Since the LVDT was mounted on a housing which in turn was mounted on the cylinder any expansion of the cylinder was reflected in the LVDT readings.

60
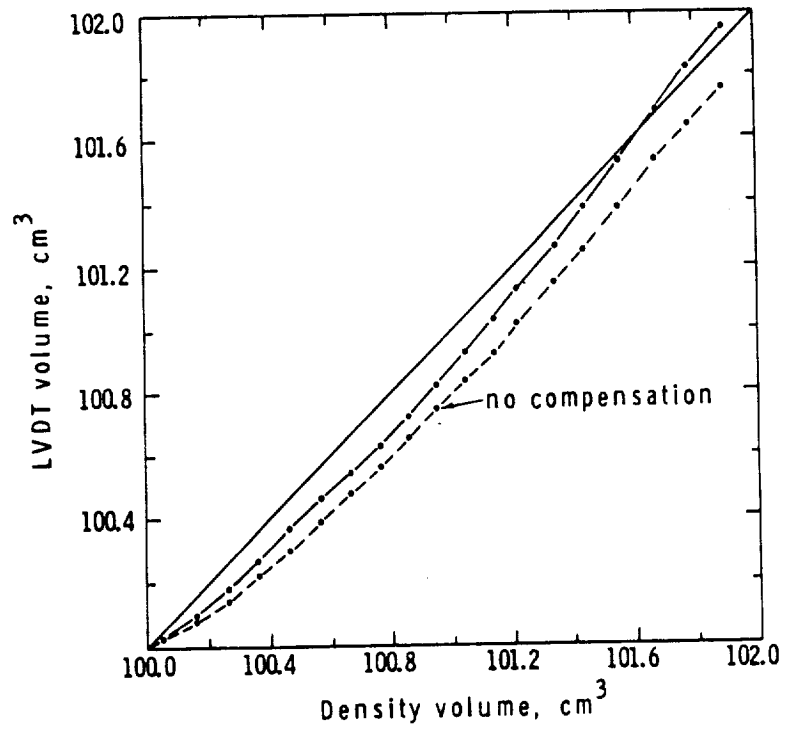
Figure 2.27 Comparison of Volume Computed from LVDT and Fluid
Temperature Data for the Expansion of Water

61

In effect, any increase in the vertical dimension of the cylinder would decrease the change in the LVDT reading. In order to compensate for this expansion a dial indicator was positioned atop the housing cover to measure the displacement due to the temperature increase. This information was recorded along with the LVDT and temperature data. Compensation for cylinder expansion was accomplished merely by adding the cylinder displacement to that recorded from the LVDT. When applied to the water expansion data results were obtained as shown in Figure 2.27. These resemble the results described in Figure 2.26 in which deviations from ideality were attributed to both the presence of a bubble and o-ring roll. A third type of test was run illustrating these problems in which a simulated polymerization was carried out by steadily withdrawing water from the reactor starting at ambient conditions while raising the temperature. The LVDT and temperature data are given in Figure 2.28a. The x's represent the corresponding LVDT position for no change in the temperature, while the dashed line is the LVDT response with no water being withdrawn. When the data were translated into 'conversion' type information (i.e. volume decrease), compensating for cylinder expansion as described above, the results of Figure 2.28b were obtained, the smooth line representing the actual syringe data and the points representing the calculation of the volume decrease from the LVDT, temperature, and gage information. The calculated conversion is shown to be higher than the actual, this being the direct result of the presence of an entrapped air bubble in the reactor. This problem and its solution will now be addressed.

An alternate loading method was developed with the object of
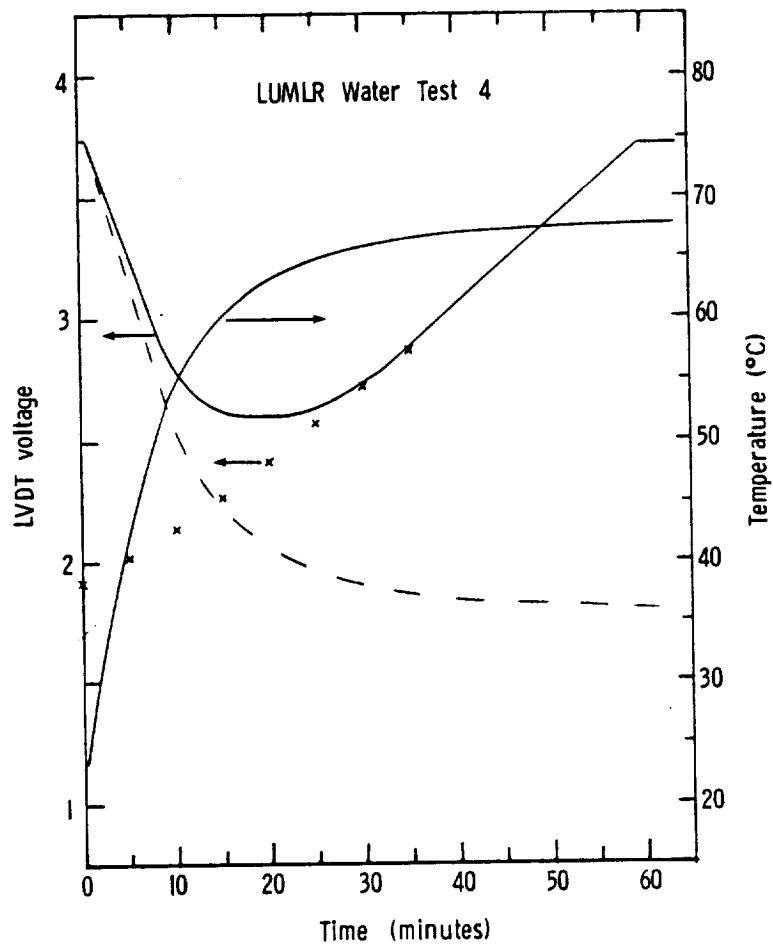
Figure 2.28a Data Obtained from 'Simulated' Polymerization by
Steadily Withdrawing H_2O from the LUMLR During Heat-up.
X'x Represent LVDT Voltage if no Temperature Rise;
Dashed Line if no H_2O Withdrawn
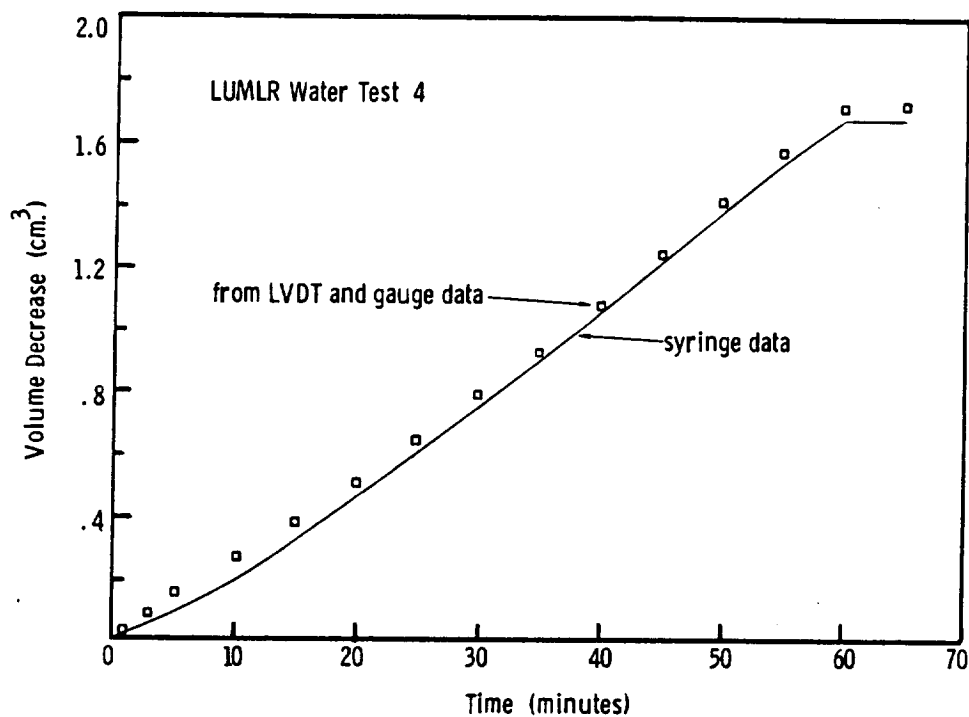
Figure 2.28b Comparison of Measured Volume Change (Syringe Data) with that Computed from the LVDT and Gauge Data ('Conversion') Corresponding to the Data of Figure 2.28a

reducing (or eliminating) air bubble entrapment in the LUMLR. The idea was that if the reactor could be loaded under conditions of reduced pressure that any entrapped bubble would be considerably reduced in volume once pressure from the piston was applied. Also, because any fluid loaded in this manner would have to be degassed at the loading pressure, it was considered that the gas (air) present as a bubble would become redissolved into the fluid, thus eliminating the expansion deviations due to this problem. Therefore, the loading hardware to achieve a low pressure/gravity fill was assembled, as diagrammed in Figure 2.29. The loading procedure was modified to accommodate the need to first degas the fluid. This was usually done around 20 mm Hg for 0.5 - 0.75 hrs, while the pressure was increased to 35 - 45 mm Hg for loading. The flow rate was adjusted so that the reactor would be filled in 15 - 20 minutes. An initial test of this loading method, using water as the working fluid, gave the results in Figure 2.30 along with the data from Figure 2.27 for comparison. These results show that a considerable improvement in the interpretation was obtained but there was still some evidence that a small bubble existed in the reactor during the test. Deviation considered to be due to o-ring roll was also in evidence.

Two separate methods were used to prevent o-ring roll. The first, not intended to solve this problem but to decrease the friction of the piston in the cylinder, made use of a Teflon sleeve which was placed over the lower Viton o-ring. The width of the sleeve was the same as the groove machined out for the o-ring. At this stage the upper o-ring was replaced by a Teflon ring to help decrease piston

65
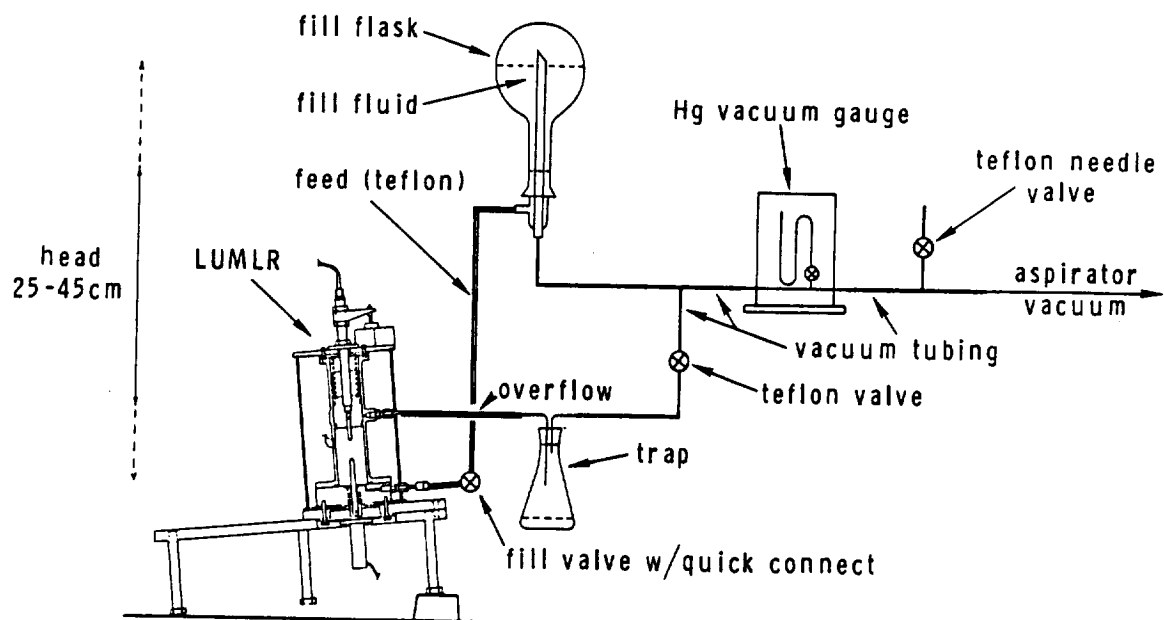
Figure 2.29   Schematic of the Low Pressure/Gravity Loading Apparatus
with the LUMLR
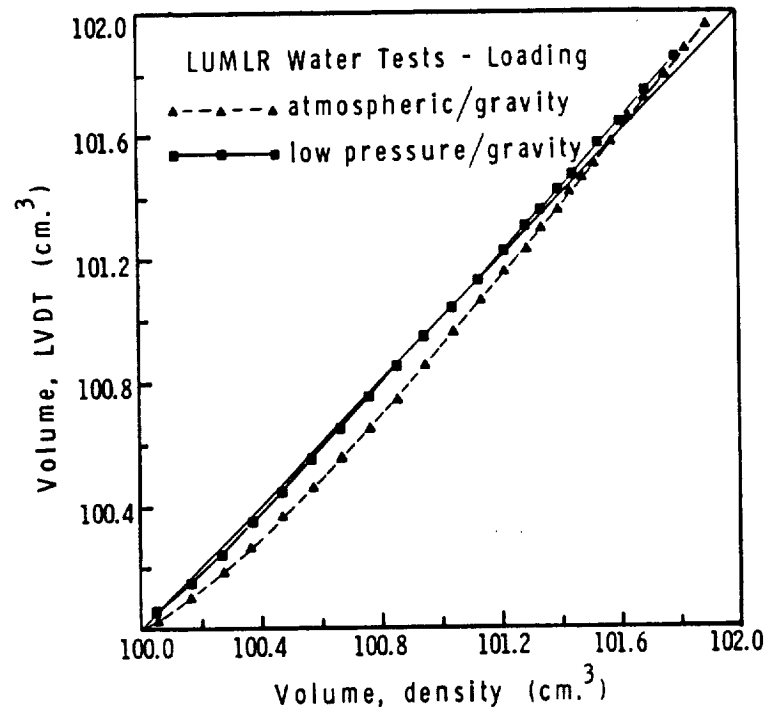
Figure 2.30   Comparison of Expansion Results Obtained for Two
Different Loading Methods

friction. The results of two expansion tests are given in Figure 2.31 where one test was performed after water was loaded at atmospheric pressure and the other at reduced pressure. The former loading method resulted in a behavior denoted by the presence of a small air bubble but did not show the phenomenon attributed to the o-ring roll, instead showing a nearly constant deviation from ideality. The reduced pressure method gave results which showed no effect of entrapped air but diverged from the expected to volumes lower than predicted by the fluid temperature. There were several possible reasons for this, including poor mixing and an initial H_2O volume greater than 100 cm^3. Instead, the real reason was that a leak had developed by which water escaped between the Teflon sleeve and the cylinder surface. Scanning electron microscopy of the sleeve surface revealed well defined grooves which were created when the sleeve passed the fill port hole during the loading operation. For this reason, the use of Teflon sleeves was abandoned.

The second approach used to counteract o-ring roll was to place a Teflon back-up ring on the upper side of the Viton o-ring which was snug and prevented any movement of the o-ring in its groove. Once again a water expansion test was run with the reactor loaded by the low pressure/gravity method. The results are illustrated in Figure 2.32 with both cylinder expansion compensated and uncompensated results being shown. The prediction with compensation was good (maximum error of 1.3%), showing not only the need for this correction but also the need to eliminate air bubbles and o-ring roll. These data gave the best results in the water expansion tests, illustrating that it was

68
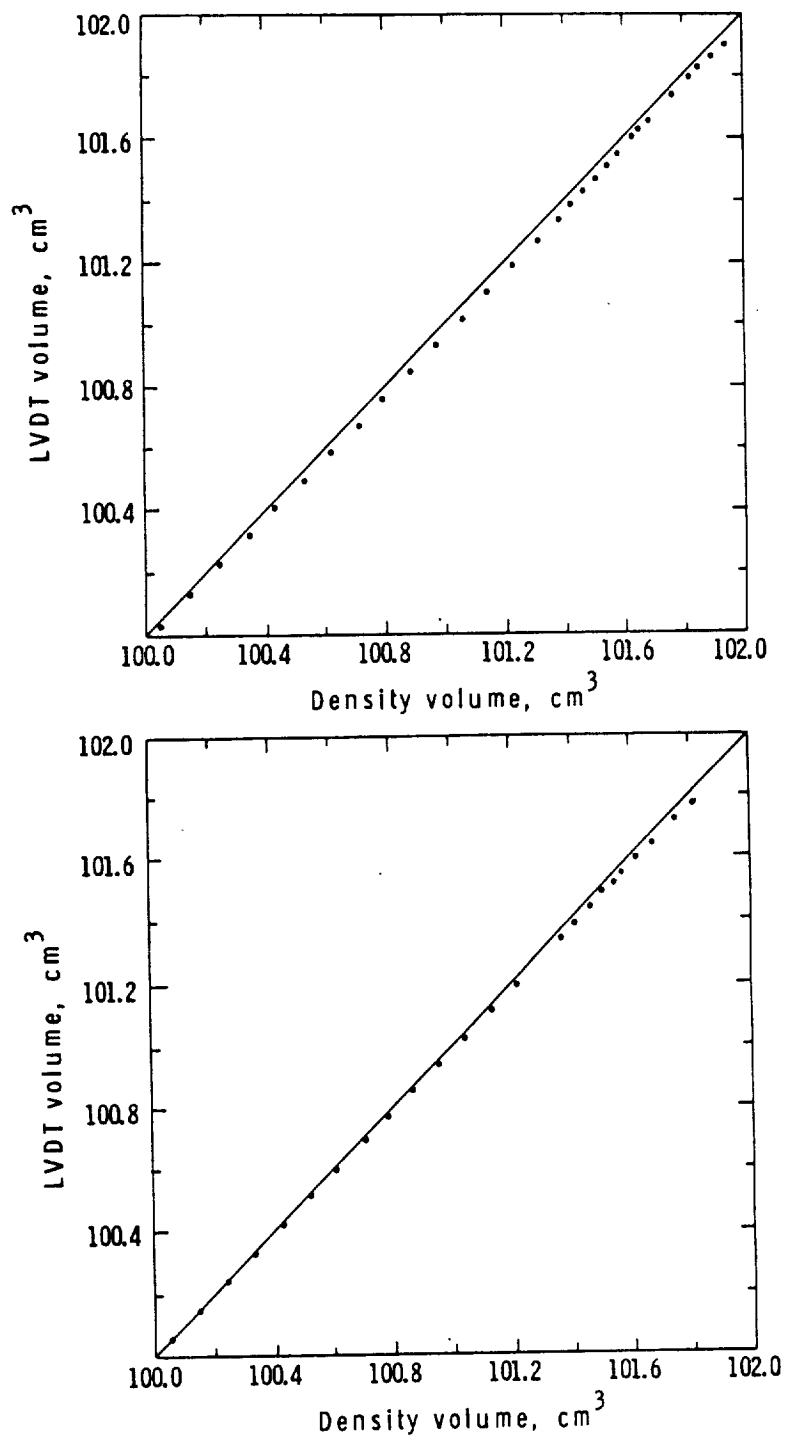
Figure 2.31   Expansion Tests   of Water Using a Teflon Sleeve on the
Lower Piston o-Ring, Atmospheric/Gravity (Top) and Low
Pressure/Gravity (Bottom) Loading Methods
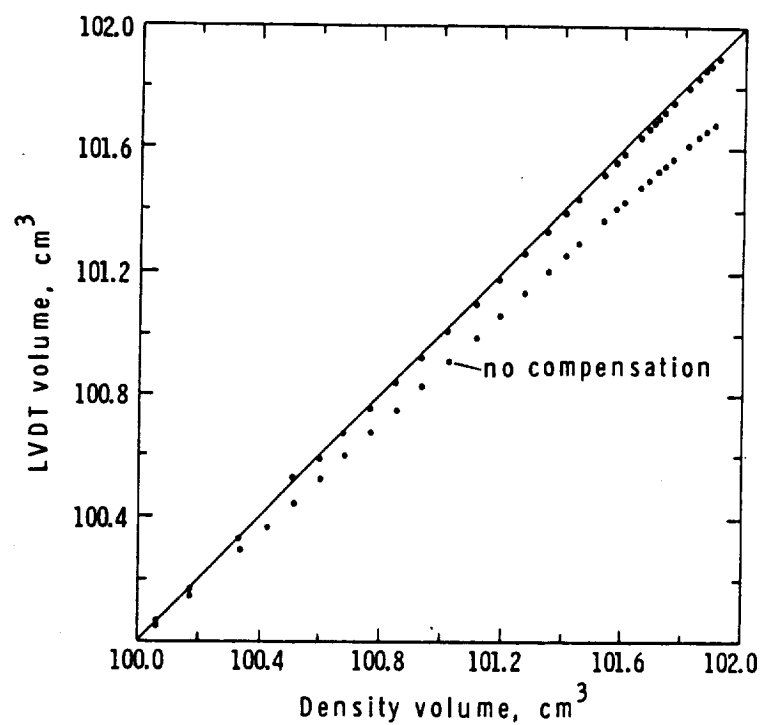
Figure 2.32 Expansion Test of Water Loaded via the Low Pressure/Gravity Technique, Teflon Back-up Ring Included. Comparison is Made with and without Compensation for Cylinder Expansion

70

indeed possible to obtain predictable expansion data from the LUMLR provided the conditions of the water test were reproduced.

Before moving on to the more complex polymerization system, a number of other concerns should be reviewed. The above results were obtained considering the effect of the expansion of the cylinder in the vertical direction by using a gage to monitor the change in height. However, the MLR Flight Hardware had no provision for recording these data and therefore, an alternate means was necessary to approximate the expansion with the data at hand. In order to calculate the expansion using the coefficient of thermal expansion for the stainless steel [10], knowledge of the temperature profile along the cylinder at any time was required. A simpler approach was taken, however, by using the wall and/or fluid temperatures to approximate a mean cylinder temperature. After exploring a number of approaches the most favorable method for approximating the cylinder expansion was found by simply assuming that the cylinder had the same temperature as the fluid along its entire length. This crude approximation is compared with several sets of gage data in Figure 2.33. In general, the expansion is underpredicted in the first minute and after 30 minutes and overpredicted in between these times. The error at long times (>60 min.) is about 10%. This increases the maximum error from 1.3 to 2.2% (error/ΔV) which would be barely perceptible in Figure 2.32. A closer approximation could nevertheless be made by using a polynomial curve fit of these data (i.e. gage = f(fluid temperature)).

The expansion of the cylinder in the radial direction along with the expansion of the stirrer blade and shaft, the temperature probe
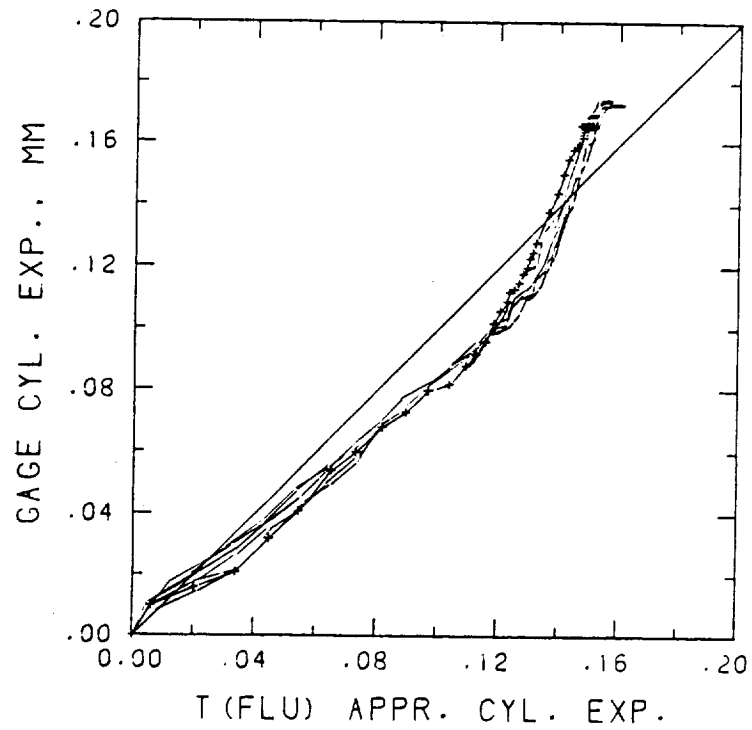
Figure 2.33 Comparison of Cylinder Expansion Data with an Approxi-
mation using T_{FLU} (Fluid Temperature)

well, the piston, and LVDT support bolt have also been considered as potential sources of errors in these measurements. The contributions of most of these were found to be negligible when compared to the major sources of error. The cylinder's radial expansion was treated using the fluid temperature approximation as proposed above for the axial expansion. A number of tests were conducted to find the contribution of the LVDT support bolt. None of these proved positive. Its contribution was therefore assumed to be negligible.

2.4.3.2.2 Expansion and Contraction in Polymerization of a Latex

In order to obtain accurate kinetic data for a polymerization conducted in a dilatometer one must have knowledge of not only the behavior of the dilatometer in recording volume changes but also the volume-temperature-composition relationships of the polymerizing phase. The characterization of the LUMLR as a dilatometer was discussed in the preceding section. The behavior of a latex during polymerization in terms of its volume is discussed in the following.

During the isothermal polymerization of styrene the decrease in volume of which dilatometry takes advantage is due to the decrease in the intermolecular distance between monomer units as they add onto growing polymer chains. When a vinyl monomer such as styrene is polymerized a double bond and a van der Waals bond are traded for two single bonds and a decrease in volume [11]. One might expect that the change in volume can be equated to a conversion merely by use of a conversion factor. This has, however, been questioned in the literature [2,5]. It has been pointed out that dilatometry is not considered an

absolute method for obtaining kinetic data but must rely on conversion factors and independent methods for determining final conversions [12]. The question of volume change and its relation to conversion has been addressed by Rubens and Skockdopole [2] in which they discuss the differences between assuming additive monomer/polymer densities and additive volumes in the interpretation of dilatometric data. In general, most studies assume the volume of the polymer and monomer are additive as in ideal thermodynamic solutions, or in terms of the density of the solution,

$$\rho_{PS} = 1/[(W_P/\rho_P) + (W_M/\rho_M)] \qquad (2.1)$$

where ρ represents density, W, weight fraction and subscripts PS, P, and M polymer solution, polymer, and monomer, respectively. The corresponding expression which assumes additive densities is,

$$\rho_{PS} = (W_P)\rho_P + (W_M)\rho_M \qquad (2.2)$$

Rubens and Skockdopole tested these by measuring densities of polystyrene/ethylbenzene solutions up to 50 wt % via pycnometry. They concluded that additive densities best described their results but their evidence was not overwhelming in that it covered only the lower conversion range. (For a seeded polymerization in which the polymer particles are swollen with twice their weight in monomer, the 'conversion' is already 33% at the start of the polymerization.) Also their densities were reported at only two temperatures (20 and 80°C) without mention of possible effects due to the proximity to the glass transition

74

temperature (T_g) at the higher temperature. A number of questions, therefore, remained. A knowledge of the density of a latex containing water, monomer, and polymer as a function of composition and temperature is necessary to obtain accurate kinetic information from the LUMLR. The densities of water and styrene are known. As in the water expansion tests, the density was obtained through a polynomial curve fit of H_2O density/temperature data. The density of styrene was computed from (13)

$$\rho_S = 0.924 - 0.000918 \ (T_F) \tag{2.3}$$

The density of polystyrene was not found to be as well established, in that a range of values was cited. Amorphous polystyrene was found to have a density varying from 1.040 to 1.065 gm/cm^3 and the crystalline form, 1.111 - 1.120 gm/cm^3. The change in density with temperature was found to be dependent upon whether the temperature was above or below the T_g. The relationships considered for ρ_{PS} were

$$\rho_{PS} = 1.050 - 0.000265 \ (T_F(^{\circ}C) - 20.0) \ \text{for} \ T_F < T_g \tag{2.4}$$

and

$$\rho_{PS} = 1.050 - 0.000605 \ (T_F(^{\circ}C) - 20.0) \ \text{for} \ T_F > T_g \tag{2.5}$$

(i.e. at $20^{\circ}C$ $\rho_{PS} = 1.050$ gm/cm^3). The reason that both of these relationships were considered was that even though the polymerization temperature ($70^{\circ}C$) was lower than any reported value for the T_g of polystyrene ($80 - 100^{\circ}C$), the presence of a solvent such as styrene is known to lower the T_g of a polymer/solvent mixture. The question was what expression applied to the polymer/monomer mixture and whether throughout the course of a polymerization a single expression was

75

adequate to describe the density of the polystyrene produced.

An attempt was made to measure the density of styrene/poly-styrene solutions as a function of temperature and weight fraction polymer via pycnometry. ASTM methods (D792 and D891) were followed in the calibration and density measurements. Styrene monomer was used without removing the storage inhibitor. The polystyrene used was ob-tained in the form of pellets (Monomer-Polymer and Dajac Laboratories, Inc.), being classified as high molecular weight ($\overline{M}_W = 3.42 \times 10^5$ via GPC). The densities of all solutions were linear with temperature. The weight fraction polystyrene could only be raised as high as 0.40 due to the high viscosity. Some results are compared in Figure 2.34 with computations using Equations 2.1 - 2.5. At 70°C there are four curves representing: 1) additive densities with ρ_P for $T < T_g$ (A) and $T < T_g$ (B), and 2) additive volumes with ρ_P for $T > T_g$ (C) and $T < T_g$ (D). At 25°C the relationships overlap to such a degree that only two curves are presented (A' and C' defined as A and C). The small circles repre-sent the data obtained via pycnometry. These results seemed to indi-cate that either additive volumes with ρ_P determined using Equation 2.4 ($T < T_g$) or additive densities with Equation 2.5 ($T > T_g$) was appro-priate for determining the volume of styrene/polystyrene solutions. However, this was not considered to be conclusive evidence in light of the sample used and its difference from a latex system (i.e. the higher molecular weight polymer, and the unknown effect of the monomer/polymer and aqueous phase interface).

Concurrent with the water testing, described in the previous section, a number of expansion tests were run using polystyrene latexes

76
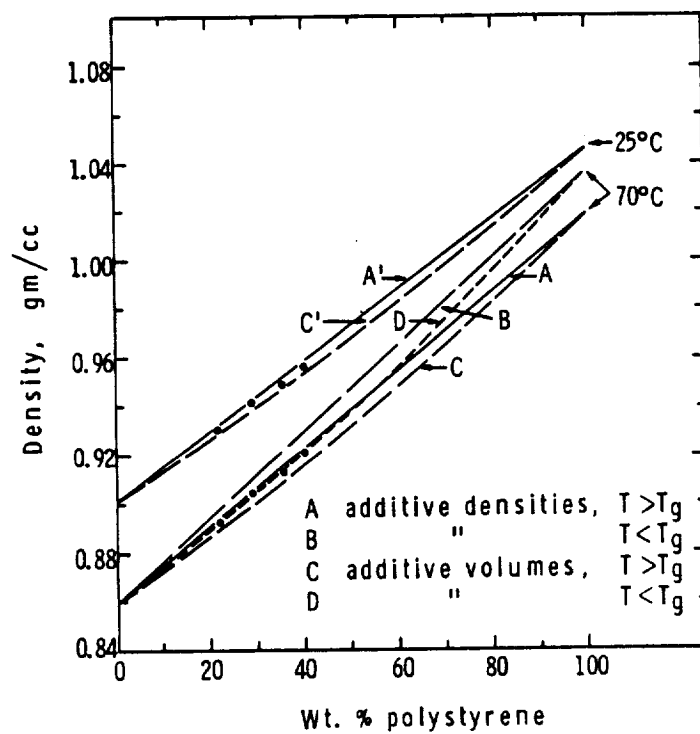
Figure 2.34 Density of Styrene/Polystyrene Solutions as a Function of Composition at 25°C and 70°C. ○ Represent Data Points

and also latexes swollen with monomer but without added initiator. The problems of air inclusion and o-ring roll, however, overshadowed the effect of the various density functions tested, only illustrating their relative differences. Subsequently, the various density functions were tested on data obtained from seeded emulsion polymerizations conducted in the LUMLR after the low pressure/gravity loading method had been developed and the back-up ring installed. The approach was empirical in nature. Each relationship was substituted into the set of equations used to compute the conversion and the results compared. The results giving not only the most satisfactory expansion prediction but also the closest final conversion when compared to an independently determined value, determined the relationships to be used in all future work.

Seeded emulsion polymerizations of monodisperse latexes were carried out in the LUMLR primarily to obtain information regarding the transition of kinetics from what was considered to be emulsion to bulk behavior. These were performed in a sequence of steps in which particles were successively 'grown' to larger sizes. These experiments will be described in detail in Chapter 3. The initial data were also used to gain some understanding of which density functions would give the closest estimation of the expected behavior in terms of volume change due to temperature changes and also due to conversion of monomer to polymer. As before, the expansion volume of the fluid as measured by the displacement of the piston (corrected LVDT data) was compared to the volume predicted from the fluid temperature and the initial contents of the reactor. The conversion was estimated in terms of the

78

grams of polystyrene produced divided by the initial grams of styrene. This was computed from the difference between the volume determined from the LVDT reading, and the volume calculated from the T_{FLU} based on the contents of the reactor considering that no conversion had taken place. A more complete description of this and how the initial fluid contents of the reactor were determined are given in Chapter 3. Data collected from initial polymerizations were analyzed to determine the effect of three variables: 1) additive densities versus additive volumes, 2) the density function of polystyrene above versus below its T_g, and 3) T_{FLU} estimation versus gage (dial indicator) compensation for cylinder expansion. The variation in results obtained using the gage versus T_{FLU} approximation was minor in comparison to the other effects and are not illustrated here. The interpretation of kinetic data via the remaining four variations are shown in Figure 2.35. The use of the computation variations involving Equation 2.5 (i.e. ρ_p for $T > T_g$) was immediately rejected for two reasons. First, the deviations during expansion increased with increasing temperature. This was a direct result of using the density expression for polystyrene at a temperature above its T_g. Apparently, one can infer from this that the density of a polymer in solution is the same as in the solid even though it is plasticized by a solvent. Secondly, the final conversions determined from the dilatometry exceeded 100% (103.8% for the case of additive volumes and 108.1% for additive densities) which of course is an impossibility. The remaining two computations using the density functions for polystyrene at a temperature below its T_g also show deviations between the predicted and measured volumes but to a lesser

79
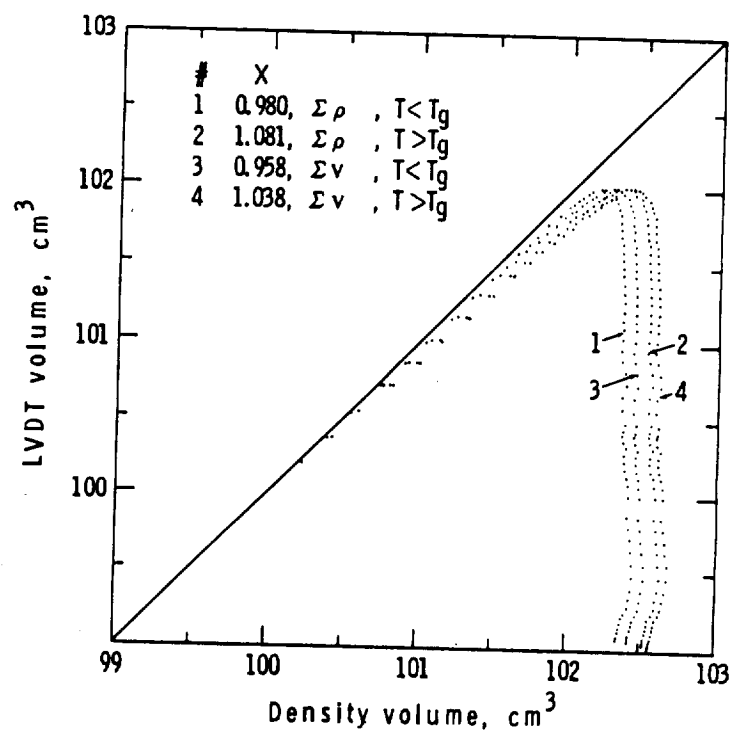
Figure 2.35 Comparison of Computation Variations for a Seeded
Emulsion Polymerization. x = final conversion.

extent for the computations assuming additive densities. One must remember that this was an actual polymerization and that some deviation could not be ruled out due to actual polymerization. The final conversions (based on total polymer) obtained via dilatometry were 95.8% for the case of additive volumes and 98.0% for additive densities. The final conversion measured by iso-octane extraction (see Section 3.5.1.5) was 97.3%. The entire conversion curve along with the fluid and wall temperature data are given in Figure 2.36 for the case of additive densities. It was concluded, in this case, that the use of additive densities was more accurate than additive volumes for characterizing the density of styrene/polystyrene solutions in a latex. Further tests on these variations were performed with other sets of data and generally the cases using additive densities proved to be the more acceptable. These findings are in line with those of Rubens and Skockdopole [2] who also found additive densities to be the more suitable relationship for describing their results. These results also show that the LUMLR dilatometer can be used to obtain accurate kinetic data from direct interpretation of the data provided that the reactor was loaded free of any air bubbles, o-ring roll was eliminated, agitation was efficient, the fluid temperature and volume were known, and the actual contents of the reactor (recipe) were determined.

2.4.4 Isothermal Character

"Temperature control loops are usually slow because of the sensor lags and the process heat transfer lags." [14] This statement can apply to large scale systems as well as small ones such as the LUMLR dilatometer. A lag in the measurement of the fluid temperature would be
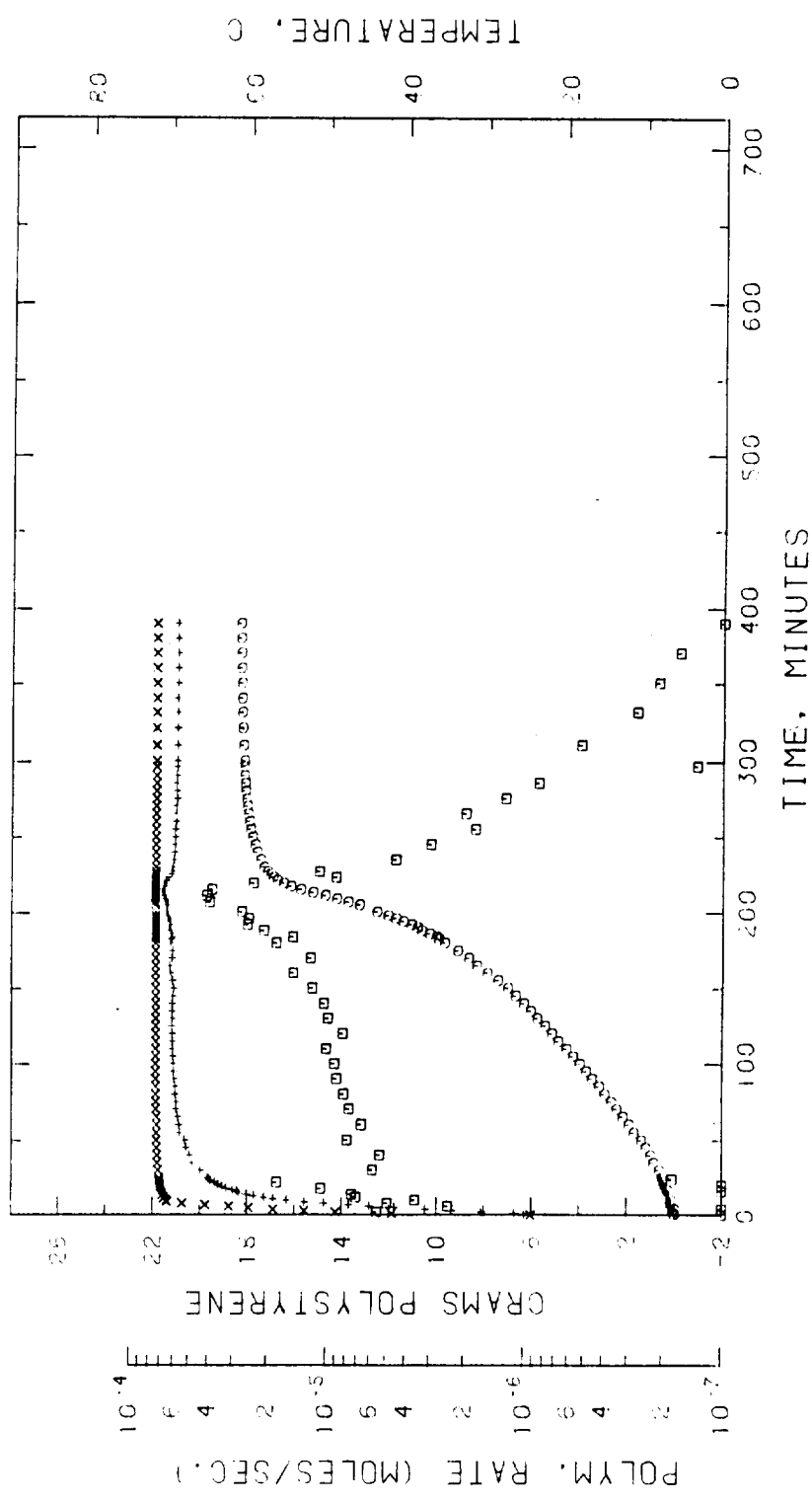
Figure 2.36 Conversion History Obtained for a Seeded Emulsion Polymerization, Assuming Additive Monomer/Polymer Densities. + and x Represent Fluid and Wall Temperatures, Respectively and ▢ , Polymerization Rates

exposed by deviations in the interpretation of expansion data. The
water expansion results given previously in Figure 2.32, however, show
only a very slight deviation which could not be attributed to any tem-
perature lag. Nonetheless, evidence for a lag was presented in Figure
2.14 which showed a difference as great as $1^{o}C$ between the T_{FLU} sensor
and a thermocouple placed next to the temperature well during a heat-up
cycle. Deliberate measurements of this sensor lag were made, the data
showing that a lag as high as $1.7^{o}C$ was possible. Figure 2.37 indicates
that this lag reaches a maximum at about 15 minutes, and then decreases
approaching zero. Apparently, this has little perceptible effect on
the interpretation of expansion data, possibly because the average tem-
perature of the fluid in the reactor lags behind the temperature mea-
sured at this point. The only perceivable effects of lag in the fluid
temperature measurement were found when the fluid viscosity in some
experiments was increased by expanded double layer effects thereby re-
ducing the mixing efficiency.

Since the controlling temperature sensor was located in the re-
actor wall and not in the fluid, severe process heat transfer lags
were possible between the reaction fluid and this sensor (i.e. temper-
ature control would be poor if a rapid exothermic reaction took place).
A measure of this lag was the degree to which the reaction fluid tem-
perature deviated from the isothermal condition. The actual control
mechanism is not known, however, a description in terms of behavior
can be offered. When the heat-up cycle in the LUMLR is initiated, a
continuous 36.5 vdc is applied across the heating wire until the wall
sensor reaches a temperature of $68.3^{o}C$ at which time (10 - 15 min. de-

83
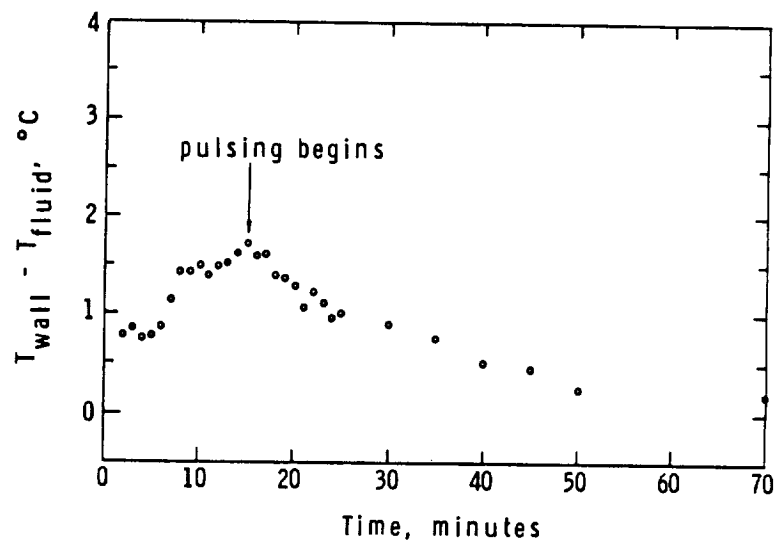
Figure 2.37   Measurement of the Lag in the Fluid Temperature
Sensor Measurement under Well Stirred Conditions
(OSC 8.0 - MLR Paddle)

pending on initial T_{FLU}) the voltage begins to pulse with a decreasing 'on' time as it approaches the 71.5°C control wall temperature. This is indicated in Figure 2.37 at the maximum temperature lag. The fluid temperature reaches about 51°C when the voltage begins pulsing and thus the approach to its steady state temperature (69.0 ± 0.5°C) takes place over an extended period of time. After 30 minutes the fluid temperature is about 66°C and at 60 minutes about 68.5°C. For a relatively slow polymerization, the fluid temperature reaches steady state and will remain there throughout the reaction. A fast reaction, however, may never truly reach a steady state temperature until after its rate maximum has passed. An example is given in Figure 2.38, which shows the kinetics of a polymerization which was essentially complete in about 2 hours. After about 50 min. the fluid temperature rose slowly, (~0.02°C/min) until the polymerization rate exceeded about 1×10^{-7} moles/cm^3 sec. As the rate increased to a maximum of 5.5×10^{-7} moles/cm^3 sec the temperature climbed to 69.9°C or about 1°C above the steady state value. No change was noted in the wall temperature until the fluid temperature was about 69.8°C (a 0.1°C change was noted) illustrating that a lag did indeed exist in heat transfer between the fluid and the wall sensor. In this case, as well as all others run in LUMLR, this problem did not have any serious consequences and therefore was not judged to be unacceptable. If, however, the reactor had been better insulated, cutting down on heat losses, the problem may have required correction. Computations were made for the imaginary case in which no heat loss took place and the fluid temperature was allowed to rise without control, due to the heat of reaction. For

85
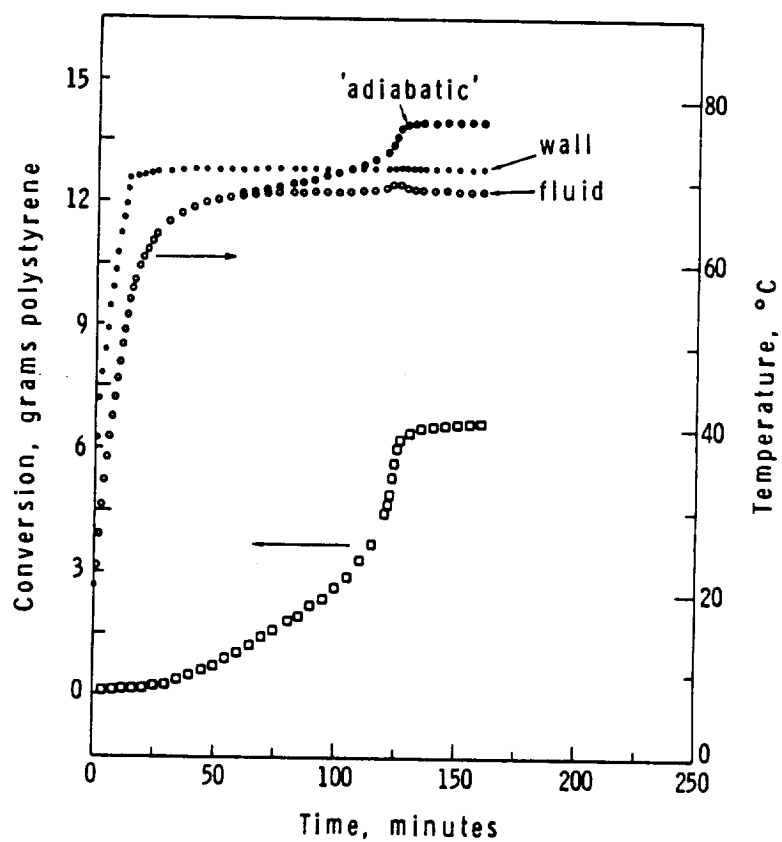
Figure 2.38 Conversion and Temperature Histories for a Seeded
Emulsion Polymerization. Adiabatic Computations
were Made Considering no Heat Loss After First 60
Minutes

this case (Figure 2.38) it was found that the temperature would rise to 78°C by the end of the polymerization. This illustrates that this method of control works satisfactorily partially because of certain heat losses from the reactor. When the net amount of heat transferred to the fluid, computed from the fluid temperature history, was compared to the heat entering the fluid due to reaction, it was seen that considerable heat must be transferred out of the system (the fluid) to maintain the given temperature profile. These results are shown in Figure 2.39 for the reaction kinetics given in Figure 2.38. A number of empirical relationships were derived to predict the temperature rise (and fall) due to high polymerization rates ($>1 \times 10^{-7}$ moles/cm^3 sec) for the purpose of being able to simulate seeded emulsion polymerizations of monodisperse latexes through a mathematical model. These contributions, based on the heat evolved from reaction versus the heat loss from the reactor, were subsequently found to be negligible in light of other kinetic considerations, however.

There was also some concern in these studies that a latex particle may be able to exist at a higher temperature than the surrounding fluid due to the internal polymerization reactions. However, in computations assuming extreme conditions, the radial temperature profile was found to be isothermal. Only extremely high polymerization rates and particle sizes on the order of 1 mm in diameter could produce any perceivable temperature gradient in the particle. This finding has been verified by others in this laboratory [15].

2.5 Summary

A stainless steel piston/cylinder type dilatometer, designed and
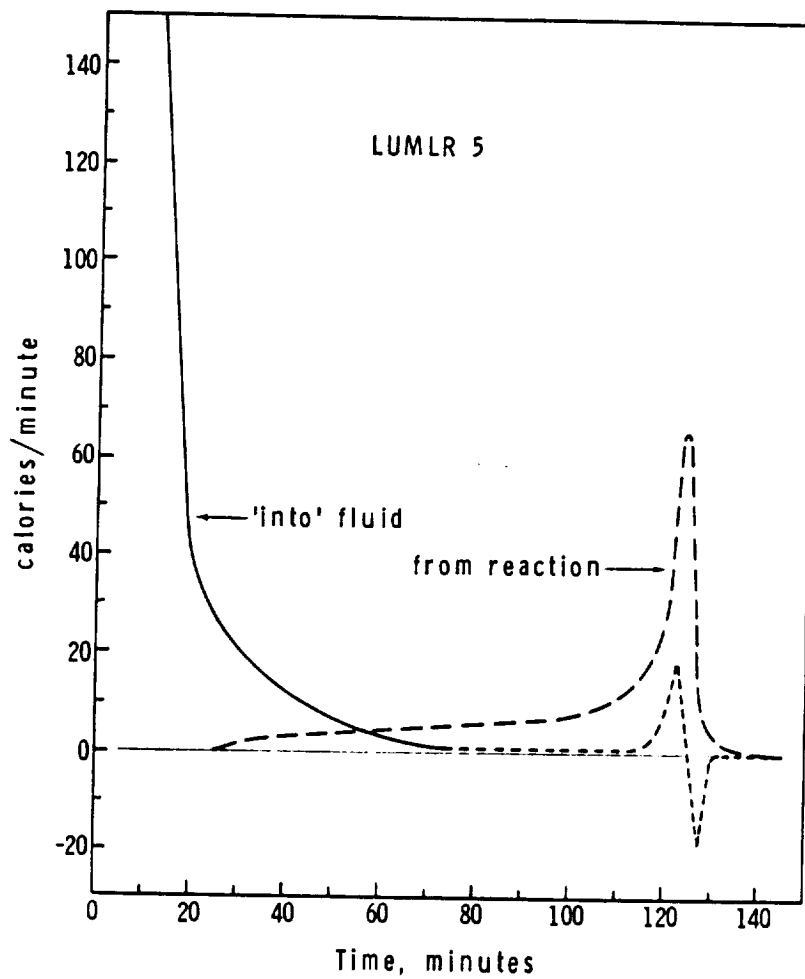
Figure 2.39   Rate of Heat Transfer to the Polymerizing Latex Computed from the Temperature History ————————— and Conversion History —— —— —— ——.

manufactured by General Electric Space Science Labs, was calibrated, modified and tested. Agitation, in an oscillatory mode, was investigated for efficiency in terms of reducing temperature gradients and the sedimentation of large size latexes. An improved stirrer paddle was designed and tested (pulse tests) and found to be much more efficient than the original design. Adequate mixing could be achieved with as low a stir speed as 10 rpm and an arc of rotation of 30° (oscillatory mode). This is recommended for polymerization experiments in microgravity.

Volume changes due to heat up and polymerization can be predicted within ~2% of their actual values provided that: 1) the reactor is loaded without air inclusion via a low pressure/gravity procedure; 2) the exact volume (± 0.2 cm^3) of the fluid occupying the reactor is known from the calibration of piston position; 3) the lower piston o-ring is held in place by a back-up ring; 4) the average temperature of the fluid is known (i.e. adequate mixing) as a function of time; 5) cylinder expansion is compensated for via gage data (or T_{FLU} approximation); 6) the exact composition of the fluid is known (i.e. styrene via iso-octane extraction); and 7) the appropriate density functions for water, monomer, and polymer are used in the interpretation of the kinetic data. The accuracy of the end point in the polymerization should be verified by independent means (e.g. iso-octane extraction).

Relatively fast reactions generally cannot be conducted under strictly isothermal conditions in the LUMLR due to the control scheme incorporated. Slow reactions, however, can be run at a constant temperature of $69.0 \pm 0.5^{\circ}$C. Steady state is reached in about 60 minutes.

C-2

The LUMLR prototype dilatometer is a rugged piece of hardware designed for a specific application, capable of providing the means for producing monodisperse latex and relevant kinetic data.

CHAPTER 3

KINETICS OF SUCCESSIVE SEEDING OF MONODISPERSE LATEX

3.1 Introduction

The emulsion polymerization of relatively water insoluble mono-
mers, such as styrene, is largely recognized to proceed through three
separate kinetics stages. Initially, the system is composed of a con-
tinuous water phase in which surfactant is present either as free mol-
ecules, micelles, or adsorbed onto large (~10 μm) monomer droplets.
The majority of the monomer is found in these droplets with the remain-
der solubilized in the micelles or in the aqueous phase. Particle form-
ation takes place in Interval I when free radicals from decomposing
initiator enter micelles and initiate polymerization. Interval I ends
when all micelles have disappeared either by particle formation or by
disbanding to support the growth of other particles. Interval II is
the growth stage, in which free radical polymerization continues to
take place in the monomer swollen particles, the monomer concentration
being maintained by diffusion from the monomer droplet reservoirs.
Once these reservoirs are depleted, the monomer concentration in the
particles begins to fall due to continued polymerization. This signi-
fies entry into Interval III. The conversion at the beginning of this
stage is known as the critical conversion, X_c, which differs depending
on the monomer/polymer system [17]. For styrene/polystyrene, X_c has
been reported to be in the 0.25 to 0.35 conversion range (i.e., 3/1 to
2/1 monomer to polymer particle swelling ratios, respectively). Partic-
le shrinkage generally takes place in Interval III because the polymer

produced is denser than its monomer. Typically, Interval III ends with the cessation of polymerization. However, another interval has been proposed to account for the possible reappearance of micelles caused by desorption of emulsifier during particle shrinkage [18]. A new crop of particles is then formed in Interval IV, and the remaining monomer is consumed.

Generally, the particles formed through emulsion polymerization have a relatively broad particle size distribution (PSD) with sizes varying from 0.1 to 0.4 µm. "Monodisperse" latexes, those with a very narrow PSD, can also be produced by this same process if the particle nucleation stage (Interval I) is kept short relative to the particle growth stage. This preparation method can only produce sizes in the 0.05 to 0.2 µm range. To grow larger sizes the method of successive seeding is used in which the small particle size latexes are swollen with monomer and polymerized in a series of growth cycles. It should be noted that an alternate method for preparing monodisperse latexes has also been developed by which particles as large as 1 µm are pre-pared in the absence of emulsifier [23]. This method, however, pro-duces latexes of relatively low solids contents.

The method of seeding is popular not only in the preparation of larger size monodisperse latexes but also in the study of the many mechanisms involved in the emulsion polymerization process [24,25,26, 27,28,29]. The use of this technique eliminates the need to treat the complex particle formation step (Interval I), thus simplifying the study of the parameters affecting particle growth. Generally, seeded emulsion polymerization is an Interval II and/or III process. If the

amount of monomer added does not exceed that required to reach saturation swelling of the particles, then Interval III predominates. The same basic kinetic expressions are applicable in both intervals as long as changes in kinetic parameters in the two intervals are taken into account [32]. Thus far, few kinetic studies have taken advantage of the method of successive seeding to study the effect the degree of subdivision of a system has on the polymerization kinetics. As the particle size is increased for a fixed solids content, the number of particles decrease and therefore, the degree of segregation of growing radicals. A decrease in the overall (measured) polymerization rate is expected from a decrease in the number of particles. A condition is reached, however, when the number of growing radicals in a particle can exceed one and thus, counter the effect of decreasing particle number. This condition is a function of particle size, as well as, the degree of conversion. An assessment of the relative strengths of these opposing effects can be determined through successive seeding from small to large particle size with monodisperse latexes. This represents a transition from emulsion polymerization kinetics, in which the polymerization rate is directly dependent on the number of particles in the system, into the region of suspension or bulk polymerization where the rate is independent of N_p. The extent to which this transition can be bridged is investigated in this research program.

In order to study the kinetics of successive seeding of monodisperse latexes, polymerization recipes must be available which can successfully produce these latexes without coagulum and small particle nucleation. A review of other efforts in successive seeding will be

93

given and their applicability to kinetic studies assessed. Some early work in this lab will be described in which a three-step sequence was used first, to obtain information regarding the nature and magnitude of the particle surface charge as a function of particle size and initiator concentration and second, to obtain polymerization kinetics as a function of the same two parameters. The problems and drawbacks to the formulation method and results will be reviewed. A more systematic recipe development will be described and kinetic results presented for seven-step sequences performed varying the initiator type and concentration and aqueous phase inhibitor type and concentration. These results will be analyzed and compared for the effects of these parameters, as well as, the particle size. The transition from emulsion to bulk kinetics will be addressed in terms of $\bar{n}$, the average number of radicals per particle, and the degree to which the polymerization rate becomes independent of particle size at the larger sizes.

3.2 Prior Developments in Successive Seeding

In order to successfully prepare monodisperse latexes via the method of successive seeding, the emulsifier concentration must be controlled in such a way as to prevent new particle generation and coagulation. For small particle sizes the operable range for emulsifier concentration is relatively broad [21,22] but above 1 µm the successful preparation of a monodisperse product becomes very sensitive to the amount of emulsifier in the system and also the degree of shearing to which the latex is subjected in order to maintain adequate mixing. At these relatively large particle sizes (i.e. for emulsion polymerization) a successful polymerization has been termed a "knife-edge" oper-

94

tion, meaning that duplicate recipes prepared under the same conditions may result in either a partially flocculated monodisperse latex or a stable latex containing a second generation of smaller particles [31].

With increasing particle size also comes the problems of creaming and settling of the monomer/polymer particles during the polymerization process. Decreasing intensity of Brownian motion coupled with the density difference between the particles and water causes creaming of highly swollen particles and settling of particles at high conversion. The accumulation of creamed or sedimented particles can result in flocculation and coalescence thereby destroying the monodispersity. Increased agitation can be used to offset these gravitational effects but with greater risk of coagulation due to mechanical shear [31]. Most studies, however, have only been concerned with the development of suitable stablization systems for each step in a sequence without much concern for the mixing characteristics of the polymerization reactor.

The pioneers of monodisperse latex first demonstrated that the successive seeding technique could be used to grow 0.1 μm monodisperse particles stepwise to a size of 2 μm [19,20,21,22]. Generally, the smaller sizes were polystyrene and the larger (>1.5 μm) were polyvinyltoluene. The latter was used to take advantage of its smaller density difference with water as compared to polystyrene. Apparently, however, the exact nature of the recipes required to accomplish this were considered proprietary and therefore remained unpublished. Of critical importance was the emulsifier and its concentration. In general, the emulsifier should be both a good wetting agent and a

good dispersing agent [33]. With any emulsifier a (more or less) trial-and-error procedure must be adopted to find the concentration range which can be used to successfully prepare monodisperse latexes (i.e. without flocculation or a new crop of particles) for each step in a sequence. In general, this has been the procedure followed in more recent publications. Deželić et al. [33] reported that mono-disperse latexes up to 0.95 μm can be prepared using Aerosol-MA emul-sifier (sodium dihexylsulfosuccinate - American Cyanamid Co.). The amount of emulsifier required to successfully produce monodisperse latexes via seeding was found to decrease with increasing particle size (.075 wt% for 0.367 μm polystyrene latex to 0.035% for 0.983 μm latex). In these experiments, potassium persulfate ($K_2S_2O_8$ was used as the initiator with sodium bicarbonate buffer ($NaHCO_3$). Monomer/ polymer ratios (M/P) varied from 9.8 to 1.38 with final solids con-tents of about 20%. The results using Aerosol-MA when compared with previous results using potassium laurate and sodium dodecylbenzene sulfonate were found to be superior.

Another extensive study using the seeding technique was performed using a mixed surfactant system of Triton X-100 (polyoxyethylene iso-oxtylphenyl ether - Rohm and Haas Co.), a nonionic emulsifier, and sodium dodecylbenzene sulfonate, an anionic emulsifier [34]. Mono-disperse latexes were produced in sizes up to 1.25 μm in diameter through a four-step successive seeding starting with a 0.29 μm poly-styrene seed and 'overpolymerizing' with polyvinyltoluene (M/P ~ 2.5). The weight ratio of anionic to nonionic emulsifier was generally about

40/60. The amount of emulsifier present in the final latexes was characterized in terms of the surface coverage of the particles as determined from soap titration. An optimum surface coverage was found to lie in the range of 50 to 70% based on the final latex surface (~50% total solids content). No information was reported on the distribution of the two surfactants between the particles and aqueous phase, however. $K_2S_2O_8$ was used as the initiator species with the pH being raised by NaOH to increase the number of chemically bound sulfate groups. No kinetic studies were reported for these or the previous studies using the formulations developed for successive seeding.

A recent study using successive seeding was conducted in this lab with the objective of investigating the surface charge density as a function of particle size [35]. An extension of this study will be reported here.

3.3 Early Work - Successive Seeding and Surface Charge Density

The effect of particle size on the surface charge density of monodisperse polystyrene latexes was investigated using the method of successive seeding to produce particles of 0.3, 0.45, and 0.70 μm diameter starting from a 0.19 μm seed (Dow LS1102A) [35]. The surface charge densities were determined via the ion exchange and conductometric titration method. The latexes were prepared using sodium lauryl sulfate emulsifier, persulfate initiator, and bicarbonate buffer. Only strong acid groups were found on the particles' surface. The surface charge density increased with increasing particle size and was said to approach an equilibrium value of 1.83×10^{-14} cm^2 (183 Å^2) per sulfate end group. This was attributed to the increased electro-

static repulsion between the particles and the charged oligomeric radicals formed from sulfate ion radicals polymerizing in the aqueous phase. Also, the emulsifier concentration range for successful preparation of monodisperse latex was found to narrow with increasing particle size. A 1 μm latex, free of new crop generation, was not successfully prepared. This work was then extended by a study of the effect of initiator type and concentration on the surface charge density using the three-step sequence.

3.3.1 Preparation and Surface Characterization Methods

Four sets of three-step successive seeding experiments were conducted starting with a monodisperse 0.19 μm polystyrene seed. This seed was first ion exchanged [36,37,38] to remove unknown quantities of emulsifier and electrolytes left over from the original preparation. The styrene monomer (Fisher Scientific Co.) used in all experiments was purified by removing the inhibitor through repeated washings with 10% NaOH solutions followed by distilled-deionized water and distillation under N_2 (Zero Grade - Linde Div. Union Carbide Corp.) at 20 mm Hg. The monomer was stored at -15°C until used. Reagent grade SLS (Onyx Maprofix S63), $K_2S_2O_8$, (both Fisher Scientific Co.) and AIBN (azobisisobutyronitrile - VAZO 64 - Dupont Co.) were used without further purification.

The latexes were prepared by bottle polymerization, first swelling the particles without initiator for two hours at 70°C by end-over-end tumbling in a constant temperature bath. Initiator was then added after cooling to room temperature and the latexes purged for 15 min. with N_2 gas. Polymerization was conducted for approximately 20 hrs. at 70°C with end-over-end tumbling. 98

Surface characterization was accomplished by the ion exchange and conductometric titration techniques. A mixed bed resin of Dowex 50W (H^+ form) and Dowex 1 (OH^- form) was prepared after each resin was subjected to a rigorous purification process [36,37,38]. Each latex (~5% solids) was contacted with the resin mixture (~1 gm/gm polymer) in 5 batch ion exchange cycles, each lasting 2 hours. Immediately following the last cycle, the latex was diluted (approximately 1 gram polymer in 200 cm^3 distilled-deionized water) and titrated with 0.02N NaOH. The titration was followed conductometrically [39]. The number of sulfate groups (strong acid) was determined from the amount of NaOH required to reach an endpoint indicated by a change in the sign of the slope of the titration curve. (See Appendix A.) Carboxyl groups (weak acid) were determined from the amount of additional NaOH added to reach a second endpoint indicated by a change in the magnitude of the slope of the curve. Additional details of this procedure can be found elsewhere [39].

3.3.2 Characterization Results

The generalized recipes used in each step of all sequences are presented in Table 3-1. In three sequences $K_2S_2O_8$ was added in concentrations of 1.34, 2.44, and 9.7 mM (in the aqueous phase) with equal amounts (wt. %) of NaHCO$_3$. The previous latexes were prepared using 4.80 mM $K_2S_2O_8$ [39]. A fourth sequence was run with AIBN as initiator (6.4 mM on monomer/polymer phase) for comparison. Note in Table 3-1 that the amount of emulsifier based on surface coverage was reduced to 42% of the initial seed surface area for step 3, this being required to reduce significant nucleation of new particles [39].

99

Table 3-1

Successive Seeding Recipes

Recipe Parameter	Step 1	Step 2	Step 3
Seed (polymer), gms	1.050	1.480	1.330
Styrene, gms	3.090	3.520	3.670
ddi water[1], gms	18.950	20.000	20.000
SLS[2], gms	0.029	0.019	0.007
Initial seed size, μm	0.19	0.30	0.45
Final particle size, μm	0.30	0.45	0.70
M/P	2.94	2.37	2.81
Final solids content[3], %	18	20	20
Emulsifier surface coverage of initial seed[4], %	80	80	42

---

[1] ddi = distilled dionized

[2] total amount added, taking into account the amount initially present in the seed.

[3] nominal

[4] assumes 50 $\overset{\circ}{A}{}^2$/SLS molecule on polystyrene and all emulsifier on particles' surface

The conductometric titration results obtained for the latexes prepared with varying initiator concentrations are presented in Figure 3.1 along with the previous results (circles). The open points represent the amount of surface charge attributable to strong acid (sulfate) groups, while the solid points indicate the total charge, i.e. strong and weak acid. The previous results showed the presence of only strong acid groups. The presence of carboxyl groups can be attributed to several possible sources, particularly the hydrolysis of sulfate groups followed by oxidation and side reactions of the initiating species [40]. Nonetheless, these additional data confirm that not
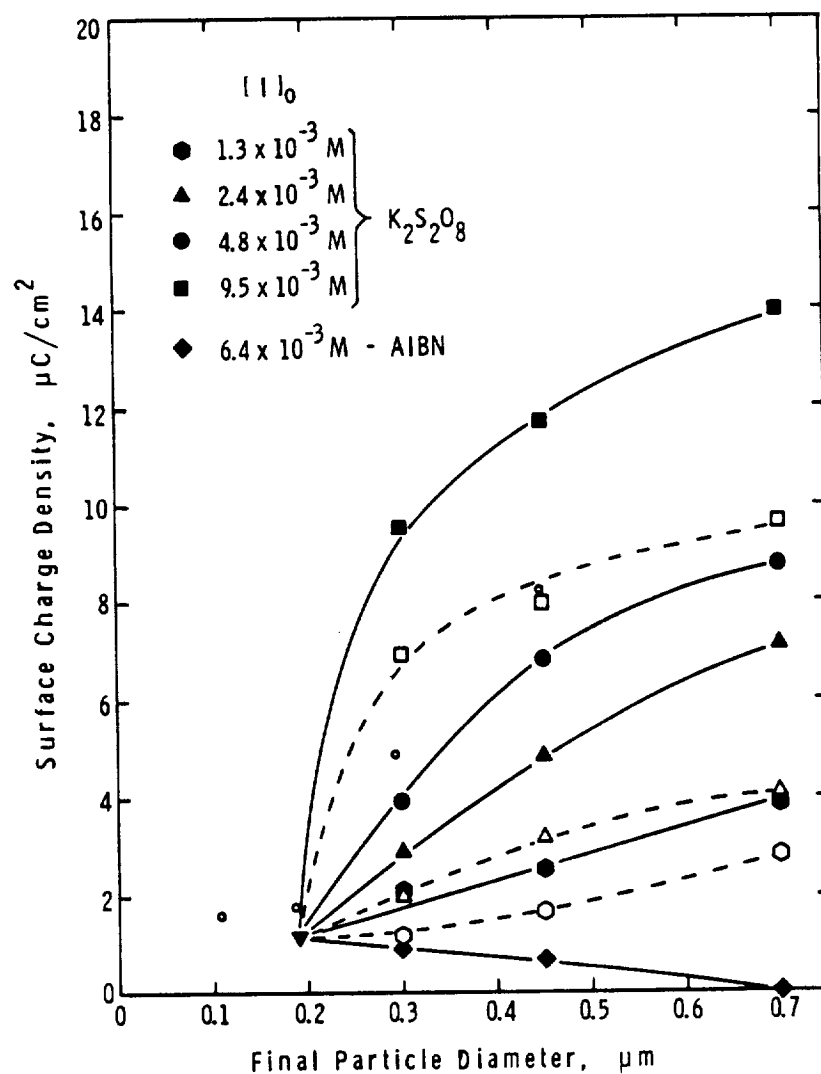
Figure 3.1 Surface Charge Density as a Function of Particle Size, Initiator Type, and Concentration for Polystyrene Latexes Prepared via Successive Seeding from a 0.19 μm Seed

101

only does the surface charge density increase with increasing particle size but also with increasing $K_2S_2O_8$ initiator concentration. Other studies have also given some indication of this same trend with particle size [41,42]. In continuous particle electrophoresis experiments, the electrophoretic mobility was found to increase with increasing particle size allowing partial separation of seven monodisperse particle populations ranging in size from 0.088 to 2.02 μm [42].

The data of Figure 3.1 can also be presented from other points of view. As a result of the original work it was proposed that the surface charge density approached an equilibrium value in terms of the average area occupied per sulfate end group. Figure 3.2 includes this data along with the results obtained in these studies. As the initiator concentration and particle size increase the area occupied per end group ($-SO_4^-$ and $-COO^-$) decreases but with less sensitivity at the higher initiator concentration. A limiting value may be approached in each sequence but it is most likely due to the recipe conditions rather than an increase in electrostatic repulsive forces preventing the adsorption of free radical oligomers bearing sulfate groups. The arrow in the bottom right corner of Figure 3.2 represents the adsorption area per SLS molecule at saturation (42 $\overset{o}{A}{}^2$/molecule) which may indeed represent a true limit due to crowding of the particle surface with charged groups.

A third manner of presenting these data is in terms of the total number of surface groups found relative to the total amount of polymer (μeq/gram). The surface charge in these terms is presented in Figure 3.3 again as a function of particle size at the various initi-
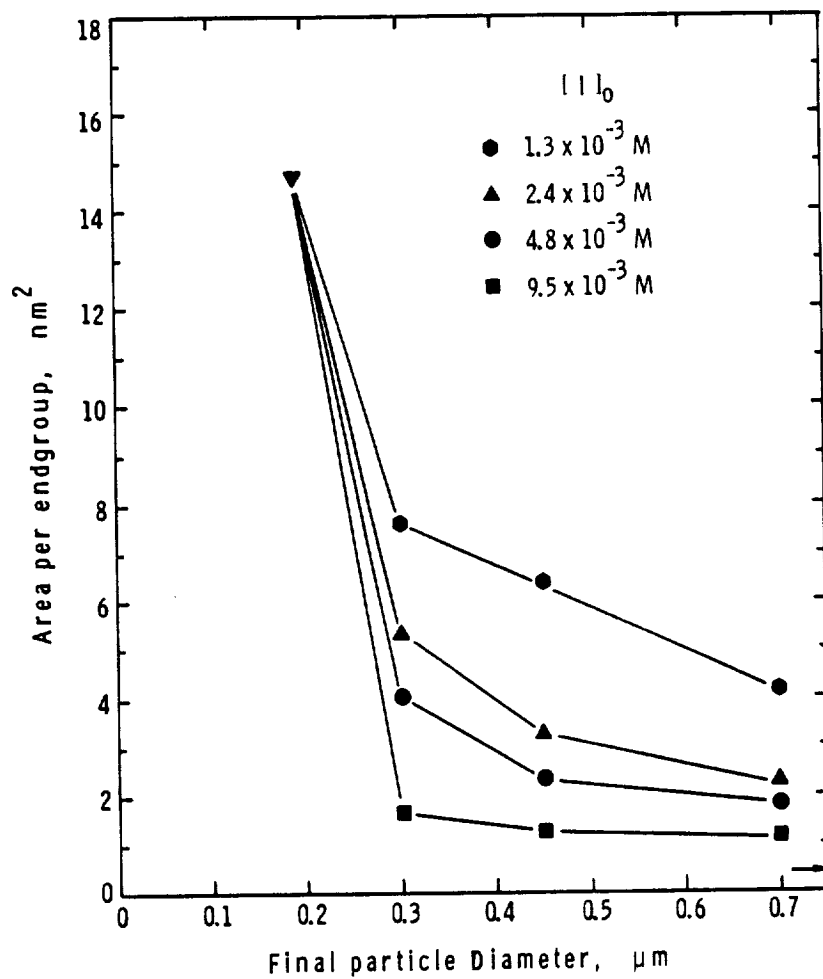
Figure 3.2 Average Area per Endgroup as a Function of Particle Size and Initial Initiator ($K_2S_2O_8$) Concentration for Polystyrene Latexes Prepared via Successive Seeding

103

Figure 3.3 Surface Charge(µeq/gm) as a Function of Particle Size and Initial Initiator ($K_2S_2O_8$) Concentration for Polystyrene Latexes Prepared via Successive Seeding

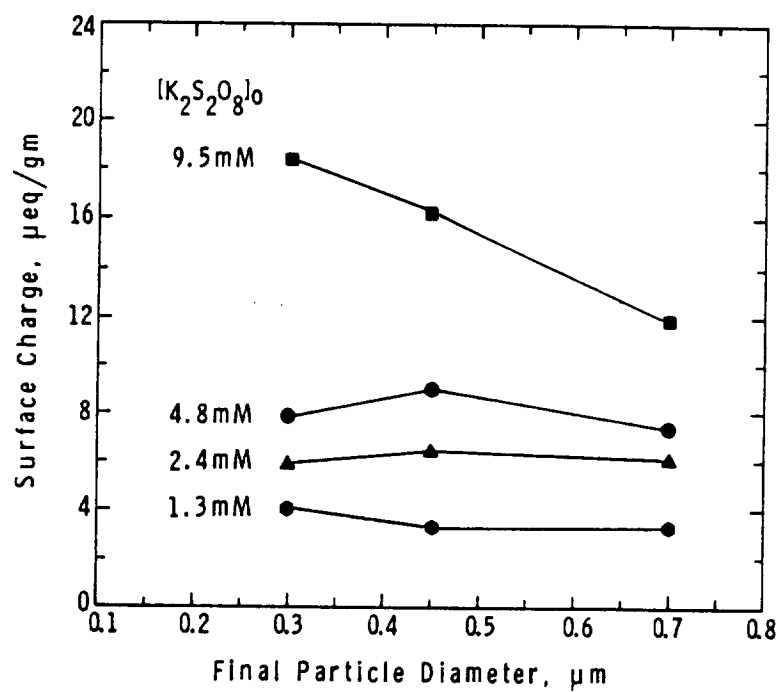ator levels. The results at the three lower initiator concentrations show some slight dependence on the particle size while the highest shows a decreasing surface charge. Speculation about the nature of the polymerization kinetics is offered based on these findings.

For small particle size latexes (~0.1 μm) the polymerization rate is generally independent of particle size and initiator concentration within certain limits (i.e., when $\bar{n} = 1/2$). As the particle size increases, however, the rate is affected due to an increasing $\bar{n}$ and a decreasing number of particles. Nevertheless, as a first approximation it was assumed that each step in a sequence required similar lengths of time to reach complete conversion (i.e., radicals would only be absorbed for this length of time). From the polymerization time, the initiator concentration and its decomposition rate, surface charge densities (μeq/gm) were computed for each step in a sequence based on the original recipes. Initially it was assumed that all decomposed initiator was absorbed by the particles and was detectable through conductometric titrations (i.e., either sulfate or carboxyl groups). The time chosen for complete conversion was based on the results of kinetic experiments having similar recipes. These will be reviewed in the following section (3.3.3). 240 minutes were used for the sequence using the lowest amount of initiator (1.37 mM). The computed surface charges at the completion of each seeding step were 12.9, 15.0, and 15.7 μeq/gm for the 0.3, 0.45, and 0.7 μm particles, respectively. The initial seed had a surface charge of 4.1 μeq/gm. These values lie well above those reported in Figure 3.3. There are several possible explanations for this: i) not all

105

groups were detected experimentally; ii) the actual polymerization time was much shorter; iii) the efficiency of the initiator radicals in terms of initiating polymerization in the aqueous phase together with adsorption onto the polymer particles was less than 100%. Even though each of these was plausible, closer attention was paid to the third one, based on accounts of lower initiator efficiency found by others [43]. The efficiency was adjusted by simply varying the fraction of decomposed initiator contributing to polymerization and re-computing the surface charge. An efficiency of 25% was thus found to result in 4.01, 3.99, and 3.98 $\mu eq/gm$ for the three successive steps, which agrees much better with the experimental data. The remaining differences may still be due to any combination of the three possibilities mentioned previously but to a smaller degree. Initiator efficiencies of 27 to 41% were reported for particles ranging in size from .221 to .364 μm [43], this being within the range of these experiments. The same procedure was applied to the next two sequences with higher initiator levels. For 2.44 mM $K_2S_2O_8$, a polymerization time of 200 minutes was used. An efficiency of 27.5% resulted in surface charges of 6.03, 6.48 and 6.63 $\mu eq/gm$ for the 0.3, 0.45 and 0.7 μm particles, respectively. Likewise, for 4.81 mM $K_2S_2O_8$ an efficiency of 25% resulted in 8.08, 9.03, and 9.32 $\mu eq/gm$ for the same three steps having a 150 min. polymerization time. The last case, that with the highest initiator level (9.77 mM), was also treated in the same way but with a fixed time and efficiency there was no way to effect a decrease in the surface charge. By varying either of these, however, reasonable results could be obtained. It is likely that a combination
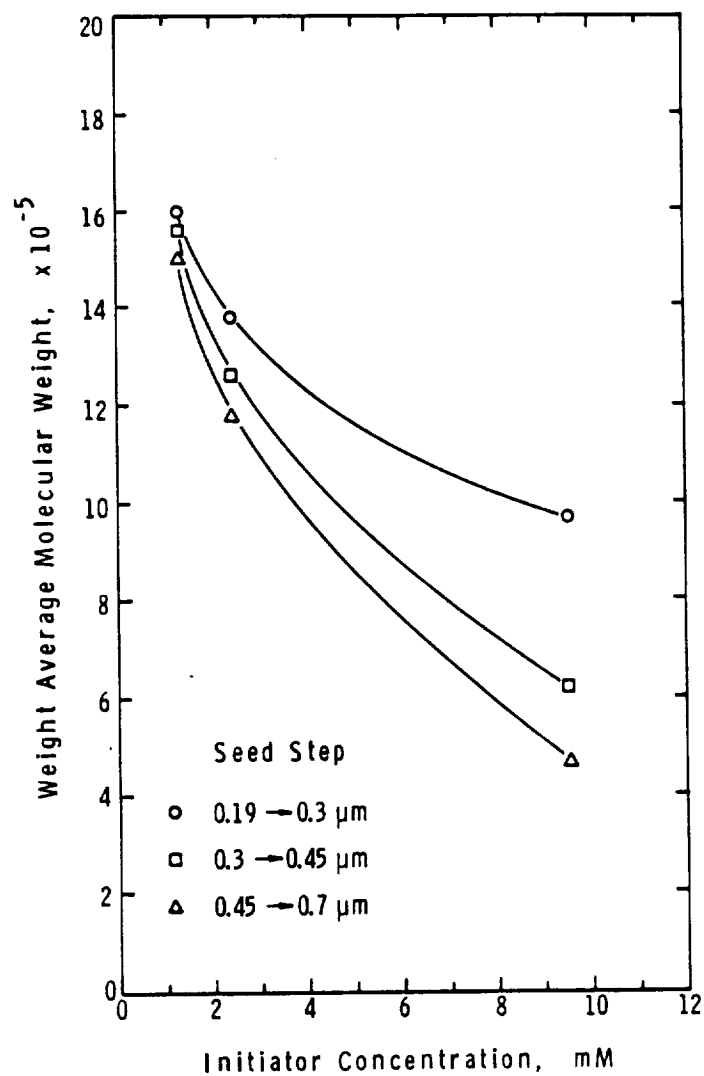
106

Figure 3.4 Weight Average Molecular Weights as a Function of
Initiator Concentration and Particle Size for Poly-
styrene Latexes Prepared via Successive Seeding

of the two is in effect. These results fit the experimental data fairly well and yet it must be noted that the assumptions made are not likely to be wholly accurate, thus requiring actual kinetic information for verification or modification of these points.

Weight average molecular weights ($\bar{M}_w$) were determined by GPC (gel permeation chromatography) as an additional characterization of the polymer produced in these sequences. As might be expected qualitatively, $\bar{M}_w$ decreased with increasing initiator concentration and increasing particle size (Figure 3.4). The molecular weight in controlled by the radical entry rate and the termination mode and rate in the particles. These data indicated that the molecular weight was most sensitive at high concentrations. Also, the $\bar{M}_w$ decreased with decreasing sensitivity to initiator concentration at a given particle size, in support of the choice of shortened reaction time (with increasing initiation concentration) given previously. The shorter the reaction time (i.e., higher the polymerization rate), the lower the number of radicals entering the particles at a given initiation rate and the greater the molecular weight. This has a tendency, therefore, to counter the effect of increasing initiator concentration, as shown in Figure 3.4.

Surface charge densities and molecular weights are only indirect indications of the nature of the polymerization kinetics in successive seeding experiments but can be important in identifying some of the mechanisms involved in emulsion polymerization.

3.3.3 Measurement of Polymerization Kinetics via Dilatometry

Three successive seeding (3-step) experiments (designated SSMLR 1,2, and 3) were conducted in the LUMLR dilatometer in order to obtain polymerization kinetics as a function of particle size and initiator concentration. The objective was to carry out the reactions with the same recipes as used in the surface charge density studies and use the kinetics to aid in the interpretation of the results, i.e., to confirm or refute the earlier speculation.

The polymerization recipes were prepared, as described in Section 3.3.1, by swelling the seed for two hours at $70^{\circ}C$. The latexes were purged with N_2 for 20 min. following cooling and the addition of the initiator and buffer. In these studies, the reactor was loaded by the atmospheric/gravity method (see Section 2.4.3). (The low pressure method was not fully developed at that time.)

A number of problems were identified in the process of performing these studies. Complete particle swelling was not consistently achieved under the conditions of the experiments as evidenced by the presence of a free monomer layer in the loading flask. This was particularly true for the first step in each sequence, in which swelling ratios averaging around 2.0 were attained as compared to the intended 2.9 ratio. There were two possible reasons for this: i) insufficient time was alloted to reach equilibrium; ii) the equilibrium swelling ratio was less than 2.9 for the given conditions of particle size and emulsifier concentration. Swelling ratios have been reported over this range depending on experimental conditions including the temperature, the specific emulsifier and its concentration, and the

particle size and concentration [44,45]. The swelling ratios were much closer to the expected values for the second and third seeding steps. Incomplete swelling (i.e., lower total surface area) had the undesirable effect of raising the aqueous phase concentration of emulsifier, thereby increasing the possibility of nucleation and stablization of a second generation of particles. Examination of the products by transmission electron microscopy revealed a few small particles in the second step and significantly more in the third step of the sequence prepared with 2.4 mM $K_2S_2O_8$.

The use of the atmospheric/gravity loading method often led to the presence of air bubbles in the reactor as seen in the interpretation of the expansion portion of the experiments. (See Section 2.4.3.) The data over the first 20 - 40 minutes were rendered useless and therefore any conversion over this period was not identified. This was not considered a significant amount for polymerizations in which the rate was low (i.e., for the lower initiator concentrations, such as 1.37 mM) but for cases with high initiator concentrations and thus, high polymerization rates, a significant amount of kinetic information was lost. For example, in the second seeding step of the sequence using 9.77 mM $K_2S_2O_8$ (SSMLR 3-2) only about the last 60% of the conversion curve was obtained. The reaction was nearly complete (i.e., conversion greater than 90%) in the first 60 minutes of the polymerization. These kinetic results are therefore of little use.

The kinetic data obtained for sequences SSMLR 1 and 2, prepared with 1.3 mM and 2.4 mM $K_2S_2O_8$, are given in Figures 3.5 and 3.6, respectively. The conversion is expressed in terms of the grams polymer
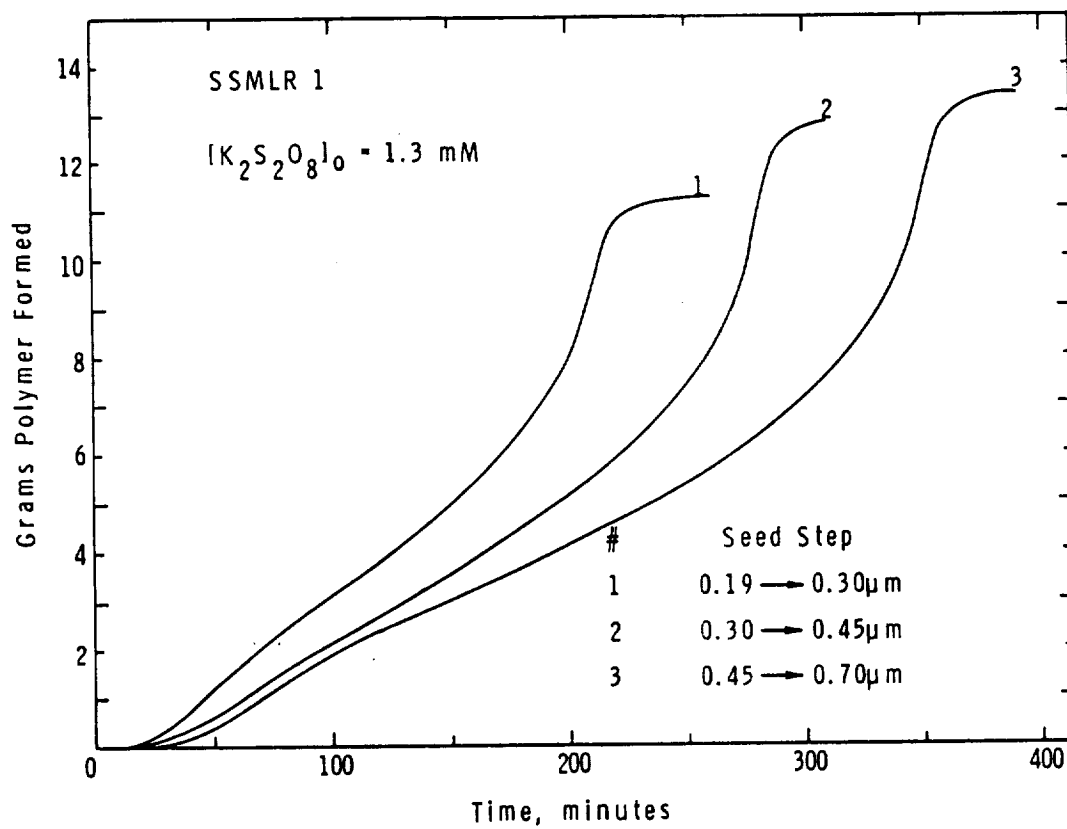
110

Figure 3.5 Conversion Histories for SSMLR 1 Prepared using 1.3 mM $K_2S_2O_8$
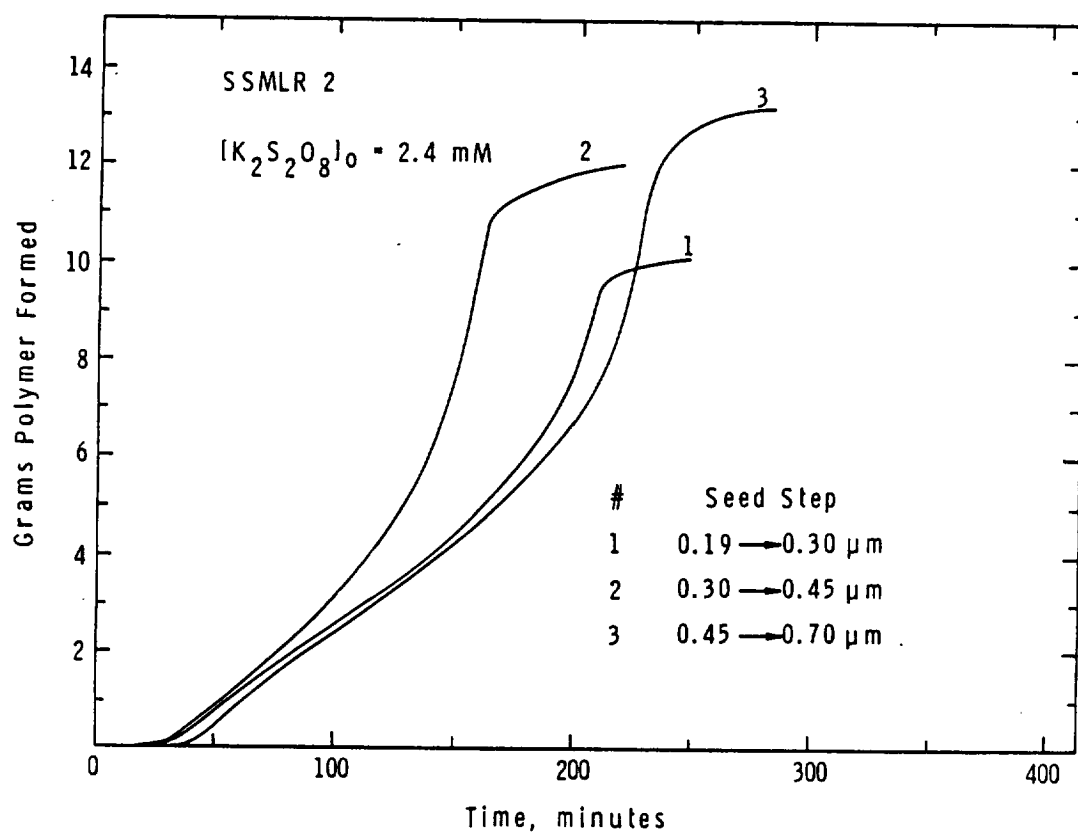
Figure 3.6 Conversion Histories for   SSMLR 2 Prepared using 2.4 mM
          $K_2S_2O_8$

produced rather than the fractional conversion so that a more valid comparison of data could be made. A number of similarities and differences were immediately obvious. Overall the two sets appeared kinetically dissimilar in that for the lower initiator concentration (SSMLR 1) the polymerizations required increasingly longer times to reach completion for increasing particle size while in SSMLR 2 there was no such trend. Also, for each sequence the amount of polymer being produced increased with particle size $(X > 95\%)$. This was due to the low swelling ratio in the first step ($\sim 2.0/1$) and the recipe design of the following two (2.4/1 and 2.8/1, respectively). This made kinetic comparisons more difficult in that the polymerization rate is known to be dependent on the fraction of polymer in a particle, particularly at larger particle sizes where more than one growing radical could be accommodated in a particle ($\bar{n} > 1/2$).

The shape of the conversion curves (Figures 3.5 and 3.6) was basically the same. The rate of polymerization initially increased, then decreased, (except for SSMLR 2-2) increased again and then fell to zero as the monomer concentration dropped to near zero. The increase in the polymerization rate at higher conversions was due to the well known gel effect brought about by the decreasing mobility of the polymer chains, in effect lowering the termination rate constant, k_t. The decreasing rate noted prior to the dominance of the gel effect was possibly real (i.e., caused by a decreasing monomer concentration in the particles prior to the gel effect) but most probably was an artifact caused by the initial presence of an air bubble in the reactor. Subsequent polymerizations performed after loading via

113

the low pressure/gravity procedure did not show this phenomenon.

The similarity of the conversion histories for the first step in the two sequences was attributed to the polymerization taking place in the proximity of Smith-Ewart Case 2 conditions ($\bar{n} = 1/2$) [46]. Obviously, these exact conditions did not exist in that $\bar{n}$ did increase somewhat from 1/2; however, this was the dominating factor in these kinetics (as opposed to the increased initiation rate from the increased quantity of initiator). With increasing particle size, Case 2 conditions were no longer fulfilled as $\bar{n}$ grew to be much greater than one (Case 3 kinetics). This represents the beginnings of the transition of kinetics from emulsion to 'bulk' which is explored in much greater depth and detail in the following sections.

3.3.4 Recommendations

An improved method of successive seeding was required in order to obtain kinetic data over a wider range of particle sizes and under conditions which produced reliable and complete kinetic information. To accomplish these ends, a number of recommendations were enacted:

1. the development of an improved successive seeding method in which:

    a) the emulsifier used was Aerosol MA.

    b) the amount of emulsifier added was based on a fractional surface coverage of the final particle surface (accounting for the amount in the aqueous phase) and held constant throughout the sequence.

    c) the M/P weight ratio was fixed at 2/1 whereby particles would be grown successively from 0.19 to 0.27 to 0.39 to 0.57 to 0.82 to 1.19 to 1.76 to 2.4 μm.

114

d) the final solids content was fixed at 30%.

e) lower initiator concentrations were used (1 mM).

f) actual amounts of monomer in swollen and product latexes were determined by independent means.

2. The LUMLR dilatometer was used to obtain reaction kinetics before which:

a) a back-up ring was incorporated on the lower piston o-ring (Section 2.4.3).

b) an improved agitator paddle was developed (Section 2.4.2.3).

c) minimal agitation speed was adopted.

d) loading was accomplished by the low pressure/gravity technique.

3.4 Recipe Development

The prevention of nucleation and coagulation in the preparation of monodisperse latexes above 1 μm by the seeding method was previously described as a "knife-edge" operation. In seeded systems where the free emulsifier concentration was known to be well below the CMC, nucleation was, nevertheless, found to occur. The mechanism by which this occurs is popularly thought to be that of homogeneous nucleation [47]. Theoretical and experimental studies of particle nucleation in seeded and unseeded systems, with and without emulsifier, were described in a series of papers [48,49,50,51]. A mathematical relationship was developed for the number of nucleated particles, N, as a function of the initiation rate, R_i, the stability ratio between primary particles and seed particles, W_{ls}, and the number N_p, and size, r_p, of the seed particles:

$$N = \frac{R_i \, 3k_p \, M_W \, r \, W_{1S}}{8D_W \, \bar{k}T \, F_S \, (N_p r_p)^2} \qquad (3.1)$$

where k_p is the propagation rate constant, M_W, the aqueous phase concentration of monomer, r, the radius of primary particles, D_W, the diffusivity of oligomers in water, $\bar{k}$, Boltzmann's constant, T, temperature, and F_S, the absorption efficiency of radicals by seed particles. The particle numer, N, at high seed concentrations should therefore be proportional to $(N_p r_p)^{-2}$. In a seed sequence in which the swelling ratio and the solids content are held constant, the number of seed particles is proportional to d^{-3} and therefore, N is proportional to d^4. N, N_p, the total particle surface area, and an average surface-to-surface distance between seed particles are shown in Figure 3.7 as a function of final particle diameter in a seed sequence. This serves to qualitatively illustrate the difficulty of maintaining a monodisperse latex in a seed sequence, without nucleating a significant amount of new particles. A number of steps can be taken to accomplish this, such as use of a low amount of initiator to reduce R_i, a low amount of emulsifier to lower W_{1S}, and an increased solids content to raise N_p. This does not, however, say anything about the coagulation of seed particles which can be equally destructive in terms of monodispersity. W_{SS}, the stability ratio between seed particles must be high enough to maintain stability. This is primarily controlled by the nature and amount of stabilizer present on the surface of the particles. In general, if all conditions are the same, this stability ratio increases with increasing particle size. However, this does not account for the increased collision energy due to the increased
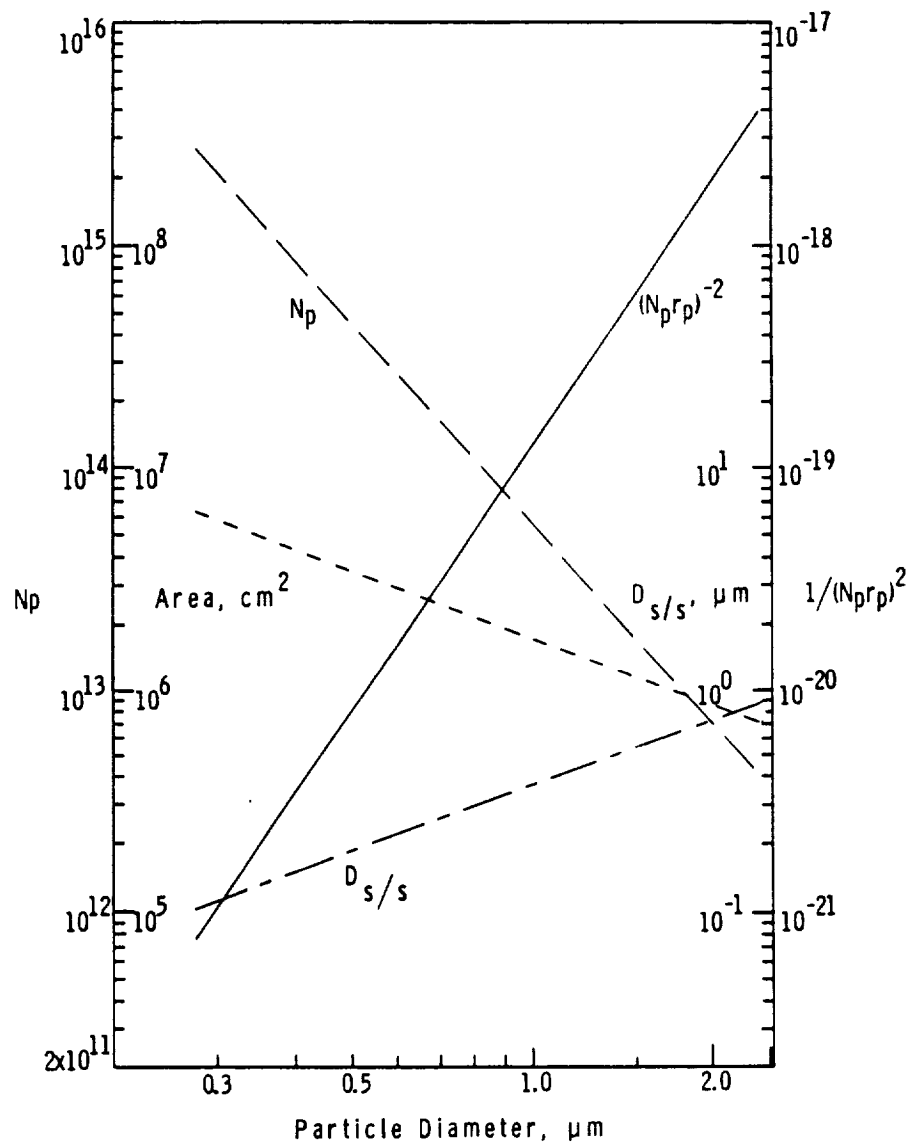
116

Figure 3.7 N_p, Surface Area, $D_{S/S}$, and $(N_p r_p)^{-2}$ as a Function of Final Particle Size in a Seed Sequence at 30% Solids
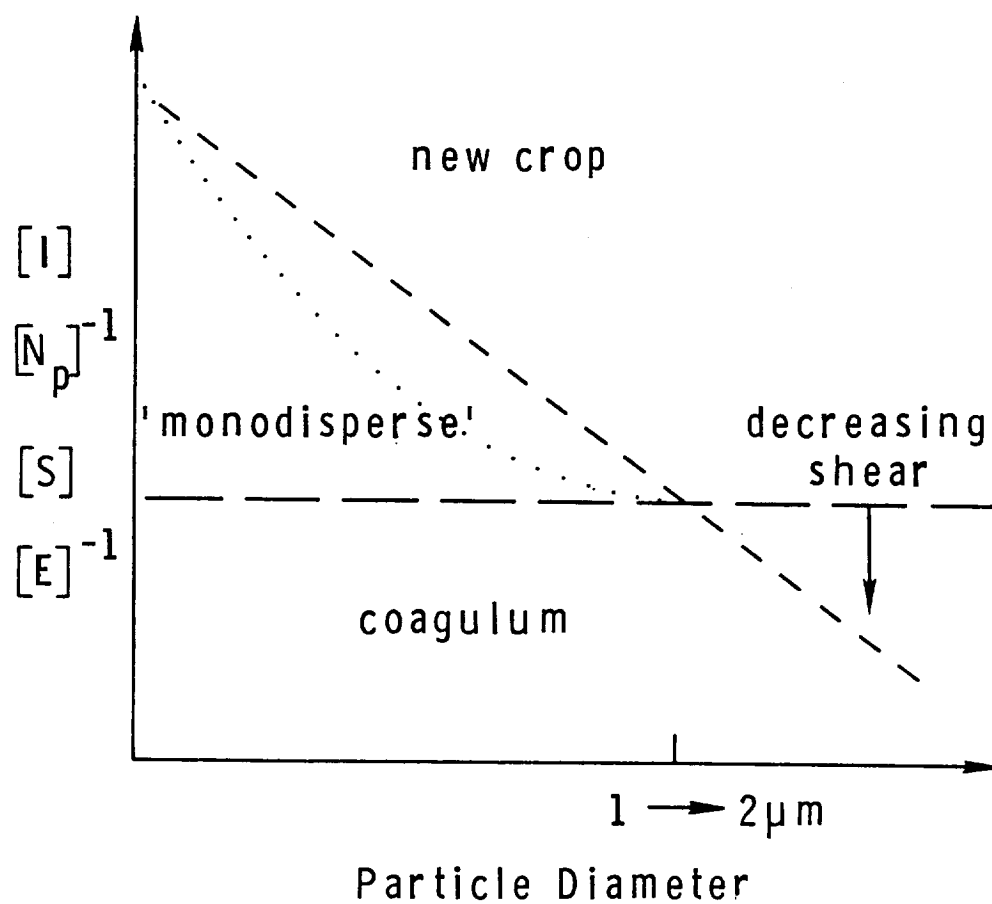
117

Figure 3.8   Factors Affecting the Preparation of Monodisperse
             Latexes via Successive Seeding.   Regions Representing
             Failure are Given by 'New Crop' and 'Coagulum'

mass of the particles moving at a given speed under identical mixing conditions.

A constant surface coverage of the particles approximates a constant surface charge density (surface potential) and ensures a constant aqueous phase concentration of emulsifier. It does not secure protection against nucleation or coagulation in a seeding sequence to large particle size unless other factors are equally controlled such as the ionic strength and shear conditions. A qualitative picture of factors influencing the successful preparation of monodisperse latexes through successive seeding is presented in Figure 3.8. Regions of success (monodisperse) and failure (new crop and coagulum) are depicted, illustrating the 'knife-edge' phenomenon in the 1 - 2 μm particle size region. A significant new crop of particles occurs with excessive levels of surfactant, [S], and initiator [I], or too low a concentration of seed particles, [N_p], and electrolyte [E]. The reverse is true for coagulum formation which is also brought about by increased shear. The shape and magnitude of the slopes of these curves is uncertain but the general trends are shown. The development of a successive seeding formulation for preparing monodisperse latexes is largely dependent on the nature of these functions.

3.4.1 Series C X-Y

This series of seeded polymerization experiments was designed to test the emulsifier limits of coagulation and new crop phenomena. The emulsifier chosen for these studies was Aerosol-MA (American Cyanamid Co.). This emulsifier had been previously shown to give good results in seeded polymerizations of monodisperse latexes up to 0.95 μm. It

119

has also been termed a "forgiving" surfactant [52], implying that it can be used successfully over a wider concentration range as compared to other surfactants. Aerosol-MA is very soluble both in water and sytrene and has a CMC around 0.6 - 0.7% [53]. It is available as an 80% active solution with 15% water and 5% isopropanol. This was used without further purification in these experiments.

In this series of experiments the emulsifier concentration was determined by the amount needed to achieve fractional surface coverages of 0.1, 0.2, 0.3, 0.4, and 0.5 based on the final particle size in each step. The equilibrium of surfactant between the aqueous phase and the particle surfaces was assumed to be that of the adsorption isotherm determined by Ahmed [54]. This isotherm was determined on a 0.19 µm PS latex (Dow Lot LS1102-A) which had been cleaned by the ion exchange method. A Langmuir type isotherm was determined with constants a_s and b equal to 39 $Å^2$ and 3.7 x 10^2 liters/mole, respectively, where a_s is the molecular area of an Aerosol-MA molecule at saturation and b is the ratio of rate constants of adsorption and desorption.

For each emulsifier level, a six step sequence was planned in which particles were grown from an initial seed size of 0.19 µm to 1.71 µm:

$$0.19 \text{ µm} \xrightarrow{1} 0.27 \text{ µm} \xrightarrow{2} 0.40 \text{ µm} \xrightarrow{3} 0.57 \text{ µm} \xrightarrow{4} 0.82 \text{ µm}$$

$$\xrightarrow{5} 1.19 \text{ µm} \xrightarrow{6} 1.71 \text{ µm}$$

An optional seventh step to grow particles to 2.5 µm was also considered a possibility depending on the success of the previous steps. The final solids content was fixed at 30% with monomer/polymer swelling ratios of 2/1. The initiator and buffer concentrations were held

120

at 0.027% by weight based on the aqueous phase ($[K_2S_2O_8]_0 = 1$ mM).

The initial seed was cleaned by the ion exchange method and concentrated using a serum replacement cell (described by Ahmed [54]). The monomer was washed and distilled as described previously. The initiator, $K_2S_2O_8$, was recrystallized once from distilled-deionized water, dried, and stored under N_2 at $-15^{\circ}C$. Reagent grade $NaHCO_3$ was used without further purification.

Swelling was accomplished in 1 oz. bottles by rotation along a tilted axis ($\sim 45^{\circ}$) at room temperature ($25 - 30^{\circ}C$) for about 24 hours. Initiator and buffer were added afterwards and the polymerizations were carried out with end-over-end tumbling (36 rpm) at $70^{\circ}C$ for another 24 hours. The products were characterized in terms of their surface tension (Wilhelmy plate method), solids content, and apparent monodispersity (i.e., qualitative examination via scanning electron microscopy).

A sequence producing all monodisperse latexes was not found in this series of experiments. A new generation of small particles was evident in all samples after the third seeding step. Complete coagulation was found only in the sixth step of the sequence with the least emulsifier (10% coverage, C6-1). This, however, was not considered a lower limit for the emulsifier since the presence of nucleated particles causes a redistribution of the emulsifier, thereby lowering the actual surface coverage.

The surface tension data were used to determine the aqueous phase concentration of emulsifier in the latexes after polymerization via a calibration curve. The results are given in Figure 3.9 by the open
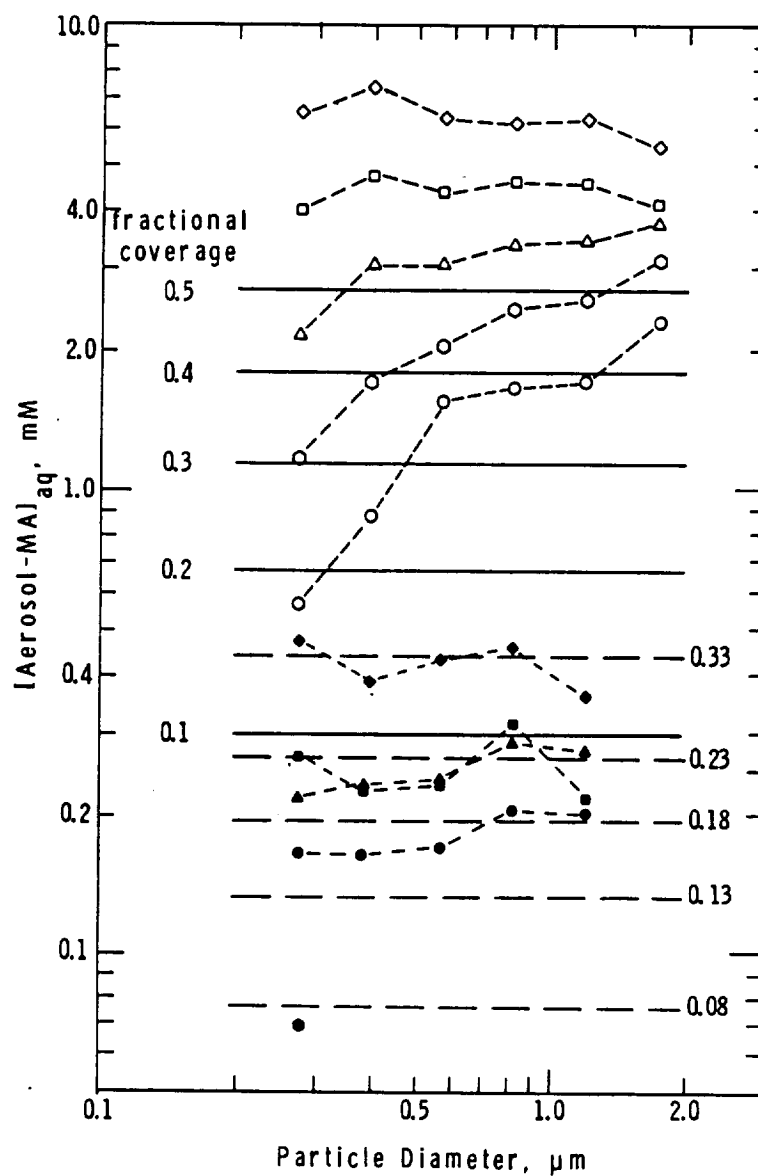
Figure 3.9   Aqueous Phase Emulsifier Concentrations as a Function
of Particle Size for Series CX-Y (Open Points) and
SDX-Y (Solid Points). The Latter are Based on a Corrected
Adsorption Isotherm.   The Horizontal Lines Represent Con-
stant Fractional Surface Coverages

122

points. Solid horizontal lines are drawn at the concentrations representing 0.1, 0.2, 0.3, 0.4, and 0.5 fractional surface coverage which represent the specifications for this series of experiments. There was no agreement between the measured and planned concentrations. It was suggested that the presence of electrolyte in the form of the initiator and buffer may have affected the adsorption behavior of the emulsifier. Using the data obtained in the initial seeding steps (in which nucleation was not evident), an adsorption isotherm was constructed for the system. A linear Langmuir plot of the data is given in Figure 3.10 along with the previously assumed isotherm. This function is described by

$$1/n = (1/N) + (1/C_A Nb) \qquad (3.2)$$

where n is the number of surfactant molecules adsorbed per unit area, N is the value of n at saturation $(a_s = 1/N)$, and C_A is the aqueous phase concentration of the emulsifier. The value of a_s, determined from the intercept, was 53.8 A^{o2}/molecule, with $b = 1.12 \times 10^3$ liter/mole, as determined from the slope and intercept. These differ somewhat from the original findings of 39 $\overset{o}{A}^2$/molecule and 3.7×10^2 liters/mole. The magnitude of these differences are not uncommon when comparisons are made between various methods and sources of information. The same research effort produced alternate values for a_s and b of 45 $\overset{o}{A}^2$ and 3.9×10^4 1/mole, determined by a variation in the serum replacement method [54]. In other studies using sodium lauryl sulfate, values were reported for a_s over a range from 42 $\overset{o}{A}^2$ [54] to 65 $\overset{o}{A}^2$ [55] while b ranged from 6.34×10^2 [56] to 8.0×10^3 [57] liter/mole.
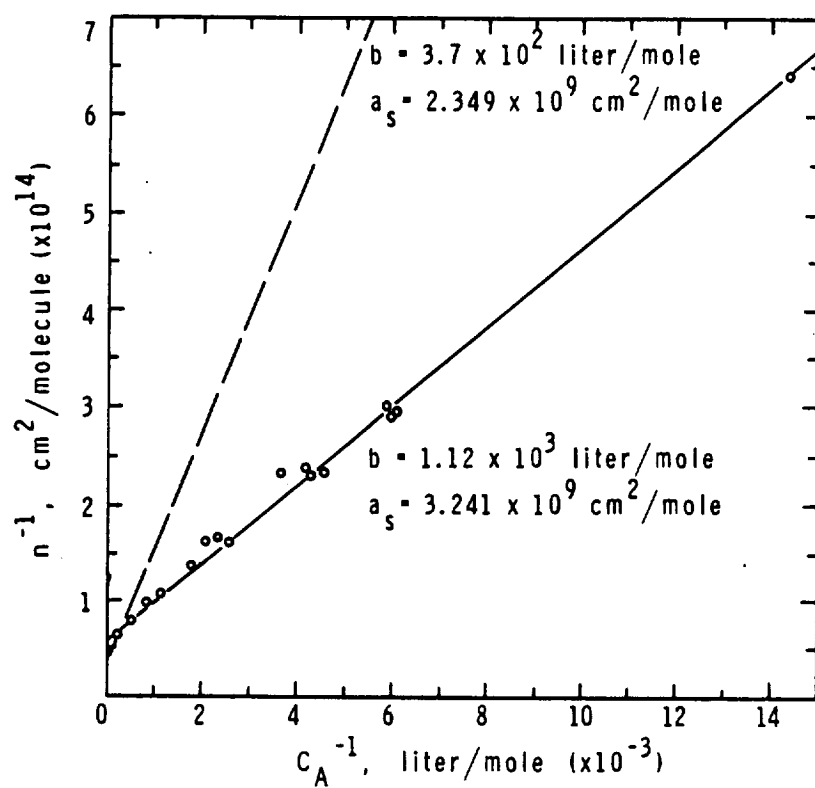
123

Figure 3.10 Langmuir Plot of Adsorption Data for Aerosol-MA. The Points were Determined by Surface Tension, the Dashed Line from Serum Replacement [54]

Methods used include serum replacement [54], surface tension [56], and conductometric titration [55]. Such differences have generally remained unexplained.

The revised adsorption isotherm was used to recompute the surface coverages of the first step of each sequence in the CX-Y series. These were found to be 0.33, 0.47, 0.58, 0.71, and 0.80 corresponding to the original 0.1, 0.2, 0.3, 0.4 and 0.5, respectively, obviously much higher than expected. A second series of experiments was planned based on the information gained in the CX-Y studies.

3.4.2 Series SD X-Y

Six additional sequences were planned by which the first four recipes would have surface coverages of 0.08, 0.13, 0.18, and 0.23 according to the revised isotherm with $K_2S_2O_8$ initiator and $NaHCO_3$ buffer at the same concentrations as used previously. The remaining two series would have coverages of 0.23 and 0.33 but initiation would be accomplished using the oil soluble initiator AIBN (azobisisobutyronitrile) (10.0 mM on monomer) in conjunction with the aqueous phase inhibitor, $NaNO_2$ (0.1 wt % on the aqueous phase). Generally, oil phase initiation is used in bulk, solution, and suspension polymerization. The inhibitor $NaNO_2$ was previously found to be successful in preventing "emulsion polymerization" from occurring in a dispersion polymerization of styrene [58] and therefore, appeared to be a good candidate for the inhibition of nucleation in seeded emulsion polyerizations.

The final solids and swelling ratios were kept constant as in the previous series, being 30% and 2/1, respectively. Initially, the

125

procedure for swelling was the same as used previously for the $K_2S_2O_8$/NaHCO$_3$ cases while in the AIBN/NaNO$_2$ cases all ingredients were added prior to swelling. After 24 hr., however, the swelling was found to be incomplete in the $K_2S_2O_8$/NaHCO$_3$ cases and that a viscous layer had formed in the AIBN/NaNO$_2$ cases. The procedures were subsequently modified by adding the buffer (NaHCO$_3$) prior to swelling (to increase the adsorption of the emulsifier, thereby lowering the particle-water interfacial tension) while the AIBN plus 5% of the styrene monomer was withheld until 5 hrs. prior to the start of the polymerization. These changes substantially reduced the extent of the problems described above. The polymerizations were once again carried out for 24 hrs. in a bottle tumbler, however, in these experiments the bottles were oriented so that rotation was around the bottle axis. This was done to provide gentler mixing thereby reducing the possibility of shear induced flocculation. The products were characterized as before.

Only four of the six sequences were carried out as far as the 6th seeding step. The two containing the least amount of emulsifier flocculated, one in the first step (0.13 fractional coverage) and the other in the second step (0.08 fractional coverage). This flocculation was complete in each case, the product having the consistency of whipped cream. There was no separate aqueous phase visible. The mechanism of this flocculation was not clear. SEM examination revealed that the particles had retained their identity (i.e., did not coalesce), indicating that the flocculation had occurred at high conversion.

126

The two remaining sequences, employing aqueous phase initiation, each resulted in significant quantities of new particles formed by the sixth step. It was not determined at which step the most significant generation of new particles occurred. It was likely that this had taken place much earlier than the sixth step.

The two sequences using the AIBN/NaNO$_2$ combination resulted in the generation of few small particles, the original particle population maintaining a narrow distribution. Scanning electron micrographs of the products of the sixth step in the two series are given in Figure 3.11. It was noted that the polymerizations in some cases were not complete after 24 hours, as evidenced by a residual monomer odor and film formation of the dried products.

Once again the surface tension was monitored for the product of each step to check on the consistency of the aqueous phase emulsifier concentration. The results, given in Figure 3.9 by the solid points, are compared to the fractional coverage specified for each series. There was some deviation or scatter of the experimental results but this seemed reasonable in light of the previous findings.

There were several observations made during the course of these experiments which seem worthy of mention. The sixth step of the two surviving K$_2$S$_2$O$_8$ sequences resulted in complete flocculation. Upon sonification these systems became fluid latexes. The mechanism of this flocculation does not seem to be shear related since shear could destroy the structure of the flocculant. A bridging mechanism was subsequently suggested for this phenomenon. The presence of additional small particles could have also played a role. In contrast, the

Figure 3.11 Scanning Electron Micrographs of PS Latexes Produced in the Sixth Step of Seed Sequences having Designed Surface Coverages of 23% (l) and 33% (r). Oil Soluble Initiator (AIBN) and Aqueous Phase Inhibitor (NaNO$_2$) Used. Particle Size Approximately 1.7 μm

AIBN initiated samples were fluid when removed from the polymerization bath (sixth step). However, when attempts were made to redisperse the particles after sedimentation the particles flocculated irreversibly (i.e., could not be redispersed by sonification). This was obviously due to shear effects.

3.4.3 Recommendations

The CX-Y and SDX-Y series revealed that fractional surface coverages as low as 0.18 could not produce monodisperse latexes free of newly generated particles in a six-step successive buildup from 0.19 μm to 1.71 μm using $K_2S_2O_8$ initiator. Flocculation was found to occur at a coverage of 0.13 in the first seeding step after 24 hrs. rotation at $70^{\circ}C$. Oil phase initiation (AIBN) with aqueous phase inhibition ($NaNO_2$) proved more successful in achieving monodisperse products without flocculation and few newly generated particles. Based on these results the following recommendations were made: 1) to perform successive seeding experiments in the LUMLR dilatometer at low fractional surface coverages (≤ 0.08) with $K_2S_2O_8$ initiator to take advantage of the controlled low shear rate and relatively good mixing; 2) to further develop successive seeding systems using oil phase initiation and aqueous phase inhibition, likewise making use of the LUMLR to obtain polymerization kinetics.

3.5 Successive Seeding in the LUMLR

Sequentially seeded emulsion polymerizations of monodisperse latexes were performed in the LUMLR prototype for a number of reasons: 1) to obtain the kinetics of polymerization of monodisperse latexes as a function of particle size and other recipe parameters and to use

this information in determining to what extent the kinetics proceeds into the transition region between emulsion and bulk kinetics; 2) to take advantage of the low shear environment for preparing latexes which would flocculate under normal polymerization conditions; 3) to prepare for the microgravity investigations in similar dilatometers by, first, establishing sound experimental techniques and, second, determining the polymerization kinetics for particles prepared under similar conditions leading up to the microgravity experiments. An experimental approach was described in the preceding section (3.4) and consequently was adopted for the successive seeding described here. A detailed description is first given of the experimental methods and data conversion computations, followed by the experimental results for successive seedings performed under various recipe conditions. Kinetic analysis and comparisons are discussed.

3.5.1 Experimental Procedures

Recipe prepration, reactor loading, polymerization, decanting, and product characterization are described here. Some of these procedures were described previously with less detail.

3.5.1.1 Recipe Preparation

3.5.1.1.1 Materials

The seed used in the first step of each sequence, SSMLR 4 through 13, was the monodisperse 0.19 μm PS (Dow LS 1102A) latex. This was diluted to about 5% solids and subjected to five ion exchange cycles with mixed bed (Dowex 1/50W) resin to remove the unknown emulsifier and electrolyte, as described previously. The clean latex was concentrated to 17 - 20% using a filtration method.

The second seeding step used the product of the first as seed without any further purification except for filtration through glass wool to remove any coagulum. This was subsequently done for all succeeding steps.

The styrene monomer was washed to remove inhibitors, as described previously. The monomer was double distilled on all glass apparatus equipped with Teflon sleeves at 20 mm Hg and $40 - 45^\circ$C under a N_2 blanket (ultra-high purity, Linde Div., Union Carbide). First distillations were preformed just prior to the start of a sequence while second distillations were done within 48 hrs. of recipe preparations. The monomer was stored at -15°C before use. The water was distilled and deionized (DDI). Aerosol-MA 80 (American Cyanamid Co.) was used without further purification. Table 3-2 lists the initiators, buffers, and inhibitors used in these studies along with the manufacturers and any purifications treatments. The initiators were stored under N_2 at -15°C.

Table 3-2

Initiators, Buffers, Inhibitors

Chemical	Manufacturer	Purity
$K_2S_2O_8$	Fisher Scientific Co.	recrys. f/DDI water
AIBN (azobisisobutyro-nitrile)	VAZO 64 Dupont Co.	recrys. f/toluene
AMBN (azobis-(2-methyl-butyronitrile))	VAZO 67 Dupont Co.	recrys. f/isopropanol
$NaHCO_3$	Fisher Scientific Co.	certified A.C.S.
$NaNO_2$	Fisher Scientific Co.	recrys. f/DDI water
NH_4SCN	J.T. Baker Chem. Co.	recrys. f/DDI water
HQ (hydroquinone)	Fisher Scientific Co.	"Purified"

3.5.1.1.2 Swelling of Seed Latexes

200 grams of each recipe was prepared for loading the LUMLR. Specified amounts of emulsifier (aqueous Aerosol-MA solution), DDI water, latex seed, monomer, and buffer or inhibitor were weighed into a 12 oz. bottle. Swelling was accomplished at room temperature by rotation of the bottle at 40 rpm with its axis oriented $30 - 45^{\circ}$ from the horizontal. Complete swelling was attained by mixing for a 20 ± 3 hrs. period. In those recipes employing oil soluble initiators, the initiator was dissolved in 5 grams of monomer and added to the latex midway in the swelling cycle (SSMLR 6 - 13). In the case of persulfate initiation, the $K_2S_2O_8$ was dissolved in 10 gm DDI water and mixed with the swollen latex immediately before loading the reactor (SSMLR 4 and 5).

3.5.1.2 Reactor Loading

The low pressure/gravity loading technique was originally developed to reduce the problems associated with the interpretation of fluid expansion data (during reactor heatup) induced by the presence of an air bubble in the reactor (see Section 2.4.3.2.1). This technique was also employed for the loading of polymerization recipes to aid in interpreting the resulting kinetic data.

The swollen latex was first filtered through pyrex glass wool (Owens-Corning Fiberglas Corp.) into a 500 ml round bottom flask to remove any viscous material which may have formed during the swelling. The latex was then degassed at at pressure of ~20 mm Hg via an aspirator for a period of 30 - 45 min. or until the degassing (bubble formation) had apparently ceased. The system was restored to atmospheric

pressure for the time it took to assemble the loading apparatus (see Figure 2.29). A 35 - 45 mm Hg pressure was then applied to the entire system (reactor, fill flask, overflow flask, and tubing). The fill valve was opened allowing latex to flow into the reactor (via a pressure head) at a rate of approximately 10 ml/min. This continued until the reactor was full and the flow into the overflow flask was free of any bubbles. With the fill valve closed, the piston was lowered until fluid was no longer discharged from the exit port and the piston came to a stop. The vacuum to the overflow flask was cut, no longer being needed, and the fill valve was opened allowing fluid to be pushed back into the fill flask, thereby lowering the piston to the pre-set 100 cm^3 position. The fill valve was then closed, and disconnected from the reactor (via the Quick Disconnect), the aspirator turned off, and the overflow flask removed. The ports were cleaned and the insulation and housing assembled.

3.5.1.3 Polymerization/Data Collection

Once loaded, the reactor was connected to the MLR Controller and the power switched on. The piston position, as determined by the LVDT reading, was recorded prior to and after releasing the piston (i.e., allowing the spring to act on the piston and thus the fluid). If the piston drop was greater than 0.15 LVDT volts, the loading was considered to be unsatisfactory and the filling procedure was repeated until an adequate response was obtained. The piston position was then monitored for any change for a period of ca. 1/2 hr. after which the agitator was switched on, provided there was no evidence of any fluid leakage. The Stir Speed setting used in all of these exper-

iments was OSC 6.0, corresponding to 14 rpm and 79° arc (see Section 2.4.2.1). The stirrer paddle used was the modified MLR Blade design (Teflon). The piston position was followed for another 1/2 hr. period, again as a leakage check.

At time zero, a set of sensor readings were recorded including the fluid and wall temperatures, the LVDT voltage, and the gauge reading (set atop the reactor housing cover for monitoring cylinder expansion, Section 2.4.3.2.1). The experiment was begun by applying voltage across the heating wire (70°C switch on Controller). Data were recorded at one minute intervals for the first 25 minutes and then every 5 minutes. If the reaction became relatively rapid (Δ(LVDT)/5 minutes $\geq$ 0.1 volt) data were taken every 2 minutes until the reaction rate slowed once again. A polymerization was judged to be complete if no change in the LVDT reading occurred over a 20 minute interval. At this time, the power was switched off.

3.5.1.4 Decanting of Product

The latex was removed from the reactor as soon as possible following termination of the experiment. The housing cover and insulation were first removed and the piston position fixed (via the nut on the support bolt). The fill port quick connect was removed and the port was cleaned out so that the small amount of latex (partially polymerized) in this region would not contaminate the product. The piston was then cranked up and pulled from the reactor. The latex was decanted and filtered through glass wool into a flask, sealed with parafilm and immediately cooled in cold running water. The time was recorded for this event for later use in computing the residual

134

initiator concentration in the latex. The reactor was cleaned thoroughly and readied for the next polymerization.

3.5.1.5 Characterization

Product latexes were characterized in terms of their final solids content (gravimetrically), surface tension (Wilhelmy plate), residual monomer content (iso-octane extraction), monodisperse quality (scanning electron microscopy), and polymer molecular weight (gel permeation chromatography). In addition, the latexes produced in the persulfate initiated sequences (SSMLR 4 and 5) were characterized in terms of their pH and particle surface charge density (ion exchange and conductometric titration). Some of these methods were described previously while others require no further description. The determination of residual monomer (as well as the initial monomer content in the swollen latex) is described here in some detail, however.

Iso-octane extractions of the styrene in the swollen and product latexes were performed to determine the initial and final 'conversions' from the monomer contents [44]. Approximately 0.2 grams of swollen latex (0.5 gms product latex) was added to 20 gms of iso-octane (Purified Grade, Fisher Scientific Co.) in a 1 oz. bottle and tumbled end-over-end for 24 hrs. A quantity of about 0.1 gms (0.6 gms from product latex extraction) of the iso-octane phase was diluted by another 20 gms of iso-octane resulting in styrene concentrations around 10^{-5} gms styrene/gm iso-octane. This solution was then pumped through the sample cell of a UV Absorbance Monitor (Model 1840 - Instrumentation Specialties Co.) set at 245 nm and the absorbance recorded. The calibration curve in Figure 3.12 was used to determine the actual styrene con-
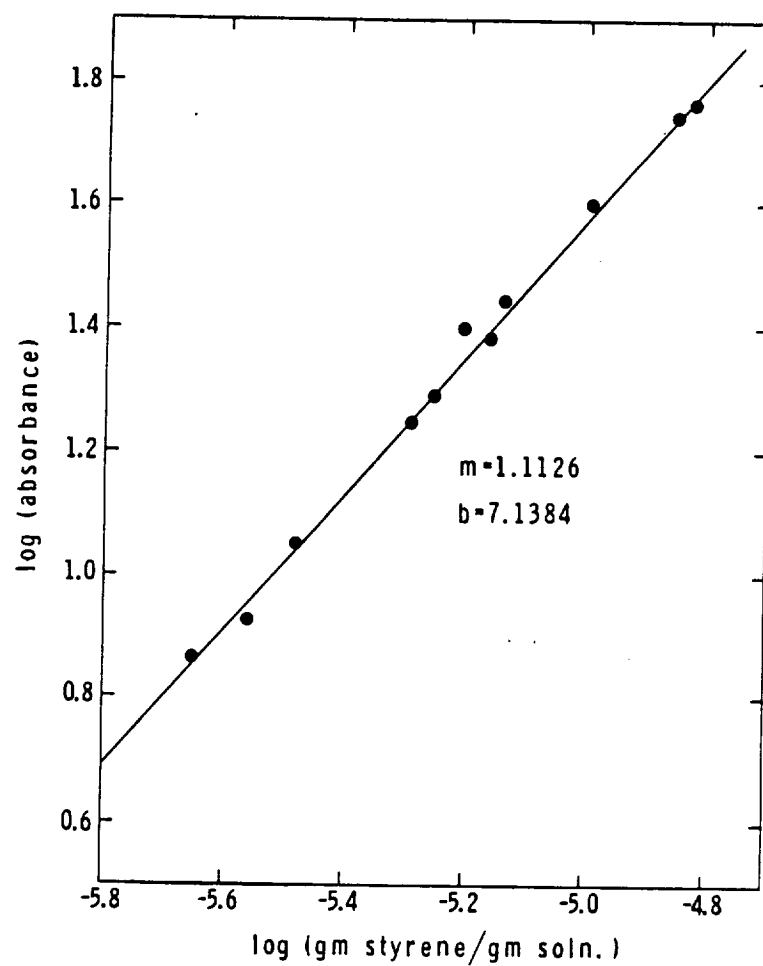
135

Figure 3.12   UV Absorbance (245 nm) as a Function of Styrene Concentration (in Iso-Octane)

136

tent in the solution. The amount of styrene in the latexes was back-calculated through the dilution data. The amount of styrene determined to be in the swollen latex was used to compute the recipe which was substituted into the kinetic interpretation program. The amount in the product was used to determine the fractional conversion for comparison to that obtained via the dilatometric data.

A Waters Associates Model ALC/GPC 201 liquid chromatography unit with μ-Styragel columns was used for determining the molecular weight distributions of the polymer produced in the successive seeding experiments. Samples of 0.5 wt % solids in tetrahydrofuran (THF) were prepared, filtered, and injected into the columns with a solvent (THF) flow rate at 2 ml/min. The resulting chromatogram was interpreted through use of a calibration curve with corrections made for spreading. Details are given in Appendix B.

3.5.2 Interpretation of Raw Data - Conversion

The conversion history for a polymerization in the LUMLR was obtained through interpretation of the LVDT, fluid temperature, gage, and recipe data collected during the experiment. Basically, the conversion was determined from the volume change due to polymerization zeroing out the effects of changing temperature. The following sequence of computations was made (via a computer program) to obtain conversion:

1. The recipe, in terms of weight fraction (W), polystyrene (PS), styrene (S), water (H_2O), initiator (WFINIT), buffer or inhibitor (BUF), and emulsifier (EMUL) was computed from the known amounts of ingredients added to the latex, the seed and its constituents, and

137

the results of the iso-octane extraction/UV analysis on the swollen latex (S);

2. the total grams of fluid in the reactor (G_T) was calculated from the known volume of the reactor (V_R), the recipes' three major components (PS, S, H_2O), and the density of each component at the time zero fluid temperature. Assuming additive densities of styrene and polystyrene (see Section 2.4.3.2.2):

$$G_T = V_R / [(W_S + W_{PS})^2 / (W_S \rho_S + W_{PS} \rho_{PS}) + W_{H_2O} / \rho_{H_2O}] \qquad (3.3)$$

The volumes of the aqueous and oil phases are considered additive in all computations;

3. the grams of each component (G_{PS}, G_S, G_{H_2O}) were calculated from the weight fractions and total grams;

4. for each data point, a volume ($V_{T,i}$) was computed based on the fluid temperature and the original recipe:

$$V_{T,i} = (G_{PS} + G_S)^2 / (G_S \rho_{S,i} + G_{PS} \rho_{PS,i}) + G_{H_2O} / \rho_{H_2O,i} \qquad (3.4)$$

$\rho_{S,i}$ and $\rho_{PS,i}$ were calculated using equations 2.3 and 2.4, respectively (Section 2.4.3.2.2). $\rho_{H_2O,i}$ was obtained from a polynomial fit of temperature-density data for water;

5. also for each data point, the actual volume (V_{LVDT}) was computed from the LVDT voltage, compensation for cylinder expansion being made by either the gage data or the approximation via the fluid temperature:

$$V_{LVDT,i} = \Delta h_i A_i + V_R \qquad (3.5)$$

where A is the cross-sectional area (cm^2),

$$A_i = \pi \left[r_{cyl} \left(1 + \alpha \left(\frac{9}{5} \right) \Delta T_{F,i} \right) \right]^2 \qquad (3.5a)$$

where α, the coefficient of thermal expansion for stainless steel (type 302) = 1.728 x 10^{-5} cm/cm $^{\circ}$K, ΔT_F = difference between the current and time-zero fluid temperature ($^{\circ}$C), r_{cyl} = radius of the cylinder at room temperature (2.05 cm). Δh is the change in piston position,

$$\Delta h_i = (v_1 - v_i)/K_{LVDT} + \Delta l_i \qquad (3.5b)$$

where v_1 and v_i are the time zero and current LVDT voltages, K_{LVDT} is the conversion factor, 14.7868 volts/cm and Δl_i is the expansion dimension of the cylinder as measured by the dial indicator atop the housing cover or as estimated from the fluid temperature,

$$\Delta l_i = l_c \, \alpha \left(\frac{9}{5} \right) \Delta T_{F,i} \qquad (3.5c)$$

where l_c is the cylinder length, 18.669 cm.

6. the difference in volumes, ΔV, was finally used to compute the change in the amount of styrene in the reactor,

$$G_{S,i} = \{ [(G_S \rho_{S,i} + G_{PS} \rho_{PS,i})^{-1} - \Delta V_i (G_{PS} + G_S)^{-2}]^{-1} - (G_{PS} + G_S) \rho_{PS,1} \} / (\rho_{S,i} - \rho_{PS,i}) \qquad (3.6)$$

where $\Delta V_i = V_{T,i} - V_{LVDT,i}$;

7. the fractional conversion was thus obtained:

$$X_i = (G_S - G_{S,i})/G_S \, . \qquad (3.7)$$

Equivalent expressions derived assuming monomer/polymer additive volumes were also used in the earlier studies for comparison. (See Appendix C.) However, results obtained assuming additive densities proved more consistent (see Section 2.4.3.2.2) and therefore were used in the interpretation of the data presented here.

139

3.5.3 Persulfate Initiated Sequences

Two sets of successive seeding experiments were conducted using potassium persulfate initiator with sodium bicarbonate buffer. The first (SSMLR 4) used 1 mM $K_2S_2O_8$ (added based on the aqueous phase) with a particle surface coverage of 8% by the emulsifier, Aerosol-MA. The second (SSMLR 5) employed halved quantities of each of these (0.5 mM $K_2S_2O_8$ and 4% coverage) to reduce the number of nucleated particles in the series.

3.5.3.1 SSMLR 4 - 8% Coverage/1 mM $K_2S_2O_8$

The experimental design for SSMLR 4 was as follows:

1) monomer/polymer swelling ratio = 2/1

2) final solids content = 30%

3) emulsifier concentration 'constant' in terms of

    a) fractional surface coverage = 0.08

    b) aqueous phase content = 7.76 x 10^{-5} M

4) <u>added</u> amount of initiator constant = 1 mM (aqueous phase)

5) <u>added</u> amount of buffer constant = 3.2 mM (aqueous phase) (i.e. equal amounts by weight of initiator and buffer)

The step-by-step particle sizes were by design:

$$0.19 \ \mu m \xrightarrow{1} 0.27 \ \mu m \xrightarrow{2} 0.40 \ \mu m \xrightarrow{3} 0.57 \ \mu m \xrightarrow{4} 0.82 \ \mu m$$
$$\xrightarrow{5} 1.19 \ \mu m \xrightarrow{6} 1.71 \ \mu m \xrightarrow{7} 2.47 \ \mu m$$

Most of the experimental recipe 'constants', varied somewhat due to the sequence design in which the product latexes were used as seed without any purification between steps. A balance was made on the emulsifier to maintain it at the design level but the initiator and buffer were added in the same quantities each time. Based on the

decomposition rate, the amount of initiator left in the product latexes was estimated from the polymerization time (until quenching under cold running water) and temperature (69°C). This was used to compute the actual amount in each step prior to polymerization. The amount of buffer was simply computed by a mass balance assuming that it was unchanged throughout the experiments. The swelling ratios were estimated from the iso-octane extraction results of the swollen latex assuming no loss of polymer during swelling. These results are presented in Table 3-3. Monomer/polymer ratios varied on both the low and high side of the 2/1 design. These were attributed to both incomplete swelling due to the formation of a viscous phase on top of the swollen latex (polymer particles dissolved in a monomer layer) and carry-over of monomer from the previous step due to conversions under 100%, respectively.

Table 3-3

Recipe 'Constants' for SSMLR 4

SSMLR4	M/P	% Solids	γ(N/cm)x10^5	$[K_2S_2O_8]_0$ (mM)	$[NaHCO_3]_0$ (mM)
1	1.82	28.2	74.5	1.00	3.23
2	2.06	28.5	73.2	1.21	4.38
3	2.06	28.4	72.8	1.25	4.76
4	2.06	28.3	73.2	1.26	4.91
5	1.91	27.8	71.4	1.25	4.96
6	2.00	26.9	70.8	1.26	4.98
7	1.90	26.7	69.7	1.26	5.08

These effects were also reflected in the final solids contents and somewhat in the latex products and surface tension values. All solids contents were below 30% and decreased significantly in the last three

141

steps. The surface tension also decreased in these three steps due to a decrease in the particle surface area available for adsorption. The initial persulfate concentration increased by 21% from step one to step two and only 3% from two to three, remaining constant thereafter. The buffer level increased from step to step (35% from 1 to 2, 9% from 2 to 3, 3% from 3 to 4, etc.) with decreasing difference. The effect of this increase in the electrolyte level on the particle stability was considered small in light of the polymerization results.

All of the latexes produced in this series were stable when decanted from the reactor (i.e., fluid with no massive coagulation). However, the products of bottle polymerizations which were run at 70°C for 24 hrs. using the left-over swollen latexes were completely flocculated (Recipes 1, 2 and 3). These bottles were tumbled end-over-end, subjecting the latexes to a shear apparently greater than experienced in the LUMLR. Also, the 24 hr polymerization time was considerably greater than the ~7 hr. experiments in the prototype. The fourth recipe was removed from the bottle polymerizer after 9 hrs. as compared to a 7 hr. 20 min. period in the LUMLR. The latex was again flocculated. However, the bottle with the fifth seed recipe was removed after the same time as the dilatometric run and the latex was stable, although the last two steps (6 and 7) each resulted in complete flocculation after parallel polymerization times. These results lend support to the previous observation that this flocculation is not only shear related but perhaps more importantly that it is a phenomenon which occurs quite late in a polymerization (>95% conversion) (see Section 3.4).

The quality of the latexes polymerized in the LUMLR, in terms of

uniformity (i.e., without small or large off-size particles), is illustrated by the scanning electron micrographs of Figure 3.13. The first step was free of small or large particle generation while the next three steps showed some evidence of relatively few small particles with no off-size larger particles. Steps 5, 6, and 7 resulted in increasingly larger amounts of small particles but without larger off-size particles. These results indicated that a further reduction in the emulsifier concentration (and initiator concentration) was still necessary if monodisperse latexes were to be prepared above 1 μm in size using aqueous phase initiation. Kinetic and characterization results will be presented for only the first four steps of this sequence in light of these findings.

The combined conversion histories for steps 1 through 4 are presented in Figure 3.14. The results are given as solid lines instead of discreet points because the data points lie within five minutes (or less) of each other. (See Figure 2.36 for an example of the fluid and wall temperature profiles, conversion and polymerization rate data given as discreet points for SSMLR 4-1.) The conversion is represented in grams polystyrene formed since actual fractional conversion scales vary due to the slightly different swelling ratios.

Within the four-step seed sequence the polymerization time increased with increasing particle size. This was due to the decreasing initial polymerization rates rather than the rates being lower throughout each successive reaction. Note that the influence of the gel effect was present throughout the entirety of each polymerization and that the polymerization rates were nearly the same at high conversion

143

SSMLR 4 $K_2S_2O_8$/NaHCO$_3$

$[I]_o = 1.0$ mM

FRCV = 0.08
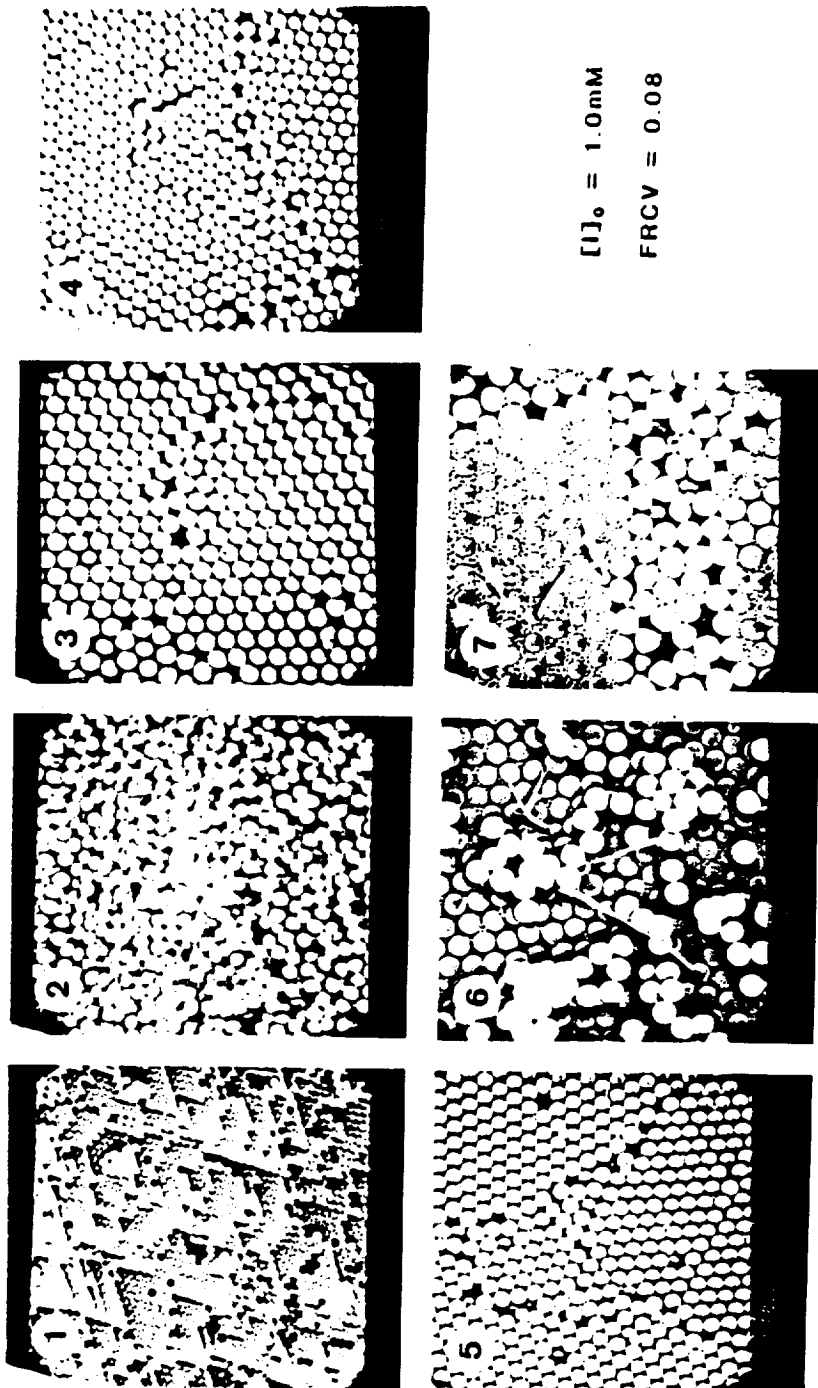
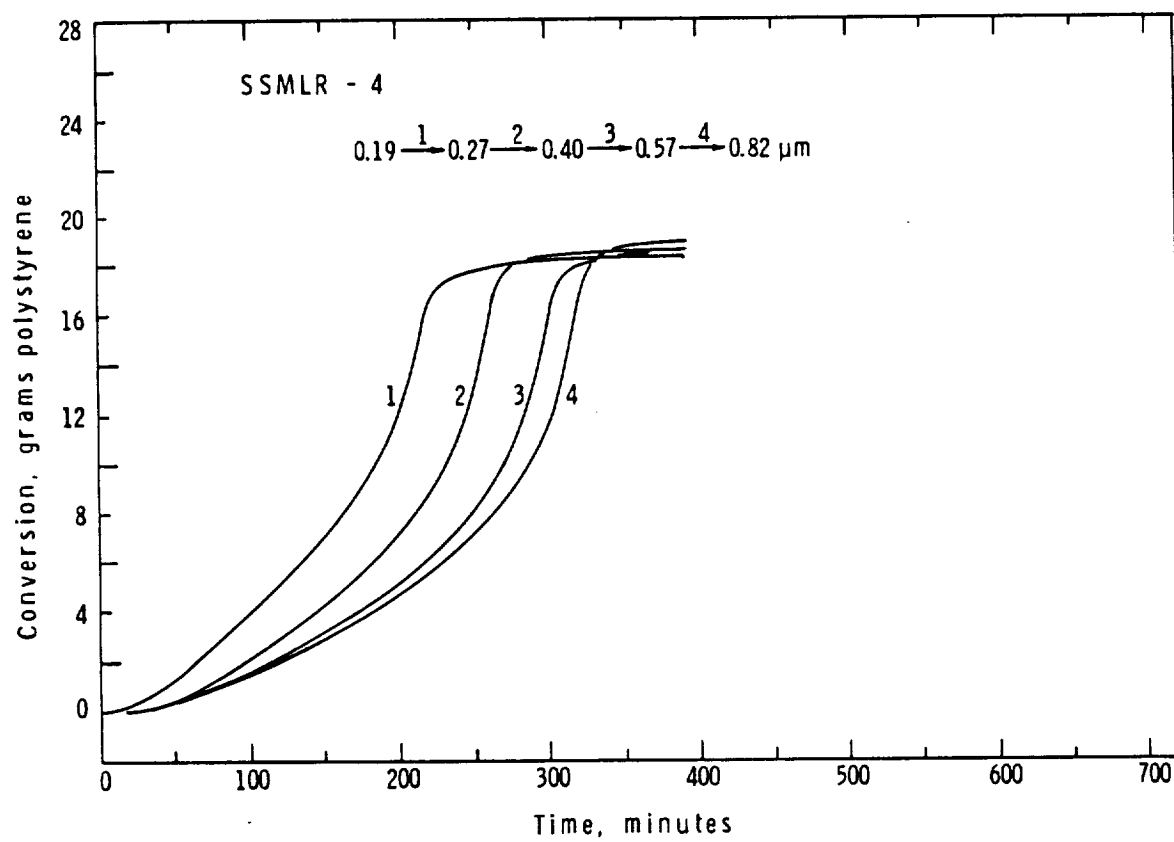Figure 3.13 Scanning Electron Micrographs of Latexes Produced in SSMLR 4, Steps 1 through 7

Figure 3.14 Conversion Histories for Seed Sequence SSMLR 4,
Steps 1 through 4

145

($\geq$10 gms polystyrene). Qualitatively, the decreasing **rates** were attributed primarily to the decreasing number of particles (N_p) in the system with increasing particle size (i.e., for a fixed solids content $N_p \alpha d^{-3}$). However, the differences in the rates between each succeeding step became smaller despite a 66% decrease in the number of particles for each step. (Step 1 = 2.65×10^{15}, Step 2 = 8.85×10^{14}, Step 3 = 2.95×10^{14}, Step 4 = 9.8×10^{13} particles in the reactor volume). This effect is related to the transition of kinetics from emulsion towards bulk kinetics as described in more detail further on.

The characterization results from the iso-octane extractions, conductometric titrations, and GPC chromatograms are given in Table 3.4.

Table 3-4

Conversion, Surface Charge, and Average Molecular Weight of SSMLR 4 Latexes

| SSMLR 4 | % Conversion[1] | | Surface Charge | | Molecular Weight | |
	On Monomer	On Polymer	μeq/gm	$\mu C/cm^2$	$\bar{M}_n \times 10^{-5}$	$\bar{M}_w \times 10^{-6}$
0.19 μm seed	--	--	3.08	.99	2.5	1.4
1	96.0	97.4	1.75	.81	2.9	1.6
2	94.6	96.4	1.32	.88	3.5	1.5
3	93.5	95.6	0.91	.88	3.7	1.5
4	94.6	96.4	0.89	1.23	3.2	1.4

[1]from iso-octane extraction/UV analysis

Limiting conversions below 100% were found for all polymerizations due to the reduced diffusivity of monomer molecules in the glassy polymer matrix. The surface charge decreased in terms of microequivalents per gram of polymer and increased only slightly in terms of

146

microcoulombs/cm^2 (i.e., surface charge density). These results are consistent with those reported previously (Section 3.3.2) except that only strong acid groups (sulfate) were found in these polymerizations as compared to both weak and strong acid groups. From this information it was possible to speculate about the efficiency of adsorption of growing free radical chains with sulfate end groups (comparable to the initiator efficiency factor, f). In order to do this, a number of assumptions were made: 1) all adsorbed groups were detectable as sulfate groups; 2) all groups present on the initial seed were still present on the particle surface (i.e., no buried groups); 3) the initiator decomposition rate and initial initiator concentration were accurate. The rate constant for decomposition is given by

$$k_d = k_{d_o} \exp (-E_{ad}/RT) \tag{3.8}$$

where k_{d_o} = 5.188 x 10^{16} sec^{-1} and E_{ad} (activation energy) = 33.5 kcal/gram-mole for persulfate [82]. R is the universal gas constant, and T the absolute temperature ($^{\circ}$K). The efficiency was computed by dividing the amount of surface groups expected assuming a 100% efficiency over the polymerization time (until quenching) into the amount actually found from the conductometric titration results. This efficiency was found to decrease from 0.59 to 0.45 to 0.32 to 0.31 for steps 1, 2, 3, and 4, respectively. These results have a number of implications which will be discussed in the following section.

The molecular weight distributions were relatively broad with high weight average molecular weights characteristic of emulsion polymerization. These decreased slightly with increasing particle size. The increased radical entry rate per particle (i.e., decreasing

147

particle number) can explain this even keeping in mind a reduced iniator adsorption efficiency.

3.5.3.2 SSMLR 5 - 4% Coverage/0.5 mM $K_2S_2O_8$

In order to improve on the monodisperse quality of the latexes produced via successive seeding the secondary generation of particles had to be reduced. The obvious directions for accomplishing this included reductions in the initiator and aqueous phase emulsifier concentrations and an increase in the particle number or solids content. For SSMLR 5 the latter remained unchanged while both the initiator and fractional surface coverages were halved to 0.5 mM and 0.04, respectively. The aqueous phase concentration was consequently reduced by 52% from 0.078 mM to 0.0372 mM by halving the surface coverage.[†] The amount of buffer added was also halved (equal wt. fractions of initiator and buffer). The recipe 'constants' for SSMLR 5, given in Table 3-5, were determined as described previously. A relatively low

Table 3-5

Recipe 'Constants' for SSMLR 5

SSMLR 5	M/P	% Solids*	γ(N/cm)*$\times10^5$	pH*	$[K_2S_2O_8]_0$ (mM)	$[NaHCO_3]_0$ (mM)
1	1.87	25.7	74.2	6.9	0.50	1.62
2	2.06	28.2	73.9	7.3	0.62	2.25
3	1.99	27.5	74.6	7.2	0.62	2.42
4	2.06	28.1	73.9	7.3	0.62	2.50
6	2.10	28.0	74.4	7.3	0.60	2.49
7	2.11	28.2	---[+]	---[+]	0.60	2.51

*measured after polymerization
[+]sample flocculated

[†]The CMC of Aerosol-MA is in the range of 15 - 18 mM.

148

swelling ratio together with a low solids content were indicative of the greater difficulty in swelling encountered with the lower emulsifier concentration in the first step of the sequence. The swollen latex contained a viscous monomer/polymer layer, the primary contributor to these losses. Subsequent swellings did not exhibit any significant loss of monomer or polymer, this being attributed to a lowered resistance to swelling due to the presence of residual monomer in the particles from the previous polymerization step. As in SSMLR 4, all solids contents were below 30%, remaining relatively constant around 28%. The surface tension of the latexes was also relatively constant in this series, indicating a nearly constant emulsifier level. (At such a low concentration of emulsifier the effect of the presence of particles resulted in surface tensions above that of water alone.) The pH of the final latexes was also monitored to confirm neutrality. Once again the initial initiator concentration was computed to remain constant after the first seeding step (0.6 mM).

All but the last step in this sequence produced stable latexes. SSMLR 5-7 was run for 12.75 hr, even though the reaction was essentially complete after 8 hrs, in order to monitor residual monomer conversion. The experiment was stopped when it was noted that the fluid temperature was dropping appreciably, a phenomenon which had not been observed previously. A completely flocculated latex ('shaving cream') was found upon opening the reactor. It was believed that the temperature drop was a direct outcome of the flocculation and the resulting poor mixing. In this way the precise moment of flocculation could be determined. This is yet another piece of evidence supporting the idea

149

of flocculation at high conversion. Furthermore, the parallel bottle polymerizations, usually run for the same length of time as the dilatometer experiment, was stopped one hour short and the latex was found to be stable. All of the latexes prepared in the previous steps via bottle polymerizations were also found to be stable after a duplicate polymerization time. It should be noted that these bottles were tumbled with their axis parallel to the axis of rotation as opposed to the perpendicular as in the previous experiments. This configuration obviously produced less shear as originally intended.

Scanning electron micrographs of the latexes produced in SSMLR 5 are reproduced in Figure 3.15. The latexes appear to be relatively free of new particle generation up to the fourth seeding step, while a few can be seen in the fifth and sixth steps and many in the last step. Significant numbers of larger off-size particles (~2 - 4% of the particle population) can also be noted throughout the sequence leading one to speculate that this is in the vicinity of the lower limit of emulsifier concentration needed to provide stability for the individual particles in the system. The improvement in the latex quality was not as significant as might be expected from the reduction in the emulsifier and initiator concentration. However, it must be remembered that the ionic strength was also reduced (initiator and buffer) which would weaken the effect of a lowered emulsifier concentration (i.e., increased stability of nucleated particles).

The polymerization conversion histories for SSMLR 5 are presented in Figure 3.16. All seven curves are presented, even though the products of the last three steps are not considered to be strictly

150

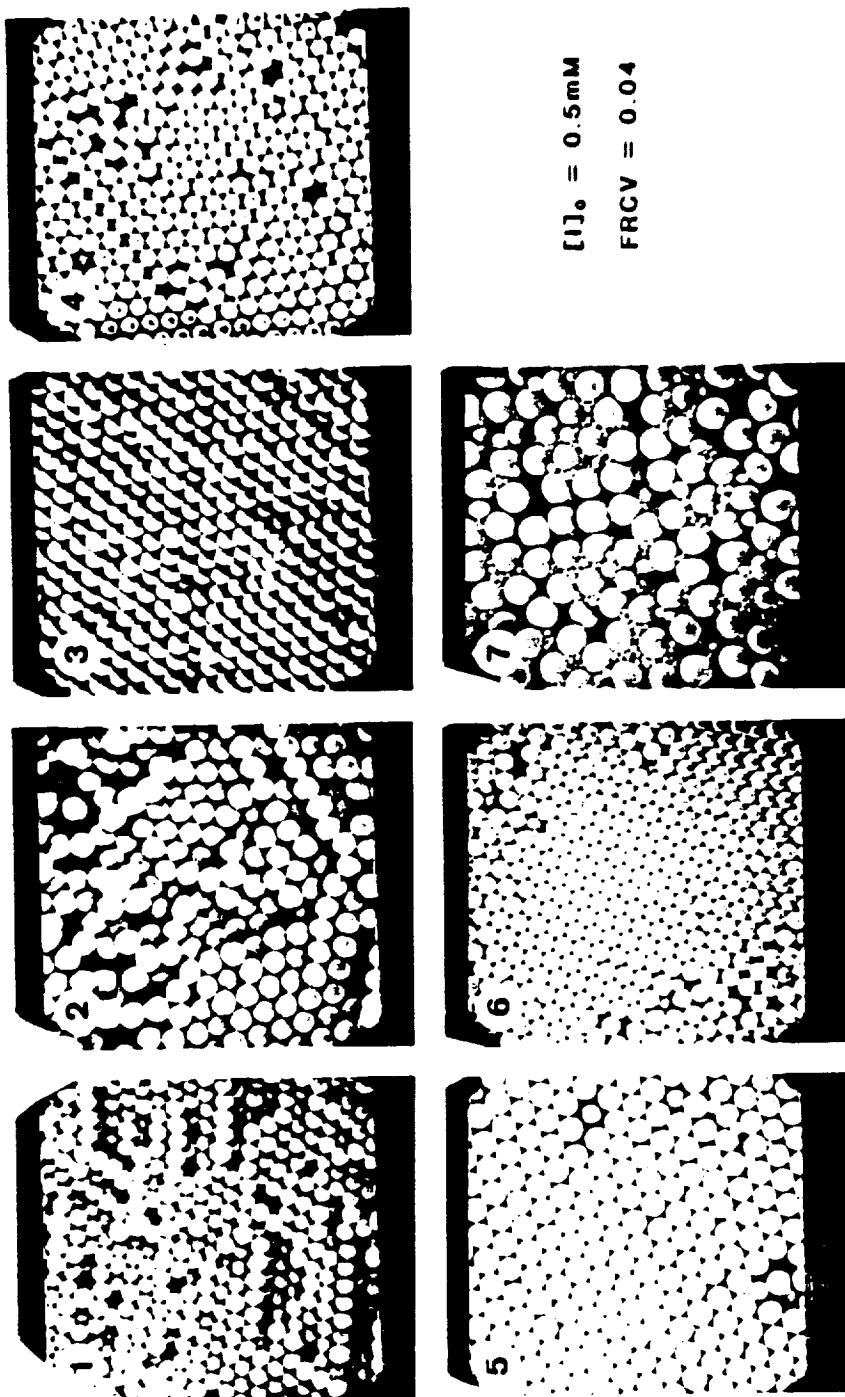SSMLR 5 $K_2S_2O_8$/NaHCO$_3$

$[I]_o = 0.5mM$

FRCV = 0.04

Figure 3.15   Scanning Electron Micrographs of Latexes Produced in SSMLR 5,
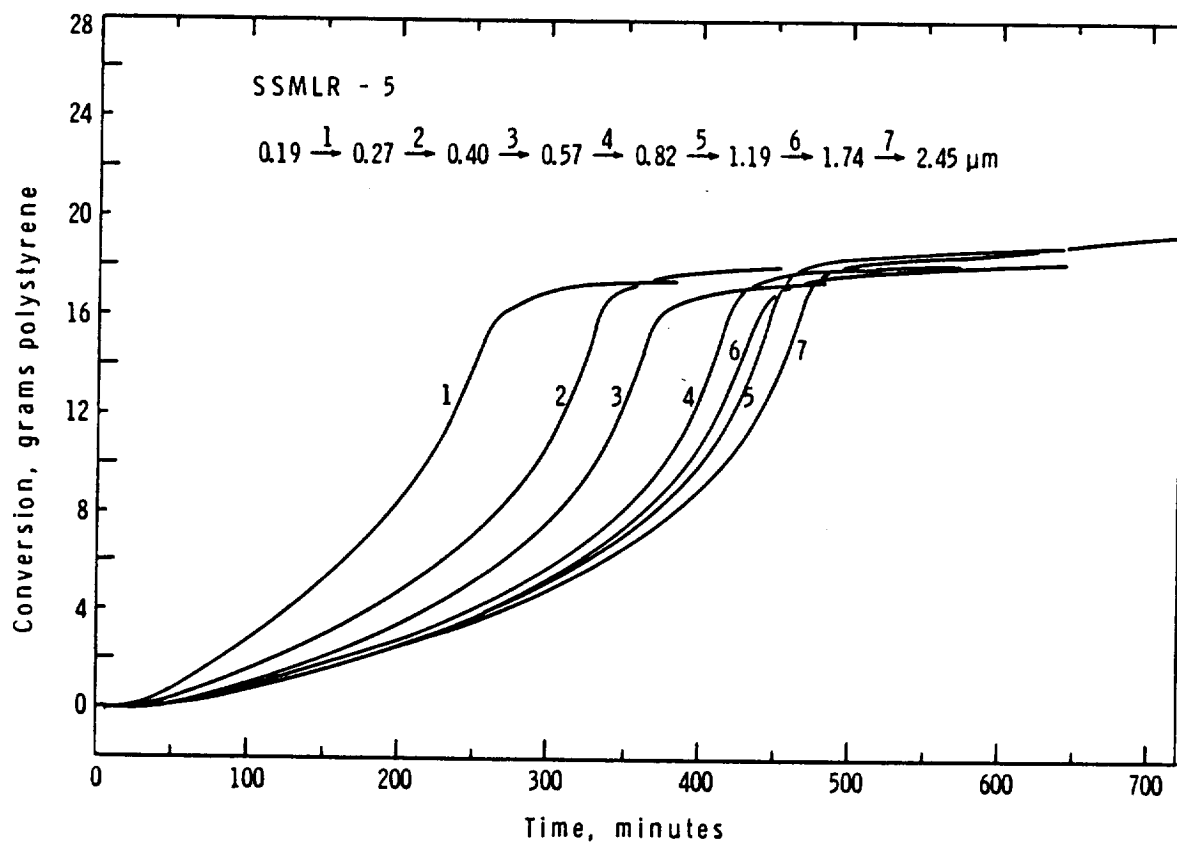Steps 1 through 7

151

Figure 3.16 Conversion Histories for Seed Sequence SSMLR 5, steps 1 through 7

'monodisperse'. As in SSMLR 4, the polymerization times increased with increasing particle size. However, the polymerizations took longer to reach high conversion for the case of SSMLR 5, indicating a dependency on the initiator concentration. The final conversions based on monomer and determined by both iso-octane extraction and dilatometry are given in Table 3-6. Agreement within 1% was obtained with the exception of the last step (3%). The average conversion was 94.9 + .4% (on monomer) indicating that the residual monomer content was about 0.035 gm monomer/gm polymer or 3.5%.

Table 3-6

Conversion, Surface Charge, and Average Molecular Weight of SSMLR 5 Latexes

| SSMLR 5 | % Conversion | | Surface Charge | | Molecular Weight | |
	Extrac-tion	Dila-tometry	$\mu eq/gm$	$\mu C/cm^2$	$\bar{M}_n x10^{-5}$	$\bar{M}_w x10^{-6}$
1	95.5	95.3	1.32	0.61	4.0	1.9
2	95.0	94.4	0.85	0.56	3.8	1.7
3	94.6	95.5	0.70	0.67	3.8	1.8
4	94.8	95.9	0.35	0.49	3.7	1.8
5	94.6	95.2	0.34	0.67	4.7	1.8
6	94.6	95.0	0.45	---	5.6	1.9
7	95.5	98.6	0.42	---	5.3	1.9

The surface charge, in terms of $\mu eq/gm$, decreased with increasing particle size through the first five steps of the sequence. This was the same behavior as noted in SSMLR 4, with the difference that lower values were found, this being consistent with the reduction in the initiator concentration. The combined data from SSMLR 4 and 5 are presented in Figure 3.17, plotting both the charge in terms of

153
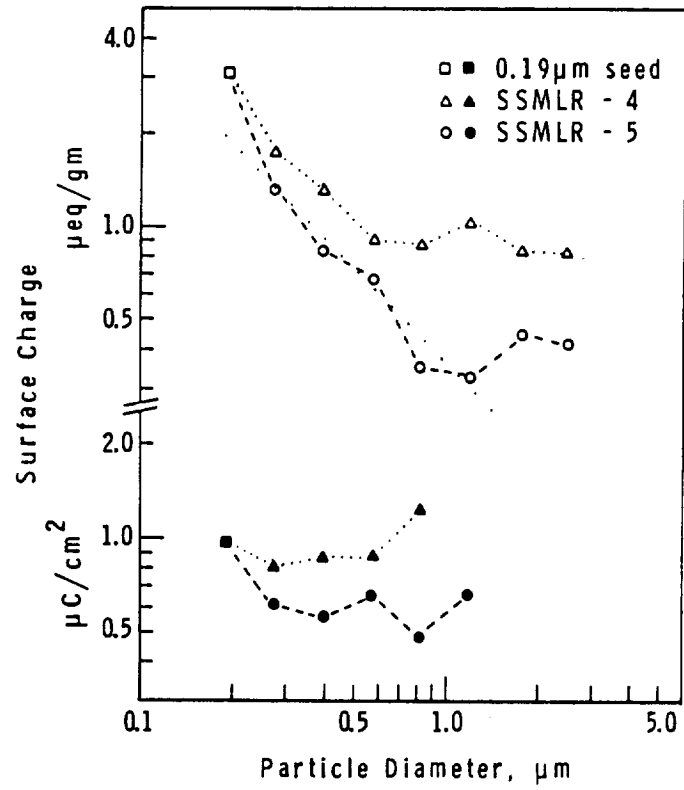
Figure 3.17   Surface Charge, μeq/gm (Open Points) and μC/cm^2
             for SSMLR 4 and 5 as Functions of Particle Diameter

μeq/gm (open points) and the surface charge density ($\mu C/cm^2$) as functions of the particle diameter. Only the significant surface charge density data are plotted (i.e., those for the steps in which little or no particle nucleation was noted). Initiator radical efficiencies were also estimated for this sequence as outlined in the previous section. These are compared with the previous results in Table 3-7.

Table 3-7

Initiator Radical Absorption Efficiencies Estimated from Surface

Charge Data

Efficiency

Sequence Step	SSMLR 4	SSMLR 5
1	.59	.68
2	.45	.50
3	.32	.44
4	.31	.21
5	--	.20

Decreasing efficiencies were computed for each sequence with increasing particle size up to the fourth and fifth steps of SSMLR 4 and 5, respectively. Greater 'absorption efficiencies' were determined for the first three seeding steps of SSMLR 5 in which both the initiator concentration and surface coverage were reduced. Both of these could conceivably contribute to the increased efficiency. A reduction in surface coverage by an anionic emulsifier decreases the total charge present on the particle surface, thus reducing the electrostatic repulsion between a particle and a charged oligomer radical and thereby increasing the capture efficiency. The absorption rate, ρ_a, is defined by:

155

$$\rho_a = k_a [R\cdot]_W \qquad (3.9)$$

where k_a is the mass transfer coefficient for free radical absorption into particles and $[R\cdot]_W$ is the concentration of radicals in the aqueous phase. The absorption of free radicals has been explained by both diffusion theory [47,48] and collision theory [46,59]. From diffusion theory k_a is a function of the particle diameter, d:

$$k_a = 2\pi D_W N_p d \qquad (3.10a)$$

where D_W is the diffusivity of a radical in the aqueous phase, while collision theory states that absorption is proportional to the available surface area:

$$k_a = 4\pi C N_p d^2 \qquad (3.10b)$$

where C is a constant. In these successive seeding experiments the number of particles is proportional to d^{-3}. If this is substituted into equations 3.10a and 3.10b the rate of absorption becomes proportional to d^{-2} for diffusion theory and d^{-1} for collision theory. The 'absorption efficiency' determined from the surface charge data is considered directly proportional to the absorption rate of free radicals. A log-log plot of the efficiency versus particle diameter using the data of SSMLR 5 (steps 1 through 5) was fitted with a linear least squares fit of slope -1.02. This result, therefore, suggests that the collision theory of radical absorption is applicable under the conditions of these experiments. The question that remains is what happens to the free radicals which are not absorbed into the particles. Aqueous phase termination and transfer reactions are likely to account for this.

The weight average molecular weights were not very sensitive to particle size, however, the effect of initiator concentration was significant. $\bar{M}_W$ increased by about 20% as a result of halving the initiator (and emulsifier) concentration. Lower radical entry rates produced higher molecular weight polymer.

3.5.3.3 Kinetic Analysis

The overall rate of reaction , R_p, in a seeded emulsion polymerization of monodisperse latex is given by:

$$R_p = k_p \ [M]_p \ \bar{n} \ N_p/N_A \qquad (3.11)$$

where k_p is the propagation rate constant, $[M]_p$, the concentration of monomer in the particles, $\bar{n}$, the average number of radicals per particle, N_p, the number of particles, and N_A, Avogadro's number. The successive seeding conversion histories obtained via dilatometry were used to obtain the rate of polymerization by computing the slope of the curve at any given point. Two numerical curve fitting techniques were tested for obtaining polymerization rate information. The first used n-th order polynomial fits of the conversion-time data (grams polystyrene) determined by the least squares method. This technique proved inadequate when applied to the entire conversion curve, resulting in poor fits up to the highest order tested (n = 10). However, improved results were achieved when the fit was applied over the range of accelerated conversion, prior to the sharp decrease in the polymerization rate. The second technique, a cubic-spline method, was also applied to the conversion data which had the advantage of being able to cover the entire curve but the disadvantage of being sensitive to

any noise in the data. An example of the results obtained using each of these methods is illustrated in Figure 3.18. The squares represent the polymerization rate computed from slopes obtained from the cubic spline method. The solid line represents the results obtained using a 7th order polynomial fit. The latter generally gives a better fit over most of the conversion range but is inaccurate after the rate maximum. Consequently, the cubic spline technique was used routinely in the interpretation of all the conversion data for these seed sequence, being supplemented at times by the polynomial fit method.

With a knowledge of the polymerization rate as a function of time and conversion and the polymerization recipe, the average number of growing radicals per particle ($\bar{n}$) was computed. In these seeding experiments N_p was determined by the experimental design and likewise the initial monomer concentration in the particles. Using these and recomputing $[M]_p$ based on the measured conversion, $\bar{n}$ was determined at each recorded point on the curve. The propagation rate constant was calculated from

$$k_p = k_{po} \exp(-E_{ap}/RT) \tag{3.12}$$

where $k_{po} = 2.2 \times 10^7$ 1/mole.sec and E_{ap} (activation energy) = 7400 cal/mole for styrene [60]. These values had been determined directly from emulsion polymerization experiments. Other values for k_{po} and E_{ap} have been reported elsewhere in the literature, with values for k_{po} as low as 4.5×10^6 1/mole.sec [61]. E_{ap} values range from 7.3 to 7.76 kcal/mole [61,62]. These inconsistencies reflect the uncertain nature of these types of determinations and therefore, any com-

158
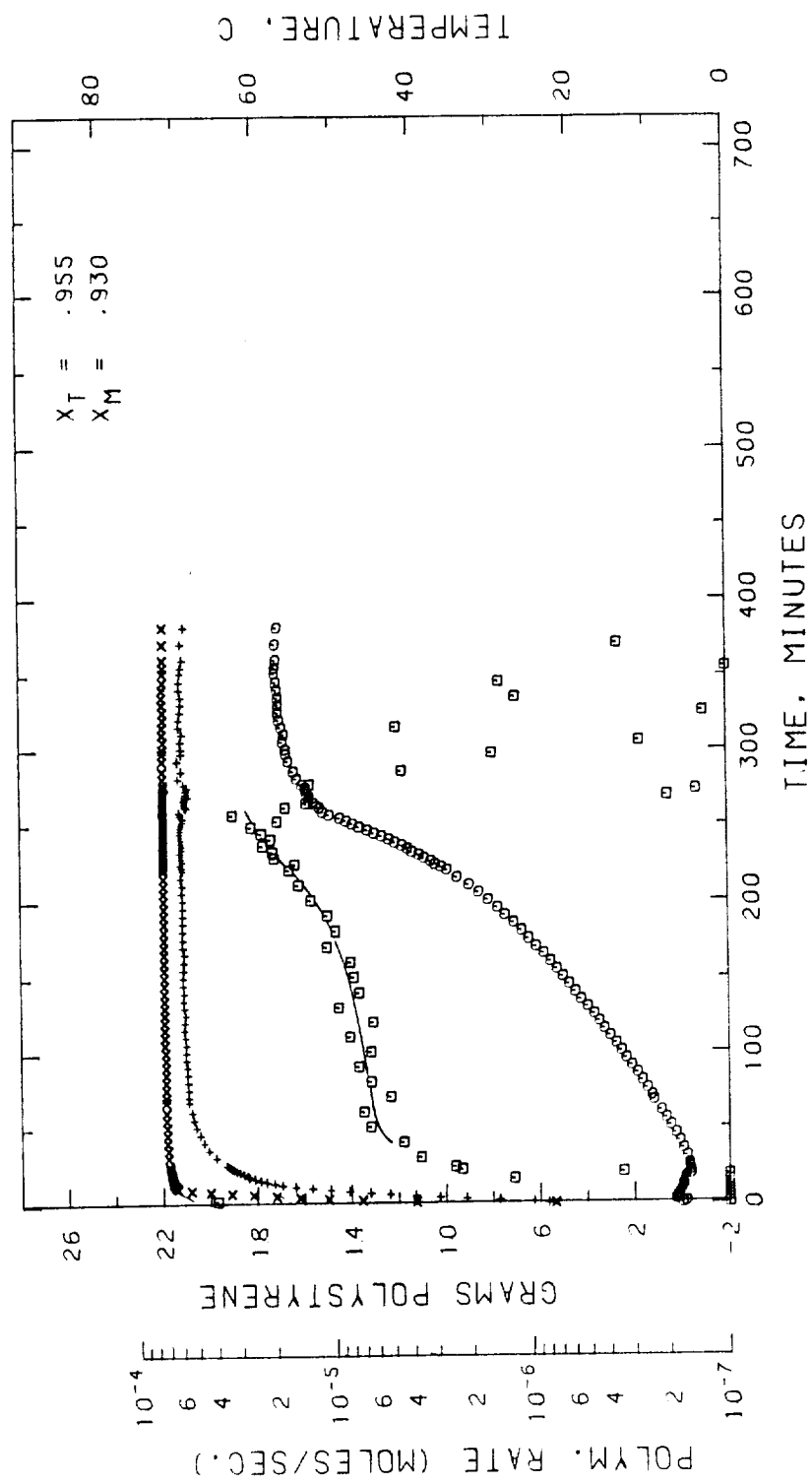
Figure 3.18   Data of SSMLR 5-1 Illustrating Differences Between a 7th Order Polynomial Fit and Cubic Spline Fit (Squares) of the Conversion Data (Circles) Used to Obtain R_p. x and + Represent Wall and Fluid Temperatures, Respectively

putations based on these must be regarded in this light. In addition, it is also known that k_p does not remain constant over the entire conversion range if the temperature of polymerization lies below the glass transition temperature of the polymer, which is in the $85 - 100^{\circ}$C range for polystyrene. This effect begins to be significant for a weight fraction polymer between 0.8 and 0.9. Beyond this point, the determination of $\bar{n}$ is meaningless without a knowledge of the k_p-conversion behavior.

The behavior of $\bar{n}$ as a function of the weight fraction polymer, W_p, ('total' fractional conversion) for the first step of sequence SSMLR 5 is presented in Figure 3.19. A log scale (left ordinate) is used for $\bar{n}$, represented by the squares, because of the wide variation experienced. The points were computed from both the cubic-spline $(x, \square)$ and polynomial fits of the conversion histories (R_p) as shown previously in Figure 3.18. As before, a certain amount of noise was produced by the cubic-spline fit while a slight oscillation was produced by the polynomial (7th order) fit. More important, however, are the results themselves. $\bar{n}$ was found to increase with conversion from an initial value in the region of 1/2 to a maximum of about 15 at W_p of 0.87 or 0.81 on monomer. Thereafter, the computed $\bar{n}$ decreased due to the inaccurate use of a constant k_p value as described above. The fact that $\bar{n}$ rose above 1/2 (Smith-Ewart, Case 2 kinetics) indicates that in 0.27 μm particles containing greater than 35% polystyrene (in styrene) instantaneous termination is no longer a reality (i.e., two or more growing radicals can co-exist in a particle). This marks the onset of the transition of polymerization kinetics from emulsion ($\bar{n} = 1/2$) to bulk ($\bar{n} \gg 1$). 160
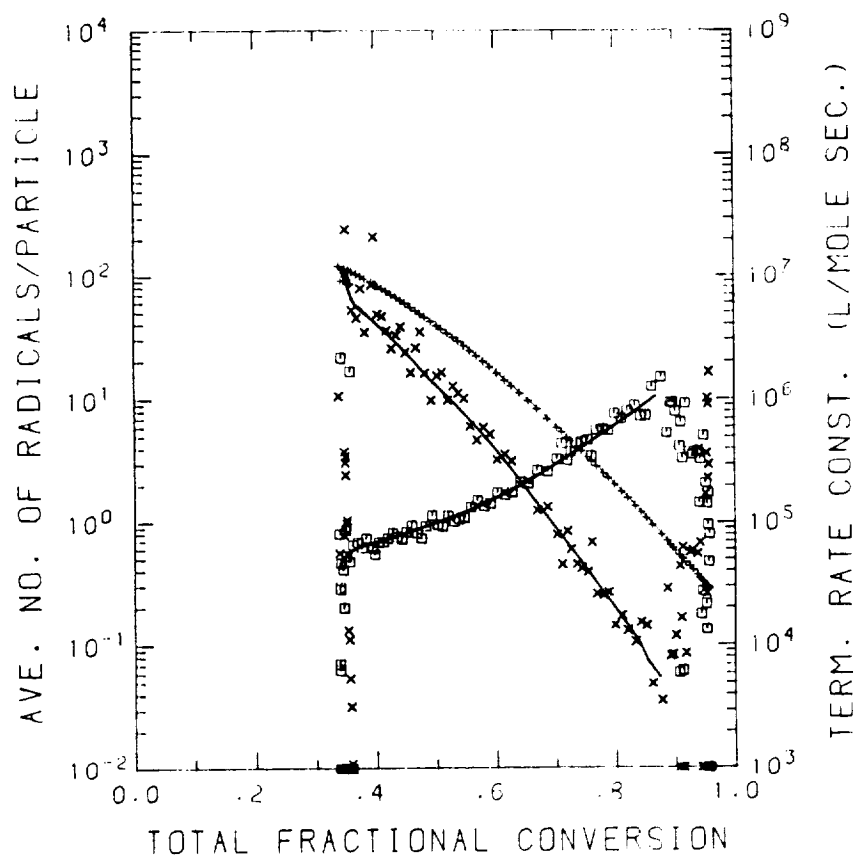
Figure 3.19 $\bar{n}$ (Squares) and k_t (x) as a Function of Total Conversion for SSMLR 5-1. Discreet Points from Cubic Spline Fit, Solid Curve from Polynomial Fit. +'s Represent Values of k_t determined from Bulk Polymerizations [63]

It seems appropriate at this point to describe more fully the nature of the transition from emulsion to bulk polymerization kinetics. The rate expression for polymerization in emulsion was given previously by equation 3.11. The equivalent expression for bulk or solution polymerization (radical chain) is

$$R_p = - \frac{d[M]}{dt} = k_p \; [M] \; [R\cdot] \; . \qquad (3.13)$$

$[R\cdot]$, the concentration of all radical species, is computed from

$$[R\cdot] = (R_i/2k_t)^{\frac{1}{2}} \qquad (3.14)$$

and

$$R_i = 2f \; k_d[I] \qquad (3.15)$$

where R_i is the rate of initiation (generally equal to the rate of decomposition), k_t, the termination rate constant, f, the initiator efficiency, k_d, the decomposition rate constant of the initiator, and [I], the initiator concentration. Therefore, for bulk polymerization,

$$R_p = k_p \; [M] \; (fk_d[I]/k_t)^{\frac{1}{2}} \; . \qquad (3.16)$$

The basic difference between emulsion and bulk kinetics is therefore the difference in the number of growing radical species which can exist in a given volume of monomer/polymer phase.

This transition can be described conceptually by considering, for example, a 1 cc volume of monomer/polymer solution at a given conversion. At that point in time free radicals are generated according to equation 3.15 which determine a certain rate of polymerization. If that volume is divided into two parts the overall R_p remains the same. Even dividing it into a thousand parts results in the same polymeriza-

162

tion rate. This is because the number of growing radicals is many orders larger than the number of parts and is therefore unaffected by this division. However, when the subdivided volumes approach that volume 'occupied' by a single growing radical an effect is felt. The summation of the number of radicals over the parts begins to exceed the number that existed in the whole. The separation due to subdividing the system acts to prevent radicals from meeting and terminating. A point is reached in which a subdivided unit can contain only one growing radical. This radical terminates when a second radical is generated (or enters) in the unit. The average number per unit is therefore 1/2 if the rate of generation is constant. If these units are further divided, the same average number of radicals still exist in each unit and therefore the polymerization rate summed over all units is doubled with each division of all units. Conversely, in a latex system of small particle size (e.g., 0.05 μm), Smith-Ewart Case 2 kinetics generally exists throughout a polymerization. The rate is controlled by the number of particles and the monomer concentration within the particles. Under these conditions, if the number of particles is halved with a corresponding doubling of particle volume, the rate of polymerization is halved. This trend continues until conditions exist in which more than one growing radical can exist in a particle at any given time. This is highly dependent on particle size (volume) and conversion (monomer concentration in the particles). $\bar{n}$ is therefore the single most important factor determining the overall rate of emulsion polymerization. The history of the theoretical approach for obtaining $\bar{n}$ will be described in Chapter 4. However,

163

some of the expressions derived for computing $\bar{n}$ will be employed here to further the analysis of the kinetic results.

The number of free radicals in a particle is determined for the most part by the rates of radical absorption, desorption, and termination. The Smith-Ewart recursion expression [46], which represents a free radical balance for the entire latex system, has been extended and solved by Stockmayer [64] and O'Toole [65] by assuming pseudo steady-state conditions:

$$\bar{n} = (a/4) \ I_m(a)/I_{m-1}(a) \tag{3.17}$$

where $I_m(a)$ is the modified Bessel function of the first kind. m is a measure of the degree of radical desorption,

$$m = k_{de} \ v \ N_A/k_t \tag{3.18}$$

k_{de} being the desorption rate constant, and v the particle volume. a is related to another parameter α, by

$$a = (8\alpha)^{\frac{1}{2}} \tag{3.19}$$

while

$$\alpha = \rho_a \ v \ N_A/N_p \ k_t \tag{3.20}$$

where ρ_a is the rate of radical absorption. This treatment was extended further by Ugelstad et al. [66] to account for the reabsorption of desorbed radicals plus aqueous phase bi-radical termination.

In the emulsion polymerization of styrene, desorption and aqueous phase termination are generally considered to be inconsequential with respect to the polymerization kinetics. Exceptions have been found, however, for very small particle sizes (.05 - .08 μm) and low

164

initiation rates [67,68]. This treatment also neglects these in light of the large particle size being dealt with in these studies. (Desorption was found to be proportional to the inverse square of the particle radius [67]). In this case, $m = 0$ and the Bessel functions of equation 3.17 are reduced to zero and first order.

Van der Hoff [69] described a subdivision factor, z, by

$$z \equiv \bar{n}/(a/4) = I_o(a)/I_1(a) \quad . \tag{3.21}$$

In other words, z is the ratio of the number of radicals in a latex particle of volume, v, to the number of radicals existing in an equivalent volume in a bulk polymerization under identical monomer/polymer conditions. Figure 3.20 presents the variation of z with a, illustrating (somewhat qualitatively) the regions of conventional emulsion, suspension, and solution (or bulk) polymerization kinetics. It can be seen that $z \sim 1$ if a is greater than about 10, this being the region of solution kinetics. Values of a between 1 and 10 are given to describe the suspension polymerization region where z is roughly between 1 and 3 (i.e., $.75 \leq \bar{n} \leq 2.5$). The region of emulsion polymerization kinetics is defined by values of a less than 1, where z is greater than 3 ($\bar{n} < .75$). Therefore, the transition from emulsion to bulk kinetics is defined to take place well within the limits of $0.1 < a < 100$ (i.e., 3 orders of magnitude in a). These correspond to values of $\bar{n}$ in the range between 1/2 and 25.

The criteria described above are applicable to water soluble initiators from which radicals are formed and enter particles singly. The case for oil soluble initiators has also been made in which radi-
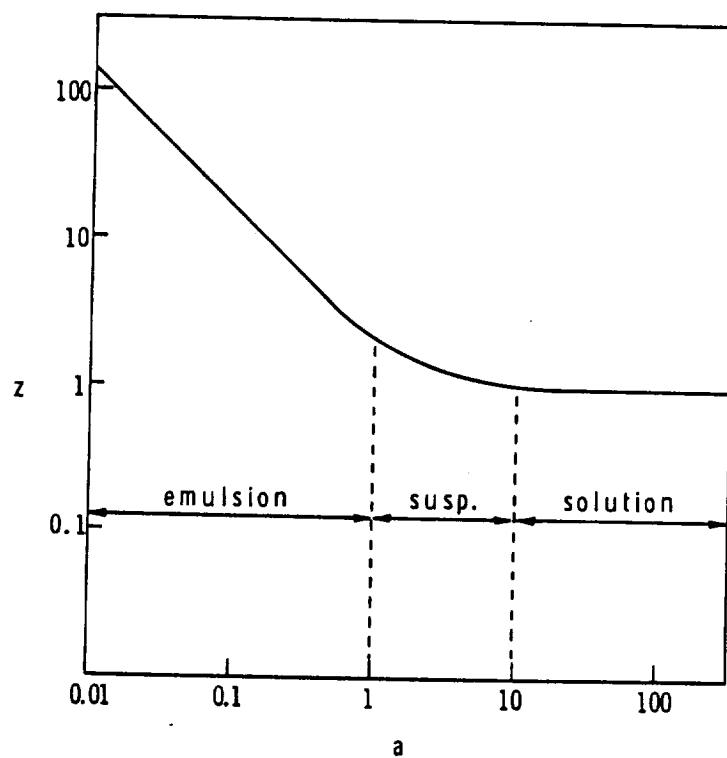
Figure 3.20 Subdivision Factor, z, as a Function of the Parameter
          a [69]

cals are created in pairs within the particles [70]. The subdivision factor for this case is given by

$$z = \tanh{(a/4)} \qquad (3.22)$$

which indicates a decreasing z with decreasing a, the opposite of the case presented above. In either case, the rate of polymerization is described by

$$R_p = k_p[M] \ (R_i/2k_t)^{\frac{1}{2}} \ z \qquad (3.23)$$

which is applicable to emulsion, suspension, solution, and bulk polymerization systems.

This transition has also been described by others from various perspectives. Friis and Hamielec [71] found that $\bar{n}$ is equal to or greater than one-half throughout emulsion polymerizations of styrene, conforming to Case 2 kinetics ($\bar{n} = 0.5$) at low conversions and Case 3 ($\bar{n} \gg 1$) at high conversions. The polymerization rate under Case 3 conditions was considered independent of the particle number and therefore corresponded to bulk polymerization kinetics. The transition range between Case 2 and Case 3 kinetics corresponded to values of $\bar{n}$ between 0.5 and 10. Saidel and Katz [72] have described stochastic and deterministic approaches to modeling the kinetics of emulsion polymerization. If the rate of radical arrival is much less than the termination rate within the particles (i.e., n = 1 or 0), the stochastic model is applicable. The deterministic model describes the opposite case in which rate arrival is much greater than the rate of temination ($\bar{n} \gg 1$). These account for Case 2 and Case 3 kinetics but not the transition region between the two. Ugelstad and Hansen [32] describe

the transition between Case 2 and Case 3 kinetics by setting bounds of $0.1 < \alpha < 10$. These correspond to values of a between .89 and 8.9 which is roughly the same as those presented for suspension polymerization kinetics by van der Hoff [69]. This can be seen in Figure 3.21 which shows the relationship between $\bar{n}$ and α for various values of m [66]. For $m = 0$ the transition between $\bar{n} = 1/2$ and $\bar{n} = (\alpha/2)^{\frac{1}{2}}$ is indicated. The lower limit on α perhaps should be reduced to 0.1 to encompass more of the transition range.

The criteria presented in both Figures 3.20 and 3.21 require knowledge of α in order to define where a specific set of polymerization conditions lies with respect to the transition region. However, the parameters ρ_a and k_t are subject to some uncertainty. Generally, ρ_a, the rate of absorption, is assumed to be equal to the rate of initiation, but this may not be true especially in the case where aqueous phase termination is important. The termination rate constant is also known to vary with conversion during Interval III where the gel effect predominates. A number of efforts have been made to better define this 'constant' through empirical means at first [68, 76,73] and then by more theoretical approaches based on free volume theory and entanglement coupling [74 - 78]. In spite of all these efforts it is obvious that the variation of k_t with conversion and molecular weight is still not wholly understood since significant differences in the results are evident.

In these studies, the variation of k_t with conversion was approximated from the experimental data by making a number of simplifying assumptions: 1) the rate of radical absorption equaled the rate

168
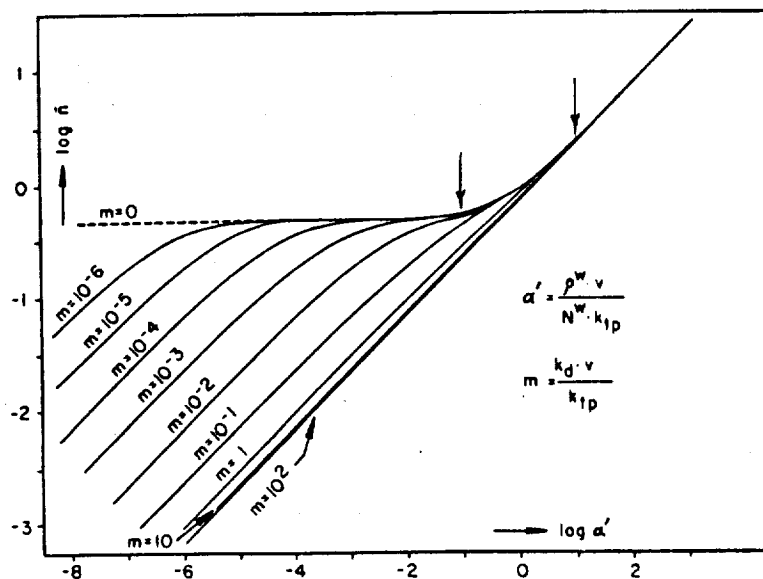
Figure 3.21   Average Number of Radicals per Particle $\bar{n}$ as a Function of the Parameters a' and m [32].

of initiation $(f = 1)$; 2) the effect of desorption and aqueous phase termination were negligible; 3) the amount of monomer in the aqueous phase was insignificant; 4) the propagation rate constant followed the relationship given by equation 3.12, permitting computations of $\bar{n}$; and 5) a simplified expression for $\bar{n}$, derived by Ugelstad and Mørk [79] was applicable for backcalculation of k_t. This expression is given by

$$\bar{n} = (0.25 + \frac{\alpha}{2})^{\frac{1}{2}} \qquad (3.24)$$

and is applicable for cases in which radical desorption and aqueous phase termination are negligible. Therefore, with knowledge of $\bar{n}$, ρ_a, v, and N_p, k_t could be calculated. An example of the results obtained following this computation method is given in Figure 3.19 (x's) for SSMLR 5-1 (right hand ordinate). k_t is shown to decrease three orders of magnitude from about 10^7 to 10^4 1/mole·sec over the range of W_p from 0.35 to 0.85. The apparent increase in k_t after W_p of 0.9 was attributed to the changing k_p which was unaccounted for in this analysis. Since these methods produced values of k_t which were dependent on the original value of $\bar{n}$ and involved a number of assumptions, some of which may be inaccurate, the evaluation of the degree to which any given polymerization proceeds into the transition region should be done independent of α (or a).

The use of $\bar{n}$, as obtained from experimental data, to determine the extent (if any) to which the kinetics proceeds into, through, or past the transition region according to the criteria of Friis and Hamielec (i.e., $0.5 < \bar{n} < 10$) can be evaluated via the results of the successive seeding experiments. The effects of particle size (seeding

170

step) and total fractional conversion (W_p) on $\bar{n}$ for the results of

SSMLR 5 are presented in Figure 3.22. The final particle size for

each seed step is the same as that given previously in Figure 3.16.

$\bar{n}$ is shown to increase with conversion for each step and in a parallel

fashion with increasing particle size. A portion of each curve for

the first four steps is in the $\bar{n}$ range of 1/2 to 10 while the remain-

ing three are outside this range. According to the criteria de-

scribed previously, this indicates that even at a particle size of

0.27 μm (swollen diameter) and an initial monomer/polymer ratio of

2/1, the polymerization kinetics are already in the transition region

and perhaps even traverse it in a single polymerization. This type

of plot, however, does not give any real indication of the degree to

which the transition was bridged in terms of the proximity to Case 3

or bulk polymerization kinetics (i.e., R_p indpendent of N_p). If the

polymerization rate as a function of the number of particles is plot-

ted at various conversion (as presented by Pramojaney [18], results

are obtained as given in Figure 3.23 (bottom). The rate is represented

by $nN_p\phi_m$ where ϕ_m is the volume fraction monomer in the particles.

Three different conversion levels (W_p) are represented: 0.35, 0.60,

and 0.80. The initial polymerization rates, approximated at $W_p = 0.35$,

show an initial large decrease with decreasing number of particles

(i.e., increasing particle size) from the first to second step, fol-

lowed by smaller and a somewhat steady decrease in the rate. Note

that a slope of 1 (dotted line) would be equivalent to Case 2 kinetics.

This indicated that some dependence on particle number was experi-

enced even when $\bar{n}$ exceeded 10. At a conversion equivalent to W_p of

0.60, the effect of decreasing particle number was found to be insig-
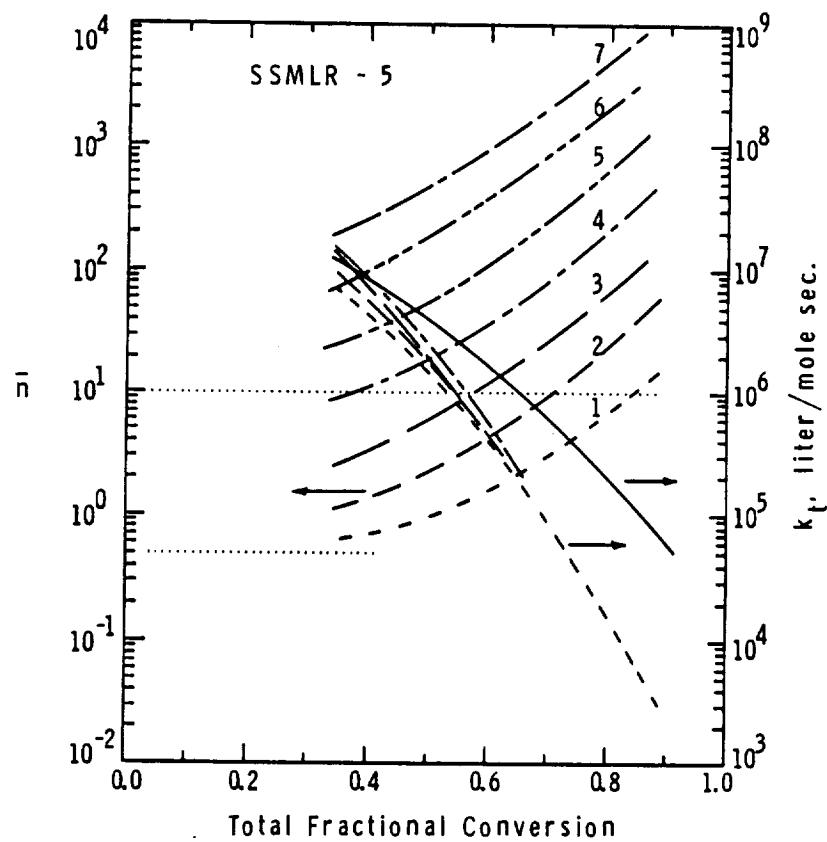
Figure 3.22 $\bar{n}$ and k_t as a Function of Particle Size (Seeding Step) and Total Fractional Conversion (W_p) for SSMLR 5

nificant after the first seeding step, while at $W_p = 0.80$ the rate was apparently independent of particle number throughout the entire sequence. These observations are in accord with the behavior of the conversion-time curves (Figure 3.16) through the fifth seeding step which show decreasing initial polymerization rates with increasing particle size and yet nearly identically shaped curves over the upper portion of the conversion scale. (Recall that steps 6 and 7 resulted in significant generation of new particles, which negates any kinetic analysis.) The kinetic transition can also be viewed from the dependency of $\bar{n}$ on particle diameter in the seeding sequence. A replot of the data of Figure 3.22 to illustrate this effect is given for the same three conversion levels in Figure 3.23 (top). Much of the data lie on straight lines with obvious divergence at low values of $\bar{n}$. These deviations can be attributed to the approach to case 2 kinetics as the particle diameter decreases. All these lines drawn through the data have a slope of 3 and any deviation of a point from these lines indicates a deviation from the proprotionality, $\bar{n} \alpha d^3$. For Case 3 kinetics $\bar{n} = (\alpha/2)^{\frac{1}{2}}$ and therefore, $\bar{n} \alpha (v/N_p)^{\frac{1}{2}}$. However, in these seed sequences $N_p \alpha 1/d^3$ as described previously, and thus $\bar{n} \alpha d^3$. This proportionality is valid provided that the same k_t vs. W_p function applies to each polymerization and also that the rate of radical absorption is likewise the same for each step at a given conversion. This last point should not be strictly true since longer times should result in lower initiation rates due to consumption of initiator. This type of plot may not be sensitive to these differences, however. Nevertheless, the transition to 'bulk' kinetics appears to be substantially complete

173
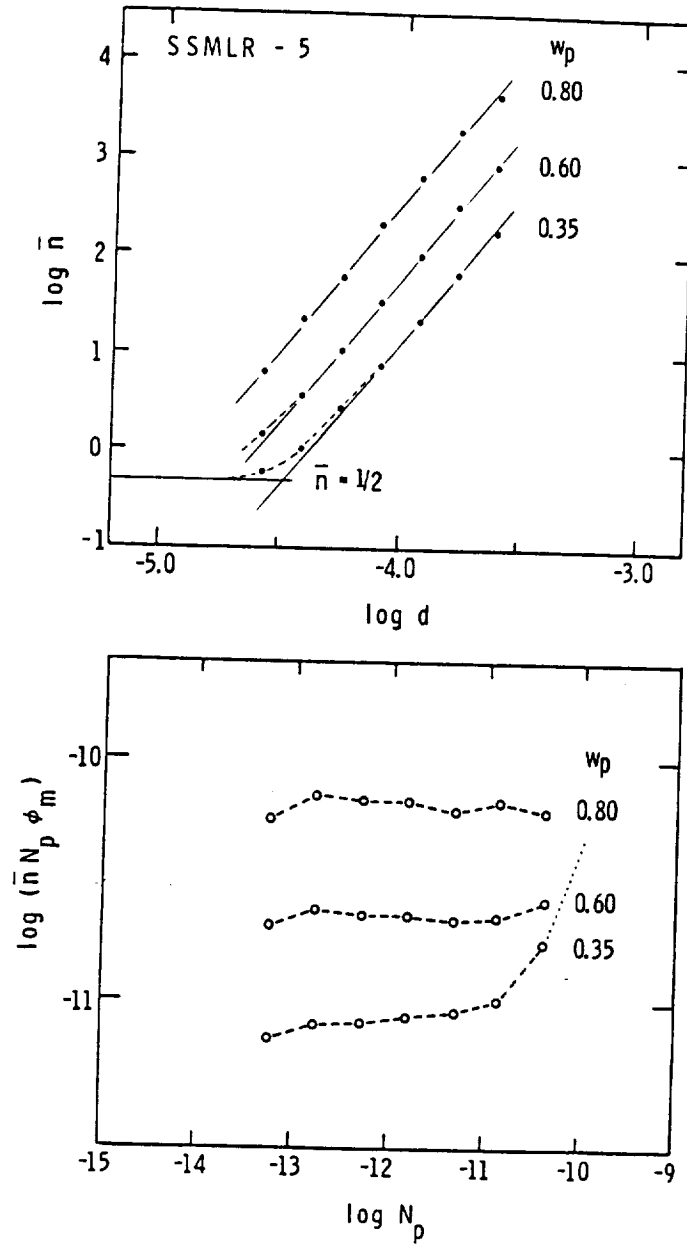
Figure 3.23 (Top) $\bar{n}$ as a Function of Particle Diameter, d, and
(Bottom) $\bar{n}$ N_p ϕ_m as a Function of N_p for SSMLR 5 at
Three Conversion Levels

174

through the fourth seeding step (0.82 μm).

The variation of k_t with conversion as back-calculated from $\bar{n}$
is given for SSMLR 5 steps 1-4 in Figure 3.22. For comparison, the
empirical relationship developed by Friis and Hamielec [73] from bulk
polymerization data is also presented (solid line). Note that the
SSMLR 5 experimental curves do not match each other at low conversions.
The apparent values for k_t increase with increasing particle size ($W_p =$
0.35). Recall that these computations assume an initiator efficiency
of 1.0 which may be incorrect in view of these results and the 'absorp-
tion efficiency' results presented earlier in Table 3.7. If these effi-
ciencies are substituted into the k_t analysis the effect is to decrease
the values of k_t to more comparable but not exact numbers. However, if
these efficiencies are used throughout the analysis of the entire con-
version histories the converging curves of Figure 3.22 would diverge
at higher conversions. It does not seem likely that there should be
any significant differences in the k_t functions from step to step be-
cause of the similarity in the weight average molecular weights of the
polymer products (Table 3.6). One possibility is that the absorption
efficiency may also change with conversion, being low initially (de-
creasing with increasing particle size or decreasing total surface
area) and increasing with conversion to comparable values for each step
in the sequence. This explanation may not be compatible from a mech-
anistic point of view with the description of the adsorption rate given
by Equations 3.8-3.10 since no dependency on conversion is present in
these expressions. Perhaps a decreasing equilibrium monomer concentra-
tion in the aqueous phase due to decreasing concentration in the par-

175

ticles plays a role in increasing the absorption efficiency. Radical loss due to precipitation or aqueous phase termination may decrease with the lower monomer level due to the increased life-time of radical oligomers with short chain lengths (i.e., the interval between additions of monomer units is increased).

3.5.3.4 Summary

A number of points should be stressed based on the results of the persulfate initiated sequences SSMLR 4 and 5:

1) 'Mondisperse' polystyrene latexes, free of significant quantities of small off-size particles, were prepared in 4 successive seeding steps up to 0.82 μm starting with a 0.19 μm seed. However, 2 - 4% of the particle population consisted of larger off-size particles attributed to the limited stability provided at the low emulsifier coverage. The recipe conditions were 2/1 monomer/polymer, 4% surface coverage via Aerosol-MA, 0.5 mM $K_2S_2O_8$, and 30% final solids content. Above 1 μm, the nucleation of small particles became significant under these conditions. These latexes could not be prepared under 'normal' bottle polymerization conditions without complete flocculation.

2) Apparent sulfate ion radical absorption efficiencies, computed from surface charge analysis, were found to decrease with increasing particle size up to 0.82 μm.

3) The initial polymerization rates decreased with increasing particle size but with decreasing sensitivity (up to 1.19 μm).

4) In all cases, R_p increased with conversion up to about 80% due to the gel effect. $\bar{n}$ exceeded 1/2 and increased with conversion and particle size.

5) The transition from 'ideal' emulsion polymerization kinetics (Case 2, $\bar{n} = 1/2$) to 'bulk' kinetics (Case 3, $\bar{n} \gg 1$) was evaluated based on several kinetic relationships. The approach to Case 3 conditions, where R_p is independent of N_p, and $\bar{n}$ is directly proportional to d^3 (v), was substantiated through the fourth seeding step (0.82 µm). At high conversion (X = 0.8) the rate was nearly independent of N_p and $\bar{n}$ was proportional to d^3. The most sensitive means for judging whether a polymerization took place beyond the transition region was by simply observing whether the conversion histories overlapped for two consecutive seeding steps.

Improvements in the monodispersity of the product latexes above 1 µm was believed possible by increased solids contents (up to 50%) and decreased initiator concentration (e.g. 0.1 mM $K_2S_2O_8$) at the same emulsifier surface coverage (4%). However, interest was shifted to oil phase initiation, being more promising for reducing particle nucleation.

3.5.4 AIBN and AMBN Initiated Sequences

The minimization or elimination of the nucleation of new particles in successive seeding experiments intended to produce monodisperse latexes up to 2.0 µm was considered more likely through the use of oil soluble initiators in combination with water soluble inhibitors. This recipe formulation strategy was proposed to reduce the presence of free radicals growing in the aqueous phase by limiting

177

the amount of initiator decomposing outside the particles and des-
troying those that did by reaction with an inhibitor. The choice of
the various initiator/inhibitor combinations for testing was based on
the results of Tseng [80]. A number of organic peroxy and azo-type
initiators were evaluated with the latter being favored due to higher
polymerization rates (initiator efficiencies) in seeded polymeriza-
tion experiments. AIBN (2,2'-azobis(isobutyronitrile) and AMBN
(2,2'-azobis(2-methylbutyronitrile)), VAZO 64 and 67, respectively,
were the two initiators chosen for these studies. The effectiveness
of a variety of water-soluble inhibitors in preventing new crop gen-
eration was also evaluated. Three of these were used in these stud-
ies; ammonium thiocyanate (NH_4SCN), sodium nitrite ($NaNO_2$), and hydro-
quinone (HQ). Five sequences were performed using AIBN initiator
(SSMLR 6 - 10) in combination with the three inhibitors plus a blank
(i.e., without inhibitor). Four sequences used AMBN as initiator,
three of which included HQ as the inhibitor.

3.5.4.1   Recipe Definition and SSMLR 6

Recipes paralleling those of SSMLR 5 were outlined for a sequence
using AIBN initiator and NH_4SCN inhibitor, these components being
substituted for the $K_2S_2O_8$ and $NaHCO_3$. The level of AIBN was chosen
as 0.4% by weight on monomer (22.1 mM based on monomer or 14.7 mM on
the oil phase) a typical value for recipe evaluation [80]. The in-
hibitor concentration was also selected on this basis, being 0.25% by
weight in the aqueous phase. As in SSMLR 5, the fractional surface
coverage was 0.04 (Aerosol-MA), the swelling ratio, 2/1, and the
final solids content, 30%. The swelling procedure was modified to

accommodate the need to dissolve the initiator in the monomer by swelling initially with 80% of the monomer for about 10 hr and the final 10 hr with initiator added in the remaining monomer. This was done to reduce the time the initiator spent at room temperature prior to the polymerization and also to reduce the chances of initiator loss due to any viscous monomer/polymer material formed during the early portion of the swelling.

The first polymerization step using the recipe as outlined above was not carried out successfully in the LUMLR. After two hours polymerization time the piston movement slowed to a stop well before the level expected from previous polymerizations. This behavior was attributed to the formation of gas bubbles in the reactor preventing movement of the piston and therefore, any kinetic measurements. The bubbles were formed from the N_2 evolved by the decomposition of the initiator:

$$CH_3 - \underset{\underset{CN}{|}}{\overset{\overset{CH_3}{|}}{C}} - N = N - \underset{\underset{CN}{|}}{\overset{\overset{CH_3}{|}}{C}} - CH_3 \xrightarrow{\Delta} N_2 + 2\ CH_3 - \underset{\underset{CN}{|}}{\overset{\overset{CH_3}{|}}{C}} \cdot$$
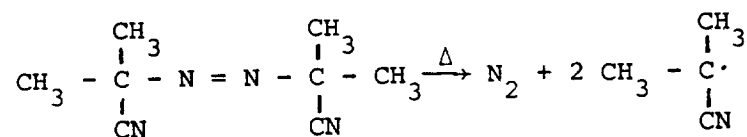
Subsequent polymerizations were conducted using initial AIBN concentrations of 4 mM based on monomer (0.072% by weight on monomer). This quantity was set by considering the amount of nitrogen gas that could be absorbed by the aqueous phase which had been degassed at a pressure of 20 mm Hg. In other words, it was determined that approximately 1.8×10^{-4} moles of AIBN (4 mM in 20 gm sytrene) would have to decompose before the aqueous phase became saturated with N_2 resulting in bubble formation and loss of kinetics.

SSMLR 6 was performed with the above revision in the initiator

concentration and also a reduction in the inhibitor level to 0.1%

based on the aqueous phase. The recipe 'constants' for this sequence

are presented in Table 3-8. Note that the solids contents were sig-

nificantly lower than those found in the previous sequences and de-

creased after the second step. There were two reasons for this:

1) monomer and polymer were lost during the swelling process due to

the development of a viscous M/P phase; 2) flocculation increased

greatly from step 4 to 5 to 6. A seventh step was not possible due

to the heavy loss of particles.

Table 3-8

Recipe 'Constants' for SSMLR 6

SSMLR 6	M/P	% Solids*	$[AIBN]_0$ (mM)	$[NH_4SCN]_0$ (mM)
1	2.01	26.0	4.00	13.14
2	1.98	26.7	4.61	18.25
3	1.86	25.7	4.68	19.97
4	1.97	25.0	4.69	20.92
5	2.35	22.5	4.63	21.38
6	2.23	16.7	4.72	20.74

*Measured following polymerization.

The flocculation as described above was an indication that the

stability of the particles decreased with increasing particle size.

The instability was verified by SEM examination of the product latexes

as shown in Figure 3.24. Off-size larger particles can be seen as

early as the second seeding step being particularly apparent in the

third step and thereafter. There are two explanations for the sta-

bility being lower in this case as compared to that of SSMLR 5. First

SSMLR 6 AIBN/NH$_4$SCN

[I]$_0$ = 4.0mM   [Z]$_0$ = 13.1mM   FRCV = 0.04
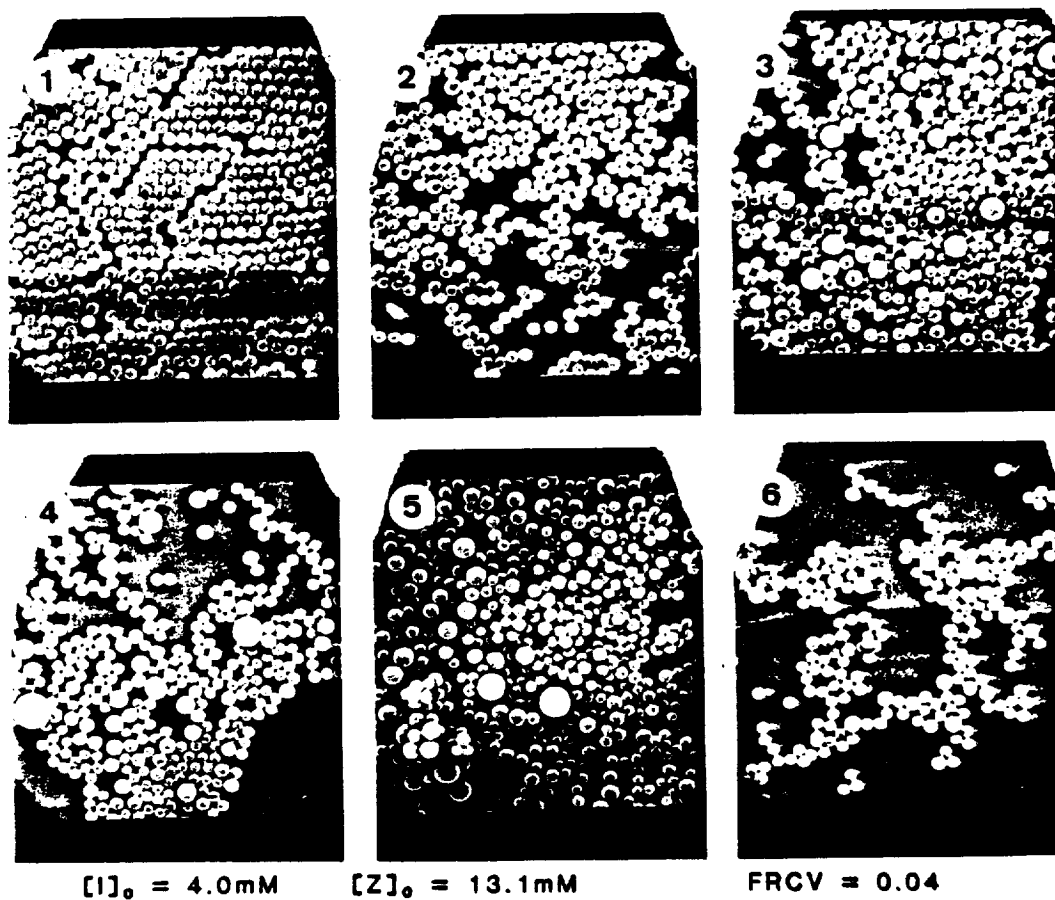
Figure 3.24   Scanning Electron Micrographs of Latexes Produced in
SSMLR 6

and foremost, the ionic strength was by the recipe design more than four times higher in SSMLR 6 than in SSMLR 5, being 1.8×10^{-3} and 0.44×10^{-3}, respectively (not accounting for surfactant or particles). An increasing ionic strength affects stability by decreasing the double layer thickness (proportional to the inverse of the square root of the ionic strength) thereby decreasing the ability of the particles to repel each other. The second reason for increased instability is also related to this factor. Since the initiator, AIBN, does not create charged radical species through decomposition, the particle surface is diluted of bound charged species (the original surface groups on the 0.19 μm seed) from step to step, thereby decreasing their concentration and contribution to the electrostatic repulsion between particles. Therefore, the stability of the latex decreased going to the $AIBN/NH_4SCN$ initiator/inhibitor system.

The polydispersity of the latexes produced in SSMLR 6 makes the kinetics of little value and therefore, will not be reported. The value in these results lies in the lesson that improved stability must be achieved to obtain monodisperse latexes. This could be achieved through a reduction in the ionic strength by lowering the inhibitor concentration and/or raising the fractional surface coverage of the particles by adding more emulsifier. The latter approach was judged to be more appropriate in light of the inhibitor concentrations used in parallel investigations [80]. The final choice of a specific surface coverage was made somewhat arbitrarily within the limits set by SSMLR 4, having 8% coverage, and the SD X-Y series using $AIBN/NaNO_2$ with 23% coverage. Consideration of the ionic strength differences

182

was also made by roughly estimating the amount of surface charge required to achieve a similar surface potential in a revised SSMLR 6 recipe as compared to the SSMLR 4 recipes. A minimum fractional coverage of 0.15 was determined and this value was used in subsequent successive seeding sequences without further consideration of ionic strengths and particle stabilities. Not only was it desirable to maintain a constant surface coverage within a sequence but also it was deemed necessary for the various sequences testing initiator/inhibitor combinations, so that comparisons could be made without undo concern over the influence of different amounts of emulsifier on the surface of the particles.

The following sequences are reported starting with the blank run in which no inhibitor was used and proceeding through the results obtained with NH_4SCN, $NaNO_2$, and HQ inhibitors.

3.5.4.2 SSMLR 9 - AIBN without Inhibitor

In order to judge the effects that an aqueous phase inhibitor may have on the polymerization kinetics of seeded emulsion polymerization, a control is required in which no inhibitor is included in the recipe formulations. SSMLR 9 was designed to maintain a 15% coverage of the particle surface via Aerosol-MA (0.15 mM in the aqueous phase) throughout the sequence as given below. The added initiator con-

$$0.19 \xrightarrow{\;1\;} 0.27 \xrightarrow{\;2\;} 0.39 \xrightarrow{\;3\;} 0.57 \xrightarrow{\;4\;} 0.82$$
$$0.82 \xrightarrow{\;5\;} 1.19 \xrightarrow{\;6\;} 1.71 \; \mu m$$

centration was 4 mM on monomer as determined from the intial AIBN testing. Some of the recipe 'constants' are reported in Table 3-9.

<div align="center">

Table 3-9

Recipe 'Constants' for SSMLR 9

</div>

SSMLR 9	M/P	% Solids	γ (N/cm) x 10^5	[AIBN]$_0^*$ (mM)
1	1.97	27.4	66.8	4.00
2	~2.00	28.6	67.5	4.54
3	1.99	28.3	66.5	4.47
5	2.04	28.2	68.0	4.40
6	1.97	27.7	68.4	4.37

*based on monomer

Swelling was found to be completed in all cases without the form-
ation of a viscous monomer/polymer phase. This was attributed to the
increased particle stability (and lowered interfacial tension) due to
the additional emulsifier surface coverage.

An interesting observation was made with regards to the physical
appearance of the latexes prior to and following polymerization. In
the first three polymerization steps the swollen and product latexes
displayed the rainbow-like iridescence characteristic of ion-exchanged
monodisperse latexes. This phenomenon is considered to be caused by
the arrangement of particles in ordered arrays resulting in Bragg re-
flection of visible light [81]. This iridescence was present in the
ion-exchanged seed latex (0.19 µm) but disappeared when the surfactant
and water were added. Reappearance occurred once the swelling was com-
plete. In this state most of the emulsifier is present on the particle
surface and apparently creates a repulsive force strong enough to in-
duce the ordering (expanded double layer). The iridescence in the
product latexes was slightly weaker in appearance in comparison to

<div align="center">

184

</div>

the swollen counterpart, perhaps being due to the slightly increased aqueous phase emulsifier content brought about by shrinkage of the particles and desorption of surfactant. A direct effect of this ordering phenomenon was an increase in the latex viscosity, which resulted in a noticeably poorer degree of mixing as revealed by the transient temperature response during heat-up.

There was no loss of product due to flocculation, the percent solids being relatively constant. The surface tension was also monitored and found to remain relatively constant with slight variations. Once again the initial initiator concentrations were computed to remain nearly constant after the first seeding step.

The monodisperse quality of the SSMLR 9 product latexes is illustrated by the scanning electron micrographs reproduced in Figure 3.25. Small particles were virtually absent through the first four seeding steps while only a few could be found in step 5 and greater numbers in step 6. Over-sized particles were also absent in this sequence. This represented an improvement over the results obtained with persulfate initiation. Not only were the number of nucleated particles reduced by the use of an oil soluble initiator but this was accomplished even in the presence of a much greater amount of emulsifier. Further improvements were, therefore, expected in terms of reduced nucleation at larger particle sizes with the addition of water soluble inhibitors.

The conversion histories for SSMLR 9 are presented in Figure 3.26. At first glance, these results appear strikingly similar to those of SSMLR 5 (Figure 3.16). The overall polymerization rates decreased with increasing particle size up to about 0.82 μm, with small differences

SSMLR 9   AIBN/No Inhibitor

$[I]_o = 4.0mM$

$FRCV = 0.15$
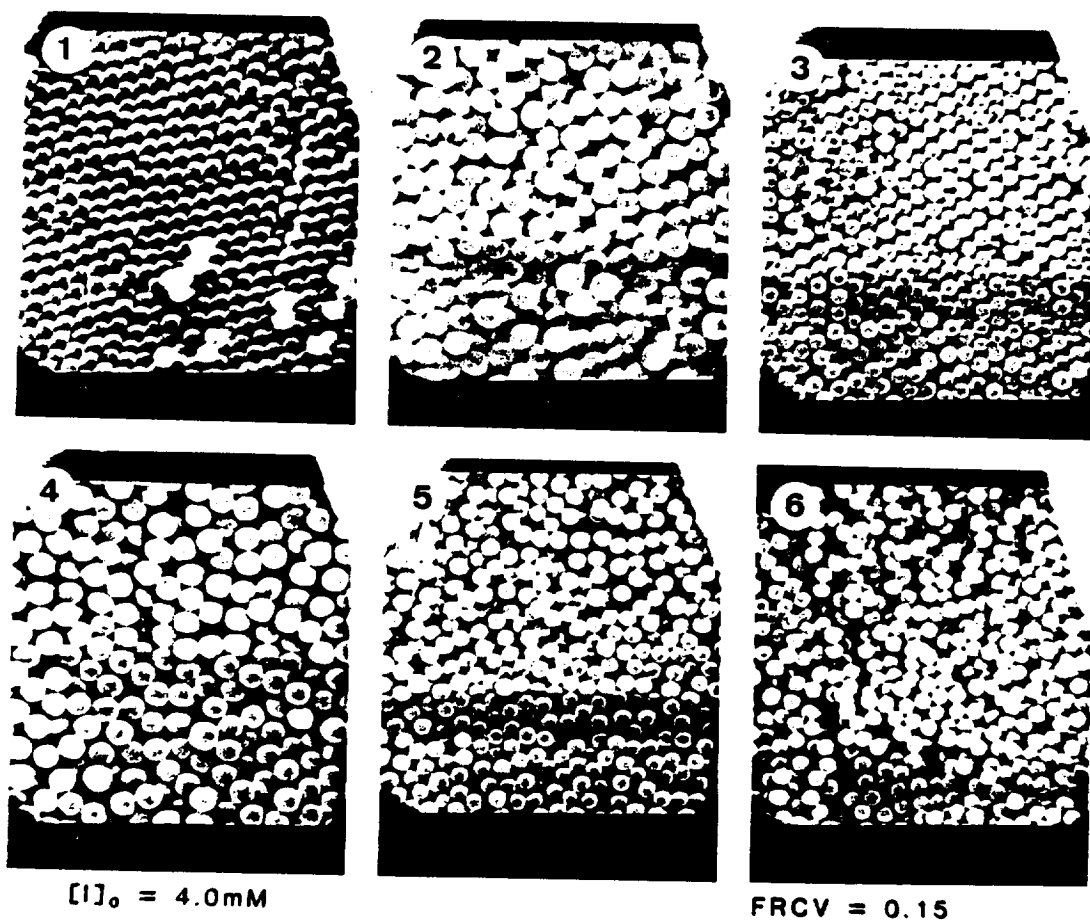
Figure 3.25   Scanning Electron Micrographs of Latexes Produced in
SSMLR 9

C-3
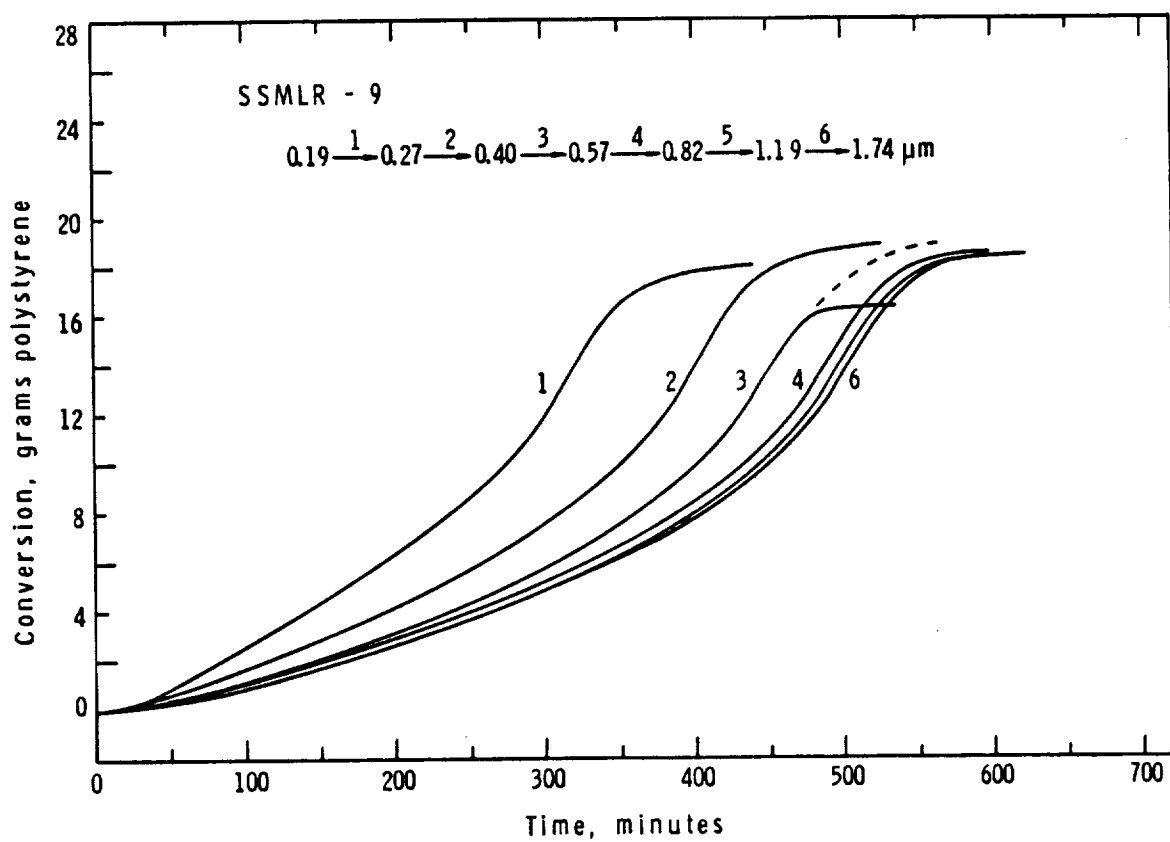
Figure 3.26   Conversion Histories for Seed Sequence SSMLR 9, AIBN
without Inhibitor

thereafter. These rates were lower than those of SSMLR 5, despite the greater amount of initiator (~2.5 times that of $K_2S_2O_8$) and its shorter half life (4.7 hrs. for AIBN vs. 8 hrs for $K_2S_2O_8$ at 70°C). (Note that for step 3, the curve was extrapolated to high conversion owing to what was believed to be a stuck piston.) It was previously indicated that for situations in which radicals were generated in pairs within the particles the polymerization rate should theoretically increase with increasing particle size (decreasing degree of subdivision). None-theless, this kinetic prediction contradicted a number of experimental results, including these, in which polymerization rates using oil soluble initiators (peroxides and azo compounds) were found to be sim-ilar to those employing persulfate initiator [69]. A number of mech-anistic explanations were postulated to account for this behavior. The central supposition of these was that radicals must appear singly in a particle, whether caused by entry from the aqueous phase, transfer to monomer followed by desorption, or an interfacial phenomenon by which radicals are formed in the emulsifier layer at the particle-water interface.

The final 'limiting' conversions, determined by the iso-octane extraction/UV absorbance analysis are presented in Table 3.10. These values average about 3% lower than those reported for SSMLR 5 (Table 3.6). The reason for this may lie in small differences in the tempera-ture profiles in the latter part of the polymerizations. All of the polymerizations using persulfate initiator had rate maxima greater than their AIBN counterparts, which caused the fluid temperature to increase at most 1°C. A higher temperature not only increases the polymerization

188

Table 3-10

Conversion and Average Molecular Weight of SSMLR 9 Latexes

SSMLR 9	% Conversion*		Molecular Weight	
	on Monomer	on Polymer	$\bar{M}_n$ x 10^{-5}	$\bar{M}_w$ x 10^{-6}
1	92.8	95.2	3.7	1.6
2	92.9	95.1	2.7	1.6
3	90.6	93.7	2.8	1.5
4	92.3	94.8	3.2	1.4
5	92.0	94.6	5.0	1.5
6	91.6	94.5	4.5	1.5

*from iso-octane extraction/UV absorption analysis

rate but perhaps more importantly changes the conditions of the passage through the glass transition. This has the direct effect of delaying the decrease in the propagation rate constant at high conversion, perhaps enough to account for this difference in conversion.

The polymerization kinetics of successive seeding using oil soluble initiators can be examined in the same manner as those performed using persulfate initiator. One would expect very similar results for SSMLR 9 in light of the resemblance of the conversion histories to SSMLR 5. The average number of radicals per particle, $\bar{n}$, as a function of the total fractional conversion (W_p) and particle size is given in Figure 3.27. In all cases, $\bar{n}$ exceeds 1/2 and increases with increasing conversion. In the first seeding step, however, $\bar{n}$ exhibits a slower rise than shown in the previous case (Figure 3.22). Of greater interest, perhaps, are the results obtained for the back-calculation of k_t as a function of conversion. These are contrasted with the bulk behavior of k_t as described previously. There are two

189
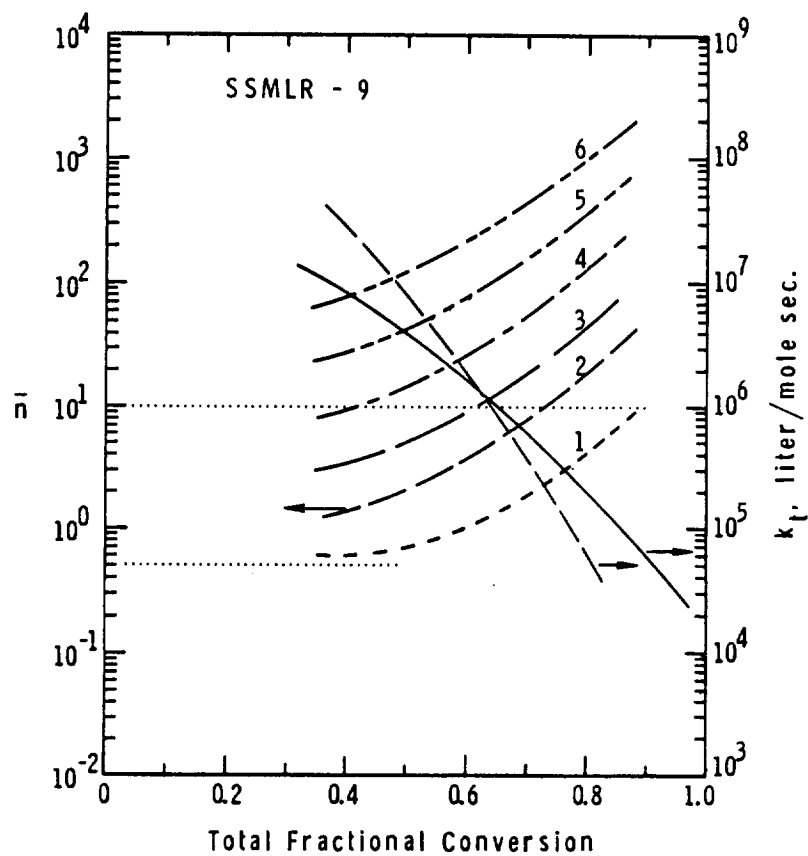
Figure 3.27 $\bar{n}$ and k_t as a Function of Particle Size (Seeding Step)
and Total Fractional Conversion (W_p) for SSMLR 9

major differences between these results and those of SSMLR 5. First, the superimposed curves were found to lie on the same line, within the experimental scatter of the data. This was expected from the similarity of the polymerization conditions and the polymer molecular weights (Table 3-10). (It should be noted that this behavior was also expected for SSMLR 5.) Second, the position of the curve with respect to the ordinate was shifted to higher values than those for SSMLR 5. This position was considered unlikely since any k_t function should extrapolate to the same value at zero conversion whether the data were obtained from bulk, suspension, or emulsion polymerization. Friis and Hamielec [73] determined a value of k_t for styrene at 70°C with zero conversion equal to 5×10^7 1/mole·sec. The k_t relationship obtained from these data obviously could not intersect the ordinate at this point without assuming an unreasonable behavior. Therefore, it was evident that some assumption(s) in the analysis was at fault. The primary source of error lay in the calculation of the initiation rate or, more accurately, the effective radical 'absorption' rate. The values of k_d for AIBN were computed using $k_{do} = 2.6141 \times 10^{14}$ sec^{-1} and $E_{ad} = 29.5$ kcal/gm-mole [17] while the efficiency, f, was assumed to be 1.0. Any of these could be inaccurate considering that little is known of the behavior of oil soluble initiators (particularly AIBN) in emulsion polymerization. Nonetheless, only f was considered 'adjustable' in this analysis. By simply reducing f the position of the k_t curve could be adjusted to levels more compatible with the expected behavior. Values for f below 0.15 were required to achieve this, indicating that AIBN may be quite inefficient under the conditions of

191

these experiments. It is generally recognized that initiator efficiencies lie below 1.0, owing to what is termed the solvent cage effect which impedes the diffusion of a radical from the site of decomposition often causing reactions other than the initiation of polymerization. Values of f for AIBN have been reported over the range 0.50 - 0.70 [83], although it has been noted that f may decrease with increasing viscosity at high conversion [84]. This decrease is likely to occur over the same region in which k_p decreases, possibly obscuring the relative effects.

The kinetics of successive seeding employing oil soluble initiators can also be examined in terms of the behavior relative to the transition between emulsion and bulk kinetics. Obviously, since the polymerization kinetics for SSMLR 9 resemble those of SSMLR 5, the results are expected to be similar. Figure 3.28 (top) presents $\bar{n}$ as a function of particle diameter for the six seeding steps at 0.75, 0.60, and 0.35 weight fractions polymer. Once again the solid lines represent the relationship $\bar{n} \propto d^3$. In this case, the points do not appear to fit this relationship as closely as the case of SSMLR 5. Dashed lines, drawn through the points, indicate the extent of these differences. For a polymer fraction of 0.35 (i.e., at the beginning of the reaction) $\bar{n}$ may approach 1/2 with decreasing particle size, however, in this case it is not as obvious, and may in fact cross over to lower values. At higher conversion some differences should also be expected since $\bar{n}$ is a function of the absorption rate or initiation rate, which decreases with time due to the consumption of initiator (eqn. 3.15). Since the polymerizations took successively longer times, $\bar{n}$ at a given

192
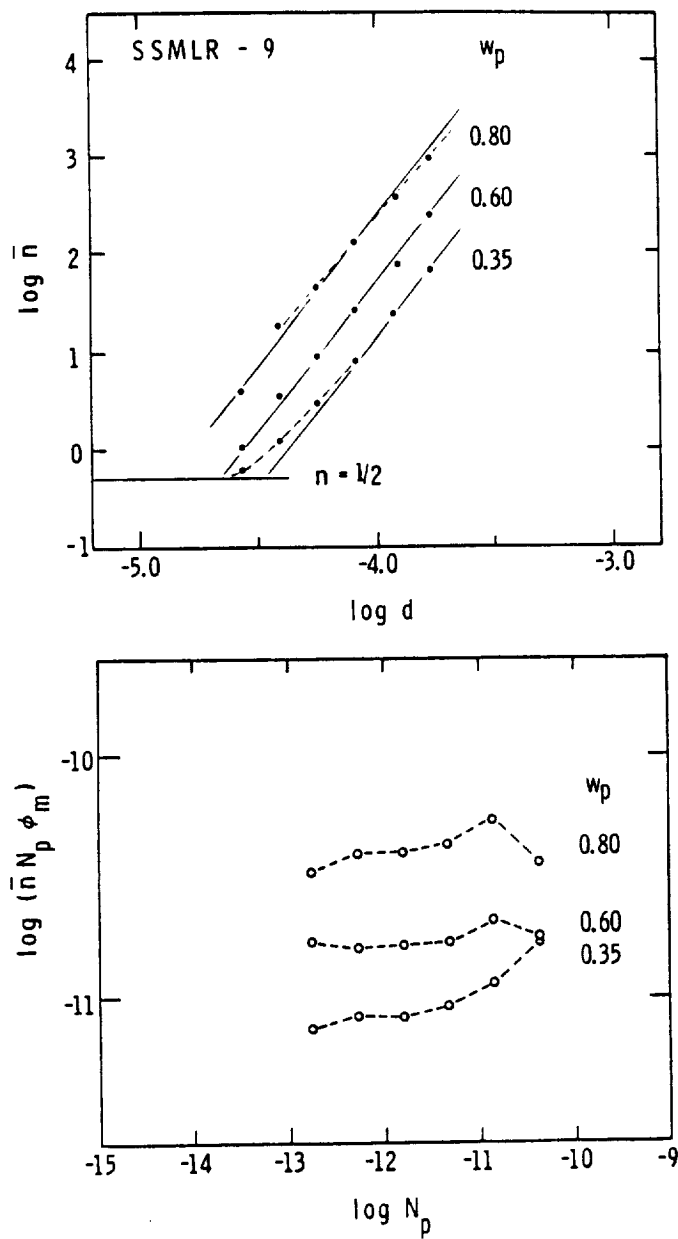
Figure 3.28   (Top) $\bar{n}$ as a Function of Particle Diameter, d, and
(Bottom) $\bar{n} N_p \phi_m$ as a Function of N_p, for SSMLR 9

193

conversion should have been slightly less than that expected merely from the $\bar{n}$ to d^3 proportionality. An alternate explanation may also account for the noted behavior. The initial initiator concentrations, as given in Table 3-9, show an increase after the first step followed by small decreases thereafter. This same pattern is also noted for the $\bar{n}$ vs. d results for $W_p = 0.75$, indicating that $[I]_0$ may be the dominant factor in explaining this behavior.

The effect of the number of particles on the polymerization rate (Figure 3.28 - bottom) is again quite similar to the results obtained for SSMLR 5 (Figure 3.23). The initial rates ($W_p = 0.35$) decrease with the number of particles (i.e., increasing particle size), but with decreasing sensitivity. At higher conversions the rate is nearly independent of particle number. Note that the jump in the rate for the second seeding step corresponds to the increase in the initial initiator concentration with subsequent decreases thereafter.

The kinetics of successive seeding of monodisperse latex using AIBN as initiator, therefore, proceed in a manner similar to the more conventional persulfate initiator. The overall polymerization rates decrease with increasing particle size but with decreasing sensitivity. For particle sizes above 1 μm the rates are nearly independent of particle size and number which is indicative of Case 3 kinetics. The initiator efficiency was found to lie below typical values quoted for bulk polymerization. It must be remembered, however, that these conclusions are specific to this polymerization system and may not be applicable if conditions are altered appreciably. Bearing this in mind, the effect of various aqueous phase inhibitors on polymerization

kinetics (and product monodispersity) are examined in the following section.

3.5.4.3 SSMLR 8, 7, 10 - AIBN with NH_4SCN, $NaNO_2$, HQ

An aqueous phase inhibitor, given the task of preventing the nucleation of a second generation of particles in the seeded emulsion polymerization of monodisperse latex, should ideally possess the following qualities:

1) It should, first and foremost, prevent the propagation of any radical present in the aqueous phase, thereby eliminating particle formation (assuming no micelles are present).

2) It should not interfere with the overall polymerization kinetics by inducing an induction period or retarding the polymerization rate. Implicit are the requirements that it not participate in the polymerization, affect the decomposition rate of the initiator, or the desorption rate of free radicals from the particles (i.e., it should not affect $\bar{n}$).

3) It should not affect the colloidal stability of the particles by causing flocculation and coalescence of particles. Included in this is the requirement that it not alter the emulsifier adsorption equilibrium behavior.

No single, water-soluble inhibitor is likely to fulfill all of these requirements. Nonetheless, three inhibitors were used in successive seeding studies, each exhibiting significantly different behaviors.

Inhibition is generally regarded to occur by one of two mechanisms. Either the inhibitor itself is a radical species which ter-

195

minates another radical, such as the decomposed initiator, or it reacts with a radical forming an essentially unreactive radical species. In many cases the exact form of the inhibition mechanism is unclear or simply unknown. Ammonium thiocyanate (NH_4SCN) was found to successfully suppress particle generation in seeded polymerizations of styrene in the presence of polyethylacrylate seed particles with benzoyl peroxide (BPO) initiator [85]. In addition, it was also found to severely reduce the emulsion polymerization rate of methyl methacrylate, again using BPO initiator [86]. In contrast, NH_4SCN has also been referred to as a polymerization catalyst [87]. This reflects the uncertainty behind the actual behavior of this compound. Other inhibitors with $^-SCN-R$ groups have also been cited in the literature [88].

Sodium nitrite ($NaNO_2$) was used in the suspension polymerization of styrene, with polyvinyl alcohol as stabilizer and lauryl peroxide as initiator, to suppress the emulsion polymerization mechanism [89]. The inhibition effect of this compound has been linked to the generation of nitrogen oxides [90]. Both SCN^- and NO_2^- are known to oxidize readily.

NH_4SCN and $NaNO_2$ are both electrolyte species which can affect particle stability in seeded emulsion polymerizations. The third inhibitor tested was hydroquinone (HQ), a non-electrolyte. The inhibiting ability of HQ has been attributed to its oxidation to quinones [91] which, in turn, act as inhibitors. HQ has been widely used as a short-stopper in emulsion polymerizations of styrene using persulfate initiator.

Kinetically, the difference between an inhibitor and a retarder is merely a matter of degree. The effectiveness of the inhibitor reaction

$$R\cdot + Z \xrightarrow{\ k_z\ } R + Z\cdot \qquad ,$$
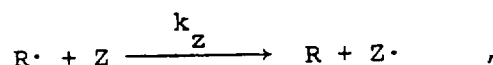
where R· is the radical species and Z the inhibitor, is characterized by the relative magnitudes of the rate constants k_z and k_p. If the inhibitor constant (k_z/k_p) is large, the polymerization generally experiences an induction period followed by an unretarded polymerization. On the other hand, if it is relatively small, the polymerization rate is retarded. Often the kinetic behavior lies between these two limits. These considerations were made for a system in which the initiator decomposed in the presence of the inhibitor. In these seeded emulsion polymerization experiments, however, the initiator is largely present in the polymer particles, while the inhibitor is located primarily in the aqueous phase. Therefore, it is possible that a more complex kinetic behavior may occur owing to interfacial phenomena, and the partitioning of initiator and inhibitor between the two phases. The kinetic results will be considered in view of these possibilities.

As in SSMLR 9, the sequences performed using NH_4SCN, $NaNO_2$, and HQ inhibitors were designed with recipes formulated to maintain a constant particle surface coverage of 15% with Aerosol-MA emulsifier. Likewise, the initial initiator concentration was set at 4 mM AIBN on monomer and the final solids content at 30%. The inhibitor concentrations were set by the addition of $NaNO_2$ as 0.1% by weight based on the aqueous phase (SSMLR 7). Equimolar amounts were then used for

the sequence employing NH_4SCN and HQ (14.5 mM on water) so that a reasonable comparison of results could be made. Recipe 'constants' for the three sequences are presented in Table 3-11. Swelling was essentially complete in all cases, as indicated by the M/P ratios. The solids

Table 3-11

Recipe 'Constants' for SSMLR 8, 7, and 10

SSMLR 8	M/P	% Solids	$\gamma(N/cm) \times 10^5$	$[AIBN]_0 (mM)^1$	$[NH_4SCN]_0 (mM)^2$
1	1.97	27.2	66.9	4.00	14.5
2	2.06	28.4	67.1	4.55	19.8
3	2.06	28.0	65.7	4.51	21.5
4	2.15	28.0	66.0	4.46	22.2
5	2.04	27.6	65.6	4.41	22.4
6	2.12	24.4	63.6	4.40	22.6
7	2.08	17.6	59.9	4.47	22.7
SSMLR 7					$[NaNO_2]_0$
1*	2.07	--	64.7	4.00	14.5
2	2.21	27.6	65.7	4.33	19.3
3	2.10	28.4	65.5	4.37	21.5
4	2.15	27.9	65.7	4.43	22.1
5	2.17	27.8	65.5	4.43	22.4
6	2.09	28.8	--	4.41	22.6
7	1.97	25.0	--	4.36	22.4
SSMLR 10					$[HQ]_0$
1*	2.16	27.5	--	4.00	14.5
2*	2.16	27.6	--	4.43	19.8
3	~2.17	26.9	--	4.35	21.7
4	2.17	28.5	--	4.29	22.6
5	2.17	17.8	--	4.18	22.4

*iridescence noted in both swollen and product latexes

[1]based on monomer

[2]based on the aqueous phase - upper limit considering no consumption

contents averaged around 28%, except in the steps where coagulum was found (i.e., SSMLR steps 8-6, 8-7, and 7-7) or the polymerization was terminated prematurely (SSMLR 10-5). The effect of coagulum formation was also noted as a drop in the surface tensions of the latexes, resulting from the displacement of emulsifier from the particles' surface (SSMLR 8-6 and 8-7). Otherwise, the surface tensions were relatively constant. The initial initiator concentrations changed slightly after the first step in both SSMLR 7 and 8, but steadily decreased for SSMLR 10. The inhibitor concentrations reported are upper limits, considering that they are unchanged during the polymerizations. This is likely to be a poor assumption, especially considering the role these are expected to have in limiting radical growth in the aqueous phase.

Iridescence of the swollen and product latexes was observed in SSMLR 7-1, 10-1, and 10-2. This was not unexpected where HQ was used as the inhibitor since it was not an electrolyte species. The occurrence of the phenomenon in the presence of $NaNO_2$ was, however, quite unexpected, particularly since it was not observed when NH_4SCN was substituted as the inhibitor under the same conditions. Each of these compounds is a 1-1 electrolyte and very soluble in water. Nonetheless, $NaNO_2$ exhibited almost no electrolyte effect with regards to particle stability while NH_4SCN had a large destabilizing effect.

Micrographs (SEM), representative of the latexes produced in sequences SSMLR 8, 7, and 10, are presented in Figures 3.29, 3.30, and 3.31, respectively. No small particles were evident in SSMLR 8, however, large off-size particles were found in steps 5, 6, and 7.

199

SSMLR 8   AIBN/NH$_4$SCN

$[1]_o = 4.0$mM

$[Z]_o = 14.5$mM
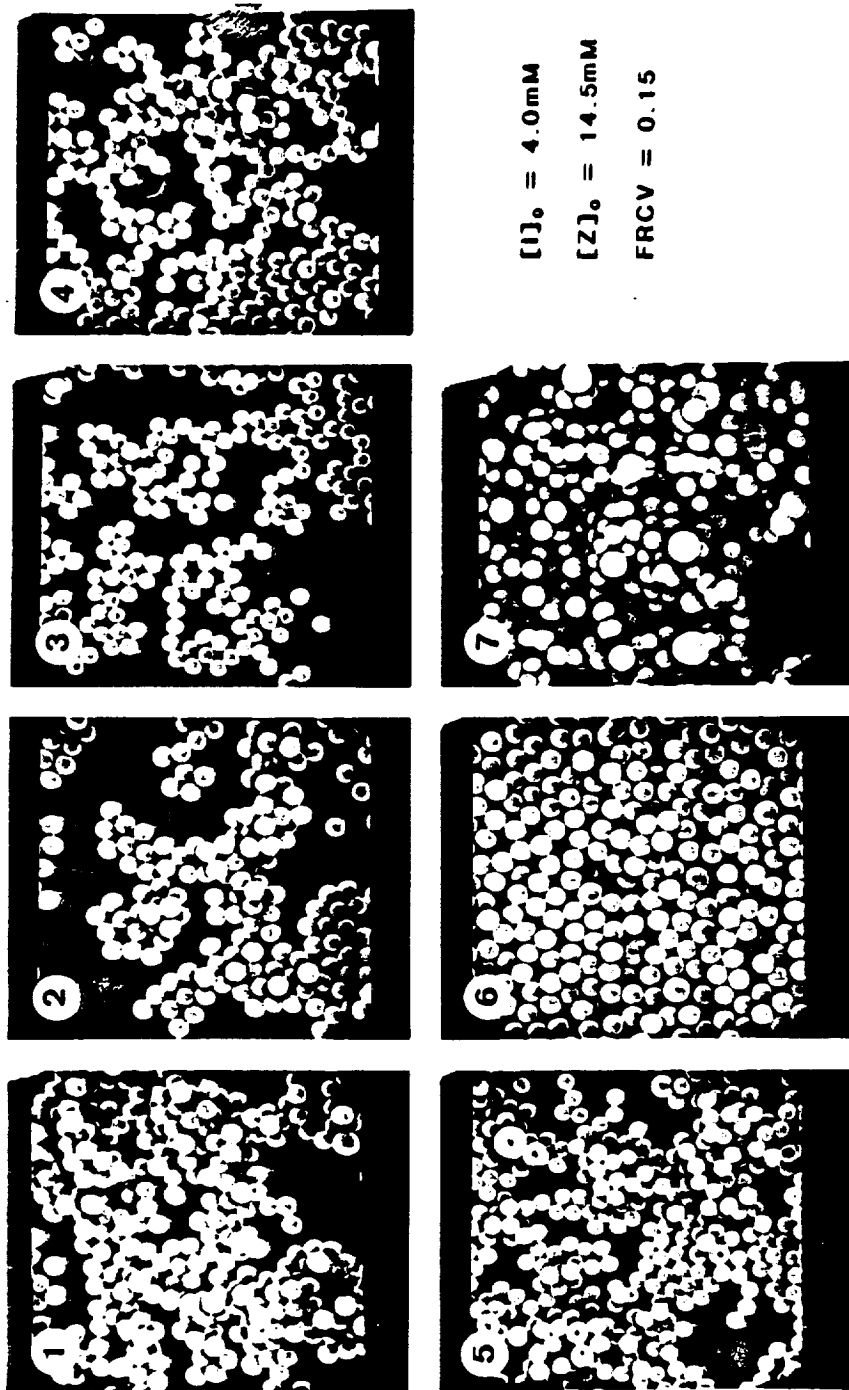
FRCV = 0.15

Figure 3.29   Scanning Electron Micrographs of   Latexes Produced in SSMLR 8

SSMLR 7 · AIBN/NaNO$_2$

$[I]_o$ = 4.0mM

$[Z]_o$ = 14.5mM
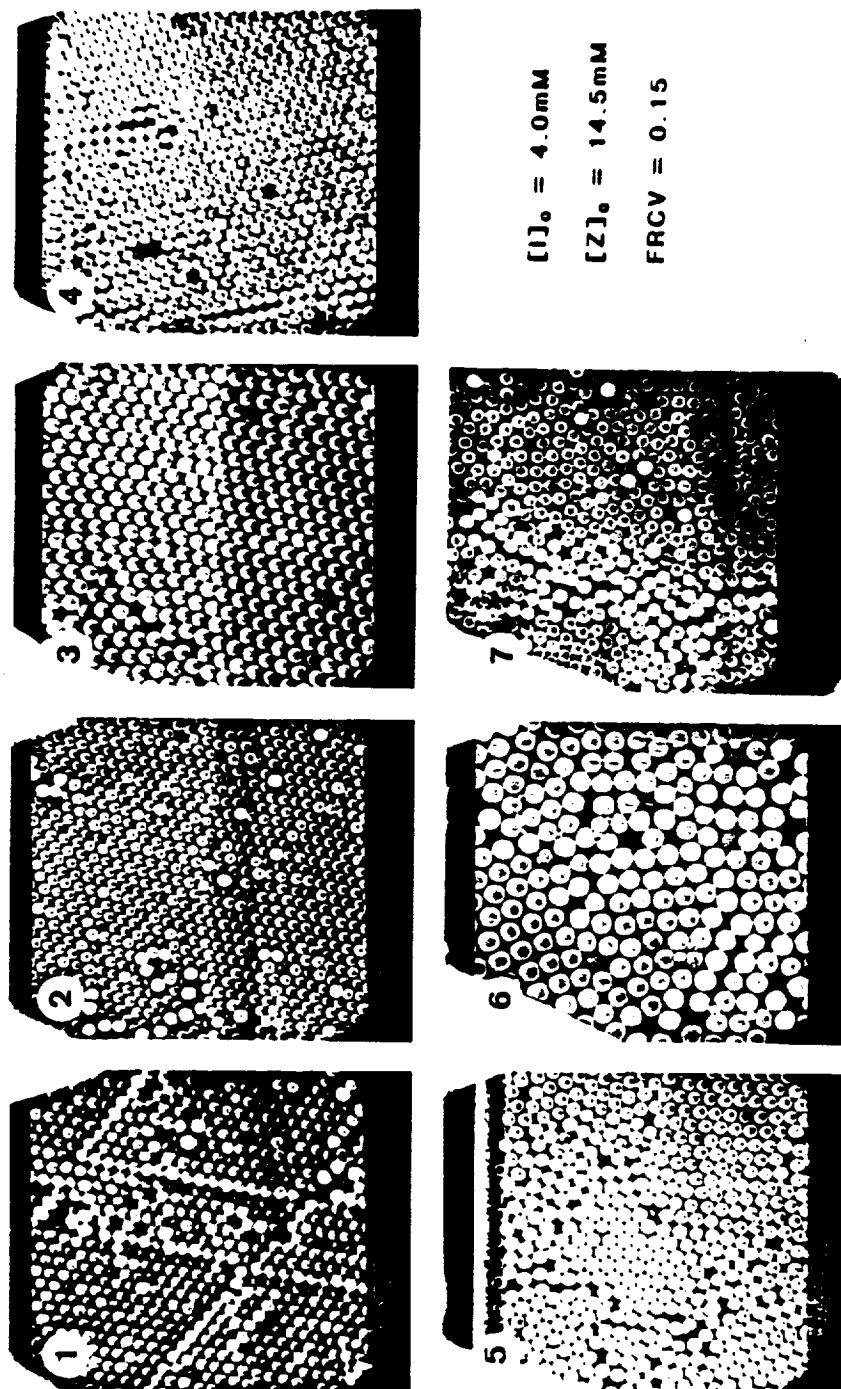
FRCV = 0.15

Figure 3.30 Scanning Electron Micrographs of Latexes Produced in SSMLR 7

SSMLR 10   AIBN/HQ
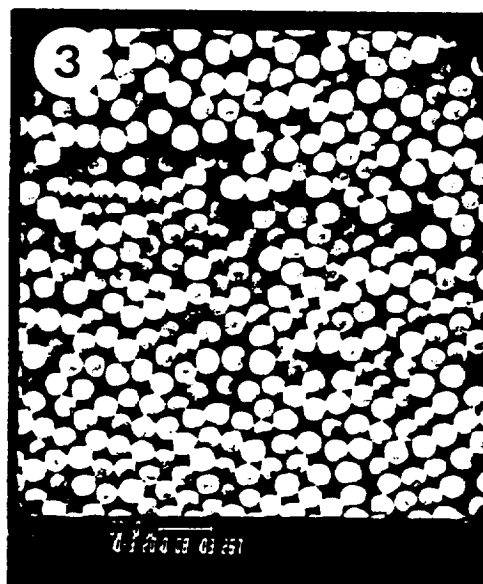
$[I]_0 = 4.0mM$

$[Z]_0 = 14.5mM$
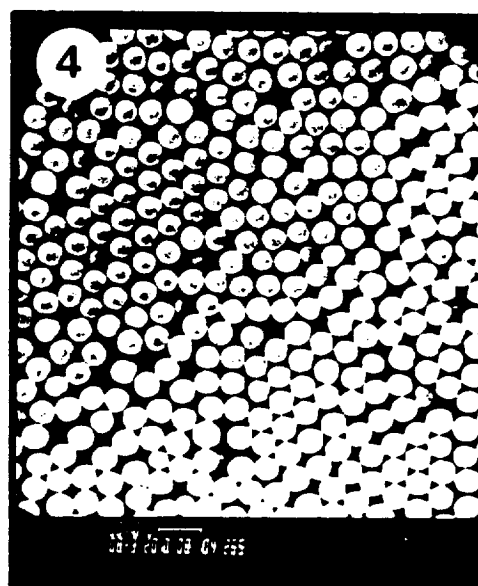
FRCV = 0.15

Figure 3.31 Scanning Electron Micrographs of Latexes Produced in
3rd and 4th Steps of SSMLR 10

Increased instability with increasing particle size was manifested as in SSMLR 6, occurring in the fifth step instead of the second owing to the increased emulsifier surface coverage. In sharp contrast are the results obtained using $NaNO_2$. Small particles were generated as early as the fourth seeding step while no off-size large particles were evident (i.e., no significant electrolyte effect). These results appear to be poorer than those obtained without any added inhibitor (see Figure 3.25). The sequence employing HQ (SSMLR 10) showed no signs of new particle generation through the first four seeding steps, remaining essentially monodisperse. Therefore, the expected improvements in the monodisperse quality of latexes prepared via successive seeding were not realized with the addition of the aqueous phase inhibitors NH_4SCN and $NaNO_2$ (i.e., within the limited scope of the experiments). No conclusion was reached in this case for HQ since the sequence was not completed.

In view of the results reported above, one might expect that the polymerization kinetics for SSMLR 8 (NH_4SCN) would behave differently from that of SSMLR 9 in which no inhibitor was added. On the other hand, one might expect SSMLR 7 and 9 to have similar kinetics based on their other similarities. The conversion histories for the three sequences are shown in Figures 3.32, 3.33, and 3.34. The results are strikingly different. A number of points can be made in comparing these with the results obtained without any inhibitor (SSMLR 9 - Figure 3.26). NH_4SCN did not have any significant effect on the polymerization kinetics through the first five steps of the sequence, in terms of an observed induction period or a retardation
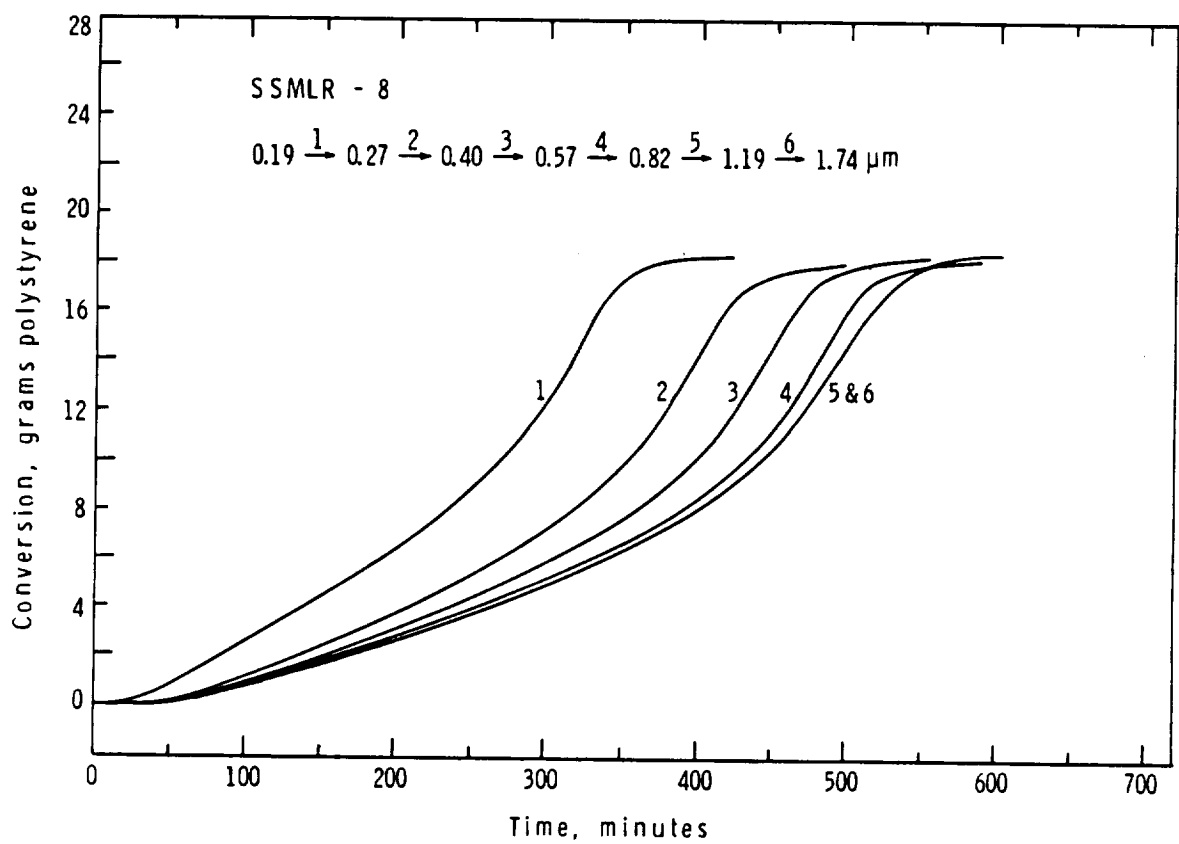
Figure 3.32   Conversion Histories for Seed Sequence   SSMLR 8, AIBN
with NH$_4$SCN Inhibitor
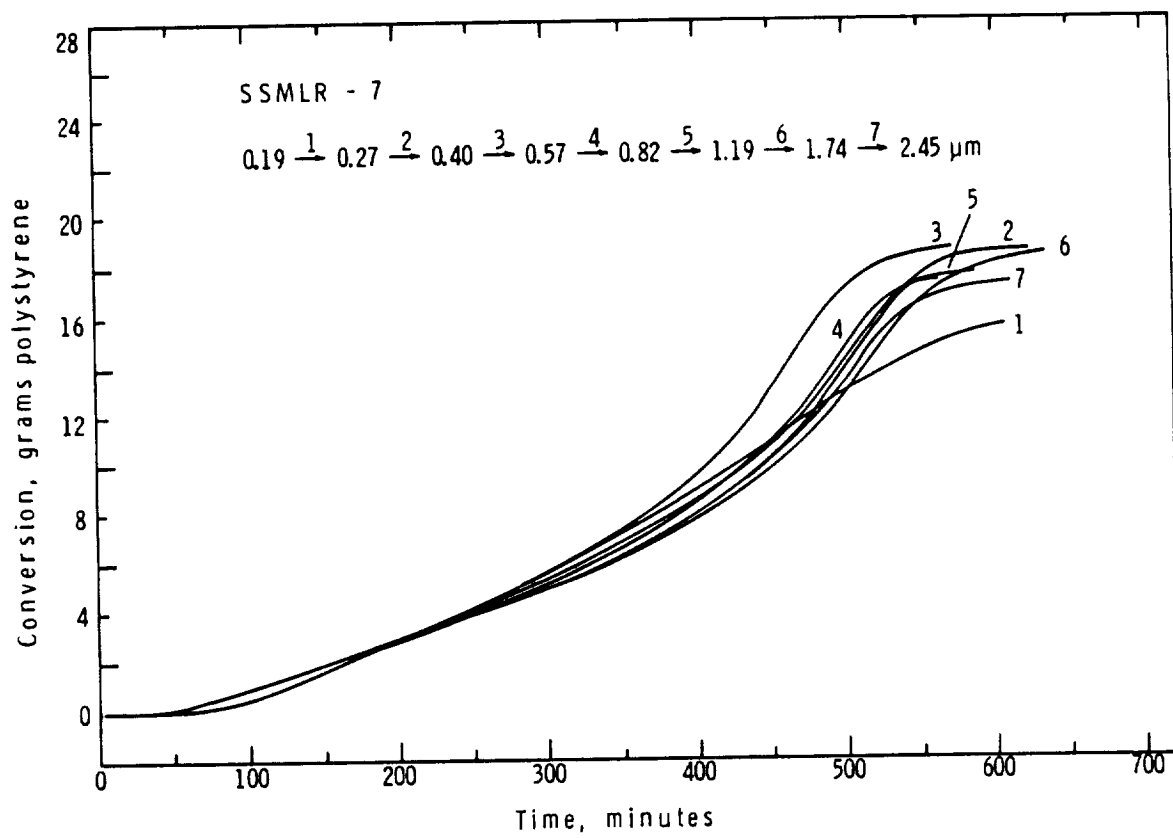
Figure 3.33   Conversion Histories for Seed Sequence SSMLR 10, AIBN
with NaNO$_2$ Inhibitor

205
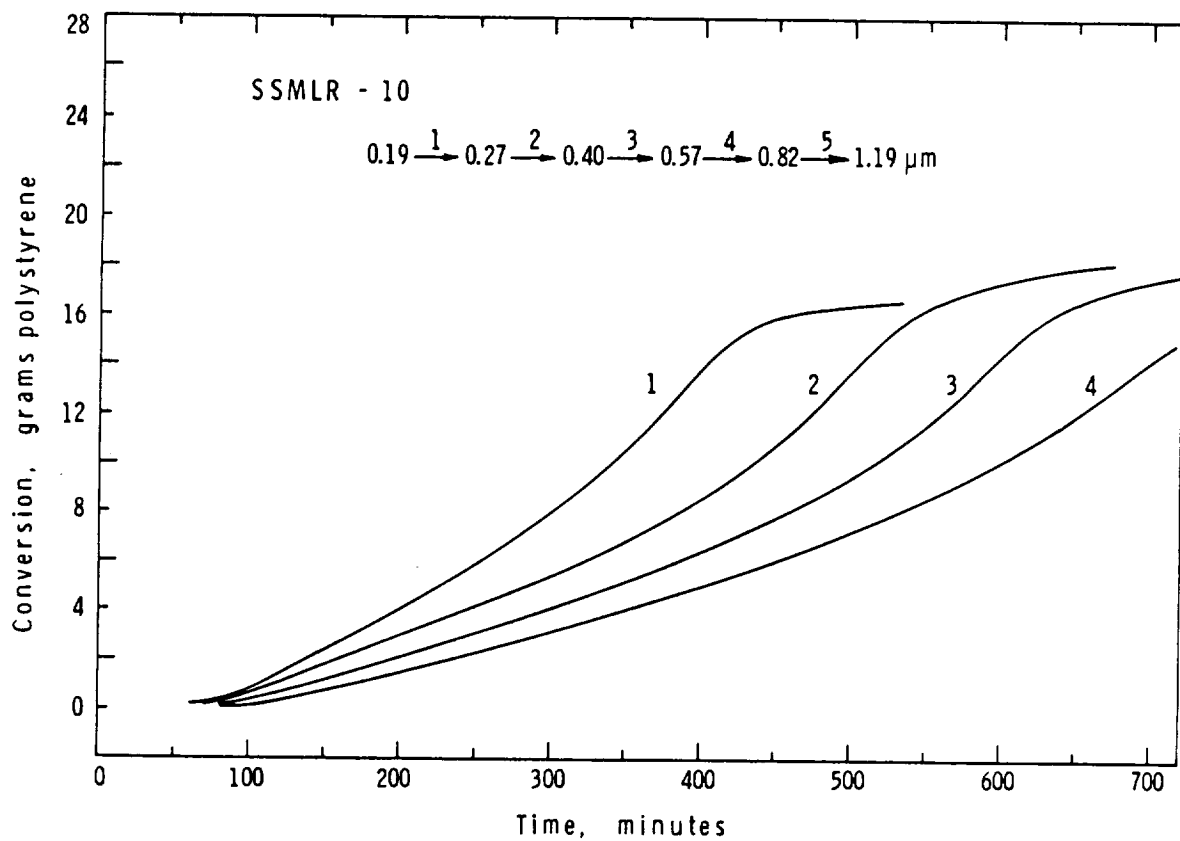
Figure 3.34   Conversion Histories for Seed Sequence SSMLR 10, AIBN
with HQ Inhibitor

effect. The results were nearly identical to those obtained without any inhibitor. Apparently this inhibitor does not induce an induction period nor significantly retard the polymerization. This would be expected for the case in which the inhibitor and initiator remain in their respective phases with no interfacial interaction. The strong electrolyte effect, as evidenced by the increased instability of the particles with increasing particle size, can also be inferred to have little significant effect on the polymerization kinetics. (Step 7 was affected by the heavy amount of coagulum.) The absence of newly generated small particles may have been a result of either an inhibition effect or an electrolyte effect, or both.

$NaNO_2$ strongly retarded the polymerization in the first seeding step and somewhat less in the second step, while apparently having little or no effect on the kinetics of the remaining steps (Figure 3.33). Recall that this inhibitor also did not exhibit the expected electrolyte effect. These results suggest that the retardation is a function of particle size which implies a surface related phenomenon. If the inhibitor acts at the particle-water interface, the effect would be expected to decrease as the surface-to-volume ratio of the particles decreases, as seen in this case. This interfacial effect may also explain the reduced electrolyte effect (i.e., lower aqueous phase electrolyte concentration). As stated previously, the mechanism of inhibition is not clearly understood.

Hydroquinone, present in the same molar quantity as the other inhibitors, caused both induction periods as well as retardation of of polymerization through the four steps of sequence SSMLR 10 (Figure

207

3.34). The partitioning behavior of the HQ between the aqueous and organic phases is not known, however, it is considered that this is likely to be a significant effect. Perhaps more important is the oxidation of hydroquinone to benzoquinone, the latter being more soluble in the oil phase. The rate and extent of this reaction may be the factors determining the inhibition and retardation effects upon the polymerizations.

The 'final' conversions, measured after the termination of the polymerizations, are tabulated in Table 3-12 along with the number and weight average molecular weights. This approach to a limiting conversion was slower in the cases using HQ, due to retardation, as reflected in the lower conversions. The molecular weights show some differences such as slightly higher values of $\bar{M}_W$ for SSMLR 8 (and 9) relative to SSMLR 7 and 10. These differences are not considered to be significant, however. (Note: the low values for $\bar{M}_W$ for 7-1 and 10-5 results from the low conversions, $\bar{M}_W$ increasing with increasing conversion.)

Differences in the polymerization kinetics are reflected in further analysis of the data. The average number of radicals per particle as a function of conversion and particle size is presented in Figure 3.35 for the cases using $NaNO_2$ and HQ (SSMLR 7 and 10). The results for the NH_4SCN inhibited sequence were nearly identical to those without inhibitor as given in Figure 3.27. The most striking difference in these results is the case of SSMLR 7-1 which indicates values of $\bar{n}$ less than 0.5 (Smith-Ewart Case 2). Generally, $\bar{n}$ is less than 1/2 under conditions of small particle size (<0.05 μm)

Table 3-12

Conversion and Average Molecular Weight of SSMLR 8, 7 and 10 Latexes

	% Conversion[1]		Molecular Weights	
SSMLR 8	On Monomer	On Polymer	$\bar{M}_N \times 10^{-5}$	$\bar{M}_W \times 10^{-6}$
1	92.6	95.1	2.9	1.4
2	91.9	94.6	3.7	1.5
3	91.8	94.5	3.6	1.6
4	91.7	94.3	3.8	1.5
5	92.0	94.7	2.9	1.5
6	92.1	94.6	3.8	1.5
7	93.2	95.4	3.1	1.6
SSMLR 7				
1	83.8	89.1	2.3	1.2
2	92.3	94.6	3.3	1.4
3	91.4	94.2	3.3	1.4
4	90.3	93.4	3.4	1.4
5	90.4	93.4	3.6	1.3
6	91.0	93.9	3.6	1.4
7	90.1	93.4	3.6	1.4
SSMLR 10				
1	90.7	93.7	3.7	1.4
2	89.7	93.0	4.8	1.4
3	89.7	92.8	4.6	1.3
4	88.6	92.2	4.5	1.3
5	36.8	57.1	2.8	1.1

[1]from iso-octane extraction/UV absorption analysis

and low initiation rates or high radical desorption rates. In this
case the inhibitor acted to eliminate active radicals from the parti-
cles at a rate of the same order as the effective radical production

rate. Therefore, growing radicals existed for less than that time between successive 'entries' of a radical and $\bar{n}$ was less than 1/2. These were the conditions during the early stages of the polymerization; however, as the conversion increased $\bar{n}$ did rise above 1/2 (gel effect) but at a lower rate than in the case without the $NaNO_2$ inhibitor. The second step of the sequence, SSMLR 7-2, also resulted in lower values of $\bar{n}$ when compared to the control. By step 4 these differences had disappeared. In the case of HQ the $\bar{n}$ vs. W_p curves all lay below those of the respective control experiments with the exception of the first step which was similar to the control up to about .75 W_p. It is likely that hydroquinone or benzoquinone acts within the particles to cause the induction period and retardation effect while acting outside the particles to inhibit the formation of new particles.

The transition from emulsion (Case 2) kinetics to bulk (Case 3) kinetics was effectively bridged by the fifth seeding step of the sequences using AIBN initiator with NH_4SCN and $NaNO_2$ inhibitors as in the previous cases using $K_2S_2O_8$ and AIBN initiators alone. This implies that the polymerization kinetics are no longer a significant function of particle size above 1.2 μm for the conditions of these seeded polymerization experiments. In other words, $\bar{n}$ becomes proportional to d^3 and $(f[I])^{\frac{1}{2}}$, while R_p is independent of particle size and number. SSMLR 10, using HQ inhibitor, does not support or dispute these findings since the fifth and sixth steps were not completed.

The preceding results indicated that hydroquinone was the most promising of the three inhibitors in terms of reducing new particle generation without affecting particle stability (i.e., satisfying two of the three requirements). From a kinetic standpoint, however, HQ proved to interfere with the polymerization kinetics by causing induction periods and retardation. Further work was done using HQ in combination with another azo type initiator, AMBN (2,2'-azobis(2-methylbutyronitrile)), because of the potential of significantly improved product latexes [80].

3.5.4.4   SSMLR 11,12,13 - AMBN with and without HQ

Three successive seeding sequences were performed using AMBN initiator with and without inhibitor. Two of these, SSMLR 11 and 12, were the analogues of SSMLR 9 and 10 while the third (SSMLR 13) was based on results obtained in the developmental work on large-particle-size latex recipes performed by Tseng [80].

The recipes for sequences SSMLR 11 and 12 were formulated as described for the previous sequences; 30% final solids content, 2/1 monomer/polymer swelling ratio, 15% surface coverage of the swollen particles, 4 mM AMBN based on monomer, and 14.5 mM HQ based on the aqueous phase. The recipe constants for the two sequences, given in Table 3-13, reflect the similarities of the sequence with the primary difference in the presence of HQ inhibitor. Note that the swollen and product latexes of steps 1 and 2 of both sequences exhibited iridescence indicative of strong double layer effects. Coagulum was generally insignificant except for the last step in SSMLR 12, as indicated by the lower solids content (24.8%). This
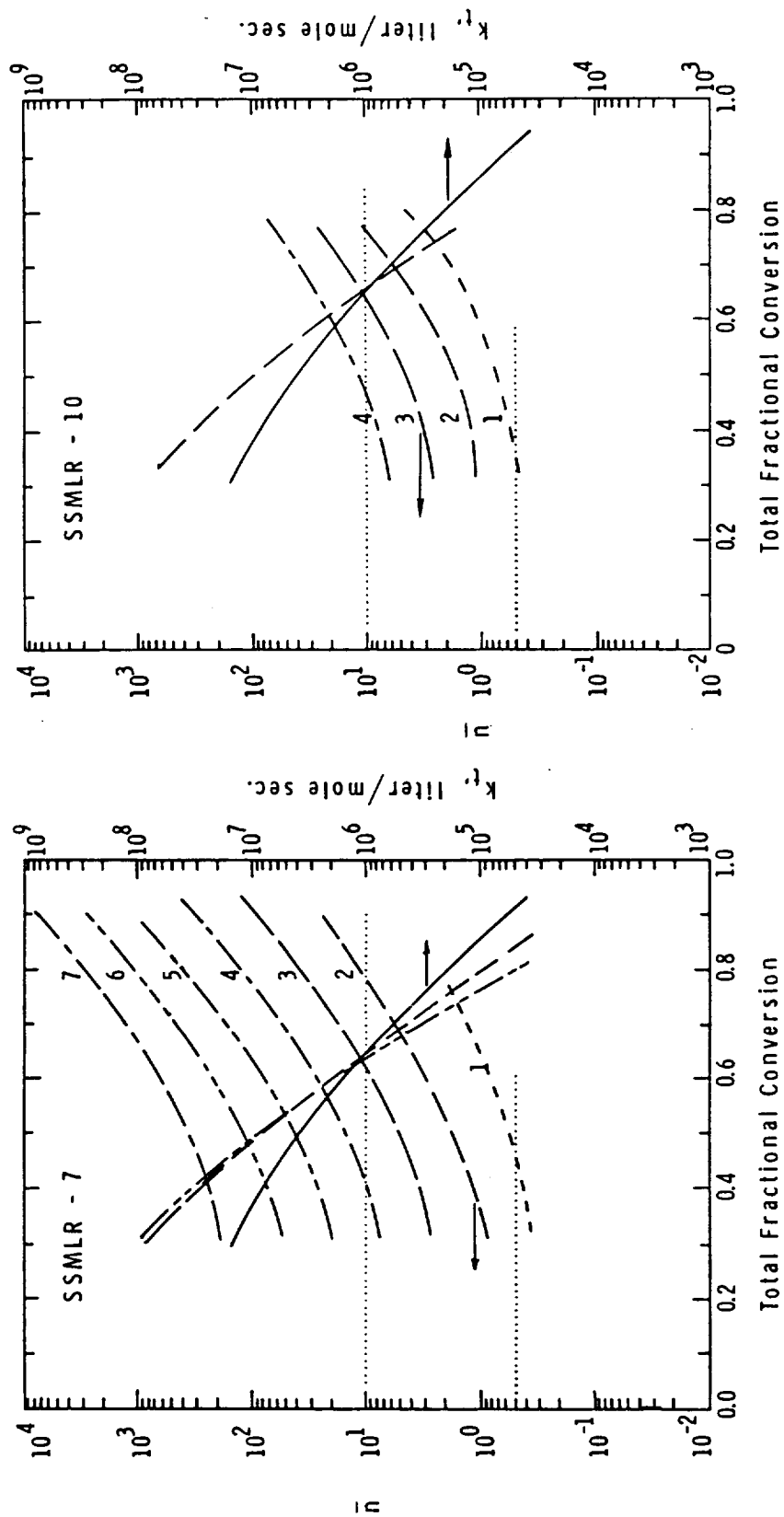
Figure 3.35 $\bar{n}$ and k_t as a Function of Particle Size (Seeding Step) and Total Fractional Conversion (W_p) for SSMLR 7 (Left) and SSMLR 10 (Right) Employing $NaNO_2$ and HQ Inhibitors, Respectively

212

suggests that the HQ does have some destabilizing influence, similar in extent to $NaNO_2$ (see Table 3-11).

Table 3-13

Recipe 'Constants' for SSMLR 11 and 12

SSMLR 11	M/P	% Solids	$[AMBN]_0$ (mM) [1]	$[HQ]_0$ (mM) [2]
1*	2.00	27.6	4.00	---
2*	2.06	28.9	4.66	---
3	2.06	28.3	4.64	---
4	2.07	28.4	4.59	---
5	2.09	28.2	4.49	---
6	2.08	27.9	4.49	---
7	2.09	27.4	4.47	---
SSMLR 12				
1*	1.93	27.0	4.00	14.50
2*	2.02	28.2	4.52	19.8
3	2.13	27.7	4.37	21.5
4	2.10	27.9	4.30	22.3
5	2.04	27.5	4.30	22.5
6	2.08	27.8	4.26	22.7
7	2.07	24.8	4.23	22.7

*iridescence noted in both swollen and product latexes
[1] based on monomer
[2] based on the aqueous phase (upper limit)

Scanning Electron Micrographs representative of some of the latex products of SSMLR 11 and 12 are reproduced in Figures 3.36 and 3.37, respectively. A few small particles were evident by the fifth seeding step (1.19 μm) without the use of HQ inhibitor while few could be seen by the seventh step (2.45 μm) when HQ was used. This

SSMLR 11   AMBN/No Inhibitor

[I]$_o$ = 4.0mM
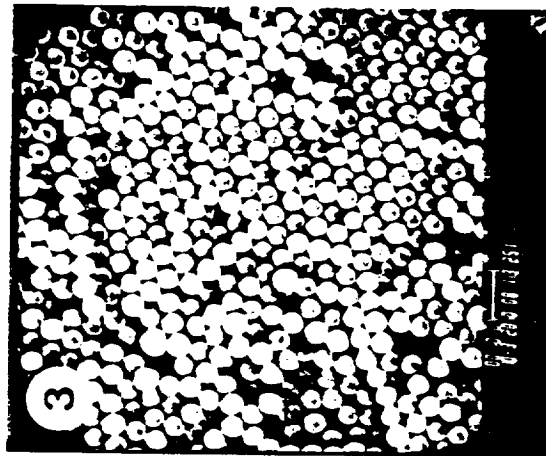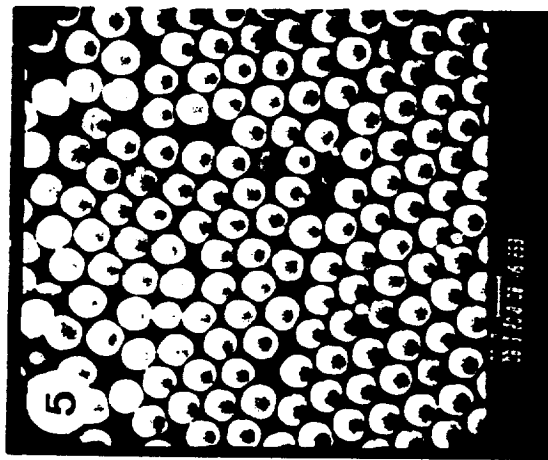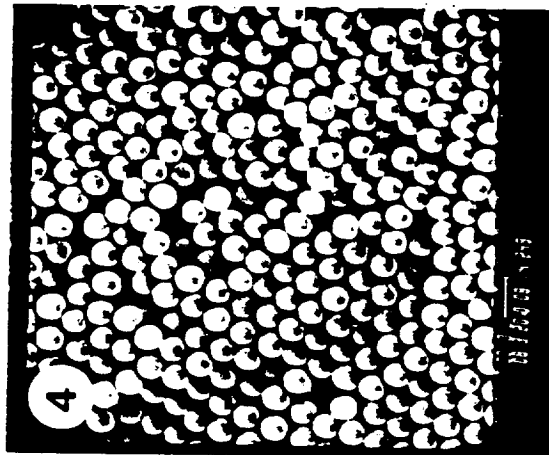
FRCV = 0.15

Figure 3.36   Scanning Electron Micrographs of Latexes Produced in SSMLR 11, Steps 3 – 5.

SSMLR 12 AMBN/HQ
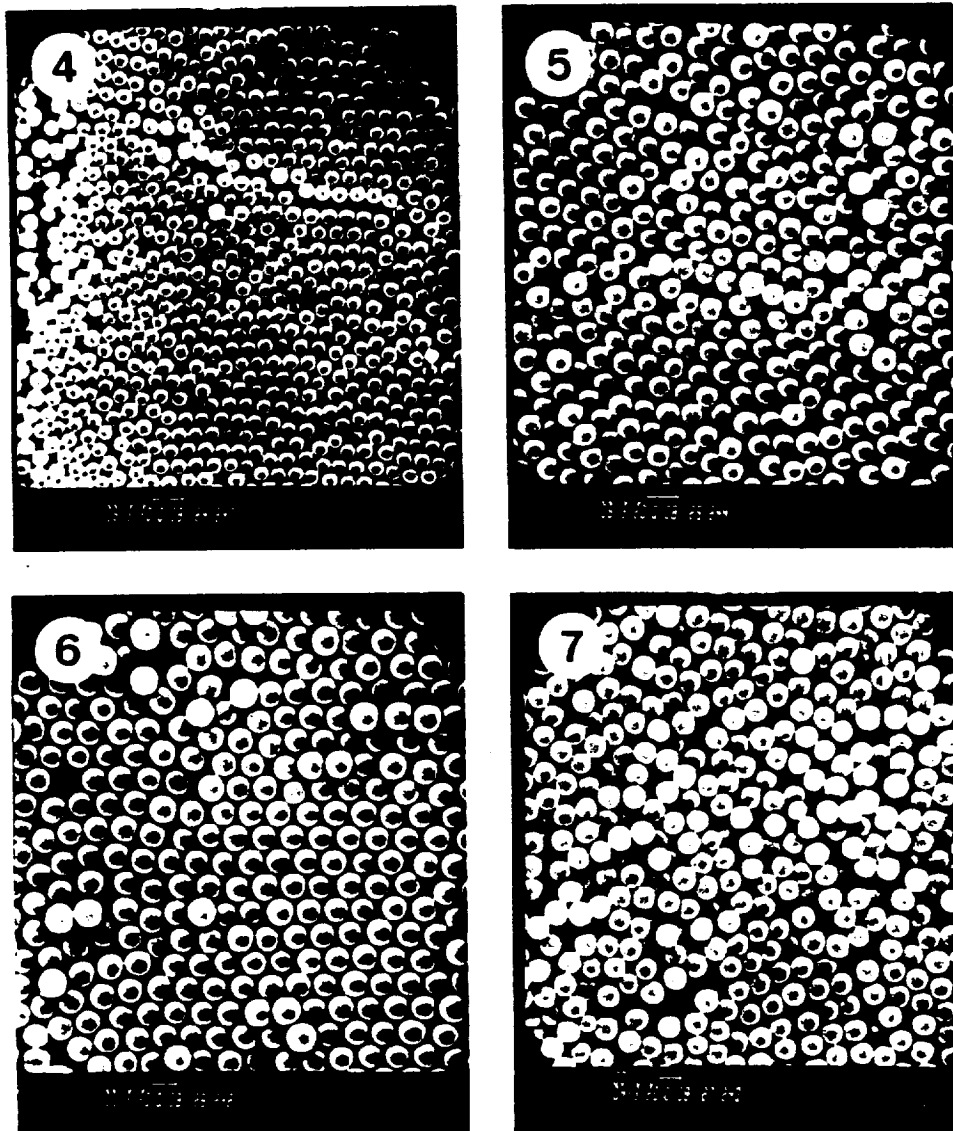
$[I]_0 = 4.0mM$

$[Z]_0 = 14.5mM$

$FRCV = 0.15$

Figure 3.37 Scanning Electron Micrographs of Latexes Produced in SSMLR 12, Steps 4 - 7

215

illustrates the relative effectiveness of HQ in preventing nucleation without causing flocculation and coalescence of the particles. No significant differences could be observed, however, between the results obtained for each of the oil soluble initiators in terms of particle nucleation.

The polymerization kinetics for the two sequences are given in Figures 3.38 and 3.39. These results are similar to the AIBN analogues but show several significant differences. The overall polymerization rates were slower for the AMBN polymerizations, showing increasing difference with increasing particle size. The lower decomposition rate of AMBN compared to AIBN accounts for this difference. At 70°C, k_d is 2.966×10^{-5} sec^{-1} for AMBN and 4.24×10^{-5} sec^{-1} for AIBN (i.e., AIBN decomposes 1.4 times faster than AMBN). This difference becomes significant for conditions in which deviation from Case 2 kinetics occurs. This also accounts for the greater induction periods observed for the AMBN/HQ systems compared to their AIBN counterparts. Note, however, that there was some variation in the induction periods for SSMLR 12, decreasing somewhat for the first three steps. This was not seen in the SSMLR 10 results (Figure 3.34). This explains the appearance that the polymerization kinetics become independent of particle size by the third seeding step which is inconsistent with all the previous findings. If the curves are shifted to achieve matching induction periods, then this phenomenon occurs closer to the fourth seeding step as seen in the preceding examples, including SSMLR 11. The difference in the induction periods is not understood, although it may be simply due to some unob-
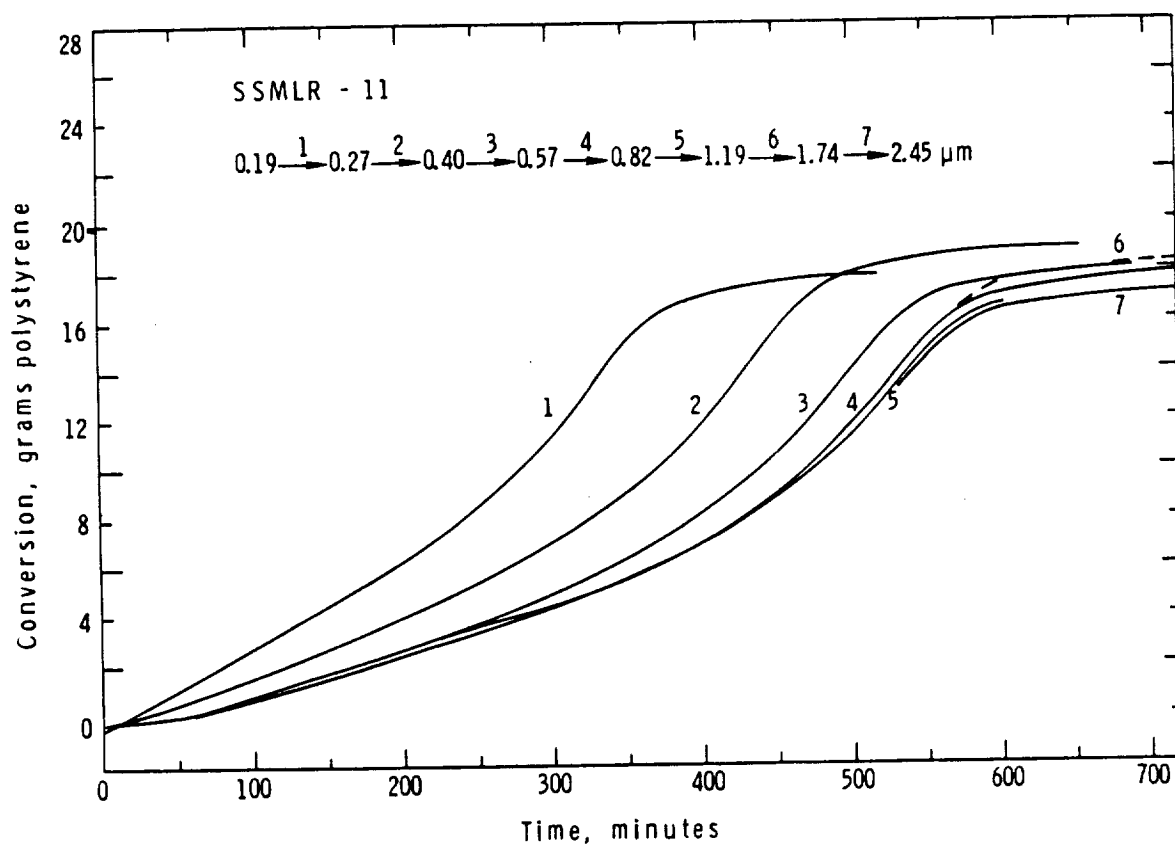
Figure 3.38 Conversion Histories for Seed Sequence SSMLR 11, Using AMBN Initiator (4 mM on Monomer) with No Inhibitor

217
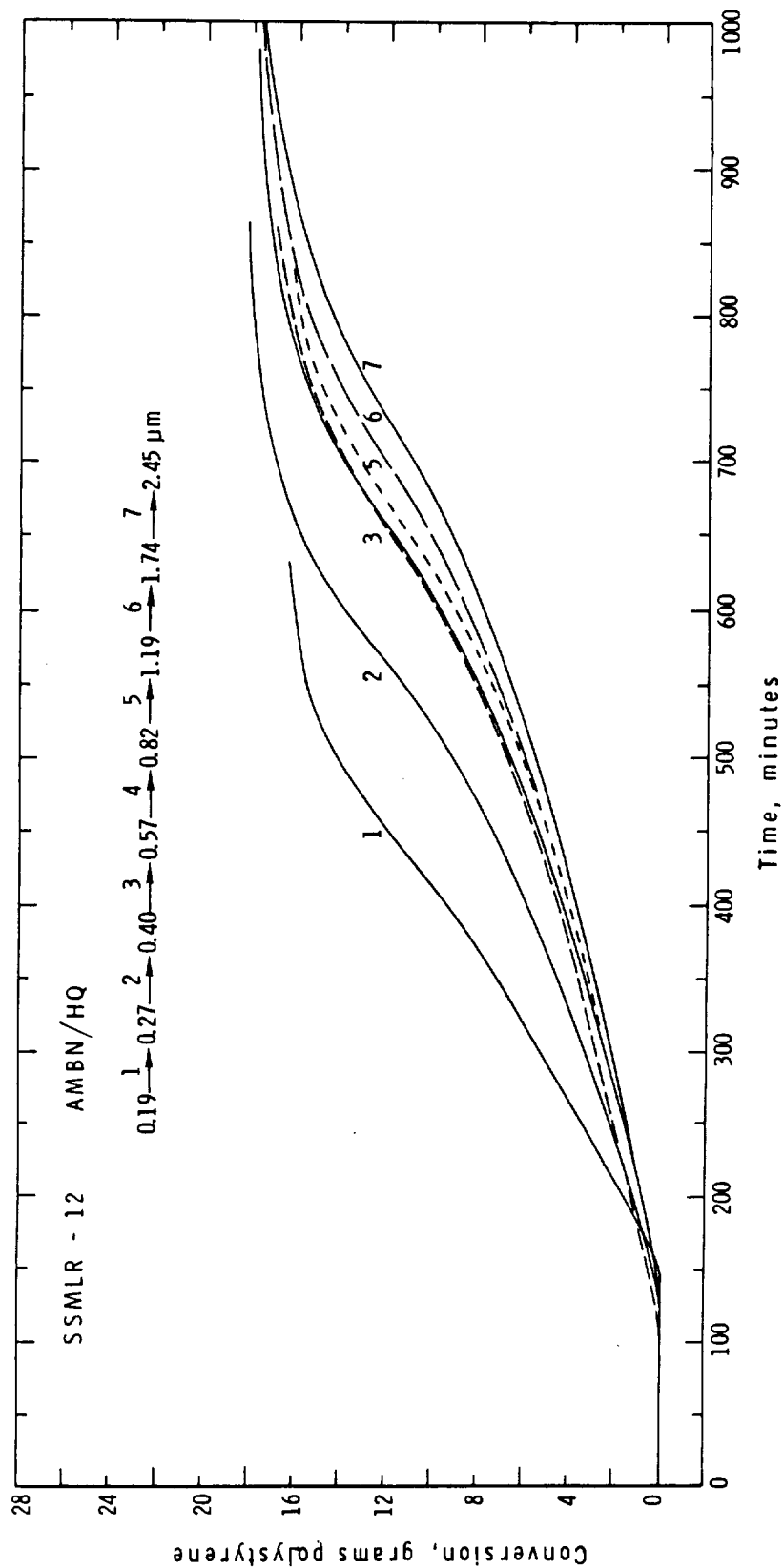
Figure 3.39 Conversion Histories for Seed Sequence SSMLR 12, Using AMBN Initiator (4 mM on Monomer) with HQ Inhibitor (14.5 mM on Aqueous Phase)

served experimental variations (such as swelling time and extent of degassing).

Further analysis of the data in terms of $\bar{n}$ and the variation of k_t with conversion suggest a low efficiency from AMBN as was the case for AIBN. This is reflected in the high values of k_t backcalculated through the data (Figure 3.40). One other important observation is that k_t does not continue accelerating to lower values as seen in previous cases but shows a bending in the opposite direction. This may be due to a real change in the k_t function, the k_p function, or even the k_d function with respect to the fraction of polymer (viscosity) in the system. This will be discussed further in Chapter 4.

The third sequence performed using AMBN as the initiator (SSMLR 13) had a number of modifications in the recipe formulation based on the developments for the STS-3 experiments [80]. The initiator concentration was increased to 5.65 mM AMBN based on monomer while the inhibitor (HQ) concentration was reduced to 3.2 mM based on the aqueous phase. The emulsifier (Aerosol-MA) surface coverage was reduced to 10% for the first five sequence steps (up to 1.19 µm) with the following four steps using a combination of stabilizers consisting of Aerosol-MA, Polywet KX-3, and PVP K-30. Polywet KX-3 (Uniroyal) is an anionic oligomeric surfactant with a molecular weight around 1500. PVP K-30 (GAF) is a polymeric stabilizer of polyvinylpyrrolidone with molecular weight of approximately 40,000. These have been shown to provide good particle stability in the growth of large-particle-size latexes without inducing significant particle nucleation when used in combination with HQ and AMBN.

219
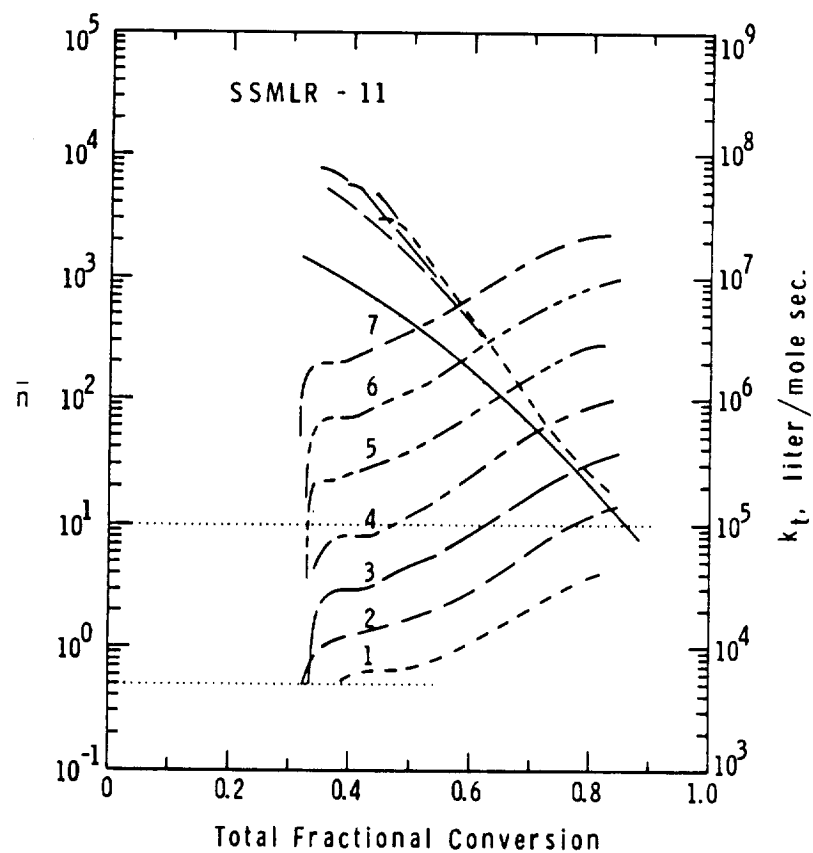
Figure 3.40 $\bar{n}$ and k_t as a Function of Particle Size (Seeding Step) and Total Fractional Conversion (W_p) for SSMLR 11, AMBN without Inihibitor

220

The nominal swelling ratios and solids contents remained 2/1 and 30%, respectively. SSMLR 13 recipe 'constants' are tabulated in Table 3-14. Note the variation in the stabilizer concentrations. Steps 6,7, and 8 varied only in the amount of Aerosol-MA (what would normally be 10% coverage). It was assumed that the total surface occupied increased for these three steps through the decreasing surface

Table 3-14

Recipe 'Constants' for SSMLR 13

SSMLR 13	M/P	% Solids	Weight % on Aqueous Phase			$[AMBN]_0 mM^1$	$[HQ]_0 mM^2$
			AMA	KX-3	PVP		
1*	1.95	27.9	0.111	---	---	5.65	3.15
2*	2.13	28.5	0.079	---	---	6.35	4.28
3*	2.09	28.1	0.056	---	---	6.35	4.65
4	2.18	29.4	0.040	---	---	6.26	4.89
5	2.25	27.4	0.029	---	---	6.26	4.89
6	2.15	27.6	0.021	0.023	0.194	6.42	4.93
7	2.13	27.6	0.016	0.023	0.194	6.30	4.94
8	2.21	27.2	0.012	0.023	0.194	6.10	4.94
9	2.23	26.9	0.010	0.016	0.136	6.24	4.97

*iridescence noted in swollen and product latexes
[1] based on monomer
[2] based on the aqueous phase

area. The recipe used in Step 8 was nearly identical to that used for the STS-3 Flight experiment #2 in which 2.5 μm polystyrene seed particles were grown to 3.4 μm (see Chapter 5). One further step (9) carried out in the sequence produced particles with nominal diameters of 5.1 μm. SEM photos of the latexes produced in Steps 4 through 9 (Figure 3.41) reveal that very few small particles were

SSMLR 13 AMBN/HQ PVP/KX-3

$[I]_0 = 5.65mM$ $[Z]_0 = 3.2mM$ $FRCV = 0.15$
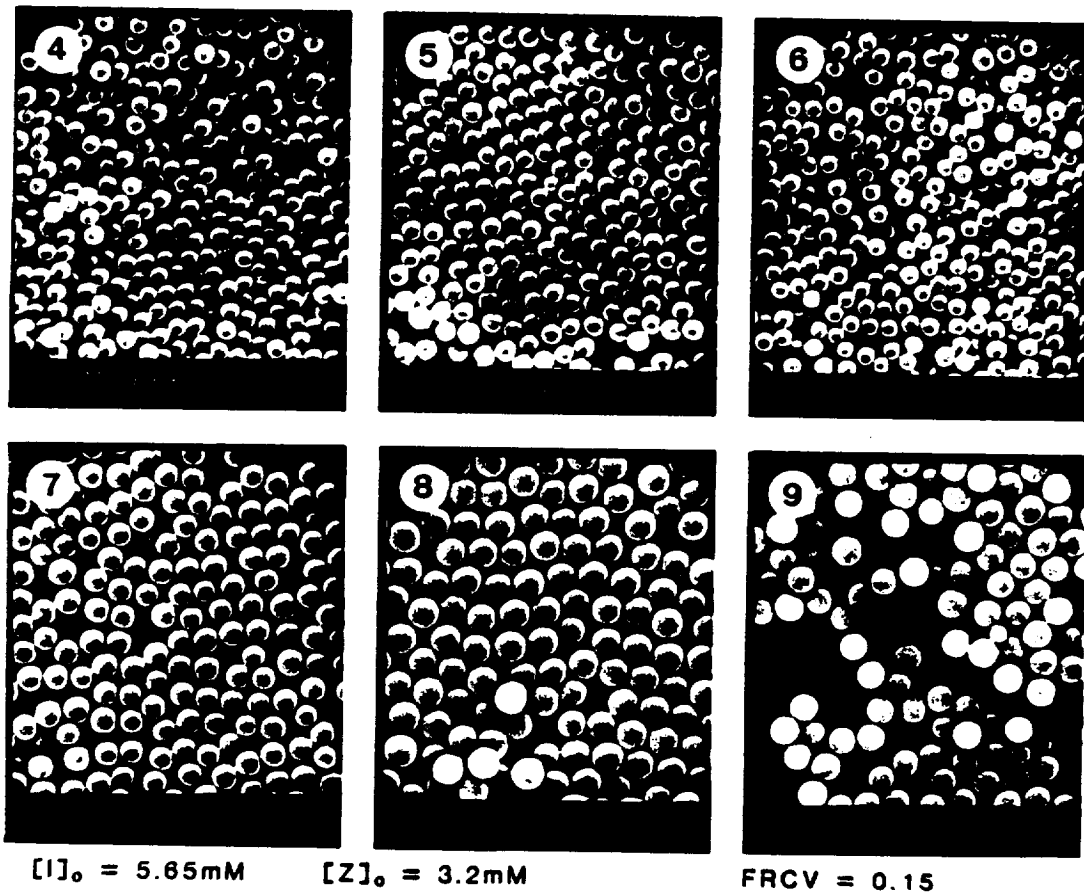
Figure 3.41 Scanning Electron Micrographs of Latexes Produced in SSMLR 13, Steps 4 - 9.

nucleated anywhere in the sequence. A close examination indicates, however, that the particle size distributions may have broadened somewhat in this series. The 'low' stir rate (OSC 6.0) coupled with a slightly higher viscosity latex (possibly due to expanded double layers and PVP polymer solution) can account for these results.

The conversion histories for SSMLR 13, shown in Figure 3.42, are similar to those reported previously for AMBN with and without inhibitor, although the latter case has the strongest resemblance. The lower hydroquinone levels (3.2 vs. 14.5 mM) induced induction periods but little retardation (the increased initiator concentration may have reduced this effect). The relative induction periods (i.e., with vs. without HQ) decreased with increasing particle size as in the case of SSMLR 12, which would confirm some kind of interfacial effect, thus decreasing with surface/volume ratio. The conversion time curves for Steps 4 and 5 (0.82 and 1.19 µm) were nearly identical, indicating completion of the kinetic transition from emulsion to bulk kinetics as found previously. This was not confirmed in the following step (6), however, taking more time to reach high conversion. Recall that this step was the first to use the more complex stabilization system of AMA, KX-3, and PVP. It is logical to assume that any interfacial effects would be significantly affected by the presence of these added stabilizers. A shift in the induction period can account for most of the difference between the results of Steps 5 and 6. Steps 7, 8, and 9 are nearly superimposed on each other, slightly shifted from Step 5 to longer times (and up from Step 6). Independence of the polymerization rate on particle

223
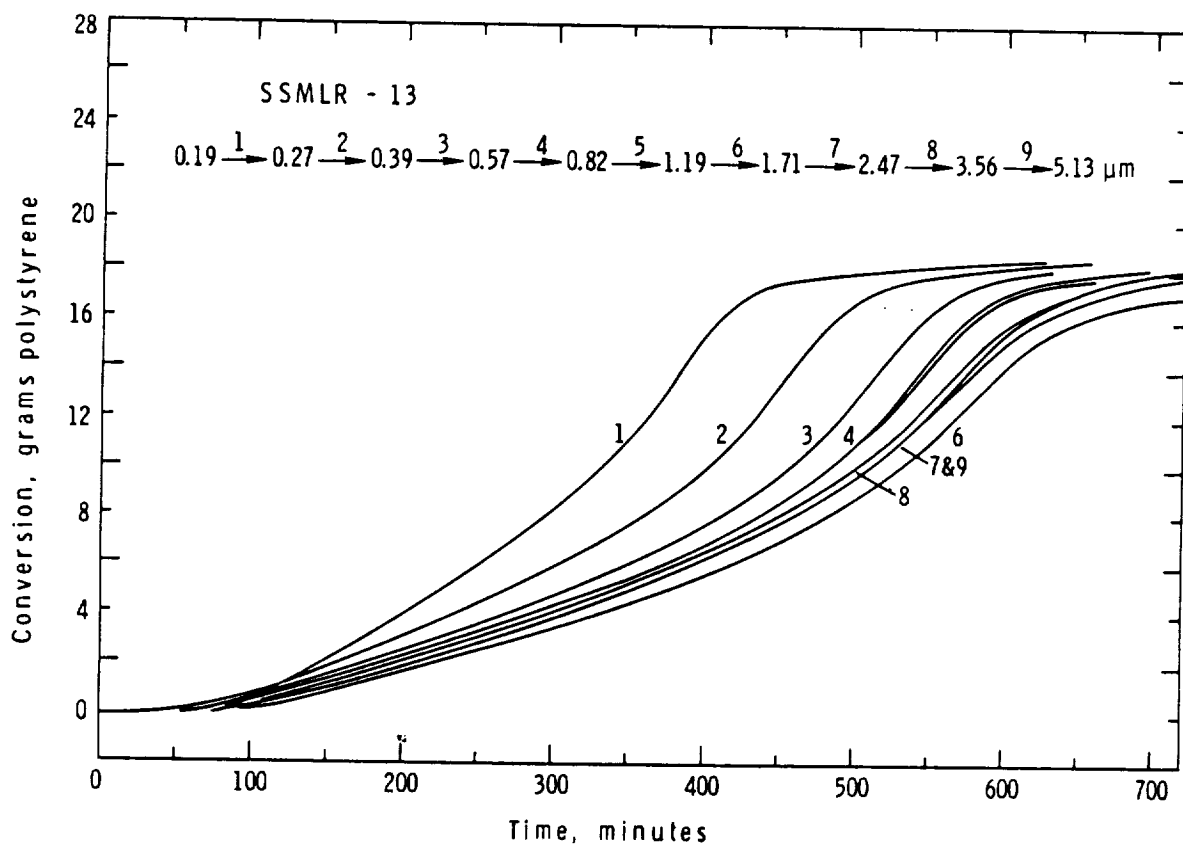
Figure 3.42   Conversion Histories for Seed Sequence SSMLR 13, using
AMBN Initiator (5.65 mM on Monomer) with HQ Inhibitor
(3.2 mM)

size and number is confirmed over this region (2.4 → 5.1 μm, and 7.3 x 10^{13} → 8.1 x 10^{12} particles/liter). A comparison of these results to the STS-3 Flight results will be made in Chapter 5.

3.5.4.5 Summary

Two oil soluble initiators and three water soluble inhibitors were employed in various combinations in successive seeding experiments designed to grow particles from 0.19 μm to 2.47 μm in seven consecutive growth cycles. Recipes designed to maintain 15% surface coverage with Aerosol-MA were used to test the effects of equimolar quantities (14.5 mM on the aqueous phase) of the inhibitors NH_4SCN, $NaNO_2$ and HQ with a 'constant' initial initiator concentration (AIBN or AMBN) at 4 mM based on monomer. The significant findings include:

1) In comparison to control experiments using AIBN without inhibitor: $NaNO_2$ was found ineffective in preventing new particle nucleation; NH_4SCN was effective but increasingly destabilized the latex particles with increasing size; HQ was unproven with only four steps completed successfully.

2) In terms of kinetics: $NaNO_2$ severely retarded the polymerizatio in the first seeding step and somewhat less in the second, having no effect thereafter; NH_4SCN had no effect on the polymerization kinetics; HQ induced induction periods and retardation of the polymerization rate.

3) Also, the general shape of the conversion time-curves was the same with decreasing initial rates with increasing size up to the fourth and fifth steps of the sequences. This indicated that the polymerization mechanism was similar to the persulfate initi-

225

ated case where radicals enter particles singly. The initiator
efficiency was determined by inference to be less than 15%.

4) AMBN was not found to be visibly different from AIBN in prevent-
ing nucleation.

5) The AMBN/HQ combinations produced monodisperse latexes up to
2.45 μm without generating significant quantities of small par-
ticles. The polymerization rate was retarded, however. Induc-
tion periods were found to decrease with increasing particle size
indicating an interfacial effect. The conversion histories were
similar to previous findings but with somewhat lower rates than
the AIBN analogues because of the lower decomposition rate.

3.6 Conclusions

A previously developed seeding method was used to study the
effect of successive seeding on the surface charge of 'monodisperse'
polystyrene latexes prepared using sodium lauryl sulfate emulsifier
and potassium persulfate initiator. The surface charge density (weak
+ strong acid groups, $\mu C/cm^2$) increased with both particle size and
initiator concentration. Particles were grown in three successive
steps from a 0.19 μm seed to 0.3, 0.45, and 0.70 μm, while the in-
itiator concentration was varied from 1.3 to 9.5 mM (on aqueous
phase). The initiator efficiency was estimated to be as low as 0.25
for these polymerizations. This could not be further verified
through kinetic measurements in the LUMLR because the specified
monomer/polymer ratios exceeded the equilibrium swelling ratios
under the conditions of the experiments. The recipe formulations
also did not extend to the desired larger particle sizes (>1 μm).

226

A more structured recipe formulation method was developed in which the emulsifier surface coverage (Aerosol-MA) was maintained constant throughout successive seeding experiments. The adsorption isotherm was constructed in order to accomplish this. Experiments were conducted to test the limits of emulsifier coverage required to maintain monodisperse latexes up to 1.7 μm (6 steps). Swelling ratios and solids contents were kept constant at 2/1 and 30%, respectively. Particles having a fractional surface coverage of 0.13 or less were unstable in 24 hour bottle polymerizations, while a coverage of 0.18 led to new crop generation during the six-step sequence. These polymerizations were initiated using persulfate. Similar sequences using AIBN initiator with $NaNO_2$ inhibitor showed reduced nucleation of small particles with a surface coverage of 0.23.

Polymerization kinetics were determined for successive seeding experiments at low surface coverage (0.08 and 0.04) through use of the LUMLR prototype dilatometer. The controlled low shear rate with relatively efficient mixing was used to obtain stable latexes. Monodisperse latexes above 1 μm were not successfully prepared using persulfate initiator due to new crop generation. The polymerization kinetics, however, were found to span much of the transition region from emulsion to 'bulk' kinetics characterized by a change from direct dependence to near independence of the polymerization rate on the number of particles (and particle diameter). Each polymerization was characterized by an increasing $\bar{n}$ with conversion due to the gel effect while the overall polymerization rates decreased, with decreasing difference, as the particle size increased. The initiator

227

efficiency (absorption) was found to decrease linearly with the decreasing available surface area, suggesting that the collision theory of radical absorption was applicable.

Reduction in the amount of nucleated particles was sought through investigation of various oil phase initiator/aqueous phase inhibitor combinations. Hydroquinone in combination with AMBN proved to be the most effective in reducing nucleation without causing flocculation. 'Monodisperse' latexes were prepared up to 2.45 μm using these together with 15% coverage by Aerosol-MA emulsifier. NH_4SCN was found to have a strong electrolyte effect in destabilizing the particles while $NaNO_2$ was rather ineffective in reducing aqueous phase polymerization. In general, the polymerization kinetics for oil phase initiation were similar to the aqueous phase case. The initiator efficiency, however, was determined to be less than 0.15 in the case of AIBN and AMBN. Hydroquinone induced both induction periods and polymerization retardation while $NaNO_2$ retarded the kinetics at small particle sizes indicating an interfacial effect. NH_4SCN had no apparent effect on the polymerization kinetics. These experiments confirmed that the kinetic transition between emulsion and bulk polymerization was complete by the fifth seeding step (particle size 1.19 μm, 2/1 monomer/polymer ratio) in which $\bar{n} > 10$ (Case 3). This was true provided that no changes in the interfacial characteristics between the particle an aqueous phase occurred at any step in the sequence.

CHAPTER 4

MODELING OF SUCCESSIVE SEEDING OF MONODISPERSE LATEXES

4.1 Introduction

The seeding technique is regularly applied in studying the var-

ious kinetic mechanisms associated with the emulsion polymerization

of styrene and other monomers. When monodisperse latexes are grown

to large size, without generation or loss of particles, the kinetic

analysis is greatly simplified. Nevertheless, complexities remain

which to date are not fully understood, particularly the effects of

increasing conversion on the various process rate constants. Succes-

sive seeding has long been used industrially to prepare monodisperse

latexes over a wide size range (0.2 - 2.0 um) but little has been pub-

lished concerning the nature of the process and the kinetics associ-

ated with such a sequence of size build-ups. The previous chapter

described the kinetics obtained for seed sequences performed using

monodisperse polystyrene seed latexes under similar conditions. The

chief variables were particle size and number, and the initiator/in-

hibitor system.

A mathematical model capable of simulating the conversion his-

tories of a sequence of seeded emulsion polymerization growth cycles

is not only valuable in confirming or elucidating the various kinetic

mechanisms involved in the process but also in modification, optimi-

zation, and scale-up for production. The model described here is a

combination of theoretically derived rate expressions along with more

empirically determined rate 'constants'. The difficulties and limita-

tions of the model will be discussed in conjunction with the predic-

tions made based on the experimental findings reported in Chapter 3.

4.2 A Description of Emulsion Polymerization

The heterogeneous nature of emulsion polymerization introduces a number of complexities beyond those found in the other types of polymerization, namely bulk, solution, and suspension. Not only are certain chemical processes involved but various physical processes involving the two phases and the interface which separates them.

The basic chemical reactions of the free radical chain polymerization are:

1) initiator decomposition

$$I \xrightarrow{\text{k}_d} 2R\cdot$$
$$\text{(initiator)} \quad \text{(initiator radicals)}$$

2) chain initiation

$$R\cdot + M \xrightarrow{\text{k}_i} RM\cdot$$
$$\text{(monomer)}$$

3) propagation

$$R(M)_n^\cdot + M \xrightarrow{\text{k}_p} R(M)_{n+1}^\cdot$$
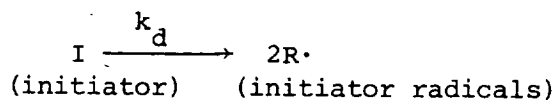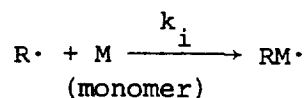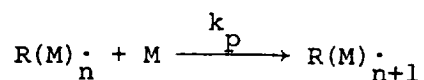
4) termination

    a) by combination

$$R(M)_n^\cdot + R(M)_m^\cdot \xrightarrow{\text{k}_{tc}} R(M)_{n+m}R$$
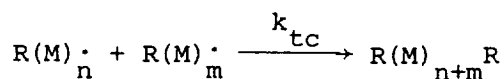
    b) by disproportionation

$$R(M)_n^\cdot + R(M)_m^\cdot \xrightarrow{\text{k}_{td}} R(M)_n + R(M)_m$$

5) transfer

a) to monomer

$$R(M)_n^{\cdot} + M \xrightarrow{\quad k_{fm} \quad} R(M)_n + M\cdot$$

b) to polymer

$$R(M)_n^{\cdot} + R(M)_m \xrightarrow{\quad k_{fp} \quad} R(M)_n + R(M)_m^{\cdot}$$
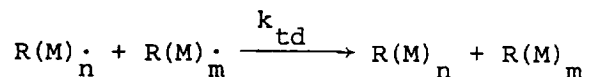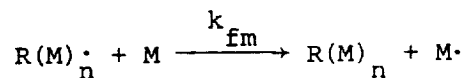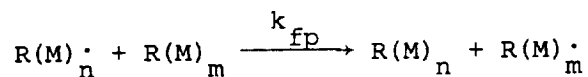
The physical processes involved in emulsion polymerization include the absorption and desorption of free radicals from particles (and micelles), the adsorption of emulsifier at the particle/water interface and its effect on the swellability of the particles, the solubility of monomer in the two phases which can affect the mechanism (locus) of polymerization, and electrostatic (double-layer) effects influencing particle stability.

Most quantitative descriptions of emulsion polymerization begin with the three-interval conceptualization proposed by Harkins [16] describing particle formation (I), particle growth (II), and monomer depletion (III). Initiation takes place in the aqueous phase where a few monomer units are added until the free radical oligomer becomes surface active and adsorbs onto a particle. Polymerization and termination occur primarily in the particle phase. The basic feature which distinguishes emulsion polymerization from the other types is the segregation of the growing polymer radicals by the interposed aqueous phase. This allows for high polymerization rates together with high molecular weight polymer production which is uncharacteristic of the others. Therefore, any attempt to model the emulsion

231

polymerization process must account for this segregation of growing free radicals.

4.2.1 Radical Balance and Steady-State Approximation

Smith and Ewart [46] derived a differential equation describing the change in the number of particles containing n radicals (N_n) with time:

$$\frac{dN_n}{dt} = \left[\frac{k_t}{vN_A}\right]\left[(n+2)(n+1)N_{n+2} - n(n-1)N_n\right]$$

$$+ \left[\frac{R_{abs}}{N_p}\right]\left[N_{n-1} - N_n\right] + k_{de}\left[(n+1)N_{n+1} - nN_n\right] \tag{4.1}$$

Solution of this equation is generally accomplished by first applying a quasi-steady state assumption (QSSA) which assumes that $dN_n/dt = 0$:

$$\left[\frac{R_{abs}}{N_p}\right]N_{n-1} + (n+1)k_{de}N_{n+1} + (n+2)(n+1)\left[\frac{k_t}{vN_a}\right]N_{n+2}$$

$$= \left[\frac{R_{abs}}{N_p}\right]N_n + nk_{de}N_n + n(n-1)\left[\frac{k_t}{vN_a}\right]N_n \tag{4.2}$$

In these equations R_{abs} represents the total rate of radical entry into the particles, k_{de} the rate constant for radical desorption, v the volume of a single particle, k_t the termination rate constant, and N_a Avogadro's number. The applicability of the steady-state assumption under conditions in which the gel effect is operative (i.e., Interval III) and $\bar{n}$ (the average number of radicals per particle) increases with conversion has been questioned [92 - 94]. It has been argued that the QSSA holds as long as the change in the

232

'equilibrium' value of $\bar{n}$ is slow compared to the rate of establishment of this 'equilibrium' value [32]:

$$\frac{d\bar{n}}{dt} << \frac{R_{abs}}{N_p} \qquad (4.3)$$

Several criteria have been derived by which this can be judged. Gardon [95] determined that the ratio of the termination to propagation rate constant (k_t/k_p) should remain above a certain value estimated from:

$$\frac{k_t}{k_p} \geq 16 \frac{\rho_m}{\rho_p} \phi_m \qquad (4.4)$$

where ρ_m and ρ_p are the densities of the monomer and polymer and ϕ_m the volume fraction of monomer in the particle. Similarly, Ugelstad and Hansen [32] concluded that:

$$\frac{k_t}{k_p} >> \frac{\phi_m \rho_m}{[4(1-\phi_m)\rho_p]} \qquad (4.5)$$

for the QSSA to be valid. These conditions are met for most monomers over nearly the entire conversion range in emulsion polymerization. Nevertheless, at high conversions where both k_t and k_p are decreasing care should be taken so that these criteria are not violated.

4.2.2 Average Number of Radicals per Particle

For a monodisperse latex swollen with monomer (Interval II or III) the polymerization rate (R_p) is given by

$$R_p = \frac{-d[M]_p}{dt} = k_p[M]_p \bar{n} N_p/N_A \qquad (4.6)$$

where $[M]_p$ is the concentration of monomer in the particles. Seeded polymerizations in which the charge of monomer is less than that re-quired to swell the particles to their equilibrium value take place

in Interval III and are characterized by a decreasing $[M]_p$ and constant N_p. k_p is generally considered constant up to high conversion (~80%), thus leaving $\bar{n}$ as the sole unknown in equation 4.6. Solution of the Smith-Ewart recursion expression (equation 4.2) was initially presented for only three limiting cases: $\bar{n} \ll 1/2$, $\bar{n} = 1/2$, and $\bar{n} \gg 1$ [46]. A more general solution was provided by Stockmayer [64] which was further modified by O'Toole [65], leading to:

$$\bar{n} = \left(\frac{a}{4}\right) \frac{I_m(a)}{I_{m-1}(a)} \quad \text{for } 0 < m < 1 \tag{4.7}$$

and

$$\bar{n} = \left(\frac{a}{4}\right) \frac{I_0(a)}{I_1(a)} \quad \text{for } m = 0 \tag{4.8}$$

where

$$a = (8\alpha)^{0.5}$$

$$\alpha = \frac{R_{abs} \, v \, N_A}{k_t \, N_p}$$

$$m = \frac{k_{de} \, v \, N_A}{k_t}$$

$I_m(a)$ is a modified Bessel function of the first kind, and k_{de} the rate constant for radical desorption from a particle. Ugelstad et al. extended this treatment to consider the readsorption of desorbed radicals and terminations in the aqueous phase through

$$\alpha' = \alpha + m\bar{n} - Y\alpha^2 \tag{4.9}$$

where $\quad \alpha' = \dfrac{R_i \, v \, N_A}{k_t \, N_p} \quad$ and $\quad Y = \dfrac{2 \, N_p \, k_t \, k_{tw}}{k_a^2 \, v}$

R_i is the rate of initiation, k_{tw} the rate constant for aqueous phase termination, and k_a the rate constant for free radical absorption. For the case in which desorption and aqueous phase termination are considered insignificant, as is generally assumed for the emulsion polymerization of styrene, $\bar{n}$ can be expressed in the form of a continued fraction:

$$\bar{n} = \frac{1}{2} \quad (1 + \cfrac{2\alpha}{2 + \cfrac{2\alpha}{3 + \cfrac{2\alpha}{4 + \ldots}}}) \qquad (4.10)$$

Mørk and Ugelstad [79] suggested a simple expression for $\bar{n}$ for the case in which desorption and aqueous phase termination are not considered:

$$\bar{n} = (0.25 + \frac{\alpha}{2})^{\frac{1}{2}} . \qquad (4.11)$$

This was shown to differ only as much as 4% from the exact solution. Expression 4.10 was used predominantly in the modeling of the successive seeding experiments. In the event that $\bar{n}$ is less than 1/2 (such as during the heat-up phase of the experiment) an alternate expression for $\bar{n}$ [32] is used:

$$\bar{n} = \frac{1}{2} \left[1 - \exp \left[- \frac{2R_{abs}t}{N_p} \right] \right] \qquad (4.12)$$

Therefore, $\bar{n}$ can be determined at any point in a polymerization provided that R_{abs}, v, k_t, and N_p are known, assuming that $m = 0$ (negligible desorption) and $Y = 0$ (negligible aqueous phase termination). Two of these are readily known from the experimental conditions, v and N_p. R_{abs} and k_t, however, are subject to a great deal of uncertainty.

4.2.3 Gel Effect

The 'gel effect', that stage in a polymerization in which chain entanglements and a decreasing free volume bring about diffusion controlled termination and propagation reactions, has in recent years become the subject of much research with the goal of a mathematical description based on known mechanisms. In emulsion polymerization the auto-acceleration noted in the polymerization kinetics is attributed to the decrease in the termination rate 'constant', as the glass transition is approached, causing an increase in $\bar{n}$ and thus the polymerization rate. Similarly, a decrease in the rate with the conversion approaching a limiting but high value is attributed to a decrease in the propagation rate 'constant'. Both of these phenomena have been related to the reduced diffusivity of the reactive species, either polymer chain or monomer molecule.

The first experessions used to describe the variation of k_t with conversion were empirical realtionships obtained through regression analysis of experimental data from bulk polymerizations [71,73,96]. Applied to emulsion polymerizations these produced much improved modeling results. In order to reduce the empirical nature of k_t, relationships were derived based on diffusivity and its relationship to free volume [74 - 77]. By assuming that k_t varies directly with the polymer diffusion coefficient, D_p, the following relationship was proposed:

$$\frac{k_t}{k_{to}} = \frac{D_p}{D_{po}} = \left[\frac{\bar{M}_{wc}}{\bar{M}_w} \right]^{2\alpha''} \left[\exp A \left[\frac{1}{v_{fc}} - \frac{1}{v_f} \right] \right] \qquad (4.13)$$

where the subscripts o and c denote the properties at zero conversion and that at the critical conversion above which the diffusion coeffi-

236

cient begins to decrease. $\bar{M}_w$ is the weight average molecular weight, v_f the free volume, and α'' and A are constants. The latter has been related to the critical free volume for a polymer segment to 'jump' but, nonetheless, has been used as an adjustable parameter which must be fitted to experimental data. The free volume is computed from:

$$v_f = [0.025 + \alpha_p(T - T_{gp})](1 - \phi_m) + [0.025 + \alpha_m(T - T_{gm})]\phi_m \qquad (4.14)$$

where T is the reaction temperature, T_{gp} and T_{gm} are the glass transition temperatures of the polymer and monomer, respectively, ϕ_m is the volume fraction monomer, α_p is the difference between the coefficient of volume expansion of polymer in the melt and glassy state and α_m is the corresponding difference for the monomer.

An expression analogous to 4.13 has been offered for the propagation rate constant, k_p [75,76]:

$$\frac{k_p}{k_{po}} = \frac{D_m}{D_{mo}} = \exp\left[B\left[\frac{1}{v_{fmc}} - \frac{1}{v_f}\right]\right] \qquad (4.15)$$

where v_{fmc} is the critical free volume below which the propagation reaction becomes diffusion controlled. Polymer molecular weight is not considered to affect the diffusion of the relatively small monomer molecules.

Reasonable agreement between theoretical predictions and experiments have been obtained using equation 4.13, neglecting any variation in molecular weight, and 4.15 for seeded emulsion polymerizations of styrene and methylmethacrylate run under various conditions [76]. Some significant differences were evident, however, in the conversion histories, particularly after the rate maxima to the limiting conversions. Nevertheless, these expressions were tested in attempts to model the

237

successive seeding experiments.

Recently, a series of papers [78] have extensively treated diffusion-controlled reactions in bulk polymerization again based on free volume theory plus entanglement coupling. Four phases of distinctly different polymerization behavior are treated quantatively: I) conventional kinetics; II) gel effect with increasing polymerization rate; III) decreasing polymerization rate; and IV) approach to a limiting conversion with the polymerization temperature being lower than the glass transition temperature of the polymer. Phase III, not considered previously, is attributed to a chain and mobility controlled termination mechanism which accounts for a slow down in the decrease of k_t with conversion. The ideas presented seem intuitively attractive, however, the predictions based on this highly complex treatment appear to be no better than found previously. The authors point out that other possible mechanisms are unaccounted for in their model, such as a decrease in the decomposition rate constant (k_d) of the oil soluble initiator due to similar diffusion limitations.

4.2.4 Radical Absorption

Quite often in simulations of emulsion polymerization the rate of radical absorption, R_{abs}, is simply equated to the rate of initiation R_i. This is done particularly when $\bar{n} \geq 0.5$ which is the case when desorption and aqueous phase termination are negligible. For the seeded emulsion polymerization of styrene at large particle sizes, (>0.2 μm) these conditions are usually assumed to be valid [17,76]. Nevertheless, absorption rates have been of some concern and a description is warranted.

238

Both diffusion theory and collision theory have been used to explain the particle absorption rate of radicals generated in the aqueous phase:

$$R_{abs} = k_a \, [R \cdot]_w \qquad (4.16)$$

where $[R \cdot]_w$ is the concentration of radicals in the aqueous phase. If absorption is considered to be irreversible (large particles) and diffusion controlled, Fick's first law gives for monodisperse particles:

$$k_a = 2\pi \, D_w \, N_p \, d \qquad (4.17)$$

where D_w is the diffusion coefficient for radicals in water, and d the particle diameter [32]. However, more often the rate of radical absorption is assumed to be proportional to the total surface available for radical capture [46,47,92]

$$k_a = 4\pi \, C \, N \, d^2 \qquad (4.18)$$

where C is a constant. These different views have yet to be resolved.

4.2.5 Rate of Radical Production

Whether generated in the aqueous or oil phase the rate of radical production is given by:

$$R_i = \frac{-d[I]}{dt} = 2f \, k_d \, [I] \qquad (4.19)$$

where k_d is the decomposition rate, [I], the initiator concentration, and f the initiator efficiency (the fraction of the initiator radicals which initiate polymer chains). The initiator concentration is therefore:

239

$$[I] = [I]_0 \exp\left[-\int_0^t f \, k_d \, dt \right] \tag{4.20}$$

and

$$k_d = k_{do} \exp\left(-E_{ad}/RT \right) \tag{4.21}$$

where k_{do} is the frequency factor, E_{ad} the activation energy, R the gas constant, and T temperature. In general, values quoted in the literature for k_{do} and E_{ad} were determined under conditions differing somewhat from actual experimental conditions which injects an unknown degree of uncertainty into any predictions based on them. Moreover, values for f also vary over a wide range, though often assumed to be 1 (or best fit) for use in modeling work.

4.3 Modeling Approach

In order to model the successive seeding experiments performed using the LUMLR prototype dilatometer a number of conditions were pre-set based on the experimental realities. Recipes specifying the weight fraction of monomer, polymer, water, and initiator were computed according to the results of iso-octane extractions of styrene in the swollen latexes and estimated initiator balances. A temperature history was imposed to account for the warm-up period. This was accomplished by curve fitting the first 80 minutes of fluid temperature data recorded in an actual polymerization. The temperature was subsequently held constant at 69.2°C over the remainder of each simulation. The initial reactor volume was set at 98.9 cm^3 as in the LUMLR experiments (offset from 100 cm^3 due to incorporation of larger stirrer paddle). Conversion was calculated both as a fraction and in terms of the total polymer produced so that direct comparisons could be made with all of the data on a single graph.

Integration of the polymerization rate equation (4.6) was accomplished numerically using the Euler method [97] with a one minute step size. $\bar{n}$ was calculated via equation 4.12 ($\bar{n} < 0.5$) or 4.10 ($\bar{n} \geq 0.5$). Various expressions for k_p and k_t were tested in a trial-and-error fashion until 'reasonable' agreement was reached between experiment and theory. The expressions derived from free volume theory were the first tested followed by more empirical expressions obtained directly from the kinetic data.

Once the first step in a given sequence was reproduced through the adjustable parameters (particularly f and $k_t(X)$) the remaining sequence was simulated initially without any further adjustments in the model. When discrepancies were found between model and experimental data, further adjustments were made as in the induction periods found in the cases using oil soluble initiator with inhibitor.

4.4 Successive Seeding with $K_2S_2O_8$ Initiator (SSMLR-5)

The successive seeding of 'monodisperse' polystyrene latexes prepared with potassium persulfate initiator was described in the preceding chapter (Section 3.5.3). The results indicated a decreasing overall polymerization rate with increasing particle size up to 1.19 µm. Surface characterization analysis also suggested a decreasing initiator radical absorption efficiency which was considered as a possible contributor to the kinetic results. Modeling attempts have been limited to the first five steps of the SSMLR-5 sequence. The generation of new crops of particles in the other experiments precluded their usefulness in any modeling study.

241

The polymerization recipes used in the modeling studies of

SSMLR-5 are given in Table 4-1. These data were obtained previously

for the interpretation of the experimental kinetic data. Values for

<u>Table 4-1</u>

<u>Recipes Used in Modeling Studies of SSMLR-5</u>

Step	Seed Diameter (cm) x 10^4	Weight Percent			
		Polystyrene Seed	Styrene Monomer	H_2O	$K_2S_2O_8$
1	0.19	10.00	18.74	71.25	0.0095
2	0.27	9.71	19.95	70.33	0.0117
3	0.39	9.67	19.20	71.12	0.0118
4	0.56	9.65	19.84	70.50	0.0118
5	0.82	9.65	20.00	70.34	0.0115

the kinetic parameters tested in these simulations studies are listed

in Table 4-2, along with other parameters used in the model.

4.4.1 <u>Termination Rate 'Constant'</u>

The simulation of Interval III kinetics in which $\bar{n}$ is dependent

on both particle size and conversion is highly sensitive to the choice

of the precise function used to describe the change in the termination

rate constant. Equation 4.13, based on reduced diffusion through

chain entanglements and reduced free volume has been used with some

limited success but nonetheless suffers from several defficiencies.

Figure 4.1 illustrates various k_t and k_p functions for styrene/poly-

styrene at $70^\circ C$ taken from the literature. The relationship of Friis

and Hamielec describes the entire conversion range through an empiri-

cally derived expression. This was obtained from bulk polymerization

experiments which generally produce polymer of significantly lower

molecular weight in comparison to that produced via emulsion polymer-

Table 4-2

Various Parameters Used in Modeling Studies

for the Styrene/Polystyrene – $K_2S_2O_8$ System

Parameter	Value	Source
M_w, styrene	104.14 gm/gm-mole	
k_{po}	2.2×10^{10} cm^3/gm-mole sec.	[73]
E_{ap}	7.4 kcal/mole	[73]
M_w, $K_2S_2O_8$	270.33 gm-mole	[73]
k_{do}	5.188×10^{16} sec^{-1}	[82]
E_{ad}	33.5 kcal/mole	[82]
f	variable ≤ 1.0	
α_p	0.48×10^{-3} $°C^{-1}$	[76]
α_m	1.0×10^{-3} $°C^{-1}$	[76]
T_{gp}	93.0 $°C$	[75]
T_{gm}	-106.0 $°C$	[76]
A	0.60	[75]
B	0.1275	[76]
$\alpha"$	0	
v_{fc}	0.1387	[76]
v_{fmc}	0.0383	[76]
d_{PS}	$1.0447 - 2.65 \times 10^{-4}$ $T(°C)$ gm/cm^3	[13]
d_S	$0.924 - 9.18 \times 10^{-4}$ $T(°C)$ gm/cm^3	[13]

243
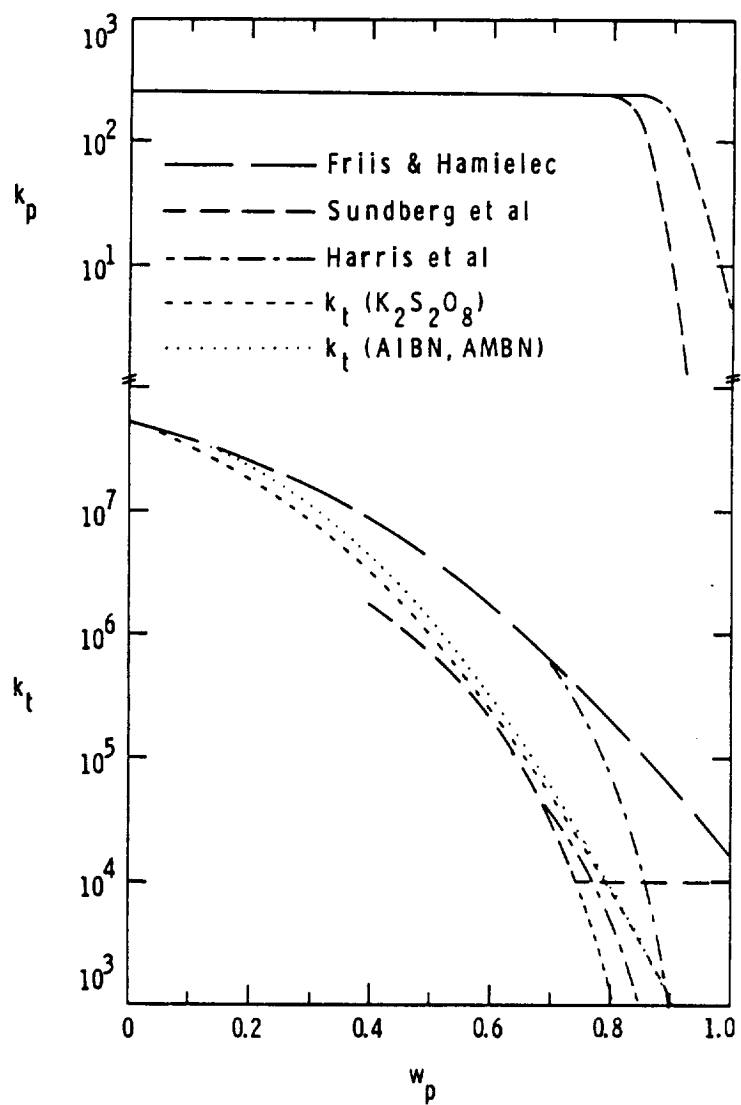
Figure 4.1 k_p (Top) and k_t as a Function of W_p (Weight Fraction Polymer) from Various Sources ($70^\circ C$)

ization. The molecular weight effect (chain entanglements) may, therefore, be of less severity than experienced in emulsion polymerizations resulting in a k_t which is a weaker function of W_p than is actually the case. The other expressions based on free volume considerations without molecular weight effects (i.e. since molecular weight does not change appreciably during the course of a seeded emulsion polymerization) do not cover the entire conversion range and also rely on empirical fitting of A and v_{fc} from data obtained in seeding experiments. It seems reasonable that any $k_t - W_p$ curve should extrapolate to the same k_t value at $W_p = 0$ where there are no molecular weight effects. This is not possible, however, for the expressions given via free volumes. This deficiency along with the sharp decrease (exponential) at high W_p contribute to the undesirability of using this method in the current model. The latter difficulty was countered by Sundberg et al. by assuming that k_t was constant after a certain conversion as illustrated in Figure 4.1. This too did not seem reasonable (although justifiable). The approach adopted in these studies was empirical, much the same as Friis and Hamielec. A k_t function was obtained by using the information gained in the sequence studies (SSMLR-5) and fitting data with a third order polynomial expression:

$$\log k_{t,69.2^\circ C} = C_1 + C_2 W_p + C_3 W_p^2 + C_4 W_p^3 \tag{4.22}$$

The least squares fit values obtained for the coefficients were:

$C_1 = 7.6871; \quad C_2 = -1.475; \quad C_3 = -3.6649; \quad C_4 = -0.4138$

245

(A slightly different function was used to model the polymerizations using the oil soluble initiators, AIBN and AMBN.) The value of k_t at zero conversion (10^{C1}) is 4.86×10^7 1/mole·sec which corresponds to the 5×10^7 liter/mole·sec value obtained by Friis and Hamielec. This expression, also given in Figure 4.1, was used to subsequently obtain all of the modeling results reported for the persulfate initiated sequences in conjunction with the k_p function of Harris et al., likewise shown in Figure 4.1.

4.4.2 Modeling Results

As pointed out previously, the most important variable in modeling the successive seeding of relatively large-particle-size monodisperse latexes is the average number of radicals per particles, $\bar{n}$. An accurate computation of $\bar{n}$ is possible only with an accurate knowledge of R_{abs}/k_t as a function of conversion. The termination rate constant defined in the previous section was determined from the data of SSMLR 5 by fitting a curve through the experimental k_t vs. W_p data, adjusting the position so that it intersected the y-axis at the appropriate k_t value.

As a starting point, the five-step sequence was modeled assuming f to be constant (0.68) throughout (i.e., particle size and number being the variables). The rate of absorption was assumed to be equal to the rate of initiation. A good match between the model and experimental conversion histories was obtained for the first step alone. The remaining curves lay nearly superimposed on each other indicating overall polymerization rates much higher than found experimentally. These results were not unexpected in view of the other experimental

246

results obtained via surface titrating indicating a decreasing initiator efficiency with increasing particle size. This efficiency, however, is more an absorption efficiency rather than the efficiency of SO_4^- radicals initiating polymer chains (f).

A decreasing radical absorption efficiency with increasing particle size was incorporated in the seed sequence based on the experimental findings (3.5.3.2). The resulting conversion histories are given in Figure 4.2 for comparison with the experimental results. The first three steps were modeled using the same efficiencies estimated from experiment while the last two steps used somewhat larger values (0.35 compared to 0.20). A marked improvement in model-experiment agreement was obtained with a correct relative placement of the conversion histories. Nonetheless, the predictions suffered from a number of dificiencies: 1) predicted overall rates of polymerization were increasingly lower than the experimental findings with increasing particle size; 2) initial polymerization rates in the last two steps were forced to be higher in the model than found experimentally in order to obtain some reasonable agreement; and 3) the predicted rates at high conversion (at $R_{p\ max}$) decreased with increasing particle size while experimentally little difference in the R_p values at this stage were noted. In other words, the concept of a decreasing radical absorption efficiency with increasing particle size appeared to be legitimate and yet was not sufficient to obtain good agreement between the model and experimental findings.

The predicted conversion histories given in Figure 4.2 were obtained based on the assumption that a given fraction (absorption effi-

SSMLR - 5 $K_2S_2O_8$

$0.19 \xrightarrow{1} 0.27 \xrightarrow{2} 0.40 \xrightarrow{3} 0.57 \xrightarrow{4} 0.82 \xrightarrow{5} 1.19$ um

#	f
1	0.68
2	0.50
3	0.44
4	0.35
5	0.35

Conversion, grams polystyrene

Time, minutes
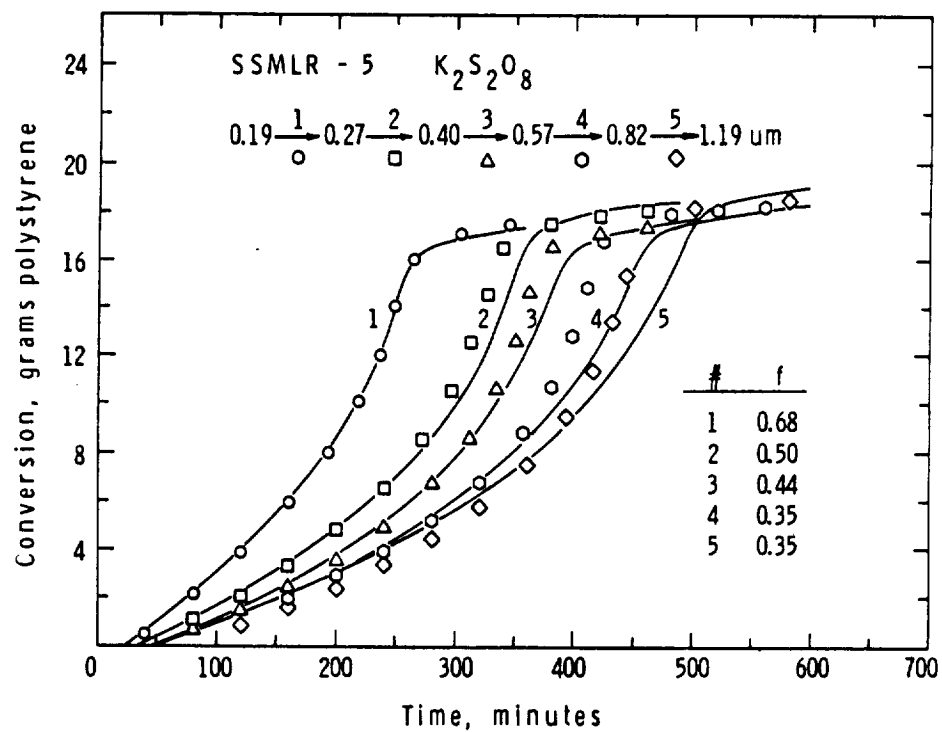
Figure 4.2   Comparison of Model Predictions (Solid Lines) with Experimental Results for SSMLR 5. Model Assumes the Absorption Efficiency is a Function of Particle Size Alone

248

ciency) of the decomposed initiator resulted in polymerization within

the particles. Knowledge of this fraction was dependent upon experi-

mental data regarding the quantity of surface sulfate groups found on

the particles. In other words, the model had no provision for pre-

dicting these efficiencies. These results, however, suggested that

the absorption efficiency may be explained by the collision theory

of absorption. Equations 4.16 and 4.18 were subsequently applied in

the model to compute the absorption rate as a function of time and

particle size. To do this, the value of C was first estimated to be

4.078×10^{14} cm/mole·sec by obtaining a fit to the first step in the

SSMLR-5 sequence. Table 4-3 lists the values obtained for the absorp-

tion rate constant, k_a, as a function of the seeding step. Also in-

cluded is a comparison of the experimentally determined absorption

efficiencies with the normalized rate constants forced to matching

values for the first seeding step. This is admittedly a rough com-

comparison but, nonetheless, the agreement is rather good.

Table 4-3

k_a as a Function of d, the Final Particle Diameter,

from Collision Theory

Step	d (cm	k_a (sec^{-1})	(k_a (sec^{-1})	f
1	0.274×10^{-4}	1.667×10^{-4}	0.68	0.68
2	0.390×10^{-4}	1.139×10^{-4}	0.47	0.50
3	0.570×10^{-4}	7.940×10^{-5}	0.32	0.44
4	0.820×10^{-4}	5.490×10^{-5}	0.22	0.21
5	1.190×10^{-4}	3.780×10^{-5}	0.15	0.20

Predictions from the revised model are again compared to the

experimental findings as shown in Figure 4.3. The agreement is quite

249
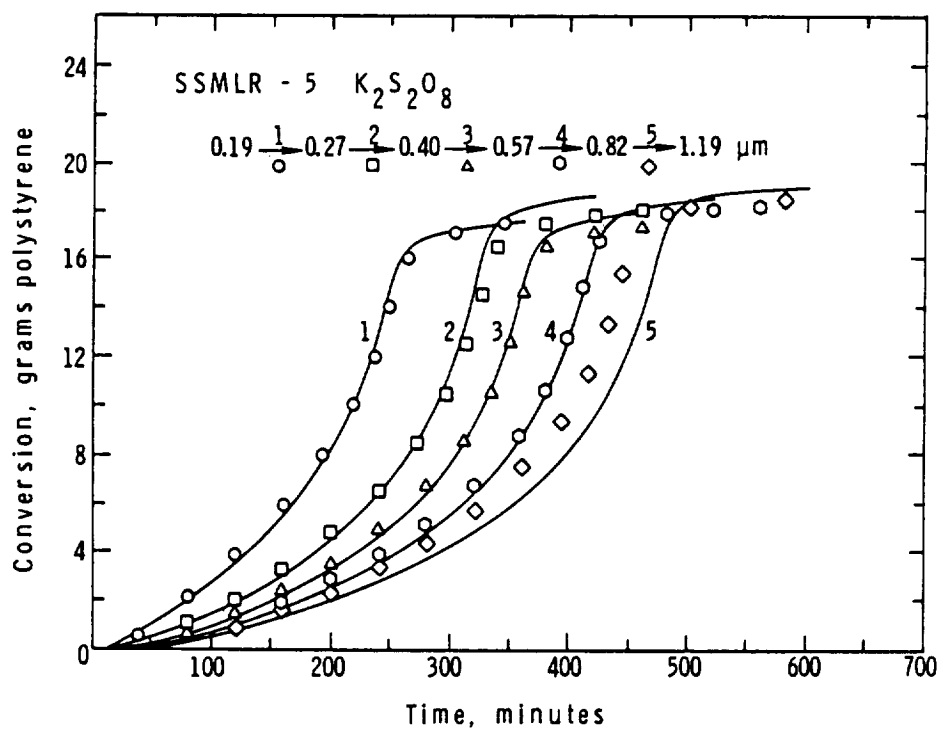
Figure 4.3   Comparison of Model Predictions (Solid Lines) with Experimental Results for SSMLR 5.   Absorption Rates Calculated from Collision Theory

close for the first four seeding steps while the last step indicates a longer predicted conversion history than found experimentally. This difference may be attributed to the effect of new crop generation in the polymerization, as illustrated in the preceding chapter (Section 3.5.3.2, Figure 3.15). Limiting conversions are generally a few percent lower than predicted from the k_p expression used from free volume theory [75]. Further adjustments (or another empirical expression) could improve the fit here.

It should be emphasized that the improvement in the model comes by considering that the radical absorption process is dependent on the number and size of the particles and the concentration of free radicals in the aqueous phase. Often this is not done in simple modeling studies of seeded emulsion polymerization. The differences in the absorption rates are illustrated in Figure 4.4 for the cases where $R_{abs} = f'R_{init}$ and $R_{abs} = k_a[R']_a$. The former method assumes the absorption efficiency factors as given previously. In either case the absorption rate should pass through a maximum, decreasing as the initiator supply is depleted. However, this is not observed over the course of the conversion histories for the case in which $R_{abs} = k_a[R\cdot]_w$. The buildup of radicals in the aqueous phase over the course of the polymerization causes the absorption rate to increase relatively slowly and appear to level out (before decreasing). This can account for the shape of the conversion histories obtained via experiment. It should be cautioned that aqueous phase termination may play a role in these kinetics, particularly in view of this proposed buildup of radicals.

251
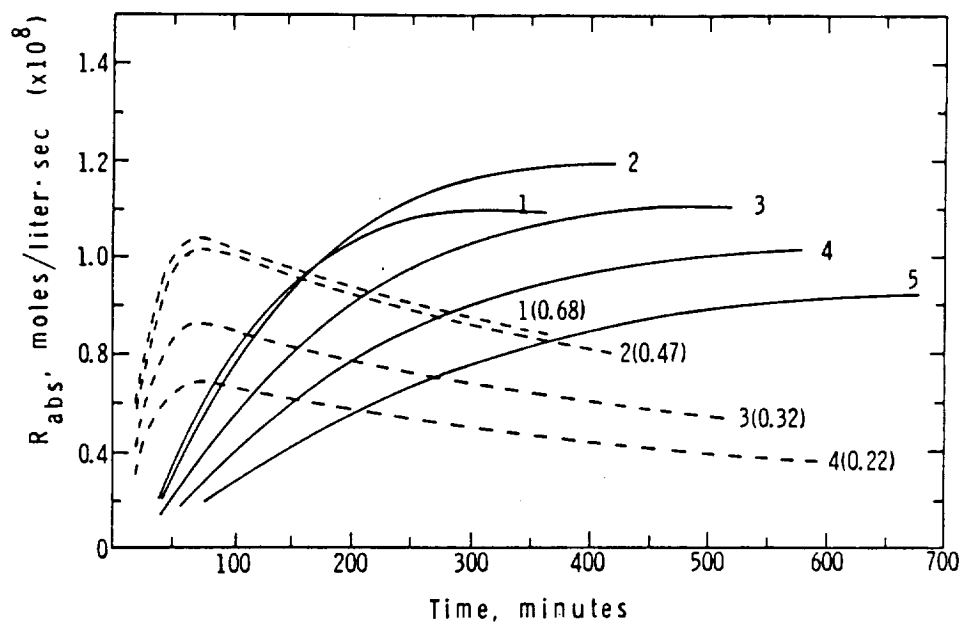
Figure 4.4   Comparison of Absorption Rates with Seeding Step Based on Collision Theory (Solid Lines) and $R_{abs} = f'R_{init}$ (f' given in Parentheses).

252

The area under a given curve in Figure 4.4 represents the quantity of free radicals absorbed by the particles during the course of the polymerization. From this, a theoretical surface charge density can be calculated assuming that all radicals have a charge (e.g., SO_4^-). A comparison between predicted and experimental values is given in Table 4-4. The predictions are significantly different for sequence steps 4 and 5. Step 5 is somewhat larger simply because the predicted conversion history is longer than found experimentally. Nonetheless, this cannot explain the whole difference. Experimental errors in the surface analysis are also conceivable, particularly since the available sample for analysis was small along with relatively low surface charge densities. Also, the possibility of hydrolysis of sulfate groups to hydroxyls or buried groups can lead to lower surface charge densities, thereby affecting the analysis. Further research is required in this area to resolve these discrepancies.

Table 4-4

Comparison of Predicted and Experimentally Determined Surface
Charge Densities for the SSMLR-5 Sequence

		Surface Charge Density uC/cm^2	
Step	X_M	σ_{exp}	$\sigma_{predicted}$
1	95.3	0.61	0.69
2	95.0	0.56	0.67
3	94.6	0.67	0.78
4	94.8	0.49	0.93
5	94.6	0.67	1.20

Other kinetic information from the model can also be compared readily with the experimental data. Figure 4.5 shows the agreement obtained for $\bar{n}$ as a function of particle size and conversion (fraction

253
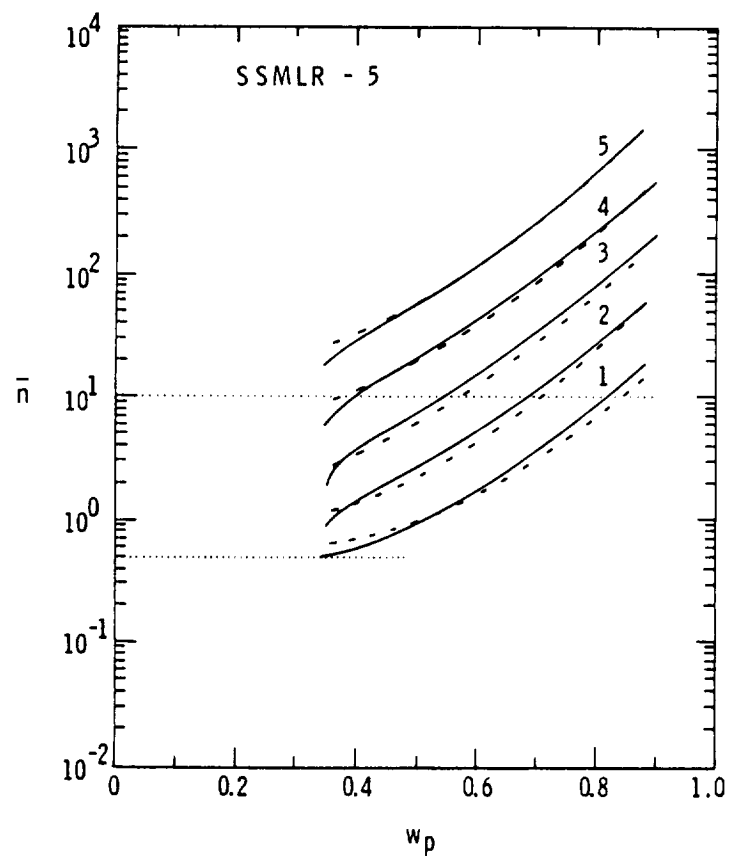
Figure 4.5 Comparison of Predicted Values of $\bar{n}$ (Solid Lines) vs. Experimental as a Function of Particle Size and Fraction Polymer (W_p) for SSMLR 5

polymer). The dashed lines represent the data as presented in the preceding chapter (Section 3.5.3.5, Figure 3.22). The closeness of the match is expected from the agreement already seen in the conversion results. Small differences can be noted, however, which are reflected in the conversion-time predictions. For example, slightly smaller or larger values of $\bar{n}$ are reflected in observably lower or higher polymerization rates, respectively.

These results suggest that in the case of aqueous phase initiation, the kinetic transition from emulsion to true bulk polymerization cannot be achieved. As long as the rate of radical absorption is a function of the particle size and number, the polymerization rate will not become totally independent of these variables. Therefore, even if $\bar{n}$ exceeds a value of 10, the criterion set by Friis and Hamielec [71], the transition to bulk kinetics is not realized. This is a direct consequence of the heterogeneous nature of the emulsion polymerization system in which free radical initiation occurs in the aqueous phase with polymerization in the oil phase. The difficulty in further verification of this observation lies in the experimental preparation of monodisperse polystyrene latexes above 1 μm using aqueous phase initiator without the generation of a new crop of particles or excessive coagulum.

4.5 Successive Seeding with AIBN and AMBN Initiators (SSMLR-9 and 11)

Much of the kinetic results described in Chapter 3 were obtained using the oil soluble initiators AIBN (2,2'-azobisisobutyronitrile) and AMBN (2,2'-azobis-(2-methylbutyronitrile)). These results appeared quite similar to those reported using persulfate. The overall

255

polymerization rates decreased with increasing particle size approaching independence on particle size and number. The kinetic transition between emulsion and bulk was considered nearly complete by the fifth seeding step.

Oil soluble initiators are rarely used in studies of emulsion polymerization, being confined primarily to suspension, solution, and bulk polymerization. The mechanism of emulsion polymerization using these initiators is not all that clear. A striking similarity in kinetic results, however, has been noted for oil and aqueous phase initiation in emulsion polymerization in these studies and others [69]. To account for this it is assumed that for small particles, a radical must be able to escape from a particle since two growing radicals cannot occupy the same small volume without immediate mutual termination. This is particularly obvious for cases in which $\bar{n} < 2.0$ such as Steps 1 and 2 in SSMLR 9 and 11 (see Figures 3.27 and 3.40). Lower initiator efficiencies in emulsion (<<0.5) when compared to bulk have been attributed to this necessity of radical escape from a particle [99]. This should not be the case, however, for large particles under conditions in which $\bar{n}$ exceeds 2. This implies that the efficiency should be greater for larger particles particularly when bulk kinetics become applicable. Initiator efficiencies in the neighborhood of 0.5 are expected for bulk polymerization, this being explained by the "cage" effect [100].

In view of the uncertainties with regards to these kinetic mechanisms, an empirical approach was adopted in these modeling studies. The efforts described here were centered on determining whether the

256

the same k_t function, as used in the modeling of the persulfate init-
iated polymerizations, was applicable to these polymerizations and
what values for the initiator efficiencies would result in reasonable
fits of the experimental data. The first five steps of sequences
SSMLR 9 and 11, using AIBN and AMBN initiators without any inhibitors,
were emphasized.

4.5.1 Modeling Results

In these studies the initiator was assumed to be distributed
homogeneously throughout the oil/particle phase. In other words, par-
titioning and interfacial effects were not considered. The recipes for
both sequences SSMLR 9 and 11 are given in Table 4-5 with a list of
the additional parameters in Table 4-6. The same set of equations was
used in modeling the conversion histories with the exception of R_{abs}
which was set equal to R_i (since no real absorption process was con-
sidered). The efficiency of the initiator species was determined in
a trial-and-error fashion from the best fit of the model to the ex-
perimental data. It was asserted in the preceding chapter (Section
3.5.4) that the efficiencies were below 0.15 by inference from the
back-calculated k_t function (f assumed equal to 1.0). This was used
as a starting point.

Good agreement between model predictions and experimental data
for sequences SSMLR 9 and 11 could not be readily achieved with the
k_t function used previously to model the persulfate initiated sequence
without unjustifiably imposing varying induction periods on the model.
This indicated that the k_t function yielded higher polymerization
rates (particulary initially) than were found experimentally (k_t too

Table 4-5

Recipes Used in Modeling Studies of SSMLR 9 and 11

Step	Seed Diameter (cm) x 10^4	Weight Percent			
		Polystyrene Seed	Styrene Monomer	H_2O	AIBN
9-1	0.19	9.80	19.32	70.87	0.0142
9-2	0.27	9.62	19.44	70.96	0.0150
9-3	0.39	9.70	19.35	71.93	0.0151
9-4	0.57	9.66	19.74	70.59	0.0149
9-5	0.82	9.66	19.73	70.59	0.0147
					AMBN
11-1	0.19	9.71	19.49	70.78	0.0165
11-2	0.27	9.68	19.92	70.39	0.0193
11-3	0.39	9.66	19.85	70.47	0.0191
11-4	0.57	9.64	19.97	70.37	0.0189
11-5	0.82	9.63	20.11	70.24	0.0186

Table 4-6

Additional Parameters for Modeling Studies using AIBN and AMBN Initiators

Parameter	Value	Source
M_w, AIBN	164.00 gm/gm-mole	[17]
k_{do}	2.6141×10^{14} sec^{-1}	[17]
E_{ad}	29.50 kcal/mole	[17]
f	0.100	this study
M_w, AMBN	192.26 gm/gm-mole	[98]
k_{do}	5.334×10^{15} sec^{-1}	[98]
E_{ad}	31.80 kcal/mole	[98]
f	0.105	this study

low at low conversions). Lower polymer molecular weights produced with use of the oil soluble initiators as compared to persulfate could account for this difference. A modified k_t function was then applied which compensated for this effect. The two functions are compared in Figure 4.1. The differences are small but significant since $\bar{n}$ (R_p) is quite sensitive to this function. The coefficients of the modified k_t function were: $C_1 = 7.6666$, $C_2 = -0.2527$, $C_3 = -5.7867$, $C_4 = 0.4118$.

Model predictions are compared to the experimental data of SSMLR 9 in Figure 4.6. These were obtained using a single value of 0.100 for the initiator (AIBN) efficiency. In Steps 1 and 2 the model diverged somewhat from the data after about 50% conversion. These differences were in opposite directions and thus not likely resolved by any single solution. Nonetheless, the fit was good in the remaining steps confirming that the assumptions made in the model were justified. This indicated that the kinetic transition from emulsion to bulk kinetics can indeed be breached with use of oil soluble initiators as opposed to water soluble ones.

In modeling the kinetics for sequence SSMLR 11 initiated with AMBN, another difficulty was encountered. In all cases the predicted limiting conversion exceeded that found experimentally by a margin as great as 5%. In the model this is controlled by the k_p function. It is not likely that this function should change merely by changing the initiator. One other possible consideration is that the efficiency of the initiator changes with conversion. Since the initiator fragments must diffuse a certain distance to encounter a monomer unit it

259
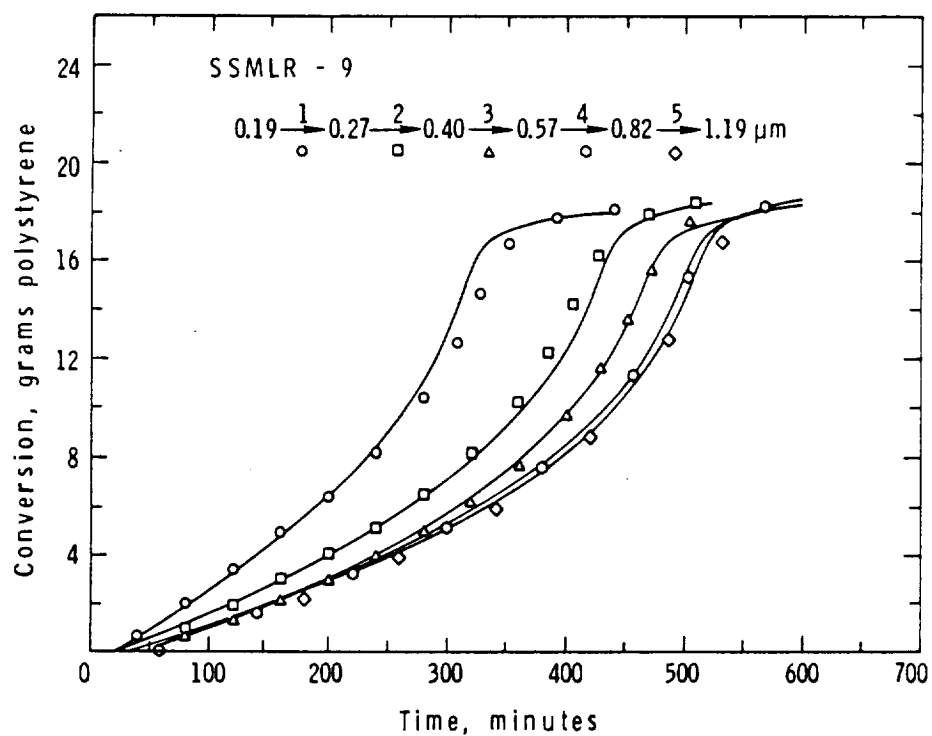
Figure 4.6   Comparison of Model Predictions (Solid Lines) with
Experimental Results for SSMLR 9, using AIBN Initiator

would seem likely that this would be affected also by the state of the system (i.e., whether rubbery or glassy). If diffusion is limited by the glassy polymer network then the possibility of radical recombination may be enhanced thereby effectively reducing the efficiency of the initiator or even the decomposition rate. The free volume approach can be used to characterize a change in k_d with conversion in a manner analogous to the treatment of k_p:

$$\frac{k_d}{k_{do}} = \frac{D_i}{D_{io}} = \exp\left[B_i\left[\frac{1}{v_{fic}} - \frac{1}{v_f}\right]\right] \qquad (4.23)$$

where D_i represents the diffusion coefficient of the initiator radical fragments and v_{fic} the critical free volume below which decomposition becomes diffusion controlled. Values of $B_i = 0.15$ and $v_{fic} = 0.077$ were used in the model. The latter corresponds to a W_p of 0.7 obtained by noting the point where the polymerization rate begins to decrease. Applying this expression resulted in the model predictions shown in Figure 4.7. For comparison, the predictions without equation 4.23 were included. The improvement in the predicted vs. experimental results was significant. The value of f for AMBN was 0.105 for this sequence, being nearly the same as found for AIBN. Note that the overall agreement is good with the exception of the second step of the sequence which shows a lower overall polymerization rate. These results are also reflected in the $\bar{n}$ vs. W_p relationships in Figure 4.8. The model (solid lines) follows fairly closely to the experimental data (dashed lines) up to $W_p = 0.85$. This is the point at which k_p begins to decrease. Note in Step 2 that the low predicted values of $\bar{n}$ vs. the experimental at low conversions is the source of

261
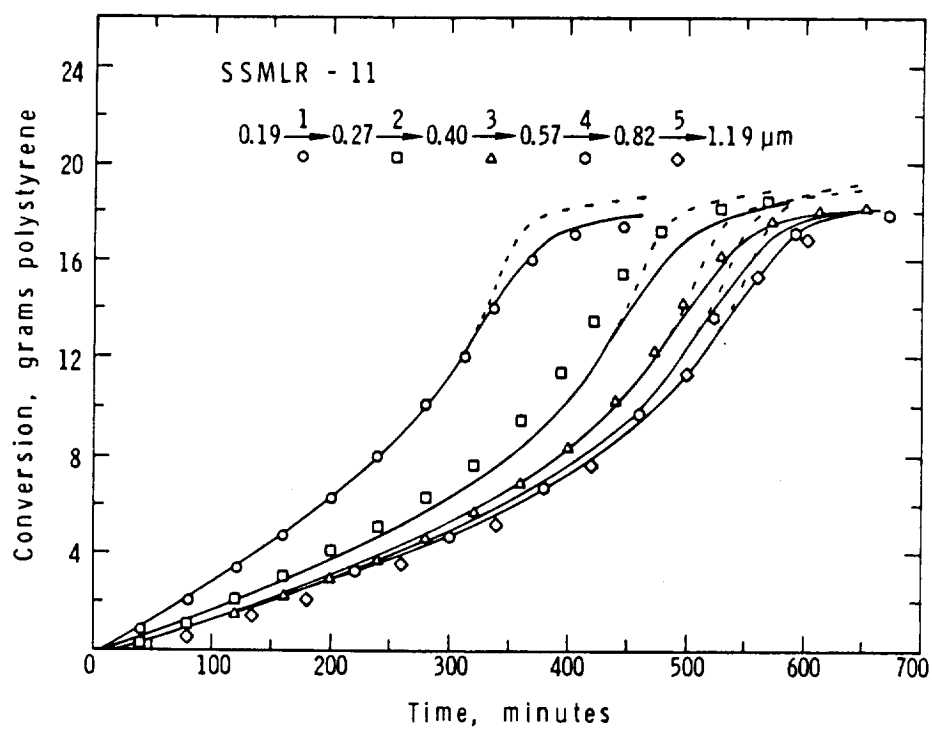
Figure 4.7   Comparison of Model Predictions (Solid Lines) with
             Experimental Results for SSMLR 11, using AMBN Initiator.
             Dashed lines without correction for k_d.

262
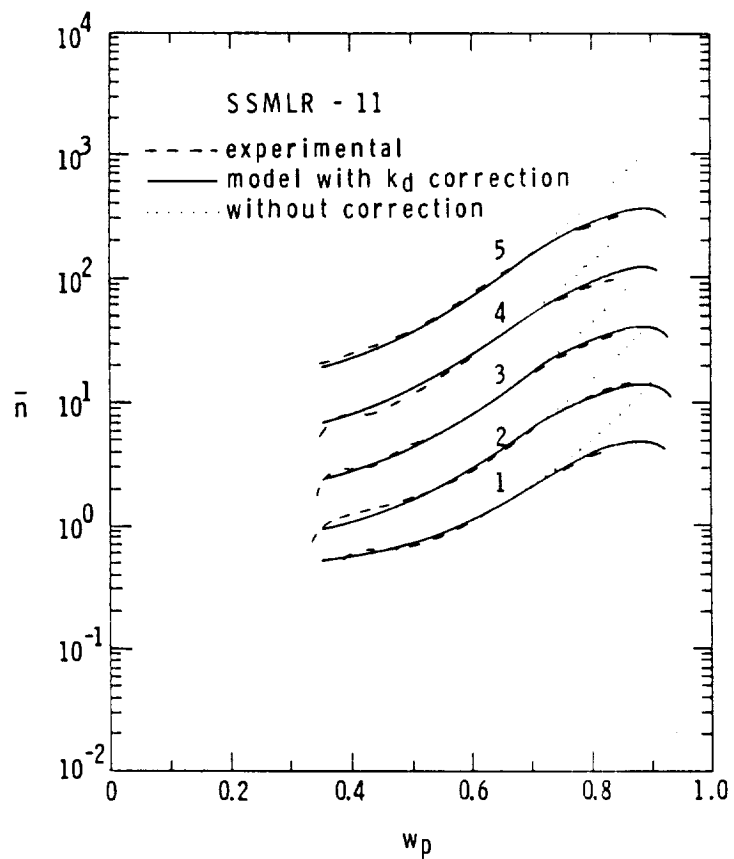
Figure 4.8 Comparison of Predicted Values of $\bar{n}$ vs. Experimental as a Function of Particle Size and Fraction Polymer (W_p) for SSMLR 11

divergence seen in the corresponding conversion history.

The correction for a reduced k_d applied in the preceding for AMBN was not found to be necessary for a reasonable fit of the data in the AIBN sequence. If this is accepted as a reasonable explanation for the phenomenon then there must be a difference between the two systems which could explain the observed behavior. One possibility is that the diffusivity of the isobutyronitrile free radical formed from the decomposition of AIBN is similar (or greater than styrene monomer and thus is affected over the same conversion range while the addition of a methyl group as on the 2-methylbutyronitrile free radical may bring about a reduced diffusivity at a lower conversion. This explanation seems reasonable but remains speculation requiring further investigation.

4.6 Discussion

The results obtained for the three sequences described above illustrate some basic differences between aqueous and oil phase initiation in seeded emulsion polymerization of large-particle-size latexes. For particles which can sustain more than one growing radical at a time, the polymerization rate is primarily governed by the rate of radical appearance in the particle whether by absorption from an external aqueous phase or by production directly within the particle. In the former case the rate of absorption is controlled by the total surface area available (collision theory) and the aqueous phase radical concentration. Initially, therefore, the absorption rate is proportional to the surface area which, in a seed sequence of constant solids content, is proportional to d^{-1}. For large particles $\bar{n}$ ($\gg 1$)

264

is proportional to $(R_{abs} \, v/N_p)^{\frac{1}{2}}$. In a sequence v/N_p is proportional

to d^6 and therefore, $\bar{n}$ is proportional to $d^{5/2}$. This corresponds to

the value found experimentally by Vanderhoff et al. in competitive

growth experiments [21,22,24] and later explained theoretically by

Poehlein and Vanderhoff [27]. To pursue this further, the rate of

polymerization in a sequence is proportional to $\bar{n}N_p$ and, therefore,

initially to $d^{-\frac{1}{2}}$ ($\bar{n} \gg 1$). This of course is not valid throughout a

polymerization since R_{abs} is a function of $[R\cdot]_w$ which changes with

time. In oil phase initiation $\bar{n}$ is simply proportional to $(v/N_p)^{\frac{1}{2}}$

or d^3 ($\bar{n} \gg 1$) and therefore, the polymerization rate is independent

of particle size. These relationships apply when $\bar{n}$ is large (>10)

due to large particle size and/or high conversion. For small particle

size latexes with case 2 kinetics, however, $\bar{n} = 1/2$ and the polymeri-

zation rate is proportional to N_p or d^{-3} for a sequence. The region

in between, therefore, represents a kinetic transtion between the

two dependencies:

1) aqueous phase initiation,

$$R_p \, \alpha \, d^{-3} \xrightarrow{\text{increasing particle size}} R_p \, \alpha \, d^{-\frac{1}{2}}$$

2) oil phase initiation,

$$R_p \, \alpha \, d^{-3} \xrightarrow{\text{increasing particle size}} R_p \neq f(d)$$

The second case represents the transition from emulsion to bulk

polymerization kinetics (i.e., independence from particle size and

number) while the first does not. These transitions can be further

illustrated by making use of the models in simulating successive seed-

ing experiments. Figures 4.9 and 4.10 illustrate conversion histories

which represent ideal sequences performed using $K_2S_2O_8$ and AIBN initiators, respectively. The initial seed size was 0.063 μm for each sequence, with constant 2/1 monomer/polymer ratios and initial iniator concentrations throughout each sequence. Two different $K_2S_2O_8$ concentrations are represented in Figure 4.9, these being the counterparts to the SSMLR 4 and 5 experiments (1.0 and 0.5 mM, respectively). These predictions are quite similar to the experimental findings (see Figures 3.14 and 3.16). Note that the predictions are nearly the same for the first three steps of all three cases due to the proximity to case 2 kinetics. Divergence of results increases with each step, thereafter. It is clear that in the case of AIBN the transition from emulsion to bulk kinetics is nearly achieved by the eighth seeding step (final diameter = 1.19 μm). For persulfate, there is likewise a transition between case 2 and case 3 kinetics but the absorption rate dependency on particle size precludes the possibility of true bulk polymerization kinetics. The overall polymerization rate continually decreases with particle size. These differences can also be seen in an R_p vs. N_p plot as given in Figure 4.11. For AIBN, the transition is represented by the shift in the slope from one to zero. This is particularly evident at low conversion (W_p = 0.4). For persulfate the shift is from one to some limiting slope which is dependent upon conversion.

These results illustrate that the basic difference between oil and aqueous phase initiation in seeded emulsion polymerization derive from the heterogeneous nature of the polymerization system which determines the locus of the initiation reaction.

266

Step	D_{seed}, μm
1	0.063
2	0.091
3	0.132
4	0.190
5	0.270
6	0.390
7	0.570
8	0.820
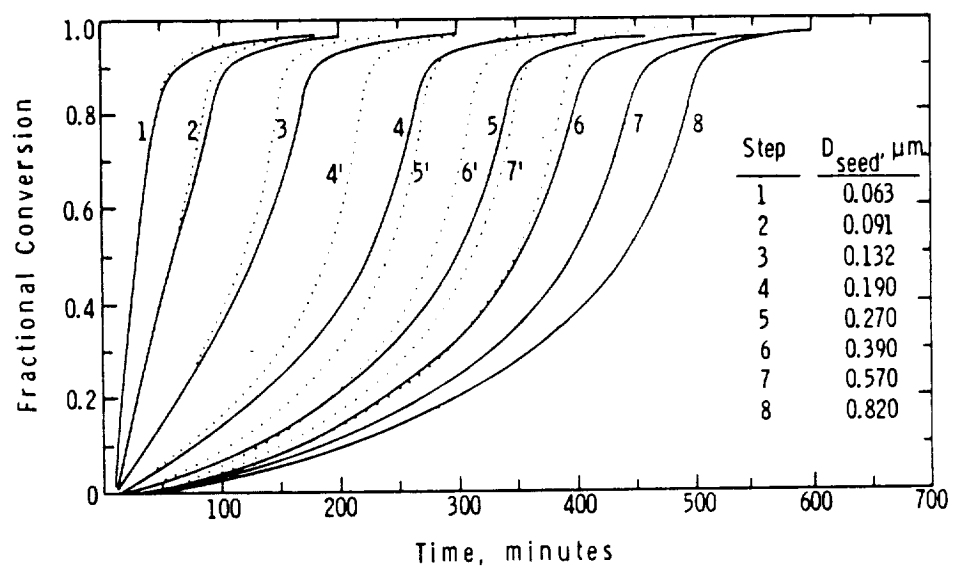
Figure 4.9   Predicted Conversion Histories for the Successive Seeding of Monodisperse Polystyrene Latexes Prepared with M/P = 2.0, 30% Final Solids, and $[K_2S_2O_8]_o$; 0.5 mM (Solid Lines) and 1.0 mM (Dotted Lines)

267

Step	D_{seed}, μm
1	0.063
2	0.091
3	0.132
4	0.190
5	0.270
6	0.390
7	0.570
8	0.820
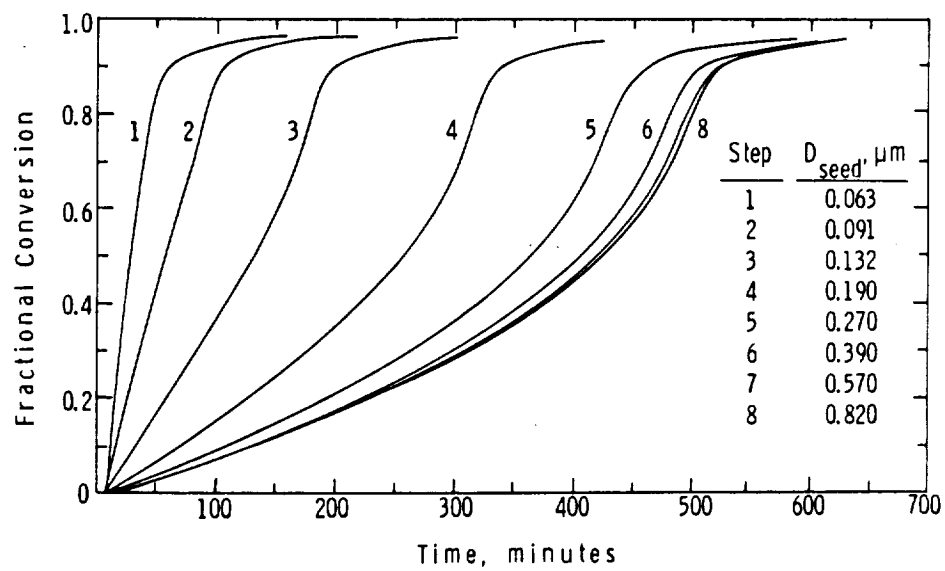
Figure 4.10 Predicted Conversion Histories for the Successive Seed-
ing of Monodisperse Polystyrene Latexes Prepared with
M/P = 2.0, 30% Final Solids and 4 mM (Based on Monomer)
AIBN.

268
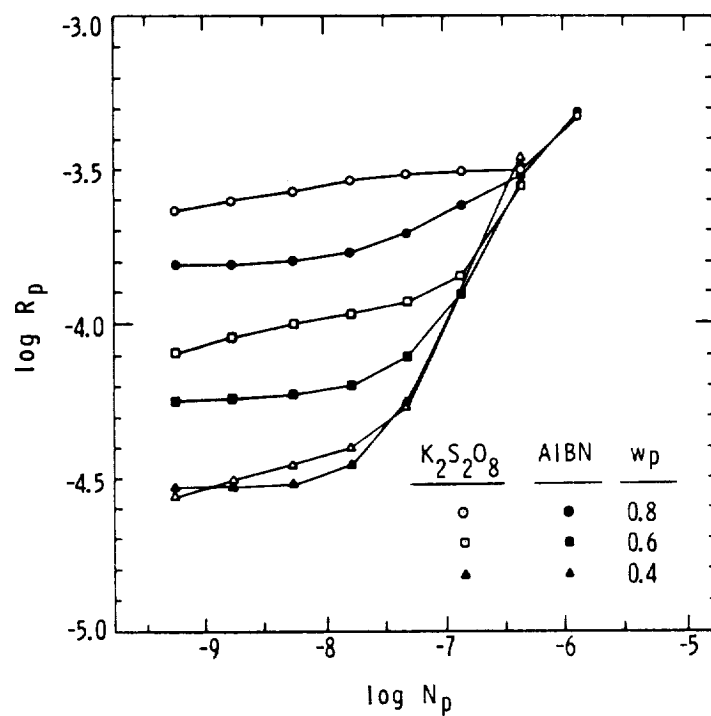
Figure 4.11 log R_p Versus log N_p at the Three Conversion Levels
for $K_2S_2O_8$ (0.5 mM) and AIBN (4 mM) Simulations

4.7 Successive Seeding using Oil Soluble Initiators with Water Soluble Inhibitors

The preceding discussion was limited to cases in which seeded polymerizations were carried out without any inhibitors added to suppress the nucleation of new crops of particles. In Chapter 3 the varying behaviors of three inhibitors, NH_4SCN, $NaNO_2$, and hydroquinone (HQ), were described in terms of their effect on particle nucleation and polymerization kinetics. Reiterating these results, NH_4SCN had no observable effect on the polymerization kinetics through five successive steps but greatly affected particle stability causing much flocculation in the last step. $NaNO_2$ retarded the polymerization in the first seeding step, somewhat less in the second, while having little or no effect on the remaining steps. It did not prevent small particle formation. Hydroquinone caused a more typical response by inducing induction periods and polymerization retardation for all seeding steps. Particle nucleation was also limited by HQ.

In order to accurately model the polymerization kinetics of these systems a number of factors should be known such as the inhibition reaction mechanism and the rate constant for the reaction. These may depend on the locus of the reaction, whether in the oil or aqueous phase, thus requiring a knowledge of the partition coefficient and the behaviors in each phase and perhaps also at the interface between the phases. As stated previously, however, little is known or published concerning these factors for the inhibitors used in these studies. Nonetheless, some conclusions were reached concerning the behavior of these materials based on the experimental data presented in the previous chapter. Since the polymerization kinetics with and

without NH_4SCN were the same, this inhibitor was considered to be present only in the aqueous phase with no partitioning or interfacial effects. One can also infer from this that the presence of radicals in the aqueous phase due to the initiator's limited solubility or desorption from the particles has no significant effects on the polymerization kinetics. A model for this system would be the same as that presented earlier for AIBN alone. The kinetic behavior with $NaNO_2$ inhibitor indicated an interfacial effect which rapidly decreased with increasing particle size. Its effectiveness as an aqueous phase inhibitor (and electrolyte) does not conflict with this idea. Modeling of this system was not pursued due to its uncertain nature and poor polymerization results. Hydroquinone, or its oxidation product benzoquinone, apparently partitions into the oil phase where it acts as an inhibitor and retarder if in relatively large quantities. The induction periods noted for these polymerizations were not always consistant with the amount of HQ added which made any predictive effort difficult without further knowledge of the mechanisms involved. Nevertheless, an attempt was made to model the kinetics of the SSMLR-13 sequence through an empirical approach to the induction period question (i.e., induction periods were chosen based on the experimental data). Figure 4.12 shows the fit of the experimental conversion histories obtained using this approach. The first four steps are represented along with the eighth seeding step, the others being excluded for the sake of clarity. The model was substantially the same as that used for SSMLR 11 with the exception of the imposed induction periods and also a modified k_d function for be-

271
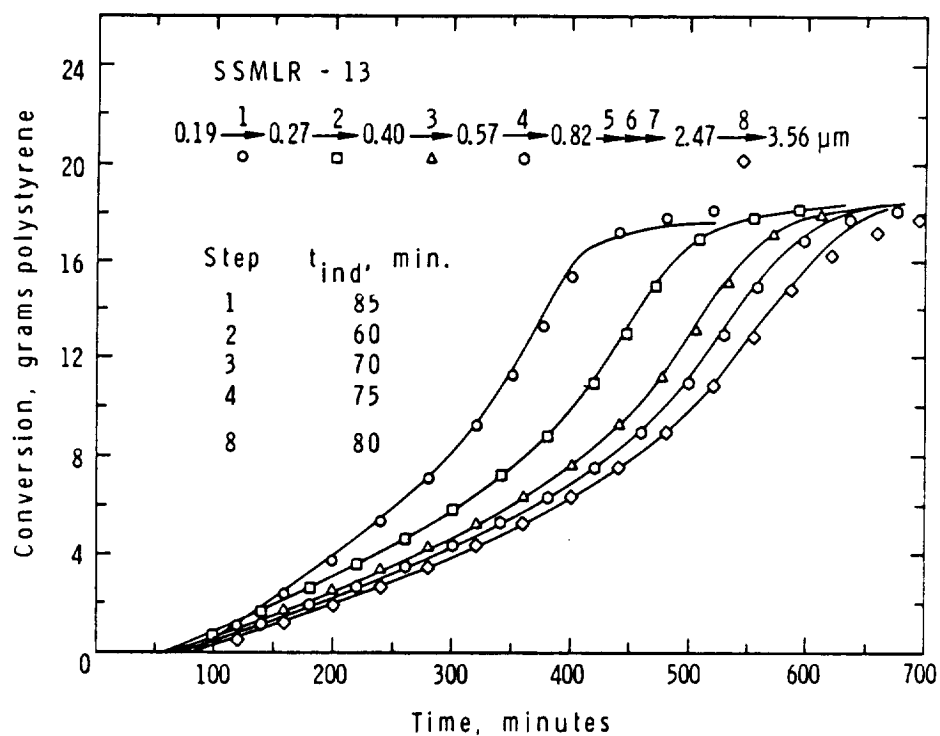
Figure 4.12   Comparison of Model Predictions (Solid Lines) with
             Experimental Results for SSMLR 13.   Induction Periods
             were Empirically Determined

272

havior at high conversions. After the first step B_i (equation 4.23) was changed from 0.15 to 0.25 to bring about a more rapid deceleration of the polymerization rate and also lowering the 'limiting' conversion (W_p 0.92). Note that this was apparently not sufficient for matching the results for Step 8 where the limiting conversion was somewhat lower. It is not likely that the actual k_d function would change under the circumstances but rather that the presence of small amounts of inhibitor would act as a retarder particularly at high conversion where diffusion limitations on small molecules is important. A true model would, therefore, have to account for this presence which involves knowledge of the inhibition mechanism, kinetics, partitioning, and diffusion limitation effects. These have not been encompassed by these studies, requiring a great amount of further work.

4.8 Conclusions

Mathematical models were developed to describe the kinetics of sequentially seeded emulsion polymerizations of polystyrene using water and oil soluble initiators. These accounted for the effects of absorption of radicals from the aqueous phase and diffusion controlled termination, propagation, and decomposition. The major findings were as follows:

1) the free volume approach to k_t was judged inadequate in describing the exact kinetics of the gel effect. Two slightly different empirical functions were used instead for the aqueous and oil phase initiated systems, the differences being attributed to molecular weight effects.

273

2) the free volume approach was used to describe a change in k_d at high conversion ($W_p > 0.7$) for the oil soluble initiator AMBN whereby lower 'limiting' conversions were defined.

3) the collision theory of radical absorption from the aqueous phase was used to successfully describe the kinetics using $K_2S_2O_8$ initiator. An initiator efficiency of 1.0 was assumed.

4) the efficiencies of the initiators AIBN and AMBN best describing the polymerization kinetics were 0.100 and 0.105, respectively.

5) the transition between emulsion ($\bar{n} = 1/2$ and $R_p \propto N_p$) and bulk ($\bar{n} \gg 1$ and $R_p \neq f(N_p, d)$) kinetics were found to occur for the case of oil phase initiation over the particle size range from about 0.1 to 1.0 μm.

6) the kinetic transition for aqueous phase initiation was not from emulsion to bulk but rather one from $R_p \propto d^{-3}$ (or N_p) to $R_p \propto d^{-\frac{1}{2}}$. The rate never became independent of particle size due to the radical absorption mechanism.

7) radical desorption and aqueous phase termination were not used to account for the polymerization kinetics of particles greater than 0.25 μm in diameter. However, aqueous phase termination most probably is relevant and could be added to form a more complete model.

8) a model accounting for the behavior of the inhibitor hydroquinone was judged to be infeasible without much added information. However, a simplified version, incorporating empirically derived induction periods and stronger reduction in k_d at high conversions (due to the presence of inhibitor) was used to describe the kinetics of successive seeding up to 3.5 μm.

274

CHAPTER 5

TOWARDS THE PRODUCTION OF LARGE-PARTICLE-SIZE MONODISPERSE LATEXES

IN MICROGRAVITY

5.1 Introduction

The preparation of 'monodisperse' latexes having particle diameters greater than ~2 μm becomes difficult due to various physical and chemical processes inherent in seeded emulsion polymerization systems. These include particle-particle stability and the generation of new particles through propagation in the aqueous phase. Interparticle stability is generally imparted by the presence of an adsorbed emulsifier layer which is in equilibrium with the surrounding aqueous medium. The presence of 'excessive' emulsifier leads to the generation of newly formed and stable smaller particles during polymerization which destroy the 'monodisperse' nature of the latex. Decreasing the amounts of emulsifier can eliminate this phenomenon but at the cost of reducing interparticle stability. This reduction can lead to the flocculation and coalescence of particles which again destroys this 'monodispersity'. Flocculation of this sort is generally caused by the shearing required to keep the suspension well mixed. This problem is compounded at the larger sizes because of density differences between the swollen and polymerized particles. Agitation sufficient to prevent creaming and settling of particles during their preparation is also sufficient to cause the flocculation of some (or all) of the particles.

Preparation of these larger size 'monodisperse' latexes in a microgravity environment could reduce the required amount of agitation

to that needed for maintaining the system at a relatively uniform temperature (i.e., temperature gradients cause particles to grow at different rates). To this end, a series of experiments were designed and performed aboard the Space Orbiters, 'Columbia' and 'Challenger'. The following describes the hardware, processing conditions, pre-flight recipe development work, and flight and ground-control exper-imental results for STS (Space Transportation Systems) 3, 4, 6, and 7.

5.2 Flight Hardware and Processing Procedures

5.2.1 'MLR' Flight Hardware

'MLR' is the acronym assigned to this program and all that is associated with it. The letters 'MLR' stand for Monodisperse Latex Reactor. In reality there are several major pieces of equipment be-sides the reactors themselves. The flight equipment consists of an Experiment Apparatus Container (EAC - manufactured by General Electric Co.) and a Support Electronics Package (SEP - manufactured by Rockwell International and Accudata). Housed within the EAC are four separate, independently operated dilatometric reactors similar to the LUMLR prototype. The EAC weighs approximately 4.23 kg and is in the form of a 0.495 m high, 0.416 m diameter cylinder. The SEP controls the experiment operation and records data from each of the four reactors on a cassette tape. It weighs 13.6 kg and has a box shape with di-mensions .346 x 0.265 x 0.300 m. These two components of the flight equipment occupy the space of three standard mid-deck lockers as shown in Figure 5.1. The two units are attached to the Orbiter bulk-head using adapter plates held by 4 bolts each. Electrical power is provided to the equipment from an overhead panel in the mid-deck.

276
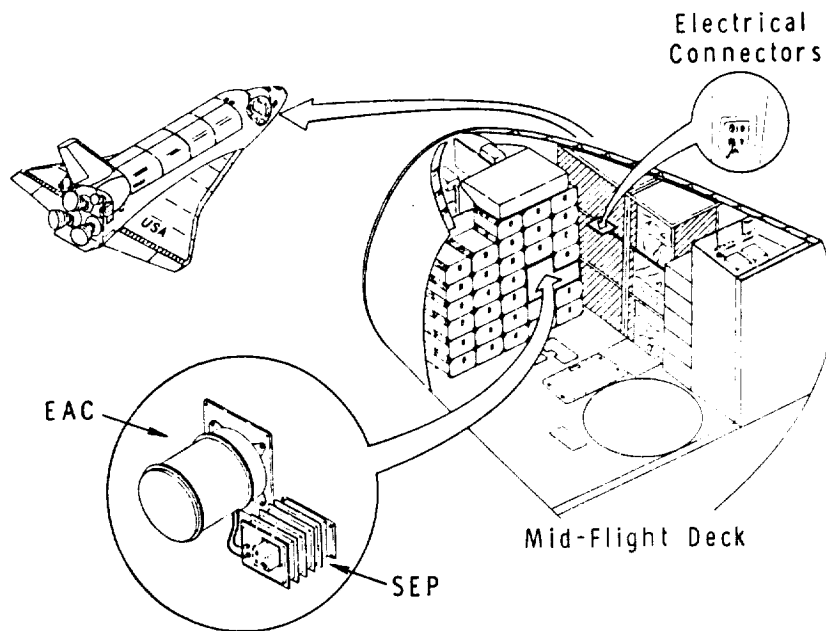
Figure 5.1 STS Accommodations for MLR (EAC and SEP) [101]

Nearly all of the operations are controlled internally with the exception of the initiation and termination of several phases of the experiment. These include the pre-processing, processing, and post-processing of the experiment. A three-position switch is provided to effect these phases: "power off", "preprocess", and "process" (pre- and post-processing use the same switch positions). The switch is maintained in the preprocess position from reactor loading through installation in the orbiter and lift off. This mode provides agitation to prevent significant latex creaming. Once in orbit the power is switched off until the designated time for processing during which the polymerizations are carried out. Following this phase, post-process agitation is performed for a designated time and then the equipment is switched off until just before the de-orbit burn. Pre-process agitation is restored at this time until power is shut off in the orbiter after it has touched down. These simple procedures indicate the small extent to which the astronauts must be attentive to this experiment.

5.2.1.1 'MLR' Dilatometers - Design and Operation

The piston/cylinder type flight dilatometers are functionally the same as the LUMLR prototype (see Chapter 1) in terms of being chemical reactors in which latexes are prepared; they were designed to be filled with ~100 cc of fluid, heated to 70°C and 90°C, and monitored for polymerization kinetics via piston movement. A number of minor design changes were made, however, to improve the performance, durability, and ease of accommodation of 13 controlling electronics modules. A cutaway view of the reactor design is reproduced

278

in Figure 5.2. Changes included: 1) single piece construction of the cylinder; 2) repositioning of the fill port, providing an inlet in the cylinder wall; 3) direct mounting of the LVDT sensor above the piston; and 4) stir blade mounting into a slotted shaft. Detailed specifications, operation, and maintenance descriptions are provided elsewhere [102].

The design changes incorporated into the flight reactors resulted in a number of changes in the behavioral characteristics and handling procedures. The former includes the temperature-time profile during heat-up and the interpretation and correction of LVDT data. The design polymerization temperature (nominally 70°C) was attained in a shorter time in the flight reactors as compared to the prototype (LUMLR); the rise was steeper and leveled out faster. Since the LVDT was configured 180° from its position in the LUMLR, a sign change (plus calibration) was required to properly interpret the expansion and contraction data. An unknown complication was also introduced by this design in that the LVDT and its sensor rod were positioned where temperature effects might become significant in the electronic behavior and thermal expansion of the components. No extensive tests were run in order to investigate this problem. Data interpretation was accomplished in a manner analogous to that of data obtained from the prototype.

Loading of the flight reactors with swollen latexes was performed in a manner similar to the method developed previously for the LUMLR prototype. The low pressure/gravity technique was applied to minimize bubble inclusion, thereby aiding in the acquisition

279

#	Description
1	fiberglass insulation
2	Viton o-rings
3	vent tube
4	heater wire leads
5	piston temperature sensor, diode
6	wall temperature sensor
7	fluid temperature sensor
8	base temperature sensor
9	LVDT -DC (Schaevitz)
10	LVDT support
11	washer, special
12	housing cover (textolite)
13	LVDT shaft
14	spring
15	piston assembly
16	quick connect (Swagelok)
17	nut
18	stirrer paddle (original)
19	stirrer drive shaft
20	Viton o-ring
21	bearings
22	cylinder assembly
23	housing
24	insulation plate (textolite)
25	quarter plate
26	base plate
27	stirrer motor

Figure 5.2 Schematic of MLR Dilatometer (Scale: 1 cm = 3.08 cm)

and interpretation of kinetic data. The initial volume of the reactor contents was not easily set at exactly 100 cm^3, as was the case for the LUMLR, but rather an LVDT voltage (~2.4 v) corresponding to a piston position which resulted in nominally 100 cm^3 of fluid volume. This voltage was then converted to fluid volume by using a calibration curve of LVDT voltage versus piston position. The LVDT in each reactor as well as all temperature measurement sensors were calibrated prior to use (Test Lab, Marshall Space Flight Center).

Agitation was provided via a stir paddle (see Figure 2.21 (top)) mounted in a machined slot in the stir shaft which was connected to a motor and gear box. Oscillatory ('washing-machine') type agitation was used in all reactors for all polymerizations. The stirrer rpm was varied by changing out the gear box.

An 'In Process Timer' (EPROM) was programmed to control the sequence of events during the processing portion of an experiment. These events included the initiation of the heat-up, the duration of the $70^{\circ}C$ portion of the experiment, the heat-up and duration of the $90^{\circ}C$ portion, and the cooling-off and shut down of data acquisition. The $70^{\circ}C$ period was initially set at ~11 hrs for STS-3, subsequently being extended to ~17 hrs for STS 4, 6, and 7. The $90^{\circ}C$ portion (intended to finish off the polymerization), lasting approximately one hour, was the same for all experiments.

Data was recorded on a cassette tape contained in the SEP or alternately could be recorded by hand for ground-based work using the Ground Support Equipment (GSE) supplied with the reactor by the General Electric Co. The cassette tape was reduced at MSFC and the

data recorded on a 9-track, 1600 bpi, unlabeled tape for subsequent processing at Lehigh University.

5.3 STS-3 Experiments

The success of any space flight experiment is dependent upon many hours of planning and preparation by a relatively large number of people as compared to an analogous ground-based experiment. Hardware design, construction, testing, and maintenance accounts for a disproportionately large fraction of the total time and budget of such a project. On the other side (and of equal importance) is the preparation and development of the experimental materials, which in this case were the latex systems (recipes) to be polymerized in microgravity. The recipe requirements for this program included: 1) a 'monodisperse' latex seed of size greater than or equal to 2 μm; 2) a stabilizer system which could ensure the stability of the particles during swelling, loading, preprocessing, processing (polymerization), post-processing, and on the shelf; 3) an initiator which would provide an adequate polymerization rate and allow for dilatometric kinetic measurement; and 4) an inhibition system which would prevent aqueous phase generation of new particles (e.g., via homogeneous nucleation) without affecting (retarding) the polymerization within the particles themselves. A submicron recipe, exhibiting well known and characterized emulsion polymerization-type kinetics was also required as a control. Besides the recipe requirements, processing in terms of agitation conditions also required specification through some experimental testing.

282

Each set of flight experiments had a number of pre-flight and post-flight experiments associated with it. These are described for each flight.

5.3.1 Pre-Flight Recipe Development

5.3.1.1 Large-Particle-Size Recipes

The development of recipes for the preparation of large-particle-size latexes was undertaken in this lab by Tseng [80]. These recipes were developed in an empirical fashion through the testing of many combinations of stabilizers, initiators, and inhibitors. These polymerizations were generally carried out by first swelling the particles overnight with all ingredients present (tumbling in a glass bottle) and then polymerizaing by tumbling end-over-end at 70°C in a constant temperature bath for approximately 20 hrs. (Any unswollen monomer was left in the bottles without separation prior to polymerization.) The latexes were qualitatively judged for the monodispersity through SEM examination and for their stability by the amount of coagulum produced. Once a general recipe was set, 'fine' tuning was done by conducting polymerizations in the LUMLR, thus obtaining kinetic information along with the behavior of the polymerization recipe in a reactor similar to the flight hardware.

Three recipes using a large-particle-size seed were planned for the STS-3 experiments. Three different swelling ratios (monomer/polymer), nominally 2, 4, and 10, would be used to grow 2.5 μm polystyrene particles to approximately 3.6, 4.3, and 5.5 μm. The stabilization system consisted of a combination of oligomeric (Polywet KX-3) and polymeric (PVP K-30) stabilizers, the former being an anionic

C-4

species. The initiator, AMBN (2,2'-azobis(2-methylbutyronitrile)), was chosen because of its low water solubility (<0.04%) and a favorable decomposition rate at $70^{\circ}C$ ($t_{\frac{1}{2}}$ = 6.5 hrs.). Hydroquinone, a nonionic and water soluble inhibitor was used to suppress aqueous phase free radical polymerization without inducing any destabilization. All of these ingredients were used without further purification (manufacturer and grade given in Chapter 3). The styrene monomer was distilled twice at reduced pressure just prior to use.

Four of the recipe parameters required further study through use of the LUMLR: 1) surfactants – types and concentrations; 2) initiator concentration; 3) inhibitor concentration; and 4) M/P swelling ratio. The final solids contents were all designed to be nominally 30%. Initially it was clear that the initiator concentration would have to be chosen such that each polymerization could be completed before the nitrogen (N_2) decomposition by-product saturated the latex and formed bubbles within the reactor. At this point no further accurate dilatometric data could be obtained. It was estimated that approximately 1.8×10^{-4} moles of N_2 would be necessary to saturate the aqueous phase (70 gms) which had been degassed at a pressure of 20 mm Hg. For a 2/1 swelling ratio this corresponds to a concentration of 4 mM based on monomer. This served as the lower limit for the initiator concentrations tested.

The first polymerizations (designated CMT-X) in the LUMLR were performed using a 2.5 µm seed which had been prepared in 3 successive seeding steps from monodisperse 0.4 µm seed (Dow LS 1103A) (see Tseng [80]). These seeds were used 'as is' without any purification, i.e.,

284

the surfactants and salts from the previous steps remained in the latex. Aerosol-MA had been a prime ingredient in the smaller particle size recipes. Additional amounts of the KX-3 and PVP were added to the 2.5 μm seed for the swelling and subsequent polymerizations. Table 5-1 lists the variation in parameters for the recipes tested. Note first CMT 4 and 5. The main difference between these two recipes was the fact that the first made use of a seed which had been cleaned (of small particles, surfactants, and salts) by repeated centrifugation/washing cycles using distilled-deionized water. As can be inferred from the final solids contents, the product of CMT 4 contained significantly more coagulum than CMT 5 which used the uncleaned version of the 2.5 μm seed. Moreover, the particle size distribution of the CMT 4 latex was obviously much broader than the CMT 5 product as evidenced by SEM examination. These results indicated that Aerosol-MA was indeed an important ingredient in the particle stabilization system and thereafter was added to any system using cleaned seed (indicated by an *).

It quickly became apparent during these tests that obtaining complete conversion histories (>90%) within the 11 hrs allotted for the polymerization at 70°C would be difficult for the low swelling ratio and impossible at the higher swelling ratios. The last two columns in Table 5-1 indicate the time required to reach a given conversion and whether or not valid kinetic measurements were hindered by the formation of a gas (N$_2$) bubble. For the 2/1 swelling ratio CMT 9 gave the most favorable results, high conversion with nearly complete kinetics. The polymerization conversion histories are

Table 5-1

Recipe Parameters and Results of STS 3 Preparation using 2.5 μm Polystyrene Seed

CMT	M/P[1]	[AMBN]$_o$[2] mM	Weight Percent Added Based on Aqueous Phase				% Final[7] Solids	% Conversion[8]	(time, hrs.)
			AMA[3]	KX-3[4]	PVP[5]	HQ[6]			
2	1.99	4.0	0	0.0107	0.1071	0.0057	25.4	85.5	(14.0)
3	1.89	5.8	0	0.0100	0.1000	0.0086	23.3	91.7	(12.0)
8*	1.87	10.9	0.0114	0.0194	0.1929	0.0164	25.6	62.8	(8.7)+
9*	1.90	6.8	0.0144	0.0233	0.1929	0.0100	29.3	91.7	(10.8)
12*	1.90	7.5	0.0144	0.0233	0.1929	0.0443	27.9	79.5	(8.7)+
4*	3.47	8.68	0	0.0150	0.1500	0.0157	20.2	~90.0	(13.3)+
5	3.80	14.14	0	0.0150	0.1500	0.0250	26.8	35.0	(7.3)+
10	3.90	11.62	0.0071	0.0176	0.1757	0.0207	25.6	59.6	(7.8)+
7	7.22	19.36	0	0.0150	0.1500	0.0393	19.61	34.6	(6.7)+
11*	7.20	14.23	0.0032	0.0166	0.1629	0.1143	22.6	21.2	(5.3)+

* Seed latex cleaned by repeated centrifugation/washing cycles.

+ Point at which N$_2$ bubble formation occurred.

[1] determined from isooctane extraction/UV analysis
[2] based on monomer
[3] Aerosol-MA
[4] Polywet KX-3
[5] Polyvinyl pyrollidone (K-30)
[6] hydroquinone
[7] measured gravimetrically
[8] measured dilatometrically

286

illustrated in Figure 5.3. The dashed part of the curves (8 and 12) are the actual data obtained, influenced by the growth of a N_2 bubble. Note also that considerable induction periods results for the smaller amounts of initiator. Nonetheless, these data follow the relationship $R_p \alpha [I]^{\frac{1}{2}}$ as measured by the initial polymerization rates. It should be pointed out that, generally, the amount of inhibitor added was in proportion to the amount of initiator (with the exception of CMT 11 and 12). This had no perceivable effect on the relative extent of the induction periods, the initiator level being the controlling factor. Recall that the inhibiting power of hydroquinone has been attributed to its conversion to benzoquinone in the presence of oxygen [88], benzoquinone being the actual inhibiting species. Moreover, benzo-quinone is much more oil soluble than water soluble and would partition mostly into the particles. Little more can be said without much more knowledge on the behavior of these species.

At the higher swelling ratios it was clear that complete polymerization kinetics could not be gained within an 11 hr. polymerization period. This was simply due to the higher value of the termination rate 'constant' (lower polymerization rate, R_p) over more of the conversion range (the gel effect decreases with increasing M/P ratio). More initiator was thus required to finish the polymerizations within the time limits with the consequence of some lost kinetic data. Only an increased reaction time would allow for the acquisition of the complete conversion-time curves.

Several other items are worth noting in Table 5-1. First, a 10/1 swelling ratio could not be achieved for the existing system,
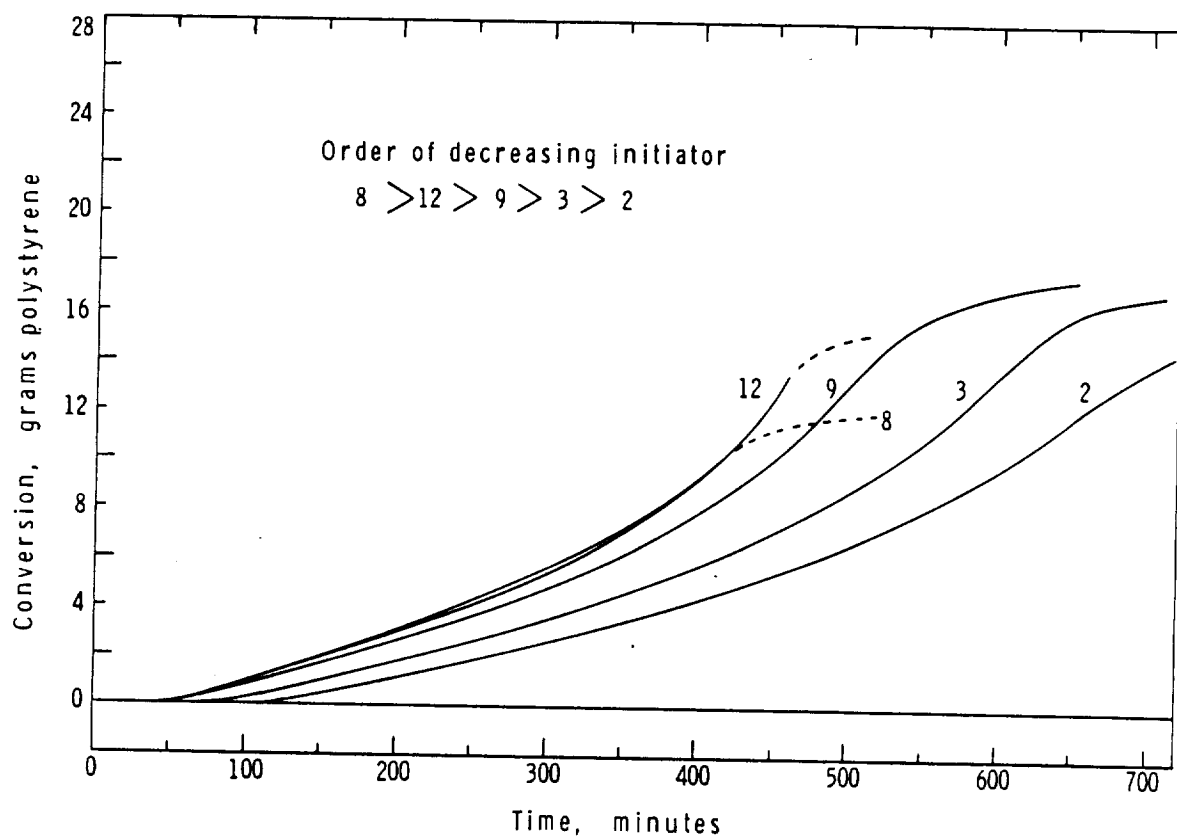
Figure 5.3   Conversion Histories for the Seeded Polymerization of a
2.5 μm PS Seed (2:1, Monomer/Polymer), Using Varying
Amounts of Oil Soluble Initiator   AMBN

7.2/1 being the maximum swelling ratio achieved. This is attribut-
able to limitations based on the thermodynamics of swelling, that is,
the balance between surface and mixing energies. This subject has been
covered extensively in the literature [30,45,103]. Second, several
inconsistencies can be seen in the observed time to loss of kinetics
and the initial concentration of AMBN; CMT 8 vs. 12 and CMT 7 vs. 11.
In the first case the initiator concentration of CMT 8 exceeded CMT
12 by 45% and yet the times were the same. In the second case, the
initiator concentration of CMT 7 exceeded that of CMT 11 by 36% and
yet had a greater polymerization time prior to bubble formation.
The other greatest difference between the two recipes in these pairs
was the level of the inhibitor, HQ. For each case with the shorter
than expected time (CMT 11 and 12) the HQ content was much higher than
its counterpart. One explanation for this would be poorer degassing
of these systems, however, this does not seem likely. Another may be
some induced decomposition of the initiator due to the presence of
the inhibitor [104]. This phenomenon has not been reported for HQ
but it is not unknown for other species (e.g., surfactants). Further
research is required to resolve this question.

5.3.1.2 Submicron 'Control' Recipe

The definition of a 'control' experiment is one which verifies
by comparison. In this case, the control was defined to be a seeded
emulsion polymerization experiment of monodisperse latex with well
defined, understood, and reproducible kinetics. The control was to
act as a check on the microgravity environment of the low earth orbit
provided in the Orbiter's mid-flight deck. No differences were ex-
pected since submicron particles were not subject to much creaming

or settling due to their small size, Brownian motion keeping them in suspension.

Conventional seeded emulsion polymerization of monodisperse polystyrene latexes has been carried out traditionally using water soluble initiators such as potassium persulfate, typically buffered by sodium bicarbonate. Anionic emulsifiers such as sodium dodecyl sulfate or Aerosol-MA are commonly used to provide stability. Solids contents may range anywhere from 20 to 50%. Swelling ratios may be as high as 3/1 depending on the system. Ideal polymerization kinetics would be the case in which $\bar{n} = 1/2$ throughout the entire polymerization, thus having no dependency on the initiator concentration or the value of the termination rate constant, k_t, (no gel effect). A system with this behavior, however, is difficult, if not impossible, to produce. An imperfect case was chosen instead, which displayed a considerable gel effect and therefore, a sensitivity to initiator concentration and particle size. A 'cleaned' (via ion exchange) monodisperse polystyrene latex (Dow LS 1102A) of particle diameter 0.19 μm, styrene monomer, Aerosol-MA emulsifier, potassium persulfate initiator, and sodium bicarbonate buffer, made up the polymerization recipe. This was based on work described in Chapter 3 (SSMLR 4-1). A 2/1, M/P swelling ratio with a projected 30% final solids content was planned. Surface coverage with Aerosol-MA was set at 8%, with a 1 mM $K_2S_2O_8$ concentration (equaled in weight by the buffer). The polymerization kinetics were presented previously in Section 3.5.3.1, Figure 3.14, curve 1.

Some concern over the survival of such a recipe in 'Orbiter' ambient conditions for the time before activation of the experiment (~4 days) led to a ground run test to check on polymerization at room temperature. The swollen recipe was purged with oxygen free N_2 gas (ultra high purity - Linde) for 20 minutes and tumbled in a glass bottle with a nitrogen blanket. Each day for eight days a sample was removed from the bottle, care being taken to purge with N_2, and analyzed for the styrene content via iso-octane extraction/UV analysis. Over eight days, no significant amount of conversion was found to occur. This was considered to be proof of the survivability of the recipe.

5.3.2 Flight and Ground Experiments

On March 22, 1982, the Space Shuttle Columbia was launched on its third orbital flight test (STS-3) carrying on board a set of four reactors containing monomer swollen latexes to be polymerized in microgravity. These experiments represented the first 'controlled heterogeneous chemical reactions' to be carried out in space. Shortly after the return of the Columbia ground-based analogue experiments were run for comparison.

5.3.2.1 'Pre-process'

The actual polymerizations in microgravity were preceded by a number of events which had to be completed successfully within a given time frame. These included both chemical and hardware related items: 1) reactor preparation; 2) seed and recipe preparation; 3) reactor loading; 4) pre-process agitation and leak check, 5) EAC and SEP preparation, sealing, and leak check; 6) EAC and SEP take-away and installation in the Orbiter; 7) Space Shuttle launch; and 8) switching

into the 'process' mode. The first two on this list required exten-

sive effort and time to accomplish, while the others could be charac-

terized as requiring 'intensive' efforts within a strictly defined

time table of events.

'Reactor preparation' covers a wide range of testing and refur-

bishment activities. Prior to the flight, a requirement was made that

each reactor be subjected to a minimum of two full polymerization

runs. These were termed 'sweetening-of-the-pot' runs [52] and, as

the name may or may not imply, were meant simply to get the reactors

in running order for preparing latexes. Seeded emulsion polymerization

recipes using a submicron seed (0.4 μm), 2.5/1 monomer-to-polymer

swelling ratio, 15% final solids content, persulfate initiator, and

bicarbonate buffer, were prepared in single batches for loading four

reactors. Loading was accomplished by the original gravity/atmos-

pheric fill procedure without degassing the latex. No back-up ring

was used behind the lower piston o-ring. (Any change in material or

procedures required much in the way of documentation, time, and paper-

work.) The former was later changed for the flight itself. An ex-

ample of the experimentally obtained conversion histories for the

four reactors designated for flight (Nos. 3,5,7, and 8) is given in

Figure 5.4. The results showed a fair reproducibility and yet indi-

cated some possible trouble spots. The first hour of data was not

reliable in terms of kinetics, this being due to the difficulty in

predicting the expansion behavior during heat-up. Much of this prob-

lem can be attributed to the absence of the back-up ring (see Chapter

2, Section 2.4.3.2.1). Extrapolation back to zero time was required

292
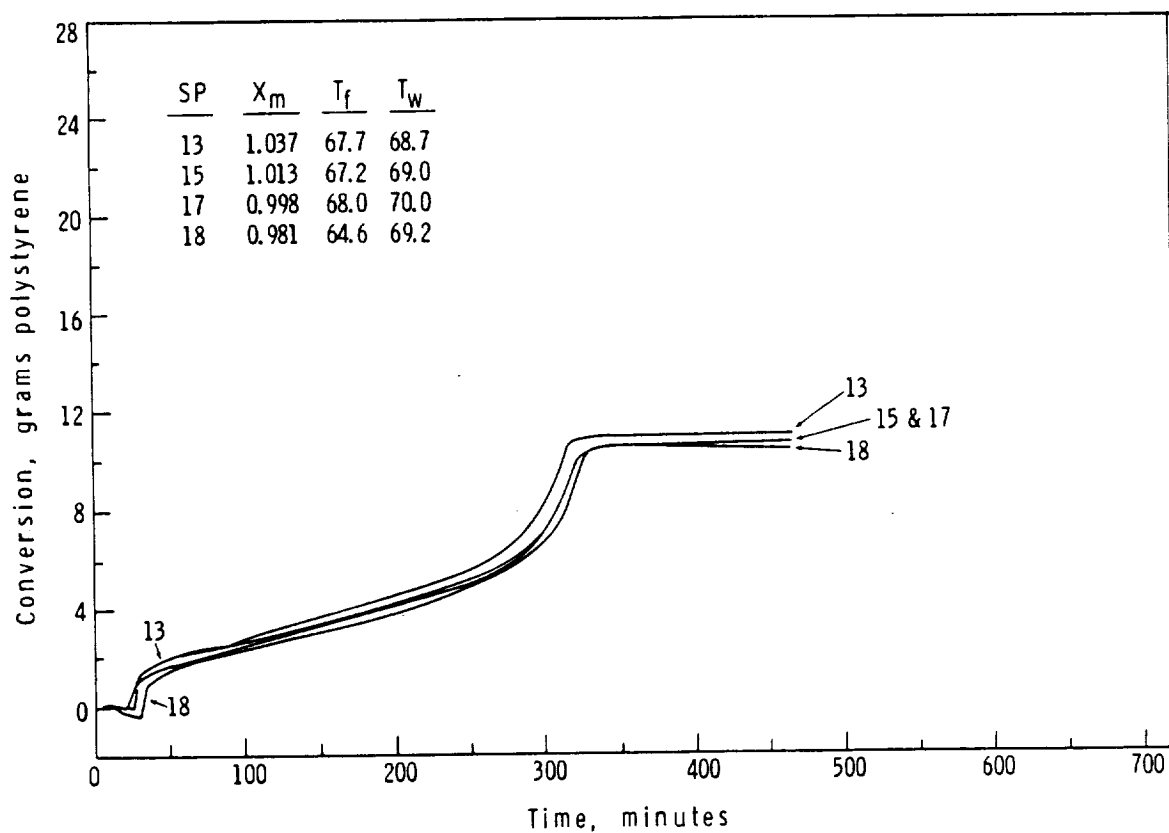
Figure 5.4 Conversion Histories for Seeded Emulsion Polymerization
of Styrene/Polystyrene Obtained in 'Sweetening-of-the-
Pot' Run in Flight Designated Reactors

293

to obtain a reasonable continuous curve. A second problem was found in the fluid temperatures at the control point (nominally 70°C). The temperatures were 67.7, 67.2, 68.0, and 64.6°C for reactors 3,5,7, and 8, respectively (as compared to 69.2°C for the LUMLR prototype). Sources of error included: 1) calibration (T°C vs. voltage); 2) voltage drop of the power source under load; and 3) controller set-point. Recalibration by MSFC later corrected the errors involved in the calibration, leaving the other two unresolved. (The set-point for reactor 8 gave a fluid temperature of 68.4°C, more in line with the other reactors.) Nonetheless, after three polymerizations in each of the flight reactors, they were judged to be acceptable for the flight experiments. Refurbishment for flight involved a thorough cleaning of all reactor components contacting the latex and replacement of all o-rings (Viton) and quick-disconnects (QD's). All bolts were torqued to specification during the re-assembly just prior to the loading.

The preparation of the flight seed and recipes was alluded to previously in the description of recipe development (Section 5.3.1.1). A brief account is given here, the details being found elsewhere [80]. The large-particle-size polystyrene flight seed had a diameter of 2.520 ± .046 µm (1.84% standard deviation) as measured from Transmission Electron Micrographs with a MOP-3 digital analyzer (Zeiss, Inc.). Prior to the flight, this seed had undergone a rigorous cleaning procedure using sedimentation to reduce the oversize particle count (doublets, triplets, etc.) and a modified form of the serum replacement technique [105] to clean out both surfactants and any small par-

294

ticles which may have been nucleated during the preparation of the
seed. (Recall that nucleation and coagulation were described as the
nemesis of the monodisperse latex formulator.)

The latexes were prepared for loading by first swelling the
particles with styrene monomer for a minimum of 17 hrs. at room tem-
perature. The recipes are given in Table 5.2. All the ingredients

Table 5-2

STS-3 Flight Recipes (Design)

Recipe #	1	2	3	4
Seed diameter, μm	2.52	2.52	2.52	0.19
Monomer/polymer	2/1	4/1	10/1	2/1
Final particle diameter, μm	3.63	4.31	5.43	0.27
$[AMBN]_o$, mM (on styrene)	5.6	7.9	13.8	--
$[K_2S_2O_8]_o$, mM (on aq. phase)	--	--	--	1.0
AMA*	0.0143	0.0071	0.0032	0.0888
KX-3*	0.0233	0.0176	0.0166	--
PVP*	0.0343	0.0343	0.0343	--

*Weight percent based on the aqueous phase.

(300 grams) were combined for the three large-particle-size recipes
while the initiator (plus 10 grams water) was withheld from the sub-
micron 'control' recipe. Swelling was accomplished by gentle tumb-
ling in 12 oz. bottles oriented at ~45° in a cannister set on a lap-
idary tumbler (Carborundum). In turn each swollen latex was filtered
through glass wool into a separatory funnel if a monomer layer was
still evident. The latex was then transferred to a round-bottom
loading flask for degassing. (At this point the persulfate initiator
was added to the submicron 'control' recipe.) A period of 45 min.

295

to one hour was required to degas a given latex to a pressure of ~20 mm Hg. Foaming was carefully controlled by adjusting the pressure and using a Teflon magnetic stir bar to provide bubble nucleation sites.

The low pressure/gravity fill technique was employed to load the flight reactors (see Section 3.5.1.2). This method was adopted to decrease or eliminate any bubble inclusion in the reactor which might jeopardize acquisition of meaningful kinetic data. In general, six to eight hours were required to fill four reactors provided no problems arose. Once a reactor was loaded, it was positioned on the EAC platform and powered into the 'pre-process' mode which provided 1.5 min. of oscillatory (13 rpm) ~20 cycles/min. agitation every 30 min. This manner of agitation was judged to be adequate in preventing destructive creaming of the swollen latexes without imparting undo shear to the system. Limited agitation testing using the LUMLR prototype and swollen flight-type latexes revealed that a completely uniform suspension could not be maintained under the 90 sec. per half hour scheme; however, complete creaming was prevented, thereby keeping the particles from packing tightly together and possibly causing some coalescence.

The loading operation was designed to be completed within 10 - 15 hours of the scheduled take-away. This served as a buffer for any difficulties that might arise in the loading and also provided a significant amount of time to check on any possible leakage from the reactors. In the event that a leak did occur, a re-load would take place. The piston positions were monitored in all re-

296

actors from the time of loading until several hours before the take-away. No leakage was noted in any reactor for the STS-3 experiments. Also within this time NASA personnel sealed the EAC and SEP covers and performed leak checks.

Installation of the EAC and SEP in the orbiter took place over several hours approximately two days before launch. Pre-processing was maintained over the entire period.

STS-3 was launched with a one hour unplanned hold at 11:00 a.m. March 22, 1982. At 6:40 p.m. on the following day, 31.7 hours after launch and 102 - 112 hours after loading, the experiment was switched to the processing mode by one of the two astronauts (J. Lousma and G. Fullerton).

5.3.2.2 'Process'

The activation of the process mode initiated a number of events: 1) continuous oscillatory agitation (13 rpm, ~20 cycles/min.); 2) recording of LVDT (piston position) and four different temperatures in each reactor (fluid, wall, piston, and base) at 64 sec. intervals; 3) after ~25 min. the heating elements were activated to raise the latexes to reaction temperature and hold them for a period of 10.5 hours (nominal); 4) followed by ~45 min. heat-up and hold at ~90°C; 5) heater shut-down and cooling for 45 min.; and 6) switch back to the pre-process mode (activated by an astronaut).

5.3.2.3 'Post-Process'

The pre-processing agitation mode was maintained until the orbiter touched down on March 29. The EAC and SEP were returned to Marshall Space Flight Center (MSFC) and opened April 1 to recover

297

the latexes and the data tape. For 24 - 48 hours before opening, the EAC was inverted periodically to redisperse the sedimented particles. The latexes were carefully decanted from the reactors avoiding any contamination, particularly from the latex trapped in the voids of the fill port. (Differing temperature history and gradients in the unstirred dead volumes would lead to lower conversion and a broadened particle size distribution.) The latexes were returned to Lehigh and characterized for particle size distribution, molecular weight distribution, and yield (solids content). The tape data was analyzed to obtain the conversion histories for each of the polymerizations.

Ground-based analogues of the flight experiments were subsequently run at MSFC following the same time-line as was documented for the flight. The results of both sets of experiments are presented.

5.3.2.4 STS-3 and Ground-Based Results, Large-Particle-Size Latexes

As each reactor was opened, the latex was examined for any significant styrene monomer odor. None was detected, indicating a high conversion was reached in all recipes. Some coagulum was found on the wall of the dilatometer which contained the 4/1 buildup (Recipe #2) while the others contained only minor amounts. The solids contents, along with the iso-octane extraction results of the swollen latexes are present in Table 5-3. Note that the coagulum found in the reactor containing recipe #2 was reflected in a lowered solids content. As in the CMT series, the 10/1 swelling ratio could not be achieved with the system of recipe #3. This accounted for the significantly lower yield.   298

Table 5-3

Solids Contents and Results of Iso-Octane Extractions

of STS-3 Flight and Ground Latexes

| | | gm styrene/100 gm latex | |
	% Solids	Experimental	Design
Flight #1	28.31	---	
Ground #1	26.00	19.15	20.0
Flight #2	24.62	23.56	
Ground #2	29.68	22.75	24.0
Flight #3	22.80	21.07	
Ground #3	25.35	23.05	27.3
Flight #4	28.27	18.96	
Ground #4	29.26	18.19	20.0

Particle size analysis of the product latexes was accomplished by measuring individual particle diameters from prints of TEM micrographs. This analysis included the determination of the relative number of over-sized particles with respect to the main distributions. These distributions, along with a representative micrograph of each (excluding the submicron control) are presented in Figures 5.5 - 5.7. The various averages given above the distributions are defined in Appendix E. The number (D_N) and weight (D_W) average diameters as well as the polydispersity index (PDI) are most often cited in this type of particle size analysis. However, the standard deviation (σ) and the coefficient of variation (σ/D_N) are more significant in the analysis of relatively monodisperse particles. Table 5-4 summarizes the particle size results while Figure 5.8 combines all the distributions. Included in this table are the results of an independent analysis of flight and ground samples for recipe #3 made by the National Bureau of Standards (NBS). The particle size

SAMPLE FLIGHT 1

D_n = 3437.4   PDI = 1.001
D_w = 3441.0 D_{min} = 3010.0
N   = 2777 D_{max} = 3990.0
D_v = 3438.6 D_a = 3438.0
S_d =   64.2   STEP =   20.0
D_q = 3442.1 D_s = 3439.8

SAMPLE GRND RUN 1

D_n = 3722.6   PDI = 1.001
D_w = 3725.1 D_{min} = 3310.0
N   = 1363 D_{max} = 4290.0
D_v = 3723.4 D_a = 3723.0
S_d =   57.3   STEP =   20.0
D_q = 3726.0 D_s = 3724.3
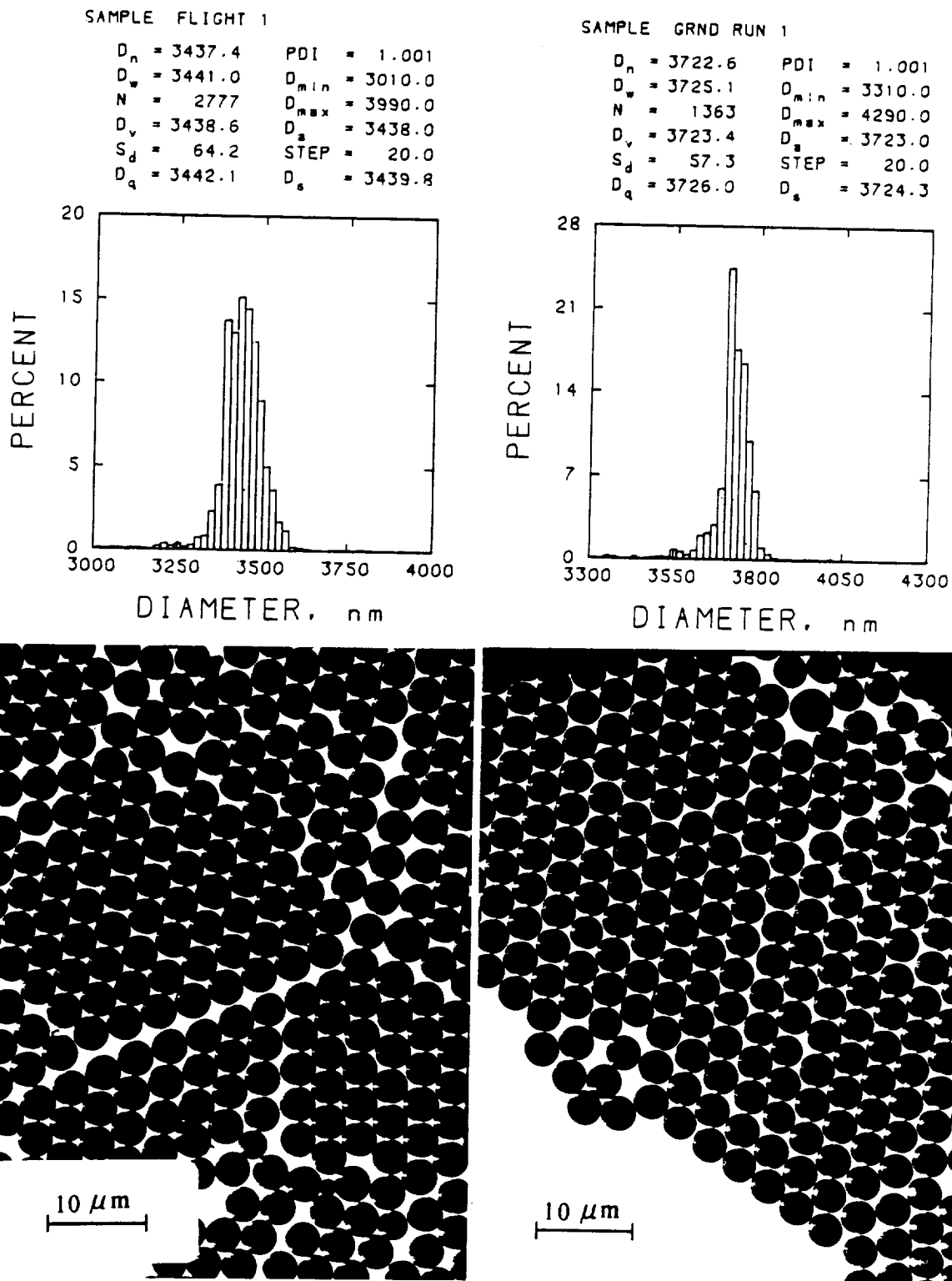
Figure 5.5   Comparison of Particle Size Distributions of the Main
Particle Populations Produced in Microgravity (FLIGHT 1)
and on the Ground (GRND RUN 1) with Representative Micro-
graphs of Each

300

SAMPLE FLIGHT 2

D_n = 4076.6   PDI = 1.001
D_w = 4079.9 D_{min} = 3510.0
N = 2256 D_{max} = 4490.0
D_v = 4077.7 D_a = 4077.1
S_d = 68.9   STEP = 20.0
D_q = 4081.0 D_s = 4078.8
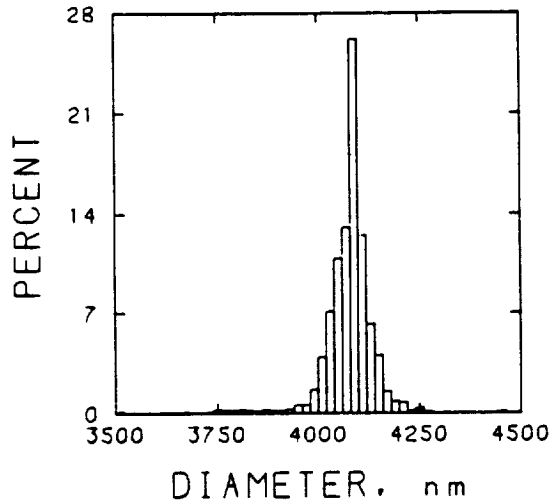
SAMPLE GRND RUN 2

D_n = 3931.6   PDI = 1.001
D_w = 3936.0 D_{min} = 3510.0
N = 913 D_{max} = 4490.0
D_v = 3933.1 D_a = 3932.3
S_d = 77.1   STEP = 20.0
D_q = 3937.4 D_s = 3934.5
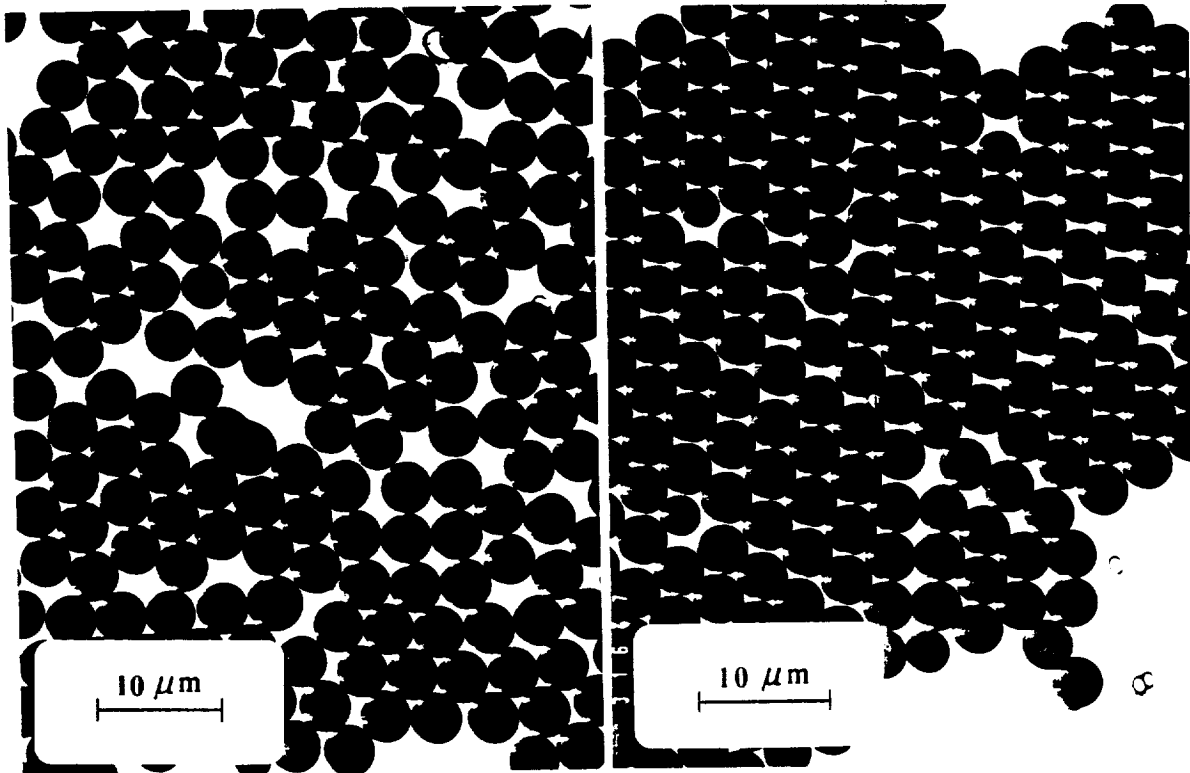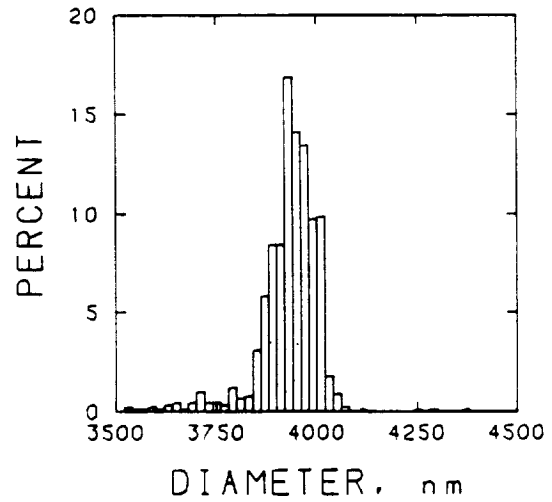
Figure 5.6   Comparison of Particle Size Distribution of the Main
Particle Populations Produced in Microgravity (FLIGHT 2)
and on the Ground (GRND RUN 2) with Representative Micro-
graphs of Each

301

SAMPLE FLIGHT 3

D_n = 4984.3		PDI = 1.001
D_w = 4988.3		D_{min} = 4510.0
N = 2095		D_{max} = 5490.0
D_v = 4985.6		D_s = 4985.0
S_d = 81.7		STEP = 20.0
D_q = 4989.6		D_e = 4987.0
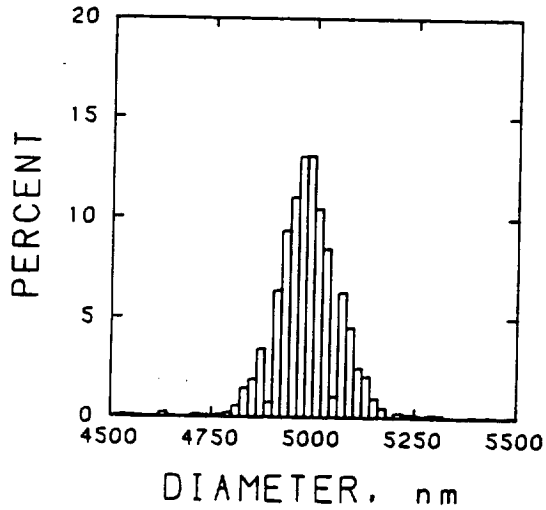
SAMPLE GRND RUN 3

D_n = 4741.1		PDI = 1.004
D_w = 4758.4		D_{min} = 4210.0
N = 1233		D_{max} = 5210.0
D_v = 4746.9		D_a = 4744.0
S_d = 166.8		STEP = 20.0
D_q = 4764.1		D_s = 4752.7
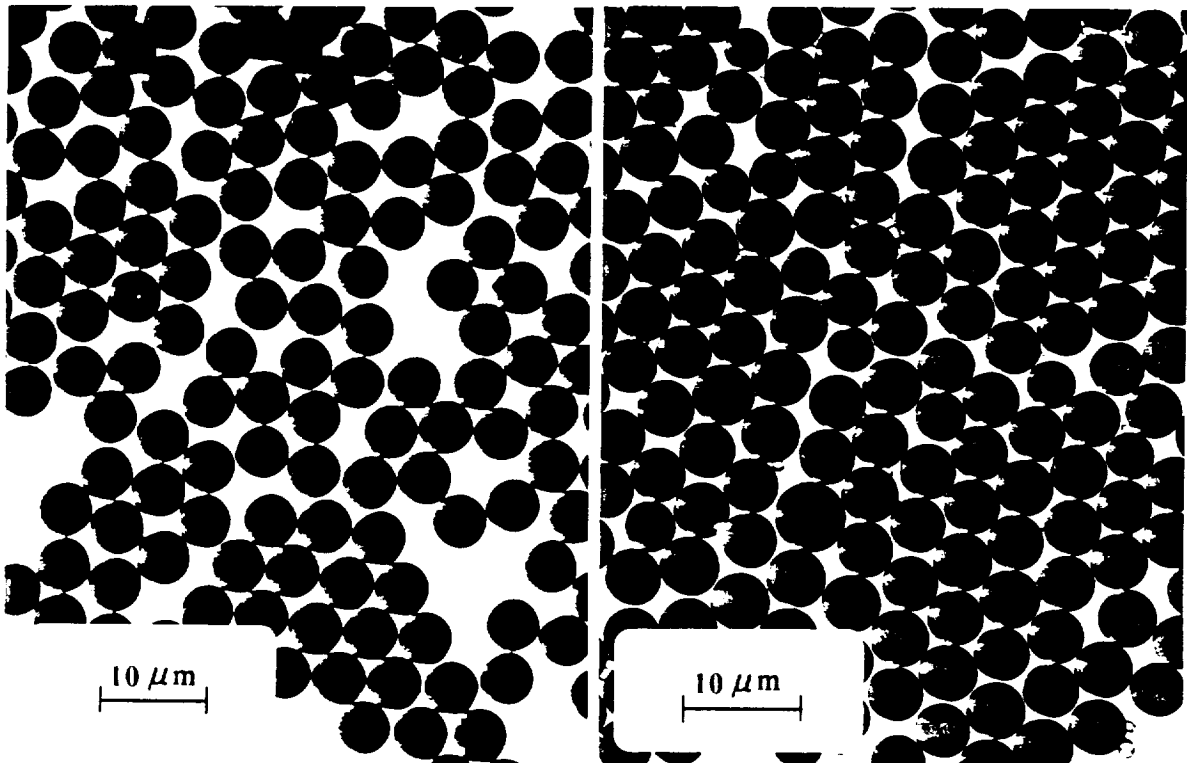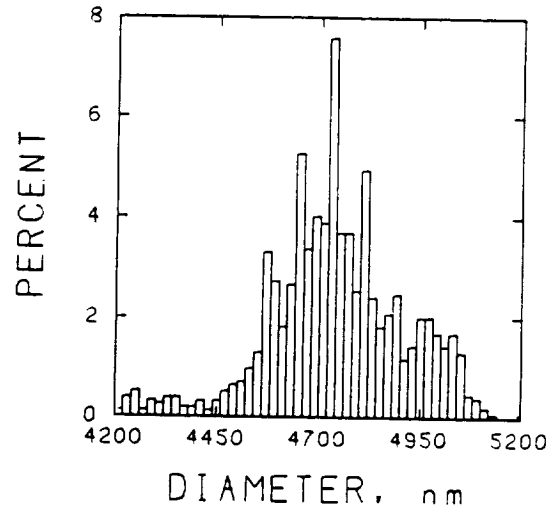
Flight 5.7   Comparison of Particle Size Distributions of the Main
Particle Populations Produced in Microgravity (FLIGHT 3)
and on the Ground (GRND RUN 3) with Representative Micro-
graphs of Each
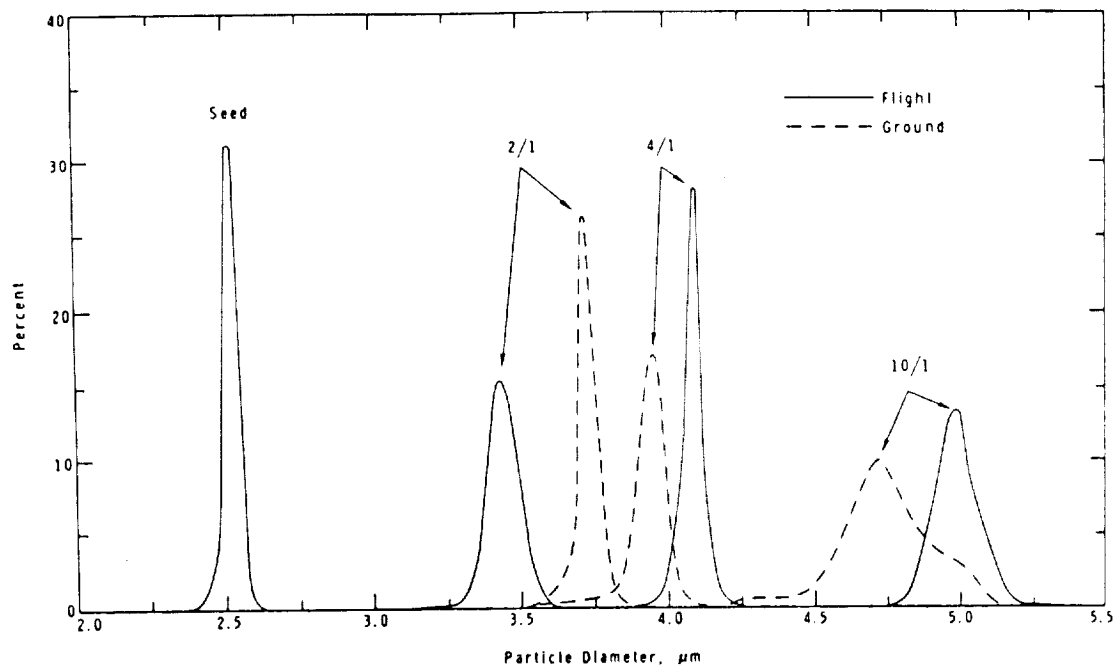
Figure 5.8 Combined Particle Size Distributions of STS-3 Seed, Flight, and Ground Latexes

Table 5-4

STS-3 Average Particle Sizes

Sample	Nominal Buildup	D_n, μm	σ, μm	n	$\sigma/\bar{D}_n$, %
Seed	--	2.52	0.046	1024	1.84
Flight #1	2/1	3.44	0.064	2777	1.87
Ground #1		3.72	0.057	1363	1.54
Flight #2	4/1	4.08	0.069	2256	1.69
Ground #2		3.93	0.077	913	1.96
Flight #3	10/1	4.98	0.082	2095	2.64
		5.04*	0.030	900	0.60
Ground #3		4.74	0.167	1232	3.51
		5.03*	0.151	900	3.00

*determined by the National Bureau of Standards (NBS)

NOTE: NBS aerodynamic particle sizing of flight and ground #3 showed 0.8 and 3.5% standard deviation, respectively.

distributions (PSD) of all samples were narrow but with some subtle differences. The uniformity, expressed as σ/D_N, was about the same for all samples except ground-based sample #3 (made with the highest monomer/polymer ratio) which had a broader distribution. This was attributed to an inadequate agitation which allowed particles to experience different temperature histories and thus different polymerization and growth rates. The absolute standard deviation (σ) increased with increasing particle size. These values reflect not only the width of the PSD but also the errors in measuring the particle images of the electron micrographs and the variation of magnification from one exposure to another. For the seed latex, when the same particle image was measured twenty times, σ was typically 0.015 - 0.018 μm or 0.6 - 0.7% of the particle diameter (D_N). This certainly contributes to a larger than 'real' standard deviation.

304

Off-sized particle analysis was limited to particles signifi-
cantly larger (≥ 2 X particle volume) than those in the main distribu-
tion. No attempt was made to analyze for undersized particles re-
sulting from particle nucleation in the aqueous phase. These were
particularly obvious in the Flight and Ground #3 samples from the
cloudiness of the aqueous phase above the sedimented particles.
Table 5-5 gives the relative numbers of over-sized particles, which
were 30 - 80% larger than those of the main distribution. These re-
sults showed that the number of over-sized particles increased with
increasing swelling ratio. No conclusion could be drawn on the ef-
fect of gravity on the production of over-sized particles.

Table 5-5

Analysis of Over-Sized Particles

Sample	Nominal Buildup	Number Related to Main Distribution
Flight #1	2/1	1/264
Ground #1	2/1	1/339
Flight #2	4/1	1/207
Ground #2	4/1	1/172
Flight #3	10/1	1/99
Ground #3	10/1	1/65

The polymerization kinetics, both flight and ground, for the
large-particle-size latexes are combined in Figure 5.9. These rep-
resent only the ~70°C portion of the experiments. There does not
appear to be any significant difference in the polymerization rates
in microgravity versus on the ground. The difference in the place-
ment of the curves was caused by interpretation difficulties during
the heat-up/expansion period. This may be partially caused by the
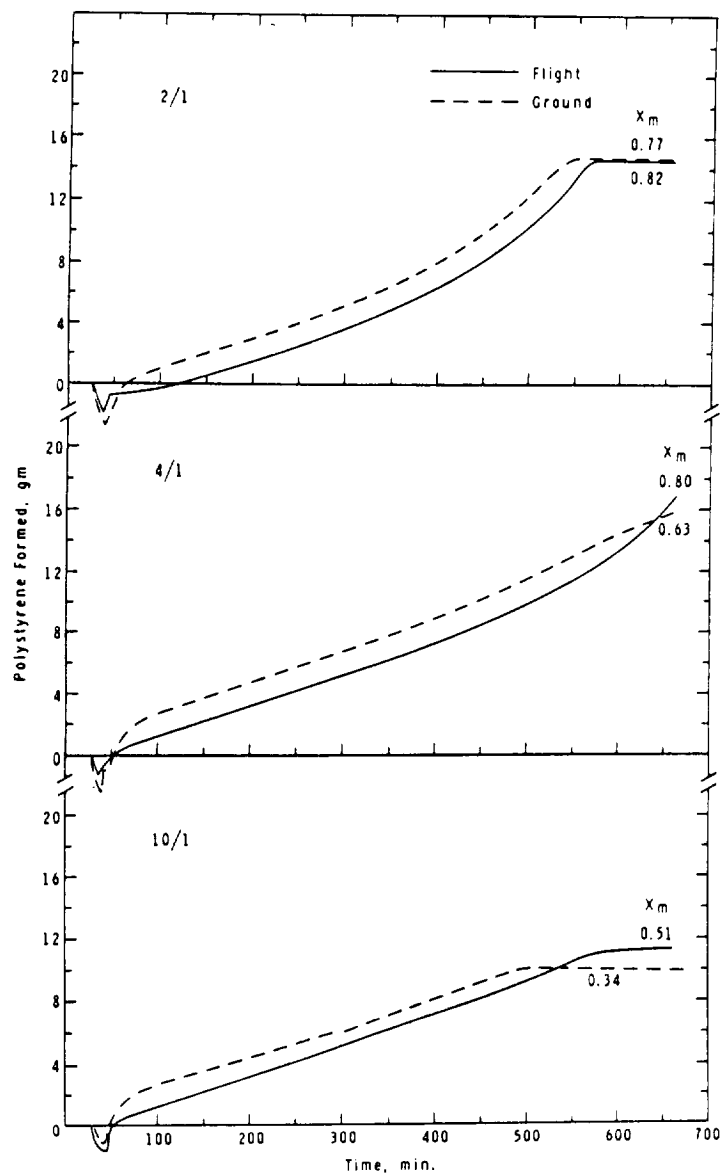
Figure 5.9 Conversion (Polystyrene Formed) Histories for STS-3
Flight and Ground-Based Polymerizations of Large-
Particle-Size Latexes

voltage drop problem mentioned previously. A $2 - 2.25^{\circ}$C higher temperature was recorded for all reactors during the ground run as compared to the flight. The lack of a back-up ring on the lower piston o-ring compounded the problem. None of the kinetics was complete in terms of the rate passing through a maximum and slowing due to the gel effect. The curves representing the 2/1 and 10/1 swelling ratios show apparent sudden cessations of polymerization. In the latter case this was caused by the formation of N_2 bubbles from the decomposition of the initiator following saturation of the fluid. In the former case, however, this was not likely and might instead be attributed to increased resistance of the piston to movement (possibly from the buildup of a polymer layer at the o-ring). Recall that a similar recipe had given nearly complete kinetics when polymerized in the LUMLR prototype (CMT 3). (A dry run in the flight reactors indicated that incomplete kinetics would be obtained using AMBN at an initial concentration of 6.8 mM on monomer (CMT 9).) The 4/1 swelling ratio experiments did not exhibit this abrupt stop in the piston movement, but the ground run did show a slowing of the rate after 575 min. which may have been caused by N_2 bubble formation.

Direct comparison of the kinetics for the three swelling ratios could not simply be done by comparing the conversion histories since each began under conditions in which $[M]_p$, $[I]$, and k_t differed. Each of these affects the rate of polymerization, $[M]_p$ and k_t being a function of conversion and $[I]$ a function of time:

$$R_p \propto [M]_p \left[\frac{[I]}{k_t} \right]^{\frac{1}{2}} \qquad .$$

(5.1)

307

For such large particles, polymerized using an oil soluble initiator, the kinetics follow the same relationships as found for bulk, solution, and suspension, independent of particle size and number. (See Chapters 3 and 4.) Deviation occurs only when significant numbers of submicron particles are nucleated in the system.

The 'initial' polymerization rates (judged to be reliable at 75 min. into the experiments) for the flight experiments are given in Table 5-6 along with some other pertinent information. An increasing polymerization rate with increasing initiator (and decreasing w_p) indicated that the change in k_t at low w_p did not override the effect of increasing initiator and increasing monomer concentration in the particles. Both of these should contribute significantly to the increase in the polymerization rate. At higher conversions, however, k_t becomes dominant in that it decreases more rapidly with time for the lower swelling ratios, giving rise to greater polymerization rates. This explains what is seen as an increasing gel effect with decreasing swelling ratio.

Table 5-6

Kinetically Related Parameters - STS-3

Sample	$[I]_o$ mM	$[M]_{po}$* mole/l.	R_p(75 min.) mole/l.sec.	$\bar{n}$(75 min.)	$\bar{M}_n$ $\times 10^{-5}$	$\bar{M}_w$ $\times 10^{-6}$
Flight #1	5.6	6.0	8.6×10^{-5}	700	2.3	1.00
Flight #2	7.9	6.9	12.4×10^{-5}	1100	2.3	0.89
Flight #3	13.8	7.5	13.6×10^{-5}	2200	1.7	0.64

*based on swelling ratios estimated from iso-octane extractions.

The average number of radicals for particle, $\bar{n}$, is commonly used to characterize the kinetics of emulsion and seeded smulsion

308

polymerizations. Table 5-6 lists some initial values of $\bar{n}$ which are much greater than those typically reported. Large particle sizes were responsible for these large values. Polymerizations (emulsion) of this nature follow Smith-Ewart Case 3 kinetics ($\bar{n} \gg 1$) [46] where $\bar{n}$ is defined by:

$$\bar{n} \doteq \left[\frac{R_i \, v \, N_a}{2 \, k_t \, N_p} \right]^{\frac{1}{2}} \quad . \qquad (5.2)$$

Figure 5.10 presents $\bar{n}$ as a function of weight fraction polymer in the particles for the three STS-3 flight experiments. The results for the two lower swelling ratios paralleled each other with the larger particle size having the greater $\bar{n}$. The upturn, of course, was due to the gel effect. Too little data were obtained for the highest swelling ratio to check if $\bar{n}$ increased similarly at high conversion.

The weight and number average molecular weights are also reported in Table 5-6. A decrease in $\bar{M}_w$ as expected, was found with increasing initiator concentration.

In the previous two chapters the results of a seed sequence (SSMLR 13) were reported which was designed to parallel the STS-3 Flight Recipe #1 in the eighth step of the sequence. Similar recipe conditions were imposed to create conditions in which a comparison would be valid. The particle seed size for SSMLR 13-8 was 2.47 µm, this being comparable to the 2.52 µm seed used in the flight experiments. Figure 5.11 combines the conversion histories obtained for each case, plus the model predictions reported earlier (see Figure 4.12). The flight results parallel the SSMLR 13-8 data quite well,
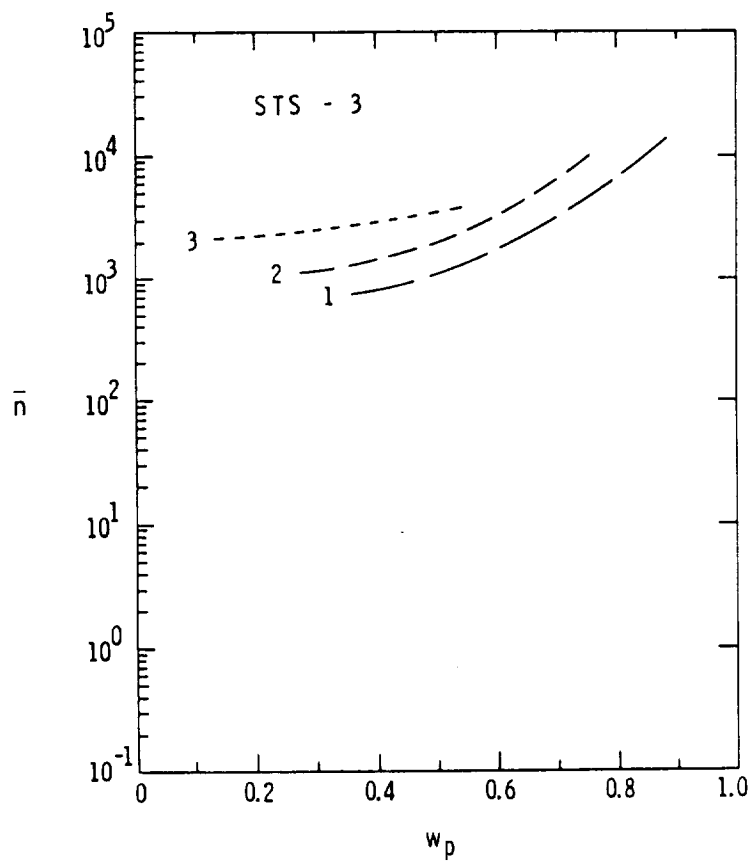
Figure 5.10 $\bar{n}$ as a Function of Weight Fraction Polymer in the Particle, STS-3 Flight Results
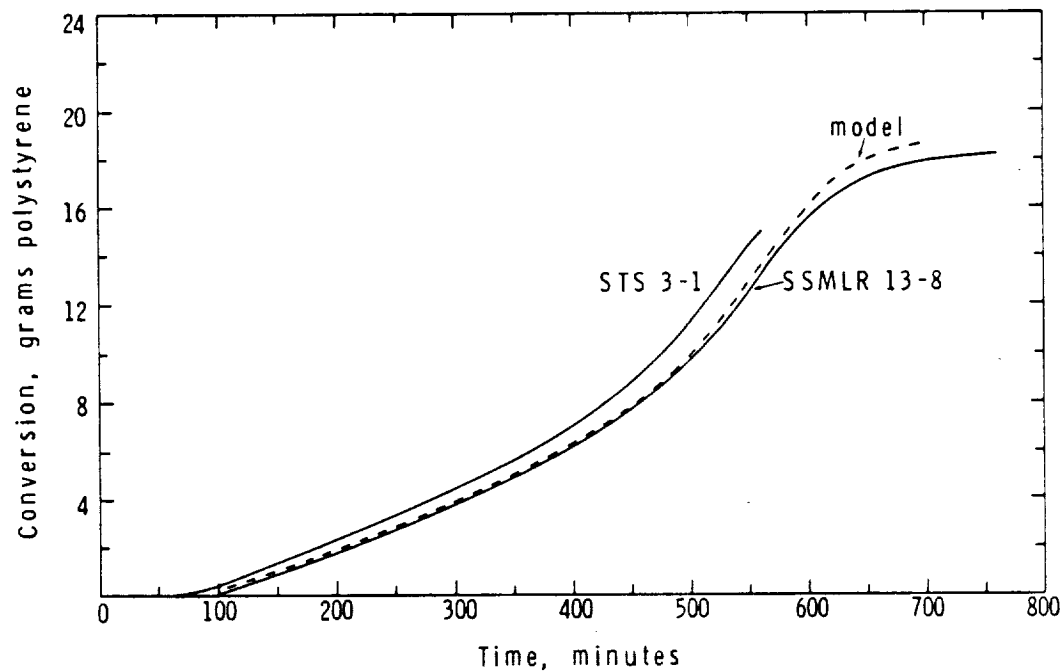
Figure 5.11 Comparison of Conversion Histories of STS-3 Flight
Recipe #1 with the Results of SSMLR 13-8 (See Figure
3.42). Model Predictions are also Included (From Figure
4.12)

311

the difference being an approximately 30 min. shorter induction period for the flight experiment, as well as the incomplete conversion history. A similar shift in the curves was noted in SSMLR 13 with the addition of the extra stabilizers. The similarity of the results, despite the different pathway for seed development, was encouraging from the view of reproducibility of kinetics of polymerization under similar but not identical conditions.

5.3.2.5 Submicron 'Control' Latex

No significant monomer odor was detected when the submicron latex (recipe #4) was decanted from the flight reactor. The data, however, indicated that no piston movement, hence polymerization, took place once the reaction temperature was reached. In contrast, the left-over, swollen flight latex was returned to Lehigh, and then loaded and polymerized at about the same time that the experiment was activated in microgravity. This sample showed little conversion (<5%) over the 4 days since preparation and gave the expected conversion history, as shown in Figure 5.12.

Two possibilities could explain the results obtained from the flight: 1) the piston stuck in the up position after fluid expansion during heat-up and polymerized normally; or 2) the latex had polymerized under ambient conditions prior to activation of the experiment. The data was examined further, particularly the expansion period. Two sets of computations were made, assuming, first, that all the monomer initially present was still present and, second, that all the monomer had been converted to polymer. The results are given in Figure 5.13, the circles representing the calculations based on
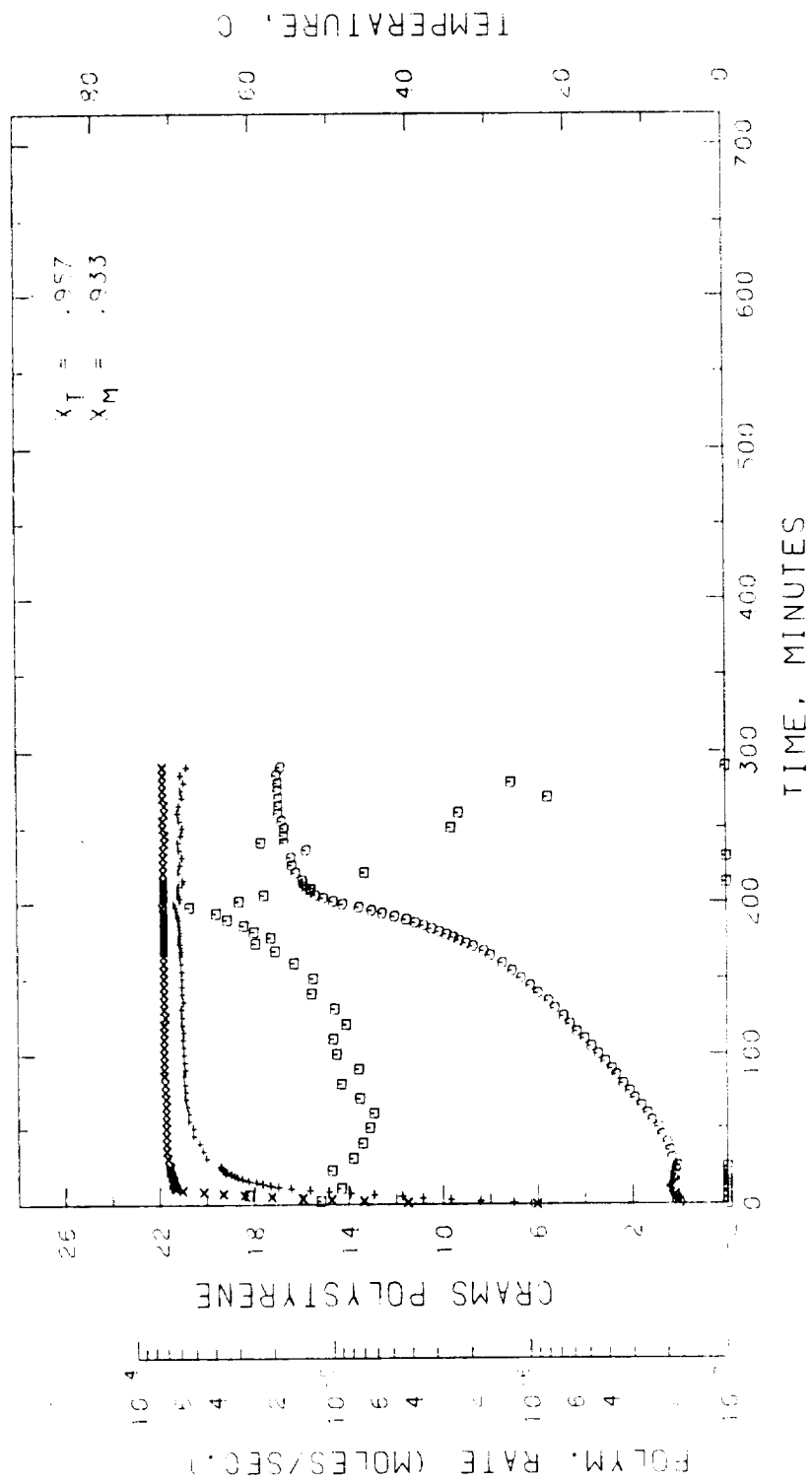
Figure 5.12   Polymerization Data Obtained for the Control Recipe (#4) in the LUMLR. ⊙ Represents the Grams PS Produced, ⊡ , the Polymerization Rate, + and x, the Fluid and Cylinder Temperatures, Respectively

313
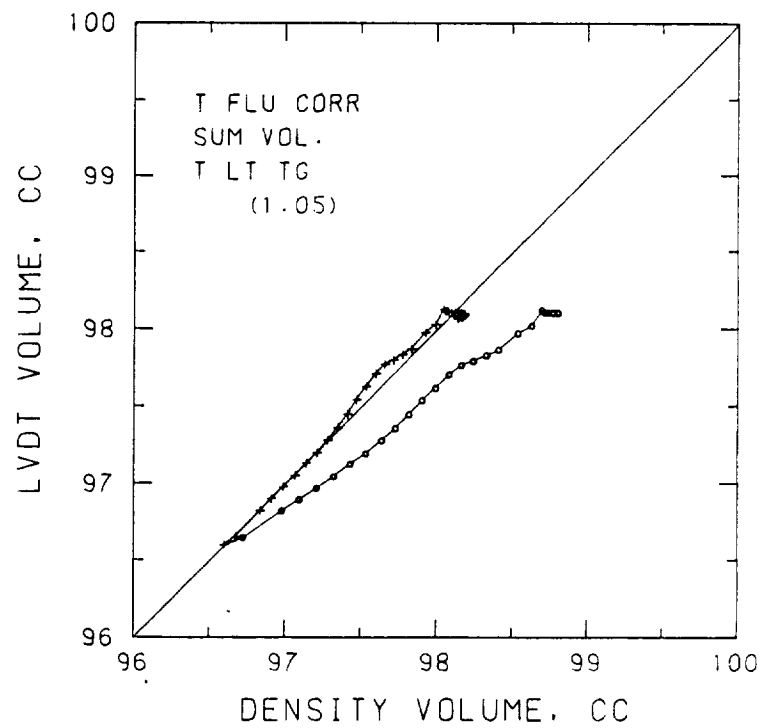
Figure 5.13 Interpretation of the Fluid Expansion for the STS-3
Submicron 'Control' Recipe #4. The Circles Represent
Computations Assuming no Conversion and the +'s Assuming
Complete Conversion

the first assumption. It was obvious from this that the second assumption was correct and that somehow complete polymerization took place at ambient conditions. This was contrary to what was found in the pre-flight testing of this recipe. Furthermore, in ground tests conducted in both the flight and prototype dilatometers, polymerization was found to occur at ambient conditions after an induction period of about 25 hrs. These results are shown in Figure 5.14. Oxygen inhibition is well known in emulsion polymerization [106] and was suspected to play a role in these results. However, degassed and undegassed samples did not show much difference in the length of the observed induction periods. Despite these results, it still appeared likely that the pre-flight test of the recipe in the glass bottle was not conducted with as much care to exclude oxygen as hindsight would dictate.

5.4 STS-6 Experiments

The STS-3 results showed that no significant advantage was gained by preparing monodisperse latexes in microgravity with particle sizes up to 4.0 μm. Some slight advantage was seen for the 5.0 μm size; however, size alone may not have been the critical factor, considering that a high swelling ratio (greater bouyancy) may have contributed more to the differences found.

In the original project outline, each successive flight latex would be prepared using seed particles which were the products of the previous flight experiments. With the improvements in the ground-based preparation process [80], however, it was decided to prepare 5.5 μm monodisperse polystyrene seed on the ground. Purifi-
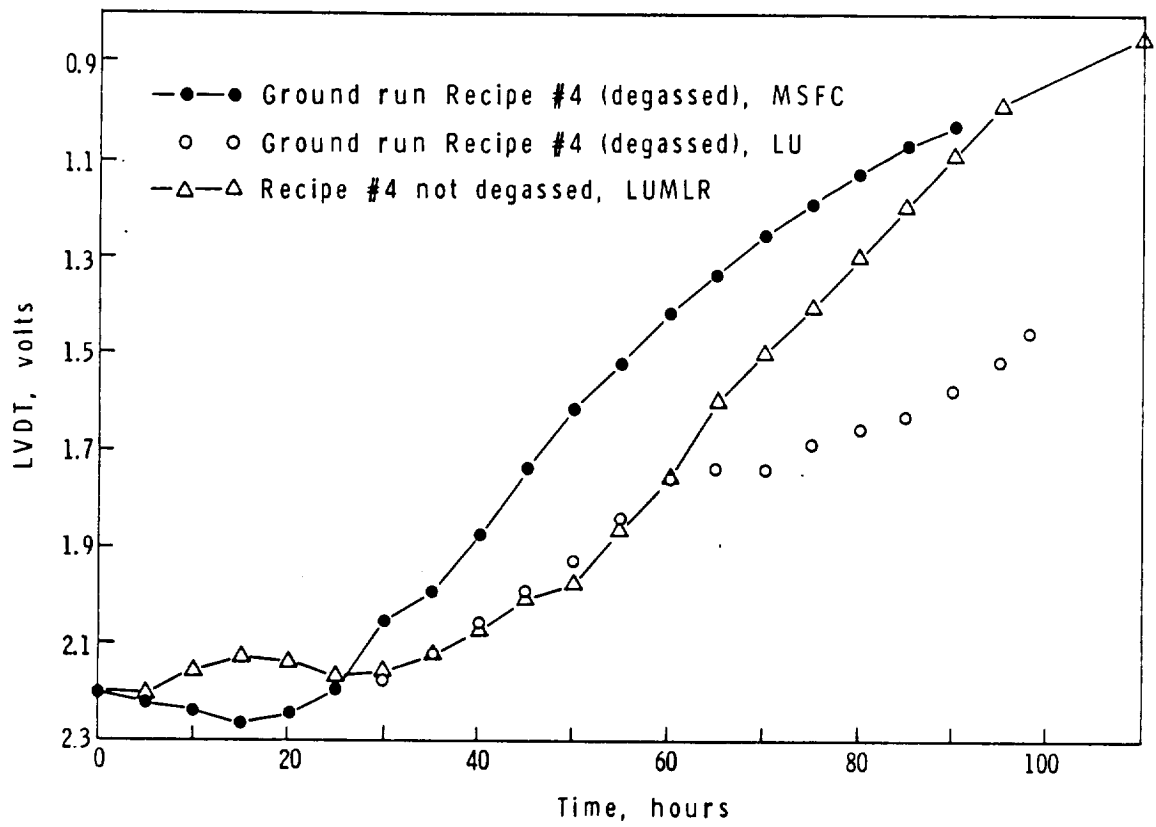
Figure 5.14   Piston Movement at Ambient Conditions with Submicron
Flight-Type Recipes (~53% Conversion per Volt)

316

cation methods ensured the absence of any significant numbers of off-size larger or smaller particles. Four recipes were developed for the STS-4 flight experiments which would grow this seed to nominal sizes of 7.9, 9.4, 10.5, and 11.4 μm (2, 4, 6, and 8 to 1 swelling ratios). STS-4 was successfully launched with these recipes on board, June 22, 1982. Upon return, however, the latexes were all found to contain high quantities of unreacted monomer and no data were found on the tape. Upon analysis, three samples were found to have polymerized to approximately 55% conversion (2, 4, and 8 to 1 swelling ratios) while the fourth had a conversion of 73%. No further analysis was performed nor any ground-based control experiments run. A power converter, one of two in the SEP, had failed some time prior to the activation of the experiment. As a consequence, the MLR experiment was de-manifested from STS-5 so that the failure could be more thoroughly diagnosed and steps taken to ensure against such a failure in subsequent flights.

5.4.1 Pre-Flight Developments

The need for a longer time at reaction temperature, demonstrated by the STS-3 experience of limited kinetic measurements, resulted in reprogramming of the process time modules on the reactors to give approximately 6½ more hours of polymerization time (total $\approx$ 17 hrs.) and data acquisition. Limitation on the time was determined by the data tape capacity. Recipes designed for the flight experiments were subsequently modified to accommodate the new time line.

317

Teflon back-up rings were mounted on all pistons to prevent o-ring roll and thereby aid in the interpretation of data, particularly during the heat-up period.

The large-particle-size recipes were quite similar to those reported for STS-3. A 5.6 μm polystyrene seed was similarly prepared on the ground, as for STS-4, but with the exception that a small amount of cross-linking agent, divinylbenzene (DVB), was included in the recipe [80]. Cross-linking of the seed was intended to provide some resistance to coalescence during the collision of swollen particles. DVB was also included in the STS-6 recipes. To supplement the hydroquinone inhibitor, a small amount of benzoquinone (BQ) was also added. Pre-flight polymerizations in both the prototype and flight dilatometers indicated that the increased reaction time was again not enough to accommodate the entire conversion histories at the higher swelling ratios.

A submicron 'control' experiment was once again planned for the STS-6 flight. It would use the same basic recipe as defined for STS -4 but also incorporate an inhibitor to prevent the premature polymerization of the styrene monomer. The inhibitor para-tert-butyl catechol (TBC) was the first tested. This is frequently used to inhibit polymerization in commercial styrene monomer. Four polymerizations were run in the flight hardware using the same submicron control recipe but with four different levels of inhibitor. The conversion histories are combined in Figure 5.15. No induction periods were induced but rather increased degrees of retardation resulted. 290 ppm represented 1/2 of the initial molar quantity of

318
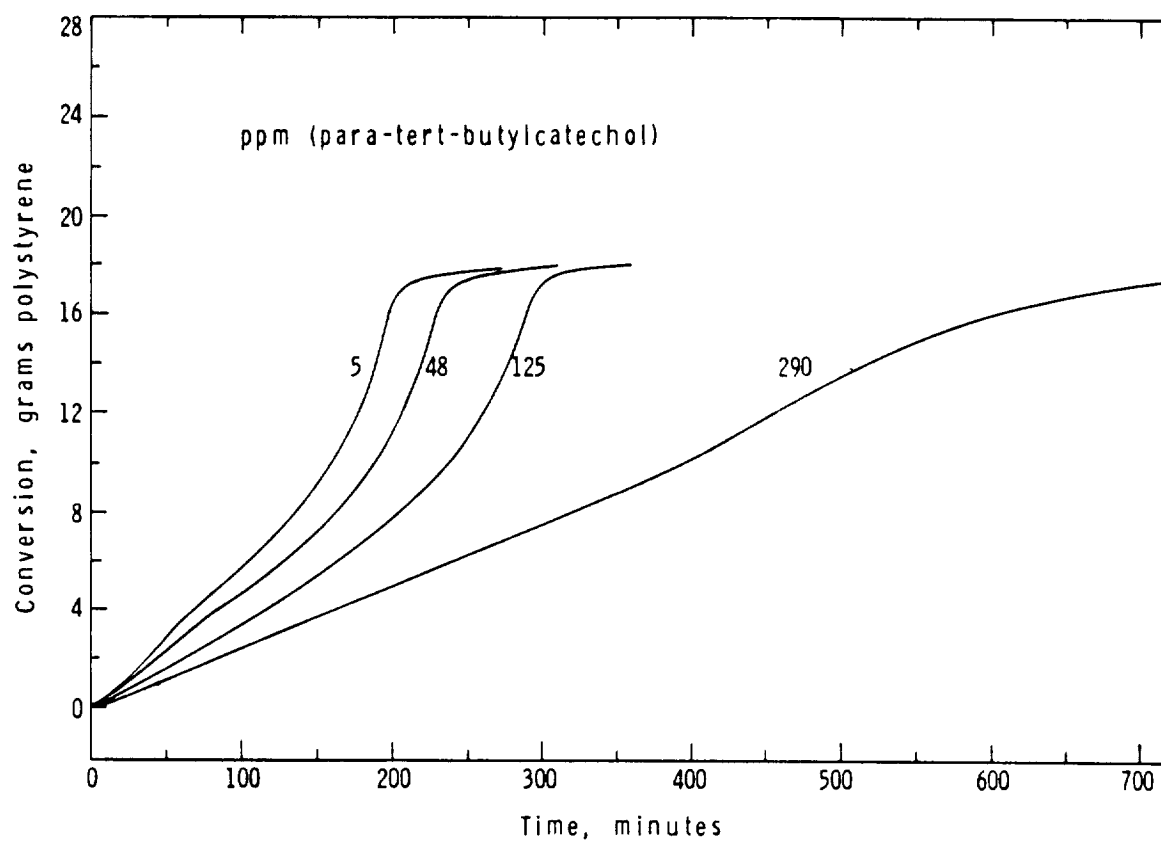
Figure 5.15   Conversion Histories Obtained for the Seeded Polymeriza-
tion of Styrene/Polystyrene in the Presence of Various
Quantities of Para-tert-butylcatechol. 2/1 M/P, 30%
Solids, 1 mM $K_2S_2O_8$

319

persulfate in the recipe. An additional test was run at ambient
conditions using 20 ppm TBC. A 35 hour induction period was found,
similar to previous findings without an inhibitor. Polymerization
occurred at a rate comparable to the non-degassed recipe in Figure
5.14.

This work was continued with a second inhibitor, hydroquinone
[107]. This was found to inhibit the seeded emulsion polymerization
of styrene/polystyrene ($K_2S_2O_8$ initiator) for lengths of time pro-
portional to its initial concentration. The observed induction per-
iods were only 1.8% of those expected for a 100% inhibition effici-
ency. This was possibly due to the slow oxidation of hydroquinone to
benzoquinone which has been postulated to be the actual inhibitor.
An initial hydroquinone concentration of 6 ppm was found to prevent
polymerization over a 4-day period at ambient conditions and yet
produce a conversion-time curve paralleling that produced without
any inhibitor. Concern over the actual ambient conditions experienced
in the Orbiter (reportedly >38°C (100°F)) at times and the possibil-
ity of a delayed launch (the EAC and SEP would not be removed unless
the delay exceeded 5 days) brought about a re-evaluation of this re-
cipe to take these into consideration. Higher quantitites of HQ
were known to cause retardation as well as induce induction periods
but this was considered to be a better alternative as long as the
polymerizations were reproducible. Two experiments were run using
25 ppm HQ, the first polymerization being conducted immmediately
after preparation of the swollen latex while the other was subjected
to a 30°C environment for 4 days in the LUMLR prototype and then

320

polymerized. The kinetics are reproduced in Figure 5.16. The curves are nearly identical in shape, the only difference being a longer induction period for the sample polymerized without a delay. These results were the basis for designating this recipe for the STS-6 Flight.

5.4.2 Flight and Ground Experiments

STS-6, the maiden flight of the 'Challenger', was launched April 4, 1983. Pre-flight activities in terms of recipe preparation, reactor loading, and hardware preparation and mounting in the Orbiter were performed as described previously. A leak in one reactor (#3) necessitated a re-load of the flight recipe. Processing began approximately four days after the loading. Post-flight latex recovery was shifted to Edwards Air Force Base (Dryden Flight Research Facility) in California from MSFC to ease the reactor handling requirements. Ground-based analogues of the flight experiments were conducted immediately after the hardware was returned to MSFC. In this case, the polymerizations were conducted the day following recipe loading, without the four-day delay as in the flight time-line.

The STS-6 recipes, as designed, are listed in Table 5-7. Note the similarities to the STS-3 recipes.

5.4.2.1 STS-6 Results

Two of the four flight latexes (Recipes 10 and 12) possessed a strong monomer odor indicative of incomplete conversion. The data indicated that the reactor containing recipe 10 had never heated up. A broken wire was subsequently found and repaired for the ground run. Recipe 12 was again found to have a monomer odor following the
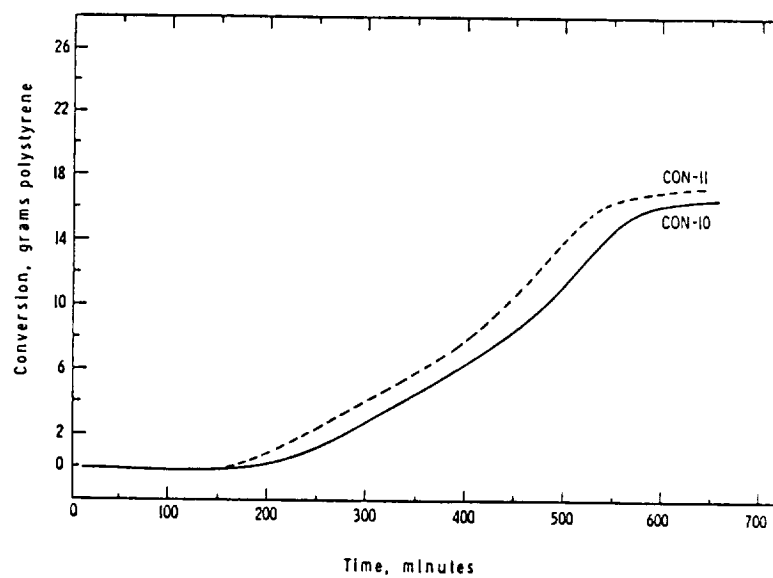
Figure 5.16   Comparison of the Conversion Histories for a Recipe
Polymerized Immediately after Loading (CON-10), and
a Recipe Exposed to a 30°C Environment for 4 Days Prior
to Polymerization (CON-11) [107]

322

Table 5-7

STS-6 Flight Recipes (Design)

Recipe #	9	10	11	12
Seed diameter, μm	5.6	5.6	5.6	0.19
Monomer*/polymer	2/1	4/1	6/1	2/1
Final particle diameter, μm	8.1	9.6	10.7	0.27
$[AMBN]_o$, mM (on styrene)	3.53	5.10	6.04	--
$[K_2S_2O_8]_o$, mM (on aqueous phase)	---	---	---	0.50
AMA[†]	0.0143	0.0071	0.0057	0.0886
KX-3[†]	0.0243	0.0186	-.0171	---
PVP[†]	0.1943	0.1771	0.1657	---
HQ[†]	0.0343	0.0343	0.0343	0.0036
BQ[†]	0.0009	0.0009	0.0009	---

*0.015% divinylbenzene added based on monomer

[†]Weight percent based on the aqueous phase

ground-based polymerization. The solids contents along with the iso-octane extraction results of the swollen latexes are given in Table 5-8.

Table 5-8

Solids Contents and Results of Iso-Octane Extractions
of STS-6 Flight and Ground Latexes

		gm Styrene/100 gm Latex	
	% Solids	Experiment	Design
Flight #9	26.9	18.41	20.0
Ground #9	17.7	20.00	
Flight #10	--	--	24.0
Ground #10	21.4	23.58	
Flight #11	22.0	23.11	25.7
Ground #11	22.9	24.04	
Flight #12	24.85	18.72	20.0
Ground #12	25.81	19.35	

The yields (nominally 30% solids) for recipes 10 and 11 were reduced due to some coagulation formed in the reactors. A small quantity of bouyant spheres 0.1 to 1.0 mm in diameter were found in the two latexes having a surface consisting of a single layer of particles. Incomplete polymerization accounts for those measured for recipe 12 (70.0 and 79.6% conversion for flight and ground latexes).

The results of the particle size analysis are presented in Table 5-9. Narrow main distributions were obtained in all cases except ground latex #11. The distribution of this latex revealed a larger tail on the small-particle-size side of the distribution. This type of broadening was also seen in the ground #3 latex (see Figures 5.7 and 5.8). Agitation insufficient to prevent creaming of the latex was considered responsible for this phenomenon.

The flight latexes contained a number of deformed particles having a barrel-type shape as well as some over-sized particles. (It was found that the barrels could be reformed into spheres by heating the latex to ~90°C with gentle agitation for an hour.) The relative numbers are also given in Table 5-9. These results are quite similar to those found for STS-3 (with the exception of the barrels). The number of over-sized particles increased with the increased swelling ratio. Particle size again does not oppear to be the dominant factor. From these experiments it was not obvious that microgravity offers a clear-cut advantage in producing monodisperse latexes up to 10 μm in diameter.

324

Table 5-9

STS-6 Particle Size Analysis-Results

Sample	Nominal Buildup	D_n, μm	σ, μm	n	σ/D_n, %	Relative # of Particles	
						Deformed[1]	Over-Sized
Seed	---	5.63	0.073	328	1.30	0	1/168
Flight #9	2/1	7.94	0.122	829	1.53	1/63	1/267
Ground #9		7.86	0.137	675	1.74	-	1/220
Flight #11	6/1	9.96	0.115	1102	1.16	1/62	1/106
Ground #11		10.04	0.281	1059	2.80	1/1410	1/93

[1] consists mostly of barrel-shaped particles.

325
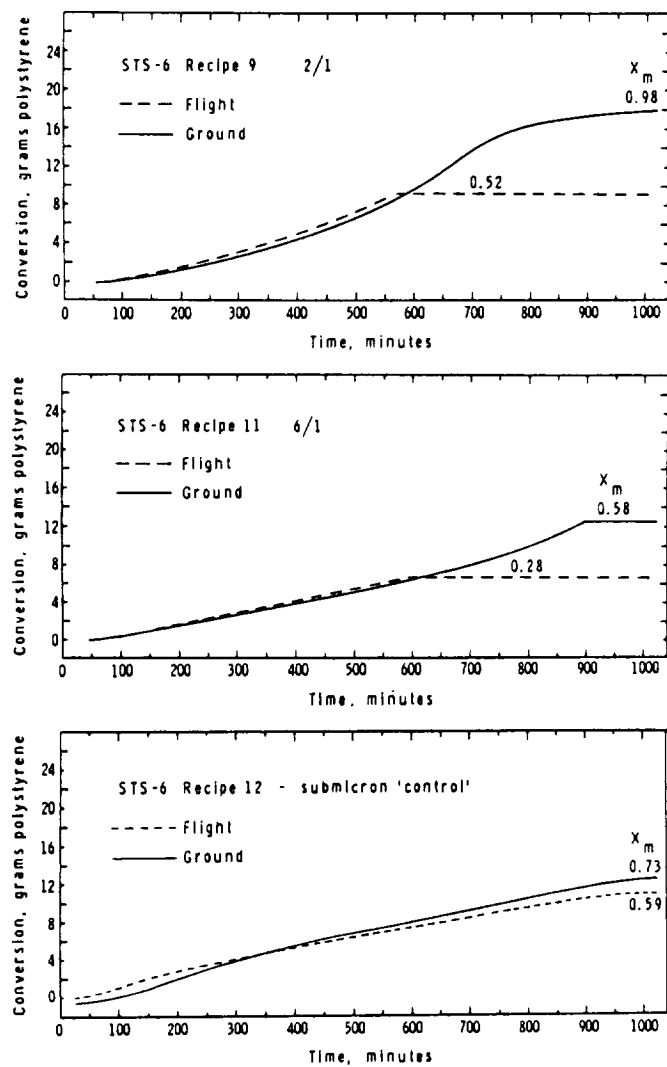
Figure 5.17 Conversion Histories for STS-6 Flight and Ground-Based Polymerizations

The polymerization kinetics for the three flight experiments (minus Recipe #10) are given in Figure 5.17 along with the ground-based results. Piston movement ceased unexpectedly early for the flight experiments 9 and 11. It was unlikely that this was caused by bubble formation. Polymer film buildup on the reactor wall during the delay from loading to activation of the experiment may have been responsible for this problem. The curves follow each other closely up to this point with the flight data showing a slightly faster polymerization rate. A slightly lower overall polymerization temperature for the poorly mixed, creamed latex on the ground could account for this difference. These results are quite similar to the STS-3 conversion histories in terms of the shape of the conversion curves but with slower rates from the decreased amounts of initiator.

The submicron 'control' polymerizations did not give the expected kinetic behavior as illustrated in Figure 5.16. Severe retardation and the absence of significant induction periods characterized these results. No gel effect was evident but rather a decreasing polymerization rate with time. Analysis of the data revealed that $\bar{n} \sim 0.3$ throughout the polymerizations, a significant deviation from Case 2 ($\bar{n} = 1/2$) kinetics. To determine whether the retardation was caused by the recipe itself, the swollen latex which remained from the ground preparation was polymerized in a glass dilatometer at $70^{\circ}C$. The kinetics did not show the severe retardation but rather the expected accelerated (gel-effect) type polymerization kinetics. This indicated that the recipe itself was not defective, but rather that the reactor in some unknown way caused the observed retardation. The re-

327

cipe without the HQ was subsequently run in the same flight reactor with no retardation detected. These results were rather baffling, leading one to suspect some interaction of HQ with the reactor components. This problem remains unresolved.

5.5 STS-7 Experiments

5.5.1 Pre-flight Developments

10.3 μm diameter monodisperse polystyrene latex particles were prepared on the ground via the recipes developed for the microgravity experiments. Seed purification was again accomplished by the repeated sedimentation separation techniques developed by Tseng [80]. Three recipes were designed to use this seed while a fourth would make use of the flight latex #9 produced on the STS-6 mission.

The 10.3 μm seed was first used to test recipes and reaction conditions prior to the flight. Polymerizations indicated that the limit to ground-based preparation of relatively monodisperse latexes within the limitations of the MLR type dilatometers was reached with the 10 μm sized particles. Massive coagulation was found in all cases for recipes having a 6/1 swelling ratio (nominal particle diameter of 19 μm). Polymerizations were conducted varying: 1) the recipe; 2) the orientation of the reactor (right side up vs. inverted) (recall that the stir blade clearance is much greater at the piston end of the reactor); 3) the stir paddle size (original vs. current design); and 4) the process oscillatory agitation speed (6 vs. 13 rpm). Partial of near-total coagulation was found in tests of the 4/1 swelling ratio (nominal particle diameter of 17 μm) but some conclusions could be drawn from the results: 1) an inverted reactor favors an increased

328

yield, i.e., agitation prior to conditions of sedimentation ($w_p > .66$ or $M/P < 0.53/1$) was the more critical factor; 2) the larger paddle size (same configuration) and greater agitation (13 rpm) favored less coagulation (through sedimentation). These tests were run without much concern for the pre-process agitation since little time was spent in this mode before experiment activation. Creaming studies, performed earlier using a 5 µm seed swollen with about 5 times its weight in styrene monomer, showed that intermittent agitation (90 sec. every 30 min.) was insufficient to prevent a significant creamed layer from forming. Moreover, continuous oscillatory agitation (13 rpm) also could not prevent some noticeable separation, particularly in the region not swept out by the stir blade. No direct evidence was obtained with regards to the effect of such conditions on the monodispersity of the swollen sample. From the results of the STS-6 flight experiments it could be inferred that the effects for that size range were negligible. Nonetheless, it was decided that all reactors would be run with continuous pre-process agitation from loading to process. Two reactors also incorporated two separate agitation speeds, one for pre-process and the other for process. The various combinations designated for STS-7 are listed in Table 5-10. Recipes 15 and 16 were

Table 5-10

Recipe and Agitation Conditions for STS-7

Recipe #	Seed diameter, µm	M/P	Oscillatory Agitation rpm	
			Pre-Process	Process
13	7.9 (STS-6 #9)	6/1	13	13
14	10.0	4/1	13	13
15	10.0	6/1	13	6
16	10.0	6/1	6	3

identical with the agitation being the tested variable. A lower agitation speed for processing was considered appropriate since mixing was only needed to reduce temperature (not particle) gradients within the latex.

5.5.2 Flight and Ground Experiments

STS-7 was launched on June 18, 1983. Within four hours after launch the continuous pre-process agitation was shut off. Twenty six hours later the experiment was activated, approximately four days after loading. Product recovery was again at Edwards Air Force Base, bad weather preventing the first scheduled landing at the Kennedy Space Center (KSC). The ground-based experiments were performed at KSC immediately after the hardware was returned. The polymerizations were again performed the day after the loading, without subjecting the swollen latexes to the full four-day delay as in the flight.

The STS-7 recipes are given in Table 5-11. Three of the four (13, 15, and 16) had the same swelling ratio and added amounts of initiator and inhibitor. These were a close match to recipe #11 of STS-6. Particle size was the major difference for the three recipes 11,13 and 15.

5.5.2.1 STS-7 Results

All four reactors functioned properly for both the flight and ground-based experiments. Little or no monomer odor was detected in any of the latexes. Various amounts of coagulum were found in each sample as indicated by the results presented in Table 5-12. Flight latexes 13 and 14 had lower yields than their ground-based counterparts, while the others (15 and 16) had much higher product yields

Table 5-11

STS-7 Flight Recipes (Design)

Recipe #	13	14	15 and 16
Seed diameter, μm	7.9[†]	10.0	10.0
Monomer*/polymer	6/1	4/1	6/1
Final particle diameter, μm	15.1	17.1	19.1
$[AMBN]_o$, mM (on styrene)	6.03	4.99	6.02
AMA**	0.0031	0.0071	0.0054
KX-3**	0.0126	0.0179	0.0164
PVP**	0.1347	0.1771	0.1657
HQ**	0.0343	0.0343	0.0343
BQ**	0.0004	0.0004	0.0004

[†]uncleaned seed, product of STS-6, Recipe #9

*0.015% divinylbenzene added based on monomer

**weight percent based on the aqueous phase

Table 5-12

Percent Solids and Estimated Coagulum of STS-7 Latexes

Recipe #	Product % Solids	Coagulum %
Flight 13	17.26	17*
Ground 13	21.78	15
Flight 14	17.12	34*
Ground 14	24.08	20
Flight 15	20.46	5*
Ground 15	12.87	43
Flight 16	19.80	10*
Ground 16	3.40	87

*estimated from the amount separated from the latex and recovered from the reactor; all others estimated from predicted versus measured product solids.

than obtained on the ground. The latter are simply explained by the ineffective agitation which led to sedimentation and irreversible flocculation of particles on the ground. The lower yields in micro-gravity are not so easily understood. One possibility was that the three days of pre-process agitation before the launch, which was not experienced by the ground-based latexes, could have acted to destab-ilize some of the particles. This did not, however, seem to have affected the larger particle size recipes (15 and 16), although re-cipe differences make this comparison questionable.

The results of the particle size analysis are given in Table 5-13. The main distributions of all flight latexes were quite narrow. The relative numbers of over-sized particles increased slightly for the samples and more so for the ground analogues. Deformed particles were also found in the flight samples as experienced previously in STS-6. Significant quantities were not found in the ground samples except for 13 which was prepared from the 7.9 μm flight seed which itself contained 1/63 deformed particles. The PSD for ground latex 16 was so broad that particles distinctly oversized were not obvious. It should be noted that in all samples a significant number of sub-micron particles were evident from the cloudiness of the aqueous phase above the sedimented particles, these being nucleated during the polym-erization process. The content of these particles was not determined.

The conversion histories are presented in Figures 5.18 and 5.19. Exact interpretation of the data was made difficult by uncertainties in the reactor contents. The method used for determining the styrene content in the swollen latexes was, as in all previous experiments,

Table 5-13

STS-7 Particle Size Analysis

Sample	Nominal Buildup	D_n, μm		σ, μm	n	σ/D_n, %	Relative # of Particles	
							Deformed	Oversized
Seed (14,15,16)	---	10.30		0.135	300	1.31	Negligible	1/130
Flight 13	6/1	13.12	(12.75)*	0.149	327	1.13	1/60	1/120
Ground 13		13.89	(13.60)	0.371	308	2.67	1/60	1/120
Flight 14	4/1	16.64	(16.21)	0.201	322	1.21	1/110	1/90
Ground 14		17.17	(16.35)	0.394	326	2.29	Negligible	1/50
Flight 15	6/1	17.81	(17.61)	0.210	3.21	1.18	1/770	1/70
Ground 15		17.68	(17.25)	0.949	275	5.37	Negligible	1/50
Flight 16	6/1	18.18	(17.73)	0.200	321	1.10	1/100	1/110
Ground 16		16.97	(17.12)	0.778	361	4.58	---	---

*calculated from the measured swelling ratios

333
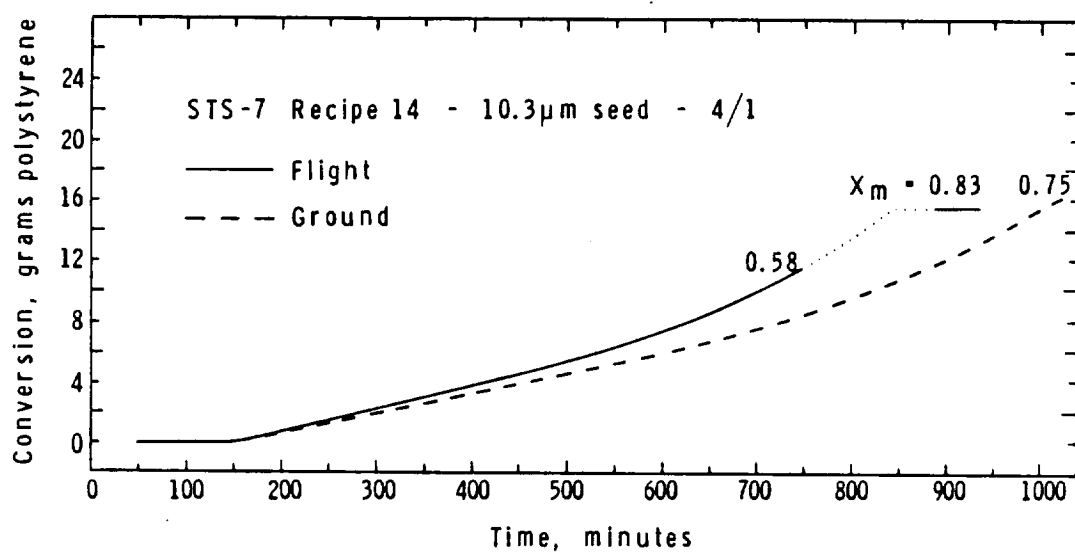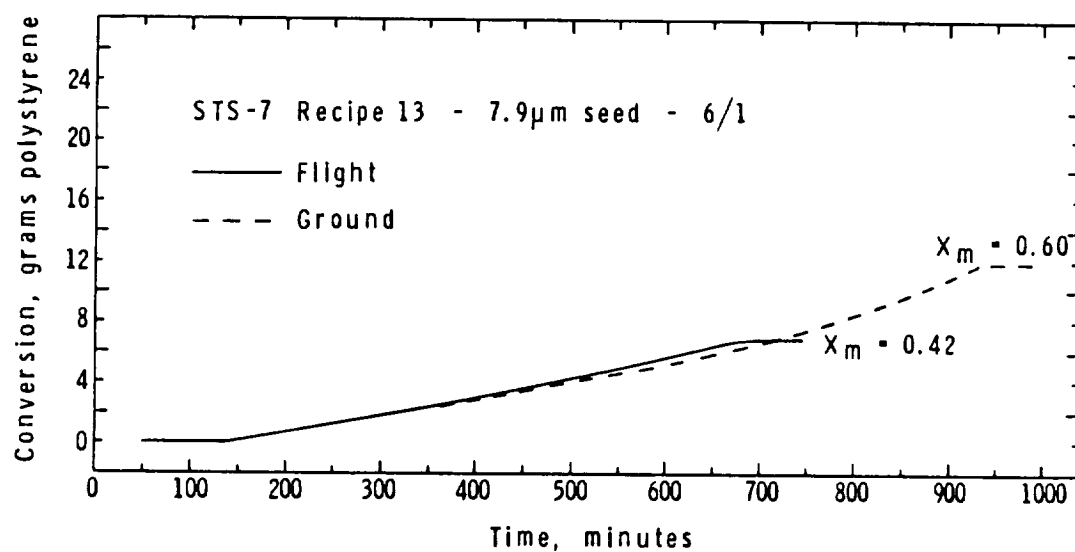
Figure 5.18 Conversion Histories for STS-7 Flight and Ground-Based
Polymerizations, Recipes 13 (Top) and 14
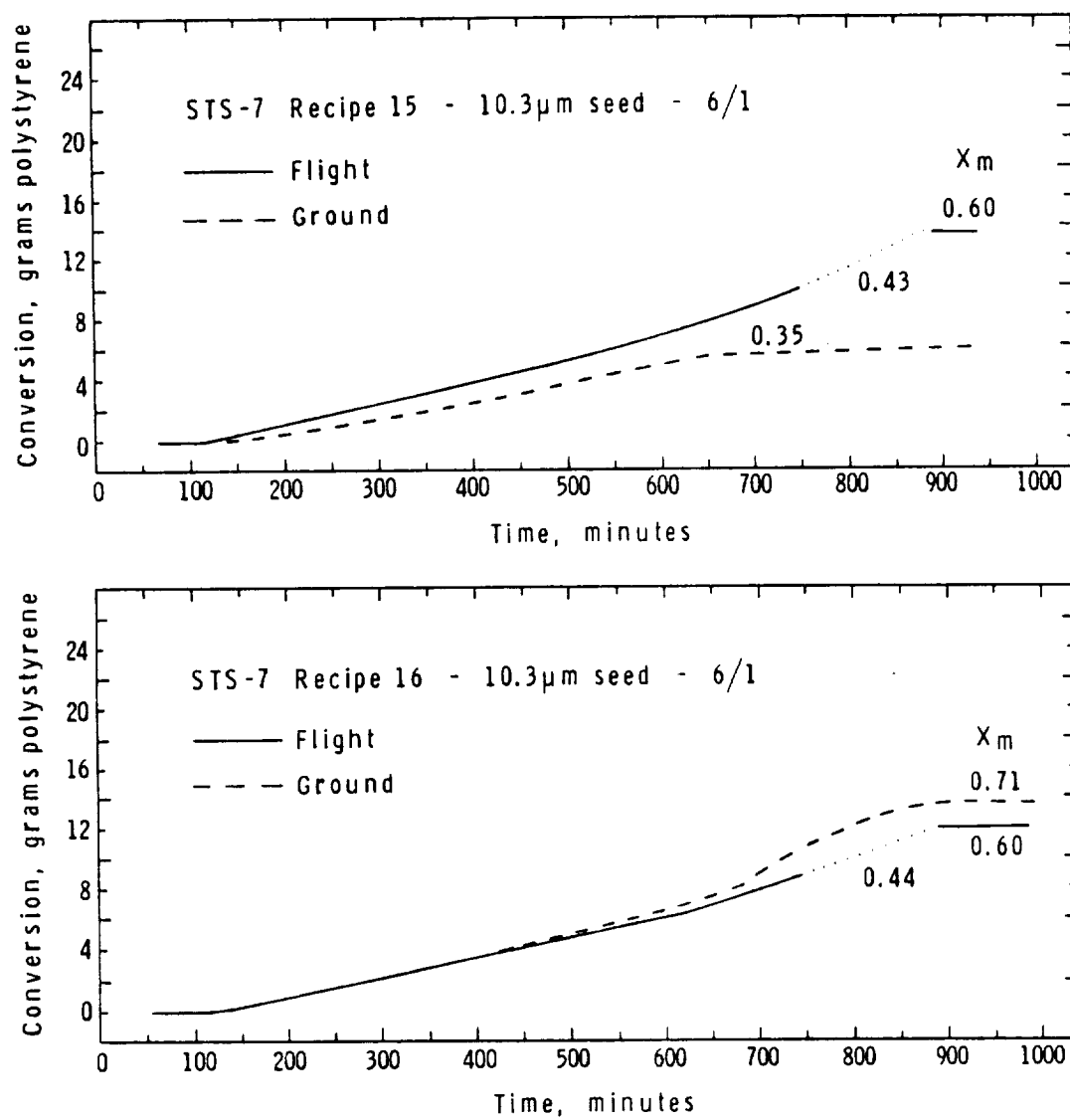
Figure 5.19   Conversion Histories for STS-7 Flight and Ground-Based
Polymerizations, Recipes 15 (Top) and 16

335

through iso-octane extraction/UV analysis of the latex expelled into the overflow flask during the loading process. The increased particle size, however, caused increased creaming rates which was visually obvious in the fill flask and also in the tubing leading to the reactor. The loading procedure did not include any agitation of the latex and thus creaming in the reactor was bound to occur. The expelled latex would, therefore, be rich in swollen particles and result in measured styrene contents on the high side. The more rapidly a reactor was filled, the more accurate would be the analysis. (This problem should be resolved for any future experiments.) The results of the iso-octane extractions are given in Table 5.14. Considerable variation is seen in these results but no consistent pattern. All results

Table 5-14

Iso-Octane Extractions and Estimation of Swelling Ratios for STS-7

Recipe #	gms Styrene/100 gms latex		% Solids Swollen Latex	M/P	
	Measured	Design		Measured	Nominal
Flight 13	17.03	25.78	5.18	3.2	6/1
Ground 13	20.72		5.00	4.1	
Flight 14	20.77	24.00	6.86	2.9	4/1
Ground 14	22.54		7.41	3.0	
Flight 15	20.79	25.78	4.96	4.0	6/1
Ground 15	17.68		4.85	3.7	
Flight 16	23.59	25.78	5.46	4.1	6/1
Ground 16	19.86		5.49	3.6	

indicate lower than designed swelling ratios, calculated from the amount of styrene and polymer content, determined by measuring the solids of the swollen latexes (oven dried at $50^{\circ}C$). The particle size calculated from these swelling ratios were, in all but one case,

336

slightly less than the measured particle size with differences ranging from 1 to 5% (see Table 5-13).

The polymerization kinetics for the flight and ground experiments were comparable for recipes 13 and 16, while significant deviations were found in the other two polymerization recipes (i.e., ground experiments had lower polymerization rates than the respective flight experiments). These results were not consistent with any line of reasoning. It was expected that differences would arise due to the creaming and settling experienced on the ground versus their absence in microgravity. Initially creaming would cause more severe temperature gradients, particularly for the lower process stirring rates (13 vs. 6 vs. 3 rpm). This should have resulted in lowered polymerization rates due to the overall lower temperatures on the ground versus in microgravity (as seen for recipes 14 and 15 and also for STS-6 recipes 9 and 11). Indeed, smaller temperature differences were measured between the wall and fluid probes in the flight experiments when compared to their ground-based analogues. Table 5-15 gives a sampling of the temperature differences experienced, measured at 350 minutes into each experiment. The second column should be independent of any error in the calibration of the temperature sensors. It was expected that this difference should increase with increasing bouyancy of the particles and decreasing process agitation. The sedimentation (or creaming) velocity is directly proportional to density differences between the particle and the medium and the square of the particle radius. The density of the swollen particle is the average of the density of the polymer and monomer weighted by their relative quanti-

337

Table 5-15

Temperature Differences Measured during Polymerization for STS-7

Experiment #	ΔT $(T_{wall} - T_{fluid})$, °C	$(\Delta T_{ground} - \Delta T_{flight}$, °C
Flight 13	1.64	
Ground 13	2.10	0.46
Flight 14	1.13	
Ground 14	2.54	1.41
Flight 15	0.02	
Ground 15	3.77	2.85
Flight 16	1.12	
Ground 16	3.27	2.15

ties. The swollen particles should, therefore, cream with increasing rates in the order $13 < 14 < 15 \simeq 16$. The temperature differences confirm this for recipes 13, 14, and 15, while 16 is somewhat low. Moreover, the decreased process agitation rate from 13 (recipes 13 and 14) to 6 (recipe 15) to 3 (recipe 16) rpm should also enhance these differences. The results for recipe 16, however, were contrary to this reasoning. This ambiguity has yet to be resolved.

The approximate conversions at the time of loss of kinetics are also indicated in Figures 5.18 and 5.19. With the exception of recipe 15, more data were obtained for the ground-based polymerizations than the corresponding flight as was seen in some previous cases (9 and 11). Longer induction periods (100 - 140 min.) were experienced in the STS-7 experiments than in STS-3 or 6, even though the HQ levels were comparable. The polymerization rates follow the same pattern as found previously. For swelling ratios greater than 2/1, R_p was initially constant and then began to increase as the gel effect became more

338

dominant. Constant rate periods have been attributed to a number of mechanisms in polymerization: 1) presence of monomer droplets serving as reservoirs and maintaining a constant $[M_p]$; 2) a balance of the decrease of $[M]_p$ with an increase of $k_t^{-1/2}$; and 3) core-shell type swollen particle morphology at the higher swelling ratios. The first was not likely since the swollen latex was always separated from any 'free' monomer prior to reactor loading. Both 2 and 3 have been used to explain such kinetic phenomena [108 - 112]. Core-shell morphology is generally recognized to exist in cases where the polymer and monomer are mutually insoluble. This is generally not the case for the styrene/polystyrene systems; however, the introduction of crosslinking in the seed and product may have some effect on this. The polymerization kinetics for these large-particle-size latexes follow bulk-type kinetics as long as severe new crop generation does not interfere by introducing typical emulsion polymerization into the system.

5.6 Conclusions

Four sets of seeded emulsion polymerization experiments were carried out on board the Orbiters 'Columbia' and 'Challenger' (2 each) yielding nine successful polymerizations of large-particle-size latexes and one submicron latex. Six other experiments were not successfully accomplished, five due to hardware failures and one recipe failure. Analogous ground-based polymerizations were also conducted. The major findings were:

1. 'Monodisperse' must be qualified. The main particle size distributions had a standard deviation of less than 2%. Off-sized larger particles were found to range from 1/360 to 1/50 relative to the

main distributions, generally increasing in number with increasing swelling ratio. Deformed particles, often barrel-shaped, were also found among the larger particle sizes (>7 μm). These existed in quantities similar to the over-sized particles. Small particle generation was not quantitatively evaluated but generally increased with particle size and swelling ratio. These could easily be removed by repeated sedimentation/separation.

2. 'Monodisperse' polystyrene latexes were also prepared on the ground up to 10.0 μm. Generally, the number of over-sized particles was in the same range as the microgravity prepared counterparts. Deformed particles, however, were virtually absent from these latexes. Post-process agitation (cooling down from ~90°C) used for the flight experiments but not for the ground-based analogues could be responsible for this phenomenon.

3. Ground-based experiments revealed that at high swelling ratios (>2/1) the process agitation (oscillatory, 13 rpm) was insufficient to prevent creaming, thus leading to significant temperature gradients and broadening of the PSD's. For particle sizes greater than 10 μm the agitation was also insufficient to prevent significant reductions in product yields due to sedimentation and irreversible flocculation. Flocculation was nearly complete for 17 μm particles prepared with an oscillatory 3 rpm agitation.

4. An oscillatory 6 rpm agitation appeared more efficient than either 13 or 3 rpm in producing 'monodisperse' latexes of large-particle size (>10 μm) in microgravity.

5. The polymerization kinetics of large-particle-size latexes showed no significant differences at the smaller sizes (≤ 5 μm) between the microgravity and gravity environments. As the size increased, the polymerization rate tended to be slightly greater for the flight versus ground experiments because the temperature was more uniform and slightly higher (0.5 to 2.85°C) in microgravity. The kinetics generally exhibited a constant rate period (M/P > 2) followed by an acceleration because of the gel effect.

6. The seeded polymerization kinetics obtained in microgravity for 2.5 μm polystyrene particles swollen 2 to 1 with styrene monomer were nearly identical (with the exception of a shorter induction period) to a similar ground-based experiment which had been the eighth step in a sequence starting with a 0.19 μm seed. A previously developed model (semi-empirical) matched the data fairly well.

7. Complete polymerization kinetics could not be obtained at the higher swelling ratios due to time limitations which determined the amount of initiator (AMBN) required to obtain complete conversions. The N_2 by-product of the decomposition of the initiator first saturated the latex and then formed bubbles, thus nullifying any dilatometric measurements.

8. A submicron 'control' (0.19 μm polystyrene, swollen 2/1 with styrene, initiated with 1 mM $K_2S_2O_8$) was unable to survive the four-day delay prior to activation of the experiments in microgravity. The addition of hydroquinone inhibitor was found to

341

prevent any significant polymerization on a subsequent flight;

however, the kinetics were, unexpectedly, severely retarded

($\bar{n} \approx 0.3$ instead of $n \geq 0.5$). This phenomenon remains unexplained.

CHAPTER 6

CONCLUSIONS AND RECOMMENDATIONS

6.1 Conclusions

Three main areas of research have been described: 1) the characterization and developments in the use of a prototype dilatometer; 2) the preparation and polymerization kinetics of monodisperse latexes obtained in a sequence of seeding steps; and 3) the microgravity preparation of large-particle-size latexes with comparison to ground-based analogues. The following is a summary of the observations and conclusions:

1) The "LUMLR", a stainless steel piston/cylinder type dilatometer, was tested and modified for use in obtaining kinetic data for the seeded emulsion polymerization of sytrene/polystyrene. Volume changes due to heat-up and polymerization could be determined within 2% of the actual values provided that a number of modifications and procedures were adopted. These included: 1) low-pressure/gravity loading; b) prevention of o-ring roll via a back-up ring; c) determining the exact volume (± 0.1 cm^3) and reactor contents (i.e., styrene monomer concentration via iso-octane extraction/UV analysis); d) use of the appropriate density functions (additivity of volume for water and particles, additivity of densities for monomer and polymer); and e) adequate agitation of the reaction mixture.

2) Agitation in the LUMLR was studied in the oscillatory mode (27 cycles/min.). A stirrer paddle was designed, tested, and found to be much more efficient than the original design, particularly at low stirring speeds. 10 rpm with an arc of rotation of 30°C was

343 .

recommended for polymerizations in microgravity.

3) Relatively 'fast' reactions cannot be conducted in the LUMLR under isothermal conditions because of the finite heat-up period, reaching a constant temperature of $60.0^{\circ}C$ (±0.5) within 60 minutes. This is a severe limitation of the device if initial polymerization kinetics (build-up to steady state) at constant temperature are desired. 'Slower' polymerizations, i.e., those in which no significant polymerization occurs over the first 6 minutes, are more suited to this dilatometer. (It should be noted that any dilatometer can suffer from this disadvantage, particularly in the case in which oil soluble initiators are used and have to be incorporated in the swollen particles prior to reaching reaction conditions.)

4) In successive seeding bottle polymerizations of monodisperse polystyrene latexes, using a previously developed recipe, the particle surface charge density (both strong and weak acid groups) was found to increase with both particle size and initiator concentration over the range 0.3 to 0.7 μm and 1.3 to 9.5 mM $K_2S_2O_8$. These experiments could not be reproduced in the LUMLR dilatometer because of limited particle swellabilities.

5) A successive seeding formulation method was developed based on constant particle surface coverages with Aerosol-MA emulsifier. Surface coverages below 13% of saturation were inadequate in providing particle stability in 24 hr. ($70^{\circ}C$) bottle polymerizations.

6) Polymerization kinetics were obtained for successive seeding experiments of styrene/polystyrene with aqueous phase initiation over the particle size range of 0.27 to 0.82 μm (four steps). Monodisperse

344

latexes, free of significant numbers of nucleated particles, could not be prepared above 1 μm despite low surface coverages (4%) and persulfate concentrations (0.5 mM). The kinetics were characterized by the autoacceleration of the gel effect (increasing $\bar{n}$) throughout each polymerization (2/1 monomer/polymer ratio). The overall rate of polymerization decreased with increasing particle size and decreasing initiator concentration. A simplified model was developed which matched the experimental data reasonably well. The collision theory of radical absorption was used to predict the radical absorption rate and the surface charge density. An empirically determined polynomial function for k_t was judged to be better than those used in more recent attempts, based on free volume theory. The transition from Case 2 to Case 3 kinetics was found to be from a dependence of the polymerization rate on d^{-3} to $d^{-1/2}$, i.e., the rate did not become independent of particle size and number and, thus, did not follow true bulk polymerization kinetics.

7) Oil soluble initiators in combination with various water soluble inhibitors were used in attempts to eliminate particle nucleation at larger particle sizes (>1 μm) in successive seeding experiments of styrene/polystyrene with 15% coverage by Aerosol-MA. Hydroquinone inhibitor and AMBN initiator were found to be effective in reducing nucleation whereby 2.45 μm monodisperse polystyrene latexes were prepared. The inhibitor NH_4SCN (with AIBN initiator) was found to destabilize the latexes via a strong electrolyte effect while $NaNO_2$ proved ineffective in reducing new crop generation. (All inhibitors were used in the same molar quantity.)

345

The polymerization kinetics were generally similar to those obtained via aqueous phase initiation but with some important differences. The autoacceleration of the gel effect was again apparent and the overall polymerization rate decreased (with decreasing difference) with increasing particle size (with the exception of $NaNO_2$ inhibited polymerizations). The initiators AIBN and AMBN, when used in successive seeding experiments without any inhibitors (controls), were judged to have efficiencies below 15%. The effects of each of the three inhibitors were contrasting: a) hydroquinone induced both induction periods and polymerization retardation; b) NH_4SCN had no apparent effect on the kinetics; and 3) $NaNO_2$ retarded the polymerizations at the smaller particles sizes (first two steps), indicating a possible interfacial effect. Both hydroquinone and $NaNO_2$ partitioned to some extent into the oil phase.

The transition between emulsion and bulk kinetics was found to occur with oil phase initiation between particle sizes of 0.3 and 1.2 μm (five seeding steps with 2/1, styrene/polystyrene, 69°C). The polymerization rate afterwards became independent of particle size and number. This was confirmed through modeling studies. Initiator efficiencies of 0.100 and 0.105 were used to successfully model the AIBN and AMBN sequences (without inhibitor), respectively. A slightly different empirical k_t function was used in the simulations, the difference being attributed to lower molecular weights. A modified k_d function, based on the free volume approach, was also employed for the AMBN initiated cases to account for the slowing of the polymerization at high conversion (unaccounted for by the decreasing k_p function).

346

8)   Nine polymerizations of large-particle-size latexes were carried out in microgravity. 'Monodisperse' polystyrene latexes from 3.4 to 18 µm were prepared by seeded polymerizations. The main particle size distributions had standard deviations less than 2%. The number of off-size larger particles generally increased with increasing swelling ratio having relative concentrations of 1/360 to 1/50 (relative to the main distribution). Small particles, nucleated during the polymerizations qualitatively increased with both swelling ratio and particle size. Ground-based counterparts showed that for the higher swelling ratios ($M/P \geq 4$), the process agitation (oscillatory at 13 rpm) was insufficient to prevent PSD broadening due to temperature gradients caused by inadequate mixing. For particle size greater than 10 µm, reduced yields were obtained from flocculation/sedimentation of the particles, particularly for the largest sizes. Standard deviations ranged from 2 to 5% while off-sized particles were of generally comparable quantity to the corresponding flight experiments.

9)   The polymerization kinetics of the large-particle-size latexes were not affected by the gravitational   environment at the smaller sizes (≤ 5 µm). At the larger sizes, the poor mixing on the ground led to lowered rates because of the temperature gradients within the creamed layer of particles. The kinetics were generally characterized by a constant rate period ($M/P > 2$) followed by the gel effect acceleration. In most cases the entire conversion history could not be obtained because the amount of initiator required to complete the polymerization within the given time frame limitations was greater than could be accommodated by the system (i.e., N_2 from initiator decomposition saturated the reaction fluid).

347

10) A submicron control recipe, consisting of 0.19 μm polystyrene seed swollen 2/1 with monomer and initiated by 1 mM persulfate, did not survive the four-day delay prior to experiment activation in microgravity. The addition of hydroquinone inhibitor subsequently remedied this, however, severely retarded kinetics were obtained. No adequate explanation has been found for this unexpected phenomenon.

6.2 Recommendation for Further Studies

Few research efforts are complete and without questions and this is by far no exception. Clarification and further substantiation of several points are recommended:

1) Mixing has been studied in a qualitative and comparative fashion in the LUMLR prototype using an oscillatory, slow-speed type agitation system. The creaming of large swollen particles has been shown to cause broadening of the PSD in ground-based experiments, indicating the inadequacy of the mixing. Other types of agitation should be studied to see if improvements can be gained without increased risks of shear induced flocculation. A helical-type mixer, running continuously, (as for moving solids) may be one type suitable for study.

2) A method for simulating low gravity conditions for solid particles dispersed in a liquid matrix has been discussed by Otto and Lorenz [113]. This method merits investigation and has been applied in some preliminary work in this laboratory. The results indicated that stable latexes in the 14 - 17 μm range can be prepared at 70°C in an 18 cm long, 0.4 cm diameter glass tube rotated about its axis at a constant 4 rpm. The same latexes had shown various degrees of floccu-

348

lation when polymerized in the LUMLR prototype. Further work is warranted based on these results.

3) Coagulation of latexes during their preparation is a common industrial problem. In these studies, a 'shaving cream' type flocculation was found in bottle polymerizations run for times longer than required to reach high conversion, while the same latexes prepared in the LUMLR did not flocculate when removed from the reactor after the rate slowed to near zero. These results suggested that this type of flocculation occurs late in a polymerization and could be prevented if the polymerization is stopped somewhat earlier. An investigation of this flocculation mechanism could be an interesting and important research area.

4) The kinetics of the successive seeding of monodisperse polystyrene latexes using potassium persulfate initiator has been investigated at two initiator concentrations and only one level of solids. The radical absorption mechanism used to model these kinetics was based on the collision theory. Further verification of this must be gained through experimentation at other initiator and particle concentrations, as well as other polymerization temperatures. Extension to larger particle sizes (>1 μm) by lowering the initiator concentration and raising the solids content should also be investigated.

5) Three inhibitors in combination with oil soluble initiators were investigated in these kinetic studies. Three different responses were noted. The mechanisms of inhibition and partitioning between the phases (and interfacial association) should be clarified to go along with the kinetic results.

6) A number of inadequacies were described in the model presented in these studies. The free volume approach to the diffusion limitation of the termination reaction was found to be inadequate, requiring instead empirical expressions. This approach was used to describe the variation of the propagation and decomposition rates at high conversion; however, the results were not always consistent. Means must be devised by which these 'constants' can be better measured. The direct measurement of $\bar{n}$ by e.s.r. has been suggested as an aid in these determinations [114].

7) In order to gain the complete reaction kinetics for the microgravity polymerizations and their ground-based analogues under the same recipe conditions, the polymerization time at $70^{\circ}C$ should be increased and the initiator concentration reduced. This time can easily be set by performing polymerizations in the LUMLR using an amount of initiator which when fully decomposed would just saturate the latex with N_2. Also, it is advised to have the controls of the flight reactors 'retuned' to obtain more closely a reaction temperature of $70^{\circ}C$.

8) The flight results indicated that off-sized larger and smaller particles increased with increasing swelling ratio. Despite the greater number of steps that would be required to achieve a certain size, it seems reasonable to use a buildup of say, 2/1 monomer-to-polymer throughout the sequence as a check on improved monodispersity. Also, ground-based experiments were more successful using this swelling ratio.

350

9) The unexpected retardation of the submicron flight recipe using hydroquinone should be examined in some detail to resolve the unknown cause of this phenomenon.

REFERENCES

(1) Collins, E.A., Bareš, Billmeyer, F.W., _Experiments in Polymer Science_, John Wiley & Sons, Inc., New York, 1973.

(2) Rubens, L.C. and Skochdopole, R.E., J. Appl. Polymer Sci., _9_, 1487-1497 (1965).

(3) Bell, C.L., J. Sci. Instr., _38_, 27-28 (1961).

(4) Voers, J.F. and Crane, R.A., Anal. Chem., _31_, 1906-1908 (1959).

(5) Rubens, L.C. and Skochdopole, 'Dilatometry', pp. 83-98 in Mark, H.F., Gaylord, N.B. and Bikales, N.M., eds., _Encyclopedia of Polymer Science and Technology_, Vol. 5, Interscience Div., John Wiley and Sons, New York, 1966.

(6) Soh, R.W., Meyer, V.E., Rubens, L.C. and Skochdopole, J. Appl. Poly. Sci., _12_, 1803-1805 (1968).

(7) Sudol, E.D., Masters Research Report, Lehigh University, 1979.

(8) Bates, R.L., Fondy, P.L., and Fenie, J.G., in _Mixing: Theory and Practice_, Uhl, V.W., and Gray, J.B., eds., Vol. 1, Academic Press, New York, 1966.

(9) Vicente, F.A., private communication.

(10) Perry, J.H., ed., _Perry's Chemical Engineers' Handbook_, 4th Ed., McGraw-Hill, 1963.

(11) Tobolsky, A.V., Leonard, F. and Roeser, G.P., J. Polymer Sci., _3_, 604 (1948).

(12) Bevington, J.C., _Radical Polymerization_, Academic Press, New York, 1961, p. 2.

(13) Bradrup, J. and Immergut, E.H., _Polymer Handbook, 2nd Edition_, Wiley-Interscience, N.Y., 1975.

(14) Luyben, W.L., _Process Modeling, Simulation, and Control for Chemical Engineers_, McGraw Hill, N.Y., 1973.

(15) Pramojaney, N., private communication.

(16) Harkins, W.D., J. Polym. Sci., _5_, 217 (1950).

(17) Fries, N., and Hamielec, A.E., _Polymer Production Technology. Part I: Polymer Reaction Engineering_, McMaster Univ., Hamilton, Ontario, 1977, Chapter 5

(18) Pramojaney, N., Ph.D. Thesis, Lehigh University, 1982.

(19) Alfrey, T., Jr., Bradford, E.B., Vanderhoff, J.W., and Oster, G., J. Opt. Soc. Am., 44, 603 (1954).

(20) Bradford, E.B. and Vanderhoff, J.W., J. Appl. Phys., 26, 864 (1955).

(21) Bradford, E.G., Vanderhoff, J.W., and Alfrey, T., Jr., J. Colloid Sci., 11, 235 (1956).

(22) Vanderhoff, J.W., Vitkuski, J.F., Bradford, E.B. and Alfrey, T., Jr., J. Polym. Sci., 20, 225 (1956).

(23) Goodwin, J.W., Hearn, J., Ho, C.C. and Ottewill, R.H., Coll. and Polym. Sci., 252, 464 (1974).

(24) Vanderhoff, J.W. and Bradford, E.B., TAPPI, 39, 650 (1956).

(25) Cetta, G., Benetta, G., Tulamini, G.P., Vianello, G., Adv. in Chem. Ser., 91, 158 (1969).

(26) Fitch, R.M., and -bin Shih, L., Progr. Coll. Polym. Sci., 56, 1, (1975).

(27) Poehlein, G.W., and Vanderhoff, J.W., J. Polym. Sci., Part A, 11, 447, (1973).

(28) Hawkett, B.S., Napper, D.H. and Gilbert, R.G., J. Chem. Soc., Faraday Trans. I, 2288 (1975).

(29) James, D.R., and Sundberg, D.C., J. Polym. Sci., Polymer Chem. Ed., 18, 903 (1980).

(30) Morton, M., Kaizermann, S., and Altier, M.W., J. Coll. Interface Sci., 9, 300 (1954).

(31) Vanderhoff, J.W., Micale, F.J., and El-Aasser, M.S., "Production of Large-Particle-Size Monodisperse Latexes", proposal submitted in response to NASA A.O. No. OA-77-3, "Space Processing Investigations for STS Missions", April 20, 1977.

(32) Ugelstad, J. and Hansen, F.K., Rubber Chem. and Tech., 49, (3), 536 (1976).

(33) Dezelic, N., Petras, J.J. and Dezelic, G., Kolloid-Z.u.Z. Polymere, 242, 1142 (1970).

(34) Dodge, J.S., Woods, M.E. and Krieger, I.M., J. Paint Tech., 40, 71 (1970).

353

(35) Misra, S.G., El-Aasser, M.S., and Vanderhoff, J.W., Graduate Research Progress Reports, 13, 59 (1980), Emulsion Polymers Institute, Lehigh University, Bethlehem, Pa.

(36) Van den Hul, H.J. and Vanderhoff, J.W., J. Colloid Interface Sci., 28, 336 (1968).

(37) Vanderhoff, J.W., van den Hul, H.J., Tausk, R.J.M., and Overbeek, J.Th.G., "Clean Surfaces: Their Preparation and Characterization for Interfacial Studies", Goldfinger, G., Ed., Marcel Dekker, New York, 1970, p. 15.

(38) van den Hul, H.J., and Vanderhoff, J.W., J. Electroanal. Chem., 37, 161 (1972).

(39) Wu, W.C., El-Aasser, M.S., and Vanderhoff, J.W., in "Emulsion and Dispersions", Becker, P. and Yudenfreund, N.M., Eds., Marcel Dekker, New York, 1978, p. 71.

(40) Vanderhoff, J.W., Preprints, A.C.S. Division Org. Coatings Plastics Chem., 42, 30 (1980).

(41) Vanderhoff, J.W., in "Emulsion Polymers and Emulsion Polymerization", Bassett, D.R. and Hamielec, A.E., Eds., A.C.S. Symposium Series, 165, 61 (1980).

(42) Krumrine, P.H., M.S. Thesis, Lehigh University, 1976.

(43) van der Hoff, B.M.E., J. Polymer Sci., 33, 487 (1958).

(44) Vanderhoff, J.W., Bradford, E.B., Tarkowski, H.L., Wilkenson, B.W., J. Polymer Sci., 50, 265 (1961).

(45) Tseng, C.M., El-Aasser, M.S., and Vanderhoff, J.W., in "Computer Applications in Applied Polymer Science", Provder, T., Ed., A.C.S. Symposium Series, 197, 197 (1981).

(46) Smith, W.V. and Ewart, R.H., J. Chem. Phys., 16, 5920 (1948).

(47) Fitch, R.M., and Tsai, C.H., "Polymer Colloids", Fitch, R.M., Ed., Pergamon, New York, 1973, p. 73.

(48) Hansen, F.K. and Ugelstad, J., J. Poly. Sci., Poly. Chem. Ed., 16, 1953 (1978).

(49) ibid, 17, 3033 (1979).

(50) ibid, 17, 3047 (1979).

(51) ibid, 17, 3069 (1979).

(52)   Vanderhoff, J.W., private communication.

(53)   Technical bulletin PRT 102, American Cyanamid Co.

(54)   Ahmed, S.H., Ph.D. Thesis, Lehigh University, 1979.

(55)   Sawyer, W.M., and Rehfeld, S.F., J. Phys. Chem., 67, 1973
       (1963).

(56)   van den Hul, H.J. and Vanderhoff, J.W., in "Polymer Colloids",
       Fitch, R.M., Ed., Plenum Press, New York, 1971, p. 1.

(57)   Brodnyon, J.G., and Kelley, E.L., J. Colloid Sci., 20, 7(1965).

(58)   Almog, Y., and Levy, M., J. Poly. Sci., Poly. Chem. Ed., 18,
       1 (1980).

(59)   Roe, C.P., Ind. Eng. Chem., 60, 20 (1968).

(60)   Morton, M., Salatiello, P.P., Landfield, H., J. Polym. Sci.,
       8, 279 (1952).

(61)   Walling, C., "Free Radicals in Solution", Chaps. 3 - 5, John
       Wiley & Sons, Inc., New York, 1957, p. 95.

(62)   Matheson, M.S., Auer, E.E., Bevilacqua, E.G., Hart, E.J.,
       J. Am. Chem. Soc., 73, 700 (1951).

(63)   Hui, A.W. and Hamielec, A.E., J. App. Polym. Sci., 16, 749
       (1972).

(64)   Stockmayer, W.H., J. Polym. Sci., 24 (106), 324 (1957).

(65)   O'Toole, J.T., J. Polym. Sci., Part C, 27, 171 (1969).

(66)   Ugelstad, J., Mørk, P.C. and Aassen, J.O., J. Polym. Sci.,
       Part A-1, 5, 2281, 1967.

(67)   Hawkett, B.S., Napper, D.H. and Gilbert, R.G., J. Chem. Soc.,
       Faraday Trans. I, 76, 1323 (1980).

(68)   ibid., 77, 2395 (1981).

(69)   van der Hoff, B.M.E., Advances in Chem. Ser., 34, 6 (1962).

(70)   Haward, R.N., J. Polym. Sci., 4, 273 (1949).

(71)   Friis, N. and Hamielec, A.E., J. Polym. Sci., 11, 3321 (1973).

(72)   Saidel, G.M., and Katz, S., J. Polym. Sci., Part C, 27, 149
       (1969).

(73)   Friis, N. and Hamielec, A.E., J. Polym. Sci., 12, 251 (1974).

(74) Marten, F.L. and Hamielec, A.E., Am. Chem. Soc. Symposium Series, 104, 43 (1979).

(75) Harris, B., Hamielec, A.E. and Marten, L., Am. Chem. Soc. Symposium Series, 165, 315 (1981).

(76) Sundberg, D.C., Hsieh, J.Y., Soh, S.K., Baldus, R.F., Am. Chem. Soc. Symposium Series, 165, 327 (1981).

(77) Cardenas, J.N., and O'Driscoll, K.F., J. Polym. Sci., Polym. Chem. Ed., 14, 883 (1976).

(78) Soh, S.K. and Sundberg, D.C., J. Polym. Sci., Polym. Chem. Ed., 20, 1299 (1982), 20, 1315 (1982), 20, 1345 (1982).

(79) Ugelstad, J. and Mørk, P.C., Brit. Polym. J., 2, 31 (1970).

(80) Tseng, C.M., Ph.D. Thesis, Lehigh University, 1983.

(81) Luck, W., Klier, M. and Wesslaw, H., Berg. Bunsenges Phys. Chem. 67, 84 (1963).

(82) Kolthoff, I.M. and Miller, I.R., J. Am. Chem. Soc., 73, 3055 (1951).

(83) Bevington, J.C., Trans. Faraday Soc., 51, 1392 (1955).

(84) De Schrigner, F. and Smite, G., J. Polym. Sci., A-1, 2201 (1966).

(85) Matsumoto, T., Okubo, M. and Imai, T., Kobenshi-Ronbunshu, 31, 576 (1974).

(86) Tromsdorff, E., Kohle, H., Lagally, P., Makromol. Chem., 1, 169 (1947).

(87) "The Condensed Chemical Dictionary", Rose, E. and Rose, A., Eds., Van Nostrand, Reinhold Co., 1966.

(88) Blackley, D.C., "Emulsion Polymerization: Theory and Practice", Appl. Sci. Publ. Ltd., London, 1975.

(89) Almog, Y. and Levy, M., J. Polym. Sci., Polym. Chem. Ed., 18, 1 (1980).

(90) Bracke, W.J.I., and Lanza, E. (to Labofina, S.A., Belgium) U.S. Patent 4,247,668 (1981).

(91) Georgieff, K.K., J. Appl. Polym. Sci., 9, 2009 (1965).

(92) Gardon, J.L., J. Polym. Sci., A-1, 6, 623 (1968).

(93) Gardon, J.L., J. Polym. Sci., A-1, 6, 665 (1968).

(94) Gardon, J.L., J. Polym. Sci., A-1, 6, 687 (1968).

(95) Gardon, J.L., J. Polym. Sci., A-1, 6, 2853 (1968).

(96) Nomura, M., Harada, M., Eguchi, W., Nagata, S., in "Emulsion Polymerization", Piirma, I. and Gardon, J.L., eds., A.C.S. Symposium Series No. 24, 102 (1976).

(97) Carnahan, B., Luther, H.A., and Wilkes, J.O., "Applied Numerical Methods", J. Wiley & Sons, Inc., New York, 1969.

(98) Technical Bulletin VAZO 67, E-44266, E.I. duPont de Nemours & Co. (1981).

(99) Al-Shahib, W.A. and Dunn, A. S., 'Polymer Colloids II', Fitch, R.M., ed., Plenum, New York, 1980.

(100) Allen, P.E.M. and Patrick, C.R., 'Kinetics and Mechanisms of Polymerization Reactions', Chichester, Ellis Horwood, 107 (1974).

(101) "Monodisperse Latex Reactor (MLR) - A Materials Processing Space Shuttle Mid-Deck Payload", Marshall Space Flight Center, Form 454, 1981.

(102) 'Operational and Maintenance and Handling Manual - Monodisperse Latex Reactor", General Electric Space Division, 1979.

(103) Ugelstad, J., Mørk, P.C., Kaggerud, K.H., Ellingsen, T. and Berge, A., Adv. Colloid Interface Sci., 13, 101 (1980).

(104) Tseng, C.M., private communication.

(105) Ahmed, S.M., El-Aasser, M.S., Pauli, G.H., Poehlein, G.W., and Vanderhoff, J.W., J. Colloid Interface Sci., 73, 388 (1980).

(106) Odian, G., "Priciples of Polymerization", 2nd ed., McGraw-Hill, New York (1970).

(107) Silwanowicz, A., M.S. Report, Lehigh University, 1983.

(108) Grancio, M.R. and Williams, D., J. Polym. Sci., Part A-1, 8, 2617 (1970).

(109) Wessling, R.A. and Harrison, I.R., J. Polym. Sci., Part A-1, 9, 3471 (197s).

(110) Napper, D.H., J. Polym. Sci., Part A-1, <u>9</u>, 2089 (1971).

(111) Gardon, J.L., J. Polym. Sci., <u>11</u>, 241 (1973).

(112) Gardon, J.L., J. Polym. Sci., <u>12</u> 2133 (1974).

(113) Otto, G.H. and Lorenz, A., Deutsche Forschungs-und Versuchsans-stalt für Luft und Raumfahrt e.V. (DFVLR), AIAA Paper <u>78-273</u>, 1 (1978).

(114) Gilbert, R.G., private communication (1983).

DETERMINATION OF SURFACE CHARGE DENSITIES VIA CONDUCTOMETRIC TITRATION

The conductometric titration of a latex (cleaned by ion exchange) containing acidic sulfate groups is characterized by a descending leg (decreasing conductance) followed by an ascending leg as the latex is titrated against NaOH. A weak acid (e.g., COOH) is noted as a change in slope of the ascending portion of the curve. The endpoints are determined by the intersection of the extrapolated linear portions of the curve. The surface charge, in terms of gram equivalents per gram of polymer (N_i) is calculated from

$$N_i = \frac{\Delta V_T \cdot N_{NaOH}}{M_p \cdot 10^3} \qquad\qquad A.1$$

where ΔV_T is the volume of titrant (NaOH), N_{NaOH} is the normality, and M_p the mass (gms) of polymer titrated. The surface charge density, coulombs/cm^2 (σ_i) is easily computed for a monodisperse latex of known particle diameter, d:

$$\sigma_i = N_i [\rho_{PS} d/6] 96500 \qquad\qquad A.2$$

where ρ_{PS} is the particle density and 96500 is a conversion factor from equivalents to coulombs.

APPENDIX B

MOLECULAR WEIGHT DISTRIBUTION AND AVERAGES OBTAINED

FROM GPC CHROMATOGRAMS

A Waters Associates ALC/GPC 201 Liquid Chromatograph, equipped with five μ-Styrogel columns (10^6 Å, 10^5 Å, 10^4 Å, 10^3 Å, and 500 Å) was calibrated using polystyrene standards (THF eluting solvent) of molecular weight 840, 2350, 3600, 17500, 110000, 200000, 470000, 650000, 1400000, and 2700000. Peak heights were obtained from the recorded chromtograms at 0.5 cm^3 intervals of elution volume. These data were converted to molecular weights using a fourth order polynomial fit of the molecular weight-elution volume calibration data. The number ($\bar{M}_n$) and weight ($\bar{M}_w$) average molecular weights were computed according to:

$$\bar{M}_n = \frac{\Sigma H_i}{\Sigma (H_i/M_i)} \qquad \text{B.1}$$

$$\bar{M}_w = \frac{\Sigma H_i M_i}{\Sigma H_i} \qquad \text{B.2}$$

where H_i represents the measured height along the chromatogram with the molecular weight (M_i) corresponding to the elution volume. A correction for instrumental spreading (axial dispersion) was applied to these averages:

$$\frac{\bar{M}_n(h)}{\bar{M}_n(\infty)} = \exp (D_2^2/4h) \qquad \text{B.3}$$

$$\frac{\bar{M}_w(h)}{\bar{M}_w(\infty)} = \exp (-D_2^2/4h) \qquad \text{B.4}$$

h is a parameter describing the width of the spreading. This is ob-

tained from a third order polynomial fit of h versus elution volume

determined from the calibration chromatograms. h represents the

square of the inverse of the peak width (leading half) measured at

36.8% of the peak maximum. D_2 is the slope of the logarithm calibra-

tion curve (molecular weight versus elution volume).

CALCULATION OF CONVERSION BY ASSUMING ADDITIVE VOLUMES

OF MONOMER AND POLYMER

The following sequence of computations was made to obtain conversion assuming additivity of monomer-polymer volumes:

1. The total grams of fluid in the reactor (G_T) was calculated from the known reactor volume (V_R), the weight fractions of the three major recipe components, polystyrene (ϕ_{PS}), styrene (ϕ_S), and water (ϕ_{H_2O}) and the density of each component at time zero:

$$G_T = V_R / (W_{PS}/\rho_{PS} + W_S/\rho_S + W_{H_2O}/\rho_{H_2O}) \qquad \text{C.1}$$

2. For each data point, a volume $V_{T,i}$ was computed based on the fluid temperature and the original recipe

$$V_{T,i} = G_{PS}/\rho_{PS,i} + G_S/\rho_{S,i} + G_{H_2O}/\rho_{H_2O,i} \qquad \text{C.2}$$

where G_{PS,S,H_2O} represent the grams of each component in the reactor.

3. The actual volume ($V_{LVDT,i}$) was also computed for each point from the LVDT voltage and compensation for cylinder expansion being made by either the gage data or the approximation via the fluid temperature (see Section 2.5.2).

4. The difference in volumes, ΔV, was used to compute the change in the amount of styrene in the reactor

$$G_{S,i} = (V_{T,i} - V_{LVDT,i} + G_S/\rho_{PS,i} - G_S/\rho_{S,i})/(1/\rho_{PS,i} - 1/\rho_{S,i}) \qquad \text{C.3}$$

5. The fractional conversion was thus obtained:

$$X_i = (G_S - G_{S,i})/G_S \qquad \text{C.4}$$

PARTICLE SIZE AVERAGES

Number
$$DN = \Sigma N_j D_j / \Sigma N_j$$

Volume-Surface
$$DS = \Sigma N_j D_j^3 / \Sigma N_j D_j^2$$

Weight
(~ light scattering)
$$DW = \Sigma N_j D_j^4 / \Sigma N_j D_j^3$$

Surface
$$DA = \left[\frac{\Sigma N_j D_j^2}{\Sigma N_J} \right]^{1/2}$$

Volume
(ultramicroscope)
$$DV = \left[\frac{\Sigma N_j D_j^3}{\Sigma N_j} \right]^{1/3}$$

Volume
(turbidity)
$$DQ = \left[\frac{\Sigma N_j D_j^6}{\Sigma N_j D_j^3} \right]^{1/3}$$

Standard Deviation
$$SD = \sqrt{ \left[\frac{N_j D_j^2}{\Sigma N_j} - (DN)^2 \right] \left[\frac{\Sigma N_j}{\Sigma N_j - 1} \right] }$$

Polydispersity Index
$$PDI = DW/DN$$

Number of Particles
$$N_j$$

Particle Diameter
$$D_j$$

APPENDIX E

NOMENCLATURE

a	$(8\alpha)^{1/2}$
a_s	surfactant molecular area at saturation, cm^2
A	empirical constant in an expression for k_t
A_i	corss-sectional area of the reactor, cm^2
b	ratio of emulsifier adsorption to desorption rate constants
B	empirical constant in an expression for k_p
B_i	empirical constant in an expression for k_d
C	constant in an expression for k_a
C_A	aqueous phase emulsifier concentration, gm-mole/cm^3
C_1, C_2, C_3, C_4	coefficients of polynomial describing k_t
d	latex partical diameter, cm (or μm)
D_M, D_p, D_i	diffusion coefficient of monomer, polymer, and initiator fragments in the particle, cm^2/sec.
D_{Mo}, D_{Po}, D_{io}	D_M, D_p, D_i at zero polymer content in the particle, cm^2/sec.
D_W	diffusion coefficient of monomer or initiator radicals in the aqueous phase, cm^2/sec.
$\bar{D}_N$	number average particle diameter, cm (or μm)
$D_{S/S}$	surface-to-surface distance between particles, μm
D_2	slope of the molecular weight-elution volume curve
[E]	electrolyte concentration or ionic strength
E_{ad}	activation energy for k_d, cal/gm-mole
E_{ap}	activation energy for k_p, cal/gm-mole
f	initiator efficiency

364

f', F_S	absorption efficiency of free radicals
G_T, G_S, G_{PS}, G_{H_2O}	total grams and grams of styrene, polystyrene and water in the reactor
h	parameter related to chromatogram spreading in GPC
Δh_i	change in piston position, cm
H_i	height along GPC chromatogram, cm
$[I]$, $[I]_0$	initiator concentration at t and t = 0, gm-mole/cm^3
$I_m(a)$	modified Bessel function of the first kind of a with order m
$\bar{k}$	Boltzmann constant, erg/molecule-$^\circ$K
k_{abs}	mass transfer coefficient for free radical absorption into a particle
k_d	rate constant for initiator decomposition reaction, sec^{-1}
k_{de}	rate constant for radical desorption from a particle
k_{fm}	reaction rate constant for transfer to monomer
k_{fp}	reaction rate constant for transfer to polymer
k_p	reaction rate constant for chain propagation in the particle, cm^3/gm-mole sec
k_t	reaction rate constant for termination in the particle, cm^3/gm-mole sec
k_{tc}, k_{td}	rate constant for termination by combination and disproportionation, respectively, cm^3
K_{LVDT}	conversion factor for LVDT signals, volts/cm
l_c	cylinder length, cm
Δl_i	axial expansion of cylinder, cm
m_p	mass of polymer, gms
$\bar{M}_n$, $\bar{M}_w$	number and weight average molecular weights
$[M]_p$	concentration of monomer in a particle, gm-mole/cm^3

I

M_W	aqueous phase monomer concentration, gm-mole/cm^3
$n, \bar{n}$	number and average number of radicals per particle
n, N	number of surfactant molecules per unit area and at saturation, cm^{-2}
N_a	Avogadro's number
N_i	surface charge, gm-equiv./gm polymer
N_n	number of particles which contain n radicals
N_{NaOH}	normality of sodium hydroxide, gm-moles/cm^3
N_p	number of particles, gm-moles/cm^3
r	radius of a primary particle, cm
r_p	radius of a particle, cm
r_{cyl}	radius of the cylinder, cm
R	universal gas constant, J/gm-mole$^\circ$K
R_{abs}	rate of radical absorption, gm-mole/cm^3 sec
R_i	rate of radical production from initiator decomposition, gm-mole/cm^3 sec
R_p	total rate of polymerization, gm-mole/cm^3 sec
$[R\cdot]_W$	concentration of free radicals in the aqueous phase, gm-mole/cm^3
$[S]$	total emulsifier concentration, gm-mole/cm^3
t	time, sec
T	reaction temperature, $^\circ$K (or $^\circ$C)
T_F, T_{FLU}	fluid temperature, $^\circ$K (or $^\circ$C)
T_g	glass transition temperature, $^\circ$K
T_{gm}, T_{gp}	glass transition temperatures of the monomer and polymer, respectively, $^\circ$K
v	particle volume, cm^3
v_1, v_i	time zero and time t LVDT voltage

v_f	free volume
v_{fc}, v_{fmc}, v_{fic}	critical free volumes indicating the onset of diffusion controlled termination, propagation, and initiation, respectively
V_{LVDT}	volume based on LVDT reading, cm^3
V_R	initial volume of reactor, cm^3
V_T	total volume of reactor at any time, cm^3
ΔV_i	volume difference between that calculated from T_{FLU} and LVDT position, cm^3
ΔV_T	volume of titrant, cm^3
W_m, W_p	weight fraction monomer and polymer
W_{IS}	stability ratio between primary and seed particles
X_i	fractional conversion at any time
z	subdivision factor
$[z]$	concentration of inhibitor, $gm-mole/cm^3$

Greek Symbols

α	coefficient of thermal expansion, cm/cm^oK
α	$= R_{abs} \, v \, N_a / k_t \, N_p$
α'	$= R_i \, v \, Na / k_t \, N_p$
α''	empirical constant in an expression for k_t
α_p, α_m	difference between coefficients of volume expansion of polymer, monomer in the melt and glassy state, cm/cm^oK
γ	surface tension, N/cm
$\phi_S, \phi_{PS}, \phi_{H_2O}$	volume fractions of styrene, polystyrene, and water in a recipe
$\rho_S, \rho_{PS}, \rho_{H_2O}$	densities of styrene, polystyrene, and water, gm/cm^3

367

ρ_a	free radical absorption rate, gm-mole/cm^3 sec
σ	standard deviation
σ_i	surface charge density, μc/cm^2
π	pi

PART B

Toward the Production of Large-Particle-Size

Monodisperse Latexes -

Studies of Swelling and Polymerization Parameters

Based on the Ph.D. Thesis

by

Chi-Ming Tseng

TABLE OF CONTENTS

ABSTRACT

Large-particle-size monodisperse latexes (>2 μm in diameter) are in demand. However, they are not easy to prepare. The difficulty lies in the sensitivity of the latexes to emulsifier concentration and mechanical shear. The largest particle size monodisperse latex prepared in large quantity by successive seeded emulsion polymerization was 2.0-2.5 μm.

To extend the successive seeded emulsion polymerization beyond the 2.0-2.5 μm upper limit, several approaches were taken: (1) Use a monomer/polymer ratio lower than the equilibrium swelling ratio to eliminate the free monomer phase, so that the chance of nucleating small particles is reduced; (2) Use an oil-soluble initiator to reduce the opportunity for the free radicals to initiate polymerization in the aqueous phase; (3) Use a water-soluble inhibitor for the same reason given in (2); (4) Use a combination of different types of surfactants to stabilize large particles without nucleating small particles; (5) Use minimum agitation to avoid the formation of coagulum by mechanical shear.

The equilibrium swelling of latex particles with monomers was studied experimentally and theoretically. Semi-empirical equations were derived for polystyrene and polymethyl methacrylate systems. A generalized thermodynamic model, which takes into account the effect of water dissolved in the monomer phase and the swollen particles, was developed. A "seeded-telomerization" swelling method using mercaptans as telogens was developed to increase the swellability of the latex

particles.

Extensive studies of initiators, inhibitors, and surfactants were carried out. It was found that an azo-type initiator, a quinoid-type inhibitor, and a combination of three surfactants, anionic, oligomeric and polymeric, gave the most satisfactory results. With these ingredients, large-particle-size polystyrene latex particles could be grown by successive seeding without generating a new crop of small particles or forming excess coagulum. Latex particles with satisfactory uniformity have been successfully grown up to 11 μm with bottle polymerization, and less successfully to 18 um and 35 um.

Four sets of microgravity experiments have been carried out in the STS missions of Space Shuttles Columbia and Challenger. Monodisperse latexes up to 18 μm (coefficient of variation = 1-2%) have been prepared in microgravity. Parallel ground-based control experiments were also conducted. All the large-particle-size ground latexes had broader main particle size distributions and much larger tails than their flight counterparts. The results indicated that much better mixing was achieved in microgravity than on ground with the same agitation design. This supports the rationale given for preparing large-particle-size monodisperse latexes in space via seeded emulsion polymerization, i.e., a minimum agitation can be used to supply enough mixing for growing large-particle-size latex particles uniformly in microgravity, without forming excess coagulum due to creaming, sedimentation, or excess shear in mixing.

CHAPTER 1

INTRODUCTION

Monodisperse latexes are those in which the particle size distribution is extremely narrow. The first monodisperse latex was the famous 580G Lot 3584 polystyrene latex, which was prepared in the pilot plant of the Dow Chemical Company in 1947. The uniformity of the latex was first noted by Backus and Williams [1, 2]. It was later investigated by electron microscopy, light scattering, small angle X-ray scattering, and ultracentrifugation. A compilation of particle-diameter determinations [3] indicated that most investigators found a diameter of about 0.259 μm. This latex gained widespread acceptance as a secondary standard in electron microscopy and other fields. Beginning in 1951, Vanderhoff undertook the deliberate preparation of monodisperse latexes and soon reproduced the 580G Lot 3584 preparation. In addition, the concept of "seeding", which had been developed earlier to delineate the mechanism of emulsion polymerization [4], was applied and developed by Vanderhoff to grow small monodisperse particles to larger sizes without broadening the particle size distribution significantly [5, 6]. A series of polystyrene latexes in ten different sizes, ranging from 0.088 to 1.171 μm diameter, were prepared in large quantity for outside distribution. The average particle diameters of the series were determined extensively by electron microscopy [6]. The results are presented in Table 1-1. The uniformity of the latexes, expressed in coefficient of variation $(\sigma/\bar{D}_n)$, actually improved with increasing particle size, as

a result of "self-sharpening" in seeded polymerization [7, 8]. The

size range of monodisperse latexes was later extended to about 2 μm by

substituting vinyltoluene for styrene.

Table 1-1.   Particle Size Distributions of Earlier
Dow Monodisperse Polystyrene Latexes [6]

Latex No.	$\bar{D}_n$, μm	σ, μm	n	$\sigma/\bar{D}_n$, %
LS-040-A	0.088	0.0080	1164	9.09
15N-23	0.138	0.0062	526	4.49
LS-055-A	0.188	0.0076	1065	4.04
LS-057-A	0.264	0.0060	577	2.27
15N-7	0.340	0.0052	415	1.53
LS-061-A	0.365	0.0079	438	2.16
15N-8	0.511	0.0074	359	1.45
LS-063-A	0.557	0.0108	373	1.94
LS-066-A	0.814	0.0105	357	1.29
LS-067-A	1.171	0.0133	315	1.14

Numerous applications have been developed for monodisperse

latexes, such as calibration of scientific measuring instruments

(e.g., electron microscopes, light scattering instruments, ultra-

centrifuges, electronic particle counters), counting of virus

particles, determination of pore size, medical serologic tests (e.g.,

rheumatoid arthritis, human pregnancy, trichinosis, histoplasmosis),

and studies of the reticulo-endothelial system [9].

Many of the applications demand monodisperse latexes of larger

particle sizes. However, monodisperse latexes with sizes greater than

2 μm are not easy to prepare. The difficulty lies in the sensitivity

of the latexes to emulsifier concentration and mechanical shear. If

the added emulsifier is insufficient to stabilize the latex particles,

4

they will flocculate to form coagulum. If too much is added, a new crop of particles will be formed, and the latex particle size distribution will be bimodal rather than monodisperse [7, 8, 10]. The range of operable emulsifier concentration is relatively broad at small particle sizes, but with increasing particle size, the operable range becomes smaller and smaller, untill at sizes above 1 μm, it becomes "knife-edge" [11]. Moreover, with increasing particle size, there is an increasing tendency for the particles to cream or settle out during polymerization because of the decreasing intensity of Brownian motion and the density difference between the particles and the aqueous phase. As the polymerization proceeds, styrene (density 0.905 gm/ml) is converted to polystyrene (density 1.05 gm/ml). Thus the polystyrene latex particles tend to cream at low conversions and to settle out at high conversions. Increasing the agitation rate to offset the creaming-settling tendency often results in the formation of coagulum, because the large particles are sensitive to mechanical shear. The densities of the particles and the aqueous phase can be matched at one end by changing the monomer composition (e.g., substituting vinyltoluene-t-butylstyrene mixtures for styrene) or by adding electrolytes or non-electrolytes to the aqueous phase. However, they can not be matched at both low and high conversions because of the continuous change of the particle density.

Since the development of Dow monodisperse latexes, there have been other developments in preparing relatively uniform (not necessarily monodisperse) latexes in the size range of 0.1-100 μm. For a comparison, four major methods are briefly reviewed:

5

1. Successive seeded emulsion polymerization –

   As described above, the method produces latexes of very narrow distribution in the particle size range of 0.1 to 2 μm. The method includes the use of a seed latex of smaller size and growing the particles to a larger size in the presence of a monomer, an initiator, and an emulsifier (usually anionic).

2. Emulsifier-free polymerization –

   This method can be represented by the works of Matsumoto and Ochi [12], Kotera et al. [13, 14], and Ottewill et al. [15, 16, 17]. The polymerization is carried out in the absence of emulsifier. Particle sizes of the latexes are controlled by the concentrations of monomer, initiator and salt. This method produces latexes of particle size 0.1 to 1 μm in low concentration (<10%). It has been claimed [18] that particles up to 4 μm can be obtained by seeded emulsifier-free polymerization.

3. Dispersion polymerization (or microsuspension polymerization) plus separation –

   The term "dispersion polymerization" was defined by Trommsdorff and Schildknecht [19] as a modified suspension polymerization that produces particles in the 10 μm range. This is the range between suspension polymerization and emulsion polymerization. Earlier works by Winslow and Matreyek [20], and later Vanzo [21], can be classified in this category. An extensive study has been carried out

6

recently by Almog and Levy [22, 23, 24, 25]. The method is similar to a conventional suspension polymerization except that a much higher concentration of stabilizer is used. The polymerization product is usually a polymer dispersion with wide particle size distribution, from several μm to tens or hundreds of μm. With subsequent separation methods, such as sieving, elutriation, sedimentation, or centrifugation, a narrower fraction can usually be obtained. The particle size distribution of the separated product is still much wider than those obtained from seeded emulsion polymerization.

4. High-swelling method plus separation -

The so-called Ugelstad two-step swelling method [26, 27, 28, 29] also starts from a seed latex. In the first step, a water-insoluble oligomeric compound is incorporated into the seed particles to increase the swellability of the particles. The second step is swelling and polymerization. The method allows high monomer-polymer swelling ratios and hence high particle size buildups. Monodisperse latexes of 2 to 50 μm have been claimed to be prepared by using this method. Although the method of increasing swellability has been frequently mentioned in publications, no details on the polymerization process itself have been given. The initiation and stabilization system used in the polymerization, the particle size distribution of the product immediately after polymeriza-

7

tion, and the separation methods involved have never been disclosed. It is believed that many small particles are generated along with the large particles during polymeriza- tion and separated out later.

The lack of a good commercial process for preparing extremely uniform latex particles with diameters >2 μm can be illustrated with Figure 1-1. The figure gives coefficients of variation $(\sigma/\bar{D}_n)$ of polystyrene and polyvinyltoluene latexes in the size range of 0.085 to 90 μm, advertised by Dow Diagnostics in 1977 [30].

According to the manufacturer, the particles smaller than 5 um are prepared by emulsion polymerization (presumably seeded emulsion polymerization) while the larger particles (>5 μm) are produced by suspension polymerization (presumably dispersion polymerization). The coefficients of variation for the suspension particles are much larger than the emulsion particles $(\sigma/\bar{D}_n = 15\text{-}30\%$ vs. 0.4-10%). Note that the coefficient of variation for the smaller particles (0.085-2 μm) decreases with increasing particle diameter and reaches a value of 0.4-1.5% as a result of "self-sharpening" in seeding. The coefficient of variation increases dramatically as the particle diameter exceeds 2.5 μm, probably due to the coalescence of normal particles in seeding.

Among the four preparation methods discussed above, method (3), dispersion polymerization, is not suitable for preparing latex particles of extreme uniformity $(\sigma/\bar{D}_n < 2\%)$. Method (2), emulsifier- free polymerization, can not be used to prepare latex particles of larger sizes (>4 um). Method (4), the high-swelling method, has never

8
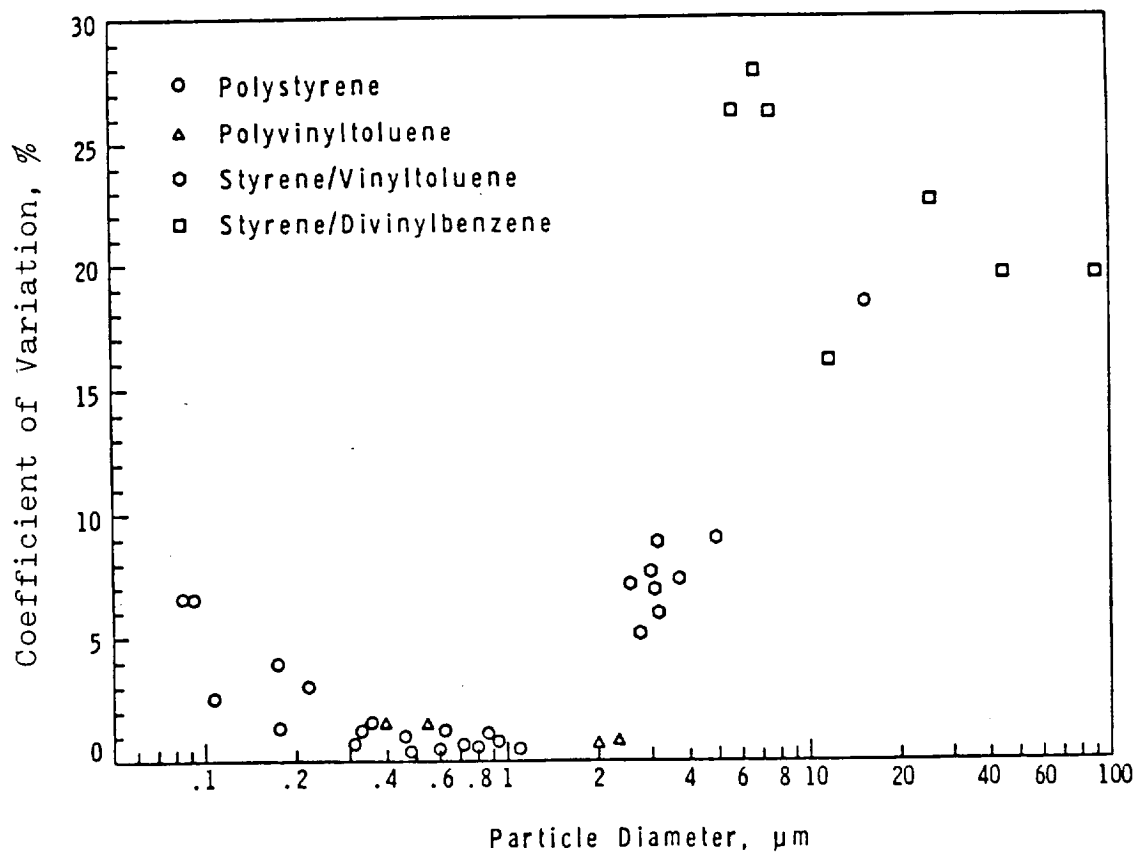
Figure 1-1.   Coefficients of variation of
polystyrene and polyvinyltoluene latexes from Dow
Diagnostics.

been well described and thus is difficult to follow. Although method (1), successive seeded emulsion polymerization, has not been used to prepare monodisperse latexes >2.5 μm in large quantity, gram quantities of 3.0 μm and 5.6 μm-diameter latexes and microscopic quantities of 12 μm-diameter latexes have been prepared by Vanderhoff [31] by recovering the stable residues from polymerizations that produced mostly coagulum. There exists a potential for further development of this method.

The objective of this study is to extend the method of successive seeding beyond the 2.0-2.5 μm upper limit, by further investigation of important polymerization parameters, so that latex particles of larger sizes (2-40 μm) with extreme uniformity ($\sigma/\bar{D}_n$ <2%) can be grown from latex particles of smaller sizes without forming excess coagulum or generating a new crop of small particles. Based on the existing information, the following approaches were outlined to achieve our goal:

1. Use a monomer/polymer ratio lower than the equilibrium swelling ratio to eliminate free monomer phase, so that the chance of nucleating small particles is reduced.

2. Use an oil-soluble initiator to reduce the opportunity for free radicals to initiate polymerization in the aqueous phase.

3. Use a water-soluble inhibitor for the same reason given in (2).

4. Use a combination of different types of surfactants to

10

stabilize the large latex particles without nucleating small particles.

5. Use minimum agitation to avoid the formation of coagulum by mechanical shear.

The equilibrium swelling ratio of a latex system is governed by the thermodynamics. The equilibrium swelling ratio in turn limits the particle volume increase which one can get from each seeding step. Further study of the swelling thermodynamics and the methods for increasing swellability are the subject of Chapter 2.

An extensive survey of polymerization initiators and inhibitors to be used to initiate seeded polymerizations in the large-particle-size range and to control small particle generation is described in Chapter 3.

A desired surfactant is one that stabilize large particles in seeded polymerization without generating a new crop of small particles, when added in a certain concentration range. Results from previous studies indicated that a single surfactant, the anionic emulsifier, did not serve this purpose in the large-particle-size range. An extensive study was therefore carried out to search for promising surfactants of other types, in the hope that another type of surfactant or a combination of different types would fulfill the requirement. Chapter 4 gives the details of this study.

As described above, large latex particles tend to cream at low conversions and to settle out at high conversions. This creaming-settling tendency can be offset by increasing the agitation rate, but these large-particle-size latexes are often sensitive to mechanical

shear, so that an increase in agitation rate often results in the formation of coagulum. One way to solve this problem is to carry out polymerization in microgravity. In microgravity, the effect of the density increase during polymerization on the creaming or settling of the particles would be obviated. The agitation rate could be reduced to the minimum level required for good heat transfer, thus minimizing flocculation by mechanical shear.

A program was proposed to National Aeronautics and Space Administration (NASA) by Lehigh University in 1977 [11], to prepare large-particle-size monodisperse latexes (2-40 µm) in microgravity. The proposal was divided into two phases with different objectives: 1. Phase I - the determination of the kinetics of polymerization of large-particle-size latexes in microgravity; 2. Phase II - the development of a practical production process for preparation of large-particle-size monodisperse latexes in microgravity. The project was funded by NASA. Two Ph.D students, E. D. Sudol and the author, and one M.S. student, A. Silwanowicz, worked on this project under the direction of Professors J. W. Vanderhoff, M. S. El-Aasser, and F. J. Micale.

Thus far, four sets of Phase I experiments have been carried out in the STS (Space Transportation System) missions of Space Shuttle Columbia and Challenger (two of each). The results of the flight experiments and parallel ground-based control experiments are described in Chapter 5. Pre-flight recipe developments and several ground-based seeding sequences are also discussed in this chapter.

Chapter 6 describes various methods involved in characterizing a

12

latex product, such as microscopy, light scattering, gel permeation chromatography and electrophoresis. Also included in this chapter are some separation methods for upgrading an imperfect latex product.

This study was concentrated on the simplest monomer-polymer system, seeding of polystyrene latexes with styrene. Most of the seed latexes used in the comparative studies were originated from a 0.40 um monodisperse polystyrene latex (Dow LS-1103-A). The polymerizations were usually carried out in glass bottles. The procedures of "bottle polymerization" are given in Appendix A.

Monodisperse colloidal systems are not only useful but also fascinating [32]. Many interesting phenomena, such as order-disorder phase transition, the iridescent colors from ordered arrays of monodisperse latex particles, have been studied by several investigators [5, 33, 34, 35, 36, 37, 38, 39, 40, 41]. The preparation of monodisperse latexes in microgravity might add more fascination to the world of monodisperse colloidal systems. Figure 1-2 shows SEM micrograph of a hollow sphere (0.76 mm diameter) comprised of an ordered monolayer of monodisperse latex particles of 7.9 μm. These particles had flocculated onto a nitrogen bubble which formed during a seeded polymerization experiment in microgravity (STS-6 flight experiment #9, see Chapter 5).
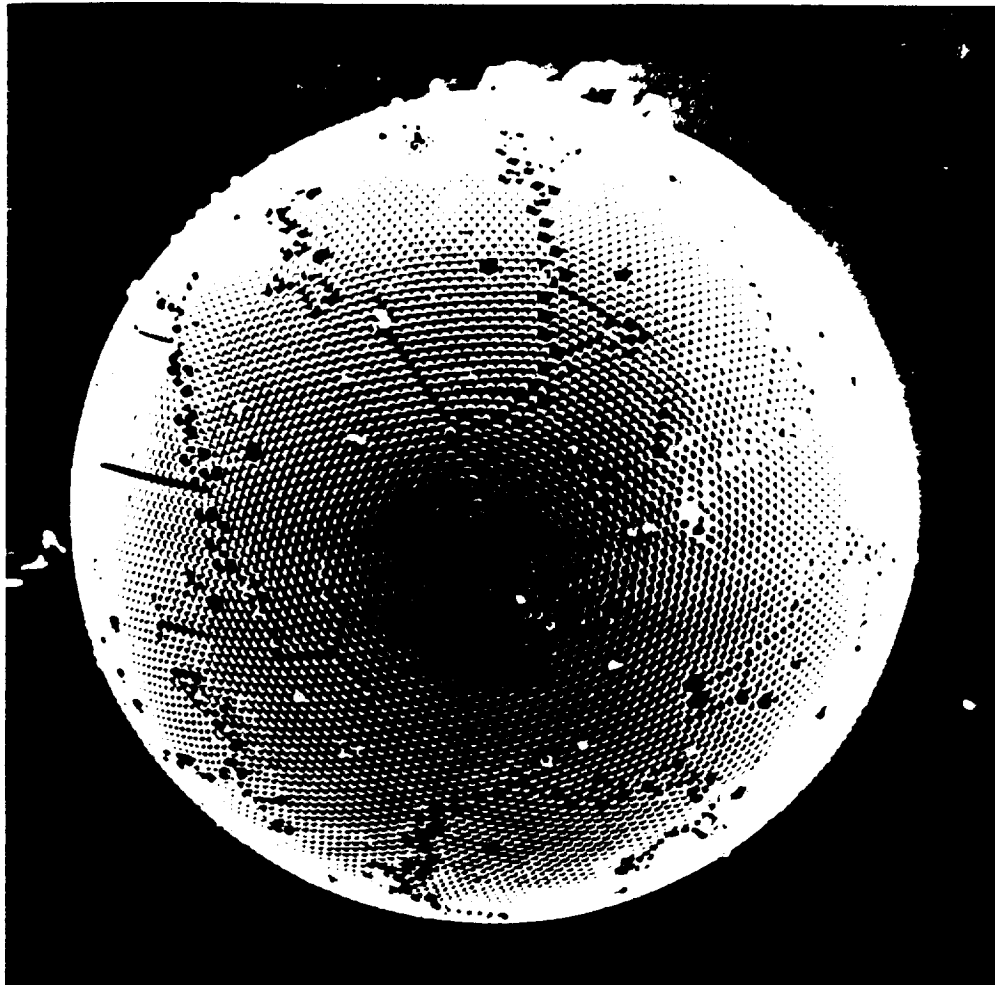
Figure 1-2.   A fascinating world of monodisperse
latex particles - SEM micrograph of a hollow sphere
comprised of an ordered monolayer of 7.9 um
monodisperse polystyrene particles, the sphere was
formed during a seeded polymerization in
microgravity.

CHAPTER 2

SWELLING OF LATEX PARTICLES WITH MONOMERS

The equilibrium concentration of monomer in latex particles during polymerization is an important parameter in the kinetic studies of emulsion polymerization. Morton et al. [42] developed a theory for the equilibrium swelling of latex particles with solvent (monomer). In this treatment, the free energy of mixing, which favors swelling, is counterbalanced by the change in interfacial energy due to the increase in the particle surface area. The system studied by Morton et al. was the swelling of polystyrene latexes by styrene, toluene, and chlorocyclohexane in the presence of potassium laurate emulsifier at the critical micelle concentration (c.m.c.).

The theory of Morton et al. has been extended to partial swelling conditions and used to obtain monomer-polymer interaction parameters and particle-water interfacial tensions by saturation swelling and partial swelling methods [43, 44, 45, 46, 47]. A complete collection of monomer-polymer swelling ratios and interaction parameters, and the interfacial tensions derived therefrom, for various monomer-polymer systems studied before 1968 were given by Gardon [45]. Unfortunately, some of the results were not consistent. For example, the interaction parameter X_{mp} ranged from 0.30 to 0.43 for polystyrene latexes swollen with styrene at room temperature, and a value of 0.55-0.58 was obtained for methyl methacrylate-polymethyl methacrylate, in contrast to the observation that methyl methacrylate is a good solvent for its polymer [45, 46]. Gardon suggested that the discrepancy in the latter

system was due to the increase of the interaction parameter by water dissolved in the monomer [45, 46]. However, no quantitative treatment considering the effect of water has been presented so far.

In practical application, swelling thermodynamics has received much attention in recent years. Ugelstad et al. [26, 27, 28, 29], using a thermodynamic treatment as well as experiments, demonstrated that the incorporation of a low-molecular-weight water-insoluble compound into latex particles allowed them to swell to a much greater extent. Therefore, latexes of large particle size could be grown by seeded emulsion polymerization in fewer steps. Guillot [48] applied a thermodynamic approach to the modeling of emulsion copolymerization processes to give a better understanding of the distribution of comonomers in the different phases and their changes with conversion, which are important in controlling the copolymerization processes.

The first section of this chapter discusses the thermodynamics of swelling in more detail. A generalized model is presented, which takes into account the effect of water dissolved in the swollen particles and in the monomer phase. The second section of this chapter describes methods of increasing the swellability of latex particles based on thermodynamic consideration.

2.1 Thermodynamics of Swelling

2.1.1 Morton-Gardon Equation -- Model I

When the swollen particle is in equilibrium with the free monomer phase, the following condition exists, according to Morton et al. [42] :

$$\Delta \bar{F} = \Delta \bar{F}_m + \Delta \bar{F}_t = 0 \qquad (2\text{-}1)$$

where $\Delta \bar{F}$ is the partial molar free energy of monomer, $\Delta \bar{F}_m$ the contribution from the energy of mixing, and $\Delta \bar{F}_t$ the contribution of the interfacial energy.

Expressing the energy of mixing in terms of the Flory-Huggins equation and the interfacial energy in terms of the Gibbs-Thomson equation gives :

$$[\ln(1-v_p)+(1-(1/j))v_p+ \chi_{mp}v_p^2] + 2\bar{V}_m \gamma/rRT = 0 \qquad (2\text{-}2)$$

where v_p is the volume fraction of polymer in the particle, j the number-average degree of polymerization of the polymer, $\bar{V}_m$ the partial molar volume of monomer, γ the particle-water interfacial tension, r the particle radius at equilibrium, R the gas constant, and T the absolute temperature.

To avoid confusion, Gardon [45] suggested that the original radius r_o be used instead of the radius at equilibrium r. Substituting $r=r_o/v_p^{1/3}$ into equation (2-2) gives equation (2-3) which is referred to as Model I in the following discussion.

$$[\ln(1-v_p)+(1-(1/j))v_p+ \chi_{mp}v_p^2] + (2\bar{V}_m \gamma /r_oRT)v_p^{1/3} = 0 \qquad (2\text{-}3)$$

It should be mentioned that, if the molecular weight of the polymer is high enough, the term $1/j$ in the above equations can be neglected.

2.1.2 A Generalized Model -- Model II

Table 2-1 lists the monomer-water mutual solubilities of some commonly used monomers. Most of the data were taken from Leonard [49]. The solubility of water in monomer followed the same order as the solubility of monomer in water for all of the monomers except vinyl acetate. The value for water in vinyl acetate appeared to be too low. The author suspects the value is erroneous - it should be 2.1 instead of 0.1 g/100g. The interfacial tension between water and vinyl acetate was measured by the author using the drop volume method and compared with the predicted values using mutual solubilities. The interfacial tension 28.3 dyne/cm predicted using a water solubility in vinyl acetate of 0.1 g/100g was too high compared with the measured value of 12.5 dyne/cm. In comparison, the interfacial tension of 13.1 dyne/cm predicted using the solubility of 2.1 g/100g was very close to the measured result. The method of predicting interfacial tensions from mutual solubilities is described in Appendix B.

Table 2-1 indicates that most of the monomers have high monomer-water mutual solubilities compared with styrene. For the swelling of these systems, neglect of the effect of water dissolved in swollen particles as well as in the monomer phase could lead to significant errors. Therefore, free energy terms describing the water-monomer and water-polymer interactions should be included in the equilibrium equations to cover a wide range of monomers.

By treating the free energy of mixing using Flory's ternary polymer solution approach [50], the following equations were obtained for the equilibrium of monomer and water inside and outside the

18

Table 2-1.   Monomer-Water Mutual Solubilities at Room Temperature

| | Solubility | |
Monomer	Monomer in Water (g/100g)	Water in Monomer (g/100g)
Styrene	0.032	0.07
Butyl acrylate	0.2	0.7
Methyl methacrylate	1.5	1.15
Ethyl acrylate	1.5	1.5
Vinyl acetate	2.5	0.1*
Methyl acrylate	5.0	2.5
Acrylonitrile	7.4	3.1

* suspected to be a misprint of 2.1

particles :

$$\ln v_m + (1-v_m) - v_w L - (v_p/j) + (\chi_{wm} L v_w + \chi_{mp} v_p)(v_w + v_p) - \chi_{wp} L v_w v_p$$
$$+ (2\bar{V}_m \gamma / r_o RT) v_p^{1/3} = \ln a_m \tag{2-4}$$

$$\ln v_w + (1-v_w) - v_m/L - (v_p/jL) + (\chi_{wm} v_m + \chi_{wp} v_p)(v_m + v_p) - \chi_{mp} v_m v_p/L$$
$$+ (2\bar{V}_w \gamma / r_o RT) v_p^{1/3} = \ln a_w \tag{2-5}$$

Most of the symbols have the same meaning as in equations (2-2) and (2-3) with the subscripts m and w denoting monomer and water. Here, L represents $\bar{V}_m/\bar{V}_w$; a_m is the activity of monomer in the separate monomer phase, which can be estimated from the solubility of water in monomer; a_w is the activity of water in the aqueous phase. For a rigorous calculation, all ingredients dissolved in the aqueous phase including monomer, surfactant, and electrolytes should be considered in estimating a_w. However, for simplicity, a_w can be approximated as unity without losing much accuracy in the prediction.

19

In this model, two more interaction parameters X_{wm} and X_{wp} have been introduced, and their values must be calculated in order to make theoretical predictions. The value of X_{wm} can be calculated from the monomer-water mutual solubilities by using equations (2-4) and (2-5) with $v_p=0$.

Since solubility data for water-polymer systems are lacking, X_{wp} can be estimated from the solubility parameters using the following equation [51]:

$$X_{12} = \bar{V}_1 (\delta_2 - \delta_1)^2/RT - z \Delta w_s/k \qquad (2-6)$$

where δ is the solubility parameter, and the constant entropic contribution, $-z\Delta w_s/k$, typically has values in the range 0.2 - 0.5. For the methyl methacrylate-polymethyl methacrylate system, X_{wm} is 3.6 as estimated from water-monomer mutual solubilities. A value of X_{wp} 5.8 can be calculated from solubility parameters of water (23.4) and polymethyl methacrylate (9.5) [52]. In the theoretical calculation, several values of X_{wp} between 3.6 and 5.8 were assumed.

Theoretical curves for Model I or Model II were obtained by solving equation (2-3) or equations (2-4) and (2-5), respectively. An iteration method was used with the aid of a CDC Cyber 720 computer. The calculated volume swelling ratio (v_m/v_p) was then plotted against the interfacial energy term $(r_0 RT/2\bar{V}_m \gamma)$.

2.1.3 Experimental Methods

The polystyrene latexes used in these swelling studies were Dow monodisperse standards : 0.19 µm (LS-1102-A), 0.40 µm (LS-1103-A), and 0.60 µm (LS-1115-B). Three polymethyl methacrylate latexes: PMMA I (0.409 µm), PMMA II (0.317 µm) and PMMA III (0.194 µm), were prepared by bottle polymerization using potassium persulfate initiator and various concentrations of Aerosol MA and Aerosol AY emulsifiers (American Cyanamid). A general description of the procedures for bottle polymerization appears in Appendix A. The particle diameters of the polystyrene latexes were determined by electron microscopy and those of the polymethyl methacrylate latexes using the Brice-Phoenix light scattering photometer by the forward angle ratio method (see Chapter 6). The latexes were used without cleaning. The surfactants added for swelling studies include sodium dodecyl sulfate (Eastman Kodak), Aerosol MA (sodium dihexyl sulfosuccinate; American Cyanamid), Triton X-100 (octylphenoxyl polyethoxy ethanol; Rohm & Haas) and poly-vinylpyrrolidone K-30 (GAF).

Excess monomer was mixed with diluted latex together with the added surfactant in a glass bottle. The swelling was carried out by tumbling the bottle end-over-end overnight. The swelling ratios were determined using the procedure of Vanderhoff et al. [53]. After swelling, the latex was mildly centrifuged to remove the excess monomer. Isooctane was then used to extract monomer from the swollen latex particles. The concentration of monomer in the extracted solution was then determined using a UV detector (Instrumentation Specialties Co. model 1840) by absorption spectra at 245nm.

21

There has been no direct method for measuring the interfacial tension between a swollen particle and the aqueous phase. However, it can be approximated by the interfacial tension between the monomer phase and the swollen latex dispersion. The latter was measured by the drop volume method. The swollen latex dispersion was dropped into the monomer phase using a microsyringe with a flat needle. The drop volume and density data were then converted to interfacial tension. Appendix C shows the device and the calculation by the drop volume method.

2.1.4 Comparison of Experimental and Model Results

2.1.4.1 Swelling of Polystyrene Latex Particles with Styrene

The swelling ratios and the corresponding interfacial tensions for the different-size latexes with added anionic surfactants Aerosol MA and sodium dodecyl sulfate are listed in Table 2-2. Those values obtained with added nonionic surfactant Triton X-100 and polymeric surfactant polyvinylpyrrolidone are listed in Table 2-3.

Figure 2-1 compares theoretical curves from Model I with all of the experimental data. It was found that the theoretical curves were almost linear and a curve corresponding to X_{mp} = 0.35 fitted the data best. Therefore, a semi-empirical equation was derived from these results :

$$v_m/v_p = 0.339 \ (r_o RT/2\bar{V}_m \gamma)^{0.594} \tag{2-7}$$

or

$$v_m/v_p = 84.9 \ (r_o/\gamma)^{0.594} \quad \text{at room temp.} \tag{2-8}$$

22

$(r_o$ in μm, γ in dyne/cm)

These data were also used to fit theoretical curves from Model II. Since the solubility of water in styrene is quite low, and χ_{wp} is quite close to χ_{wm}, the effect of the interaction terms involving water are negligible. The theoretical curves from Model II are essentially the same as those from Model I with same value of χ_{mp}.

Table 2-2.   Swelling of Polystyrene Latexes with Styrene in the Presence of Anionic Surfactants

r_o (μm)	Surfactant Conc. (% on polymer)	γ (dyne/cm)	Swelling Ratio (v_m/v_p)	$r_o RT/2\bar{V}_m \gamma$
0.095	AMA,6.0	28.7	3.02	36
0.095	SDS,6.0	23.2	3.04	45
0.20	AMA,6.0	28.1	4.31	78
0.20	SDS,6.0	21.4	4.77	102
0.30	AMA,6.0	26.6	5.73	122
0.30	SDS,6.0	19.5	6.66	168
0.30	AMA,1.4	30.6	5.14	107
0.20	AMA,1.4	31.2	4.76	70
0.095	AMA,1.4	31.6	2.77	33

AMA = Aerosol MA, SDS = Sodium Dodecyl Sulfate

In comparison, the swelling data of the styrene-polystyrene system from Morton et al. [42] were examined. In their work, a monomer-polymer interaction parameter of 0.43 and an interfacial tension of 4.5 dynes/cm was obtained by plotting $-[\ln(1-v_p)+v_p]/v_p^2$ vs. $1/rv_p^2$ and extrapolating to get the intercept and the slope. However, the result was erroneous, probably due to the mix-up of r and r_o. Morton et al. carried out the swelling experiments with potassium laurate at the c.m.c.. An attempt was thus made by the author to

Table 2-3.   Swelling of Polystyrene Latexes with
Styrene in the Presence of Nonionic and Polymeric
Surfactants

r_o (μm)	Surfactant Conc. (% on polymer)	γ (dyne/cm)	Swelling Ratio (v_m/v_p)	$r_o RT/2\overline{V}_m\gamma$
0.30	Triton,6.0	27.9	5.00	117
0.095	Triton,6.0	27.4	3.35	38
0.20	Triton,1.5	33.9	4.18	64
0.095	Triton,1.5	33.6	2.96	31
0.30	PVP,1.9	35.0	5.68	93
0.20	PVP,1.9	33.6	4.59	65
0.095	PVP,4.5	31.4	3.30	33
0.30	PVP,7.5	21.1	7.46	155
0.20	PVP,7.5	19.7	4.23	111
0.095	PVP,7.5	20.1	3.84	52

Triton = Triton X-100, PVP = Polyvinylpyrrolidone

Table 2-4.   Swelling of Polystyrene Latexes with
Styrene   - Analysis of Data from Morton et al.

r_o (μm)	Surfactant Conc. (% on polymer)	γ (dyne/cm)	Swelling Ratio (v_m/v_p)	$r_o RT/2\overline{V}_m\gamma$
0.019	K laurate,cmc	7.2	2.10	28
0.040	K laurate,cmc	7.2	3.40	61
0.087	K laurate,cmc	7.2	5.34	131

measure the interfacial tension under similar conditions, recalculate
the swelling data, and compare the results with Model I. The
interfacial tension was measured to be 7.2 dyne/cm by the drop volume
method. Table 2-4 presents the combined results: the volume swelling
ratios converted from the weight swelling ratios, the measured
interfacial tensions, and the calculated interfacial energy terms.
These data along with the theoretical curves are shown in Figure 2-2.
By comparing Figures 2-1 and 2-2, it was found the data from this work
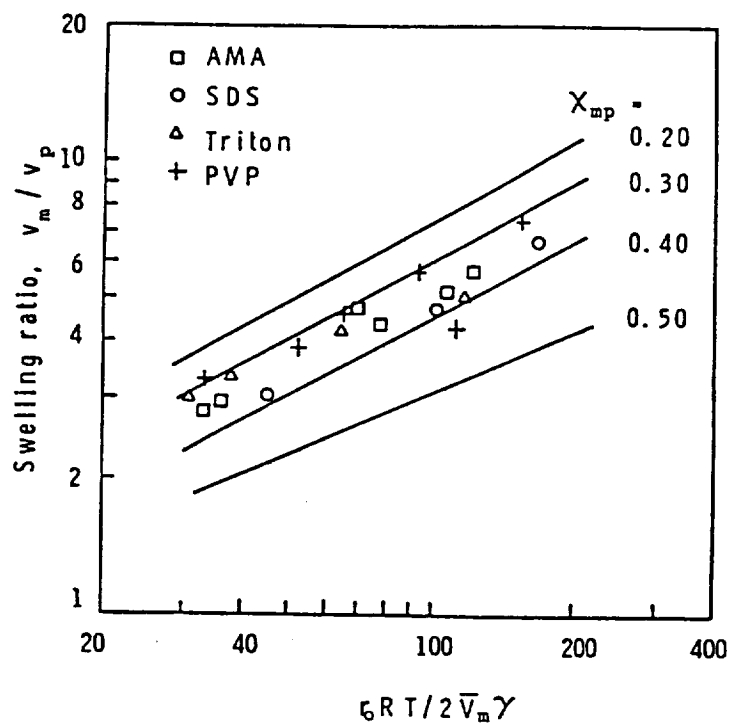
Figure 2-1.   Swelling of polystyrene latexes with styrene: comparison of experimental data with theoretical curves from Model I.

and the re-analyzed data of Morton et al. were in good agreement.

2.1.4.2 Swelling of Polymethyl Methacrylate Latex Particles with Methyl Methacrylate

Table 2-5 lists the swelling ratios and interfacial tensions for the different-size polymethyl methacrylate latexes with added Aerosol MA and sodium dodecyl sulfate emulsifiers.

Comparison of the data with the theoretical curves from Model I (Figure 2-3) defines an apparent interaction parameter X_{mp} of 0.45 and the semi-empirical equation :

$$v_m/v_p = 0.361 \ (r_o RT/2\overline{V}_m \gamma)^{0.512} \tag{2-9}$$

or

$$v_m/v_p = 43.9 \ (r_o/\gamma)^{0.512} \quad \text{at room temp.} \tag{2-10}$$

These experimental data are fitted equally well by Model II by using several pair combinations of the interaction parameters X_{mp} and X_{wp}. Figures 2-4 to 2-7 show the experimental data compared to theoretical curves from Model II with the following pairs of the interaction parameters X_{mp} and X_{wp}: 0.42, 4.5; 0.38, 5.0; 0.33, 5.5; 0.29, 5.8. It should be pointed out that Model II gives the same result as Model I when $X_{wp} = X_{wm} = 3.6$ and $X_{mp} = 0.45$. These data, however, are not sufficient to determine which pairs of parameters are closest to the actual values.

It is interesting to compare the monomer-polymer interaction parameters derived from this study with the literature values obtained by other methods. Very few data are available for styrene-polystyrene

26
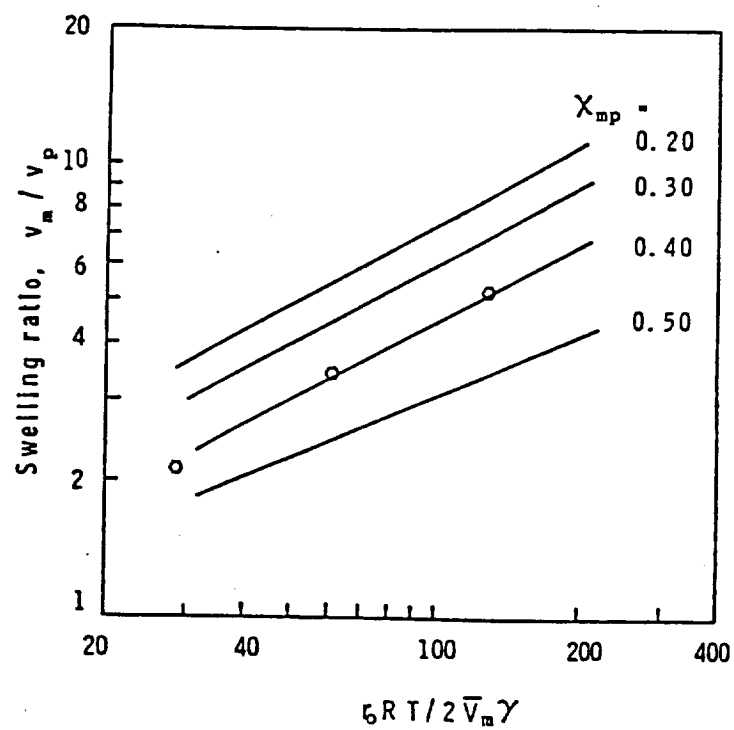
Figure 2-2.   Swelling of polystyrene latexes with styrene: comparison of the re-analyzed data from Morton et al. with theoretical curves from Model I.

Table 2-5.   Swelling of Polymethyl Methacrylate
Latexes with Methyl Methacrylate in the Presence of
Anionic Surfactants

r_0 (μm)	Surfactant Conc. (% on polymer)	γ (dyne/cm)	Swelling Ratio (v_m/v_p)	$r_0 RT/2\overline{V}_m \gamma$
0.097	AMA,1.1	10.5	4.11	109
0.097	SDS,1.1	9.2	3.88	124
0.097	SDS,3.2	7.2	4.63	159
0.16	AMA,1.1	12.3	5.04	152
0.16	SDS,1.1	9.8	5.12	191
0.16	SDS,3.2	6.6	6.91	283
0.20	AMA,1.1	12.1	5.96	197
0.20	SDS,1.1	9.4	5.89	256
0.20	SDS,3.2	6.0	8.35	402

and methyl methacrylate-polymethyl methacrylate systems. Boyer [54]
reported a value of 0.42 from the swelling of polystyrene gel
(crosslinked with divinylbenzene) by styrene. Fox [55] obtained a
value of 0.47 for methyl methacrylate-polymethyl methacrylate by the
viscosity method. More reliable interaction parameters from polymer
solution studies would give a better understanding of the swelling of
latex particles.

In summary, the thermodynamic Model I, which is based on the
theory of Morton et al., has been used to successfully fit
experimental data and obtain semi-empirical equations for the swelling
of polystyrene and polymethyl methacrylate latexes. The semi-
empirical equations provide a quick estimate of the swelling ratio
from particle size and interfacial tension. The generalized form of
Model II might prove to be more suitable for describing the swelling
phenomena of relatively hydrophilic systems .
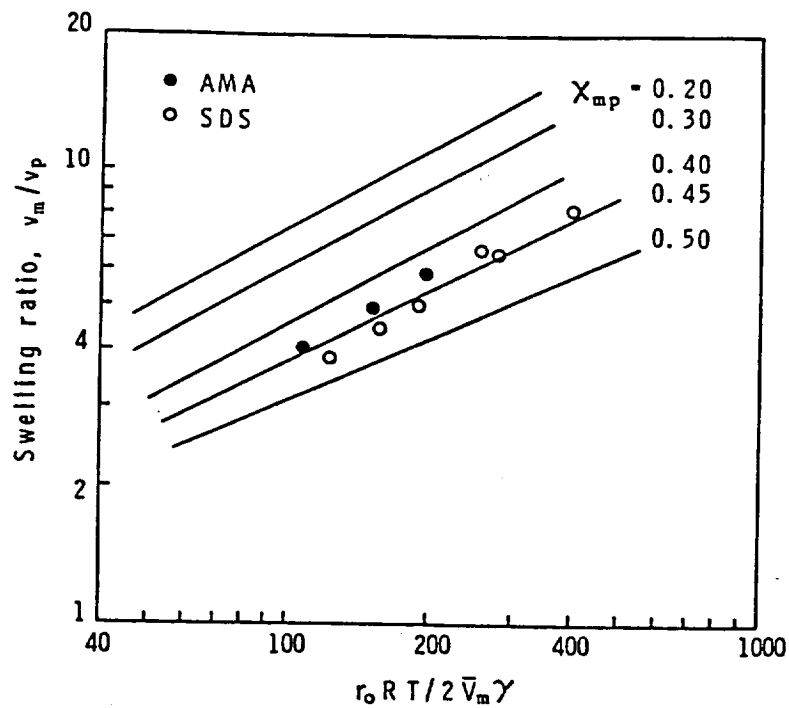
Figure 2-3. Swelling of polymethyl methacrylate latexes with methyl methacrylate: comparison of experimental data with theoretical curves from Model 1.
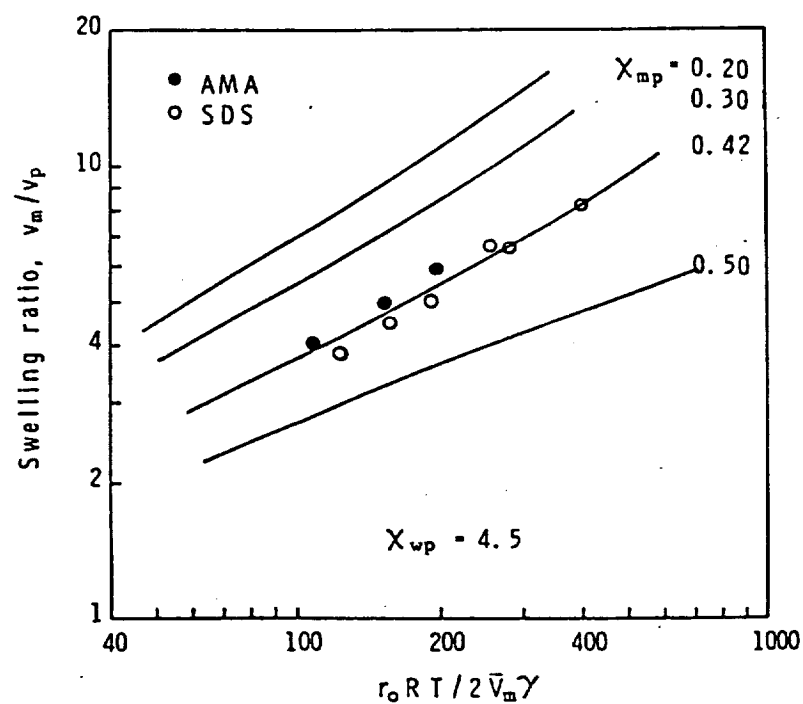
Figure 2-4. Swelling of polymethyl methacrylate latexes with methyl methacrylate: comparison of experimental data with theoretical curves from Model II for $X_{wp} = 4.5$.
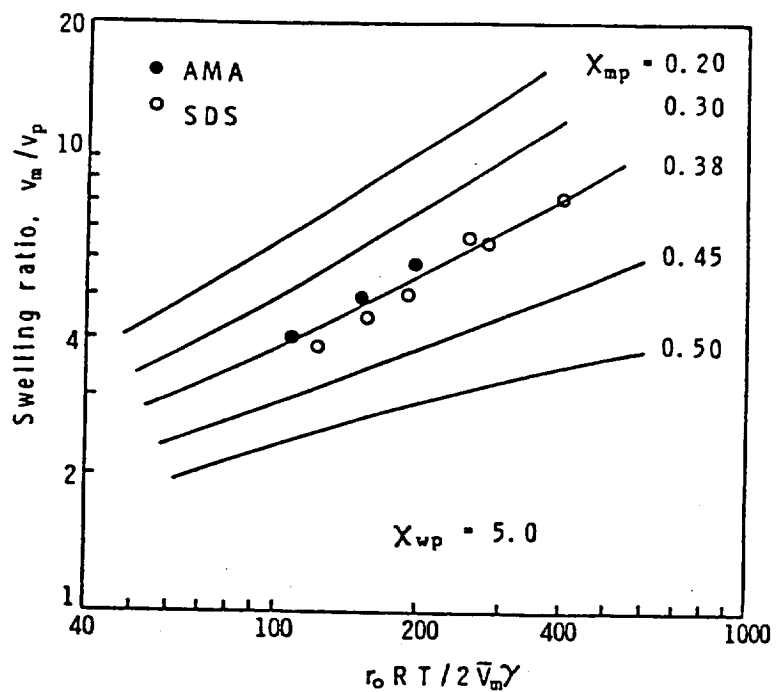
Figure 2-5. Swelling of polymethyl methacrylate latexes with methyl methacrylate: comparison of experimental data with theoretical curves from Model II for X_{wp} = 5.0.
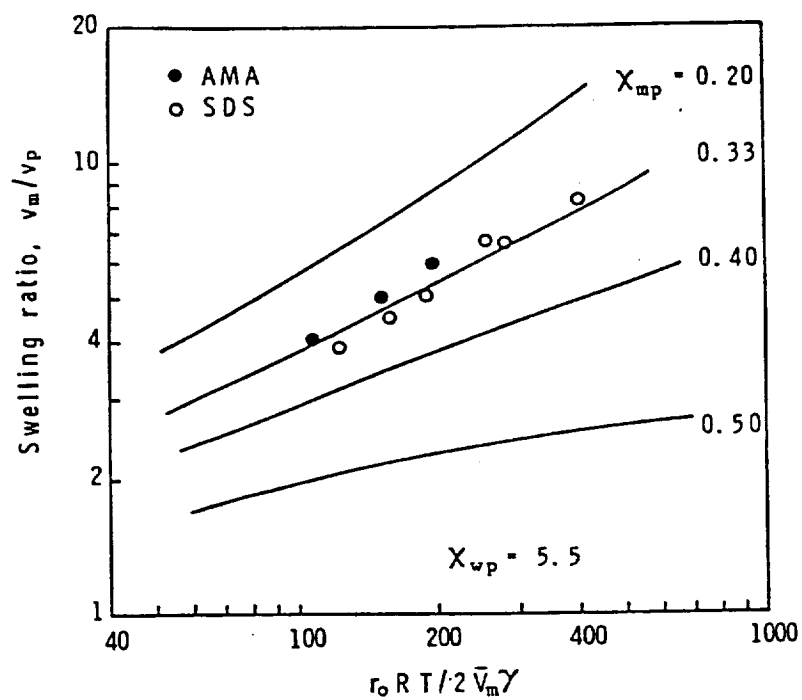
Figure 2-6.   Swelling of polymethyl methacrylate
latexes with methyl methacrylate: comparison of
experimental data with theoretical curves from Model
II for X_{wp}= 5.5.
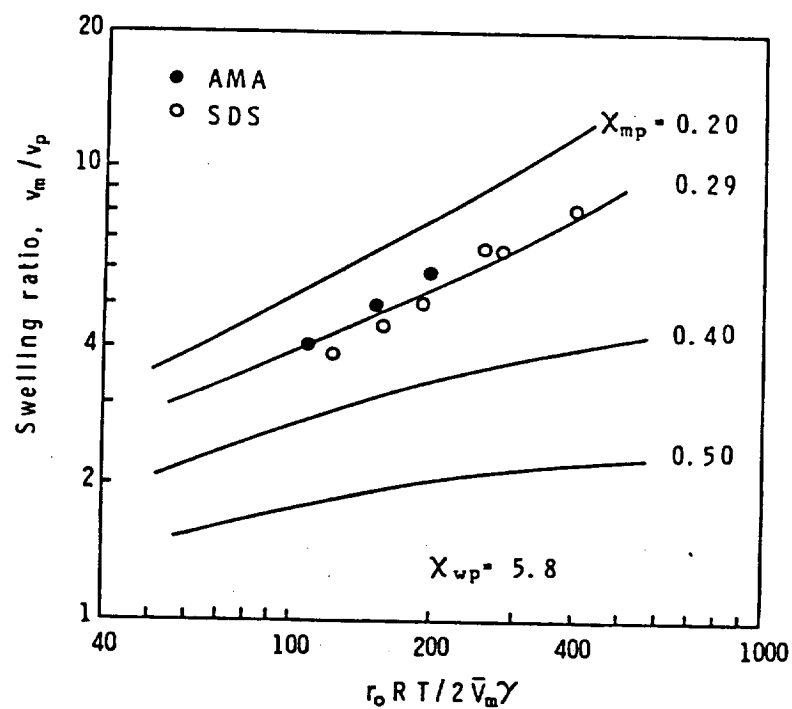
Figure 2-7.   Swelling of polymethyl methacrylate
latexes with methyl methacrylate: comparison of
experimental data with theoretical curves from Model
II for X_{wp} = 5.8.

2.2 Increasing the Swellability of Latex Particles

From the results obtained in the previous section, polystyrene latex particles can be swollen by styrene to a volume ratio of 2.1 to 7.5, depending on the particle size, and surfactant type and concentration. These results were obtained under normal conditions, i.e., molecular weight of the polystyrene was high enough so that $1/j$ in equation (2-3) could be neglected. It is clear from the equation that, if the molecular weight of the polymer were lowered to such an extent that the $1/j$ term is not negligible, the free energy of mixing can be increased and the swelling enhanced.

2.2.1 Two-Step Swelling

Ugelstad et al. [26, 27, 28, 29] used a different form of the equation to demonstrate that, by introducing a water-insoluble low-molecular-weight compound into the particle, the swelling ratio could be increased to a great extent:

$$\ln v_1 + (1-1/j_2)v_2 + (1-1/j_3)v_3 + v_2^2 X_{12} + v_3^2 X_{13}$$
$$+ v_2 v_3 (X_{12} + X_{13} - X_{23}/j_2) + 2\bar{V}_1 \gamma /rRT = 0 \qquad (2-11)$$

where 1, 2, and 3 represent monomer, water-insoluble "oligomer", and polymer, respectively. The so-called "oligomer" used by these authors was usually a long-chain hydrocarbon or chlorinated hydrocarbon such as chlorododecane. This process is outlined in Figure 2-8.

In the first stage of the process, an "oligomer" emulsion was prepared by homogenizing in the presence of an emulsifier. The emulsion was then mixed with a seed latex, added emulsifier, and a "carrier" solvent. After the "oligomer" diffused into the latex

34
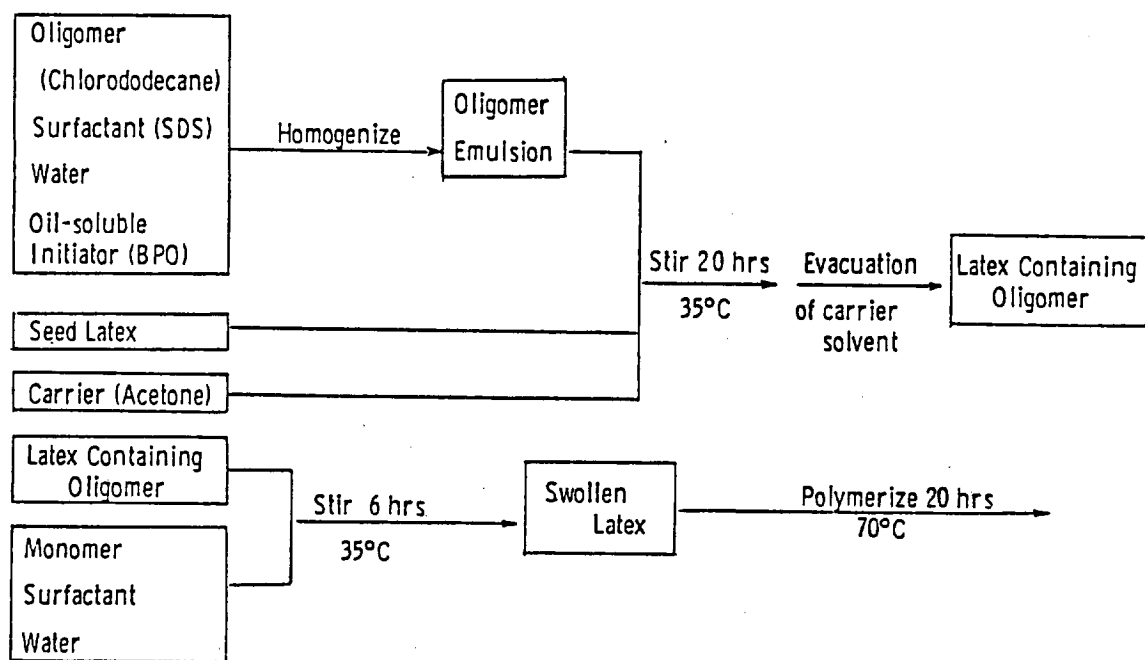
Figure 2-8.   Schematic diagram of the two-step
swelling method.

particles, the "carrier" solvent was removed by vacuum distillation. In the second stage of the process, the "oligomer"-containing latex was mixed with monomer to give a high swelling ratio.

With the two-step swelling method, an overall swelling ratio which was the volume ratio of the final particle to the initial particle (before introducing the "oligomer") greater than 100 could usually be obtained. In a recent report [28], swelling ratios greater than 1000 were claimed.

2.2.2 "Seeded-Telomerization" Swelling Method

An alternative approach to increase the swellability of latex particles is to form low-molecular-weight polymers _in situ_, i.e., to swell the latex particles with monomer and a high concentration of chain transfer agent and carry out "telomerization" in the particles. Polymerization in the presence of a chain transfer agent (telogen) to yield a series of low-molecular-weight polymers (usually <5000) is termed "telomerization" [56]. The term "oligomerization" is sometimes used instead of telomerization, but here the term "oligomer" refers only to a low-molecular-weight compound which does not incorporate elements of chain transfer agents into its structure.

Telomerization describes a kinetic situation where the rates of chain growth and chain transfer are in near-balance. The balance is quantitatively stated in terms of chain transfer coefficients or constants, C_n, defined by [56]:

$$C_n = \text{rate constant for chain transfer for } T_n \text{ / rate constant for chain growth for } T_n \qquad (2\text{-}12)$$

where T_n is the telomer radical containing n monomer units. As the length of the telomer radical increases, and the endgroup is progressively removed from the radical, C_n tends toward a limiting value, designated by C_∞ and termed the polymer-type chain transfer constant. Polymer-type chain transfer constants have been measured for a large number of compounds because of their obvious relevance to polymer molecular weight [57].

Mayo [58] has shown that the average degree of polymerization ($\bar{P}$) is related to the polymer-type chain transfer constant (C_∞), the molar ratio of chain transfer agent to monomer (R), and the average degree of polymerization in the absence of chain transfer agent ($\bar{P}_0$) by equation:

$$1/\bar{P} = C_\infty R + 1/\bar{P}_0 \tag{2-13}$$

The decrease of the chain transfer agent concentration with increasing monomer conversion is important in practice, because very reactive transfer agents are used up preferentially, giving a broad molecular weight distribution if they can not be replenished. In analogy to the initiator "half-life" of decomposition, one can define a "half-conversion" $U_{1/2}$ as that monomer conversion where the transfer agent is half consumed [57]:

$$U_{1/2} = 100 \, (1 - 0.5^{1/C_\infty}) \tag{2-14}$$

Table 2-6 demonstrates that the "half-conversion" $U_{1/2}$ decreases with increasing transfer constant C_∞ [57].

A large number of chain transfer agents and their transfer constants C_∞ for styrene can be found in the "Polymer Handbook" [57].

Table 2-6.　The "Half-Conversion" of Chain Transfer
Agents as a Function of Transfer Constants

C_∞	$U_{1/2}(\%)$	C_∞	$U_{1/2}(\%)$
0.1	99.9	5	13.0
0.2	96.8	10	6.7
0.5	75.0	20	3.4
1	50.0	50	1.4
2	29.3	100	0.7

However, there are not many transfer agents suitable for telomeriza-tion. Transfer agents with $C_\infty < 1$ are inefficient in reducing the molecular weight. On the other hand, transfer agents with $C_\infty \gg 1$ would be consumed too fast, yielding a broad molecular weight distri-bution, as described above. Carbon tetrabromide with $C_\infty = 2.5$ and various mercaptans with $C_\infty = 3$ to 20 appear to be the most promising telogens.

The use of carbon tetrabromide in seeded telomerization has been described by Ugelstad et al. [29]. However, it was found in our study that the telomerization rate in the presence of carbon tetrabromide was very low; a low conversion was obtained after a 20-hour reaction period. The effect of carbon tetrabromide on the kinetics of seeded emulsion polymerization of styrene has been discussed by Gilbert et al. [59]. Nomura et al. [60] compared the effect of carbon tetra-bromide, carbon tetrachloride, and four primary mercaptans (with 2, 4, 7, and 12 carbon atoms) on the emulsion polymerization kinetics. The decrease of polymerization rate by the chain transfer agents was explained in terms of desorption from the polymer particles of the

small radicals formed by chain transfer.

Table 2-7 lists commercially available mercaptans with 4 to 20 carbon atoms, and their transfer constants. In general, a primary mercaptan has a C_∞ value in the range of 15 to 20, while a secondary or tertiary mercaptan has a value of 3 to 4.

A "seeded-telomerization" swelling method using mercaptans as telogens, developed in this study, is outlined in Figure 2-9. A seed latex, monomer, telogen, and emulsifier was loaded into a glass bottle, which was sealed and rotated end-over-end in a 70°C water bath for 1.0-1.5 hours. The bottle was then taken out and an initiator solution was injected through the rubber gasket. The telomerization was then carried out in the same bath for 20 hours. The telomerized latex could thus be swollen to a greater extent than the untreated latex.

Table 2-7.   Mercaptans and Their Chain Transfer Constants

Mercaptan	C_∞ (T°C)
Dodecyl	14.8 (60)
t-Dodecyl	2.9 (50)
Octyl	19.0 (50)
s-Octyl	3.2 (99)
t-Octyl	4.3 (50)
Hexyl	15.3 (99)
Cyclohexyl	– –
t-Amyl	– –
s-Butyl	– –
t-Butyl	3.1 (60)

Table 2-8 compares products of seeded telomerization using
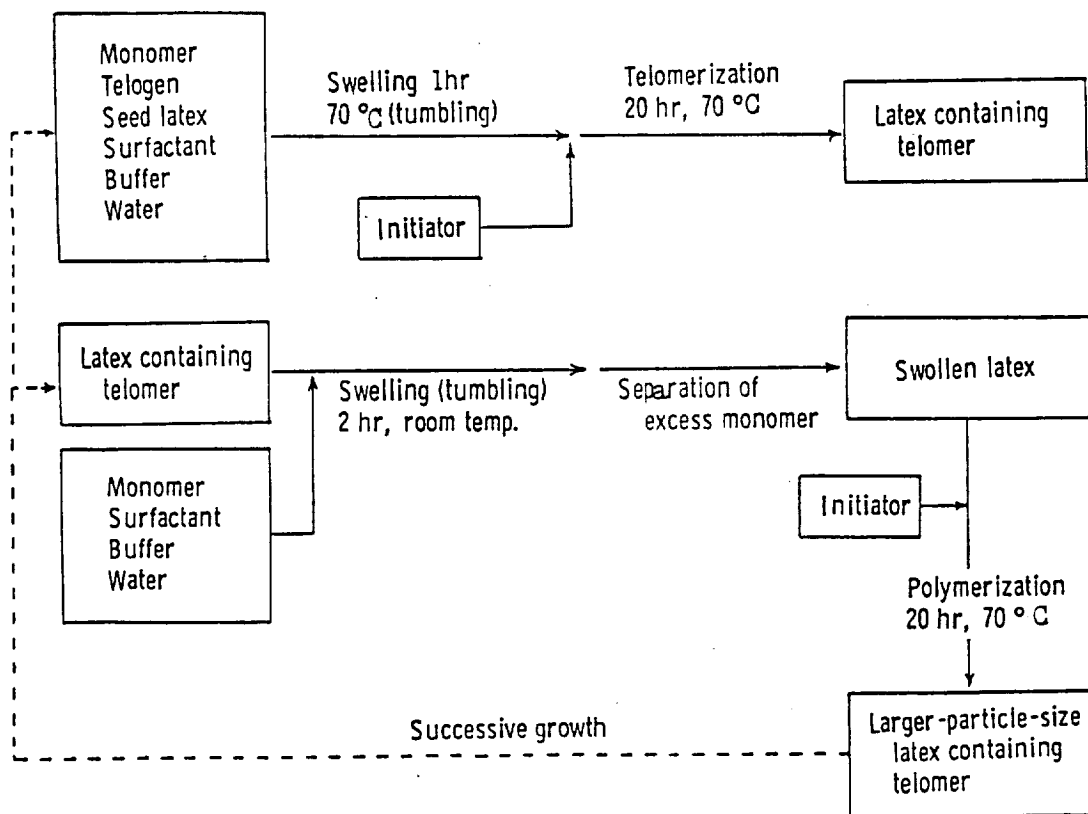
Figure 2-9.   Schematic diagram of the "seeded-
telomerization" swelling method.

40

different types and concentrations of mercaptans, and monomer/polymer ratios. The seed latex used was the polystyrene latex of 0.40 μm diameter (LS-1103-A). Aerosol MA and potassium persulfate were used as surfactant and initiator. At the begining of the study, dodecyl mercaptan and t-dodecyl mercaptan were used as telogens. Because of their low efficiency in reducing the molecular weight of the product, an attempt was made to enhance the chain transfer reactivity by lowering the chain propagation rate of the monomer. A second monomer, -methyl styrene, which has a lower propagation rate constant than styrene, was introduced into the recipes. The ratios of the two monomers are listed in the third column of the table.

The telomerized latexes were examined using cold-stage TEM. In general, a narrow particle size distribution was maintained after telomerization. Typical micrographs are presented in Figure 2-10. Molecular weight distributions of the latexes along with the seed were determined by GPC. A few typical distribution curves are given in Figures 2-11 to 2-15. A high-molecular-weight polymer peak and a low-molecular-weight telomer peak could be found in the distribution curve of each telomerization product. A major part of the polymer peak was from the seed; the rest of the peak was formed during the seeded telomerization. Columns 6, 7 and 8 of Table 2-8 show the peak molecular weight of telomer, estimated volume ratio of telomer to polymer, and overall average molecular weight of the telomerized latex. Several conclusions can be drawn from these results:

1. Incorporation of the α-methyl styrene always gave a low

Table 2-8. Products of Seeded Telomerization Using Different Mercaptans

Sample No.	M/P	α-MSt/St Monomers Ratio	Telogen (wt% on Monomer)	Conv. (%)	Peak MW of Telomer	Telomer/Polymer Volume Ratio	Overall $\overline{M}_n$
Seed	-	-	-	-	-	-	160,000
1067-3	1	0.33	t-DM(10)	76.6	3000	0.72	4000
1067-2	1	0.33	OM(15)	71.7	580	0.24	3200
1057-1	1	0	OM(10)	100	650	0.19	4100
1059-1	1	1.00	OM(5)	43.0	700	0.19	4200
1074-1	1	0.33	t-OM(10)	95.0	800	0.78	1700
1074-3	3	0.33	t-OM(6.7)	47.0	1300	1.28	1500
1109-1	1	0	s-BM(10)	100	350	0.52	1200
1109-2	1	0	t-AM(10)	100	980	0.91	1900
1109-3	1	0	CHM(10)	100	330	0.42	1100
1109-4	1	0.33	s-BM(10)	56.0	380	0.59	1100
1109-5	1	0.33	t-AM(10)	78.0	890	0.77	1600
1109-6	1	0.33	CHM(10)	90.0	380	0.40	1600
1131-1	1	0	t-OM(10)	100	1300	0.73	2500
1131-2	2	0	t-OM(10)	100	1300	1.34	2000
1131-3	3	0	t-OM(10)	100	1450	1.76	1900

St = Styrene, α-MSt = α-Methylstyrene

DM = Dodecyl Mercaptan, OM = Octyl Mercaptan, BM = Butyl Mercaptan,

AM = Amyl Mercaptan, CHM = Cyclohexyl Mercaptan
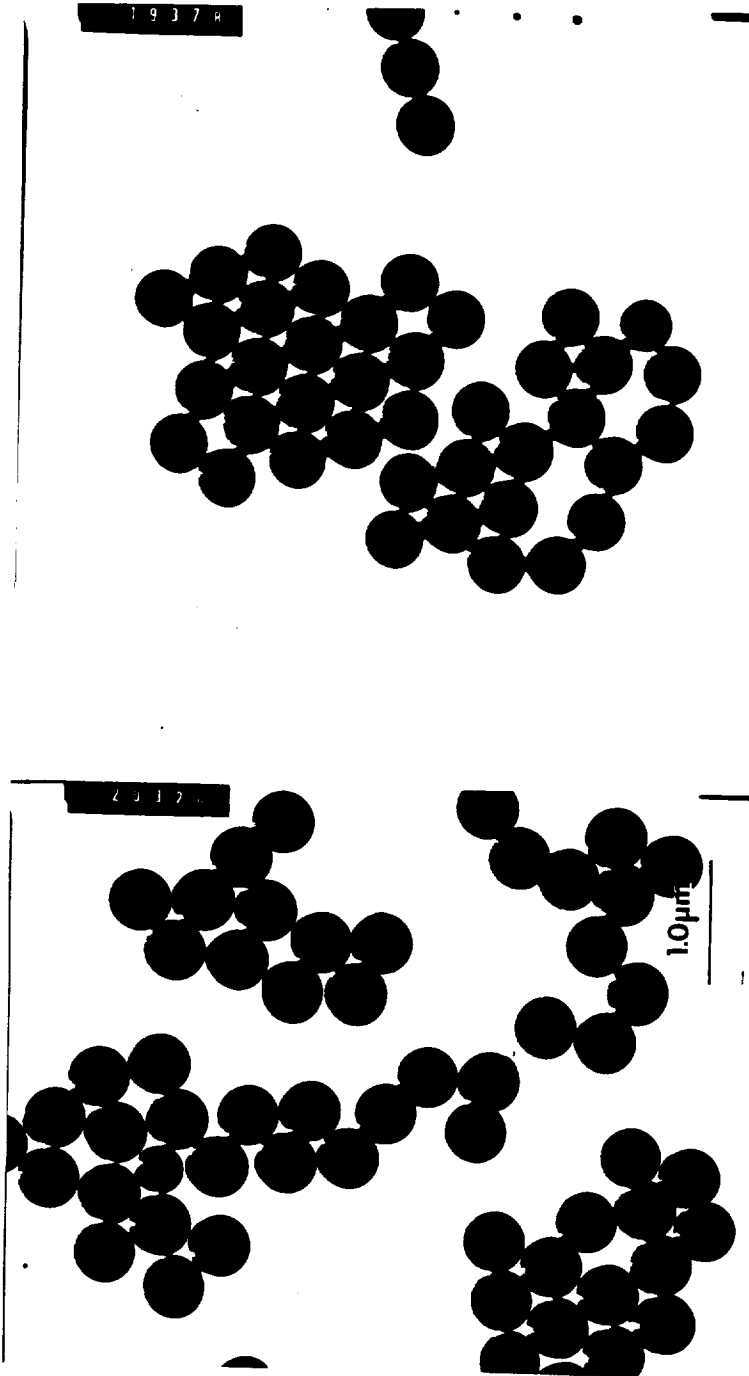
Figure 2-10. Cold-stage TEM micrographs of telomerized latexes #1057-1 (left) and #1067-3 (right).

0.4 UM SEED

NUMBER AVERAGE MWT = .16E+06
WEIGHT AVERAGE MWT = .13E+07
DISPERSITY,D = 8.14
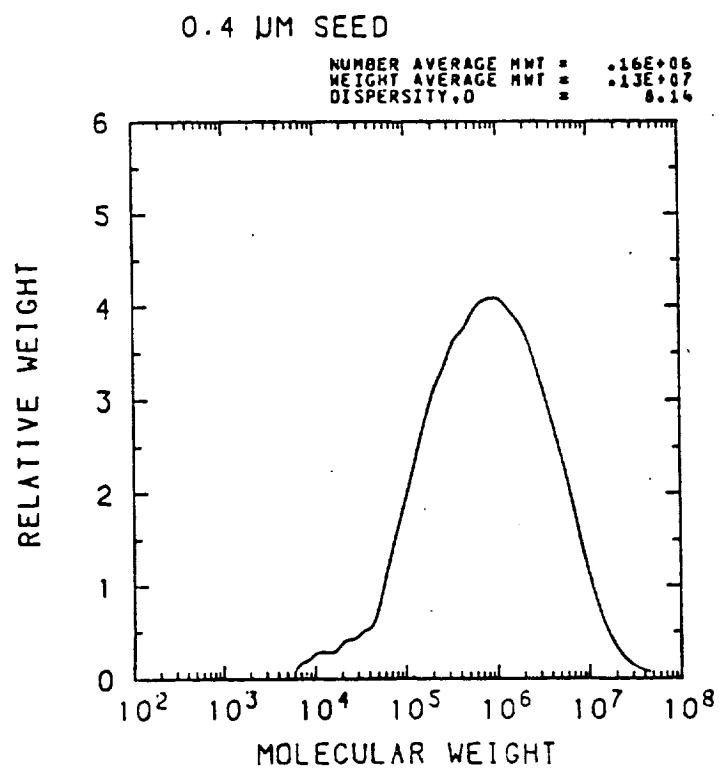
Figure 2-11. Molecular weight distribution of the 0.40 μm seed latex.

44
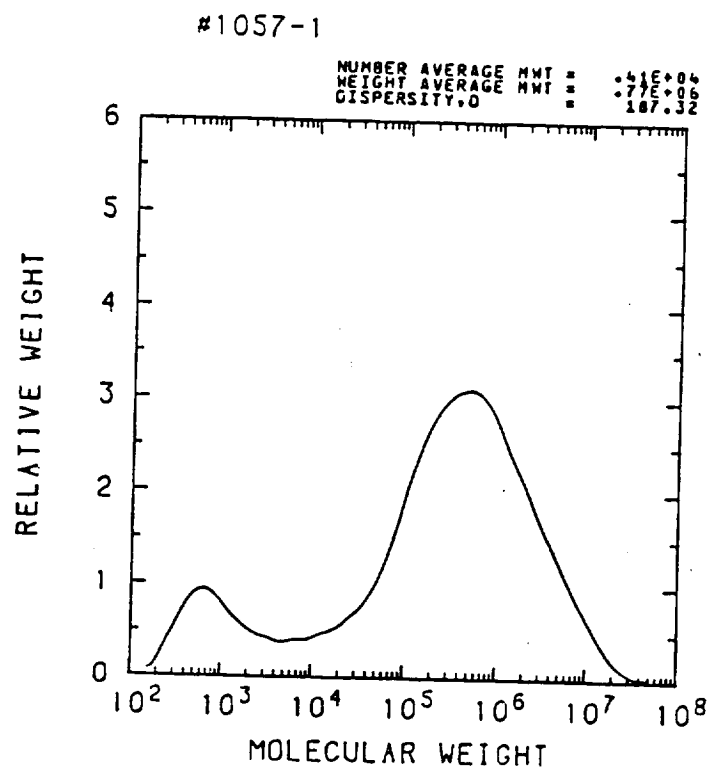
#1057-1

Figure 2-12.   Molecular weight distribution of
telomerized latex #1057-1.
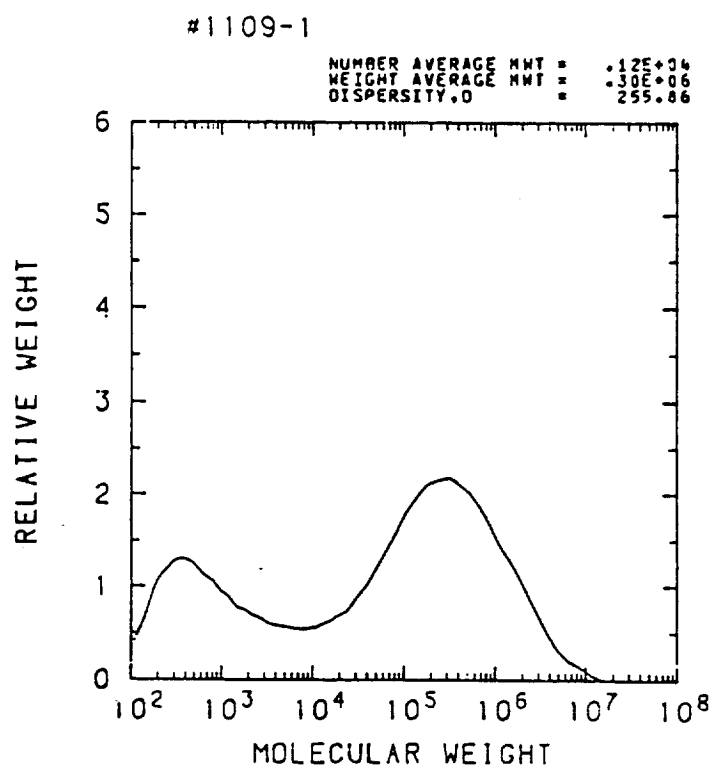
Figure 2-13. Molecular weight distribution of
telomerized latex #1109-1.

#1131-1

NUMBER AVERAGE MWT = .25E+04
WEIGHT AVERAGE MWT = .44E+06
DISPERSITY,D = 177.33
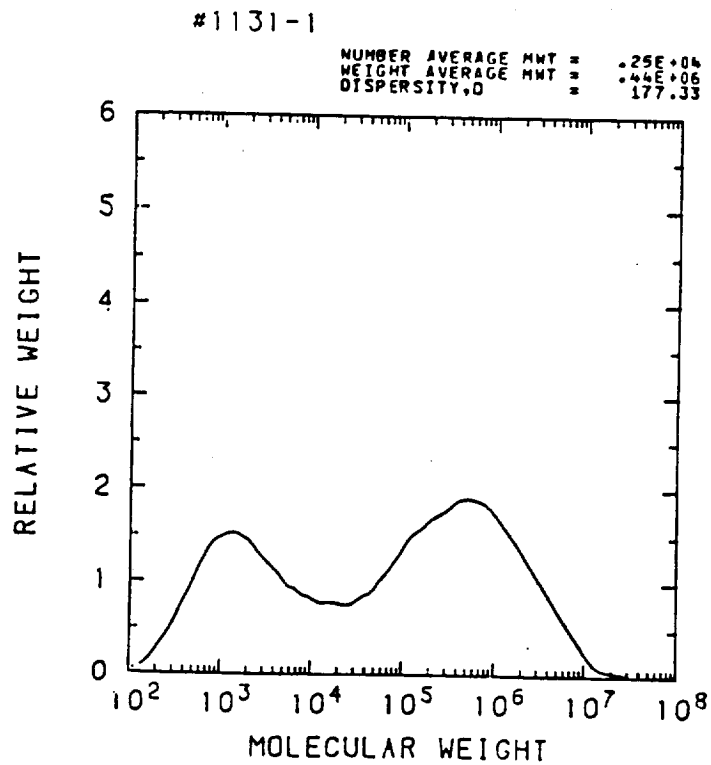
Figure 2-14.   Molecular weight distribution of telomerized latex #1131-1.

#1131-3

NUMBER AVERAGE MWT = .19E+04
WEIGHT AVERAGE MWT = .30E+06
DISPERSITY,0 = 152.87
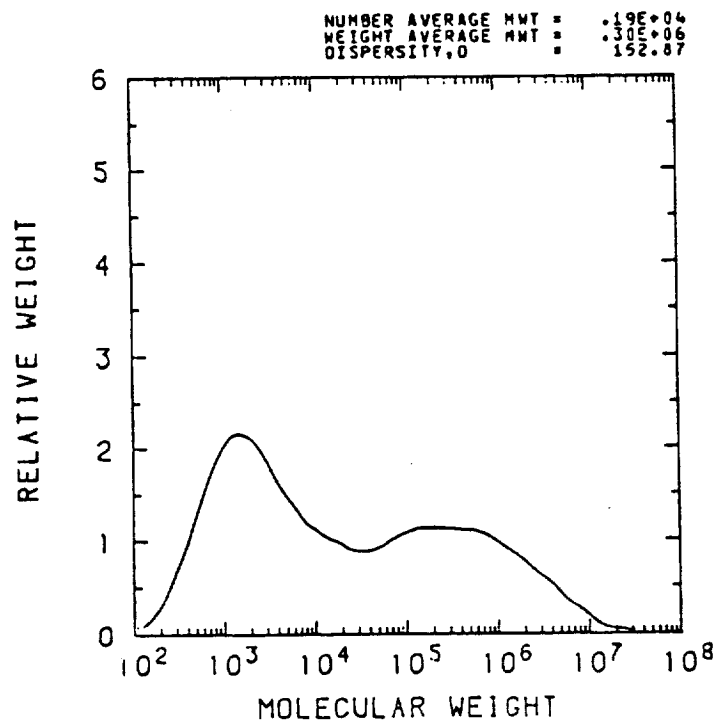
Figure 2-15. Molecular weight distribution of telomerized latex #1131-3.

monomer-to-telomer(polymer) conversion in the seeded telo-
merization.

2. A higher alkyl mercaptan usually resulted in telomer of
higher molecular weight than that from a lower alkyl
mercaptan, although the two mercaptans had similar transfer
constants (cf. t-dodecyl mercaptan in #1067-3 and t-octyl
mercaptan in 1074-1). The low chain transfer efficiency of
the higher alkyl mercaptan may be attributed to its slow
diffusion to the reaction loci. The effect of mercaptan
structure and chain length upon the rate of diffusion
through aqueous medium, the rate of mercaptan consumption
during emulsion polmerization of styrene and butadiene, and
the efficiency of mercaptan in modifying the properties of
rubbery polymers have been the subject of several studies
[61].

3. A tertiary mercaptan, which had a lower transfer constant
than its primary isomer, gave a more pronounced telomer
peak, i.e., a higher telomer/polymer ratio, than the
latter. A good example was the t-octyl mercaptan in sample
#1131-1 compared with the octyl mercaptan in sample
#1057-1. Although the former product had a slightly higher
telomer peak molecular weight, the overall average
molecular weight $\overline{M}_n$ was lower for the former. This result
agreed with the rationalization that a chain transfer agent
with $C_\infty \gg 1$ would be used up at low conversion, yielding a
broad molecular weight distribution. In other words, with

49

a chain transfer agent of high C_∞, a small fraction of monomer was converted to telomer of very low molecular weight at an early stage of reaction and a large fraction of monomer was converted to polymer after the transfer agent was used up.

4. Secondary and tertiary lower alkyl mercaptans, s-butyl mercaptan, t-amyl mercaptan, and cyclohexyl mercaptan, were effective in producing low-molecular-weight telomer.

Equation (2-3) can be used to predict swellability of the telomerized latexes based on particle size, interfacial tension, and average molecular weight. Figure 2-16 shows the theoretical relationship between volume swelling ratio and the interfacial energy term for telomerized latexes with $\bar{M}_n$ = 2000 (j = 20). The curve was generated with the computer using X_{mp} = 0.35. An interfacial tension of 26-32 dyne/cm was usually obtained when Aerosol MA surfactant was used in the swelling (cf. Table 2-2). With particle diameters of 0.50-0.63 μm, an interfacial energy term $r_o RT/2\bar{V}\gamma$ = 85-119 was obtained. Thus, from Figure 2-16, a swelling ratio in the range of 11 to 16 could be predicted for these latexes.

Table 2-9 lists the results of the swelling experiments from some of the telomerized latexes. The swelling experiments were conducted in the presence of Aerosol MA surfactant, except for sample #1152-3 in which polyvinylpyrrolidone was used. The swelling ratio (column 3) was measured volumetrically by separating excess monomer from the swollen latex with a separatory funnel. The table shows that three latexes, samples #1131-2, #1131-3 and #1109-2, with $\bar{M}_n \cong 2000$ were

50
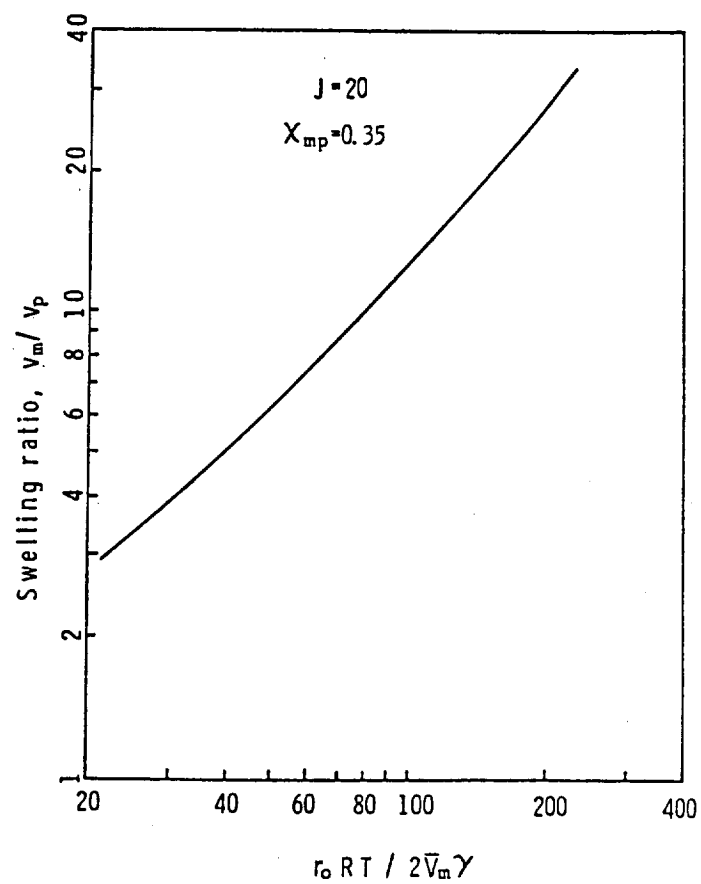
Figure 2-16. Theoretical relationship between swelling ratio and interfacial energy term for latexes with $\bar{M}_n$ = 2000.

Table 2-9. Swelling of Telomerized Latexes and Final Latexes after Polymerization

Telomerized Latexes			Swelling Ratio (v_m/v_p)	Final Latexes		Overall Volume Increase
Sample No.	Dia.(μm)	$\bar{M}_n$		Sample No.	Dia.(μm)	
1057-1	0.50	4100	10.4	1101-5	1.09	20
1109-1	0.50	1200	11.5	1128-1	1.07	19
1109-2	0.50	1900	11.5	1128-2	0.98	14
1109-3	0.50	1100	9.7	1128-3	0.96	14
1131-1	0.50	2500	12.4	1139-1	1.07	19
1131-2	0.58	2000	14.0	1139-2	1.33	37
1131-3	0.63	1900	15.7	1139-3	1.48	51
1131-3	0.63	1900	15.7	1141+	1.46	49
1152-3	0.63	1500	-	2051-3*	1.59	63

+ polymerized with AIBN initiator instead of persulfate
* swollen and polymerized in the presence of AIBN and polyvinylpyrrolidone instead of persulfate and Aerosol MA

swollen 11-16 times, which was exactly the same range predicted from the theory (Figure 2-16).

According to the theory, a lower average molecular weight should give a higher swelling ratio if other conditions are similar. However, this is not always true. Latex #1109-1 (prepared with s-butyl mercaptan) and #1109-3 (prepared with cyclohexyl mercaptan) had the lowest average molecular weights among the latexes listed in Table 2-9, but these latexes did not give higher swelling ratios than other latexes of similar sizes (cf. #1131-1 and #1109-2). One possible reason was that the molecular weight of telomers was too low. Instead of remaining inside the particles and contributing to the swelling, the telomers may have been extracted by the monomer in the free monomer phase during the swelling process. By comparing the GPC chromatograms of latex #1109-1 before and after swelling, it was found that a large fraction of the very low-molecular-weight telomers was lost after swelling. Among the mercaptans evaluated in this study, t-octyl mercaptan, which gave a clear telomer peak of reasonably low molecular weight and therefore a reasonably high swelling ratio, appeared to be the best choice as a telogen for the "seeded-telomerization" swelling process.

The swollen latexes listed in Table 2-9 were further polymerized by adding persulfate initiator or AIBN (for #1141 and #2051-3) and heating at 70°C for 20-24 hours. Typical TEM micrographs of the final latexes are shown in Figures 2-17 to 2-18. The overall volume increases from the initial seed (0.40 μm), calculated from the particle diameter, are listed in the last column of the table.

Beside the main population of large particles, some new small particles can be found in the micrographs of the final latexes, especially for those prepared with persulfate initiator and Aerosol MA surfactant. The problem of small particle generation can be controlled by a proper selection of surfactant, initiator, and aqueous phase inhibitor. This will be discussed further in Chapters 3 and 4.

The discussion on the "seeded-telomerization" swelling method so far has been limited to the growth of latex particles in 1.0-1.6 μm size range from the 0.40 μm seed latex. The method can also be applied in the large-particle-size range, i.e., >2 μm. Figure 2-20 shows SEM micrographs of the products from two consecutive "seeded-telomerization" swelling cycles. Figure 2-19 gives the key ingredients in each step of this process. Latex #3138 (~1.5 μm) was grown from the 0.40 μm seed in the first cycle; it was then grown to #3141-2 (~7 μm) in the second cycle. An overall volume increase > 5000 was obtained after two cycles of "seeded-telomerization" swelling.

As particles grow bigger and bigger, it becomes more and more difficult to prevent coagulation of the latex and generation of small particles at the same time. One major drawback of using this swelling method in the large-particle-size range is the limited shelf-life of the telomerized latex. Telomerized particles are soft and sticky; once they settle, they can coalesce into a big rubbery ball.

In summary, a "seeded-telomerization" swelling method using mercaptans as telogens has been developed. This method allows the growth of latex particles with a volume increase of >60 in one cycle.

With two consecutive "seeded-telomerization" swelling cycles, an overall volume increase > 5000 can be achieved.
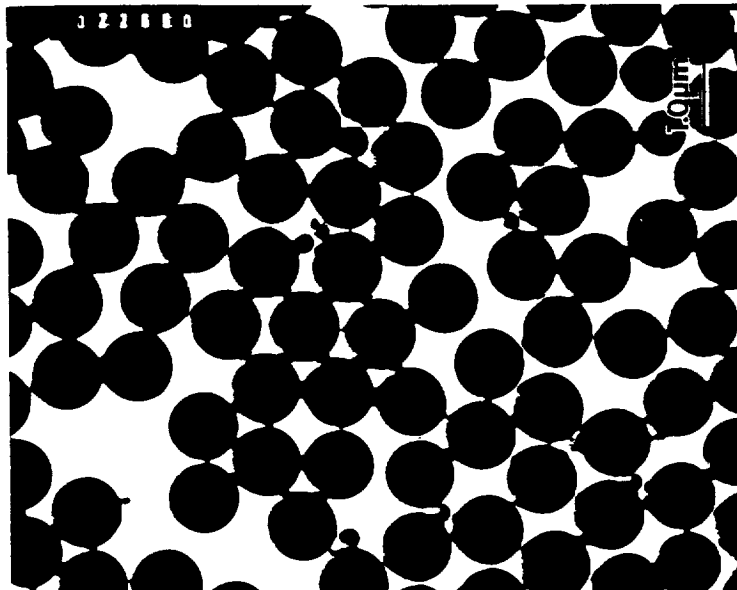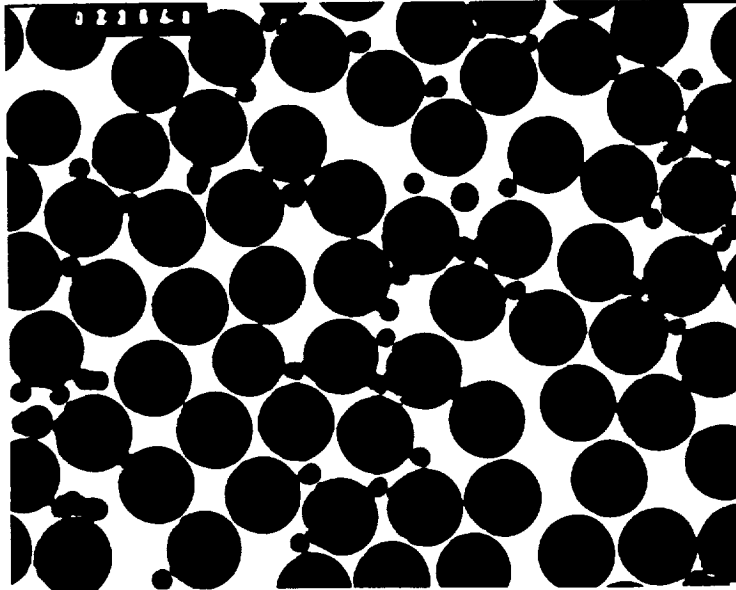
Figure 2-17. TEM micrographs of latexes #1139-2 (left) and #1139-3 (right).
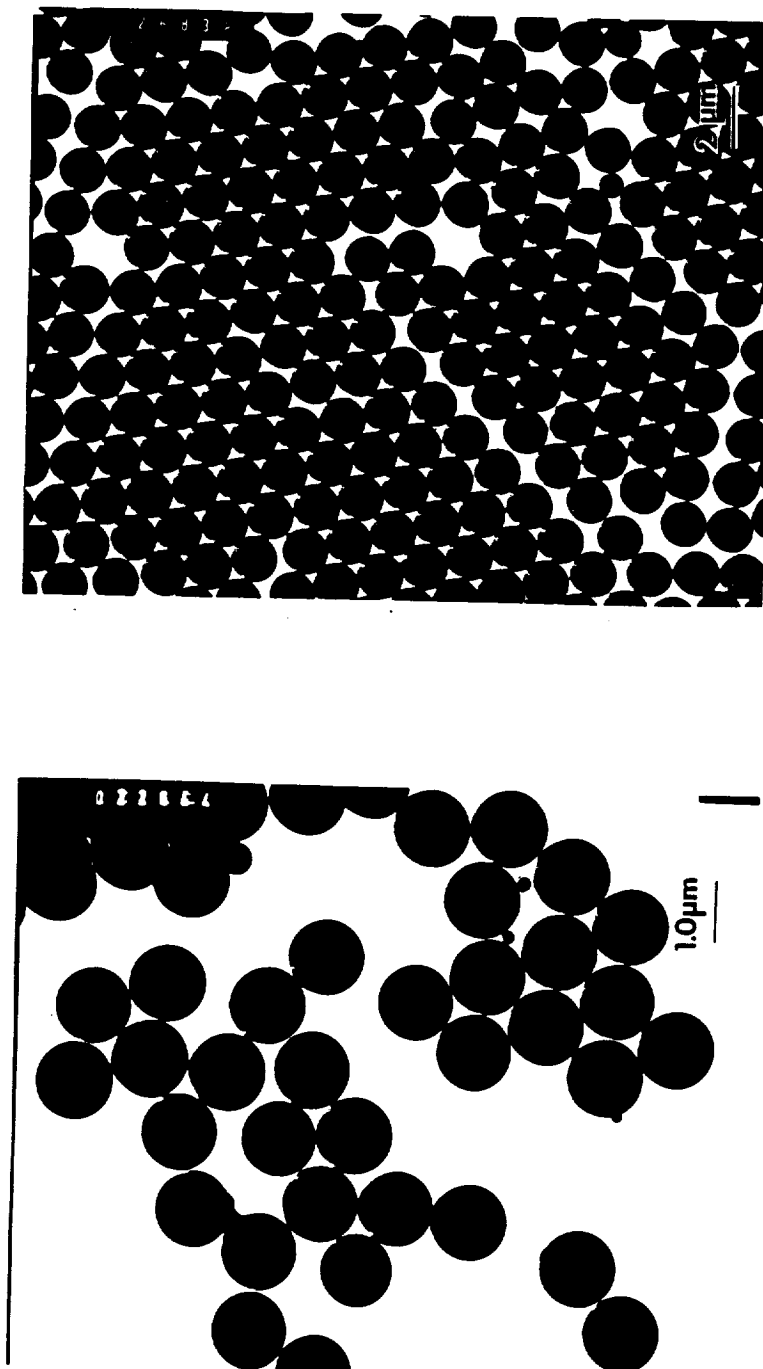
Figure 2-18.   TEM micrographs of latexes #1141 (left) and #2051-3
(right).

M/P=4   M/P=15   M/P=5   M/P=20

t-OM=10%M   t-OM=10%M

0. 40μm seed ———————→ #3017-1 ————→ #3138 ———————→ #3139-3 ————→ #3141-2

$K_2S_2O_8$=0. 1%aq   AIBN=0. 39%M   AIBN=0. 38%M   ACPA=0. 3%M

AMA=0. 14%aq   AMA=0. 12%aq   PVP=0. 15%aq   PVP=0. 15%aq

                       NH_4SCN=0. 1%aq NH_4SCN=0. 1%aq NH_4SCN=0. 1%aq
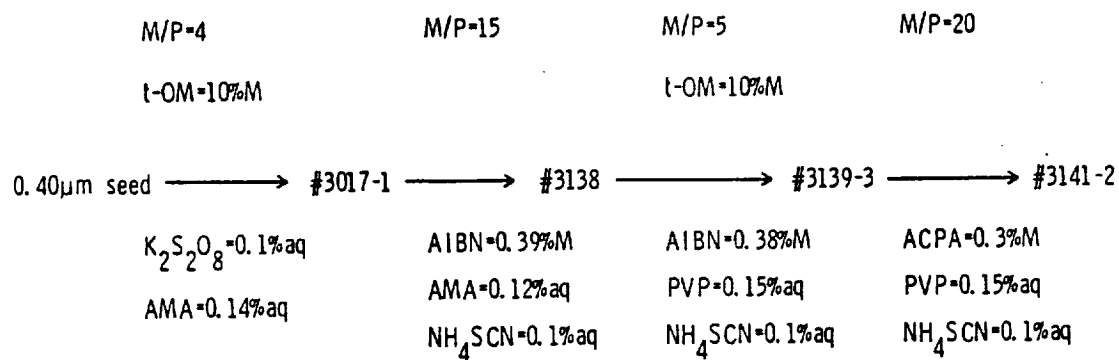
Figure 2-19.   Key ingredients used in the
consecutive "seeded-telomerization" swelling process.

58
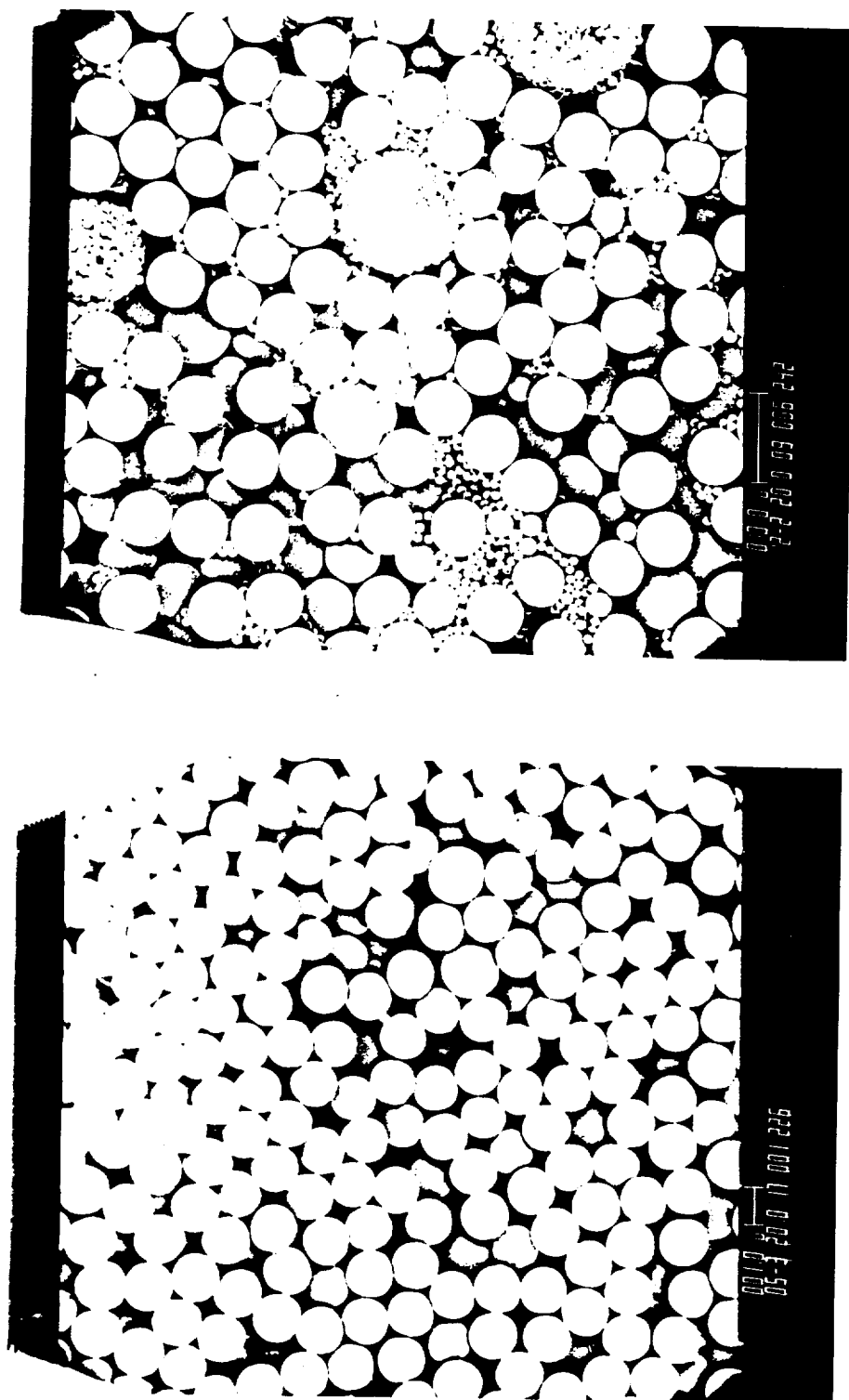
Figure 2-20. SEM micrographs of latexes from two consecutive "seeded-telomerization" swelling cycles, #3138 (~1.5 μm, left) and #3141-2 (~7 μm, right).

CHAPTER 3

INITIATORS AND INHIBITORS

3.1 Initiators

The most commonly used initiators in preparing monodisperse latexes have been inorganic peroxy salts derived from persulfuric acid, especially potassium persulfate. Oil-soluble peroxy and azo initiators such as benzoyl peroxide (BPO) and 2,2'-azobis(isobutyronitrile) (AIBN) have been used in emulsion polymerization but less commonly in preparing monodisperse latexes.

Some interest has been shown in recent years in the use of water-soluble analogues of AIBN as dissociative initiators for emulsion polymerization. Blackley [62] listed some suitable water-soluble analogues in his book: 4,4'-azobis-4-cyanovaleric acid or 4,4'-azobis(4-cyanopentanoic acid) (ACPA) and its alkali-metal salts, disodium 2,2'-azobis-2-cyanopropane-1-sulphonate, α , α' -azobisisobutyramidinium chloride, and azobis-(N,N'-dimethyleneisobutyramidine) and its salts with strong acids. Examples in which anionic and cationic azo initiators were used can be found in the work of Goodwin et al. [63], and Liu and Krieger [64].

In this work both water-soluble and oil-soluble initiators have been evaluated for preparing monodisperse latexes. Some of the initiators used in this study, along with their 10-hour half-life temperatures, are listed in Table 3-1.

Table 3-1.   Polymerization Initiators

Trade Name	Abbrev.	Manufacturer	Identity	10hr. $T_{1/2}$ °C
– –	–	Fisher	Potassium persulfate	68
– –	CHP	Lucidol	Cumene hydroperoxide	150
– –	ACPA	Du Pont	4,4'-Azobis(4-cyanopentanoic acid)	–
Vazo 64	AIBN	Du Pont	2,2'-Azobis(isobutyronitrile)	64
Vazo 67	AMBN	Du Pont	2,2'-Azobis-(2-methylbutyronitrile)	67
Lupersol 70	TBP	Lucidol	t-Butyl peroxyacetate	102
– –	BPO	Fisher	Benzoyl peroxide	73
Alperox-F	LPO	Lucidol	Lauroyl peroxide	62

61

3.1.1 Persulfate and Oil-soluble Initiators

In an earlier study, three different initiators were compared using a high-swelling-ratio polymerization recipe. Latex #1131-3 was prepared from a 0.40 μm seed latex by telomerization in the presence of Aerosol MA surfactant, persulfate initiator, and the telogen t-octyl mercaptan. Three latexes were then grown from latex #1131-3 with monomer/polymer ratios in the 15-20 range, in the presence of three different initiators. These were potassium persulfate, a water-soluble initiator, AIBN, an oil-soluble initiator, and cumene hydroperoxide (CHP). The latter has a high water solubility and is believed to decompose at the particle/water interface in such a way that the organic radical enters the particle while the hydroxyl radical remains in the aqueous phase [65, 66]. Table 3-2 summarizes the differences in particle size between the product latexes. The corresponding TEM micrographs are presented in Figures 3-1 and 3-2. Both persulfate and CHP gave bimodal distributions, while the oil-soluble AIBN produced fewer and smaller new particles.

Table 3-2.   Effect of Initiators on Small Particle Generation

Latex #	Initiator	Avg. dia. of large particles, μm	Avg. dia. of small particles, μm	No. ratio of small to large particles
1139-3	Persulfate	1.48	0.48	1/1.6
1142-2	CHP	1.42	0.54	1/0.9
1141	AIBN	1.46	0.20	1/8.3

Although organic peroxy initiators have been used successfully in
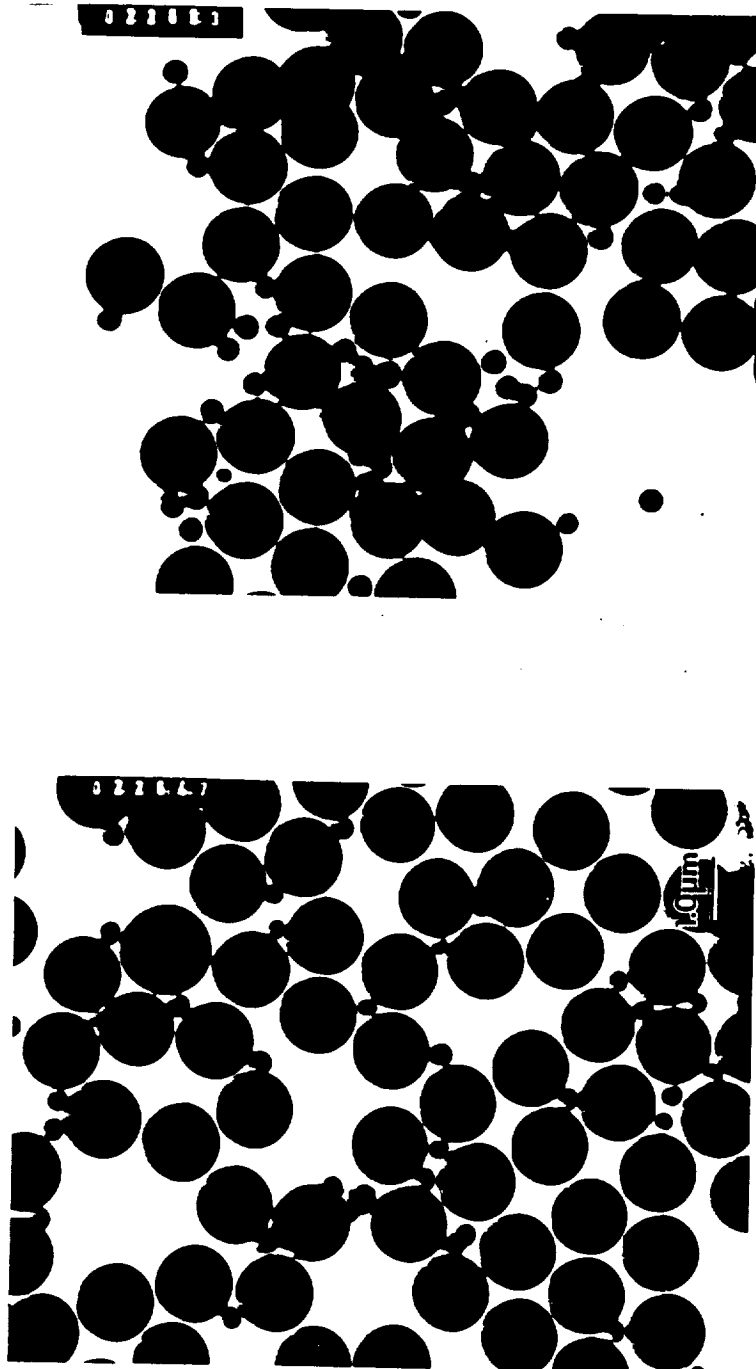
Figure 3-1. TEM micrographs of latexes grown from latex #1131-3: (1) #1139-3 (left), with persulfate initiator; (2) #1142-2 (right), with CHP initiator.

63
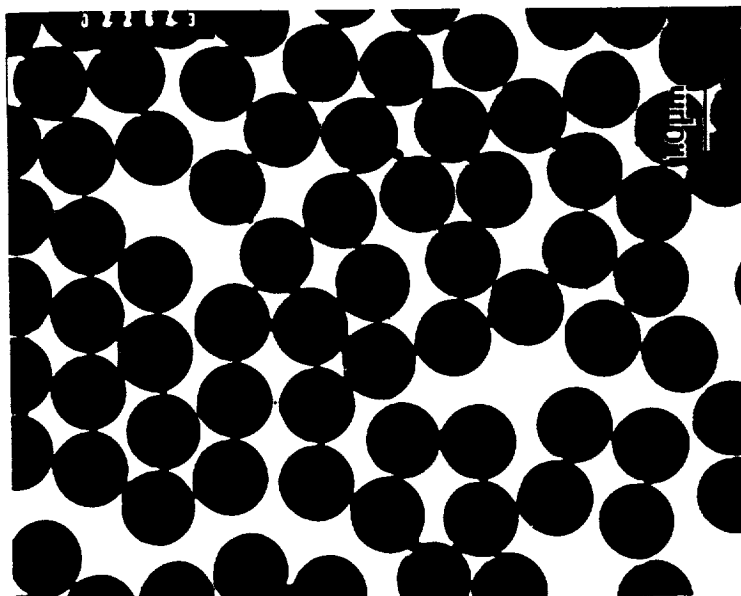
Figure 3-2. TEM micrograph of latex grown from latex #1131-3: (3).
#1141, with AIBN initiator.

emulsion polymerization as well as in suspension polymerization, they are not suitable for seeded polymerization; because of the low polymerization rate especially in the large-particle-size range ($>$ 1 μm). Figure 3-3 compares the decomposition rates of three oil-soluble initiators: AIBN, BPO, and lauroyl peroxide (LPO). LPO has approximately the same decomposition rate as AIBN, while BPO has a slightly lower value.   Figure 3-4 shows the conversion-time curve of polystyrene/styrene seeded polymerization obtained using a dilatometer which will be described later in this chapter.   The polymerization was carried out with a 0.40 μm seed latex (LS-1103-A), 1/1 swelling ratio, Aerosol MA surfactant and 0.4% BPO based on monomer.   As shown in Figure 3-4, it took about 9 hours for the conversion to reach 80%, while a similar polymerization with AIBN took only 2.5 hours to reach the same conversion.   A seeded polymerization using LPO proceeded even more slowly than BPO, despite the fact that the former has a higher decomposition rate.   Another peroxy initiator, t-butyl peroxyacetate, also gave a low polymerization rate.

The disadvantages of using oil-soluble peroxy initiators became more obvious when seeded polymerizations were carried out at larger particle sizes and with higher swelling ratios: the polymerizations took longer and longer times.   The low polymerization rates obtained with peroxy initiators may be attributed to one or more of the following factors: (1) the slow diffusion of the initiator molecule into the latex particles because of its bulkiness;   (2) the low efficiency of initiation in the swollen particles;   and (3) the decrease in decomposition rate due to the accumulation of carbon

65
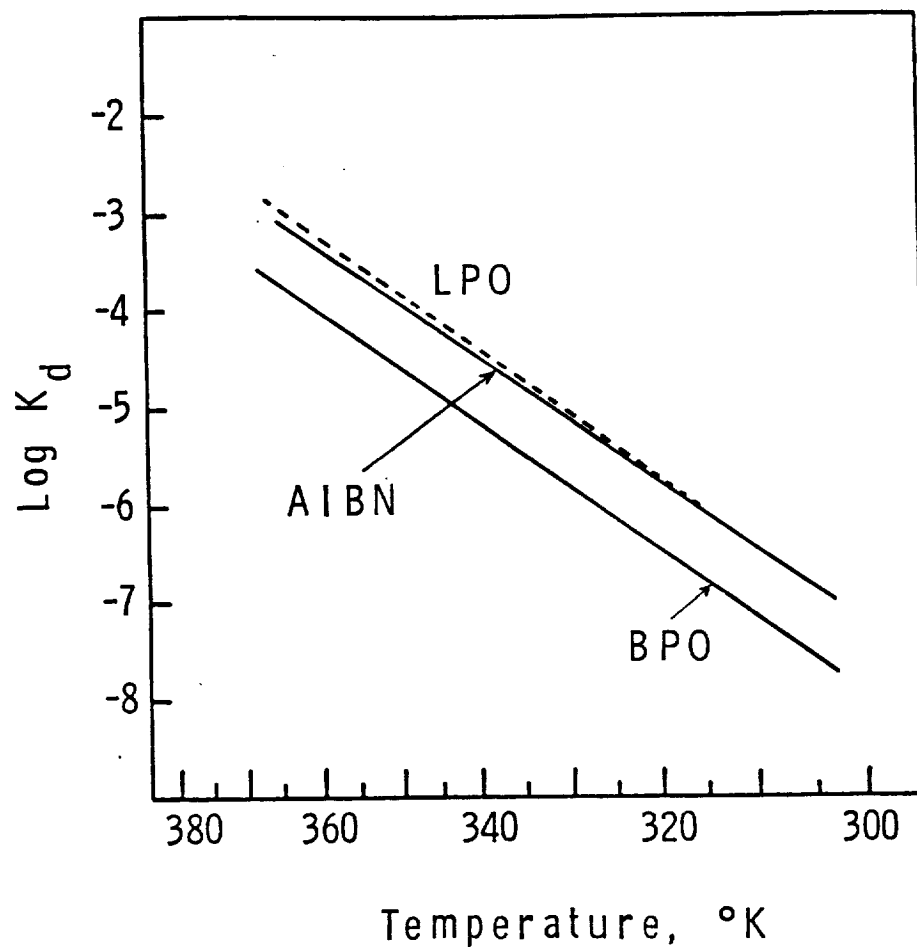
Figure 3-3.   Decomposition rates of oil-soluble
initiators: AIBN, BPO and LPO.
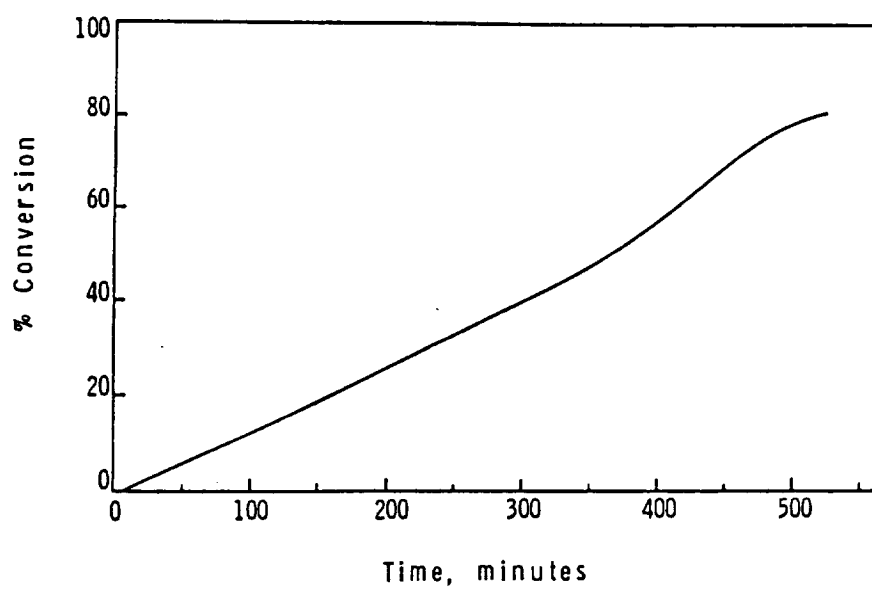
Figure 3-4.   Percent conversion-time history of a
polystyrene/styrene seeded emulsion polymerization
using BPO initiator.

dioxide as a byproduct of decomposition in the closed reaction system.

3.1.2 Analogues of AIBN: Less Water-Soluble or More Water-Soluble

Recently, a new azo initiator, AMBN (Vazo 67, see Table 3-1), has been introduced into the market. The initiator has a structure similar to AIBN, but with one additional methyl group on each side of the azo group. Because of this slight difference, AMBN has a slightly lower decomposition rate than AIBN (10 hour half-life at 67°C compared to 64°C for AIBN), and a slightly lower solubility in water. Although the difference may be small, its effect on the elimination of new particle generation was significant. Figures 3-6 and 3-7 compare two latexes, #4034 and #4066-2, grown from the seed latex #4003-2 (Figure 3-5) with Aerosol MA surfactant, hydroquinone inhibitor, and (a) AIBN and (b) AMBN initiators, respectively. Latex #4003-2 in turn was grown from a 0.40 μm seed latex by seeded telomerization. Tiny new particles were found on the edge of the SEM specimen of latex #4034, even though the latex was polymerized in the presence of water-soluble inhibitor hydroquinone. In comparison, the edge of the latex #4066-2 specimen was clean, indicating that the nucleation of small particles was substantially reduced by hydroquinone when the polymerization was initiated by the less water-soluble initiator, AMBN.

As already mentioned, water-soluble analogues of AIBN have become used in recent years. Since the latex stability worsened as the particles were grown to larger sizes, an attempt was made to use a water-soluble analogue, ACPA, to introduce acid groups onto the particle surface, in the hope that the stability of large particles

68
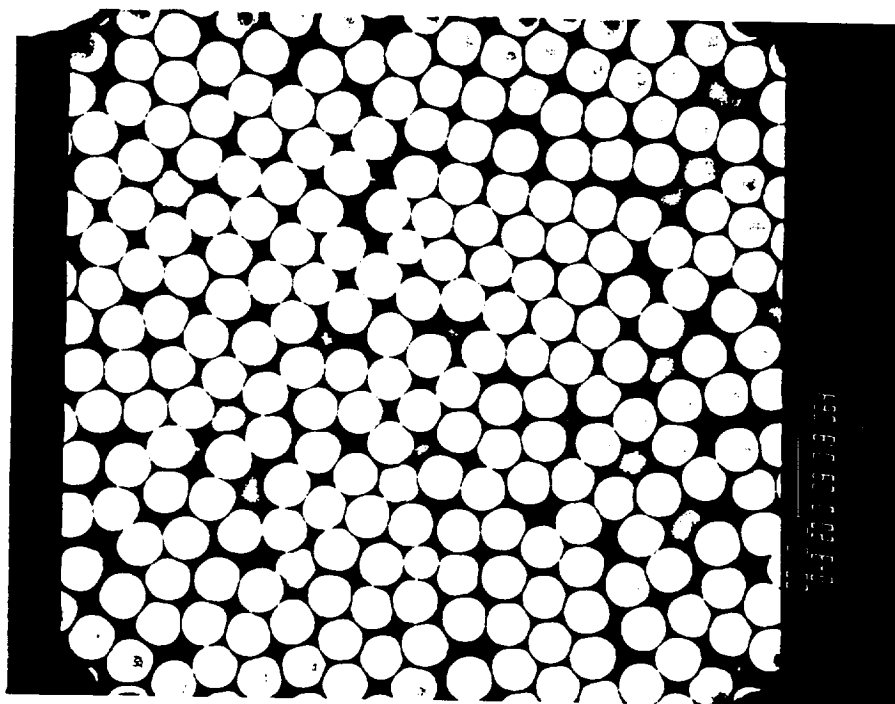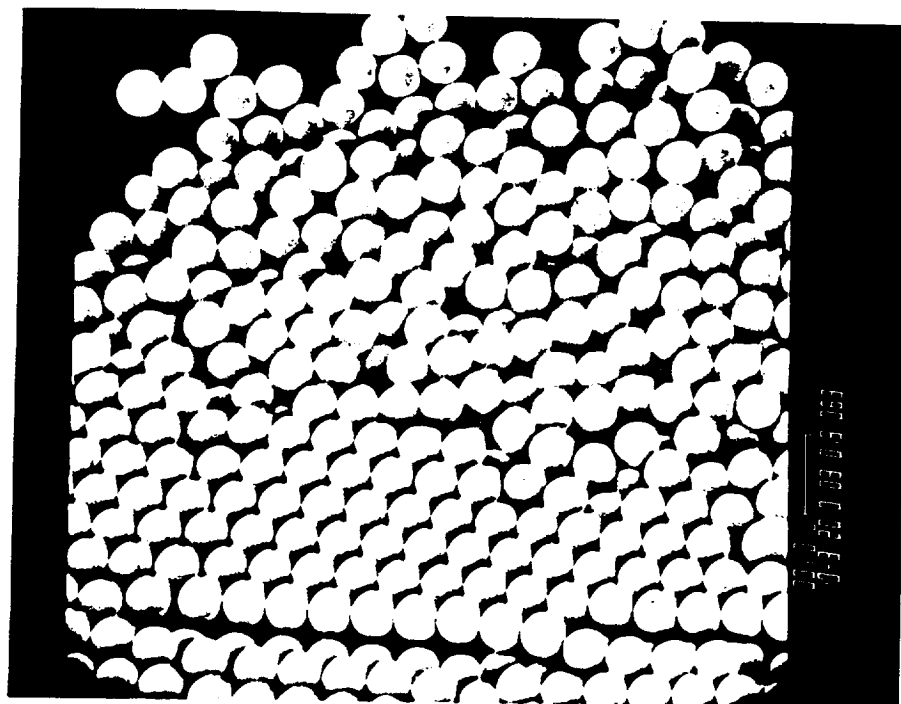
Figure 3-5. SEM micrographs of telomerized latex #4003-2.
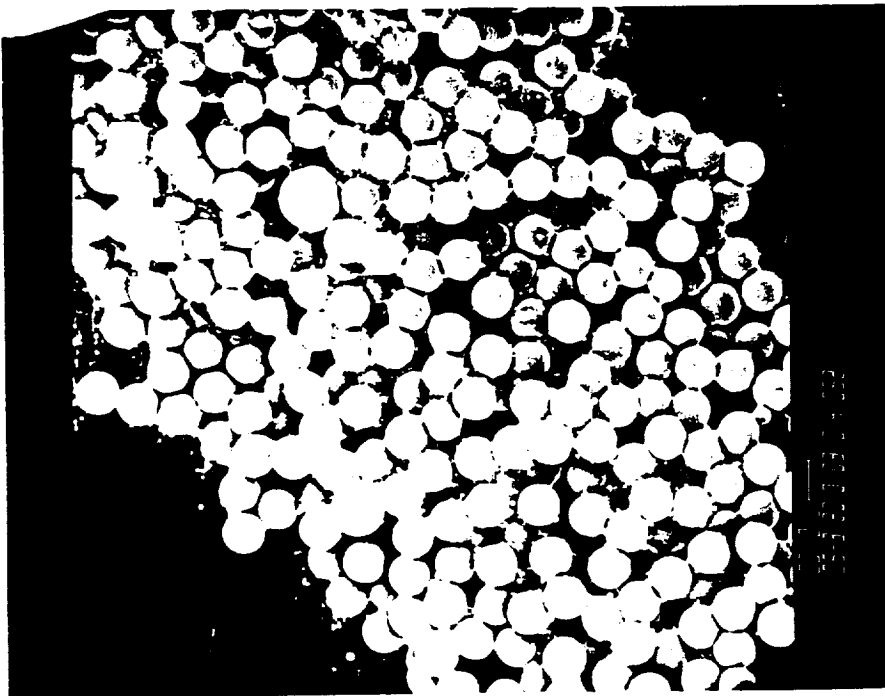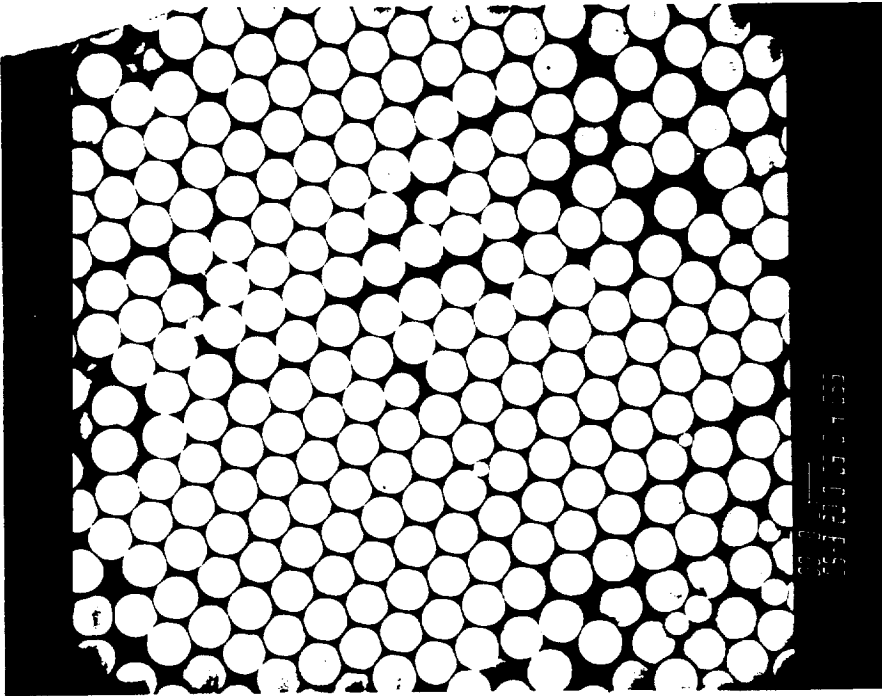
Figure 3-6. SEM micrographs of latex #4034, grown from #4003-2 with AIBN initiator.
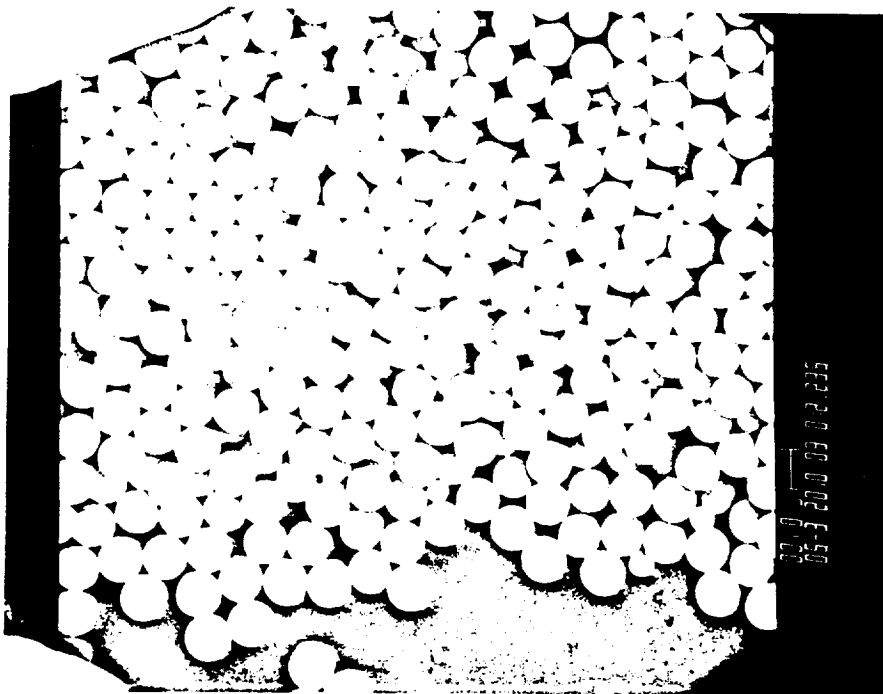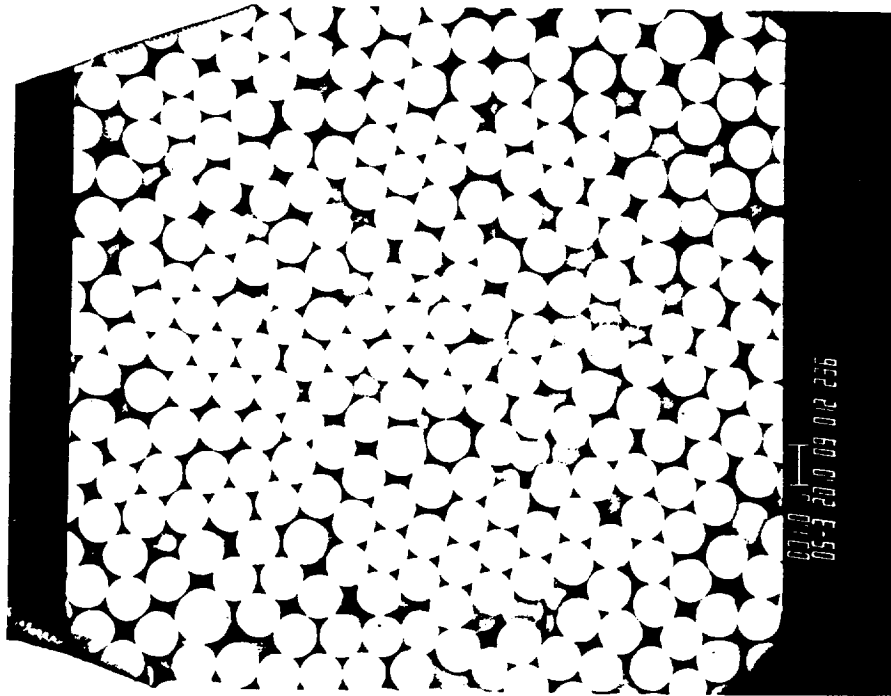
Figure 3-7. SEM micrographs of latex #4066-2, grown from #4003-2 with AMBN initiator.

would be increased without generating new small particles. Some of the earlier results with ACPA were promising. Figure 3-8 shows SEM micrographs of two latexes grown from a 2.02 μm polyvinyltoluene (PVT) seed latex. The one on the left, latex #2061-4, used Aerosol MA surfactant and ACPA initiator; the initiator was added to the recipe dissolved in a 5% sodium bicarbonate solution. The one on the right, latex #2061-1, used AIBN initiator. There was no significant difference in monodispersity between these two latexes. The off-size larger particles observed in both micrographs were believed to be carried over from the seed latex. However, there were some subtle differences between these two products in terms of latex stability and product yield. The ACPA-initiated latex was completely coagulum-free, while the AIBN-initiated latex had some coagulum as a result of particle coalescence plus bulk polymerization in free monomer drops.

Another comparison between the two initiators is demonstrated in Figure 3-9. Starting from 1.5 μm polystyrene seed latex #3138 (see Figure 2-20), four latexes were prepared with and without t-octyl mercaptan telogen, using AIBN or ACPA as initiator. Again, ACPA was added as a solution in 5% sodium bicarbonate solution. SEM micrographs of the latexes #3139-1, #3139-2, #3139-3, and #3139-4 are presented in Figures 3-10 and 3-11. As expected, the ACPA-containing recipes resulted in more stable latexes containing less coagulum. However, the ACPA samples also contained more new small particles than the AIBN samples. The telomerized latex #3139-3 was grown one more step to latex #3141-2 (see Figure 2-20) with a high swelling ratio and ACPA initiator. It is interesting to note that the new small

72
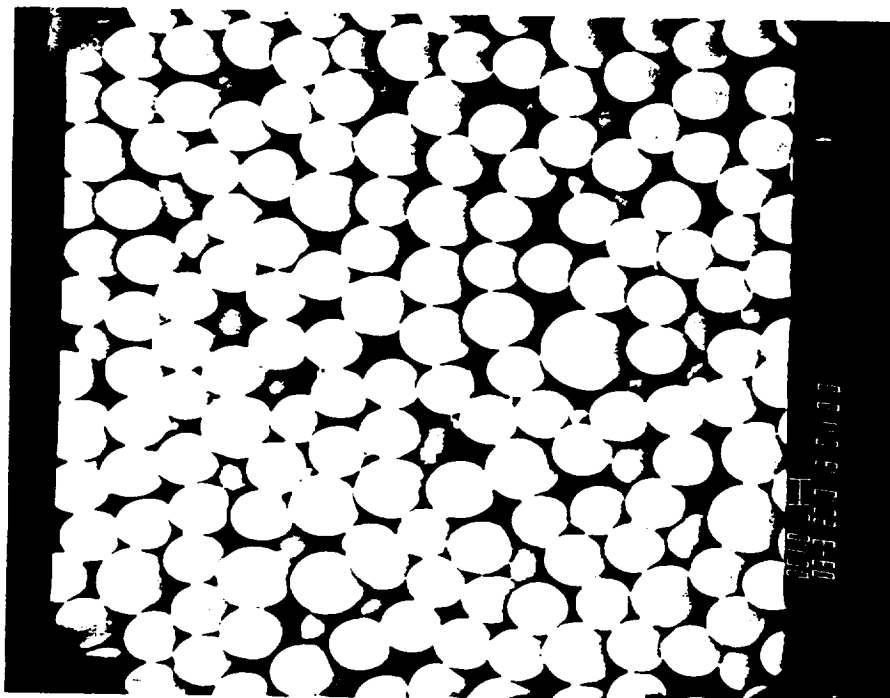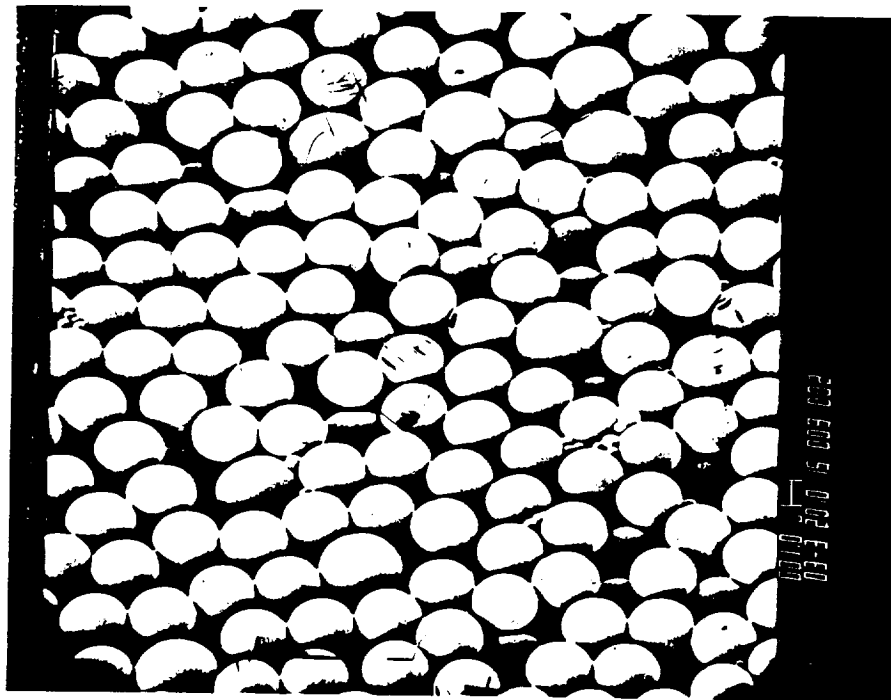
Figure 3-8. SEM micrographs of latexes grown from 2.02 μm PVT seed: #2061-4 (left) with ACPA initiator; and #2061-1 (right) with AIBN initiator.

AIBN=0.38%M   → #3139-1

ACPA=0.38%M   → #3139-2

#3138 —

AIBN=0.38%M   → #3139-3   ACPA=0.3%M   → #3141-2

t-OM=10%M

ACPA=0.38%M   → #3139-4

t-OM=10%M

M/P=5   M/P=20

PVP=0.15%aq.   PVP=0.15%aq

NH_4SCN=0.1%aq NH_4SCN=0.1%aq
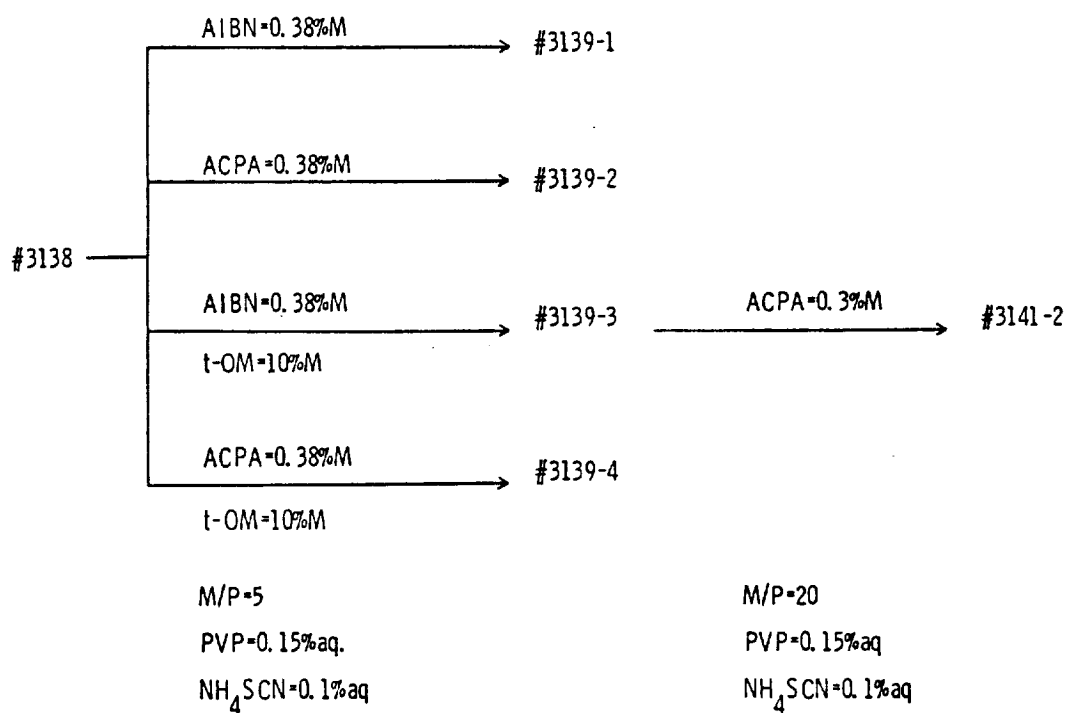
Figure 3-9.   Particle growth using AIBN and ACPA
initiators.
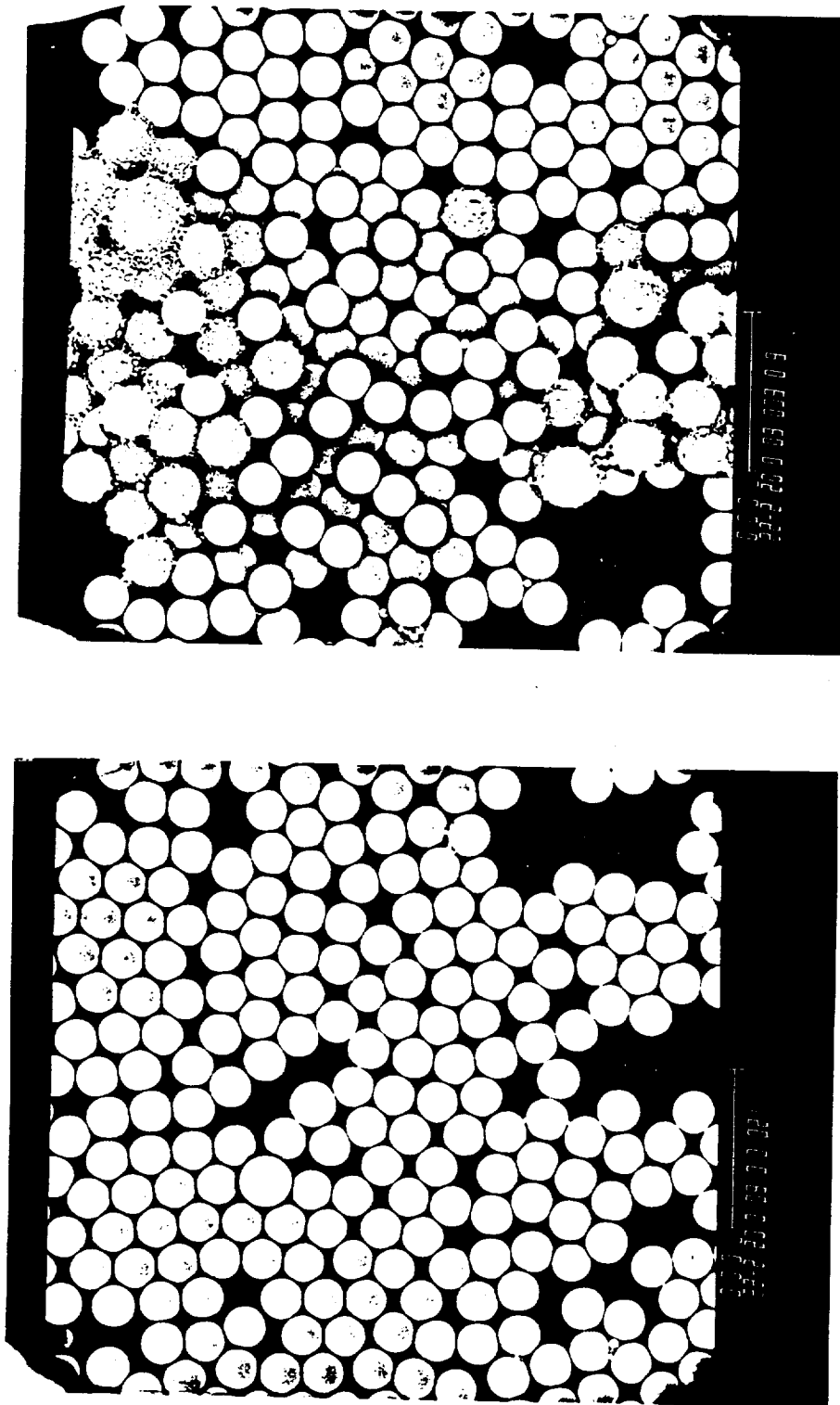
Figure 3-10. SEM micrographs of latexes grown from 1.5 μm seed latex #3138: latexes #3139-1 (left), with AIBN initiator, and #3139-2 (right), with ACPA initiator.

75
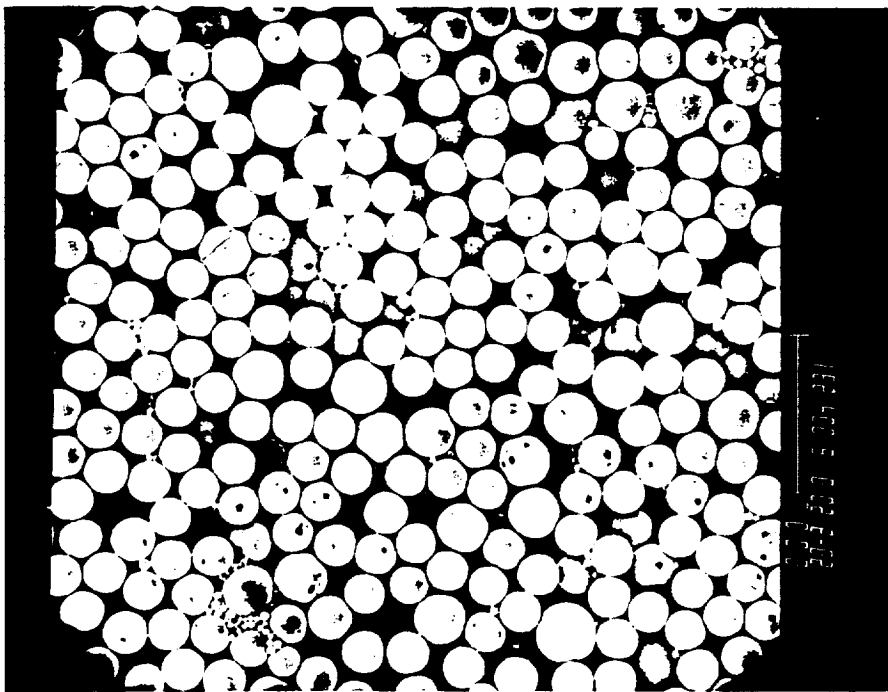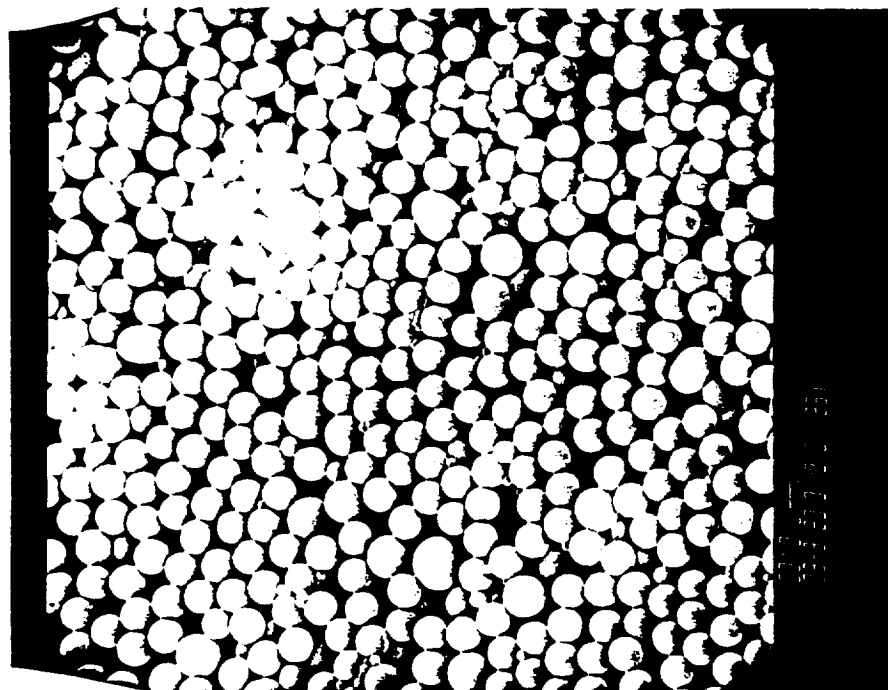
Figure 3-11. SEM micrographs of latexes grown from 1.5 μm seed latex #3138: latexes #3139-3 (left), with AIBN and t-octyl mercaptan, and #3139-4 (right), with ACPA and t-octyl mercaptan.

particles clustered on the surface of the large particles in the dried films of the ACPA-initiated latexes.

Several experiments were also carried out using ACPA initiator along with a non-inhibiting and inhibiting electrolytes, in the hope that the generation of small particles would be suppressed while maintaining the stability of large particles. The results were unsatisfactory, because of small particle generation.

3.2 Inhibitors

The objectives of including inhibitors in the seeded emulsion polymerization recipes are twofold: (1) to prevent premature polymerization; and (2) to prevent generation of small particles. In the earlier stages of this work, the proposed procedure for preparing flight experiments required that the recipe ingredients be mixed and shipped for loading two to three weeks before the experiment was to be performed in microgravity. Under these circumstances, an inhibitor was required, which would inhibit a polymerization recipe at ambient temperature for two to three weeks, but which would not change the polymerization kinetics after the recipe was heated to reaction temperature. Later, the procedure for preparing flight experiments was changed. The monomer distillation, mixing of the ingredients, and swelling of the seed particles was scheduled to be carried out within the one-week period before the launching of the Space Shuttle. The prevention of premature polymerization became less critical, and the study of inhibitors was then concentrated on prevention of small particle generation in a seeded polymerization. Table 3-3 lists the

inhibitors used in both aspects of the inhibition study.

3.2.1 Inhibition Time and Effect of Inhibitors on Polymerization Rate

Dilatometric polymerizations were carried out to search for an appropriate initiator/inhibitor combination that would prevent premature polymerization and to determine the effect of inhibitor on the polymerization rate. The idea was to use the observed induction periods at 70°C for estimating the inhibition times at ambient temperature.

The first dilatometer used in this work was a commercial dilatometer, which had been commonly used in oil chemistry. As shown in Figure 3-12, the dilatometer contained an 11 ml bulb and a 1.4 ml capillary. A small magnetic bar was placed inside the bulb, which was driven by a magnetic stirrer outside the water bath. The commercial dilatometer had several disadvantages: (1) the volume of the bulb was too small; (2) agitation was poor; and (3) it was difficult to load the latex into the dilatometer in such a way that no air bubbles were entrapped.

An improved dilatometer was then designed to eliminate these disadvantages. As shown in Figure 3-13, the home-made dilatometer consisted of a 25 ml flask, a 2 mm ID capillary with a 50 cm scale attached, and a Teflon adapter. The agitation was improved with a submersible magnetic stirrer. After filling the flask with swollen latex , any air bubble could easily be squeezed out by tightening the adapter seal. The following is a typical operating procedure for the dilatometer, using a recipe with an oil-soluble initiator:

Table 3-3.   Polymerization Inhibitors

Abbrev./Formula	Manufacturer	Identity
HQ	Fisher	Hydroquinone
MEHQ	Fisher	Hydroquinone monomethyl ether
BQ	Fisher	p-Benzoquinone
--	Fisher	Catechol
--	Fisher	Pyrogallol
DPPH	Eastman Kodak	2,2-Diphenyl-1-picrylhydrazyl
NH$_4$SCN	Baker	Ammonium thiocyanate
NaNO$_2$	Fisher	Sodium nitrite
NaDMDTC	Eastman Kodak	Sodium dimethyldithiocarbamate
DMHAHCl	Aldrich	N,N-Dimethylhydroxyamine hydrochloride
--	Baker	Thiourea
--	Aldrich	1-Ascorbic acid
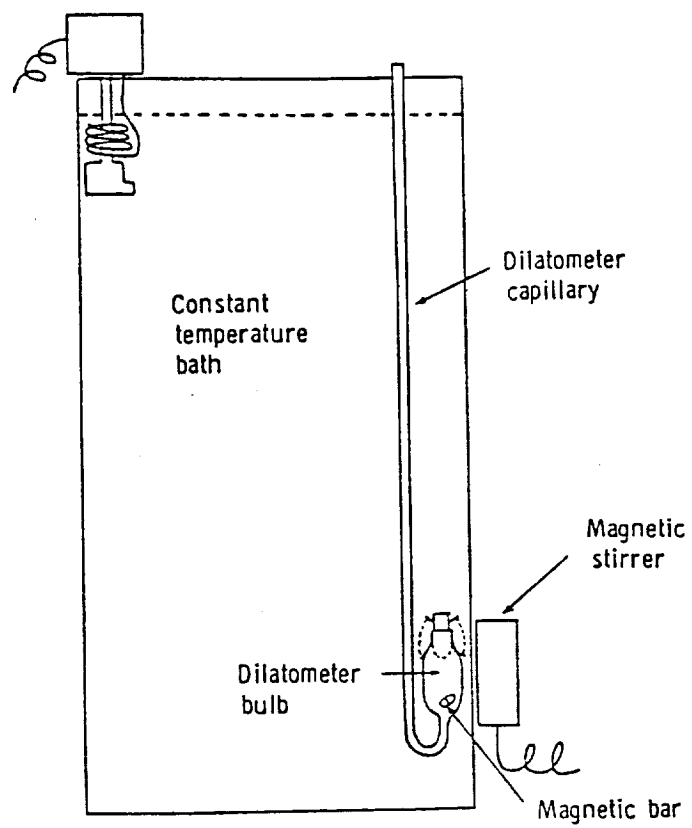
Figure 3-12. A commercial dilatometer in a constant temperature bath.

To pressure regulator
& N$_2$ cylinder

Tygon tubing

2mm ID capillary

50cm wood scale

Teflon adapter with O-ring

25ml flask

Submersible Magnetic
stirrer
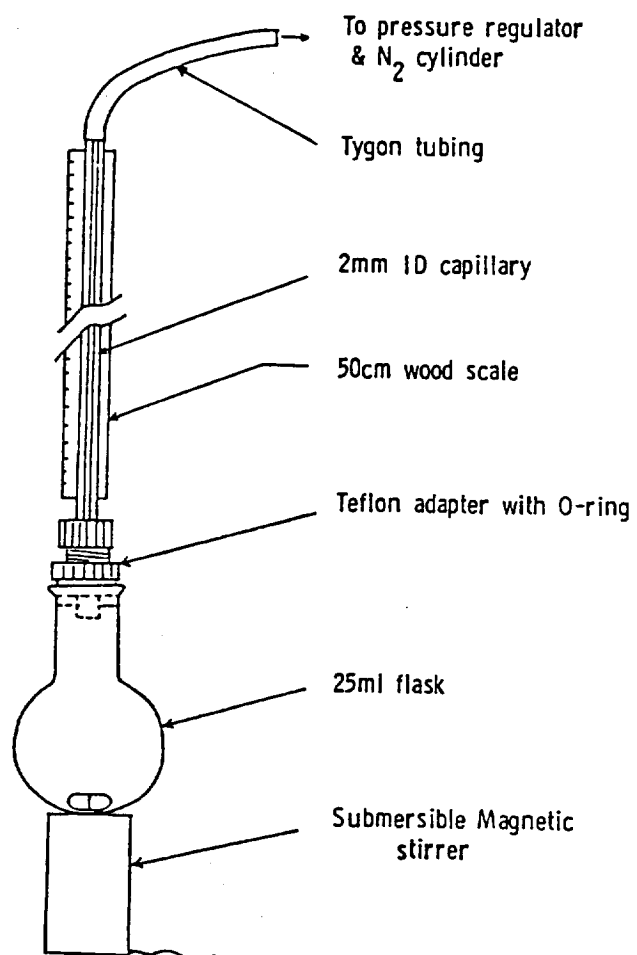
Figure 3-13.   The dilatometer developed for this
inhibitor study.

1. Dissolve the inhibitor in the monomer.

2. Weigh all ingredients, except for the initiator, in a 4-oz bottle.

3. Tumble the bottle in a water bath at 60°C for 1.5 hours to swell the latex particles with monomer.

4. Cool the bottle to room temperature. Dissolve the initiator in a small amount of monomer and add it to the bottle.

5. Tumble the bottle for 1.5 hours at room temperature.

6. Fill dilatometer flask with the monomer-swollen latex.

7. Attach the capillary tube and adapter to the dilatometer flask. Tighten the adapter seal.

8. Place the dilatometer in a 70°C water bath. Record the level change in the capillary as a function of time.

9. After stopping the reaction, check the solids content to obtain the final conversion.

10. Convert the level change data to percent conversion.

In the case of water-soluble initiators, the procedure was slightly different. The ingredients, except for the initiator, were first mixed by tumbling and loaded into the dilatometer. After the sample reached the same temperature as the water bath, i.e., the level in the capillary remained constant, an aqueous solution of initiator was injected through a very small-diameter Teflon-tubing leading down through the capillary into the dilatometer bulb or flask.

The dilatometer worked well with seeded polymerization recipes containing no inhibitor. Figure 3-14 shows a volume change and

82

conversion history for a seeded polymerization with 0.40 μm seed, M/P=1, and 0.1% persulfate in aqueous phase.

Figure 3-15 shows the volume change curve of a similar system in the presence of BQ inhibitor (inhibitor/initiator mole ratio = 0.1). The shape of the curve is quite different from the one without BQ. The capillary level first rose instead of dropping for 8 minutes after injecting the initiator solution. The level then stopped for 20 minutes before it started dropping. The overall percent conversion after 100 minutes of reaction, obtained by checking the solids content, was comparable for the inhibited polymerization and the non-inhibited polymerization. However, the overall volume shrinkage was much smaller for the inhibited polymerization than for the non-inhibited case.

The initial volume expansion and smaller value of overall volume shrinkage in the presence of BQ inhibitor could be attributed to gas evolution as a result of the reaction between the inhibitor and the initiator. The following mechanism has been proposed for the decomposition of persulfate by Kolthoff and Miller [67]:

$$S_2O_8^{2-} \text{ ---> } 2 \text{ } SO_4^{-}$$

$$SO_4^{-} + H_2O \text{ ---> } HSO_4^{-} + \cdot OH$$

$$2 \cdot OH \text{ ---> } H_2O + 1/2 \text{ } O_2$$
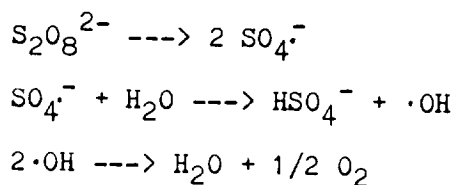
The decomposition of the initiator might be accelerated by the presence of a relatively high concentration of inhibitor. In this case, not all of the radicals generated would initiate polymerization. Excess sulfate ion-radicals and hydroxyl radicals would end up

83
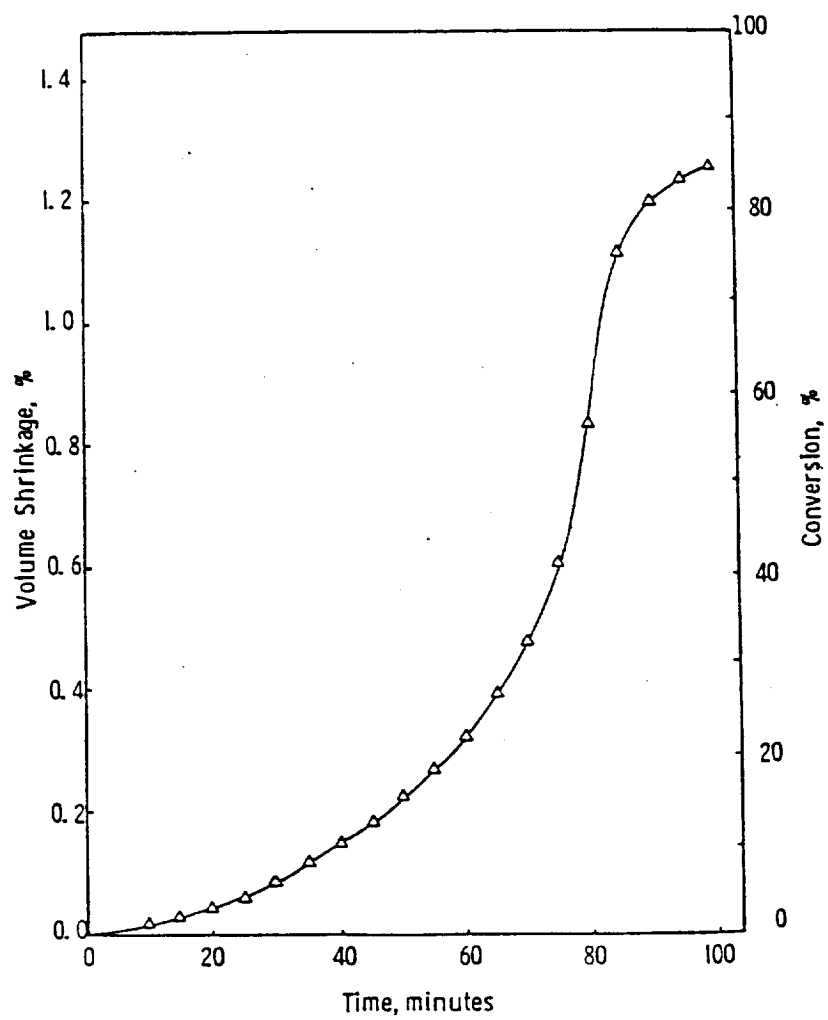
Figure 3-14. Volume change and conversion history for a persulfate-initiated seeded emulsion polymerization.
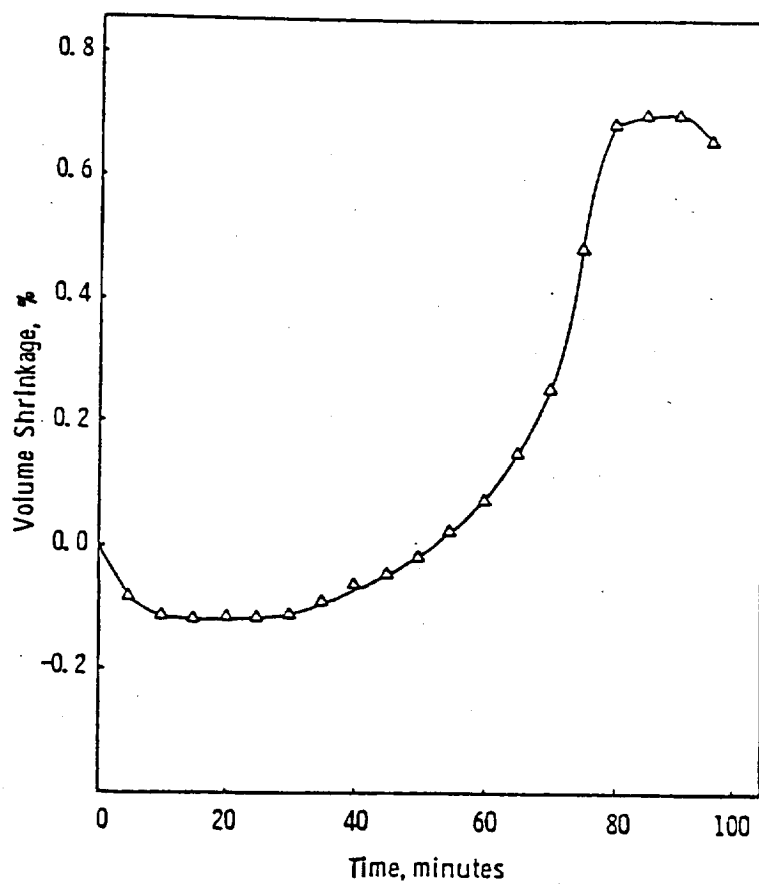
Figure 3-15.   Volume change history for a
persulfate-initiated seeded emulsion polymerization
with BQ inhibitor.

85

generating oxygen. A volume increase from oxygen generation thus dominated the earlier stages of polymerization and reduced the volume shrinkage at the latter stage of polymerization.

In a similar polymerization with hydroquinone (HQ) inhibitor (87 ppm in aqueous phase), the effect of inhibitor on volume change was even more significant. The capillary level rose rapidly during the first 50 minutes of reaction. The overall volume change after polymerization was expansion rather than shrinkage, indicating a strong reaction between the initiator and the inhibitor in the aqueous phase.

Gas evolution also occurred with the oil-soluble initiators. Nitrogen and carbon dioxide are byproducts of the decomposition of organic azo and peroxy initiators. If the concentration of the initiator is high enough, the gas evolved may exceed its solubility in water. As a result, bubbles will be formed in the reaction flask, and the measurement of volume change will yield erroneous kinetics. To minimize the effect of gas evolution, a low nitrogen pressure (about 10 cm Hg) can be applied on the capillary, as shown in Figure 3-13.

Several oil-soluble inhibitors were tested with BPO initiator. Table 3-4 shows a typical recipe for testing initiator/inhibitor combinations. The concentration of inhibitor was calculated to inhibit polymerization at ambient temperature for at least 2 weeks, according to initiator/inhibitor mole ratios and the decomposition rate of BPO. Table 3-5 lists the theoretical inhibition times, equivalent induction periods at $70^{\circ}C$, and observed results. As mentioned before, the original idea was to use the observed induction periods at $70^{\circ}C$ to predict inhibition times at ambient temperature.

Table 3-4.   Recipe for Dilatometric Study of Initiator/Inhibitor Combinations

Ingredients	Parts
0.4 μm PS seed latex (41%)	17.07
Water	44.25
Aerosol MA (5%)	0.56
Sodium bicarbonate (5%)	1.12
Styrene	7.00
Inhibitor	0.0028
Initiator	0.028

Final solids content	=20%
Monomer/polymer	=1
Inhibitor/monomer	=0.04%
Initiator/monomer	=0.4%
Surfactant/monomer	=0.4%
Buffer/aq. phase	=0.1%

Figure 3-16 shows conversion-time curves of polymerizations at 70°C with BQ, chloranil, and DPPH inhibitors. The curve for the control experiment containing no inhibitor appears in Figure 3-4. Time zero was taken as the time when the capillary level first stopped rising after the dilatometer containing the swollen latex was heated up in the water bath. The induction period was defined as the period between time zero and the time when the capillary level started dropping; in other words, when measured conversion was first observed. BQ and chloranil did not give the expected induction periods, and the polymerization rates were accelerated slightly. On the other hand, DPPH did give an induction period which was about half of the theoretical value, but the polymerization rate was severely retarded.

The disagreement between observed and theoretical induction
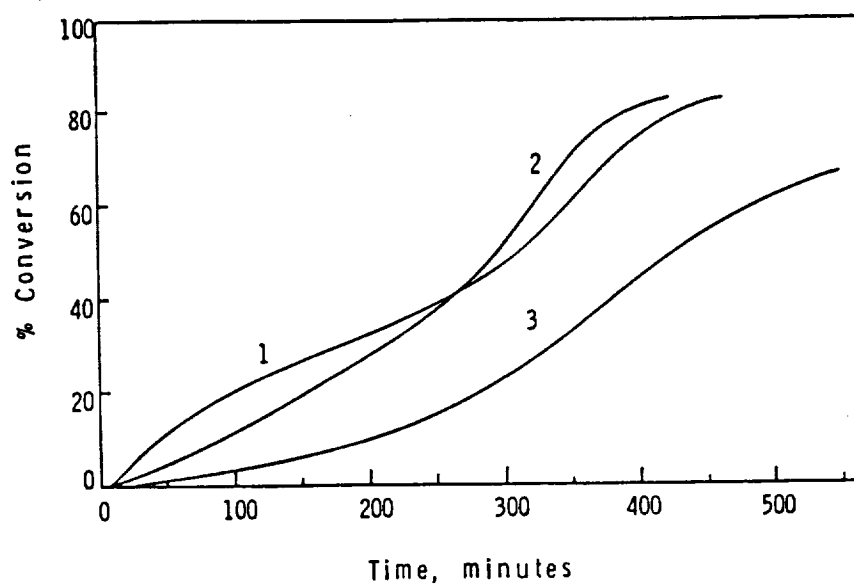
Figure 3-16. Conversion histories of seeded poly-
merizations using BPO initiator and different
inhibitors: (1) benzoquinone (2) chloranil (3) DPPH.

periods for all of the inhibitors, and the retardation of polymerization by DPPH, may be explained by the distribution of inhibitor and initiator between the phases. Although these inhibitors are classified as oil-soluble, they all have some degree of water-solubility, as indicated in Table 3-5. The bulky structure of the inhibitors, especially DPPH, prevents them from diffusing readily into the monomer/polymer particles. The distribution of initiator and inhibitor among the swollen particles, the aqueous phase, and the particle/water interface merits further investigation.

In summary, the inhibitors tested may retard or slightly accelerate a seeded emulsion polymerization depending on the nature of the inhibitor. An ideal induction period was not observed with the common inhibitors tested, owing to the complexity of distribution of initiator and inhibitor between the different phases. To predict inhibition times at ambient temperature based on observed induction periods at higher temperatures is not possible in these systems.

3.2.2 Prevention of New Particle Generation in Seeded Polymerization

In the preparation of large-particle-size monodisperse latexes by seeded polymerization, secondary particle growth is highly undesirable. However, complete elimination of new particle generation is very difficult, even when low-surface-activity surfactants and oil-soluble initiators are used. The use of water-soluble inhibitors to suppress polymerization outside the swollen polymer particles is necessary for seeded growth at particle sizes greater than 1 μm.

Similarly, the generation of latex particles during a suspension

Table 3-5. Comparison of Inhibitor Behavior in the Presence of BPO Initiator

Inhibitor	Theoretical induction period at 70°C, min.	Observed induction period at 70°C, min.	Theoretical inhibition time at 30°C, days	Effect on polymerization rate	Observed solubility in aq. phase
BQ	368	Negligible	145	Slightly accelerated	Completely dissolved
Chloranil	152	Negligible	59	Slightly accelerated	Partly dissolved
DPPH	46	20	18	Strongly retarded	Slightly dissolved

* Inhibitor/initiator = 10 wt%

** Theoretical values were calculated on 1:1 stochiometry basis, i.e., 1 mole of quinone to 1 mole of initiator decomposed, 1 mole DPPH radical to 1 mole of initiator radical.

*** Decomposition rate constant of BPO
$k_d(70°C) = 1.0 \times 10^{-5}$
$k_d(30°C) = 1.8 \times 10^{-8}$

polymerization is usually undesirable. It has been suggested that emulsion polymerization can be be retarded by addition of water-soluble inhibitors such as ammonium thiocyanate (NH_4SCN) or copper salts. Trommsdorff [68] compared the polymerization rate of suspension polymerization initiated by BPO with that of persulfate-initiated emulsion polymerization of methyl methacrylate, in the presence as well as in the absence of NH_4SCN. The results indicated that the water-soluble inhibitor NH_4SCN did not affect the suspension polymerization rate, but severely retarded the emulsion polymerization.

Matsumoto et al. [69] used NH_4SCN in the seeded emulsion polymerization of styrene in the presence of polyethyl acrylate seed latex and BPO initiator. They found that the new particle generation was suppressed by the use of NH_4SCN.

Other inorganic salts have also been used for similar purposes. Almog et al. [22] used sodium nitrite ($NaNO_2$) in "dispersion polymerization" of styrene with polyvinyl alcohol stabilizer and LPO initiator. Dispersion droplets of 2 μm and 10 μm average diameter were formed by agitating at high rpm. They found that the high-molecular-weight peak in the GPC chromatogram of the resulting polymer, which was believed to be the result of an emulsion polymerization mechanism, could be eliminated by using the inhibitor $NaNO_2$.

In a process for preparing rubber-reinforced styrenic resins, which required absorption of acrylic monomers by polystyrene beads at temperatures ranging from 110°C to 130°C for a sufficient time, Bracke and Lanza [70] used $NaNO_2$ to inhibit premature polymerization during

the absorption stage. They related the inhibition effect to the generation of nitrogen oxides. It was found that another inhibitor, hydroquinone monomethyl ether (MEHQ), alone was ineffective in inhibiting the polymerization.

NH_4SCN and $NaNO_2$ were the first two inhibitors evaluated in this study to prevent new particle generation in seeded polymerization. Figure 3-17 shows SEM micrographs of two latexes prepared from a 2.02 μm polyvinyl toluene seed latex, with AIBN initiator and PVP stabilizer, and in the presence of (a) NH_4SCN and (b) $NaNO_2$ inhibitor, respectively. Both inhibitors were used at a level of 0.1% in the aqueous phase. Apparently, NH_4SCN was more effective than $NaNO_2$ in preventing small particle generation under these conditions.

A study of the effect of inhibitor concentration on latex stability and small particle generation is outlined in Figure 3-18. Comparison of the SEM micrographs of latexes #2144 and #2149 (Figures 3-19, 3-20) indicated that $NaNO_2$ was relatively ineffective at the lower concentration (0.05% aqueous phase, $NaNO_2$/AIBN mole ratio = 0.65), but was more effective at the higher concentration (0.1% aqueous phase, $NaNO_2$/AIBN mole ratio = 2.5). However, latex #2144 (with the higher concentration of $NaNO_2$) was film-forming at 70°C, a temperature far below the T_g of polystyrene, indicating the presence of residual monomer in the latex. Apparently, the polymerization rate was retarded in the presence of a high concentration of $NaNO_2$.

Figures 3-21 to 3-23 show SEM micrographs of three latexes, about 2.5 um diameter, prepared in the presence of different NH_4SCN concentrations. An increasing number of off-size larger particles and a
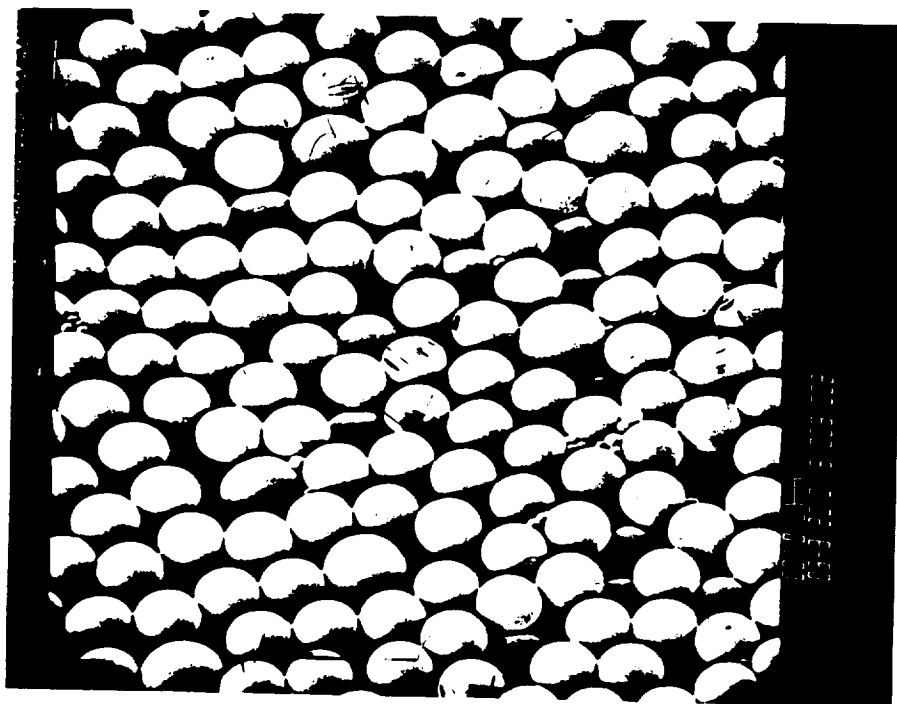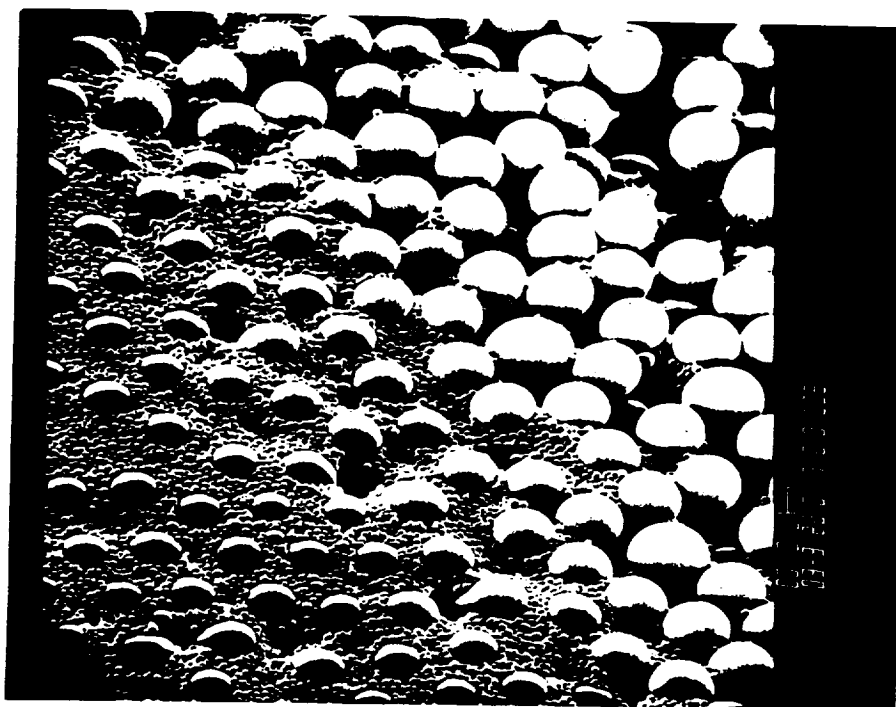
Figure 3-17. SEM micrographs of latexes grown from 2.02 μm PVT latex seed: latexes #2061-1 (left), with NH_4SCN inhibitor; and #2061-2 (right), with $NaNO_2$ inhibitor.

M/P=5
AIBN=0.38%M
PVP=0.11%aq

M/P=4   M/P=15   #4012-1
t-OM=10%M   AIBN=0.39%M   NH$_4$SCN=0.1%aq
                                                                        #4012-2
K$_2$S$_2$O$_8$=0.11%aq   #3017-1 →   #3148   NH$_4$SCN=0.2%aq
AMA=0.14%aq   AMA=0.12%aq
                        NH$_4$SCN=0.1%aq   #4012-3
                                                   NH$_4$SCN=0.3%aq

0.40μm seed

                                                   AIBN=0:38%M
                                          #2139   #2144
M/P=3   NaNO$_2$=0.1%aq
t-OM=10%M   #2137-1
                                                   AIBN=0.75%M
K$_2$S$_2$O$_8$=0.07%aq   #2147-1   #2149
AMA=0.08%aq   NaNO$_2$=0.05%aq

                        M/P=12
                        AIBN=0.36%M
                        AMA=0.08%aq   M/P=5.5
                        NaNO$_2$=0.1%aq   PVP=0.2%aq
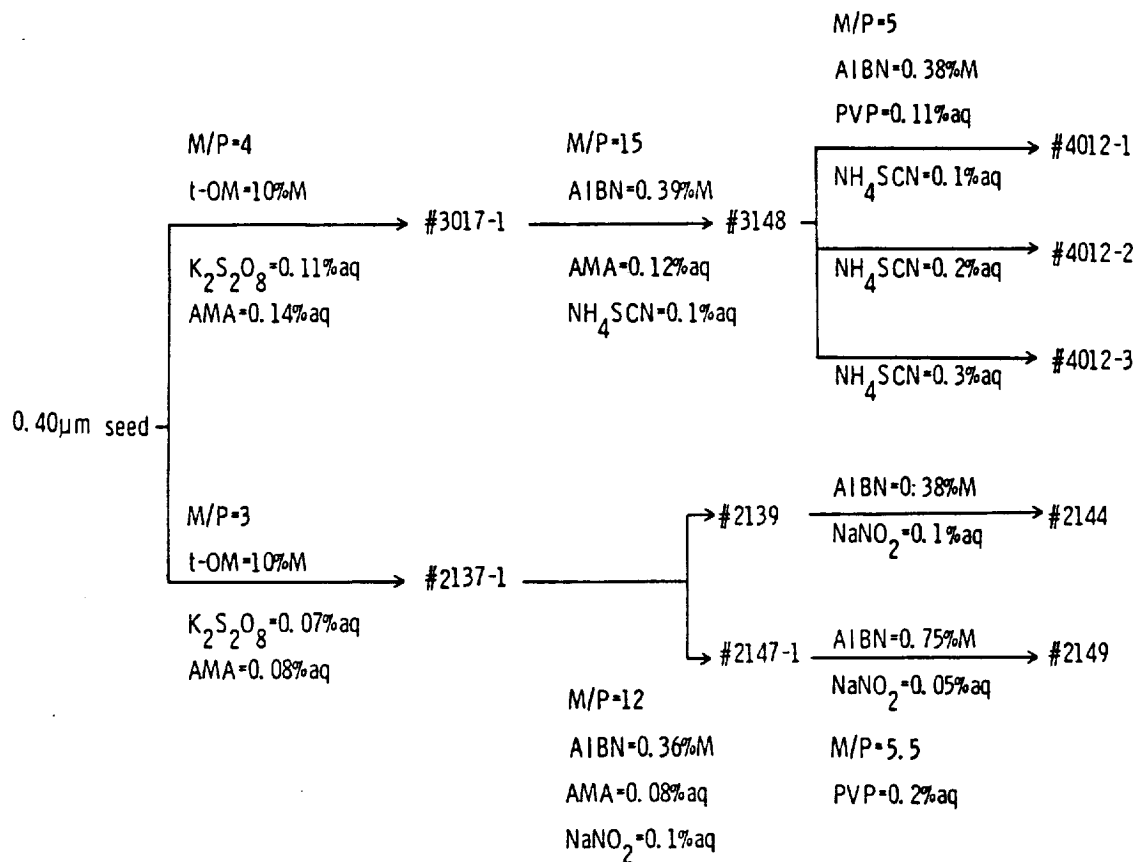
Figure 3-18.   Seeded polymerizations with different
inhibitor concentrations.

94
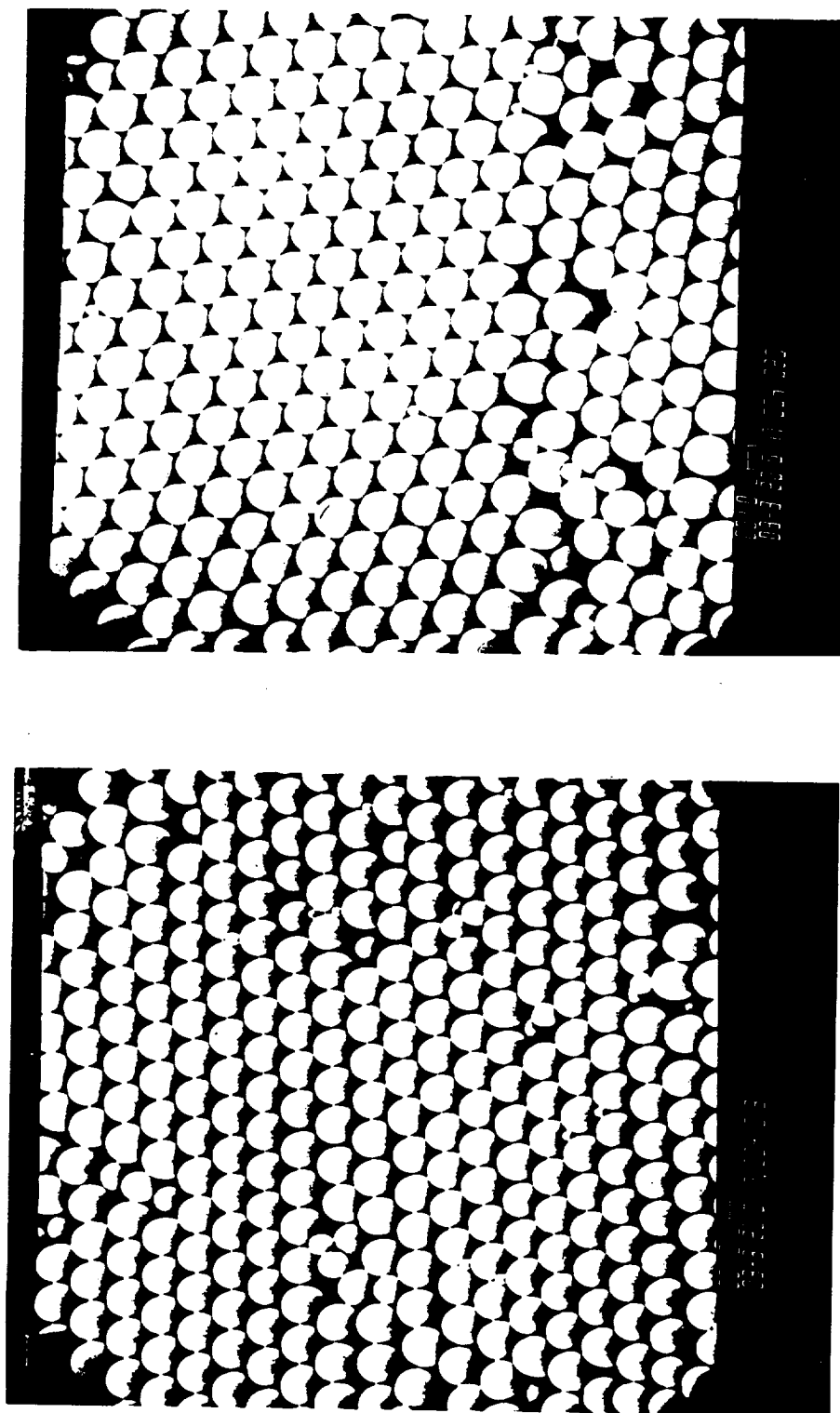
Figure 3-19. SEM micrographs of latex #2144, grown with the high NaNO$_2$/AIBN ratio.

95
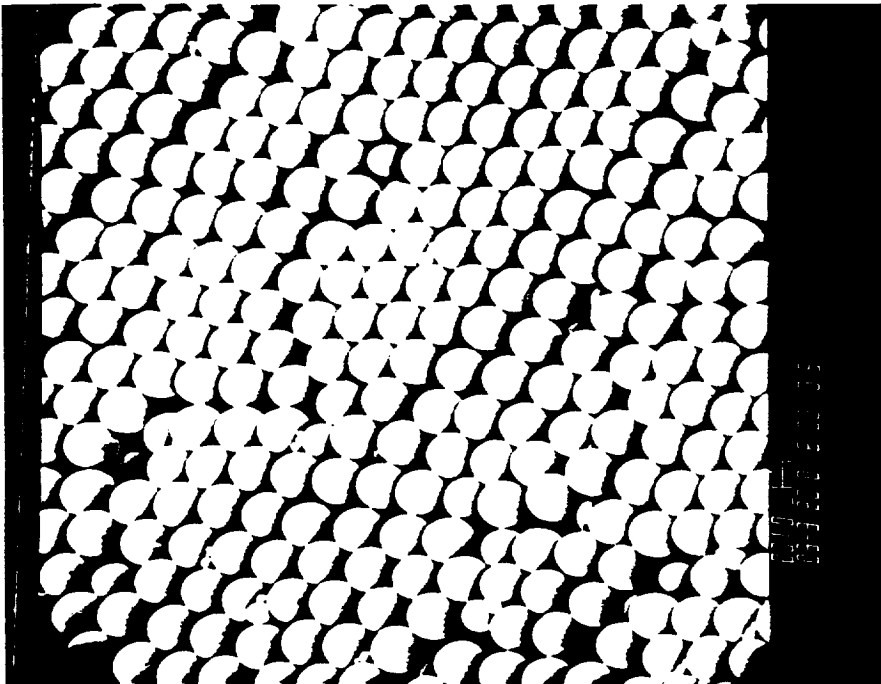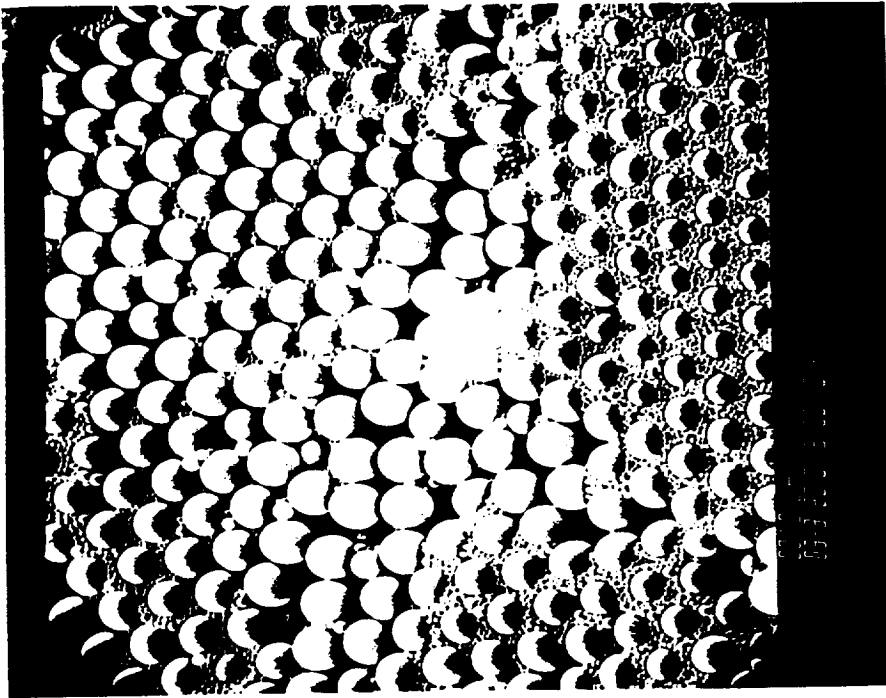
Figure 3-20. SEM micrographs of latex #2149, grown with the low NaNO$_2$/AIBN ratio.
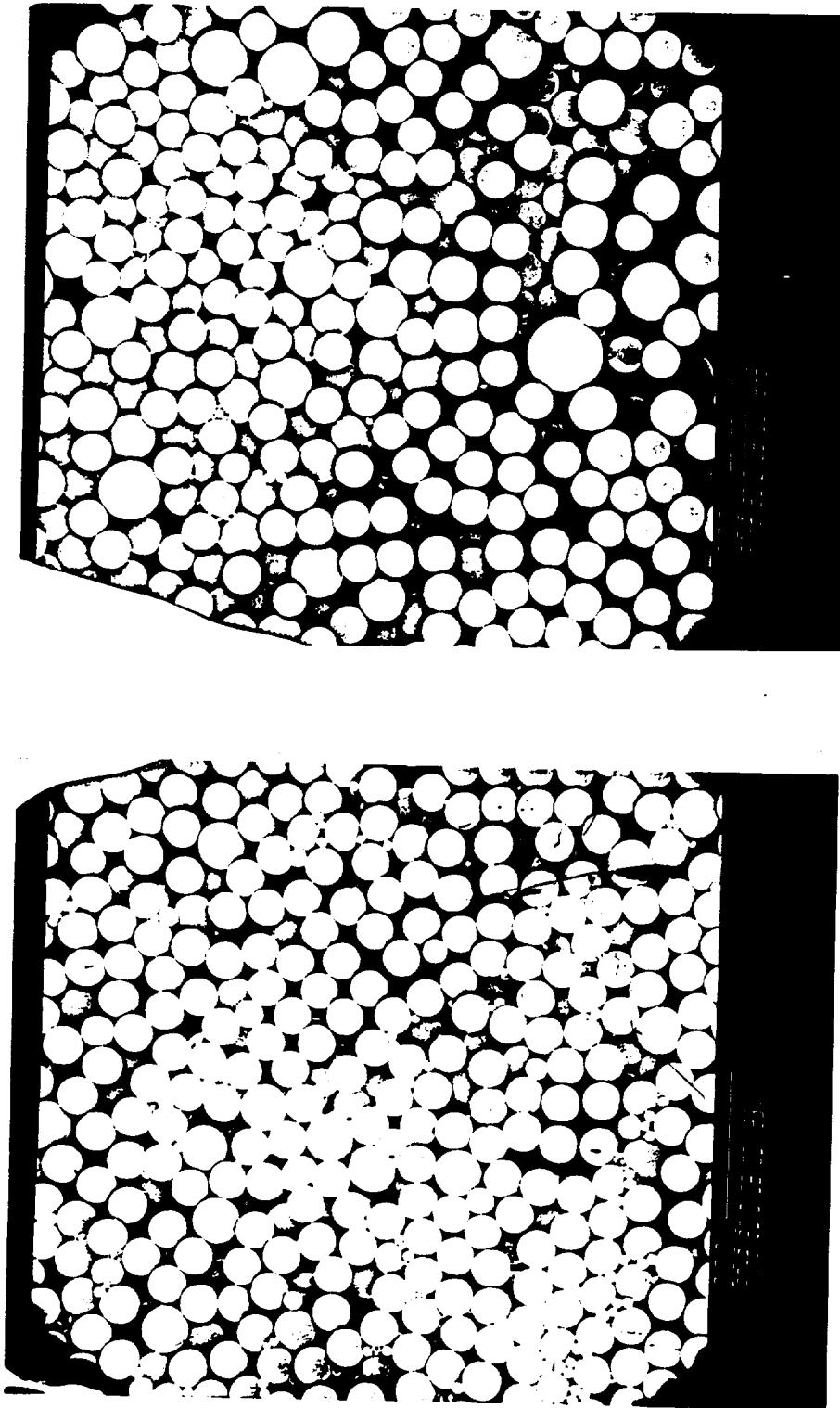
Figure 3-21. SEM micrographs of latex #4012-1, grown from latex #3148 with 0.1% aqueous NH_4SCN.
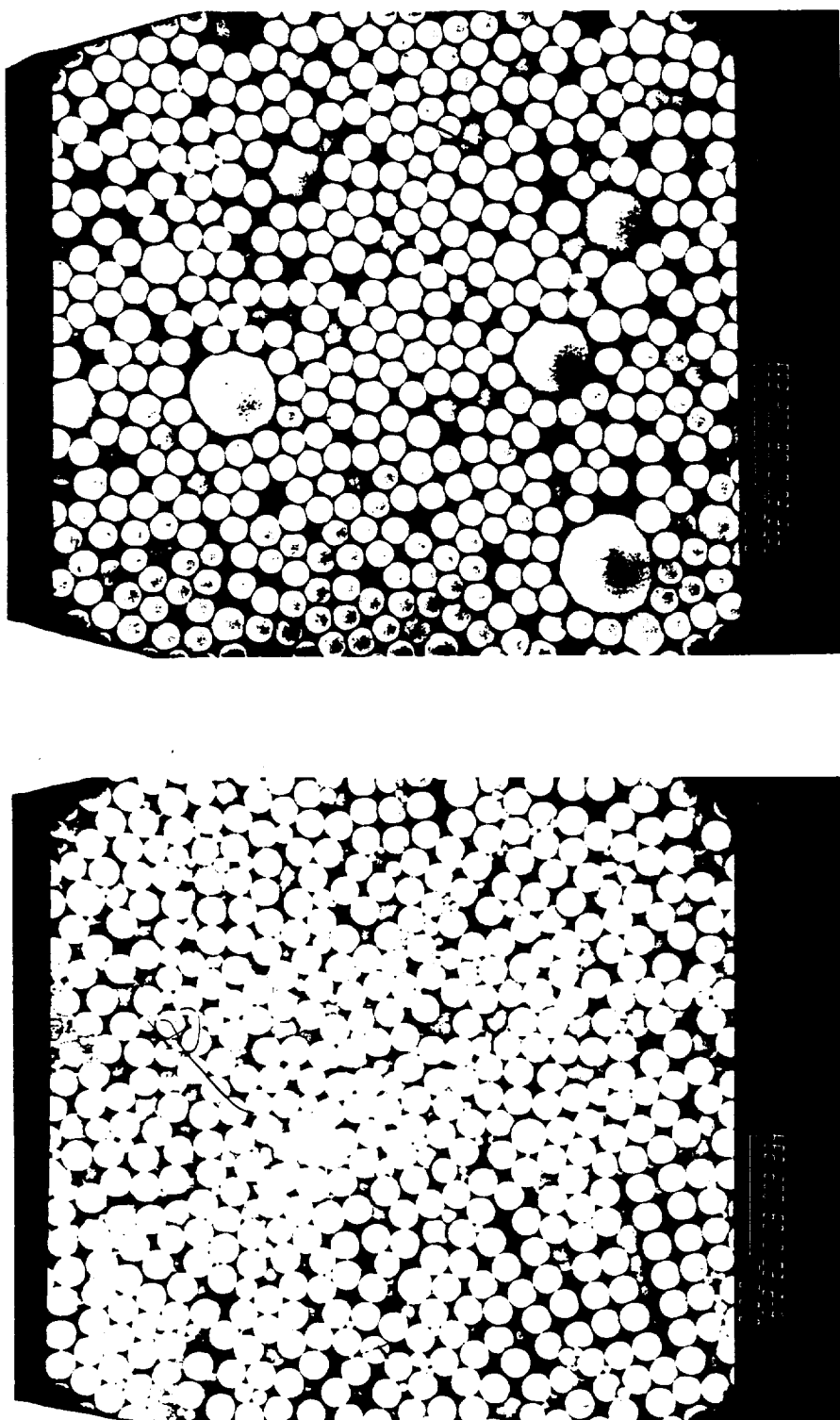
Figure 3-22.   SEM micrographs of latex #4012-2, grown from latex #3148 with 0.2% aqueous NH$_4$SCN.
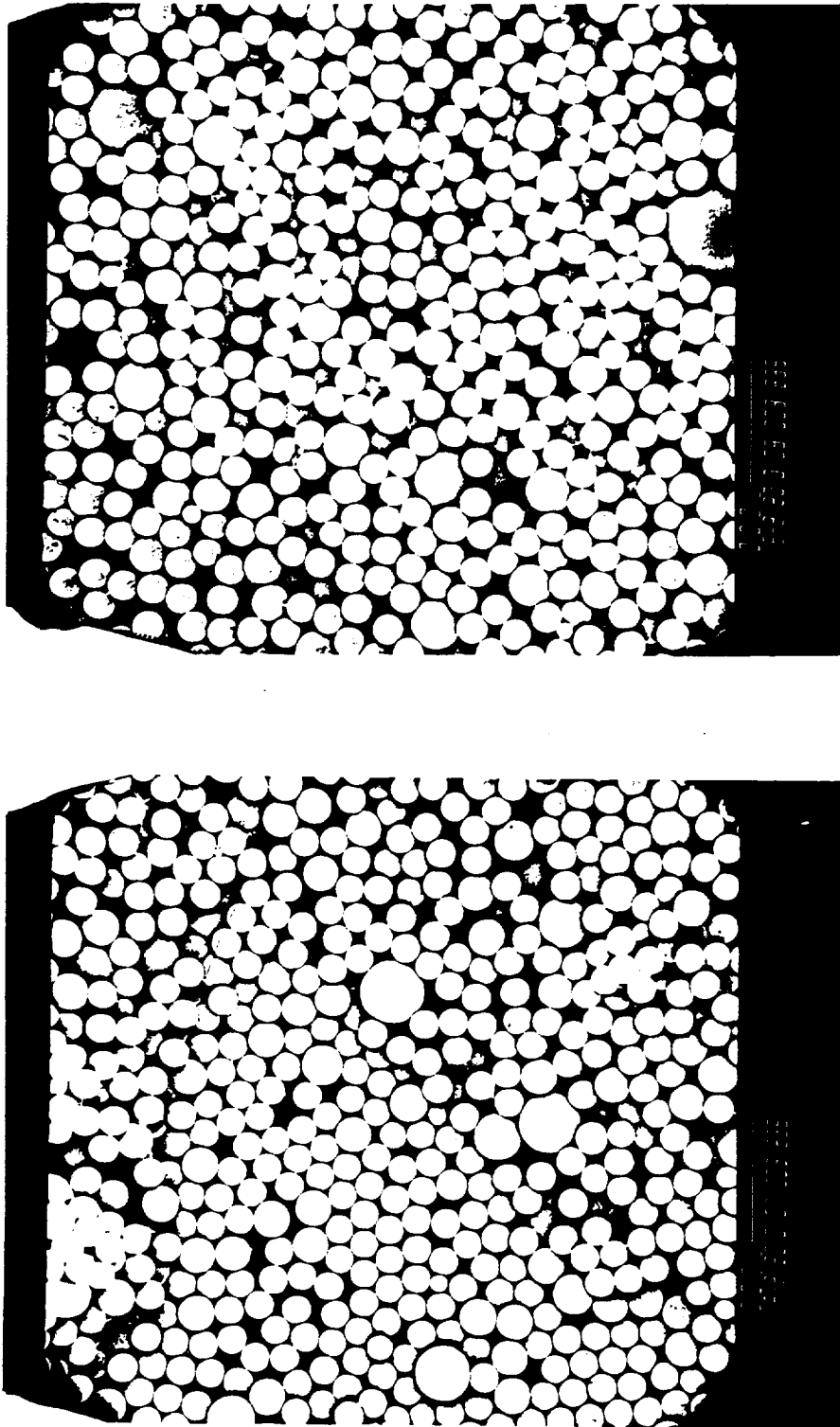
Figure 3-23. SEM micrographs of latex #4012-3, grown from latex #3148 with 0.5% aqueous NH_4SCN.

decreasing number of new small particles was observed with increasing NH_4SCN concentration. The off-size larger particles were believed to be formed from the coalescence of two or more particles. Coalescence of particles was enhanced by the addition of the NH_4SCN electrolyte, owing to the reduction of inter-particle electrostatic repulsion.

A parallel study of inhibitors in our laboratory [71] using a recording dilatometer and the laboratory prototype of the reactor used for the Space experiments, confirmed that $NaNO_2$ strongly retarded the polymerization rate at small particle size, while NH_4SCN had very little effect on the polymerization rate. On the other hand, the SEM micrographs of the product latexes indicated that NH_4SCN had a strong electrolyte effect, resulting in the formation of more over-size particles, while $NaNO_2$ had no such effect. The differences between these two inhibitors may be attributed to the ability of $NaNO_2$ to form gaseous nitrogen oxides.

In butadiene-styrene emulsion polymerization systems, there is an optimum conversion beyond which the polymer becomes increasingly branched and crosslinked [72]. Therefore, the polymerization is generally stopped at predetermined conversions. Stopping of the polymerization is achieved by the addition of suitable chemicals which react with the free radicals in the system to terminate further reaction. Such chemicals are known as shortstoppers. A wide range of substances have been used for shortstopping styrene-butadiene emulsion polymerizations. These include compounds containing, or capable of forming, quinoid structures, nitro and nitroso compounds, oxygen, aromatic polyhydroxy compounds such as catechol and pyrogallol (which

could be classified as the compounds which are capable of forming quinoid structures), water-soluble dithiocarbamates, sulphur, and 2,4-dinitrochlorobenzene and certain of its derivatives [73]. Kluchesky and Wakefield [72], Wakefield and Bebb [74], and Antlfinger and Lufter [75] have described the results of extensive surveys of various shortstopper types. An ideal shortstopper should fulfill the following requirements, according to Blackley [73]:

1. It should swiftly bring the polymerization reaction to a halt when added to the reaction system in small quantity.

2. It should discourage further chemical modification of the polymer (e.g., by degradation or crosslinking) once polymerization has ceased.

3. It should not affect the colloid stability of the latex.

4. It should not adversely affect the physical or chemical properties of the polymer obtained from the latex.

5. It should not remain behind in reactors after the short-stopped latex has been removed; otherwise the subsequent polymerization batch may be severely retarded or inhibited.

6. It should not cause discoloration.

7. It should be cheap, readily available, and have no hazards associated with its use.

8. For convenience of handling, it should be readily soluble in water, and should be capable of being stored as an aqueous solution over long periods of time.

Similar properties are also desired for inhibitors used in seeded

101

polymerization. The requirements for an ideal shortstopper would become the requirements for an ideal "new particle inhibitor" if requirements 1 and 2 were removed and the following requirement were added:

1. It should inhibit aqueous phase polymerization effectively when added to the system in a small quantity.

Thus an effective shortstopper can also be an effective "new particle inhibitor". Figure 3-24 outlines a systematic comparison of various inhibitors and shortstoppers in a seeded polymerization starting with seed latex #4003-2 of 0.63 μm diameter. SEM micrographs of the latexes are shown in Figures 3-25 to 3-36. Comparison of Figures 3-25 and 3-26 proved once again that NH_4SCN was more effective than $NaNO_2$ in preventing nucleation of new particles. Latex #4030-3, which was prepared with 0.1% aqueous NaCl, served as a control to demonstrate the effect of an electrolyte on latex stability, the formation of off-size larger particles, and the elimination of small particle generation. The latex contained not only many new small particles but also a significant number of off-size larger particles, as shown in Figure 3-27. Compared to this, other inhibitors such as NH_4SCN and NaDMDTC appeared to inhibit new particle generation by mechanisms other than just an electrolyte effect.

Hydroquinone (HQ) has been widely used as a shortstopper in styrene-butadiene emulsion polymerization. The results of Kluchesky and Wakefield [72] confirmed its effectiveness in concentrations greater than 0.05 pphm. In our study, HQ has also been found to be a

M/P=14.7

AIBN=0.39%M

AMA=0.12%aq

NH_4SCN=0.1%aq → #4030-1

$NaNO_2$=0.1%aq → #4030-2

NaCl=0.1%aq → #4030-3

HQ=0.1%aq → #4030-4

M/P=4.3

AIBN=0.38%M

PVP=0.11%aq

HQ=0.2%aq → #4034 — HQ=0.2%aq → #4035-1

Pyrogallol=0.1%aq → #4072-4

Catechol=0.1%aq → #4072-5

#4003-2

MEHQ=0.1%aq → #4066-1

Ascorbic acid=0.1%aq → #4087-1

DMHAHCl=0.1%aq → #4096-1

NaDMDTC=0.1%aq → #4099-1

Thiourea=0.1%aq → #4112-4
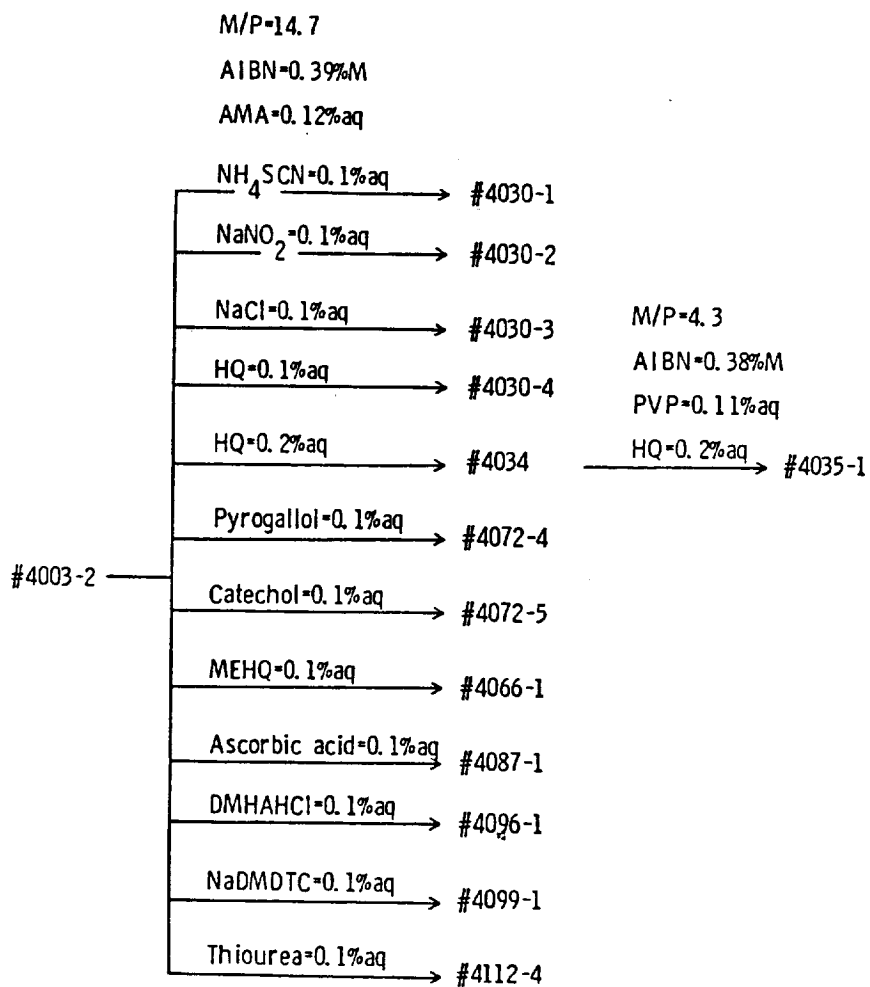
Figure 3-24.   Seeded polymerizations in the presence of different inhibitors, starting with seed latex #4003-2 of 0.63 µm diameter.

103
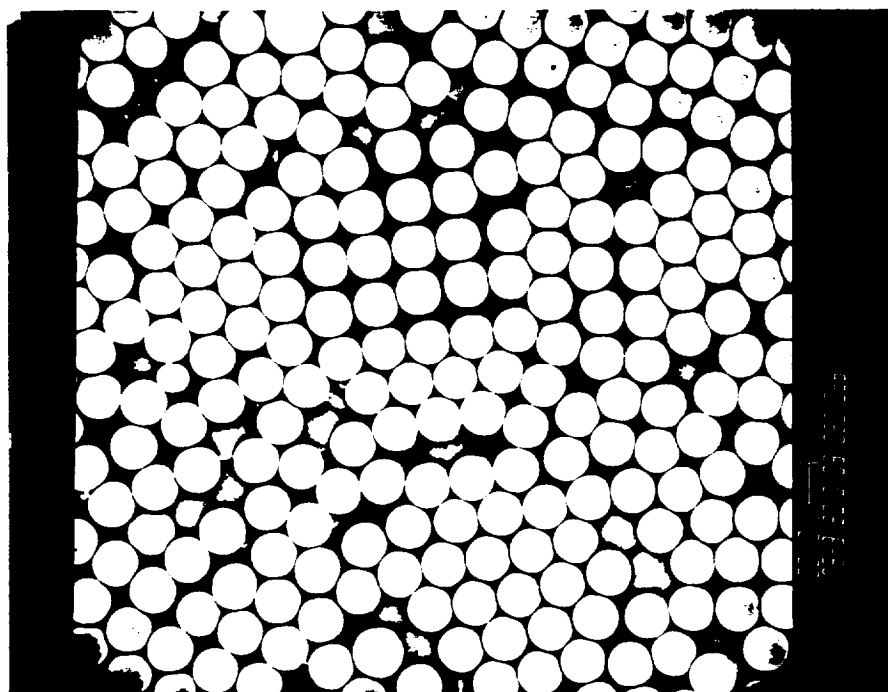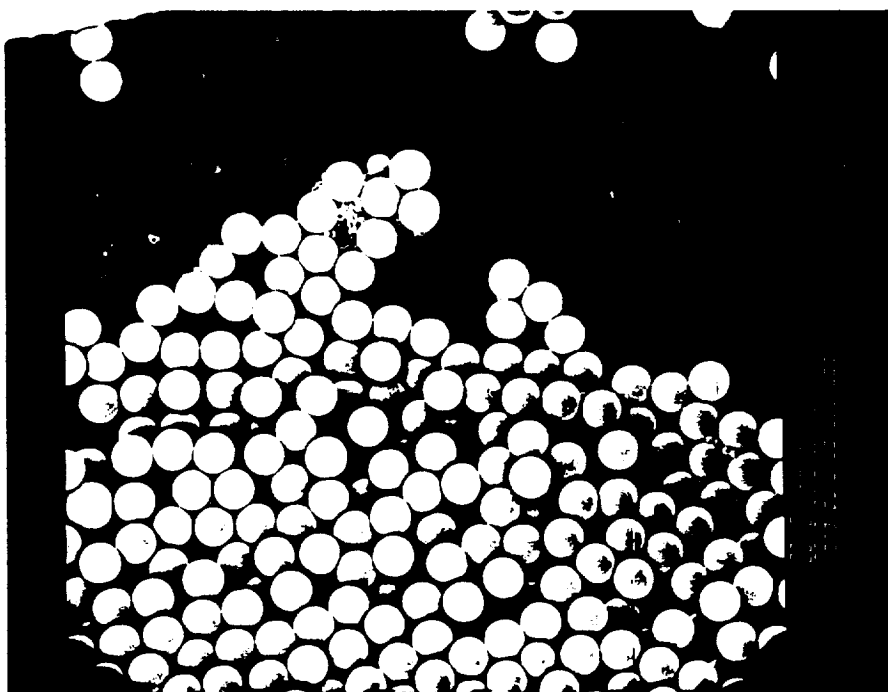
Figure 3-25. SEM micrographs of latex #4030-1, grown from latex #4003-2 with 0.1% aqueous NH₄SCN.
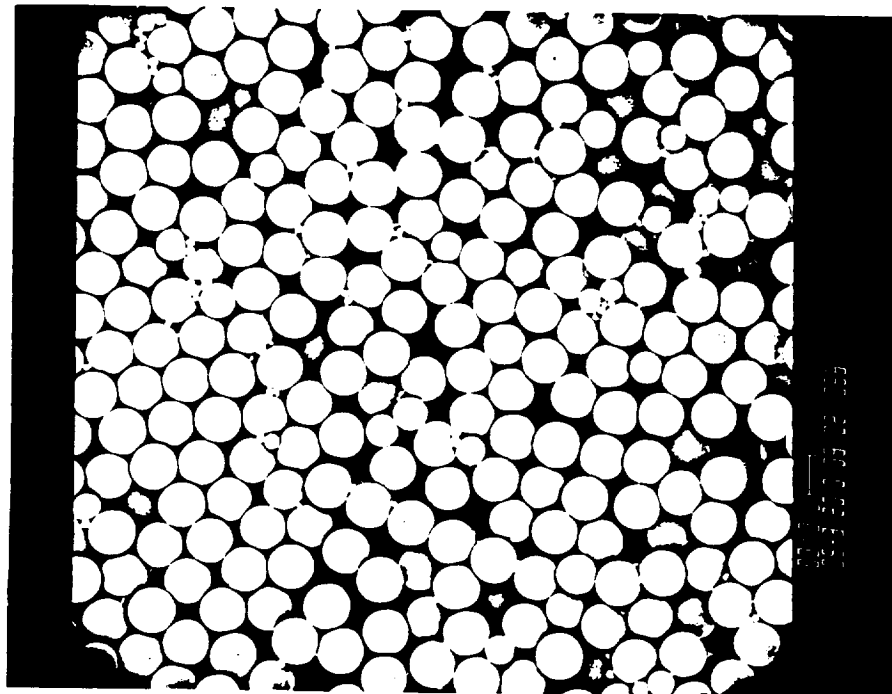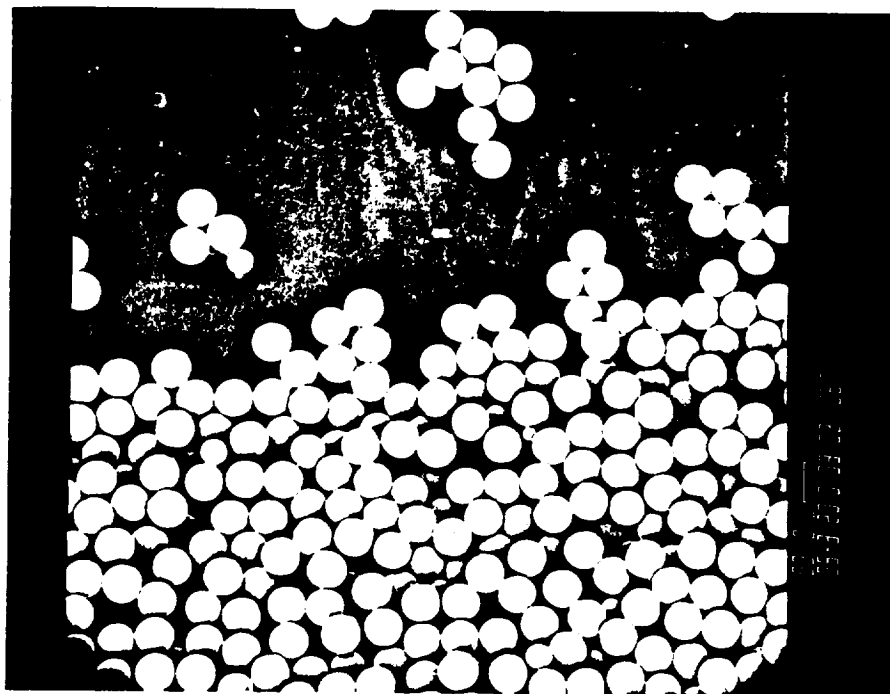
Figure 3-26. SEM micrographs of latex #4030-2, grown from latex #4003-2 with 0.1% aqueous $NaNO_2$.

105
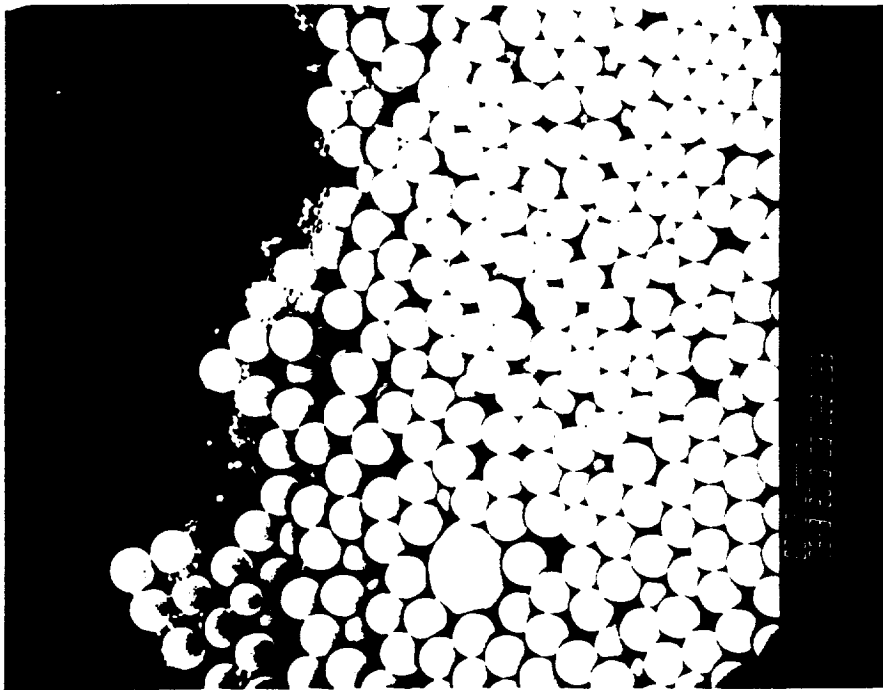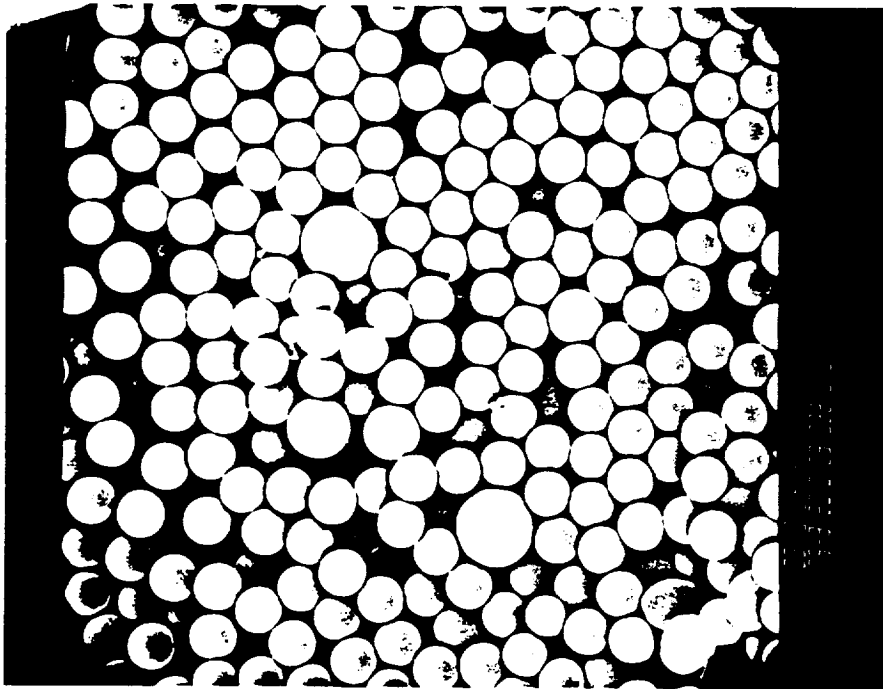
Figure 3-27. SEM micrographs of latex #4030-3, grown from latex #4003-2 with 0.1% aqueous NaCl.
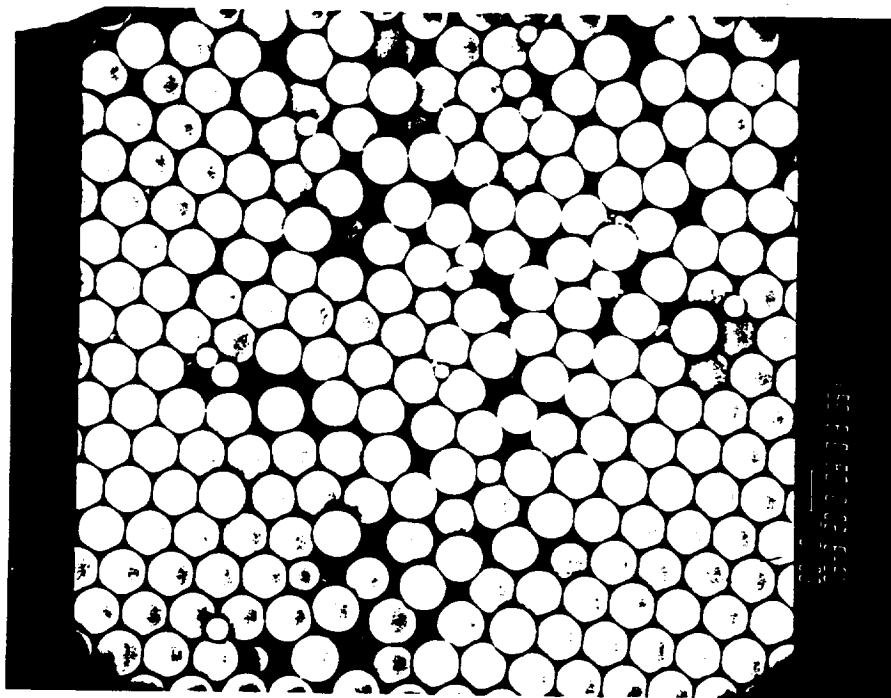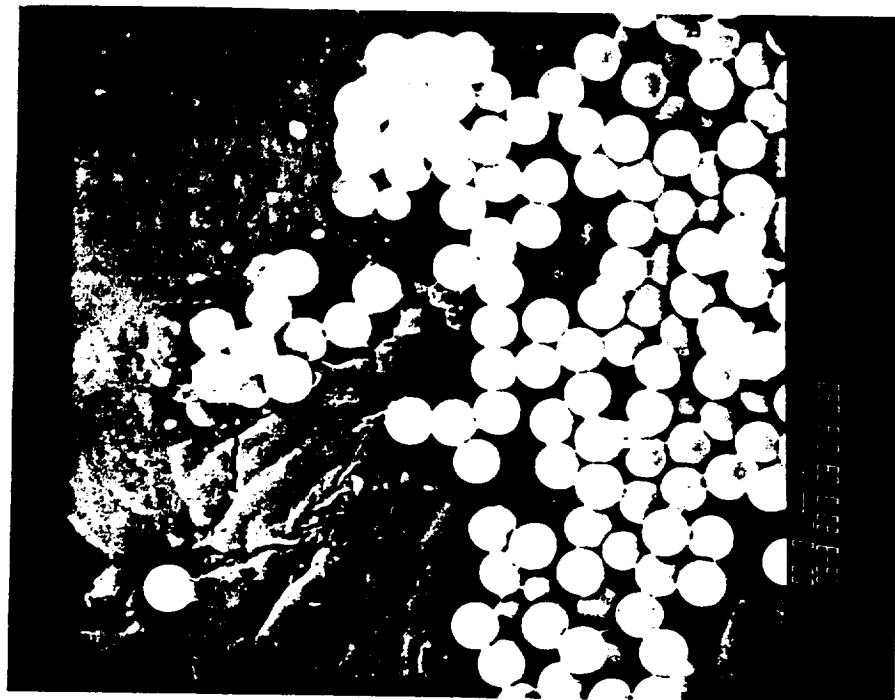
Figure 3-28. SEM micrographs of latex #4030-4, grown from latex #4003-2 with 0.1% aqueous HQ.
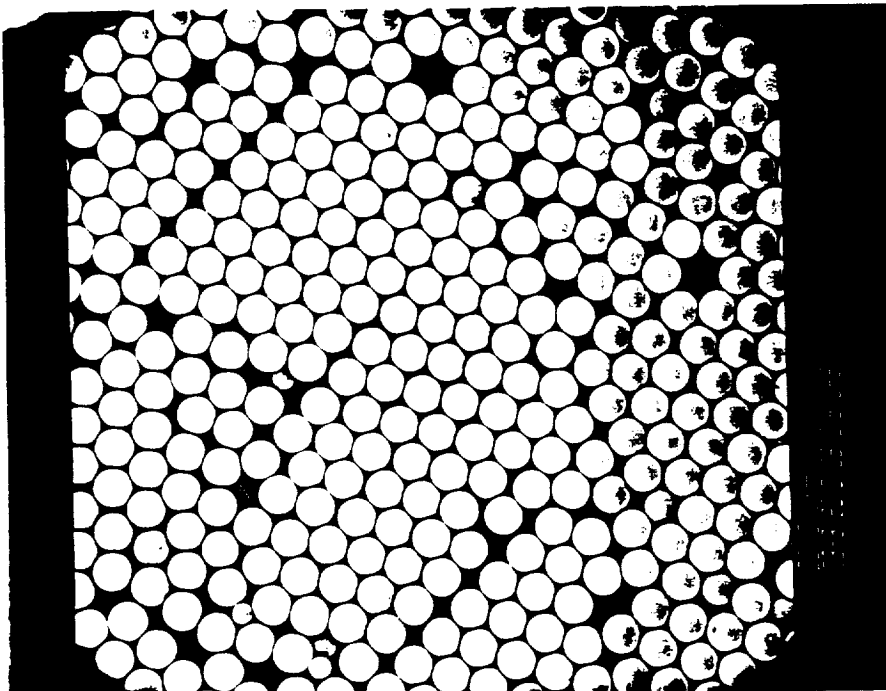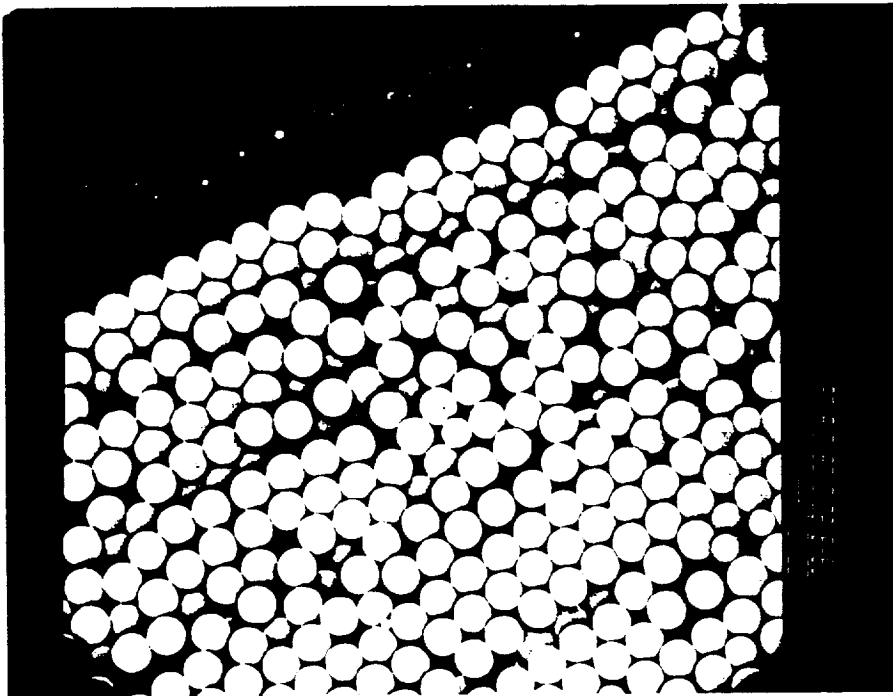
Figure 3-29. SEM micrographs of latex #4035-1, grown from latex #4034 with 0.2% aqueous HQ.
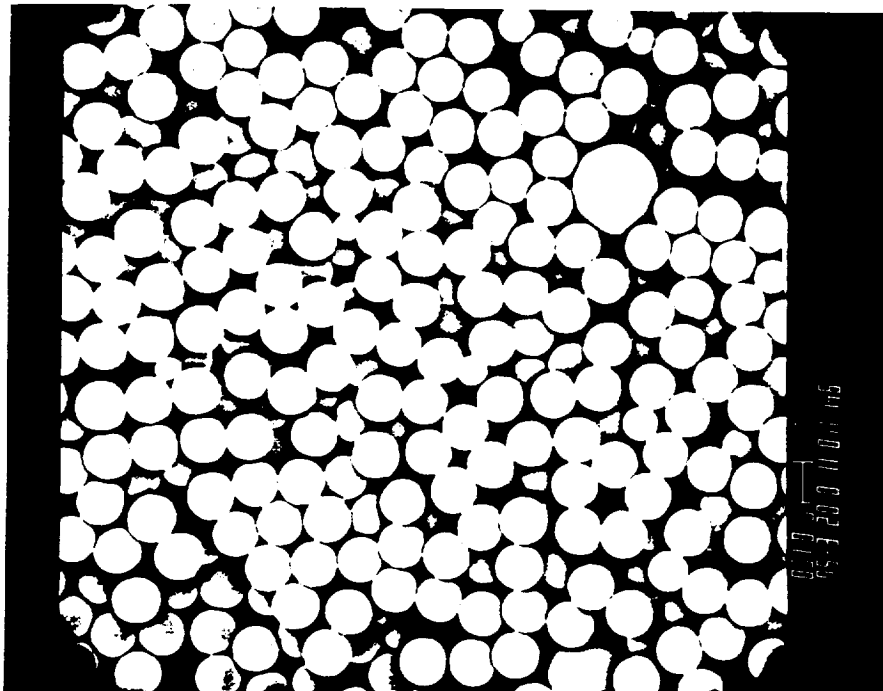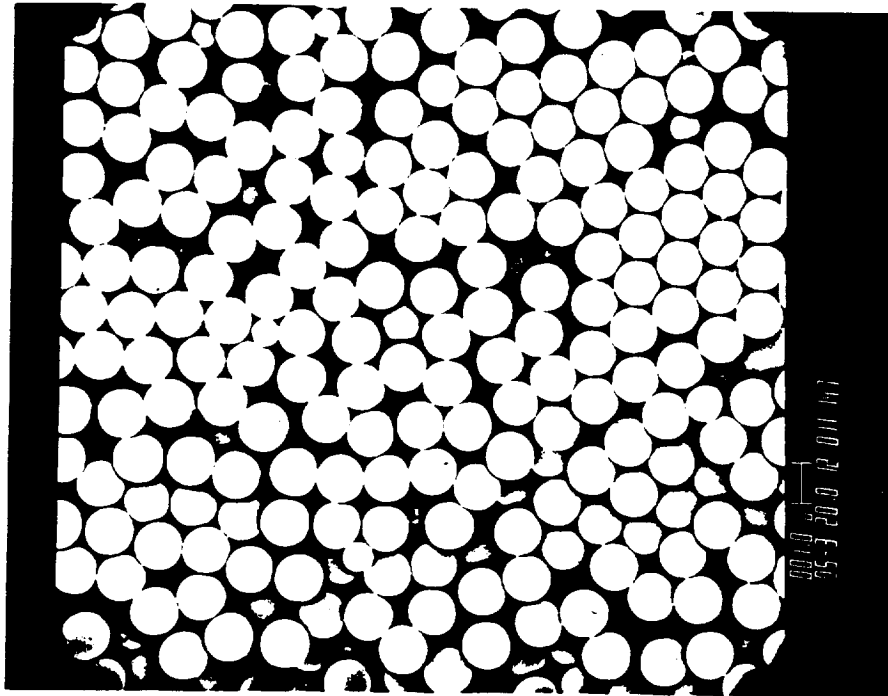
Figure 3-30. SEM micrographs of latex #4072-4, grown from latex #4003-2 with 0.1% aqueous pyrogallol.
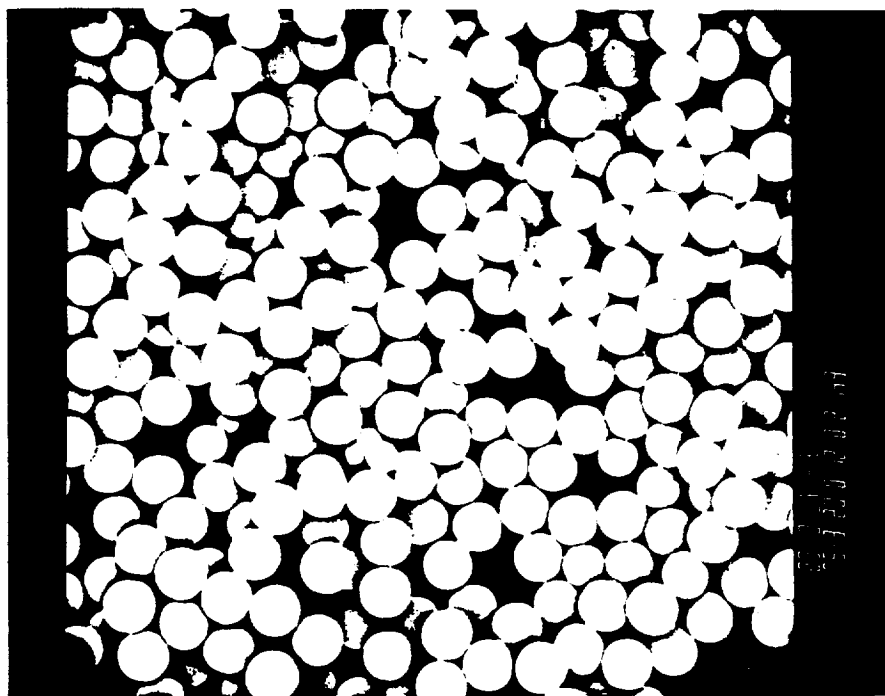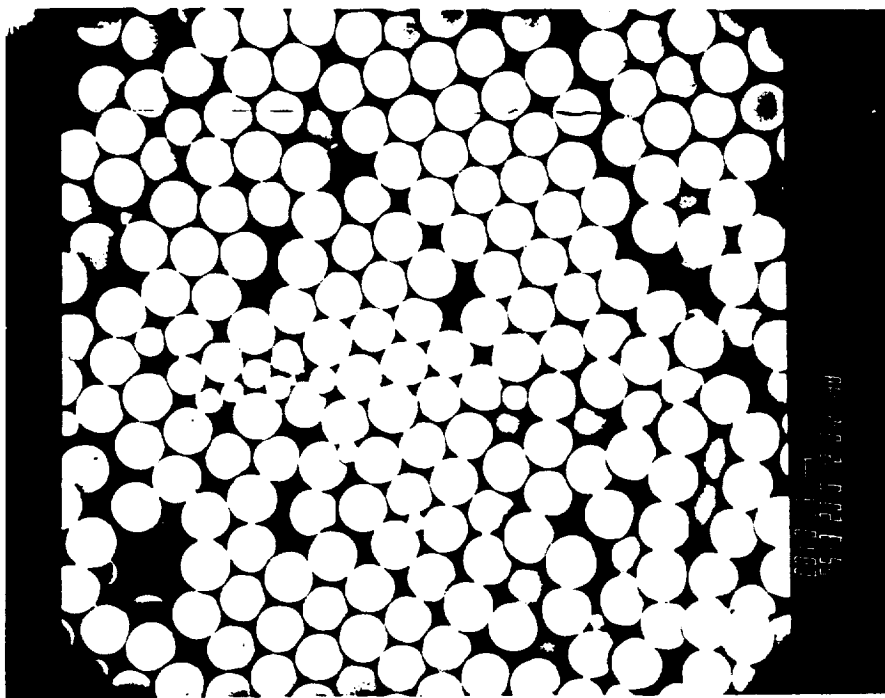
Figure 3-31. SEM micrographs of latex #4072-5, grown from latex #4003-2 with 0.1% aqueous catechol.
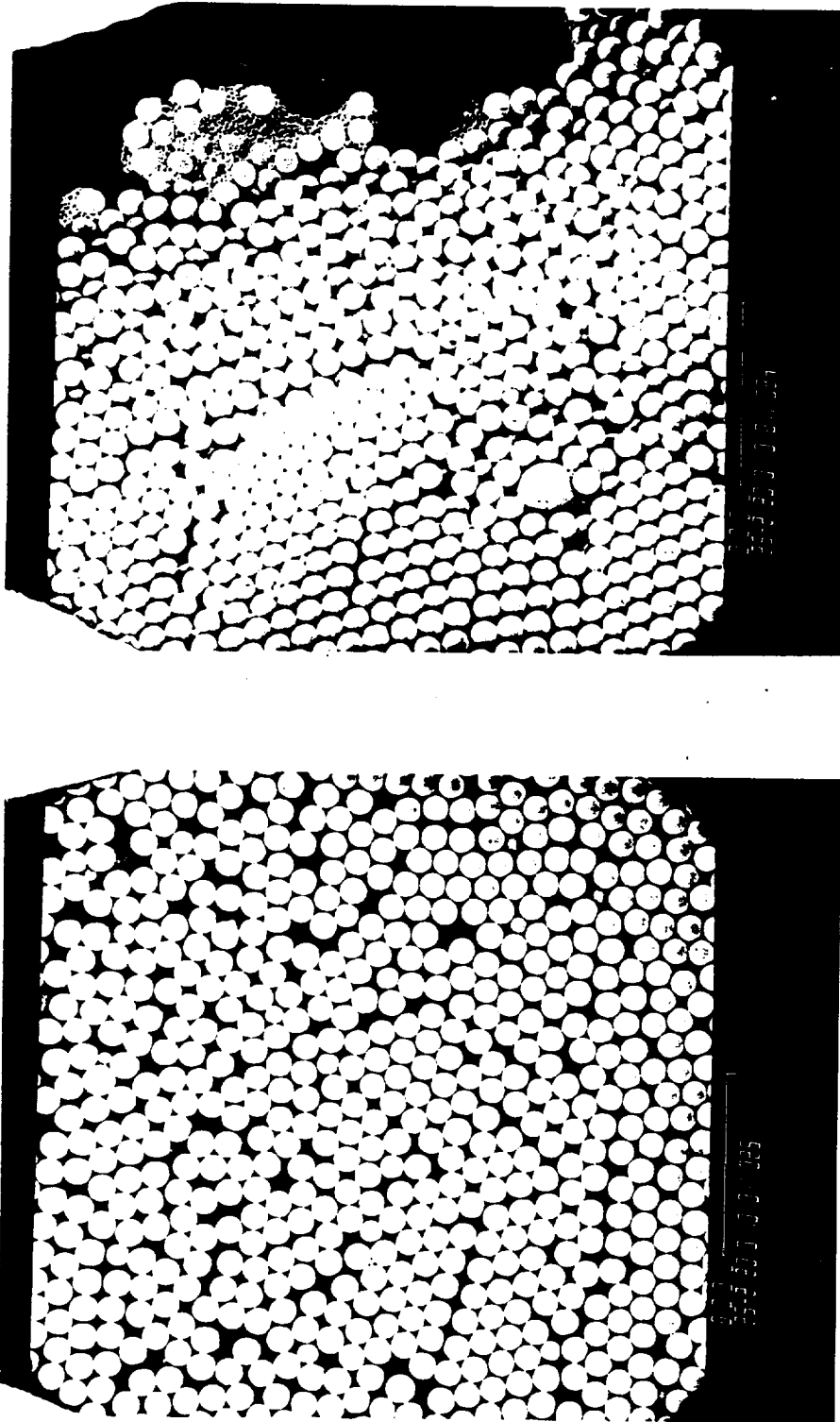
Figure 3-32. SEM micrographs of latex #4066-1, grown from latex #4005-2 with 0.1% aqueous MEHQ.
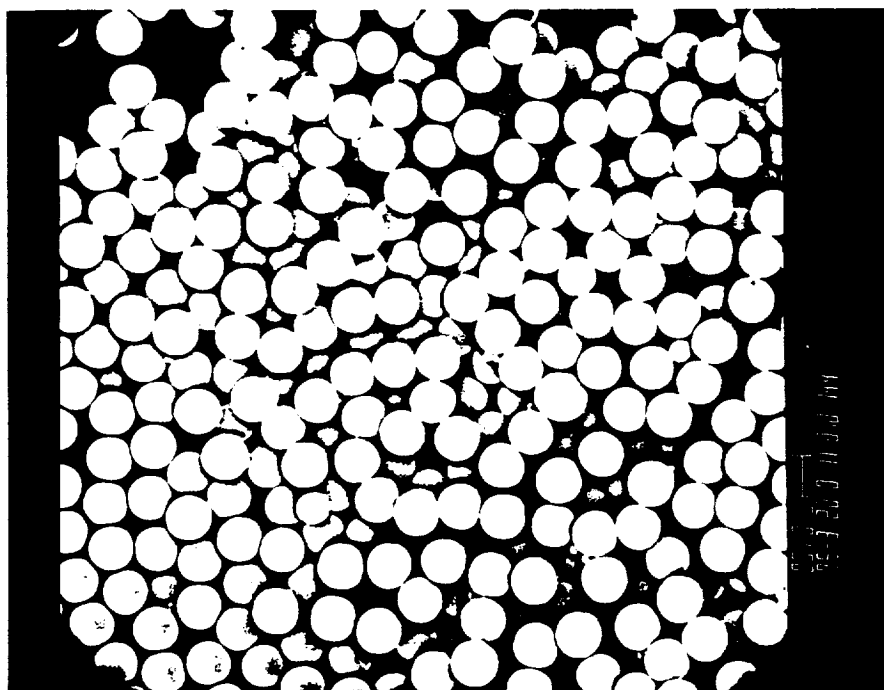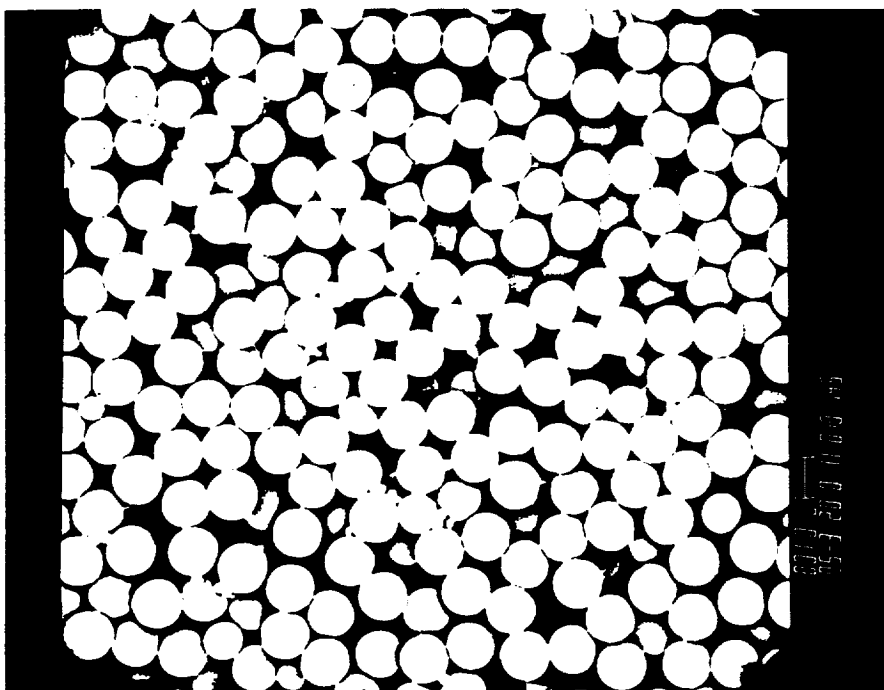
Figure 3-33. SEM micrographs of latex #4087-1, grown from latex #4003-2 with 0.1% aqueous sodium ascorbate.
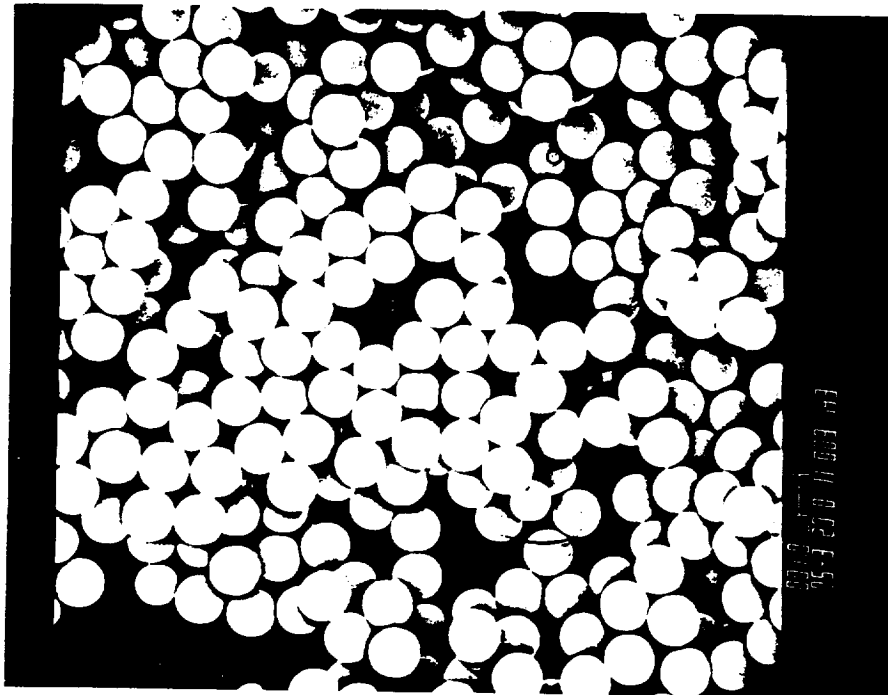
Figure 3-34. SEM micrographs of latex #4096-1, grown from latex #4005-2 with 0.1% aqueous DMHAHCl.
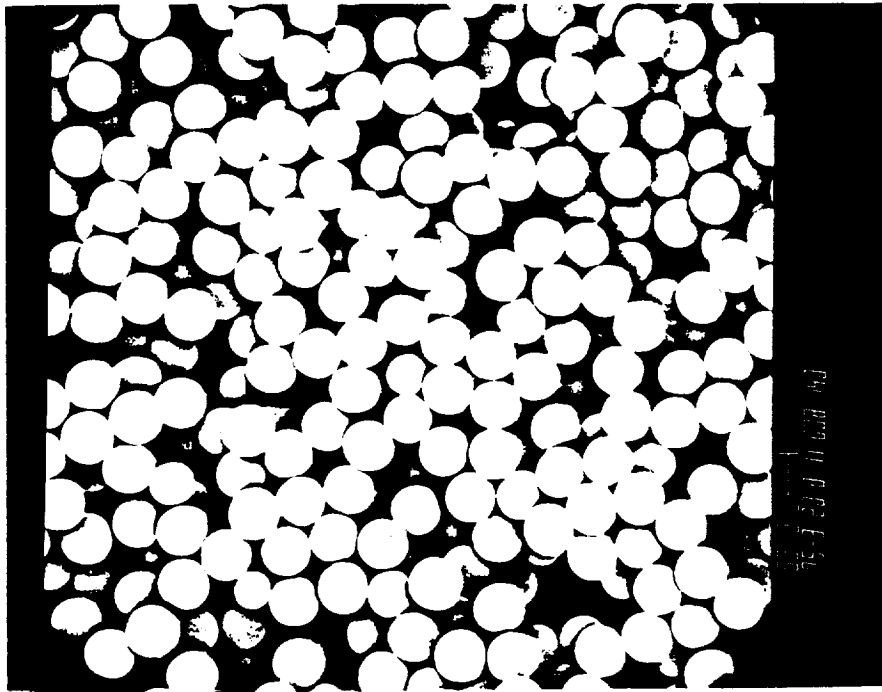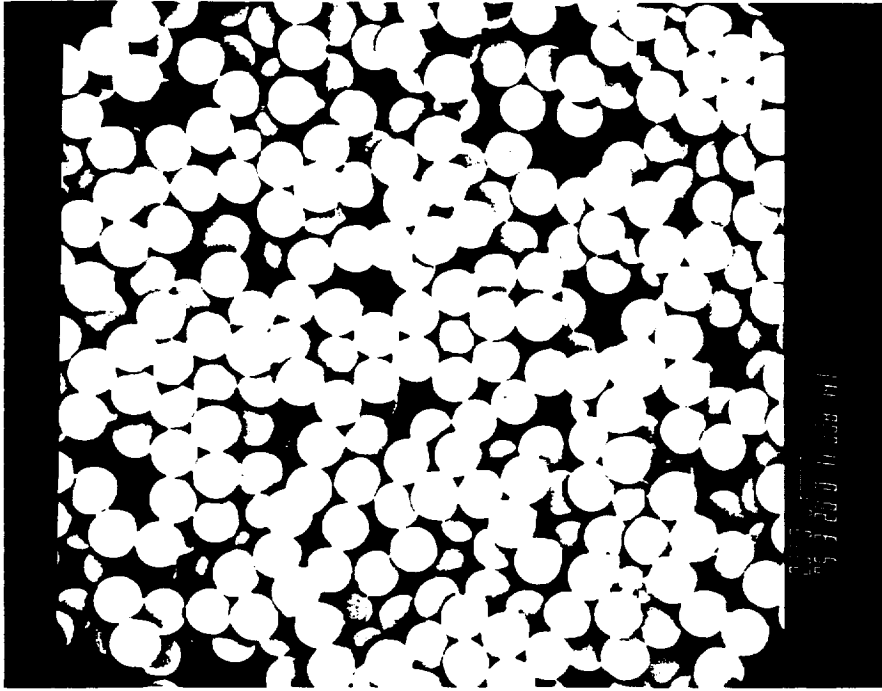
Figure 3-35. SEM micrographs of latex #4099-1, grown from latex #4005-2 with 0.1% aqueous NaDMDTC.
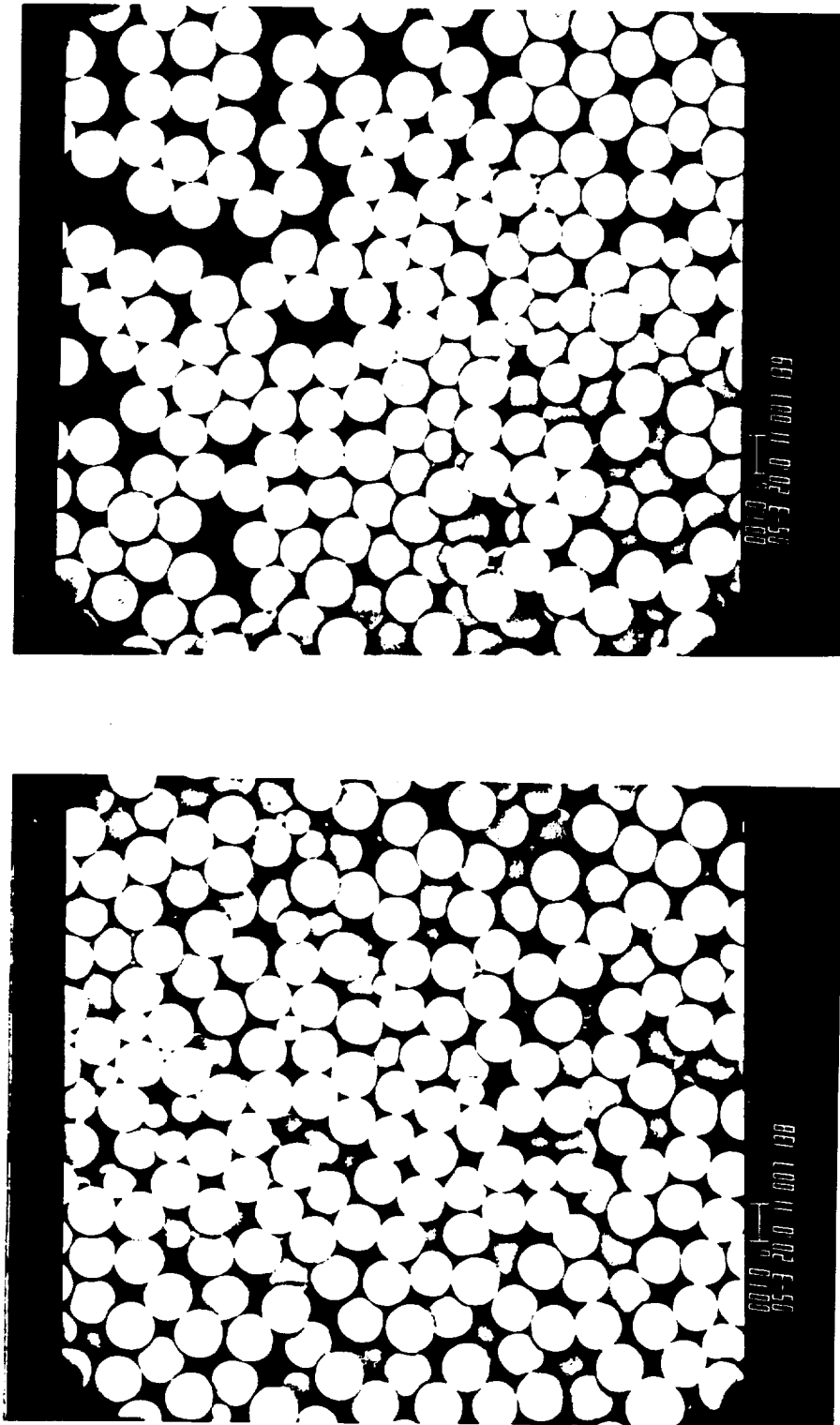
Figure 3-36. SEM micrographs of latex #4112-4, grown from latex #4003-2 with 0.1% aqueous thiourea.

115

promising "new particle inhibitor". One significant advantage of HQ over other inhibitors is that it is not an electrolyte; therefore, it should not affect the latex stability by suppressing the interparticle electrostatic repulsion. Latexes prepared with HQ along with an appropriate initiator and surfactant combination usually had a clear supernatant layer after the particles of the main distribution settled, indicating the absence of a large population of small particles. However, SEM micrographs of HQ-inhibited latexes #4030-4 and #4034 showed some tiny "aborted" particles, especially around the edge of the specimen (Figures 3-6 and 3-28). These "aborted" particles were not observed in latex #4035-1 (Figure 3-29), which was prepared from latex #4034 with the same initiator/inhibitor combination. Latex #4066-2 (Figure 3-7), an analogue of latex #4034 using AMBN as initiator instead of AIBN, did not contain tiny "aborted" particles.

The other two quinoid-type inhibitors, pyrogallol and catechol, showed inhibiting power similar to that of HQ. They also have the same advantage of not affecting latex stability, and therefore mono-dispersity, by an electrolyte effect. For comparison, SEM micrographs of latexes #4072-4 and #4072-5 are shown in Figures 3-30 and 3-31, respectively. Another quinoid-type inhibitor, MEHQ, did not inhibit new particle generation effectively, as many small particles were observed in the SEM micrographs (Figure 3-32). The poor inhibiting effect may be attributed to its low water solubility compared to other inhibitors. A minor disadvantage of using quinoid-type inhibitors is that some of them may cause discoloration, e.g., the aqueous phase of

HQ-inhibited latexes turned dark-brown on aging, while pyrogallol gave a yellow color.

Thiourea and ascorbic acid are two relatively new shortstoppers. Koski et al. [76] reported that the emulsion polymerization of styrene and butadiene using persulfate initiator was effectively shortstopped by the addition of ascorbic acid or its sodium or potassium salt. In this study, sodium bicarbonate-neutralized ascorbic acid was used instead of ascorbic acid itself, which lowered the pH significantly, resulting in massive coagulum. Product latexes using thiourea and sodium ascorbate as "new particle inhibitors" are compared in Figures 3-36 and 3-33.

The use of water-soluble dialkyldithiocarbamates as shortstoppers has been described in detail by Smith et al. [77] and by Howland et al. [78]. They are not only convenient to use, relatively cheap, and very effective as shortstoppers for low-temperature polymerization, but they are also non-toxic, non-discoloring, and non-staining. According to Howland et al. [78], some of them tend to cause the formation of coagulum when added to the latex, and others show no tendency to cause colloidal instability. In this study, sodium dimethyldithiocarbamate (NaDMDTC) was found to be one of the most effective "new particle inhibitors" in this comparison series. Another strong inhibitor was N,N-dimethylhydroxyamine hydrochloride (DMHAHCl). Hardly any small particles can be found in the SEM micrographs of latexes #4099-1 (NaDMDTC; Figure 3-35) and #4096-1 (DMHAHCl; Figure 3-34). Unfortunately, both inhibitors, especially DMHAHCl, exhibited a strong electrolyte effect, which resulted in a

high level of coagulation and therefore a low product yield.

Comparisons in a larger particle size range demonstrated further the differences among different types of inhibitors, as described in Figure 3-37. Four latexes were grown from a cleaned seed latex of 2.5 μm diameter, using AMBN initiator and a three-surfactant stabilization system, each with a different inhibitor. SEM micrographs of the product latexes are presented in Figures 3-38 to 3-41. Among these four latexes, the DMHAHCl-containing latex #5049-3 (Figure 3-40) contained the largest population of off-size larger particles and also the highest level of coagulum. Although not many off-size larger particles were observed in any of the other latexes, the NaDMDTC-containing latex #5049-2 (Figure 3-39) had a significantly higher level of coagulum than the HQ-containing latex #5049-1 (Figure 3-38) and the BQ-containing latex #5057-2 (Figure 3-41). HQ and BQ seemed to have comparable inhibiting power; however, BQ retarded the polymerization rate somewhat.

In summary, an ideal "new particle inhibitor" which fulfills all of the foregoing requirements has not yet been found and, indeed, may not exist. Therefore, a compromise must be made. Latex stability and monodispersity should definitely be considered first. Quinoid-type inhibitors, especially HQ, which inhibit new particle generation quite effectively without affecting colloid stability and monodispersity, appear to be the best choice for this purpose.

```
                    HQ=0.1%aq
                  ┌──────────────────────────→ #5049-1
                  │
                  │ NaDMDTC=0.1%aq
                  ├──────────────────────────→ #5049-2
   #4140C ────────┤
                  │ DMHAHCl=0.1%aq
                  ├──────────────────────────→ #5049-3
                  │
                  │ BQ=0.1%aq
                  └──────────────────────────→ #5057-2
```
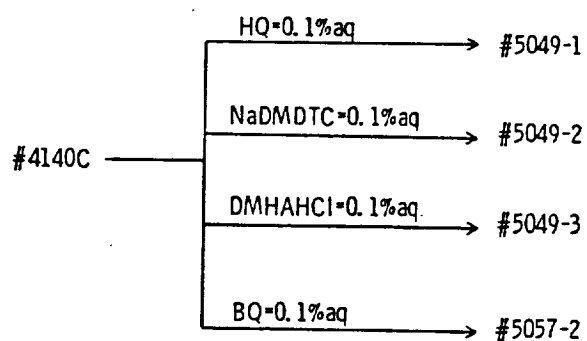
M/P=4
AMBN=0.17%M
AMA=0.007%aq
KX-3=0.018%aq
PVP=0.18%aq

Figure 3-37.   Particle growth from 2.5 μm seed latex
#4140C in the presence of different inhibitors.
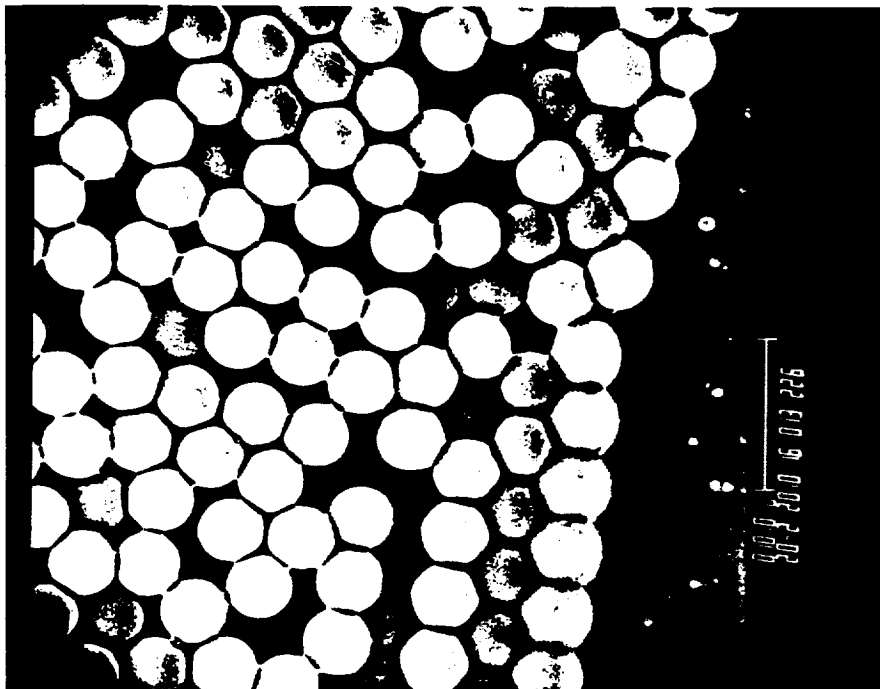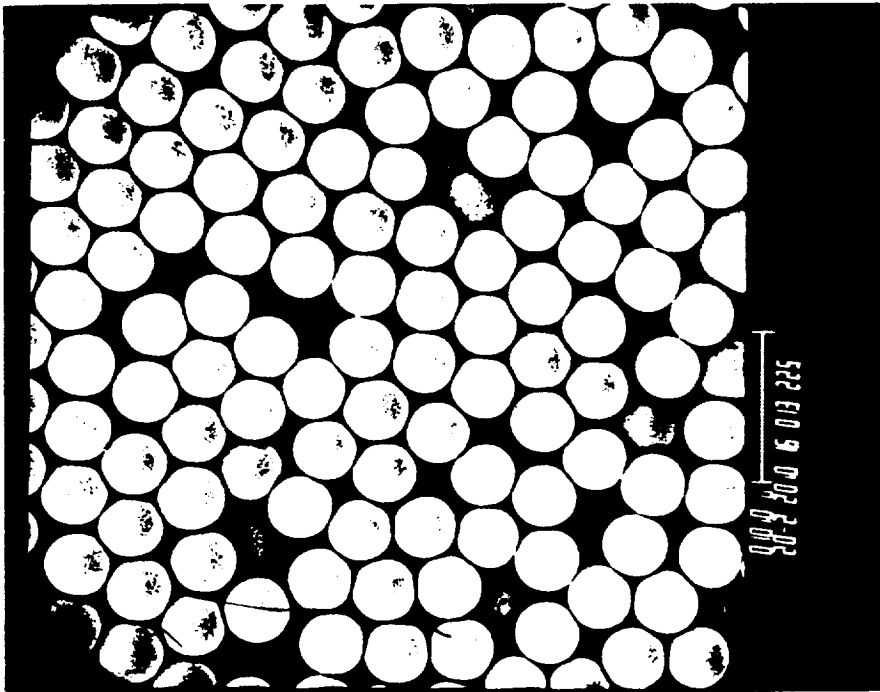
Figure 3-38. SEM micrographs of latex #5049-1, grown from latex #4140C with HQ inhibitor.
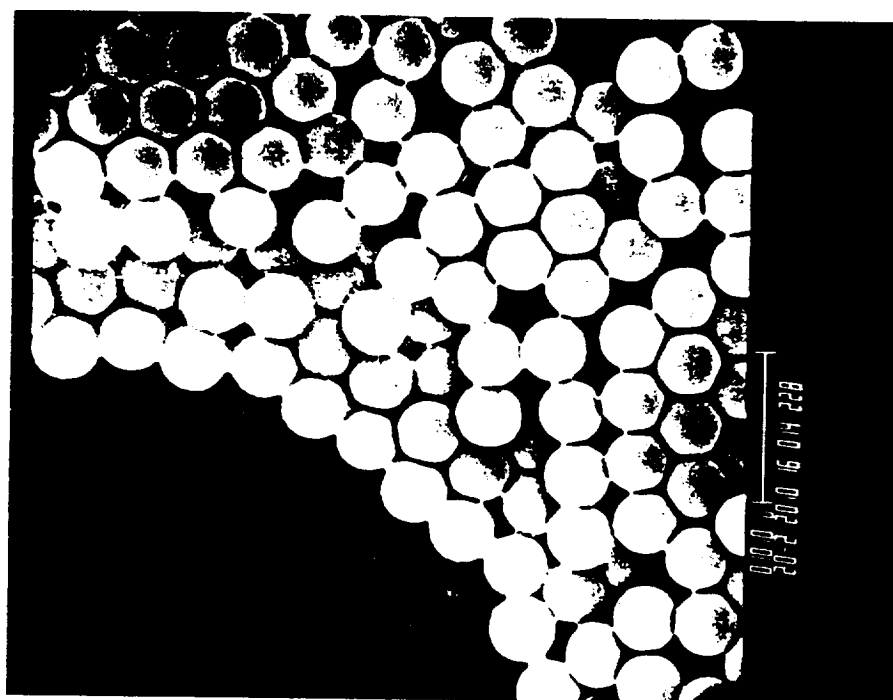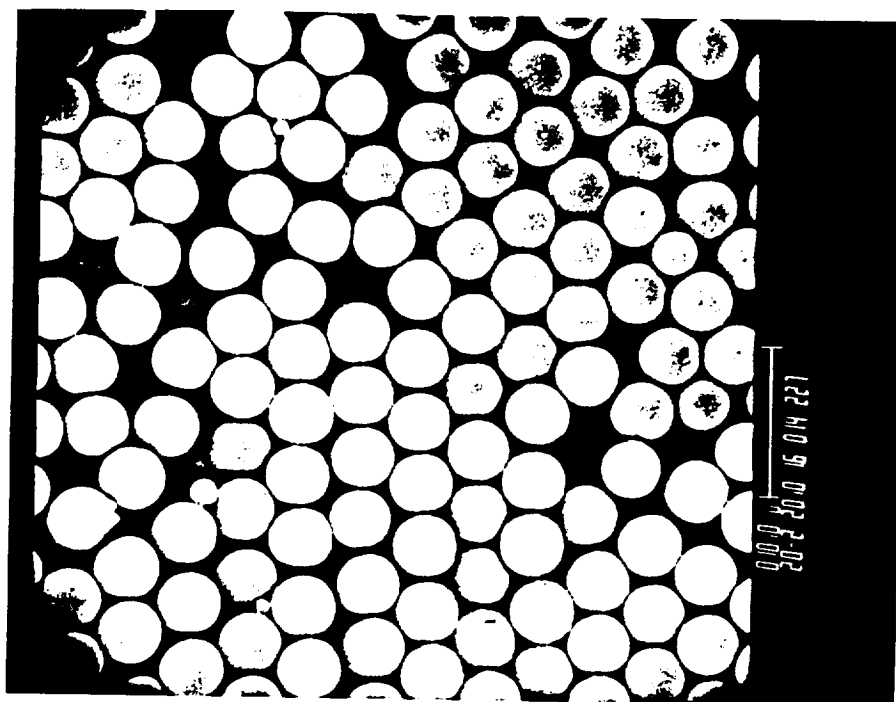
Figure 3-39. SEM micrographs of latex #5049-2, grown from latex #4140C with NaDMDTC inhibitor.
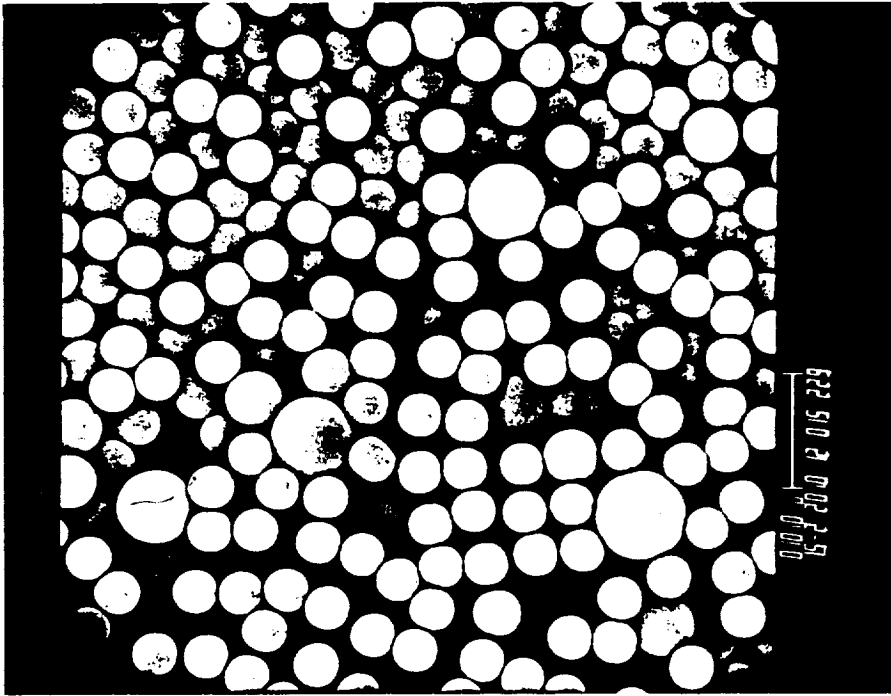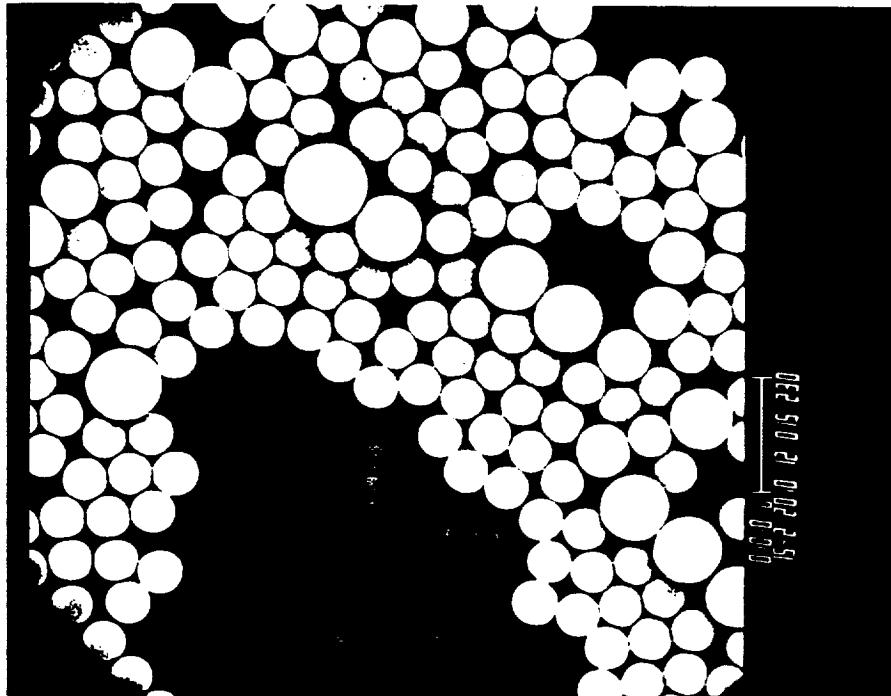
Figure 3-40. SEM micrographs of latex #5049-3, grown from latex #4140C
with DMHAHCl inhibitor.
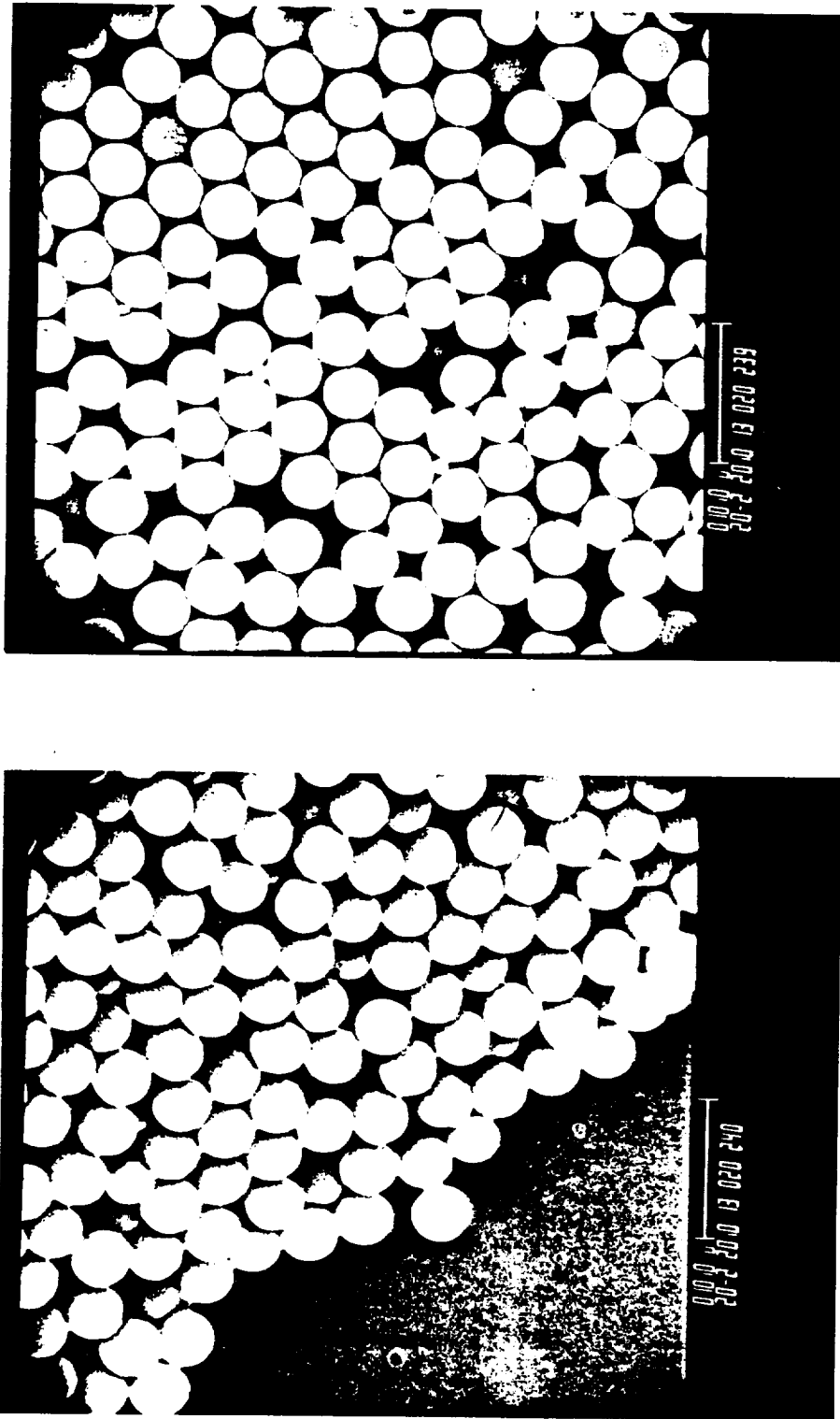
Figure 3-41. SEM micrographs of latex #5057-2, grown from latex #4140C with BQ inhibitor.

CHAPTER 4

SURFACTANTS

Surfactants play important roles in the preparation of monodisperse latexes. One of the requirements in preparing monodisperse latexes from monomer by direct emulsion polymerization is that the particle nucleation stage be short relative to particle growth stage. Emulsifiers with high critical micelle concentrations (c.m.c.'s) are preferable to those with lower c.m.c.'s. On the other hand, the emulsifier must have enough surface activity to stabilize latex particles. In seeded polymerization, careful control of the emulsifier concentration would eliminate the nucleation stage, thus allowing the growth of the seed particles to a larger size without generating a new crop of particles.

4.1 The "Forgiving" Surfactant, Operable Concentration Range, and "Knife-edge"

Every emulsifier has an operable concentration range for a given seeded polymerization system. If the added emulsifier is insufficient to stabilize the latex particles, they will flocculate to form coagulum. If too much emulsifier is added, a new crop of small particles will be formed, and the particle size distribution will become bimodal rather than monodisperse. Vanderhoff et al. [8] showed that, for 0.26 μm polystyrene seed particles grown to 0.36 μm, 1.0-2.5% emulsifier (based on monomer) gave no coagulum and no new particles in the seeding step; lower concentrations gave significant coagulum, and higher concentrations, a new crop of particles.

124

Although the type of emulsifier used in their studies, and in the preparation of Dow monodisperse polystyrene and polyvinyltoluene latexes, has never been revealed, it appeared that Aerosol MA was one of the emulsifiers commonly used [79]. Vanderhoff [80] called Aerosol MA a "forgiving" surfactant, because it gave a relatively wide operable concentration range in which to work. Dezelic et. al. [81] have described in detail the procedures for preparing monodisperse latexes from 0.20 μm to 0.95 μm diameter by seeding. They confirmed that the best results were obtained using Aerosol MA in concentrations smaller than 0.1% (based on total recipe) and monomer/polymer ratios smaller than 10.

The range of operable emulsifier concentration is relatively broad at small particle sizes, but with increasing particle size it becomes smaller and smaller, until at sizes above 1 μm it becomes a "knife-edge", i.e., duplicate polymerizations may give either a partially-flocculated monodisperse latex or a stable latex containing a new crop of small particles [11]. It is widely accepted that the emulsifier concentration in the aqueous phase must be lower than the c.m.c., or the emulsifier surface coverage on the particles (NB: in discussing surface coverage, earlier workers usually assumed that all of the added emulsifier adsorbed on the particle surface and disregarded the equilibrium between adsorbed and solute emulsifier) must be below 100%, to avoid the formation of a new crop of particles [8, 82, 83], although in some cases, especially at small particle sizes, the surface coverage may be greater than 100% using certain combination of anionic and nonionic surfactants [84, 85]. Dodge et al.

125

[86] used a combination of anionic emulsifier, sodium dodecylbenzene sulfonate, and nonionic emulsifier, Triton X-100, to prepare monodisperse latex particles of 1.25 μm diameter by four successive seeded polymerizations of vinyltoluene on 0.24 μm diameter polystyrene seed particles. They found that, at 50% solids, final surface coverages of less than 50% resulted in unstable latexes, while surface coverages greater than 70% resulted in the generation of new particles. Attempts by those authors to obtain larger particles by further seeding were unsuccessful owing to the generation of a crop of new small particles.

The difficulties of preparing monodisperse latexes larger than 1 μm in size can be explained in more detail. First, the particle population density decreases with increasing particle size for seeded polymerizations at a constant solids content, so that the probability of the particles capturing radicals generated in aqueous phase or transfered out of particles also decreased. Figure 4-1 compares the number of styrene molecules dissolved in the aqueous phase (assuming that emulsifier has little effect on the solubility) and the number of polystyrene particles in latexes of 20% solids with particle sizes ranging from 0.1 to 10 μm diameter. The particle population density for latexes of microscopic size is several orders of magnitude lower than for latexes in submicroscopic size while the concentration of monomer in the aqueous phase remains the same. Therefore, the probability of a free radical reacting with monomer in the aqueous phase and growing to a new particle instead of being captured by an existing particle increases rapidly with increasing particle size.
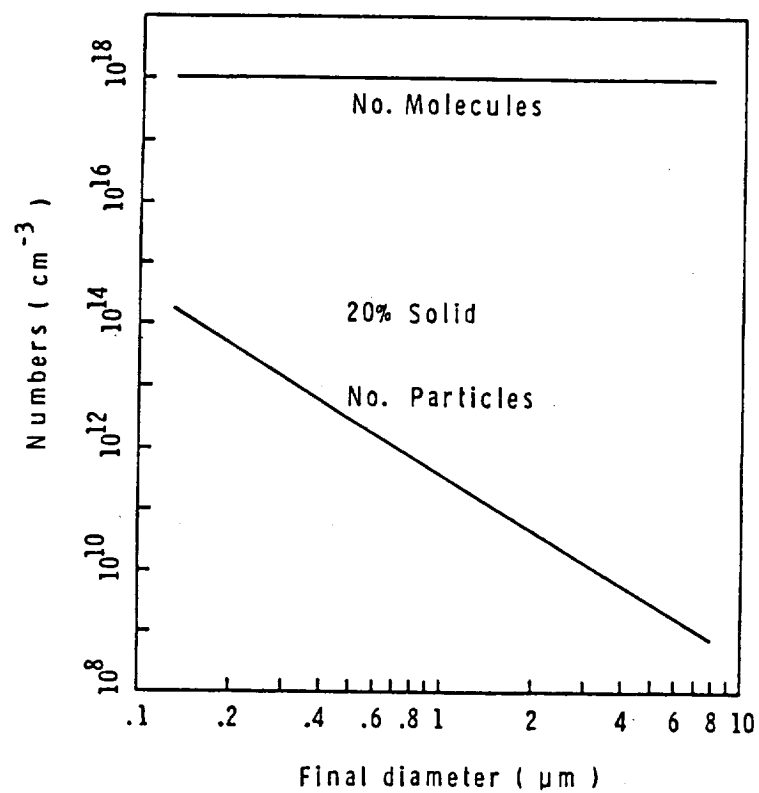
Figure 4-1. Number of polystyrene latex particles and number of aqueous solute styrene molecules in a 20% solid polymerization recipe.

The second problem arises from the free emulsifiers in the aqueous phase. Figure 4-2 shows the amount of the Aerosol MA emulsifier adsorbed on polystyrene particle surface, $[E]_{ads}$, and the equilibrium emulsifier in the aqueous phase, $[E]_{aq}$, at 50% surface coverage in 20% solids latexes of various sizes. The equilibrium concentrations were calculated based on the adsorption isotherm obtained by Ahmed [87] using the serum replacement method. A sample calculation is given in Appendix E. It is clear that, for a given surface coverage and solids content, the adsorbed fraction of the total emulsifier, $[E]_{tot}$, decreases rapidly as the particle size increases. Instead of being adsorbed on the surface and contributing to the stability of the existing particles, the free aqueous emulsifier would participate in nucleation of small particles. Figure 4-3 is a schematic diagram for the operable range of Aerosol MA emulsifier concentration in a 20% solids polymerization recipe. The $[E]_{tot}$ curve for 30% surface coverage is set as the lower limit of the emulsifier concentration, based on an arbitrary assumption that the total emulsifier concentration required to achieve 30% surface coverage, including the emulsifier in the aqueous phase, is the minimum to give a stable product in a seeded polymerization. The $[E]_{ads}$ curve for 70% surface coverage is set as the upper limit of emulsifier concentration, based on the assumption that a new crop of small particles would be generated if the total emulsifier concentration exceeds the amount required for 70% particle surface, excluding the emulsifier in the aqueous phase. The region between these two curves then is the operable emulsifier concentration range

in seeded polymerizations for preparing stable latexes without generating small particles. These two curves intersect at particle size about 2 μm, in good agreement with the "knife-edge" emulsifier concentration range observed in the 1-2 μm size range. This diagram illustrates qualitatively the narrowing of the operable emulsifier range with increasing particle size. The actual upper and lower limit of the emulsifier concentration depends on many factors, such as the type of emulsifier, the solids content, and the criteria for stability and nucleation.

Another factor which makes the preparation of large-particle-size latexes difficult is that larger particles usually require more stabilization than smaller particles polymerized under similar mechanical shear. The London-van der Waals attraction between two particles is directly proportional to particle size. In addition, a larger particle has a greater kinetic energy than a smaller particle travelling at the same speed. Therefore, larger particles have a greater tendency to collide with one other and form coagulum than smaller particles, even when they have similar repulsion energies. Moreover, the oil soluble initiators preferred in the preparation of large-particle-size latexes, to eliminate new small particle generation (as discussed in Chapter 3) usually do not contribute to the particle surface charge. The lack of electrostatic repulsion except that from adsorbed ionic emulsifier makes the particles even more difficult to stabilize.
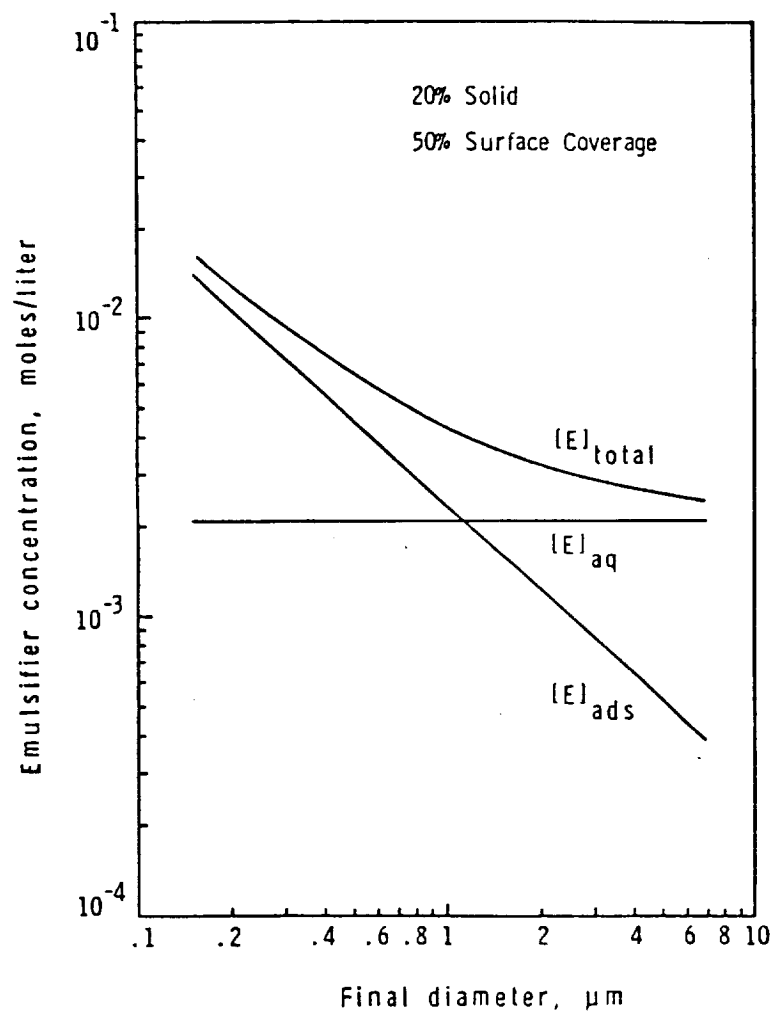
Figure 4-2.   Distribution of Aerosol MA emulsifier
between the particle surface and the aqueous phase in
a 20% solids latex with 50% surface coverage.
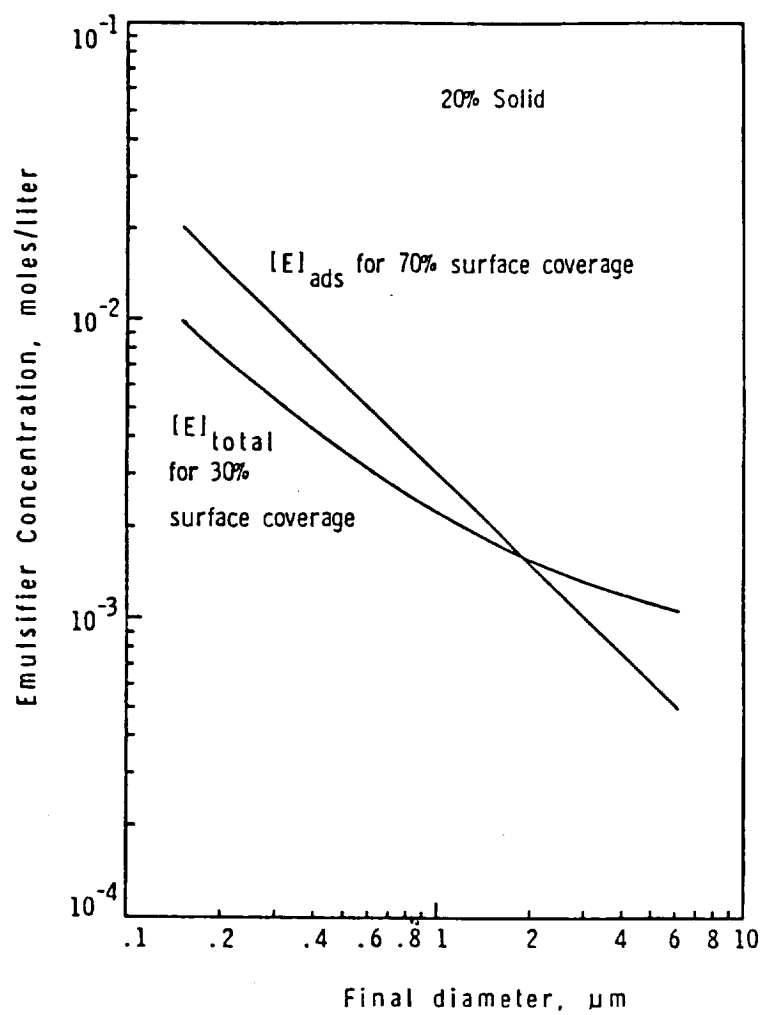
Figure 4-3. Operable range of Aerosol MA emulsifier concentration in a 20% solid polymerization recipe.

4.2 Anionic, Nonionic, Copolymerizable, and Polymeric Surfactants

A thorough search has been conducted in order to find surfactants for stabilizing large-particle-size latex particles (>2 μm) in a seeded polymerization without generating new particles. Table 4-1 lists the anionic, nonionic emulsifiers and copolymerizable surfactants used in this study. Table 4-2 lists the water-soluble polymers and oligomers evaluated as colloid stabilizers, which will be referred to hereafter as polymeric surfactants.

Surface tension-concentration curves of several surfactant solutions determined by the du Nouy ring method, are presented in Figure 4-4. Those curves without symbols were based on the values from the technical bulletins of the suppliers. Among these surfactants, Triton X-100 showed the highest surface activity while Cops I showed the lowest surface activity.

It is the fraction of surfactant adsorbed on the particle surface that contributes directly to the particle stability. The amount of surfactant adsorbed on the surface of a monomer-swollen latex particle could probably be correlated with its ability to reduce the interfacial tension at the monomer-water interface. The drop volume method (see Chapter 2) was used to determine the interfacial tension as a function of surfactant concentration. Figure 4-5 presents the results for several anionic surfactants. Low-molecular-weight surfactants, Aerosol OT and Aerosol MA, reduced the interfacial tension continuously and smoothly with increasing concentration. Even surfactants of higher molecular weight, such as poly(acrylamide-acrylic acid) and Polywet KX-3, followed the same trend. On the other

Table 4-1.   Anionic, Nonionic and Copolymerizable Surfactants

Trade Name	Abbrev.	Manufacturer	Identity
Aerosol MA	AMA	American Cyanamid	Sodium dihexyl sulfosuccinate
Aerosol OT	AOT	American Cyanamid	Sodium dioctyl sulfosuccinate
- -	SDS	Eastman Kodak	Sodium dodecyl sulfate
DS-10	SDBS	Alcolac	Sodium dodecylbenzene sulfonate
Triton X-100	-	Rohm & Haas	Octylphenoxyl polyethoxy ethanol
Tween 20	-	ICI Americas	Polyoxyethylene sorbitan laurate
Tween 80	-	ICI Americas	Polyoxyethylene sorbitan oleate
Cops 1	-	Alcolac	A short-chain vinyl sulfonate
- -	NaSS	Dow	Sodium styrene sulfonate
- -	NaVTS	Dow	Sodium vinyltoluene sulfonate

Table 4-2.   Polymeric Surfactants

Trade Name	Abbrev.	Manufacturer	Identity
Methocel MC	MC	Dow	Methyl cellulose, 10 cps
Cellosize WP-09	HEC	Union Carbide	Hydroxyethyl cellulose
PAM 50	PAM	American Cyanamid	Polyacrylamide
Polyox WSR N-10	PEO	Union Carbide	Polyethyleneoxide, $MW=10^5$
Vinol 205	PVOH	Air Products	Polyvinyl alcohol, 88% hydrolyzed
PVP K-30	PVP	GAF	Polyvinylpyrrolidone, $MW=4 \times 10^4$
CMC 7L	CMC	Hercules	Carboxymethyl cellulose
— —	—	Polyscience	Polyacrylic acid, $MW=8 \times 10^4$
— —	—	Aldrich	Polyacrylic acid, $MW=2 \times 10^3$
— —	P(AM-AA)	Polyscience	Poly(acrylamide-acrylic acid), $MW=2 \times 10^5$
Gantrez An-119	P(MVE-MA)	GAF	Poly(methyl vinyl ether-maleic anhydride)
Polywet KX-3	KX-3	Uniroyal	$RX(CH_2CR^1Y)_a-(CH_2CR^2Z)_b$, $MW=1.5 \times 10^3$

hand, carboxymethyl cellulose, 7L, had very little effect on the interfacial tension.

Figure 4-6 compares interfacial tension-concentration curves of solutions of nonionic polymeric surfactants. Among them, polyvinyl alcohol, Vinol 205, showed an unusual interfacial activity, it reduced the interfacial tension continuously as the concentration increased, reaching 10 dyne/cm at high concentrations. For polyvinylpyrrolidone, K-30, and hydroxyethyl cellulose, Cellosize WP-09, the interfacial tension decreased to 21-26 dyne/cm at concentrations <0.01% and then leveled off. Polyacrylamide, PAM 50, had a much smaller effect on the interfacial tension than the other three surfactants. Polyvinylpyrrolidone, K-30, and hydroxyethyl cellulose, Cellosize WP-09, turned out to be the most satisfactory polymeric surfactants evaluated in this study.

Although Aerosol MA is an excellent surfactant for the preparation of monodisperse latexes in submicron sizes, it is ineffective in stabilizing particles >2 μm for swelling and subsequent polymerization. Swelling of large-particle-size latexes with monomer in the presence of this surfactant usually gave a viscous layer on the top of the dispersion, indicating that the stability was poor. Polymerization with this type of recipe always resulted in the formation of much coagulum and many new small particles. Anionic surfactants with higher surface activity such as Aerosol OT and sodium dodecyl sulfate improved the stability to some extent, but they resulted in the generation of small particles.

Nonionic surfactants, including Triton X-100, Tween 20, Tween 80,

135
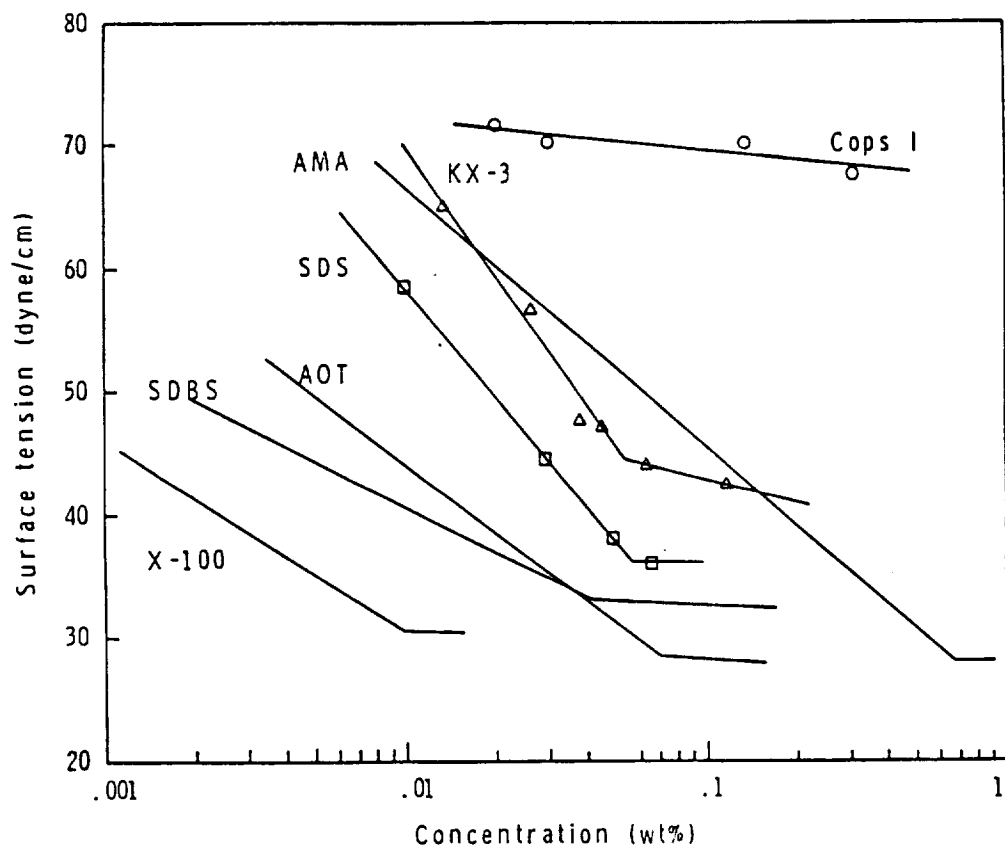
Figure 4-4. Surface tension-concentration curves of surfactant solutions.

136
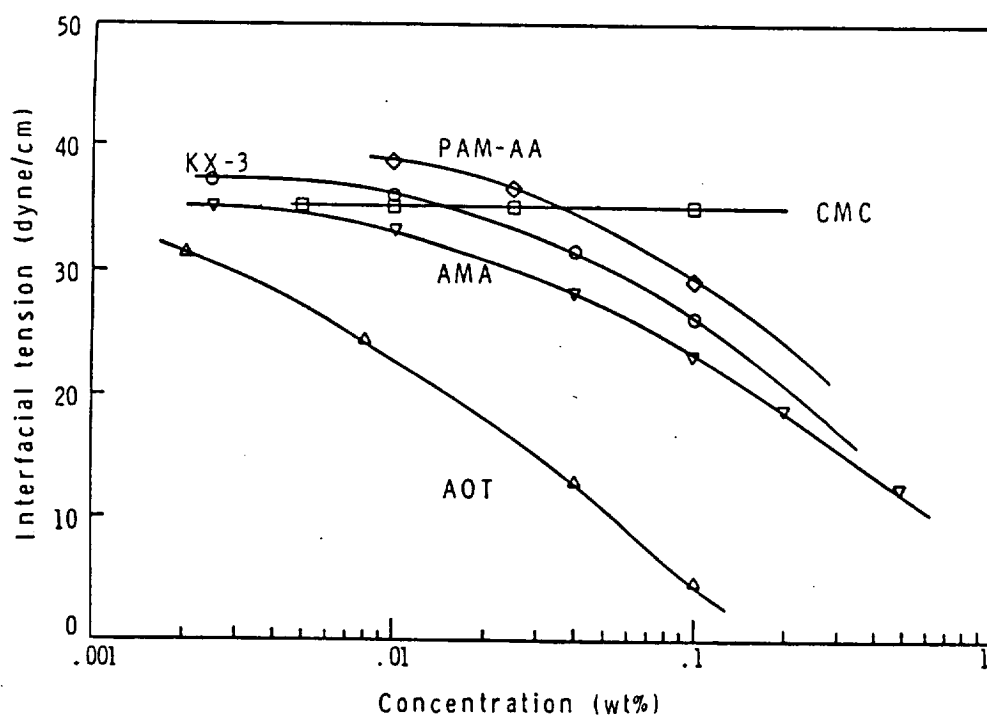
Figure 4-5. Interfacial tension-concentration curves of styrene-anionic surfactant solutions.
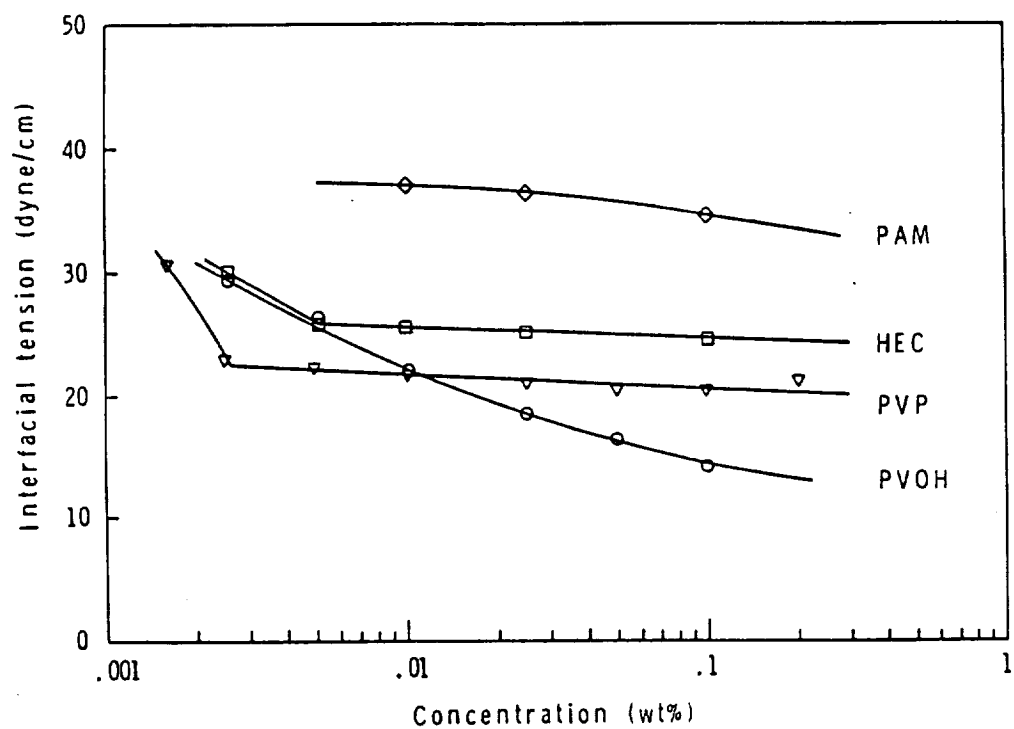
Figure 4-6.   Interfacial tension-concentration
curves of styrene-nonionic polymeric surfactant
solutions.

and their combinations with anionic surfactants, were tried as substitutes for Aerosol MA in stabilizing latex particles larger than 2 μm. None of them were found to be satisfactory; they resulted in the generation of new small particles without improving the stability of the large particles.

Some copolymerizable surfactants (ionic comonomers) have been used in emulsion polymerization to control surface charge and improve mechanical stability. For example, Greene et al. [88, 89, 90] investigated styrene-butadiene copolymer latexes stabilized with varying amounts of in situ polymerized sodium 9-(and 10)-acrylamido stearate. Krieger et al. prepared emulsifier-free polystyrene latexes using ionic comonomers sodium styrene sulfonate, sodium 2-sulfoethyl methacrylate [91], and sodium vinylbenzenesulfonate [64]. Schild et al. [92] prepared polystyrene latexes using the ionic comonomer sodium 2-acrylamido-2-methyl propane sulfonate. Ahmed [87] compared emulsifier-free polystyrene latexes prepared using ionic comonomers sodium styrene sulfonate, sodium 2-sulfoethyl methacrylate, sodium vinyltoluene sulfonate, and COPS II (an acrylic sulfate; from Alcolac).

Copolymerizable surfactants Cops I, sodium styrene sulfonate and sodium vinyltoluene sulfonate were used in some of our polymerization recipes to increase the surface charge and thus improve the particle stability. Figure 4-7 (left) gives an example of a latex stabilized with Cops I. This latex #2016-3 was grown from a 0.40 μm seed (LS-1103-A) with the telogen t-octyl mercaptan. The telomerized latex was later grown to latex #2051-1 (Figure 4-7 (right)) using polyvinyl-
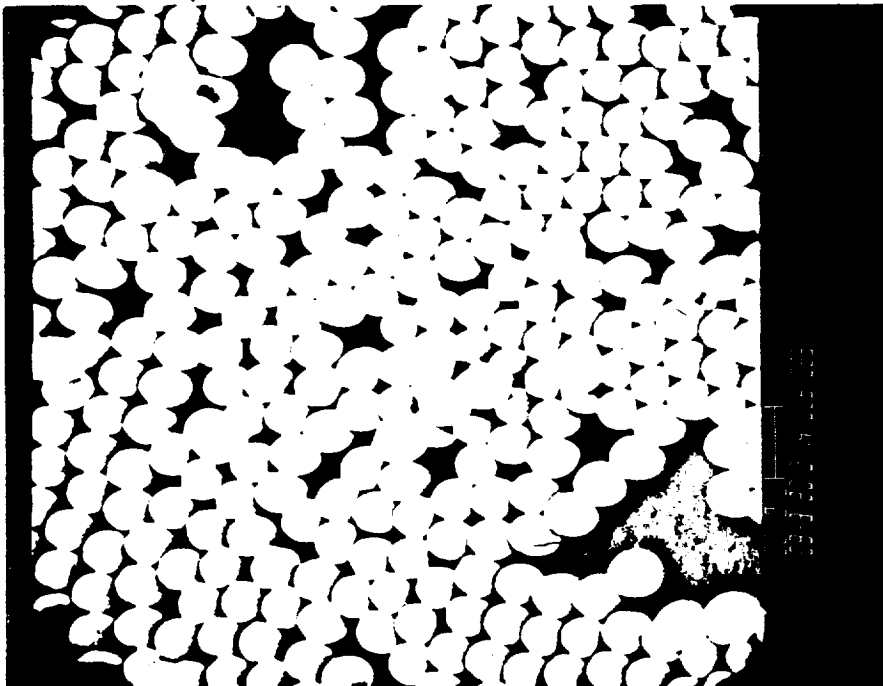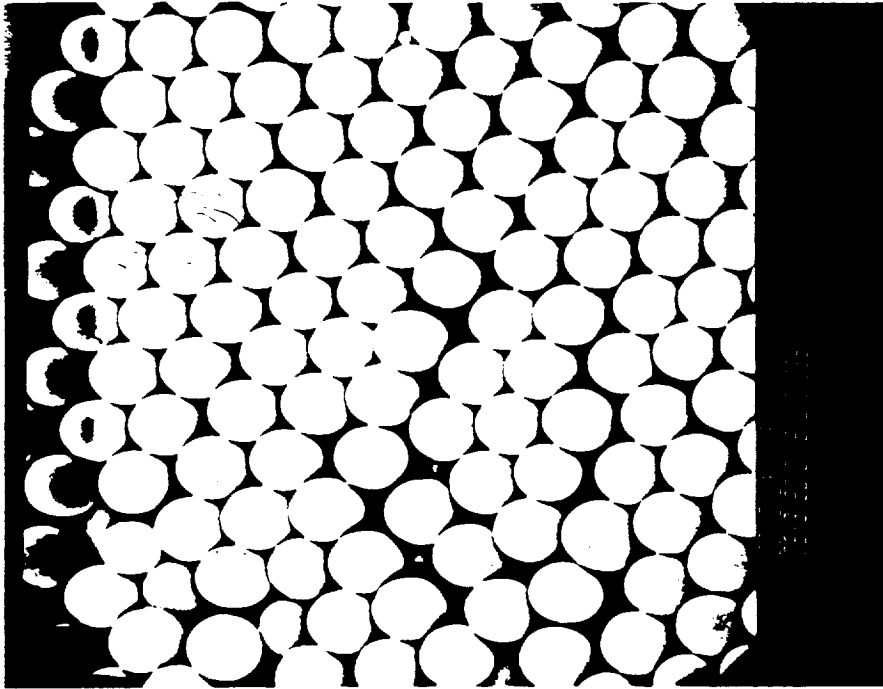
Figure 4-7. SEM micrographs of latex #2016-3 (left) grown from 0.40 μm seed with Cops 1 and latex #2051-1 (right) grown from #2016-3 with PVP.

#4003-2

M/P=14.7
AIBN=0.39%M
AMA=0.13%aq

→ #4061

PVOH=0.11%aq → #4068-2

HEC=0.11%aq → #4068-1

CMC=0.11%aq → #4086-1

P(MVE-MA)=0.11%aq → #4086-2

P(AM-AA)=0.11%aq → #4086-5

PAM=0.11%aq → #4100-3

PAM=0.11%aq
KX-3=0.01%aq → #4108-6

M/P=4.3
AMBN=0.38%M

PVP=0.11%aq
KX-3=0.01%aq → #4100-1

M/P=4.3
AMBN=0.38%M

PVP=0.11%aq
KX-3=0.01%aq → #4108-5

→ #4034

M/P=4.3
AIBN=0.38%M
HQ=0.2%aq

PVP=0.11%aq → #4046

#4035-1

PVP=0.11%aq
Cops I=0.12%aq → #4050-2

PVP=0.11%aq
NaSS=0.12%aq → #4052-1

PVP=0.11%aq
NaVTS=0.12%aq → #4052-2

M/P=4.3
AIBN=0.38%M
HQ=0.2%aq

Figure 4-8.   Polymerization series to grow latex particles from #4005-2 seed particles of 0.63 μm diameter up to 7.4 μm using various surfactants and combinations.

pyrrolidone, K-30, as the stabilizer.

The copolymerizable surfactants used in this study do not adsorb strongly on monomer-swollen latex particles; therefore, they contribute little to the stabilization of the particles during swelling and the early stage of polymerization. For best results, these surfactants should be used in combination with other types of surfactants in seeded polymerization of large-particle-size latexes. Examples of using copolymerizable surfactants with polymeric surfactants to grow latex particles up to 7.4 μm can be found in the polymerization series outlined in Figure 4-8.

Water-soluble polymers have been widely used in suspension polymerization as stabilizers [19, 93]. Winslow and Matreyek [20] in an earlier study showed that the particle size in the suspension polymerization of divinylbenzene could be controlled by agitation, and the type and concentration of stabilizers. They found that high concentrations of high-molecular-weight partially-hydrolyzed polyvinyl alcohol gave spherical particles of small diameter, e.g., 2% polyvinyl alcohol and 740 rpm agitation gave 7 to 38 μm diameter particles and a homogenizing mixer gave 3 to 8 μm diameter particles.

Trommsdorff and Schildknecht [19] defined the modified suspension polymerization that produced particles in 0.5-10 μm range, i.e., the range between suspension and emulsion polymerization, as "dispersion polymerization". Polyvinyl alcohol and a number of other polymers have been used in the dispersion polymerization of vinyl butyrate, methyl vinyl ketone, methyl acrylate, vinyl acetate, methyl methacrylate, and styrene [19, 94, 21, 22, 23, 24, 25].

Numerous studies have been carried out on the adsorption of polyvinyl alcohol onto polystyrene latexes and other substrates. Lankveld and Lyklema [95] studied the adsorption of polyvinyl alcohol on the paraffin-water interface by measuring the interfacial tension as a function of time and concentration. The interfacial tension curve obtained for PVA-88 was similar to the curve obtained in this study for Vinol 205 at the styrene-water interface (Figure 4-6). Both polyvinyl alcohol samples have the same degree of hydrolysis.

Although polyvinyl alcohol is the best known polymeric surfactant, it is not suitable for our system. A seeded polymerization using polyvinyl alcohol, Vinol 205, as stabilizer resulted in a polydisperse product; particles of varying sizes, including a new crop of small particles, were found in the SEM micrograph of the latex (Figure 4-11). Other grades of polyvinyl alcohol were also tried; none of them gave satisfactory results.

Polyvinylpyrrolidone and hydroxyethyl cellulose were found to be promising for stabilizing latex particles >2μm, at the early stages of this study. Figure 4-9 shows micrographs of two latexes prepared with these two surfactants. Both were grown from a 1.5 μm seed, using AIBN initiator and NH_4SCN inhibitor. Latex #2034-2 prepared with hydroxyethyl cellulose contained more new small particles than latex #2034-1 prepared with polyvinylpyrrolidone.

Figure 4-8 outlines a series of seeded polymerizations conducted with various polymeric surfactants and combinations. Several potential polymeric surfactants, including polyvinyl alcohol, hydroxyethyl cellulose, polyacrylamide, carboxymethyl cellulose,

143

poly(acrylamide-acrylic acid), poly(methyl vinyl ether-maleic anhydride), and polyvinylpyrrolidone, were compared in seeded polymerizations usind AIBN initiator and HQ inhibitor to grow particles from 1.5 µm to 2.5 µm. SEM micrographs of the product latexes are given in Figures 4-11 to 4-18. In general, nonionic polymers polyvinylpyrrolidone and hydroxyethyl cellulose resulted in more stable latexes than polyacrylamide and other polymers, judging from the product yields and particle aggregation observed by optical microscopy. Ionic polymers resulted in less stable latexes.

An interesting phenomenon was observed for the recipes using ionic polymeric surfactants: the swollen particles tended to cream and the polymerized particles tended to settle much faster than the particles in the recipes using nonionic polymeric surfactants. The phenomenon was observed even with a very low-molecular-weight polyacrylic acid (MW=$2x10^3$) and the oligomeric surfactant, Polywet KX-3 (MW=$1.5x10^3$). This phenomenon may be attributed to a volume restriction mechanism due to strong charge interaction between ionic polymers. The volume restriction mechanism has been considered theoretically by Asakura and Oosawa [96, 97], and studied experimentally by Sperry et. al. [98, 99].

Other polymeric surfactants evaluated did not give satisfactory results, e.g., polymerization with methyl cellulose gave a dispersion of mm size particles and polyethyleneoxide gave complete coagulation.

Although latexes of 2.5 µm size were successfully prepared with several nonionic polymeric surfactants, a further step to grow the particles to 4.4 µm size could not be achieved with the polymeric

144

surfactant alone. Massive coagulum was formed owing to the lack of electrostatic repulsion between the particles. Since the polymerizations were carried out with an oil-soluble azo initiator, the surface charge density diminished as a result of particle growth. It was then decided to combine a polymeric surfactant with a second type of surfactant in the polymerization recipe to provide both steric and electrostatic stabilization. A few successful examples can be found in Figure 4-8. These include combinations of polyvinylpyrrolidone and polyacrylamide with oligomeric surfactant polywet KX-3, and ionic monomers sodium styrene sulfonate, sodium vinyltoluene sulfonate, and Cops I. SEM micrographs of the product latexes are given in Figures 4-19 to 4-22.

Further polymerization to grow the latex particles to 7.4 μm and larger sizes was eventually achieved with the most promising surfactant combination, polyvinylpyrrolidone and Polywet KX-3. SEM micrographs of the 7.4 μm latex (#4108-5) are given in Figure 4-23. The main particle size distribution appeared to be quite narrow; however, significant numbers of over-size particles were found in the micrographs. The over-size particles are believed to result from coalescence of normal particles during polymerization. The coalescence could be reduced by incorporating a crosslinking agent to harden the seed particles (see Chapter 5).

Polyvinylpyrrolidone is manufactured in the United States in four viscosity grades identified by their K-values [100], K-15, K-30, K-60, and K-90. The number average molecular weights are about 1×10^4, 4×10^4, 1.6×10^5, 3.6×10^5, according to the manufacturer (GAF). All

145

four grades were evaluated in the early stages of this study. It was found that K-30 gave the most satisfactory result in terms of particle-particle stability and prevention of new particle generation. These polyvinylpyrrolidone samples were further analyzed in this laboratory using aqueous GPC (see Chapter 6). The molecular weight distributions are given in Figures 4-24 to 4-27. It was found that the distributions were very broad. At least two peaks were observed in each sample. The number average molecular weights followed the same trend as the values reported by the manufacturer, but the the absolute values were not in good agreement.

The use of polyvinylpyrrolidone in combination with other dispersants as suspension stabilizers had been described earlier [101, 102]. Typical secondary dispersants used with polyvinylpyrrolidone included anionic surfactants, nonionic surfactants, and various water-soluble polymers.

Polyvinylpyrrolidone forms molecular adducts with many other substances [100]. Its ability to interact with the anionic surfactant sodium dodecyl sulfate in aqueous phase has been well-studied [103, 104, 105, 106, 107, 108]. The combination of polyvinylpyrrolidone with other types of surfactants in seeded polymerization has given satisfactory results in this study. The possibility of interaction between these surfactants and the stabilization mechanism of the combination is worth further study.

The adsorption of polyvinylpyrrolidone onto the surface of polystyrene latexes has been studied recently. Kellaway and Najib [109] determined the adsorption isotherms by measuring the polymer

146

content in aqueous phase using refractometry. They found that the adsorption was of Langmuir-type and the extent of adsorption increased with increasing molecular weight; the adsorption reached the saturation plateau at a concentration of 0.75-1.0 g/l.

To determine the conformation of molecules at the interface, Kellaway and Najib correlated the adsorption of polyvinylpyrrolidone and carboxymethyl cellulose with their molecular weights. They made use of the equation developed by Perkell and Ullman [110]:

$$A_s = KM^\alpha, \tag{4-1}$$

where A_s is the monolayer saturation value, M is the molecular weight, and K and α are constants. For polyvinylpyrrolidone, α was found to be 0.16, indicating that the polymer was adsorbed as random coils; for carboxymethyl cellulose, α was found to be 1.0, indicating that the polymer molecule was attached to the latex surface at only one point and the remainder of the molecule protruded into the surrounding medium. The difference in conformation between these two polymers could account for their different effects in lowering the styrene-water interfacial tension (Figures 4-5 and 4-6).

Kellaway and Najib also measured the adsorption layer thickness for various polyvinylpyrrolidone fractions using viscometry and photon correlation spectrometry. The thickness obtained ranged from 4.45 nm to 20.09 nm for MW 1.0-70x10^4 (Table 4-3). Two methods agreed well.

The Polywet surfactants are a family of patented oligomers prepared from one or more polymerizable functional monomers and contains a hydrocarbon end group [111]. Figure 4-28 compares the

147

Table 4-3.   The Adsorption Layer Thickness for
Various PVP Fractions [109]

Molecular Weight	Thickness(nm)
10,000	4.45
24,500	8.25
44,000	16.34
360,000	18.72
700,000	20.09

stabilization mechanism of the Polywet surfactants with conventional
anionic surfactants [112].   The hydrophilic end of the oligomer
adsorbed on particle surface extends far out into the aqueous phase.
The charged chain segments repel each other at greater distance,
creating a more stable dispersion.   The surface activity of this type
of surfactant, and the emulsion polymerization using the surfactant as
the sole emulsifier, has been studied by Roe [113], and White and Jung
[114].   The latexes produced with these surfactants exhibit high
surface tensions, good mechanical stability, and low foaming
tendencies, according to these authors.   Among the different grades of
Polywet surfactants, KX-3 was found to be the most suitable for our
system.
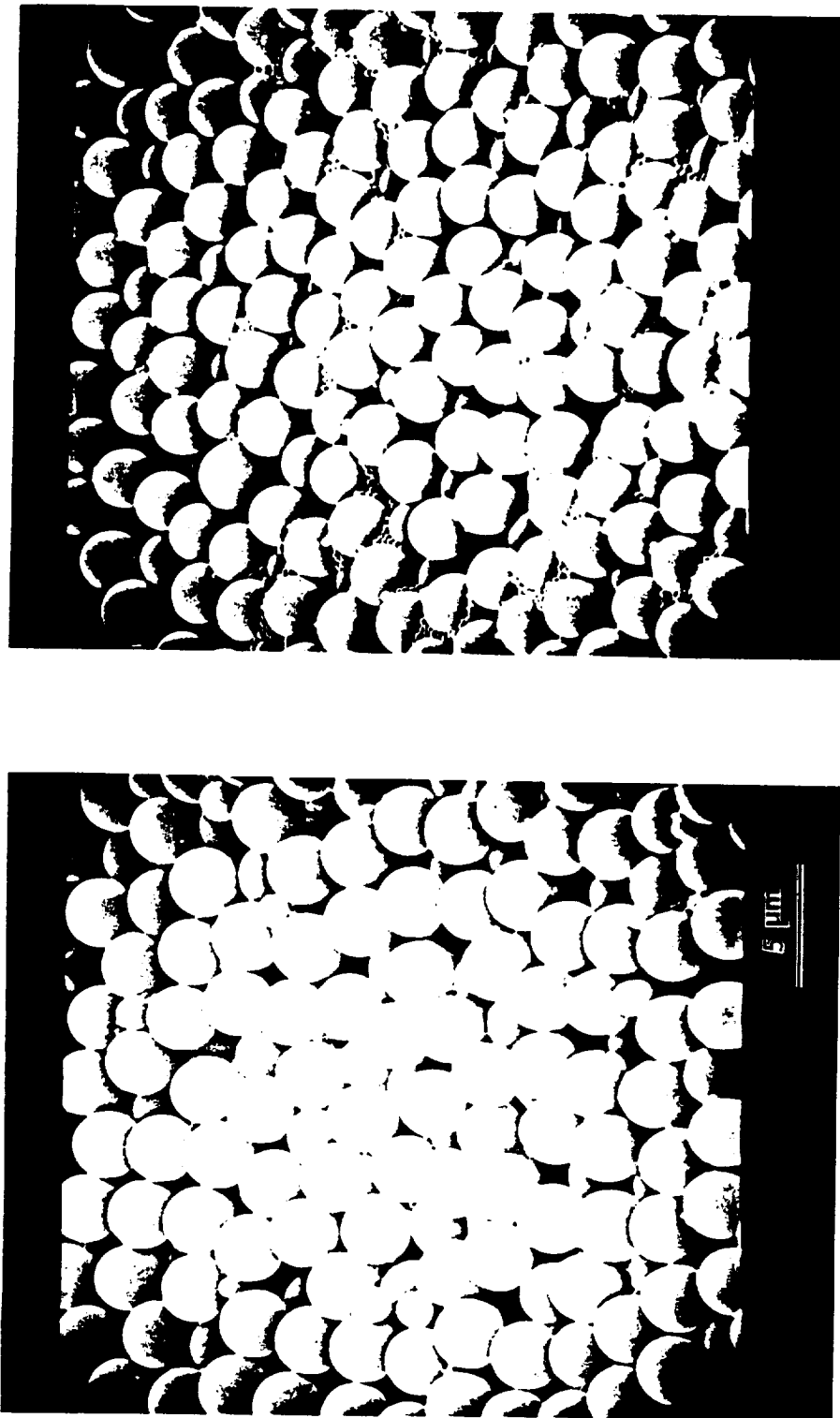
Figure 4-9. SEM micrographs of latex #2034-1 (left) prepared with PVP and latex #2034-2 (right) prepared with HEC.
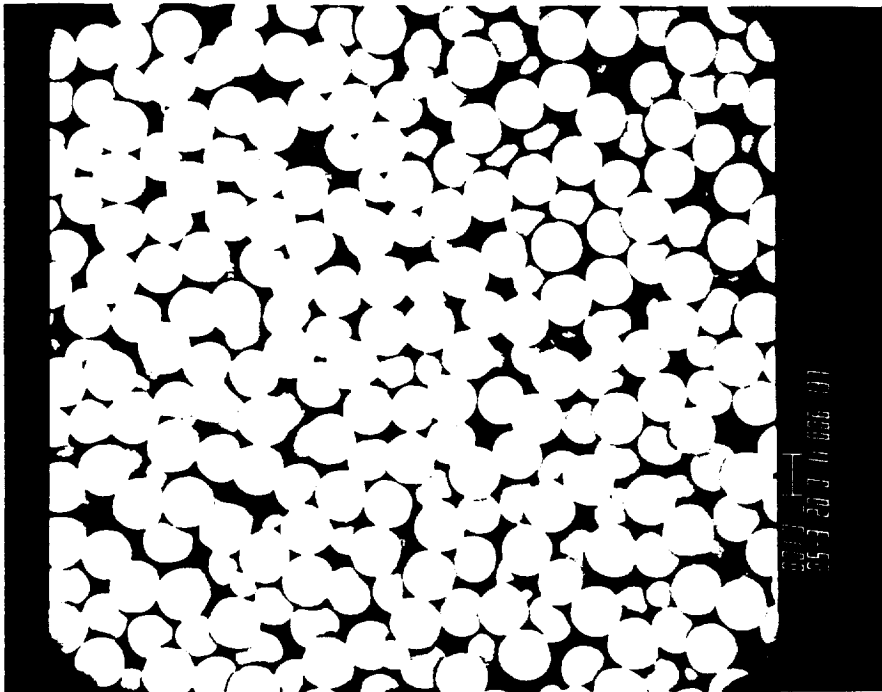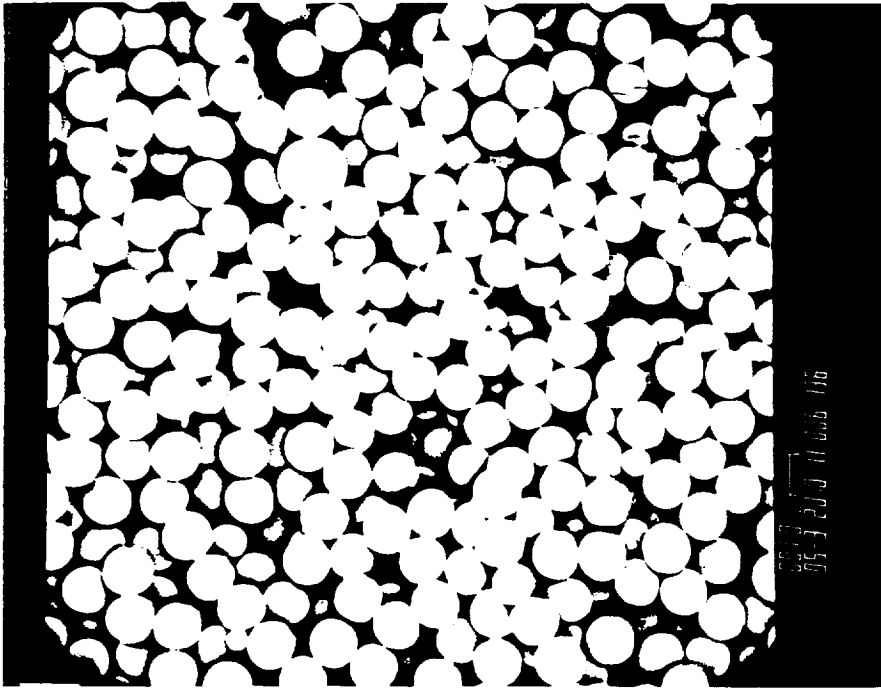
Figure 4-10. SEM micrographs of latex #4061.

150
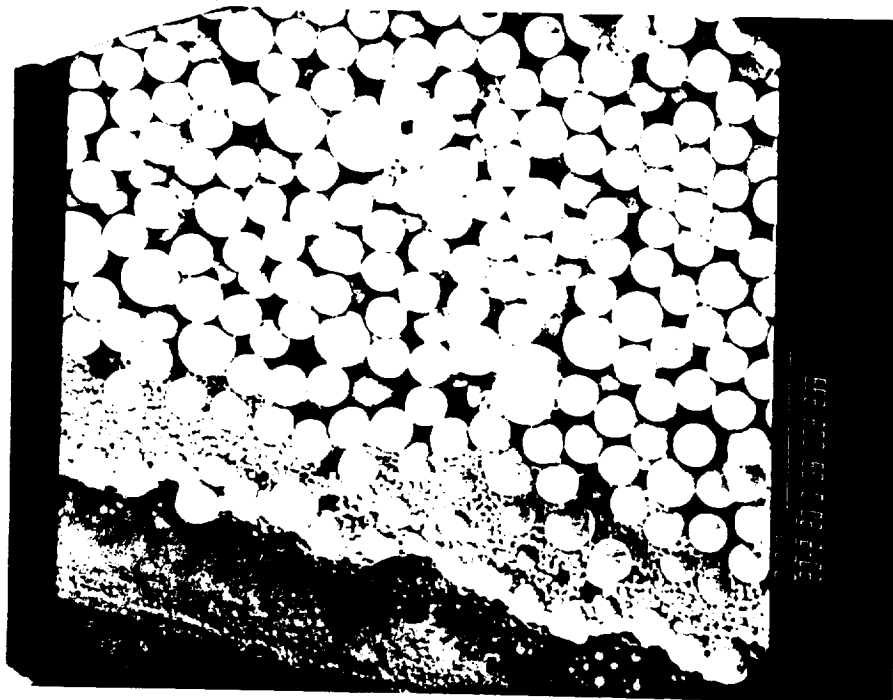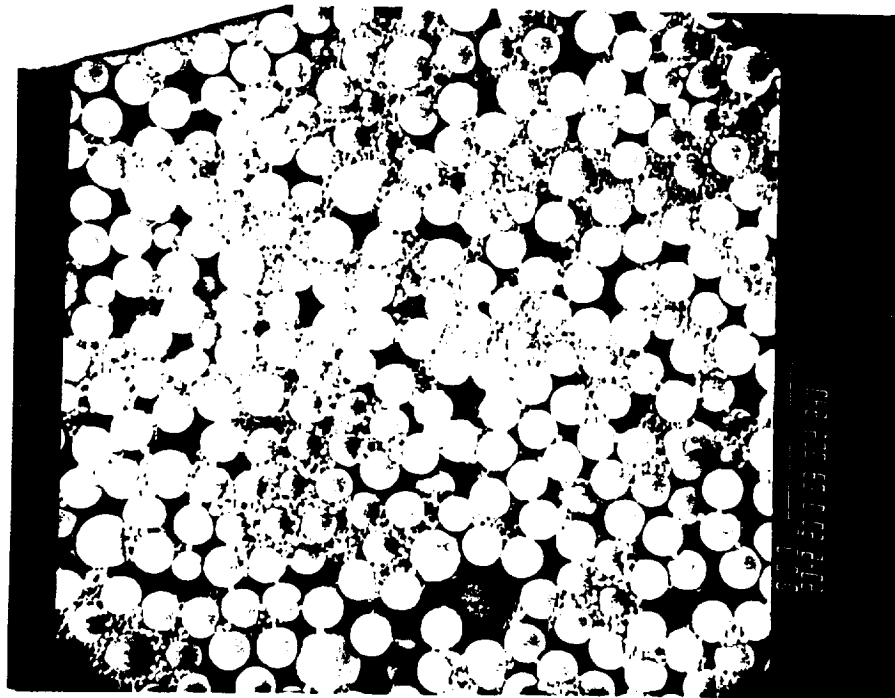
Figure 4-11. SEM micrographs of latex #4068-2 grown from latex #4061 with PVOH.
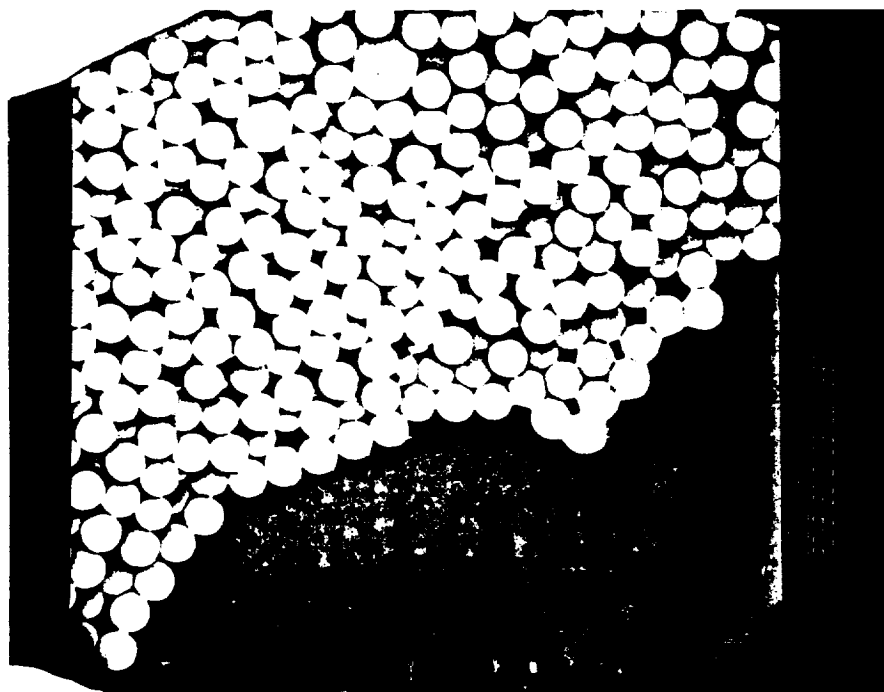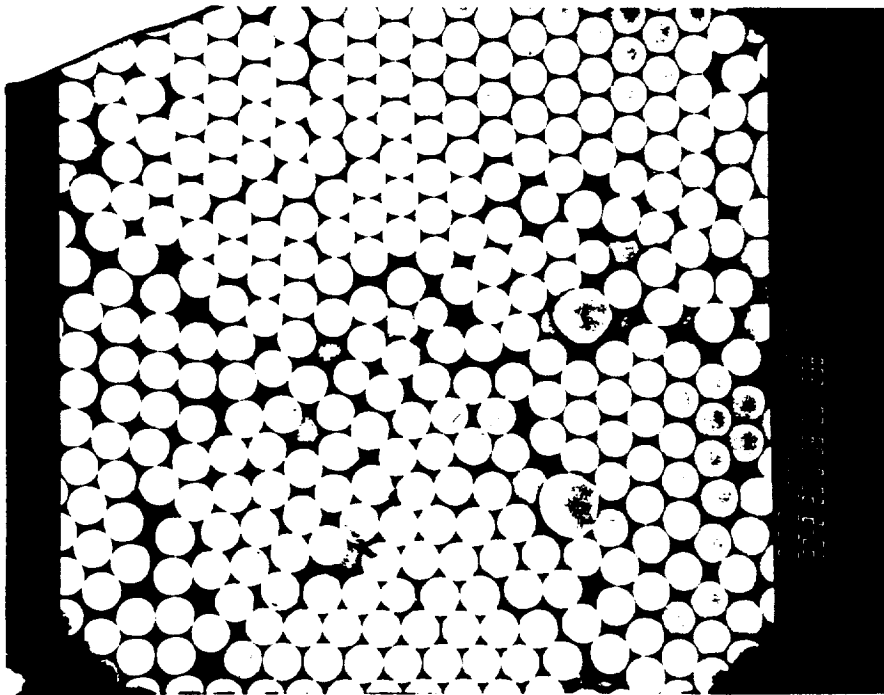
Figure 4-12. SEM micrographs of latex #4068-1 grown from latex #4061 with HEC.
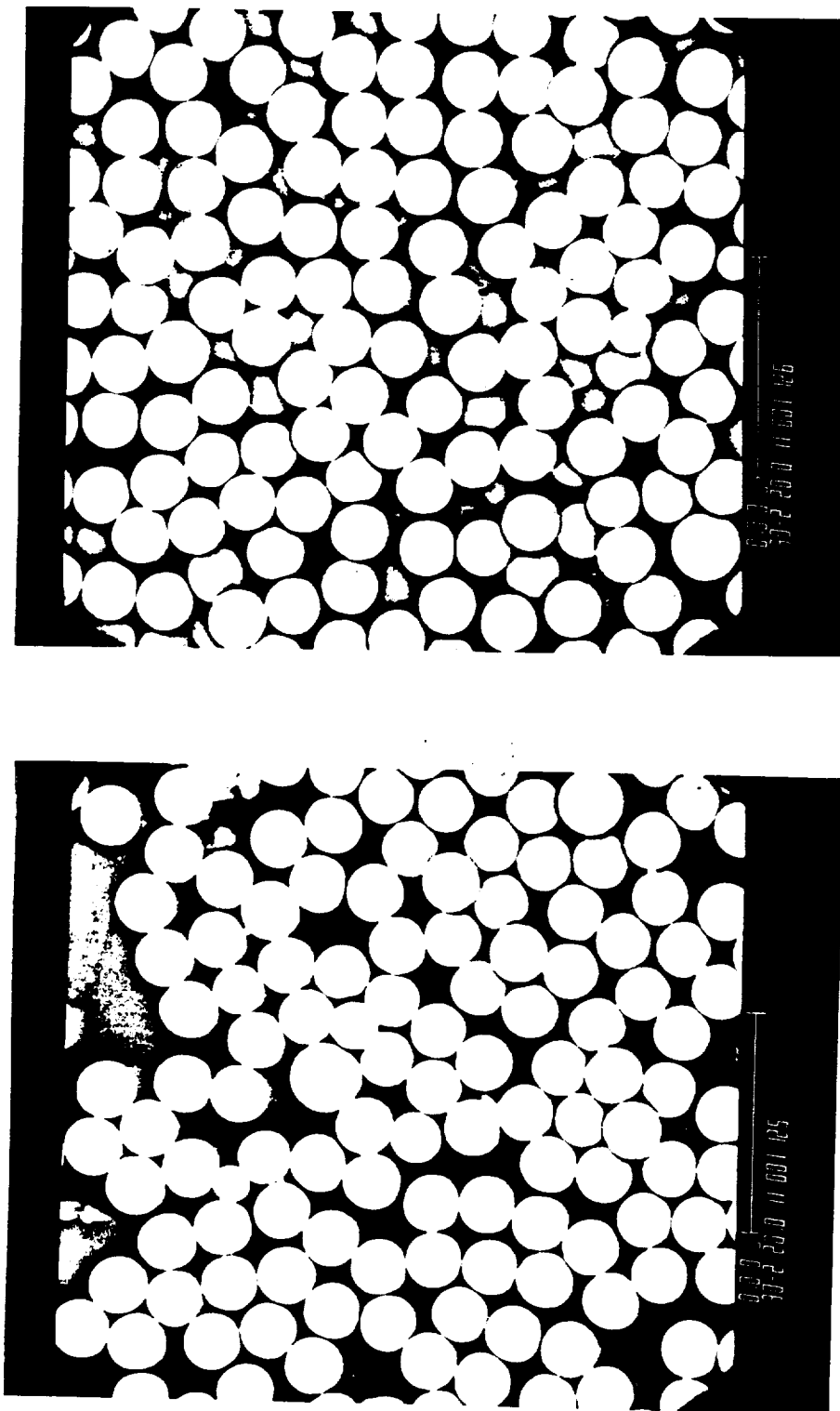
Figure 4-13. SEM micrographs of latex #4086-1 grown from latex #4061 with CMC.
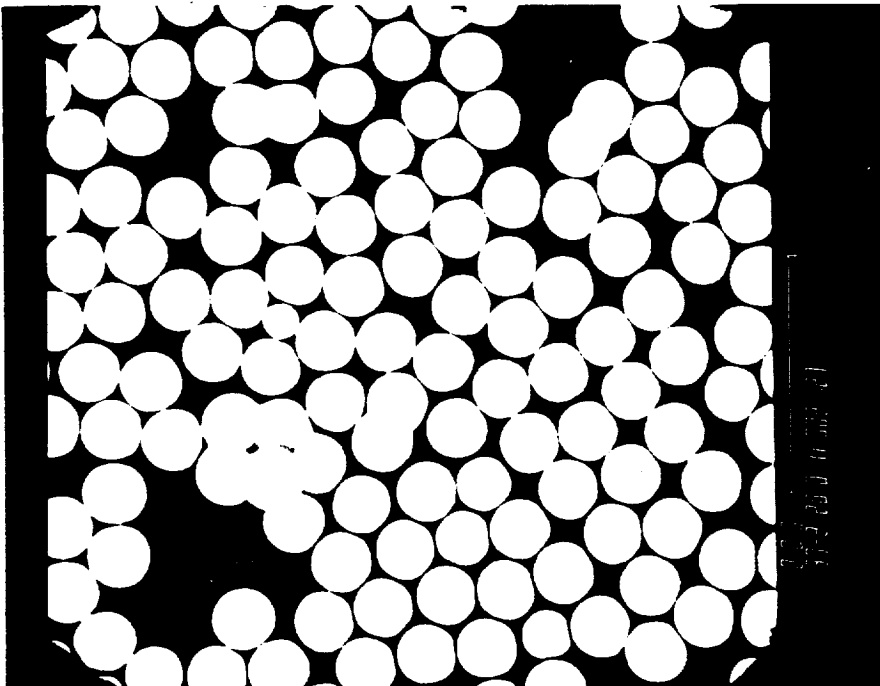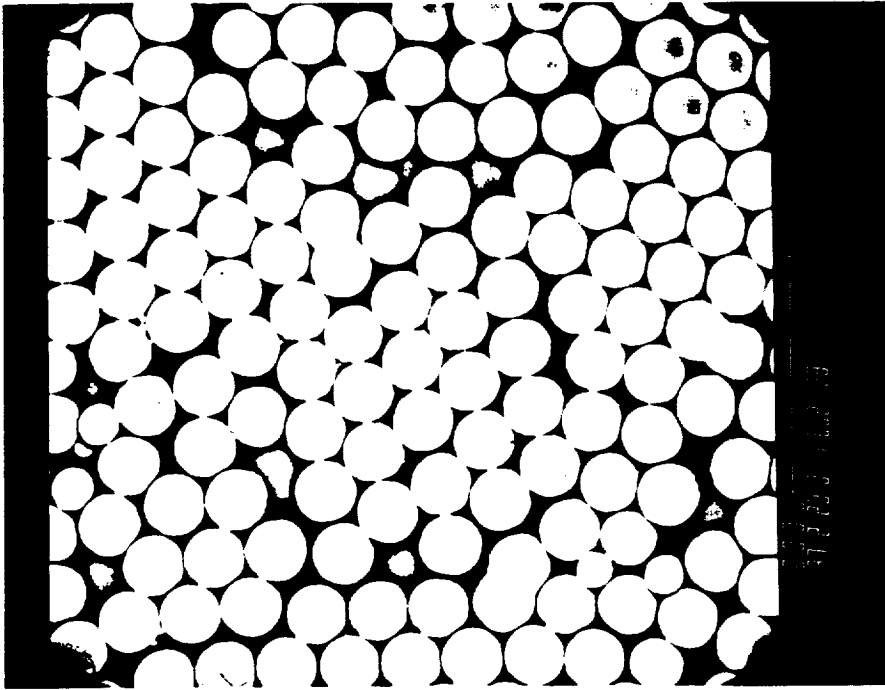
Figure 4-14. SEM micrographs of latex #4086-2 grown from latex #4061 with P(MVE-MA).
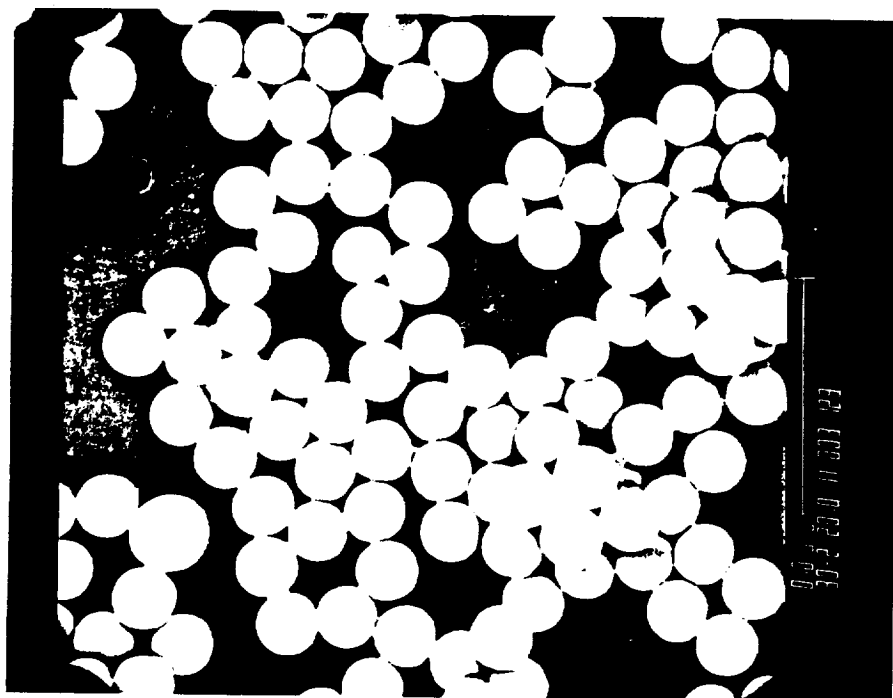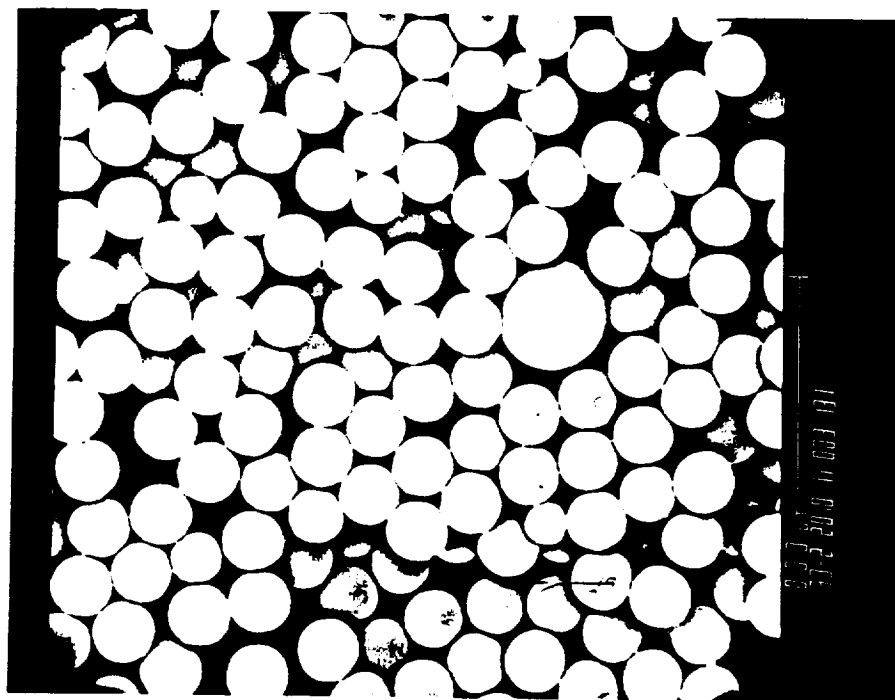
Figure 4-15. SEM micrographs of latex #4086-5 grown from latex #4061 with P(AM-AA).

155
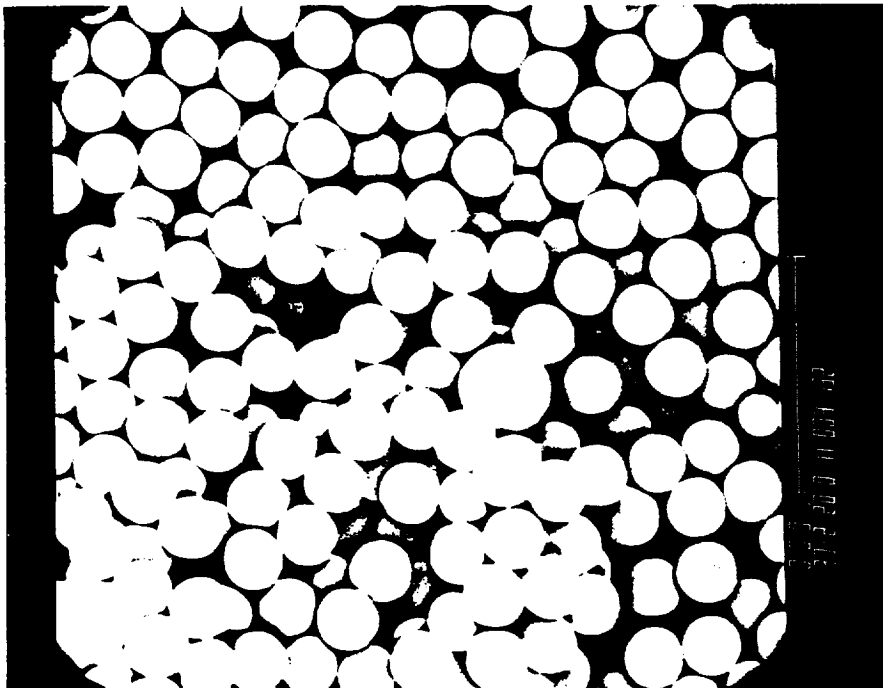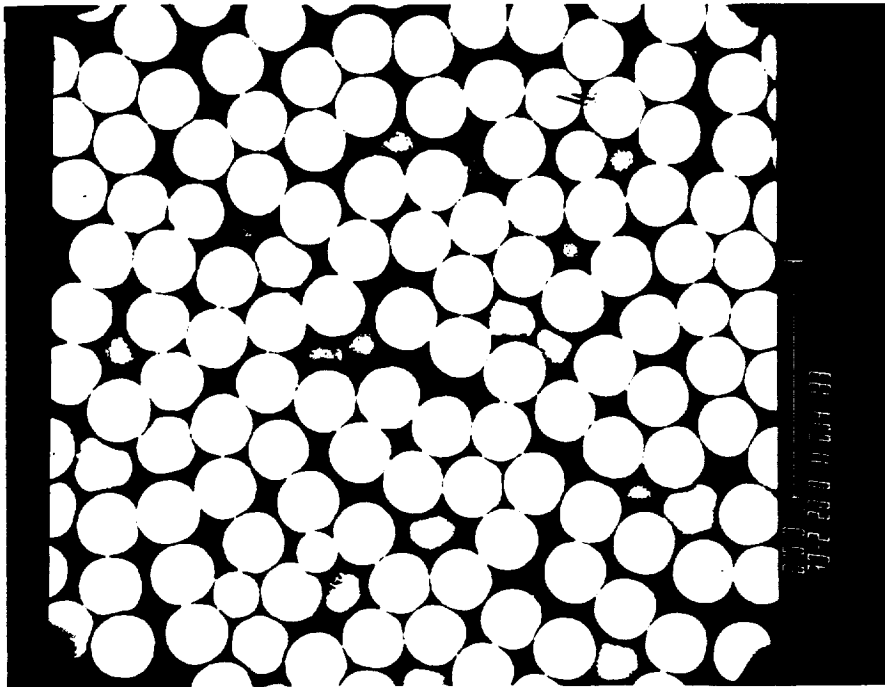
Figure 4-16. SEM micrographs of latex #4100-3 grown from latex #4061 with PAM.
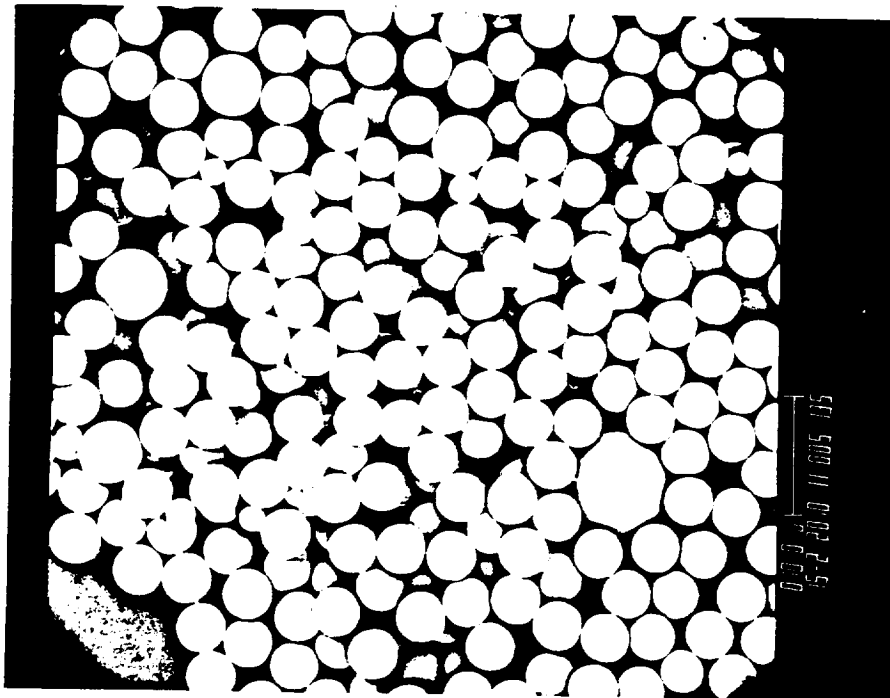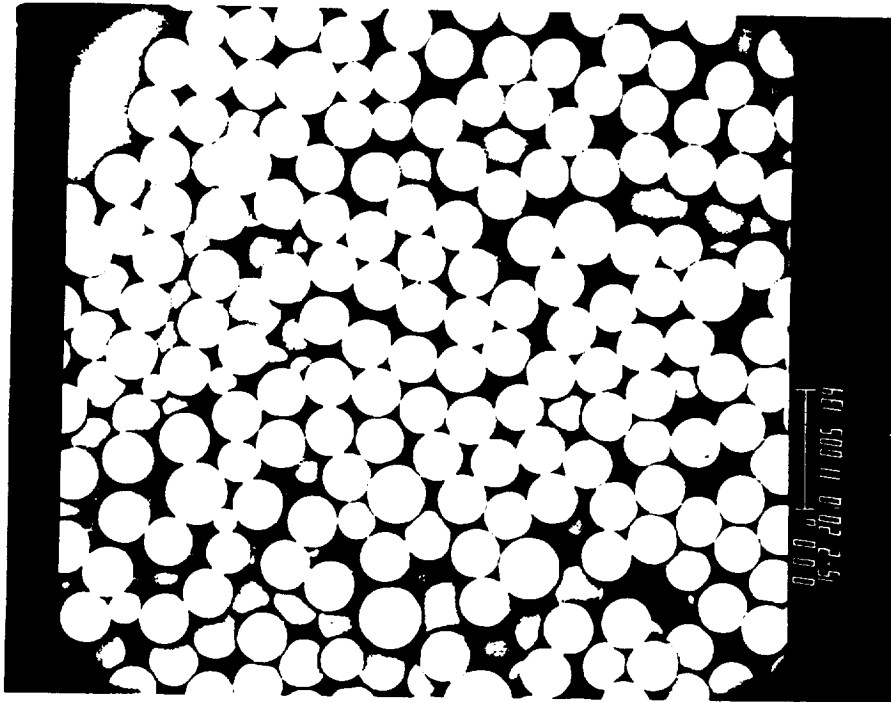
Figure 4-17. SEM micrographs of latex #4108-6 grown from latex #4100-3 with PAM and KX-3.
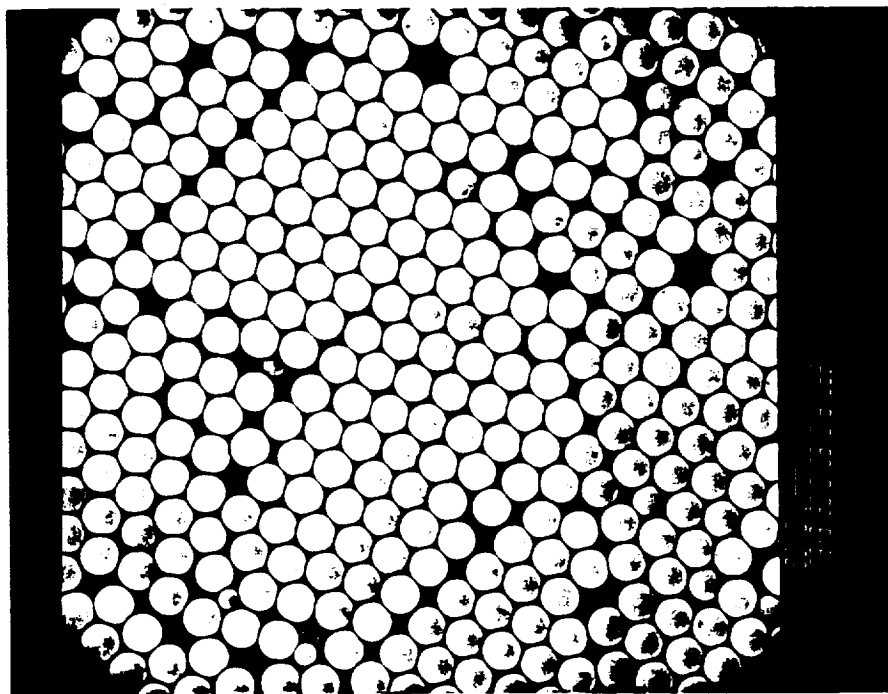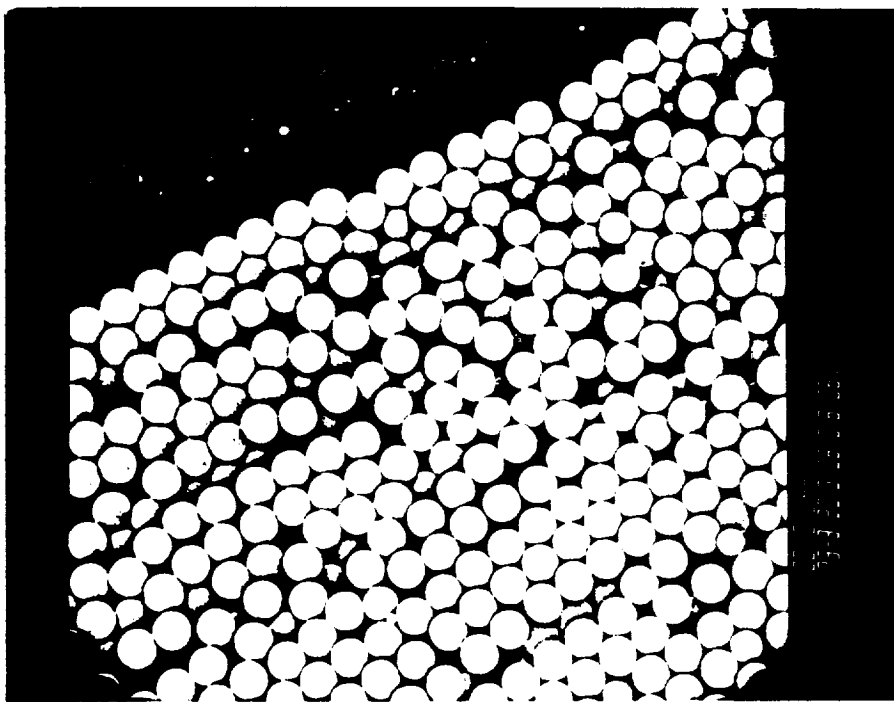
Figure 4-18. SEM micrographs of latex #4035-1 (same recipe as #4046) grown from latex #4034 with PVP.
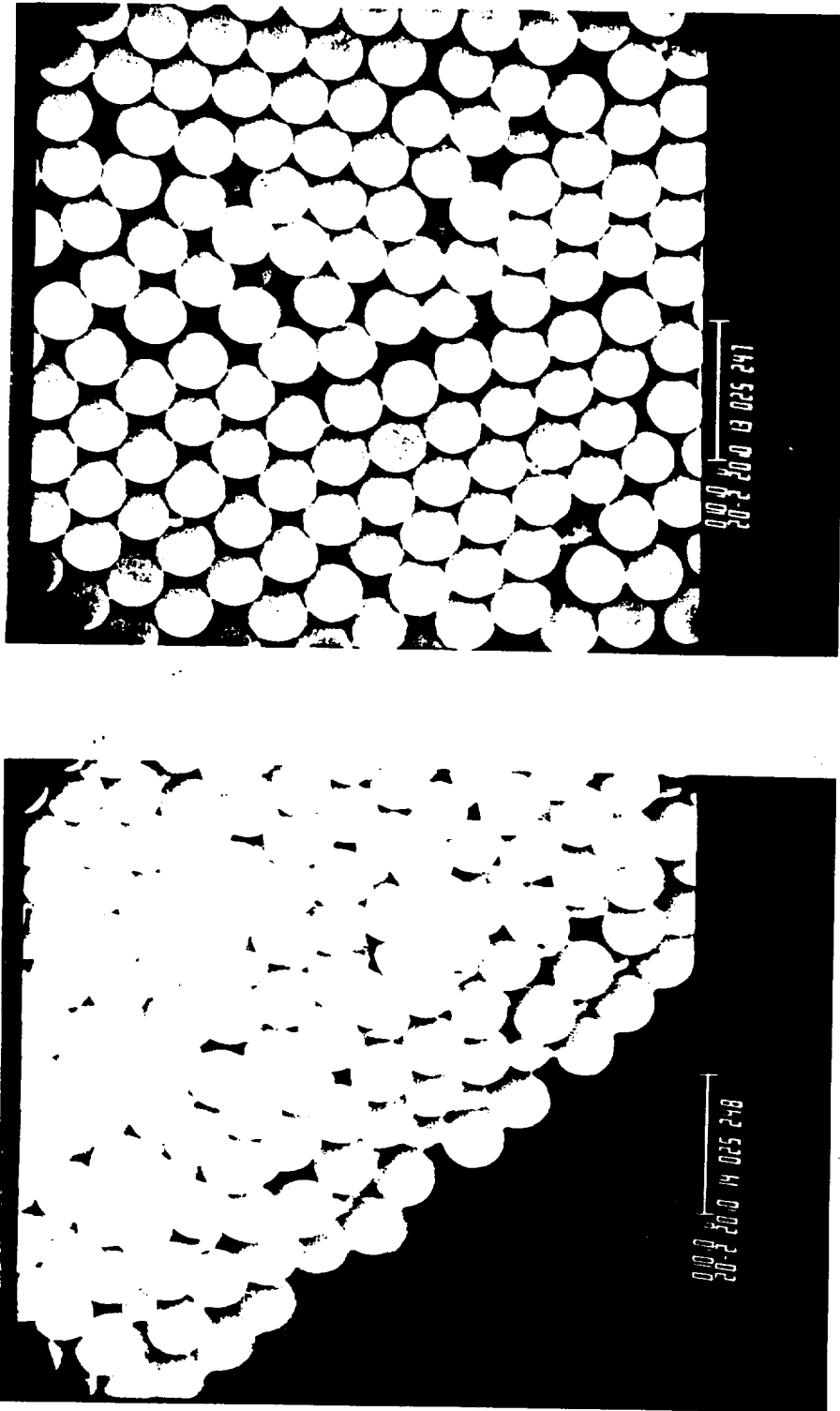
Figure 4-19. SEM micrographs of latex #4100-1 grown from latex #4046 with PVP and KX-〉.
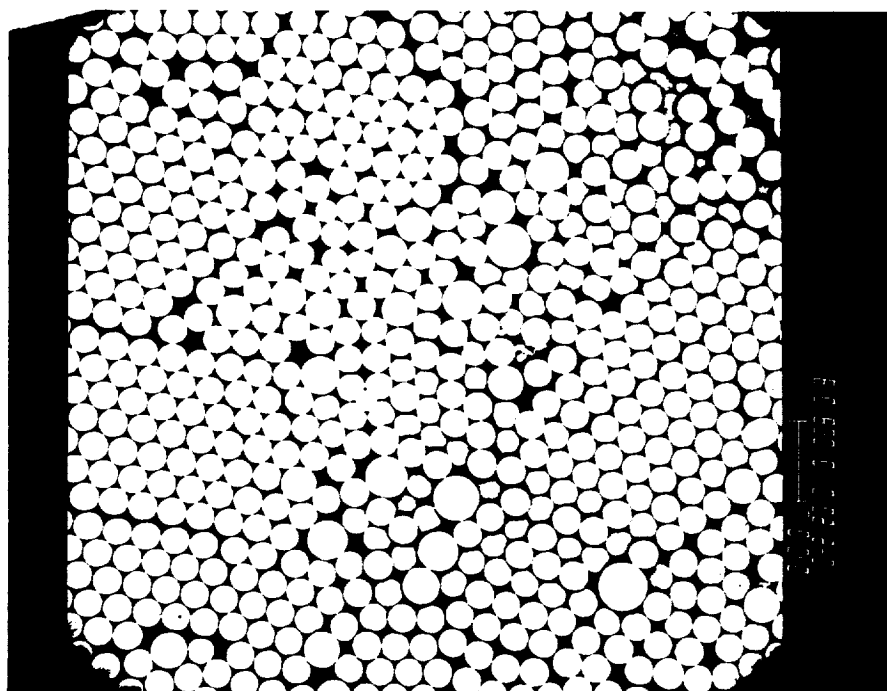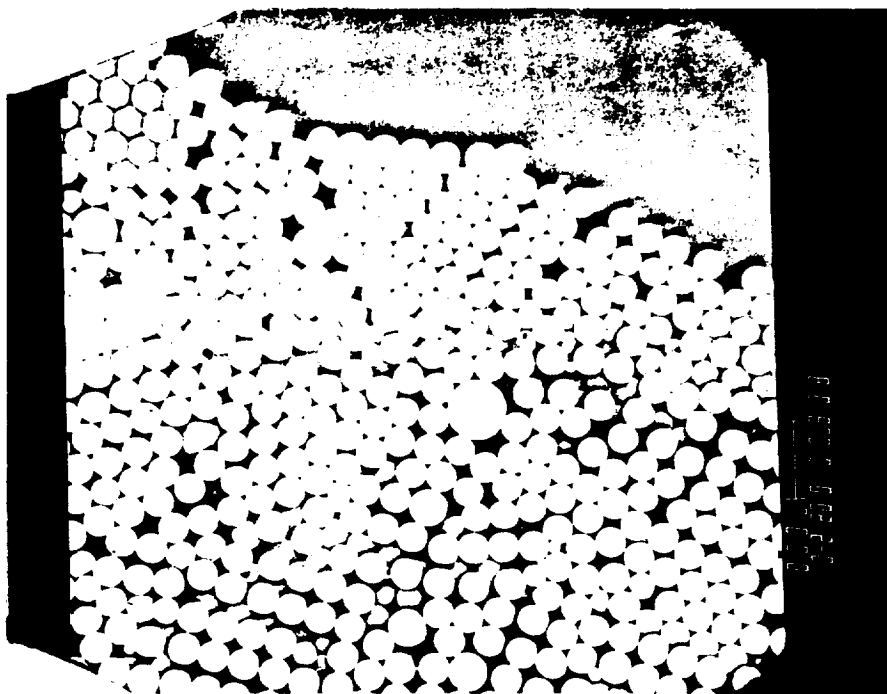
Figure 4-20. SEM micrographs of latex #4052-1 grown from latex #4046 with PVP and NaSS.
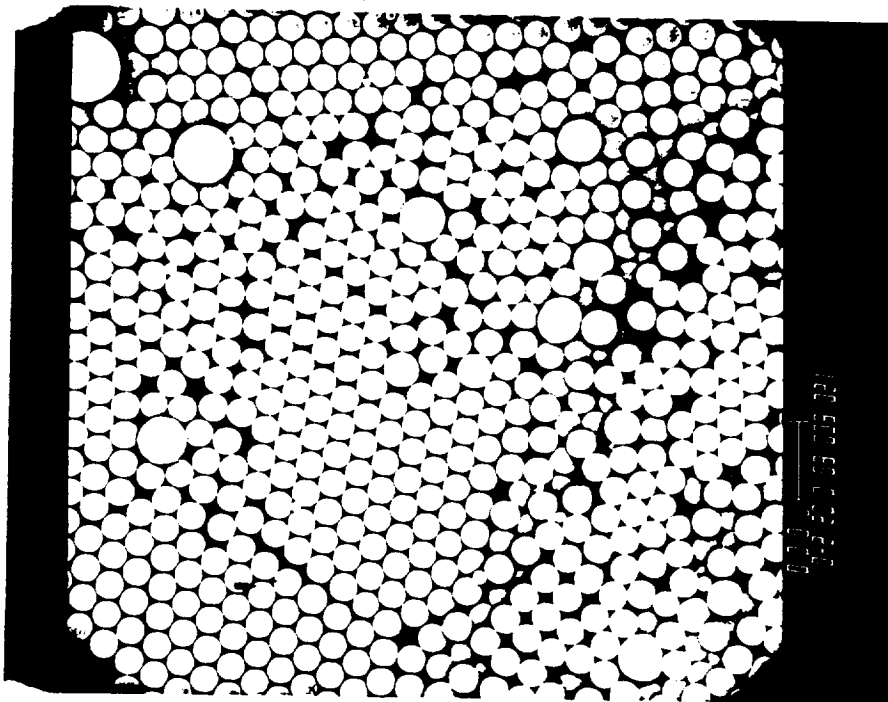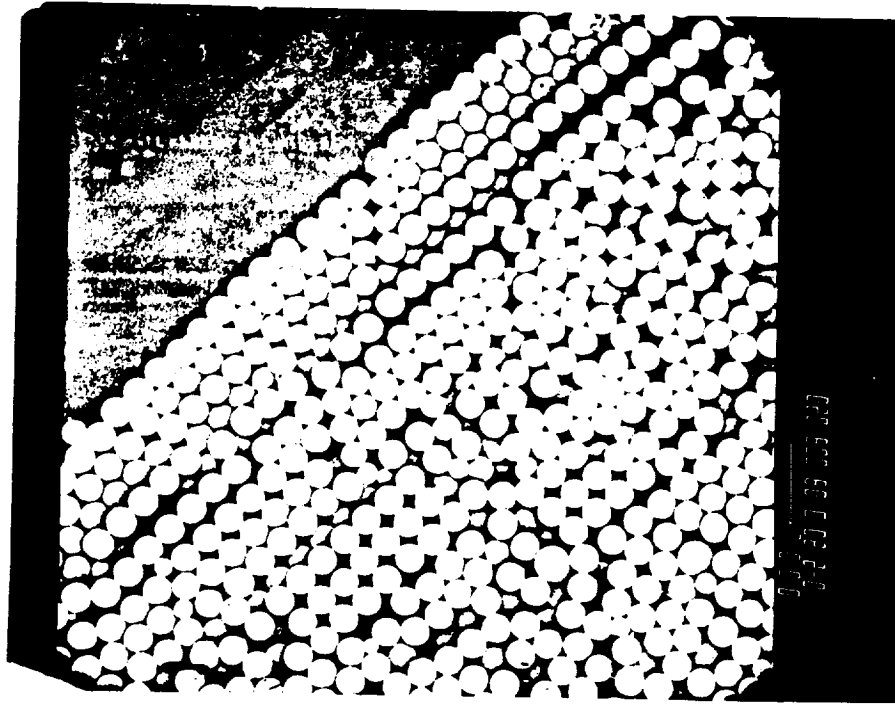
Figure 4-21. SEM micrographs of latex #4052-2 grown from latex #4046 with PVP and NaVTS.
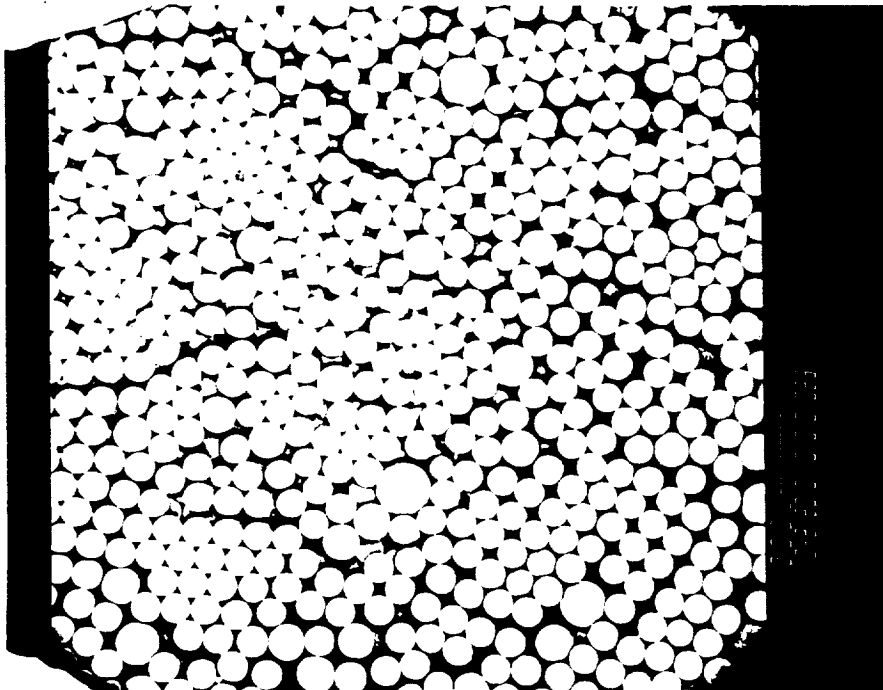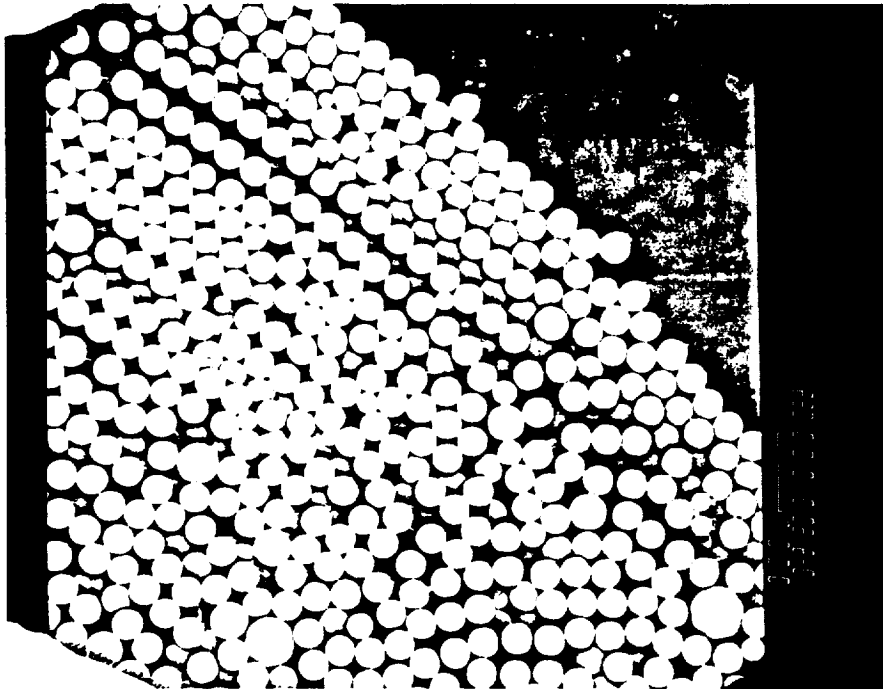
Figure 4-22. SEM micrographs of latex #4050-2 grown from latex #4046 with PVP and Cops 1.
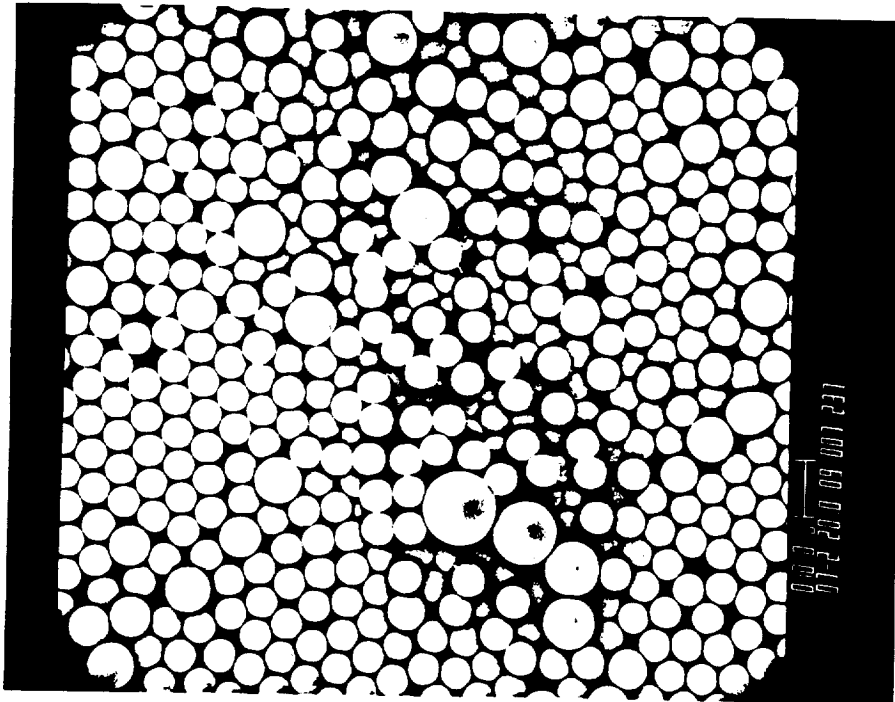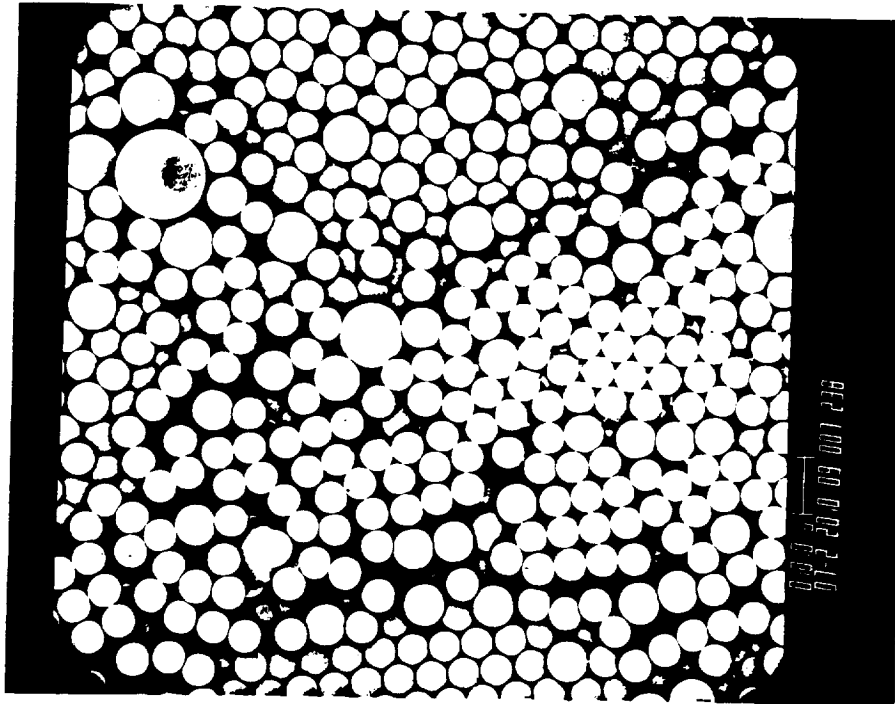
Figure 4-23. SEM micrographs of latex #4108-5 grown from latex #4100-1 with PVP and KX-3.

PVP K-15

NUMBER AVERAGE MWT = .56E+04
WEIGHT AVERAGE MWT = .13E+06
DISPERSITY,D = 23.76
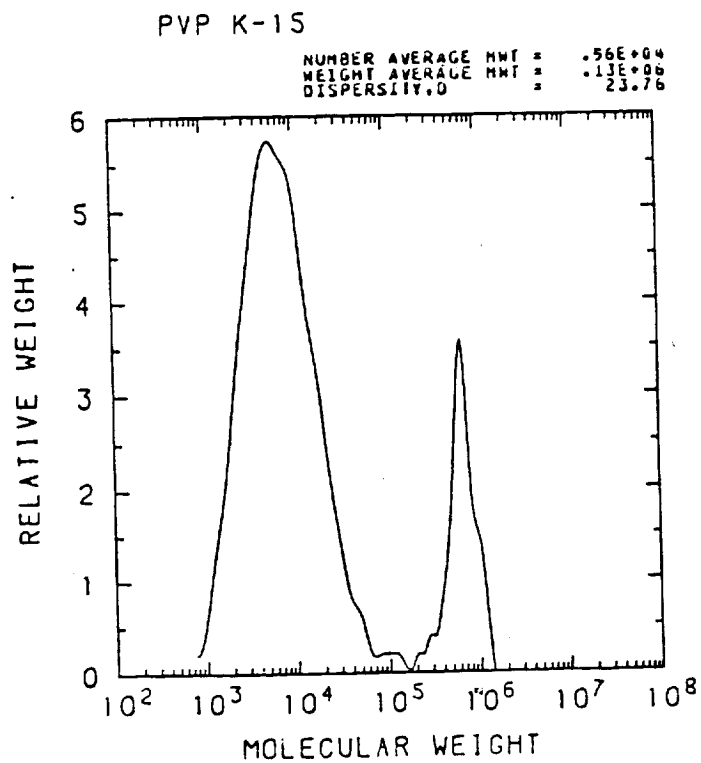
Figure 4-24.   Molecular weight distribution of poly-
vinylpyrrolidone K-15.

PVP K-30

NUMBER AVERAGE MWT = .13E+05
WEIGHT AVERAGE MWT = .25E+06
DISPERSITY,D = 18.48
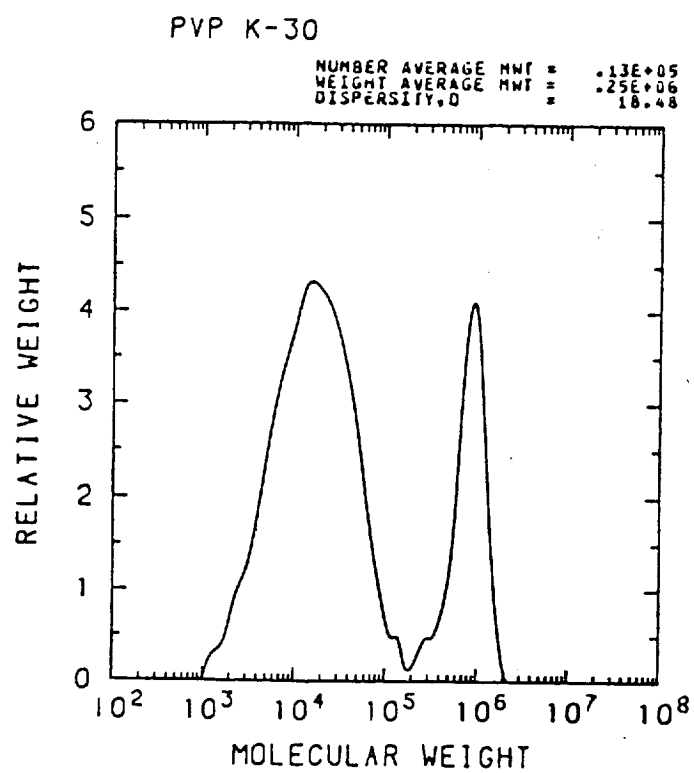
Figure 4-25.   Molecular weight distribution of poly-
vinylpyrrolidone K-30.

165
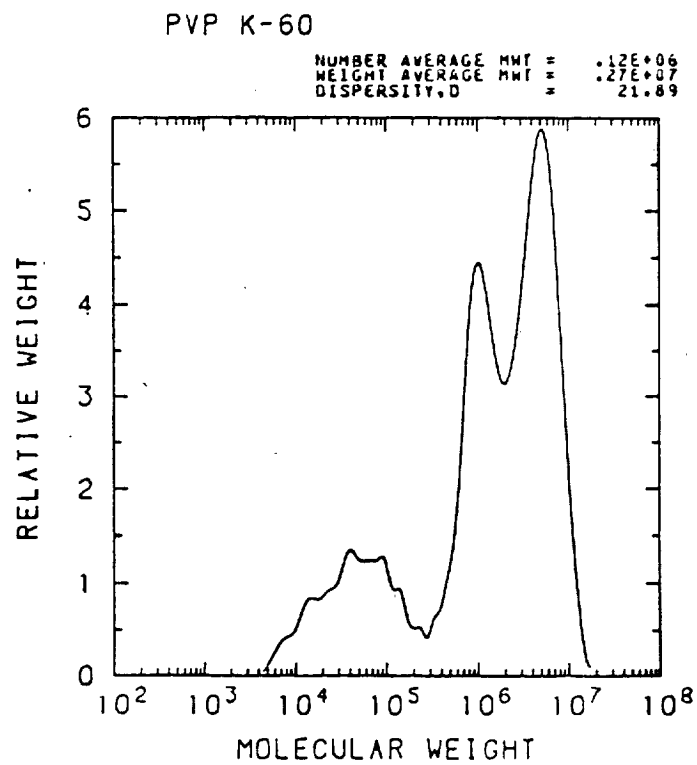
Figure 4-26.   Molecular weight distribution of poly-
vinylpyrrolidone K-60.

PVP K-90

NUMBER AVERAGE MWT = .15E+05
WEIGHT AVERAGE MWT = .18E+07
DISPERSITY,D = 11.98
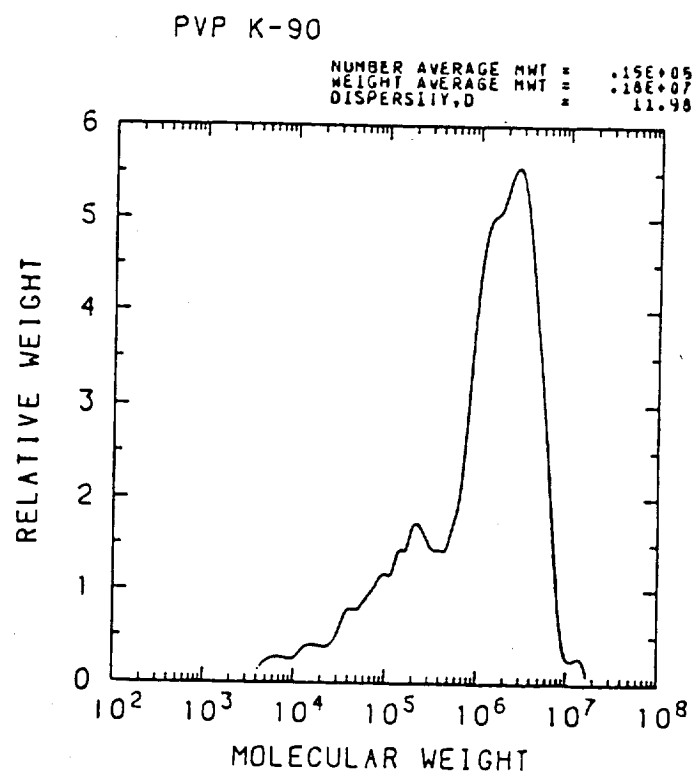
Figure 4-27. Molecular weight distribution of poly-vinylpyrrolidone K-90.
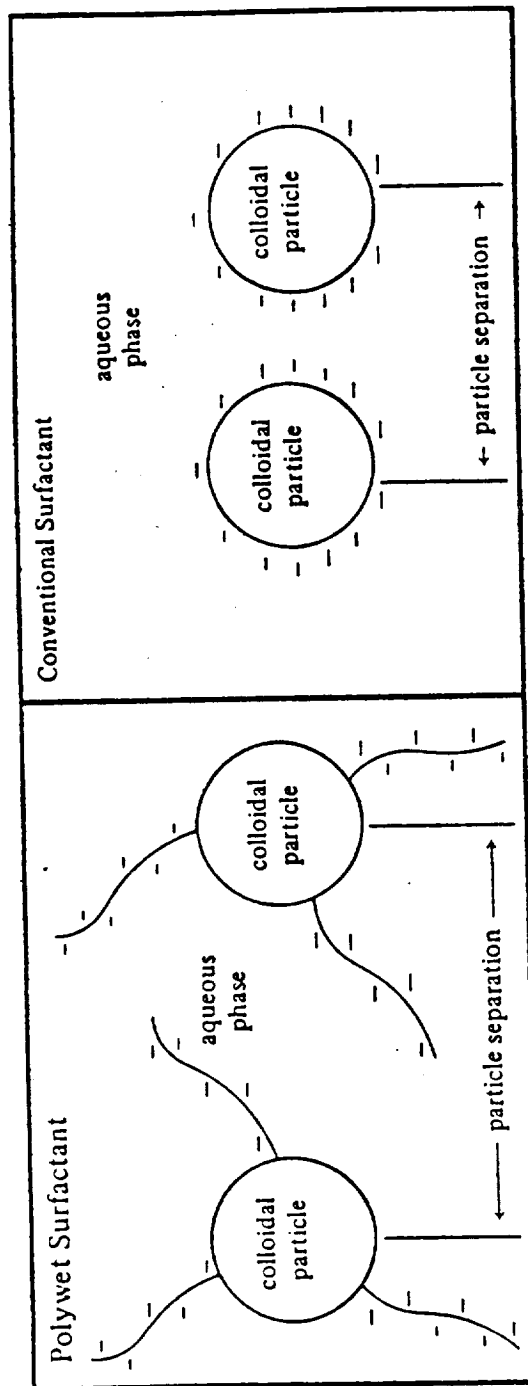
Figure 4-28. Schematic representation of latex particles stabilized with Polywet surfactants and conventional emulsifiers [112].

168

CHAPTER 5

PREPARATION IN MICROGRAVITY AND ON EARTH

5.1 Recipe Development

The basic studies on important variables in preparing large-particle-size monodisperse latexes, such as swelling ratio, initiator, inhibitor and surfactant, have been described in the previous chapters. From these studies, the following ingredients were chosen for the microgravity experiments: oil-soluble initiator 2,2'-Azobis-(2-methylbutyronitrile) (AMBN), (partially) water-soluble inhibitors hydroquinone (HQ) and benzoquinone (BQ), oligomeric surfactant Polywet KX-3, and polymeric surfactant PVP K-30. Before each flight experiment, a number of pre-flight experiments were conducted. The recipes developed from bottle polymerizations were fine-tuned in the laboratory prototype reactor, LUMLR, to obtain kinetic data and observe the behavior of the polymerization recipes in a reactor similar to the flight hardware. Details of the LUMLR design and operation can be found elsewhere [71]. This section will describe the results from the recipe testing in the LUMLR.

5.1.1 Initiator Concentration and Polymerization Kinetics

According to the original specifications, the flight reactor polymerization schedule was 11 hours at 70°C and one hour at 90°C. With this time limit, the initiator concentration must be adjusted so that the polymerization be close to completion within 11 hours and the full conversion-time curve can be measured. During the recipe tests before STS-3, it became apparent that obtaining complete conversions

(>90%) within 11 hours alloted for the polymerization at 70°C would be difficult for the lower swelling ratios and impossible at the higher swelling ratios, because of the formation of nitrogen bubbles due to the decomposition of the initiator.

Figure 5-1 presents the conversion-time curves of a series of polymerizations (designated as CMT-X) conducted in the LUMLR using a 2.5 μm seed latex and 2/1 monomer/polymer swelling ratio. The AMBN concentrations used were in the decreasing order: CMT-8 (0.225% based on monomer) > CMT-12 (0.155%) > CMT-9 (0.140%) > CMT-3 (0.120%) > CMT-2 (0.085%). The dashed parts of the curves are the actual data, which were influenced by the growth of a nitrogen bubble. With the higher initiator concentrations (CMT-8 and CMT-12), the polymerization could be completed within 11 hours, but with part of the kinetic curve lost. With the lower initiator concentrations (CMT-3 and CMT-2), the full conversion-time curve could be measured but in a time longer than 11 hours. Only recipe CMT-9 gave high conversion and a nearly complete kinetic curve within the 11-hour period. Note that the initial polymerization rates vary approximately with the square root of initiator concentration.

Similar tests were carried out with higher swelling ratios (4/1 and 10/1). At these higher swelling ratios, the polymerizations could not be completed within the 11-hour period at 70° because of the lower polymerization rate over more of the conversion range. Thus more initiator was required to finish the polymerization within the 11-hour period with the consequent loss of some kinetic data. Only an increased reaction time would allow for the acquisition of the

170
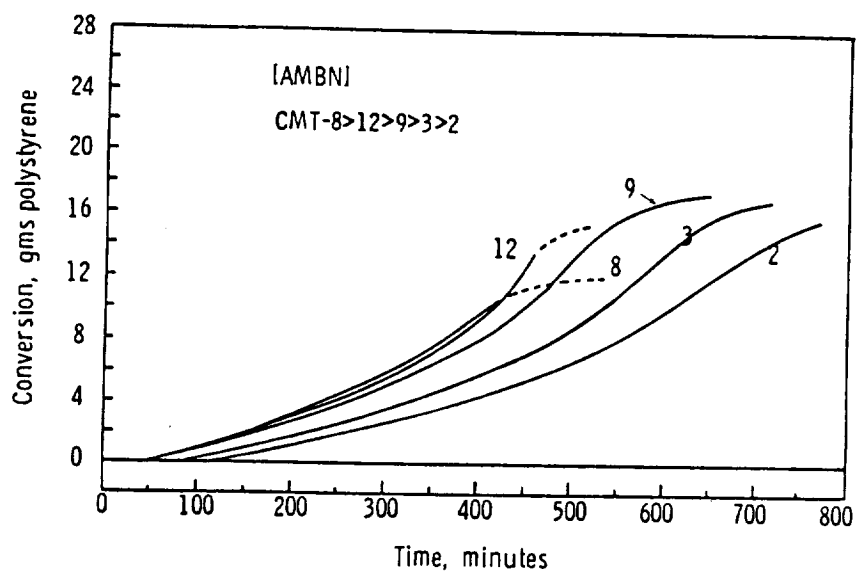
Figure 5-1. Conversion-time curves for the seeded polymerization of a 2.5 μm seed (M/P=2/1), using varying amounts of AMBN initiator: CMT-8 0.225%; CMT-12 0.155%; CMT-9 0.140%; CMT-3 0.120%; CMT-2 0.085%.

171

complete conversion-time curve. This conclusion led to reprogramming of the flight hardware after STS-3 to extend the 70°C period to 17 hours for the STS-4, STS-6 and STS-7 flights.

5.1.2 Aerosol MA Surfactant and Particle-Particle Stability

It was pointed out in Chapter 4 that a surfactant combination such as PVP K-30 (polymeric) and Polywet KX-3 (oligomeric) worked well in stabilizing the particles without generating new small particles during the seeding polymerization for preparing large-particle-size latexes. At the beginning of the CMT-series experiments in the LUMLR, the 2.5 µm seed latex was used without cleaning. Additional PVP and KX-3 surfactants were added to the seed for the swelling and subsequent polymerization. In one of the latter experiments (CMT-4; 4/1 swelling ratio), an "upgraded" seed latex, cleaned by centrifugation and serum replacement (see Chapter 6) was used. Unlike the products from uncleaned seed, a polydisperse product was obtained and the yield was lowered. It was soon realized that the removal of the residual Aerosol MA surfactant from the seed latex diminished the latex stability thus causing more coalescence and coagulation. Although the residual Aerosol MA concentration in the uncleaned seed latex was low compared with the added concentrations of the other two surfactants, it played a crucial role in stabilizing the particles. From that time on, Aerosol MA was added to any polymerization recipe using cleaned seed latex.

5.1.3 Crosslinking and Over-Size Particles

During the recipe test prior to STS-4, it was found that it was difficult to prevent the formation of over-size particles, which were formed by coalescence of two or three normal particles. It was decided that a crosslinking agent should be incorporated to decrease the tendency of particles to coalesce. A crosslinking agent divinylbenzene (DVB) was added to the seed latex recipes. The effect of crosslinking was then evaluated by examining the products grown from the crosslinked seed. Unfortunately, it was found that a high degree of crosslinking caused the formation of odd-shaped particles due to the uneven swelling and growth from the highly crosslinked core. Figure 5-2 shows SEM micrographs of latex #5090 grown from a 5.5 μm crosslinked (0.06% DVB) seed and an 8/1 swelling ratio. All the particles were pear-shaped as a result of uneven swelling. Two other latexes (#5108-1 and #5108-2) were prepared from seed latexes of the same size but of lower crosslinking density (0.015% and 0.003% DVB, respectively) and compared to latex #5068-4 grown from an uncrosslinked seed. SEM micrographs of these latexes are presented in Figures 5-3 to 5-4. No pear-shaped particles were found in these latexes. Fewer over-size particles were found in latexes #5108-1 and #5108-2 grown from crosslinked seed than latex #5068-4 grown from uncrosslinked seed. After the STS-4 flight, 0.015% DVB was included in every recipe for preparing latexes of diameter greater than 5 μm.
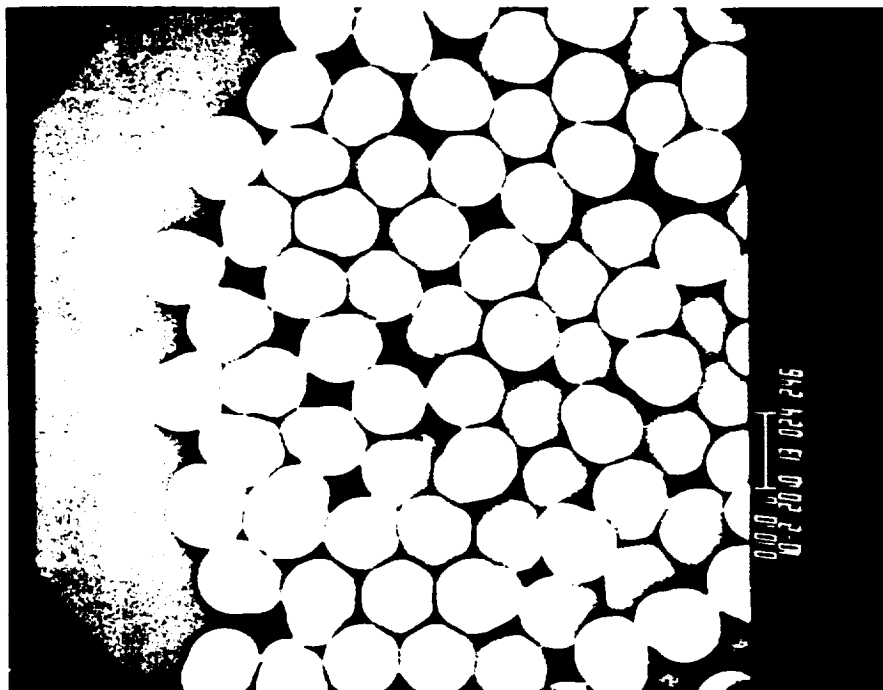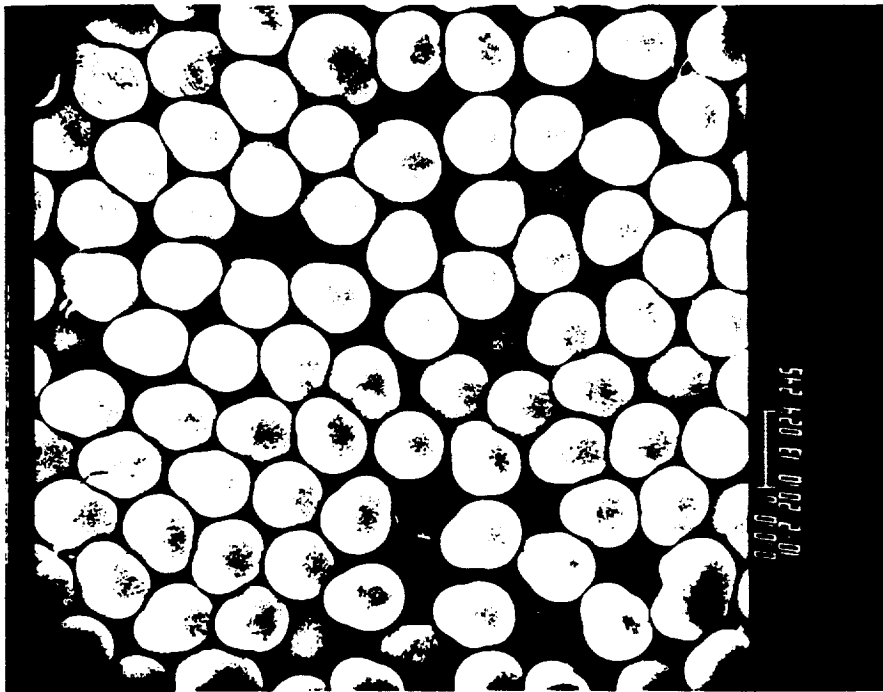
Figure 5-2. SEM micrographs of latex #5090 grown from a 5.5 μm crosslinked (0.06% DVB) seed latex with 8/1 swelling ratio.
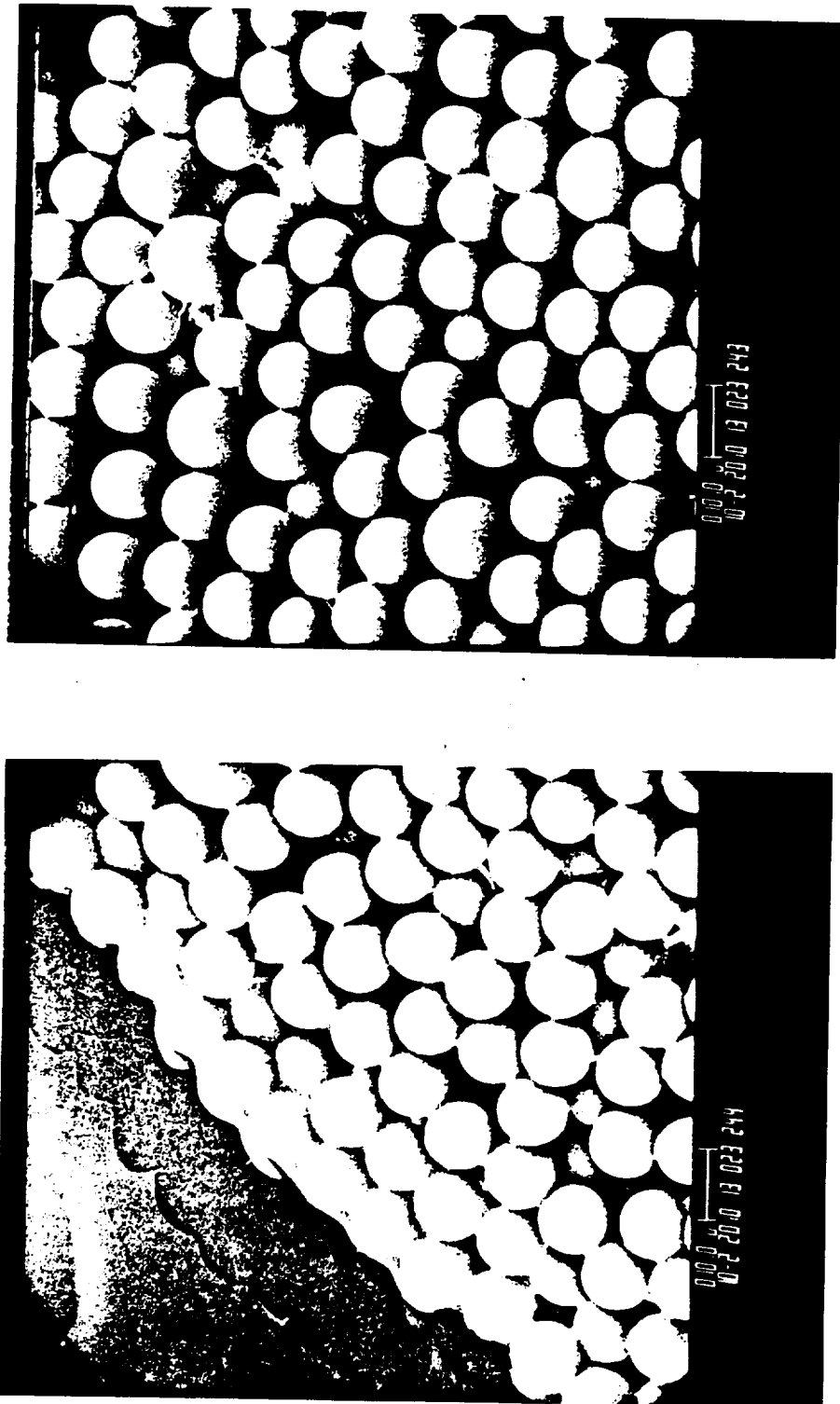
Figure 5-3. SEM micrographs of latex #5068-4 grown from a 5.5 μm un-crosslinked seed latex with 8/1 swelling ratio.
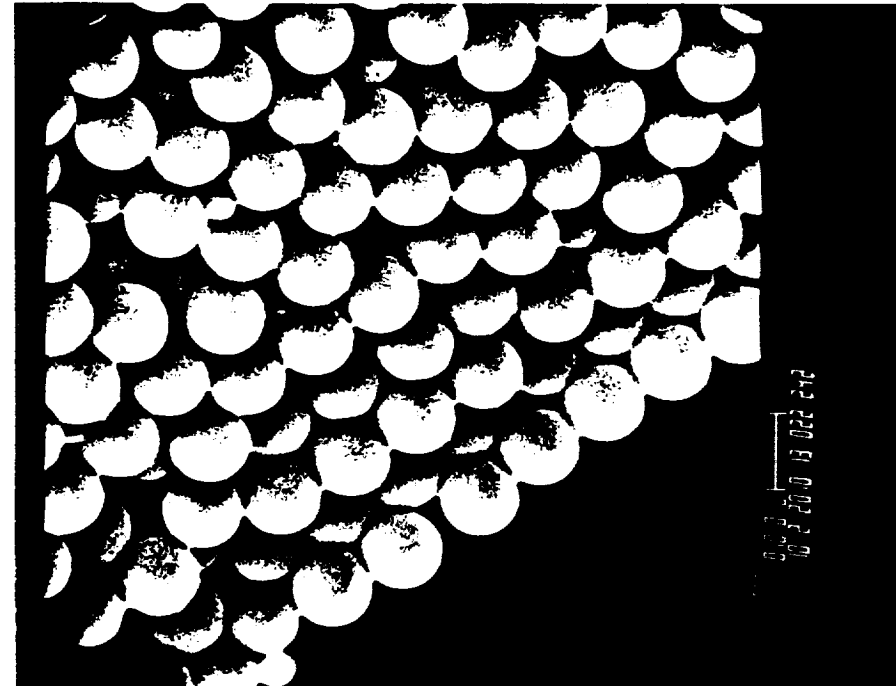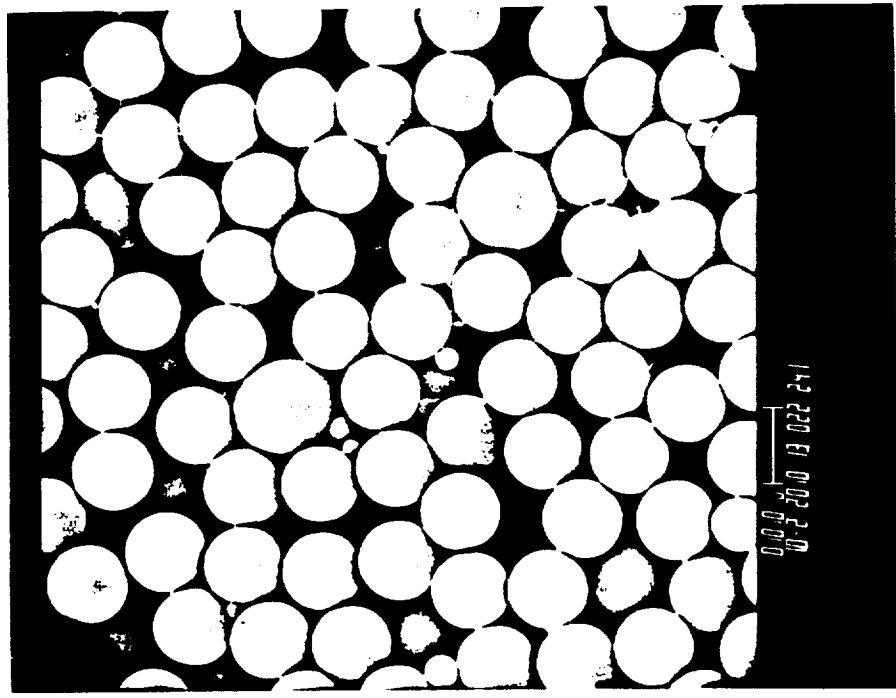
Figure 5-4.   SEM micrographs of latex #5108-2 grown from a 5.5 μm
crosslinked (0.003% DVB) seed latex with 8/1 swelling ratio.
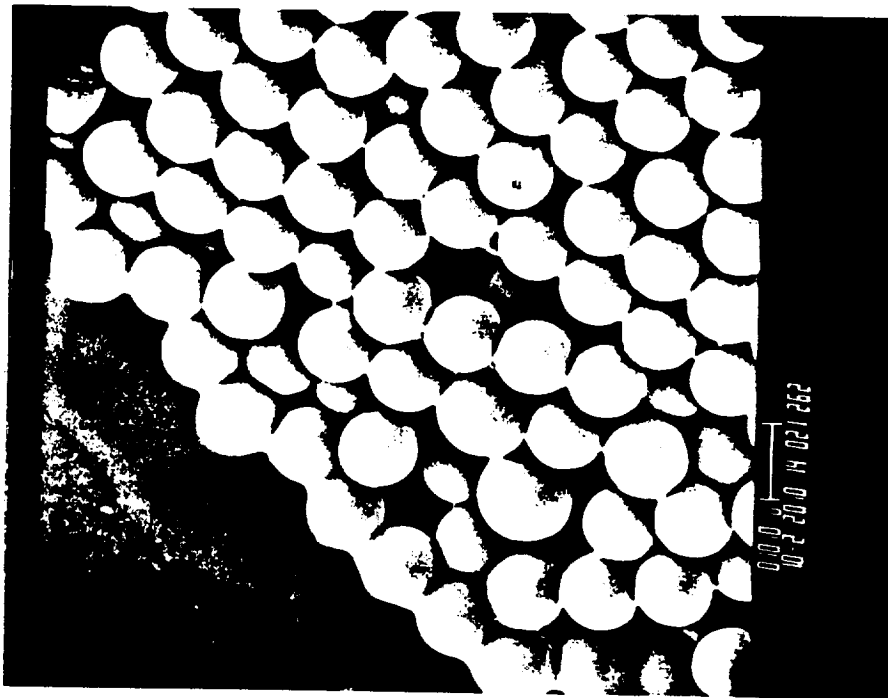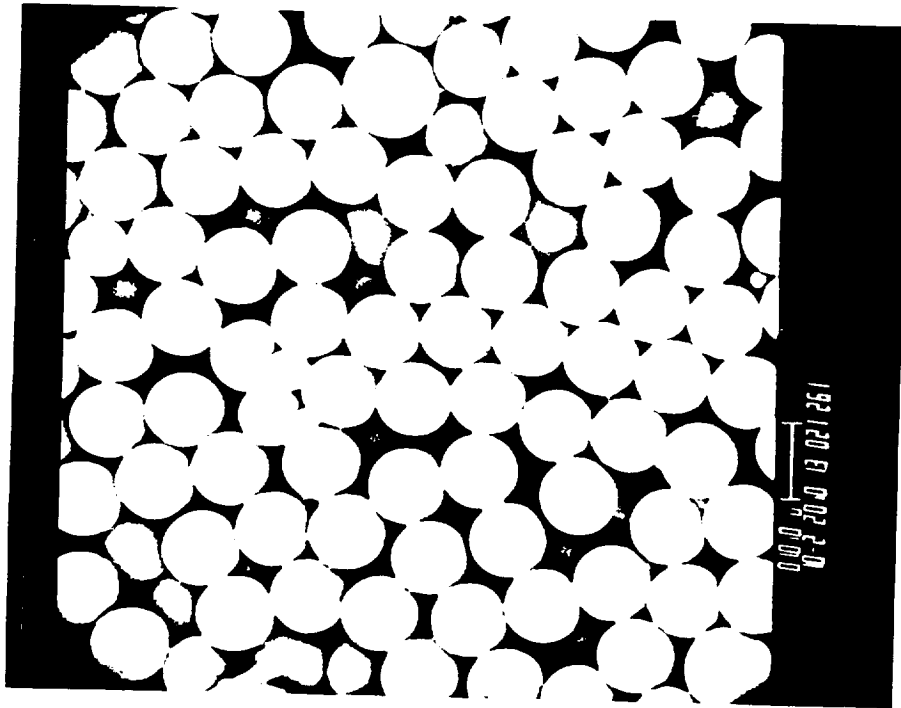
Figure 5-5. SEM micrographs of latex #5108-1 grown from a 5.5 μm crosslinked (0.015% DVB) seed latex with 8/1 swelling ratio.

5.2 Comparison of Flight and Ground Experiments

Microgravity experiments were conducted with the Monodisperse Latex Reactor (MLR). The flight hardware consists of an Experiment Apparatus Container (EAC) manufactured by General Electric Co. and a Support Electronic Package (SEP) manufactured by Rockwell International and Accudata. Housed within the EAC are four independently-operated dilatometer-reactors. Each reactor is surrounded with 13 electronic modules. Each piston/cylinder-type reactor was designed to be filled with 100 ml of fluid. A stirring blade connected to a motor on the bottom of the reactor provides the fluid with oscillatory agitation at low rpm. The SEP controls the experimental operations and records data from each of the four reactors on a tape cassette. Figure 5-6 is a photograph of the flight hardware. Figure 5-7 shows that the flight hardware occupies the space of three standard mid-deck lockers in the Space Shuttle. Further details on the design and operation of the flight hardware can be found elsewhere [71].

Four sets of microgravity experiments have been carried out to prepare monodisperse latexes of large particle size. Shortly after each flight, ground-based control polymerizations were carried out in the same flight hardware. The polymerization kinetics and particle size distributions of the flight and ground latexes were compared. Table 5-1 summaries the launch dates, seed particle size, and swelling ratios used in each flight.
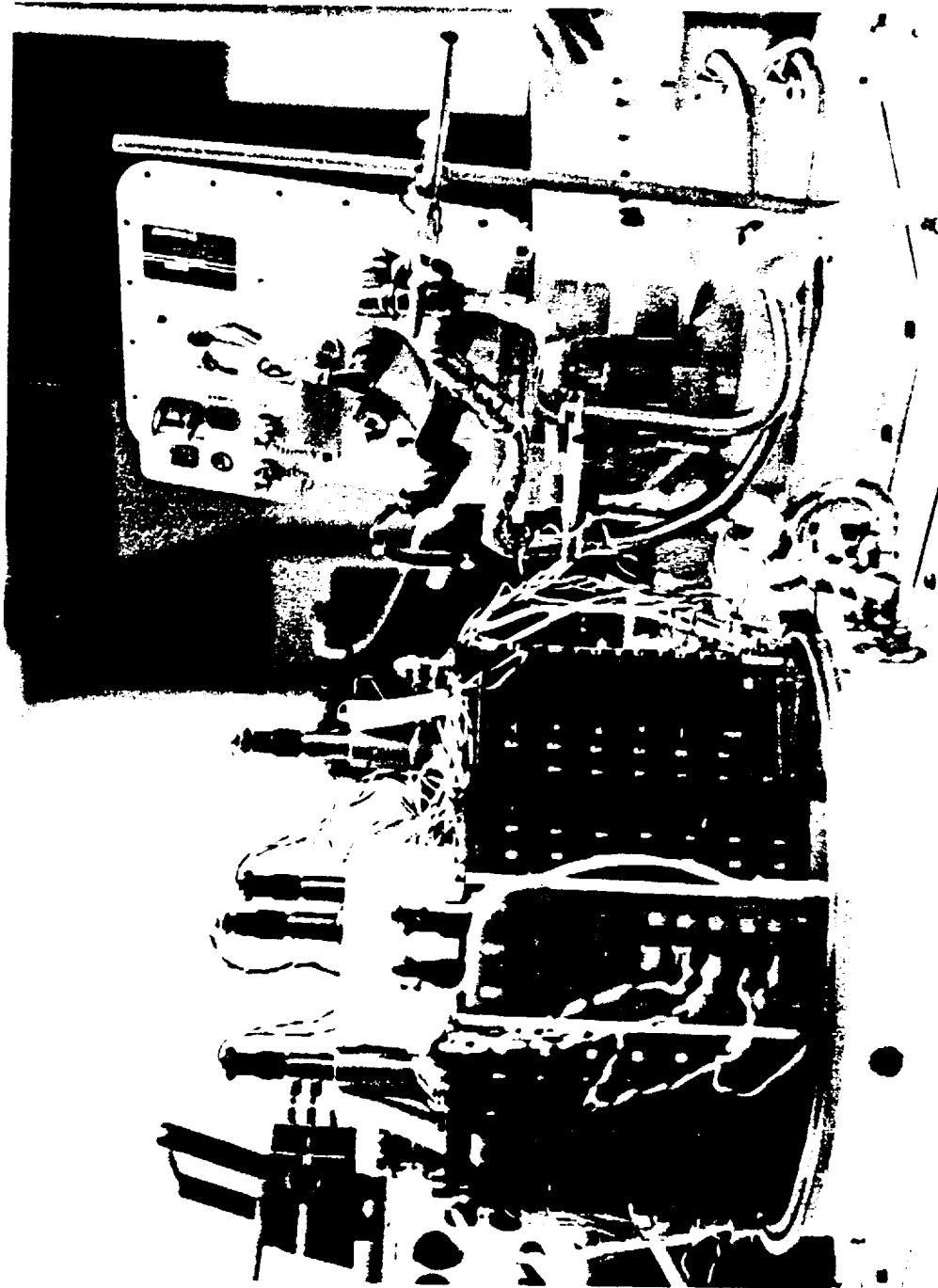
Figure 5-6. Photograph of the flight hardware: four reactors on the EAC platform (left) and the SEP (right).

EAC

SEP

Mid-deck
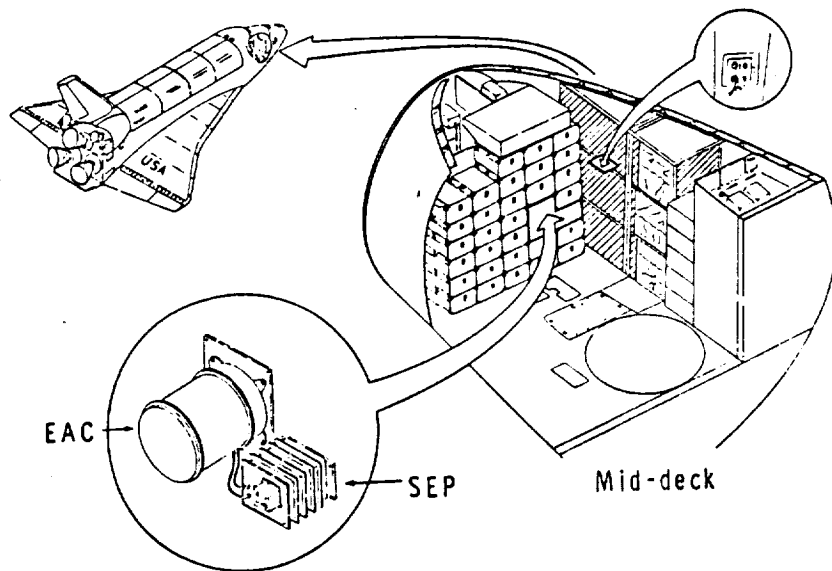
Figure 5-7.   Accommodation of the flight hardware
in the Space Shuttle.

Table 5-1.   Launch Dates, Seed Sizes, and Swelling
Ratios Used in Microgravity Experiments

Flight	Launch Date	Seed Size, μm	Monomer/Polymer
STS-3 (Columbia)	3/22/82	2.5	2/1,4/1,10/1
STS-4 (Columbia)	6/27/82	5.5	2/1,4/1,6/1,8/1
STS-6 (Challenger)	4/4/83	5.6	2/1,4/1,6/1
STS-7 (Challenger)	6/18/83	7.9 & 10.3	4/1,6/1

5.2.1 STS-3

Three large-particle-size recipes were used in the STS-3 flight experiments. A 2.5 μm polystyrene latex (#4131-2C), prepared in this laboratory from a 0.40 μm seed latex (LS-1103-A) by three seeding steps, was used as seed. The flight seed latex was cleaned by centrifugation and serum replacement (see Chapter 6) to remove most of the off-size particles. The recipes were designed to have a final solids content of 30%. The variations of these polymerization recipes are given in Table 5-2.

The seed latex, the remaining water, and the other ingredients were weighed into a 12-oz bottle and tumbled with a Lortone tumbler overnight. The monomer-swollen latex was filtered with glass wool into a separatory funnel to remove excess monomer. After degassing in a flask at a pressure of 20 mm Hg, the swollen latex was loaded into the reactor. The reactor was then mounted on the EAC platform. In the "preprocess" mode, the fluid in the reactor was agitated for 1.5

Table 5-2.   STS-3 Flight Recipes

		Initiator	Inhibitor	Surfactants		
Recipe #	M/P	AMBN (%M)	HQ (%aq)	AMA (%aq)	KX-3 (%aq)	PVP (%aq)
1	2/1	0.12	0.034	0.014	0.023	0.194
2	4/1	0.17	0.034	0.007	0.018	0.176
3	10/1	0.29	0.034	0.003	0.017	0.163

min. of oscillatory motion (13 rpm) every 30 min. After the Shuttle reached its orbit, the equipment was switched to the "process" mode by the astronaut. The latex was then subjected to continuous oscillatory agitation (13 rpm) and heated for 11 hours at 70°C and one hour at 90°C. The equipment was then switched back to the "preprocess" mode and agitated intermittently until the Shuttle landed. After landing, the latexes and the data tape were recovered from the flight hardware. The flight hardware was refurbished and the ground-based control experiments were carried out.

The product analysis included estimation of the product yields from solids contents and the measurement of particle size distributions by electron microscopy. The solids contents along with the styrene contents measured by isooctane extraction of the orginal swollen latexes are presented in Table 5-3.

The particle size analysis of the product latexes was accomplished by measuring individual particle diameters from prints of the TEM micrographs (see Chapter 6). Representative micrographs and particle size distributions of the seed and product latexes are

Table 5-3.   Solids Contents and Results of
Isooctane Extraction of STS-3 Flight and Ground
Latexes

Sample	% Solids	gm styrene/100gm latex	
		Exp.	Design
---------	--------	----	----
Flight #1	28.3	--	20.0
Ground #1	27.0	19.2	
Flight #2	24.6	23.6	24.0
Ground #2	29.7	22.8	
Flight #3	22.8	21.1	27.3
Ground #3	25.4	23.1	

presented in Figures 5-8 to 5-21. Table 5-4 summarizes the particle size results, the number-average diameter $(\bar{D}_n)$, the number of particles measured (n), the standard deviation (σ), the coefficient of variation $(\sigma/\bar{D}_n$, in%), and the relative number of over-size particles. Also included are the results of an independent analysis of flight and ground samples of recipe #3 made by the National Bureau of Standard (NBS) [115]. The standard deviations obtained by NBS were smaller than the standard deviations obtained in this laboratory for both flight and ground samples. The difference may be attributed to the treatment of measurement uncertainties. The standard deviations reported by NBS were corrected for the edge determination uncertainty and magnification distortion while no corrections were made for our results.

The particle size distributions of all samples were narrow but with some subtle differences. The uniformity expressed as $\sigma/\bar{D}_n$ was
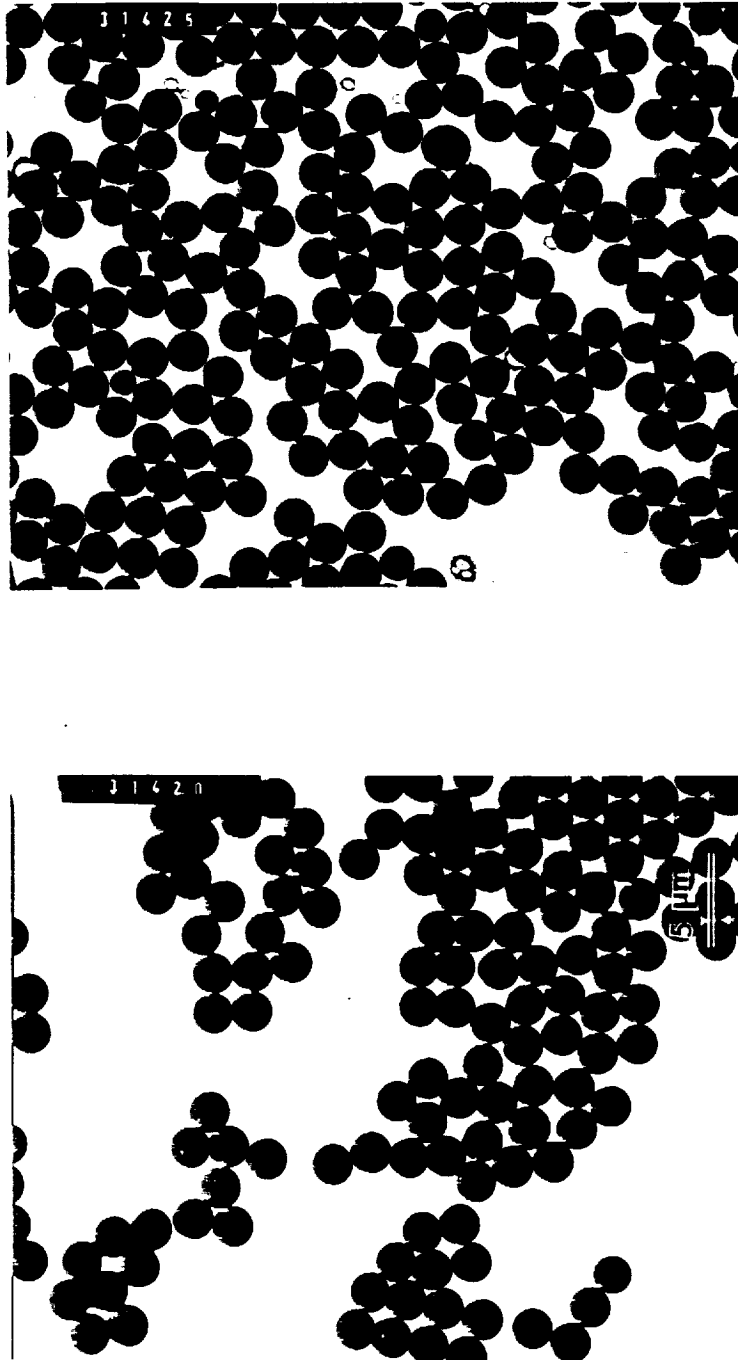
Figure 5-8. TEM micrographs of STS-3 flight seed latex #4131-2C.
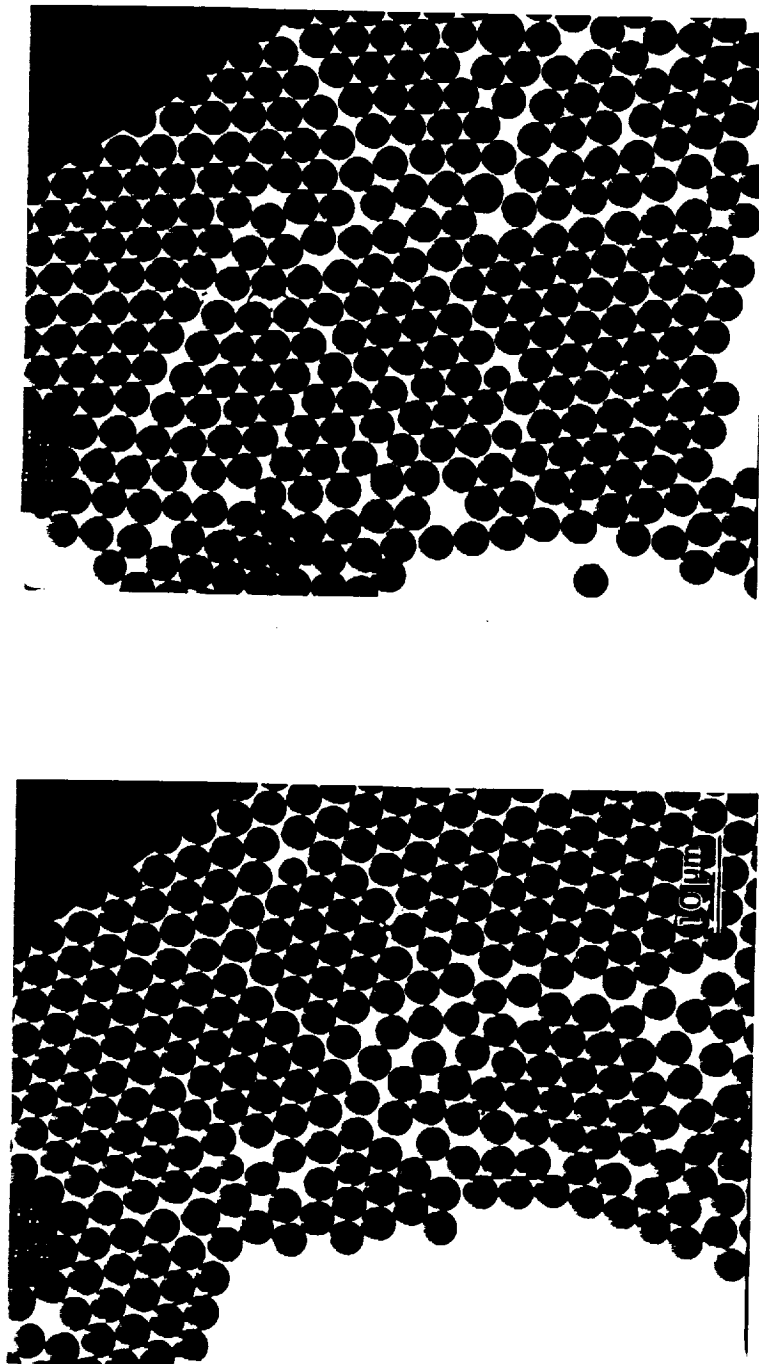
Figure 5-9.   TEM micrographs of STS-3 flight latex #1.
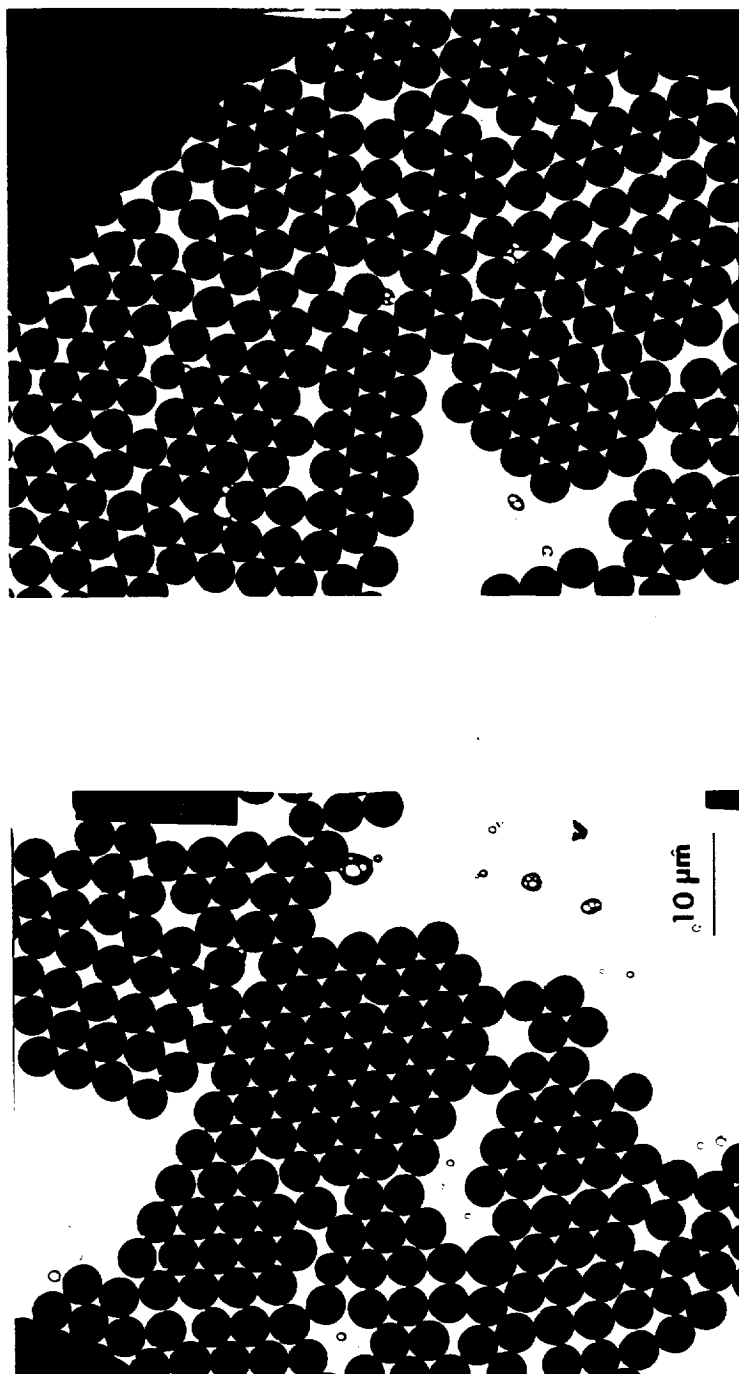
Figure 5-10. TEM micrographs of STS-3 ground latex #1.

10 μm
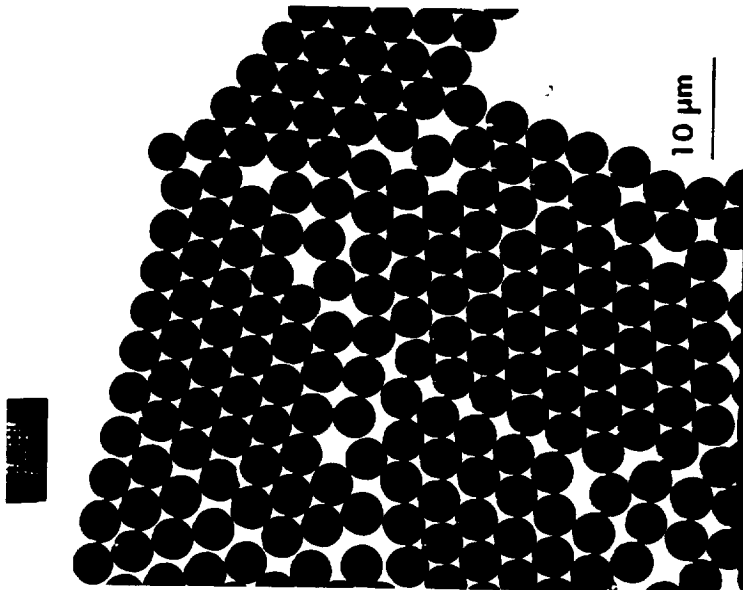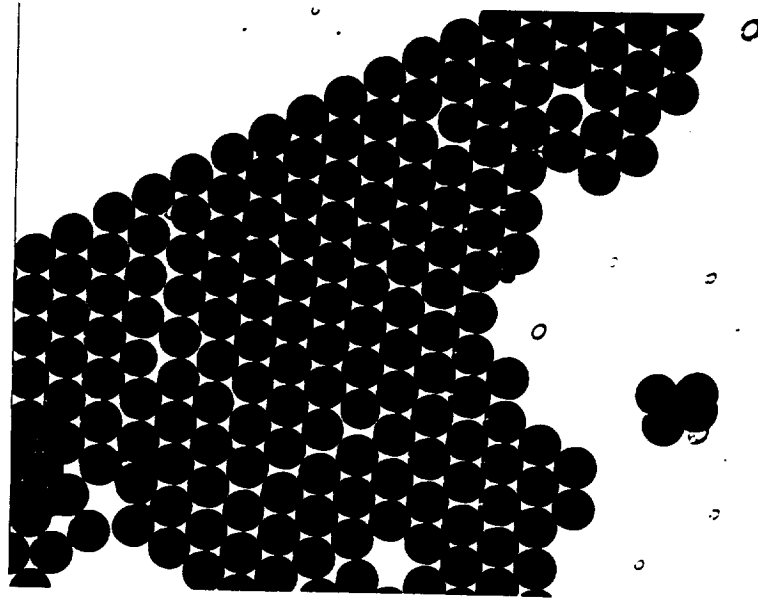
Figure 5-11. TEM micrographs of STS-3 flight latex #2.

187
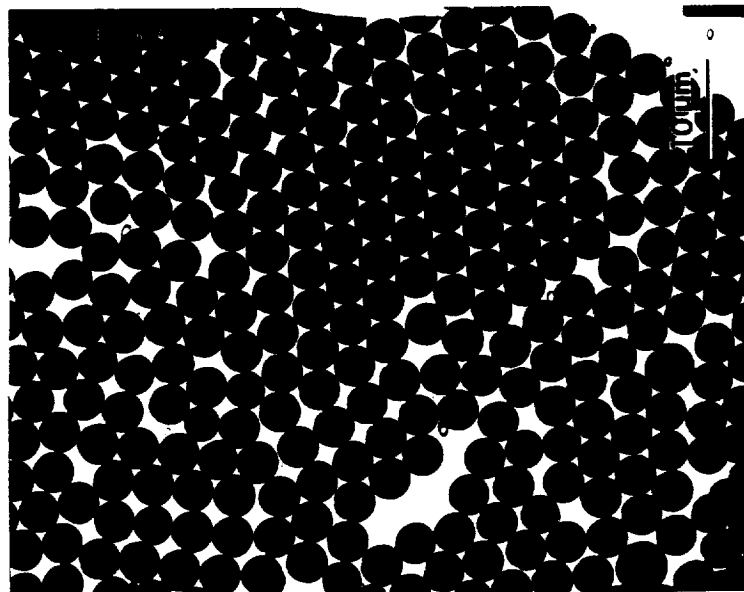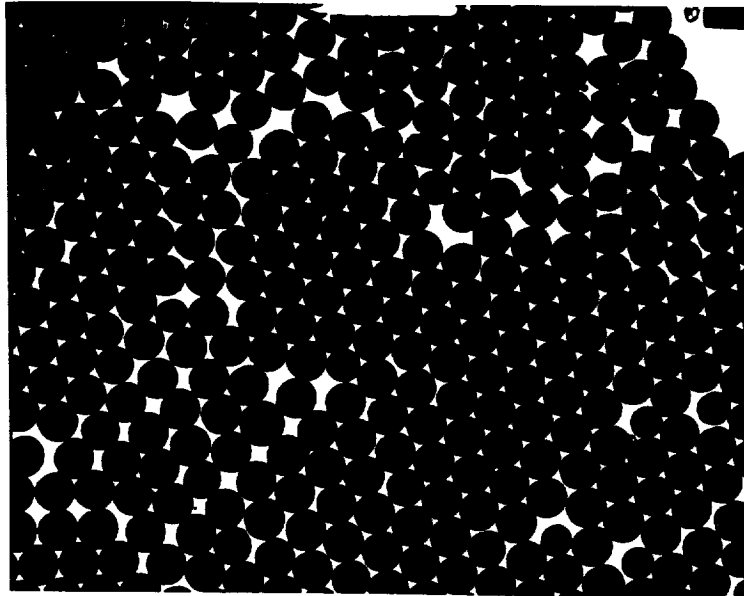
Figure 5-12. TEM micrographs of STS-3 ground latex #2.

188
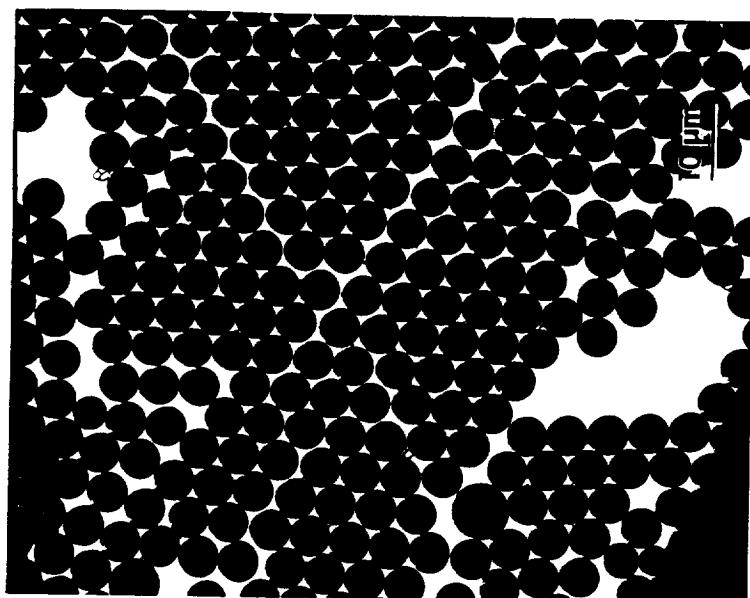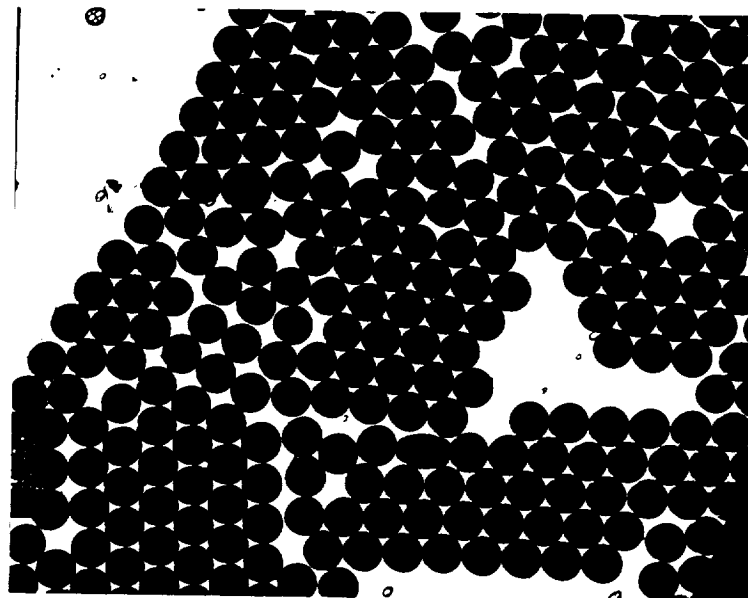
Figure 5-13. TEM micrographs of STS-3 flight latex #3.
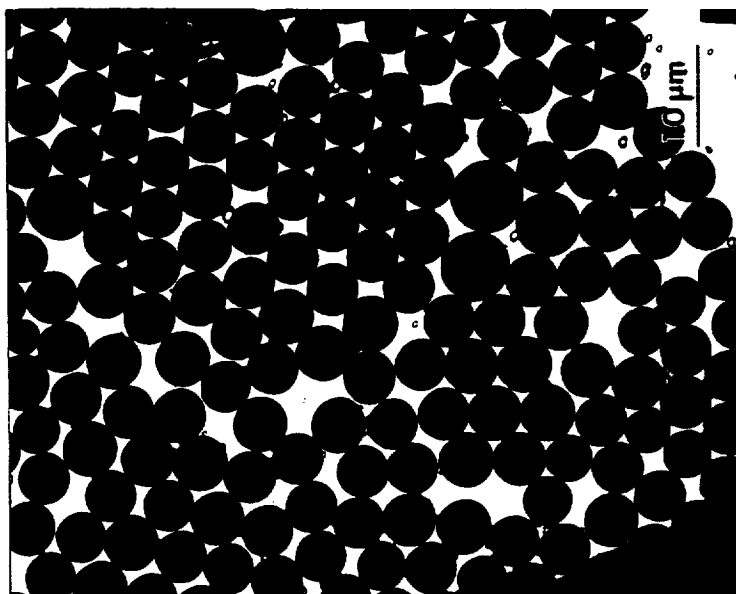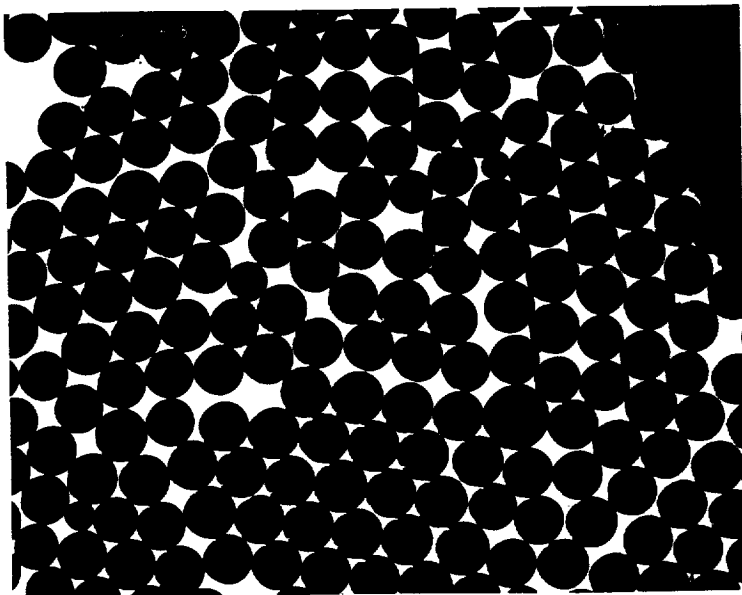
Figure 5-14. TEM micrographs of STS-3 ground latex #3.

SAMPLE SEED STS3

$D_n = 2519.1$ PDI $= 1.001$
$D_w = 2521.6$ $D_{min} = 2010.0$
$N = 1024$ $D_{max} = 2990.0$
$D_v = 2519.9$ $D_a = 2519.5$
$S_d = 46.3$ STEP $= 20.0$
$D_q = 2522.4$ $D_s = 2520.8$
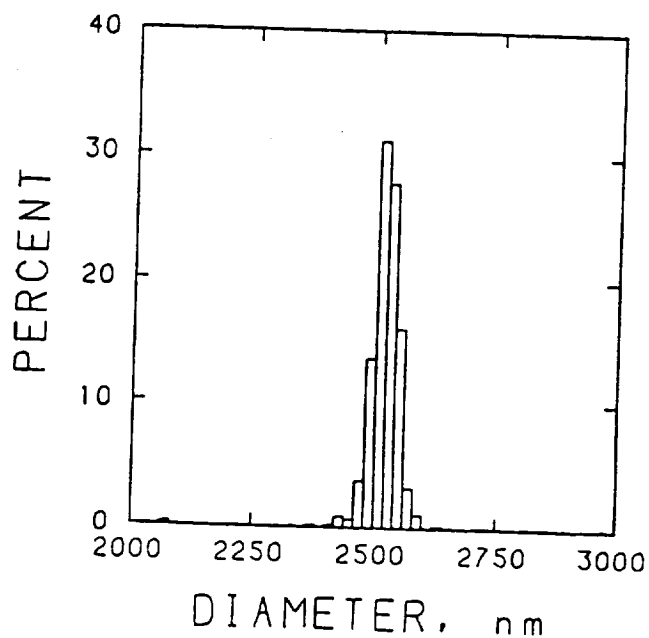
Figure 5-15. Particle size distribution of STS-3 flight seed latex #4131-2C.

SAMPLE FLIGHT 1

D_n = 3437.4	PDI = 1.001
D_w = 3441.0	D_{min} = 3010.0
N = 2777	D_{max} = 3990.0
D_v = 3438.6	D_a = 3438.0
S_d = 64.2	STEP = 20.0
D_q = 3442.1	D_s = 3439.8
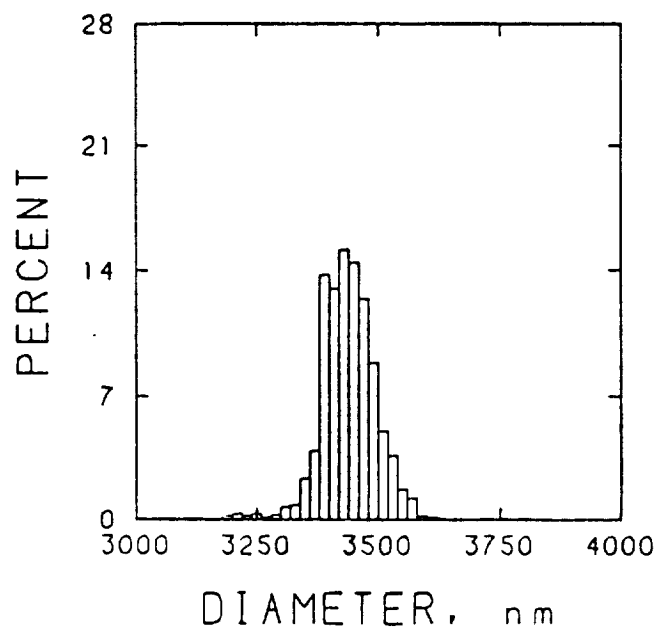
Figure 5-16. Particle size distribution of STS-3 flight latex #1.

SAMPLE GROUND 1

D_n = 3722.6   PDI = 1.001
D_w = 3725.1 D_{min} = 3310.0
N = 1363 D_{max} = 4290.0
D_v = 3723.4 D_a = 3723.0
S_d = 57.3   STEP = 20.0
D_q = 3726.0 D_s = 3724.3
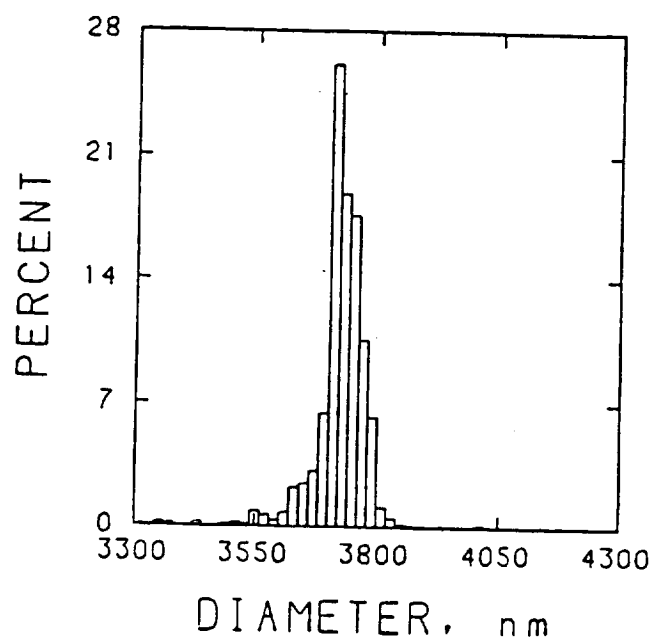
Figure 5-17.   Particle size distribution of STS-3 ground latex #1.

SAMPLE   FLIGHT 2

D_n = 4076.6   PDI = 1.001
D_w = 4079.9 D_{min} = 3510.0
N = 2256 D_{max} = 4490.0
D_v = 4077.7 D_a = 4077.1
S_d = 68.9   STEP = 20.0
D_q = 4081.0 D_s = 4078.8
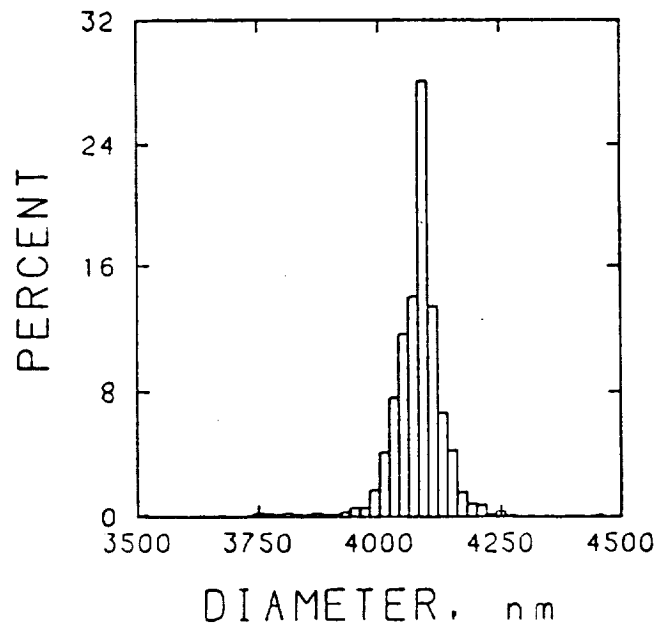
Figure 5-18.   Particle size distribution of STS-3 flight latex #2.

SAMPLE GROUND 2

D_n = 3931.6   PDI = 1.001
D_w = 3936.0 D_{min} = 3510.0
N = 913 D_{max} = 4490.0
D_v = 3933.1 D_a = 3932.3
S_d = 77.1   STEP = 20.0
D_q = 3937.4 D_s = 3934.5
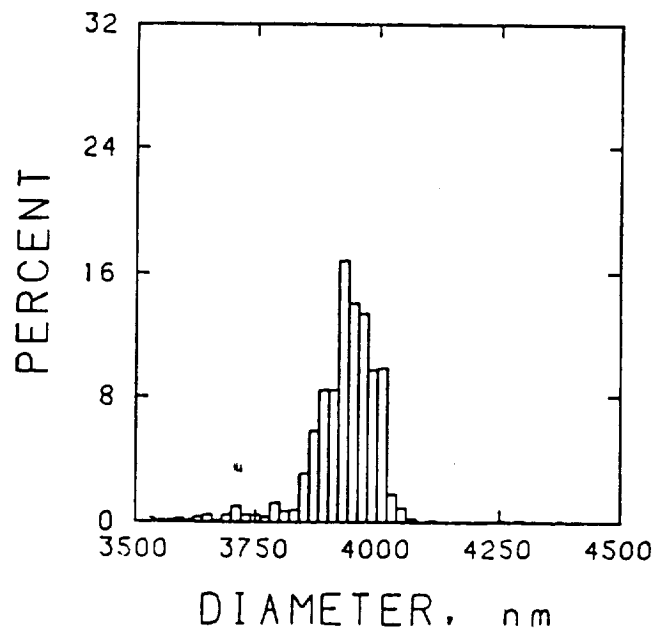
Figure 5-19.   Particle size distribution of STS-3
ground latex #2.

SAMPLE FLIGHT 3

D_n = 4984.3   PDI = 1.001

D_w = 4988.3 D_{min} = 4510.0

N = 2095 D_{max} = 5490.0

D_v = 4985.6 D_a = 4985.0

S_d = 81.7   STEP = 20.0

D_q = 4989.6 D_s = 4987.0
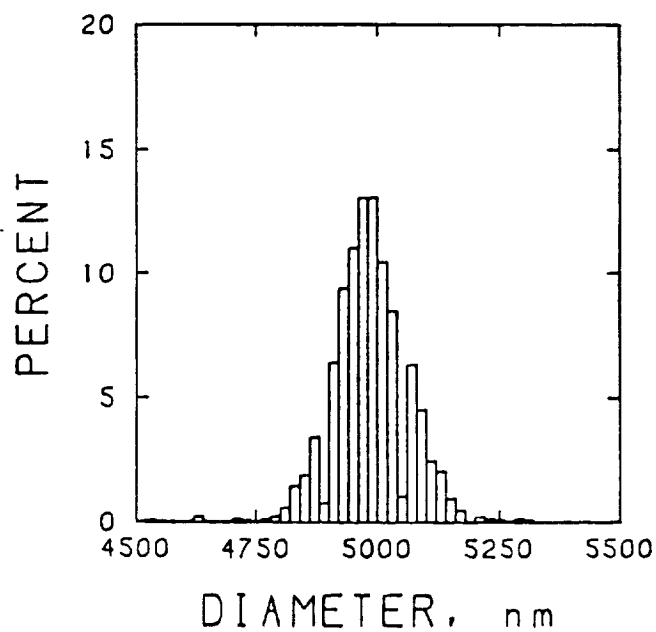
Figure 5-20.   Particle size distribution of STS-3 flight latex #3.

196

SAMPLE GRND RUN 3

D_n = 4741.1	PDI = 1.004
D_w = 4758.4	D_{min} = 4210.0
N = 1233	D_{max} = 5210.0
D_v = 4746.9	D_a = 4744.0
S_d = 166.8	STEP = 20.0
D_q = 4764.1	D_s = 4752.7
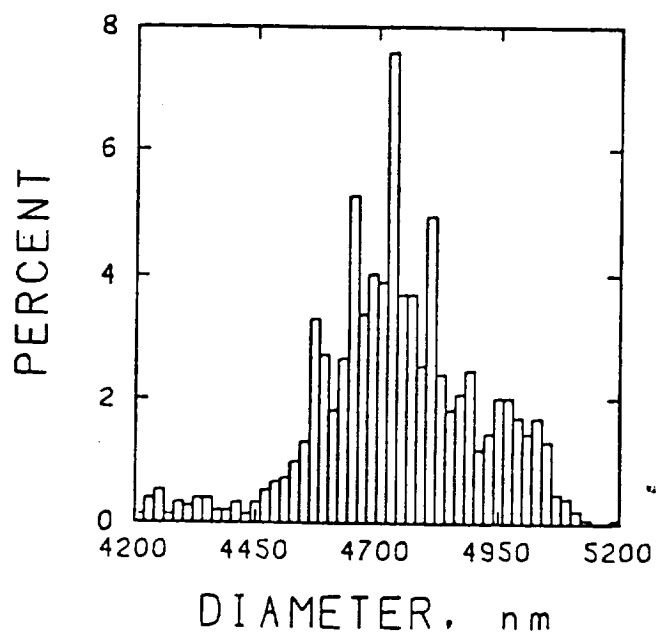
Figure 5-21.   Particle size distribution of STS-3
ground latex #3.

Table 5-4.   Results of STS-3 Particle Size Analysis

Sample	$\bar{D}_n$, μm	σ, μm	n	$\sigma/\bar{D}_n$, %	Relative No. of Over-Size Particles
Seed #4131-20	2.52	0.046	1024	1.84	0
Flight #1	3.44	0.064	2777	1.87	1/264
Ground #1	3.72	0.057	1363	1.54	1/339
Flight #2	4.08	0.069	2256	1.69	1/207
Ground #2	3.93	0.077	913	1.96	1/172
Flight #3	4.98 5.04 *	0.082 0.030	2095 900	1.64 0.60	1/99
Ground #3	4.74 5.03 *	0.167 0.151	1232 900	3.51 3.00	1/65

* determined by the National Bureau of Standards (NBS)

198

about the same (1.5-2.0%) for all samples except ground #3, which was made with the highest monomer/polymer ratio. The ground #3 latex not only had a broader main distribution than the flight latex, but also had a larger tail in the distribution curve. This was attributed to inadequate agitation, which allowed particles to experience different temperature-time histories and thus different polymerization and growth rates.

The off-size particle analysis was limited to particles significantly larger (two- or three-times larger in volume) than those in the main distribution. The results showed that the number of over-size particles increased with swelling ratio. No attempt was made to determine the number of off-size smaller particles resulting from particle nucleation in the aqueous phase.

The polymerization kinetics of both the flight and the ground polymerizations of large-particle-size latexes are shown in Figure 5-22. These curves represent only the 70°C portions of the experiments. There was no significant difference between the poly-merization rates in microgravity and on the ground.

5.2.2 STS-4

Four large-particle-size recipes were developed for the STS-4 flight experiments. Two of the recipes (#5 and #6) used the 5.5 μm crosslinked (0.06% DVB) seed latex #5084C; the other two recipes (#7 and #6) used the 5.5 μm uncrosslinked seed latex #5053C. The recipes are given in Table 5-5. The operation of the STS-4 flight experiments was similar to that of the STS-3 experiments.
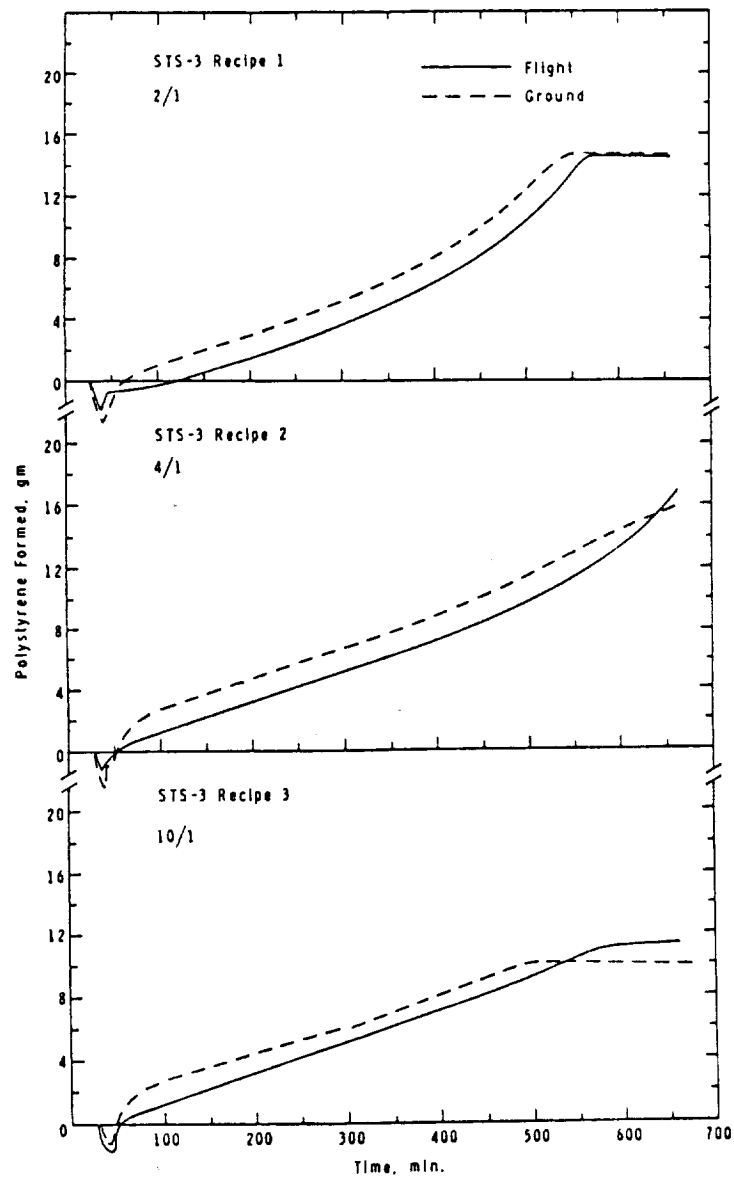
Figure 5-22. Conversion-time curves for STS-3 flight and ground polymerizations.

Table 5-5. STS-4 Flight Recipes

Recipe #	M/P	Initiator AMBN (%M)	Inhibitors HQ (%aq)	BQ (%aq)	Surfactants AMA (%aq)	KX-3 (%aq)	PVP (%aq)
5	2/1	0.075	0.034	0.005	0.014	0.024	0.194
6	4/1	0.106	0.034	0.005	0.007	0.018	0.177
7	6/1	0.129	0.034	0.005	0.005	0.016	0.166
8	8/1	0.149	0.034	0.005	0.004	0.018	0.182

The STS-4 experiments were carried out using the same procedure established for the STS-3 experiments; upon unloading, however, all of the latexes had the distinct odor of styrene monomer, and no data was found on the tape. The problem was traced to the failure of a DC voltage converter in the SEP, with the consequent failure of other electronic components, so that the monomer-swollen latexes were heated to some indeterminate temperature instead of 70°C. The conversions of these latexes determined by isooctane extraction were between 54% and 73% (Table 5-6).

Portions of each of the incompletely polymerized latexes in capped bottles were tumbled end-over-end in a water bath for 20 hours at 70°C and 3 hours at 70-82°C to complete the polymerizations. The latexes before and after heating were examined by SEM. Representative micrographs of the latexes along with the flight seeds are presented in Figures 5-23 to 5-27. Significantly more over-size particles or partially coalesced (dumbbell-shaped) particles were found in the latexes after heating on the ground. The particle diameters estimated

Table 5-6.   Conversions and Particle Sizes of the
STS-4 Flight Latexes

Sample	% Conversion	Particle Diameter, μm	
		Before	After *
---------	-------------	------	-------
Flight #5	56.1	7.5	7.5
Flight #6	72.9	8.3	9.0
Flight #7	53.5	8.7	9.3
Flight #8	55.0	9.0	10.8

* after heating for 20 hours at $70^{o}C$ and 3 hours at $70-82^{o}C$
on the ground

from the SEM micrographs, both before and after heating, are given in

Table 5-6.   No further analysis were carried out on these latexes and

the parallel ground-based experiments were not performed.

5.2.3 STS-6

Three of the STS-4 flight experiments were repeated in STS-6 but

with some modifications.   The 5.6 μm crosslinked (0.015% DVB) seed

latex #6010C was used.   The crosslinking agent DVB was also included

in the flight recipes.   The recipes are listed in Table 5-7.

The   polymerization   conditions   were   similar   to   the   STS-3

experiments except that the reaction time at $70^{o}C$ was extended from 11

to 17 hours.   Two of the recipes (#9 and #11) were successfully

polymerized to high conversions in microgravity, but the third recipe

(#10) was never heated owing to a broken wire in the heating element.

The latexes and data tape were recovered for analysis.   The ground-

based control experiments were also carried out shortly afterwards for

comparison with the flight results.

202
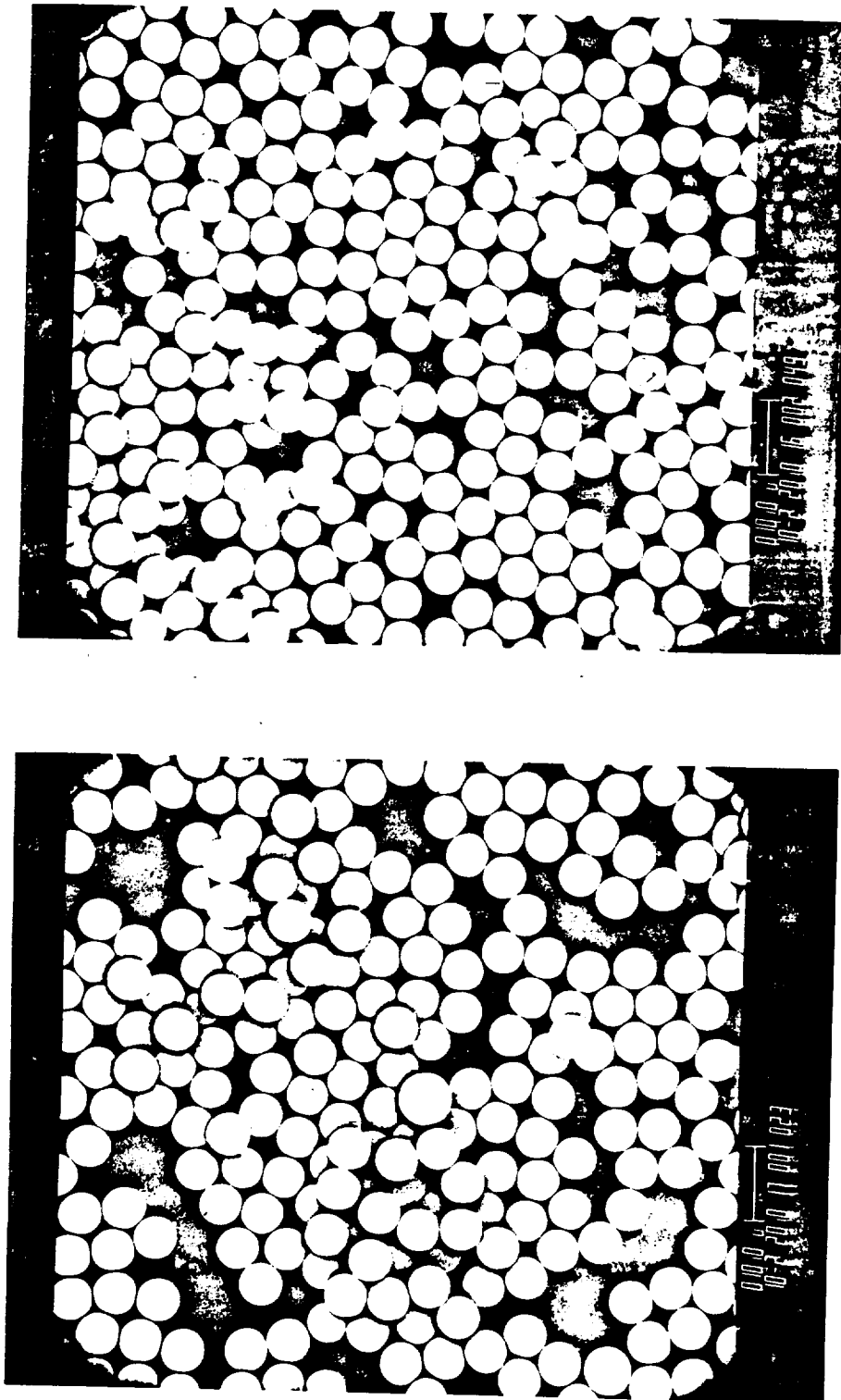
Figure 5-23. SEM micrographs of STS-4 flight seed latexes #5084C (left) and #5053C (right).

203

C- 7
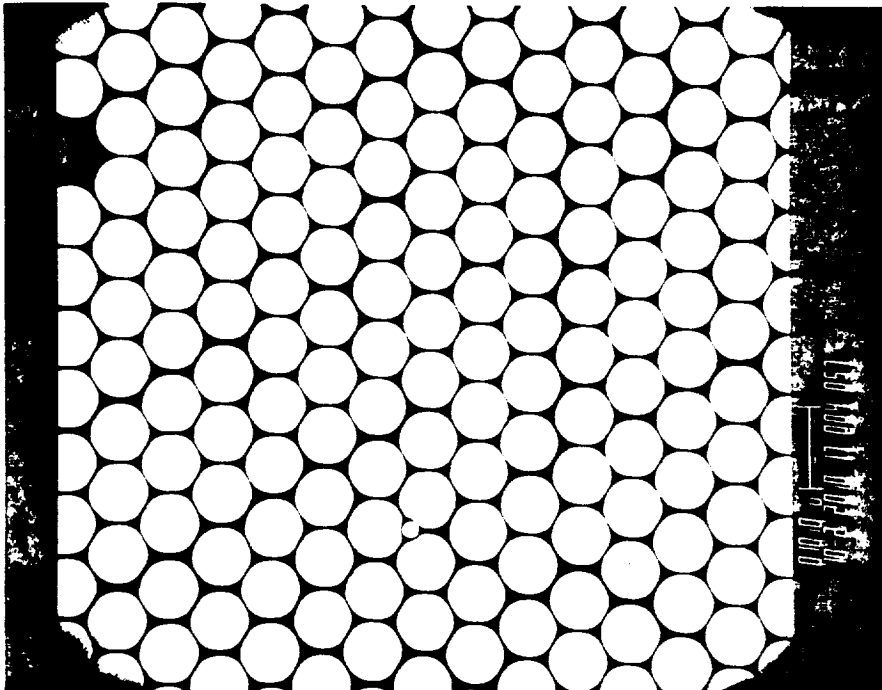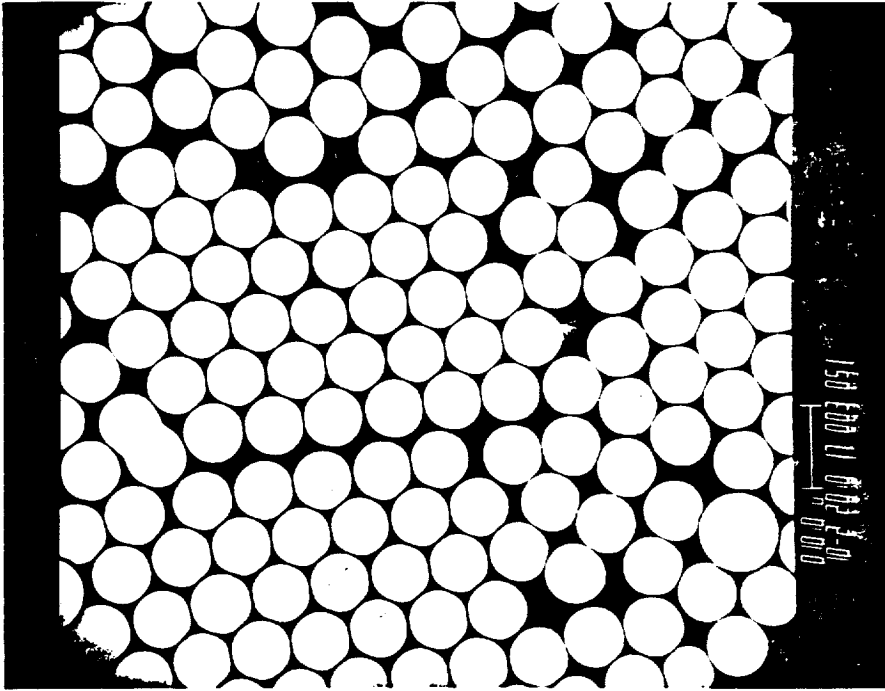
Figure 5-24. SEM micrographs of STS-4 flight latex #5, before (left) and after (right) heating on the ground.
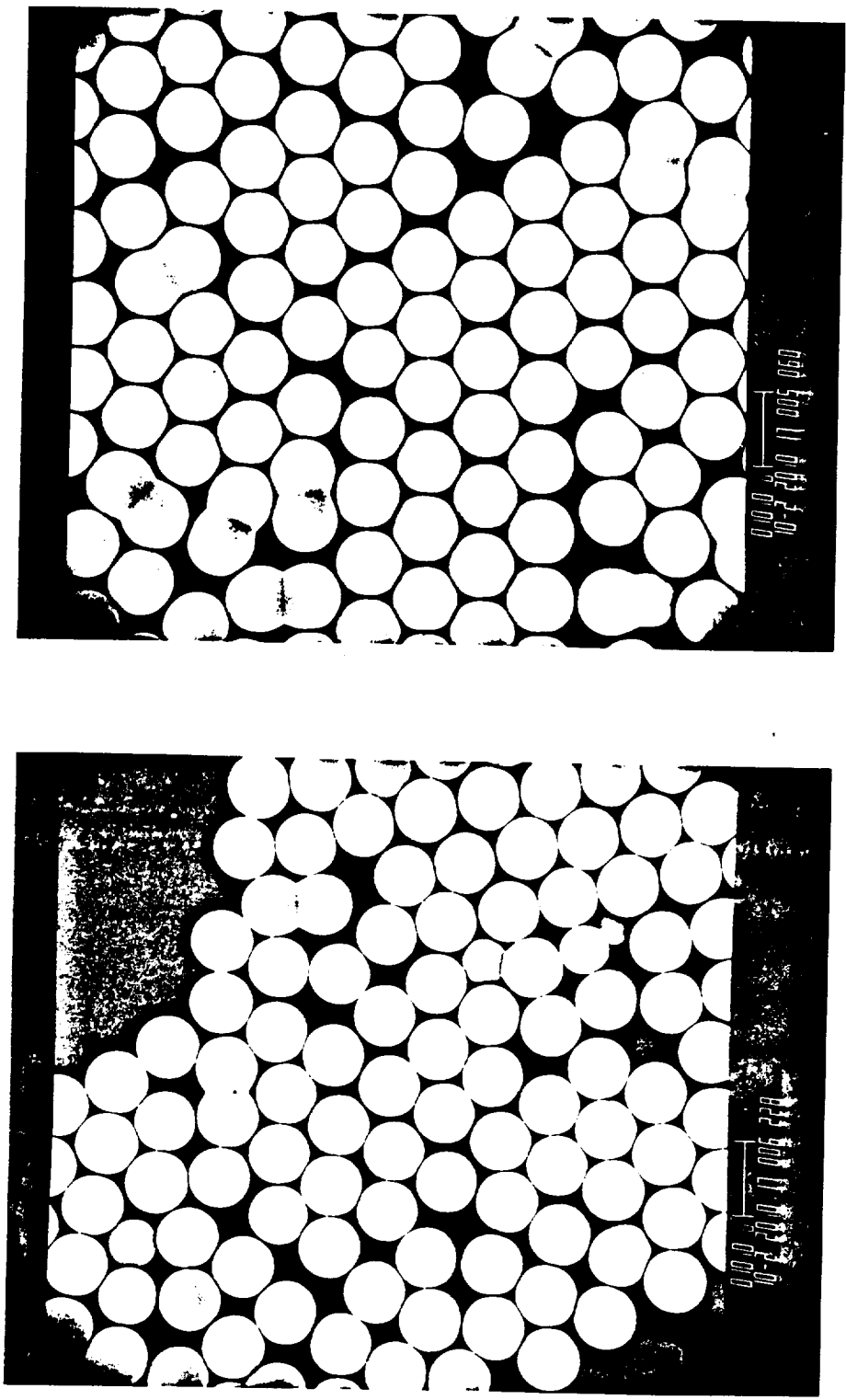
Figure 5-25. SEM micrographs of STS-4 flight latex #6, before (left) and after (right) heating on the ground.
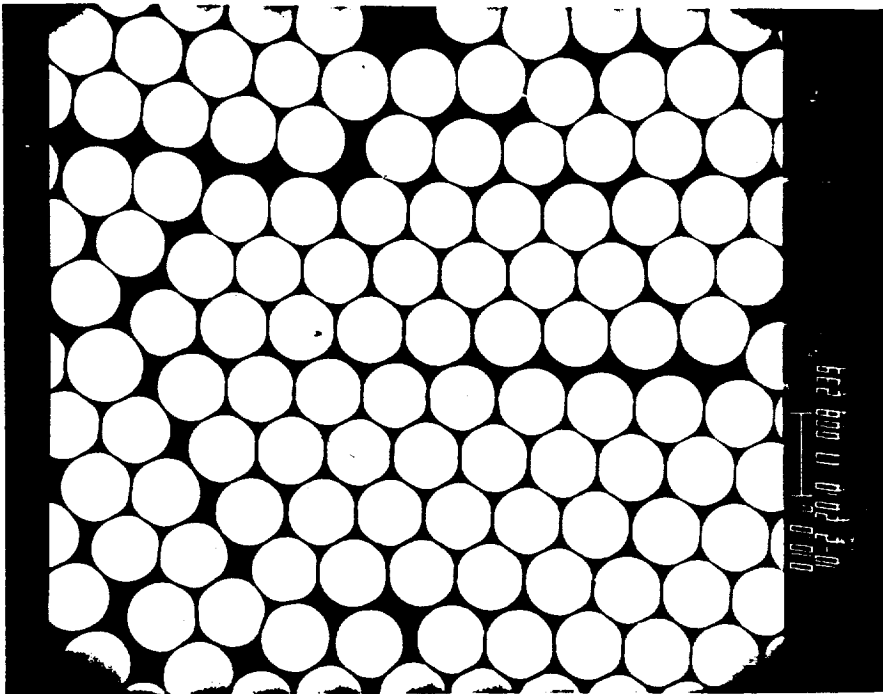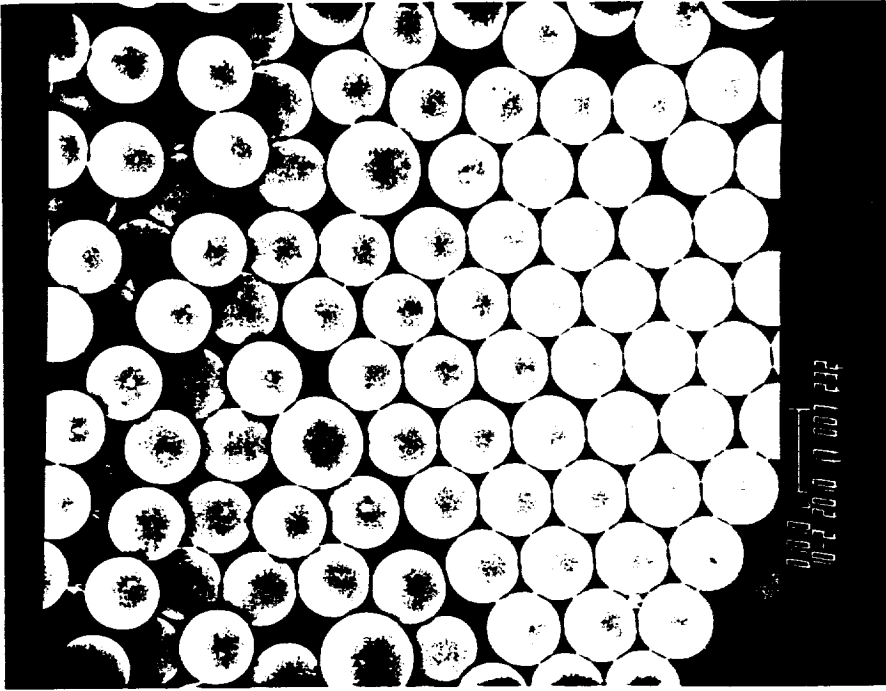
Figure 5-26. SEM micrographs of STS-4 flight latex #7, before (left) and after (right) heating on the ground.
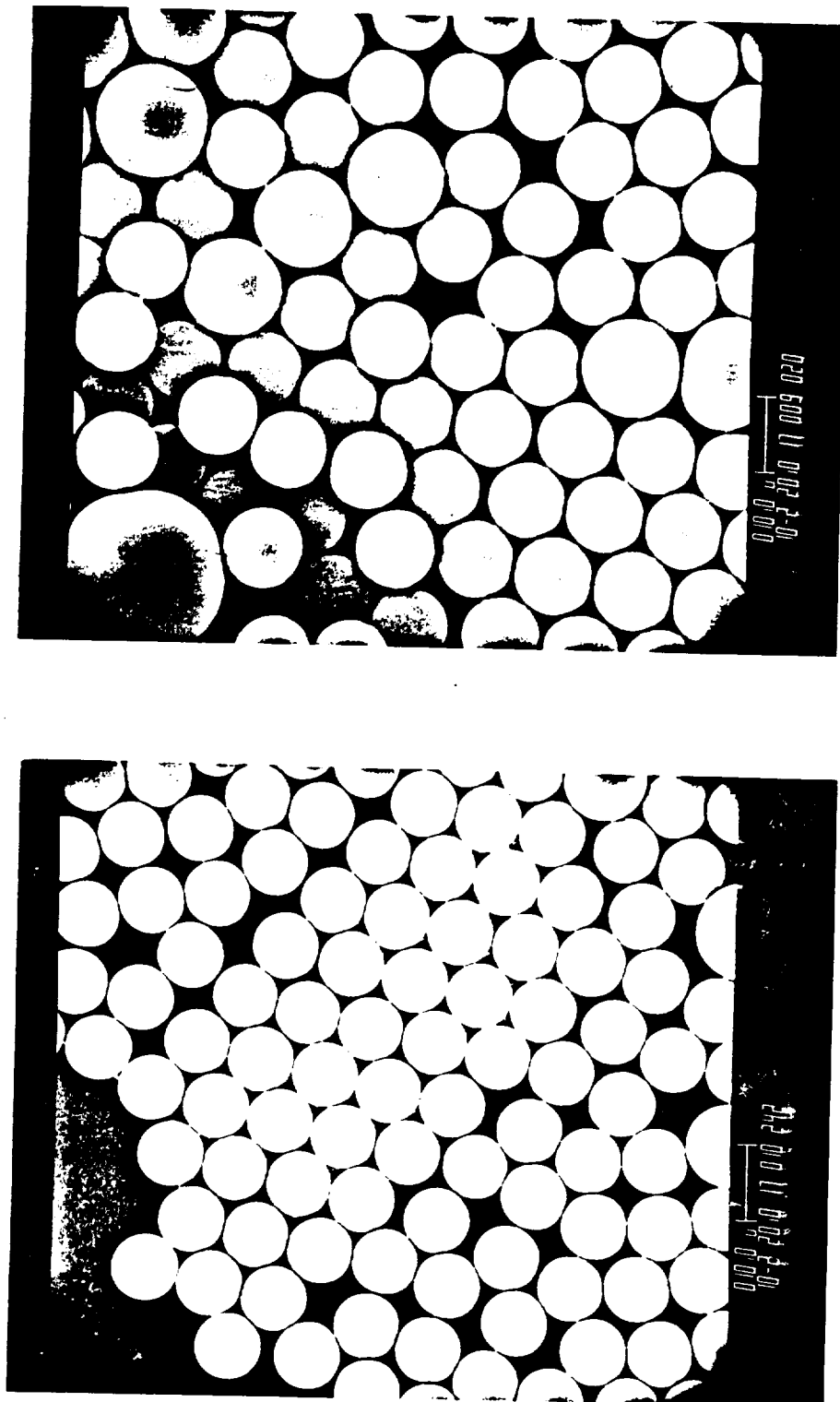
Figure 5-27. SEM micrographs of STS-4 flight latex #8, before (left) and after (right) heating on the ground.

Table 5-7.   STS-6 Flight Recipes

Recipe #	M/P	Initiator AMBN (%M)	Inhibitors HQ (%aq)	BQ (%aq)	Surfactants AMA (%aq)	KX-3 (%aq)	PVP (%aq)	Crosslinker DVB (%M)
9	2/1	0.075	0.034	0.0009	0.014	0.024	0.194	0.015
10	4/1	0.106	0.034	0.0009	0.007	0.019	0.177	0.015
11	6/1	0.128	0.034	0.0009	0.006	0.017	0.166	0.015

The solids contents of the product latexes along with the isooctane extraction results of the monomer-swollen latexes are given in Table 5-8.

Table 5-8.   Solids Contents and Results of Isooctane Extraction of STS-6 Flight and Ground Latexes

Sample	% Solids	gm styrene/100gm latex exp.	design
Flight #9	26.9	18.4	20.0
Ground #9	27.7	20.0	
Flight #11	22.0	23.1	25.7
Ground #11	22.9	24.0	

Representative TEM micrographs and particle size distributions for the STS-6 seed, flight, and ground latexes are presented in Figures 5-28 to 5-37. The results are summarized in Table 5-9. All of the latexes comprised narrow main distributions except for ground latex #11, which had a small-particle-size tail. This type of distribution-broadening, which was also seen in the STS-3 ground latex

#3, was attributed to insufficient agitation to prevent particles from creaming and sedimenting and to keep a uniform temperature-time profile in the reactor.

The flight latexes contained a number of deformed (barrel-shaped) particles as well as some over-size particles. The relative numbers are given in Table 5-9. The number of over-size particles increased with the increasing swelling ratio, as was the case for the STS-3 experiments. The reason for the formation of these barrel-shaped particles was not known, but may be related to the post-process agitation in the flight experiments: the barrel-shaped particles were made deliberately by mechanical shear, e.g., by smearing a drop of large-particle-size latex over a microscopic slide with a glass rod; the barrel-shaped particles were reformed into spheres by heating the latex with gentle agitation (shaking or tumbling) at 90°C for 15 minutes to one hour.

The polymerization kinetics of the flight and ground recipes #9 and #11 are shown in Figure 5-38. The first parts of the conversion-time curves were similar for the flight and ground runs. However, the flight curves levelled off much earlier than the ground curves. The reason for this difference is not clear. One possibility is that a thin polymer film formed on the cylinder wall of the reactor between the loading and the Shuttle launch (~3 days), which prevented the piston from moving all the way down as the polymerization proceeded and the latex volume shrank.
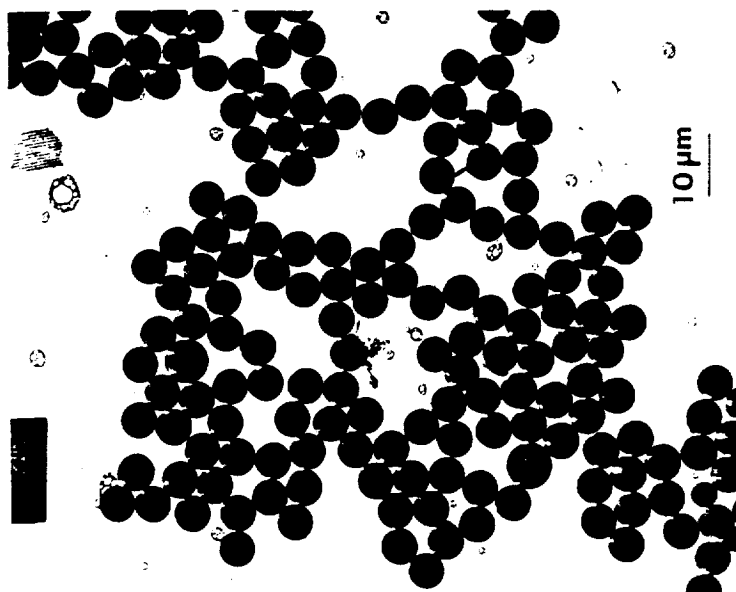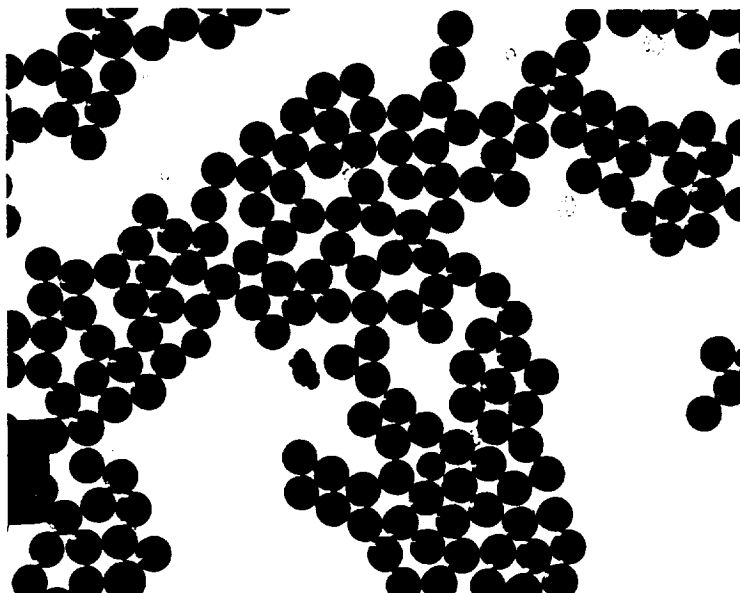
Figure 5-28. TEM micrographs of STS-6 flight Seed #6010C.

10 μm
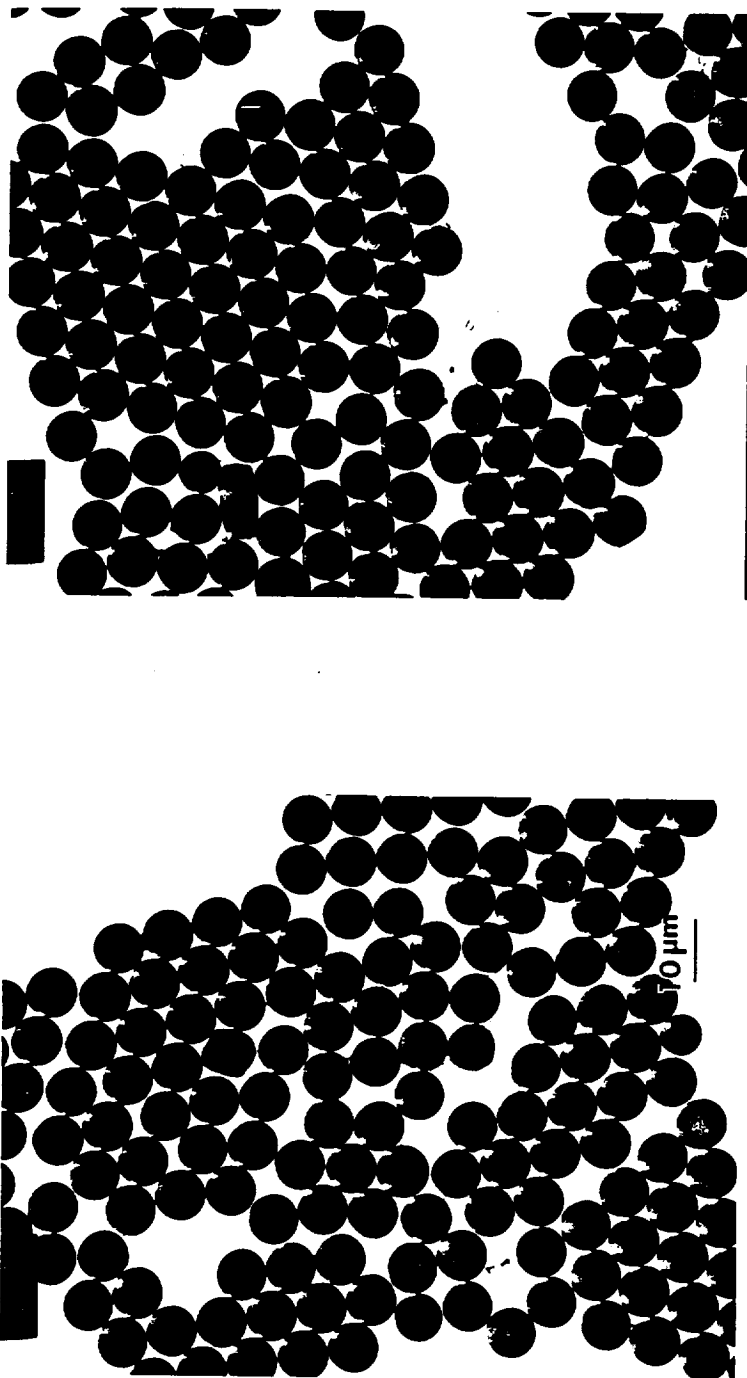
Figure 5-29.   TEM micrographs of STS-6 flight latex #9.
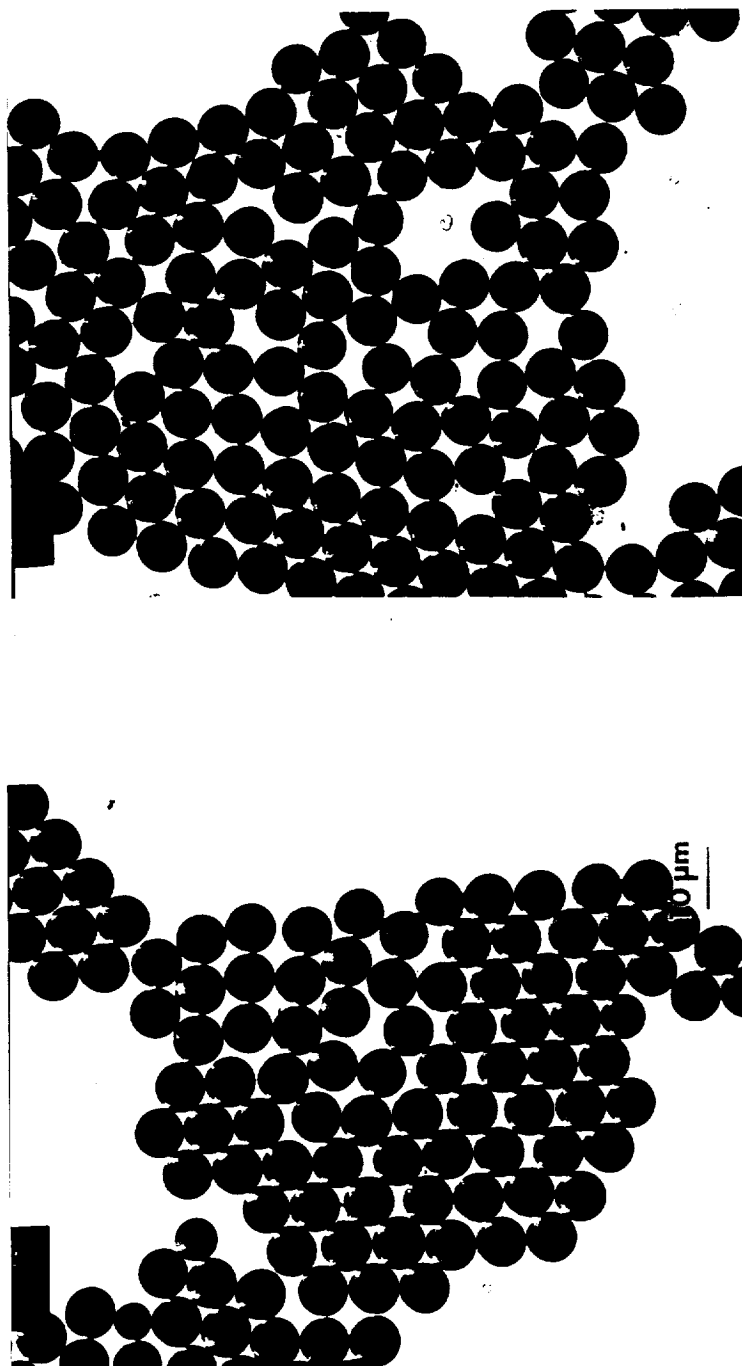
Figure 5-30.   TEM micrographs of STS-6 ground latex #9.
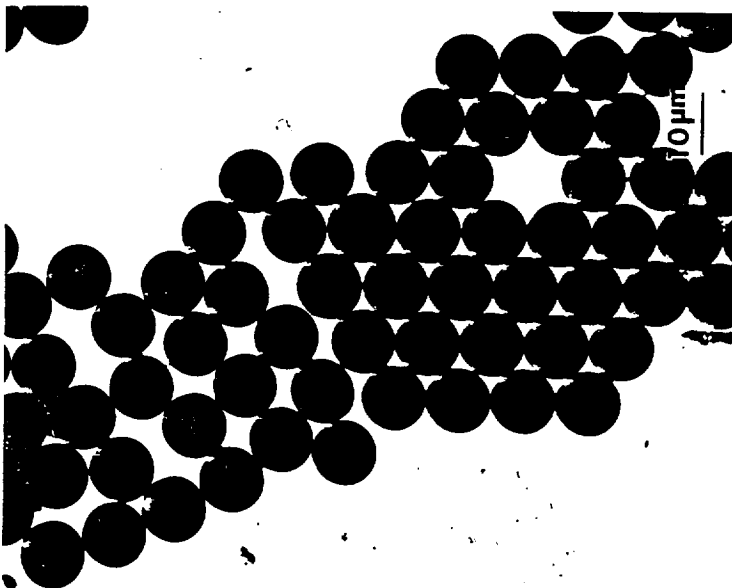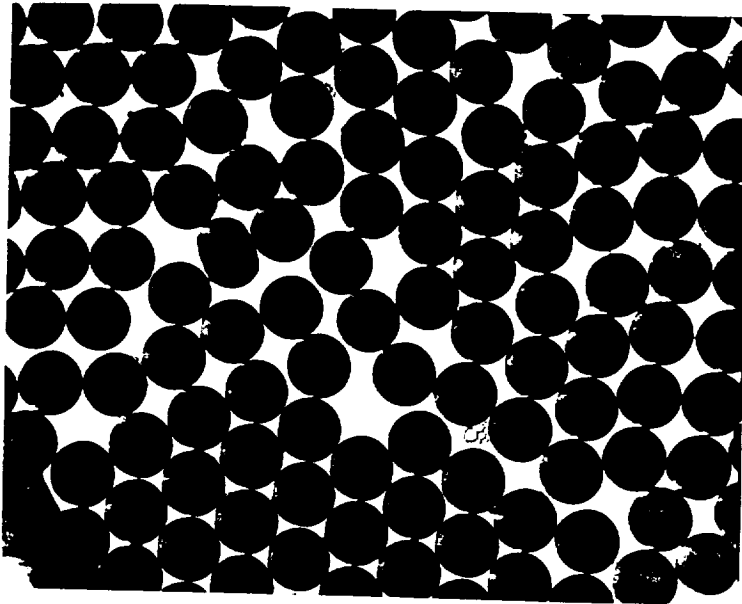
Figure 5-31. TEM micrographs of STS-6 flight latex #11.

10 μm
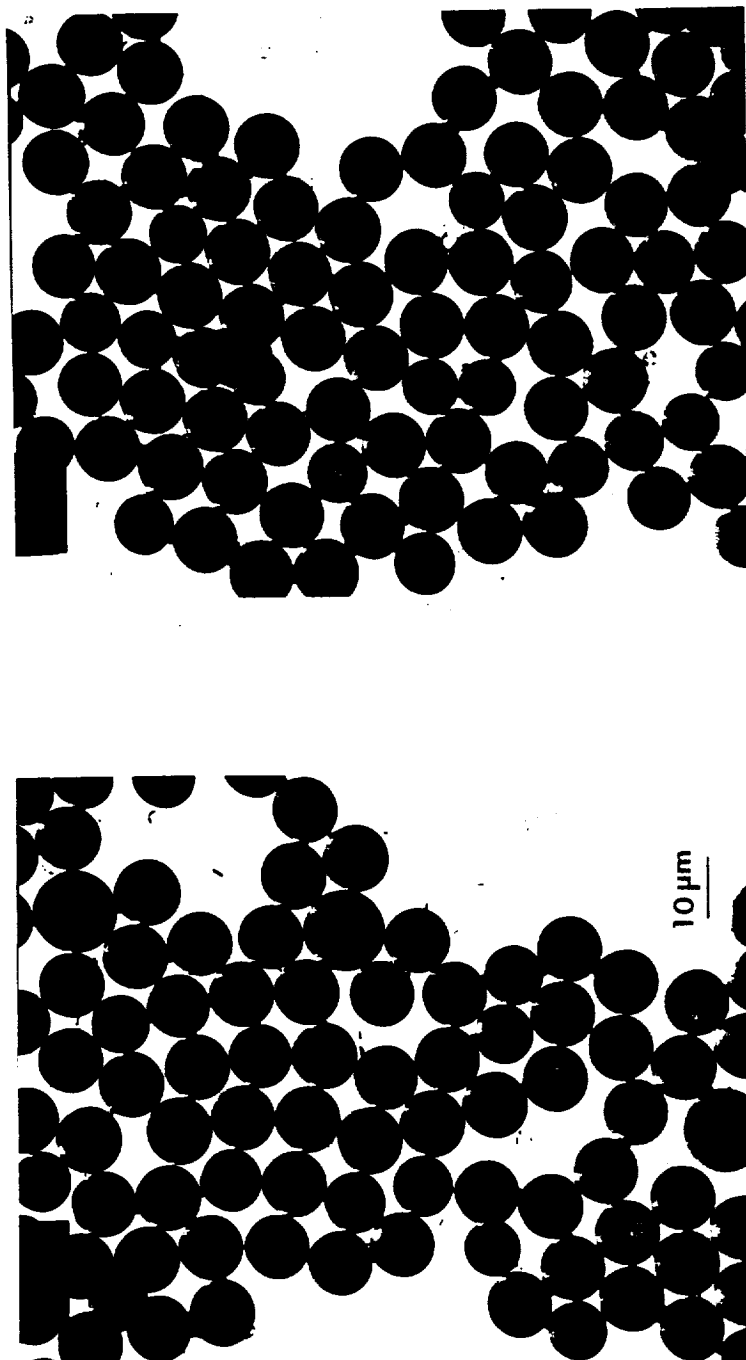
Figure 5-52. TEM micrographs of STS-6 ground latex #11.

SAMPLE SEED STS6

D_n = 5631.9   PDI = 1.000
D_w = 5634.7 D_{min} = 5200.0
N =   328 D_{max} = 5980.0
D_v = 5632.8 D_a = 5632.4
S_d =   73.0   STEP = 30.0
D_q = 5635.6 D_s = 5633.8
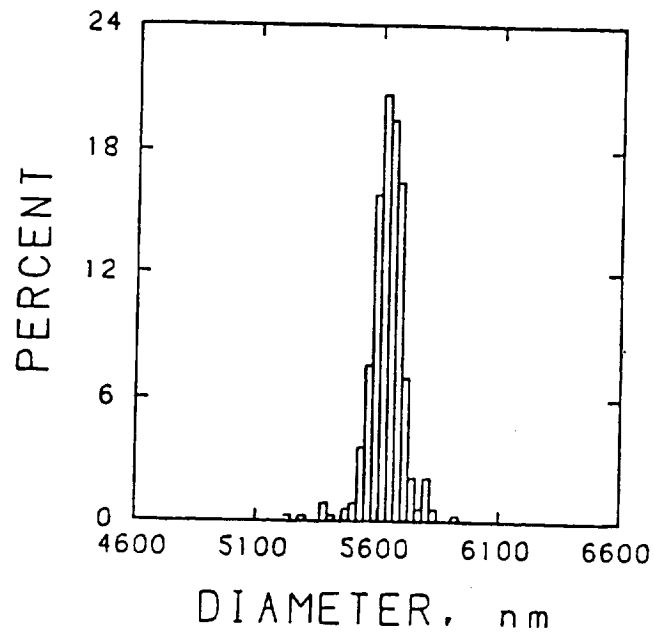
Figure 5-33.   Particle size distribution of STS-6
flight seed #6010C.

SAMPLE FLIGHT 9

D_n = 7939.7   PDI = 1.001
D_w = 7945.3 D_{min} = 7040.0
N   =   829 D_{max} = 8990.0
D_v = 7941.5 D_a = 7940.6
S_d = 121.8   STEP =   30.0
D_q = 7947.2 D_s = 7943.4
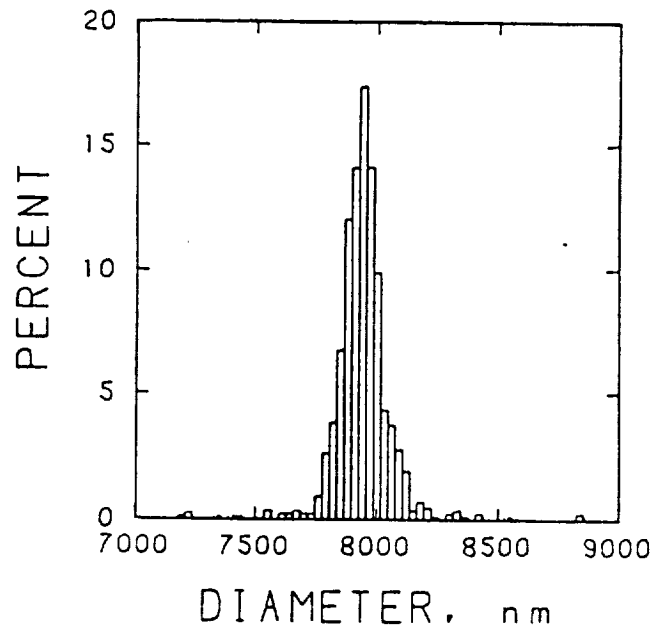
Figure 5-34.   Particle size distribution of STS-6
flight latex #9.

216

SAMPLE GROUND 9

D_n = 7863.6   PDI = 1.001
D_w = 7870.7 D_{min} = 7040.0
N =   675 D_{max} = 8960.0
D_v = 7865.9 D_a = 7864.7
S_d = 137.0   STEP =   30.0
D_q = 7873.0 D_s = 7868.3
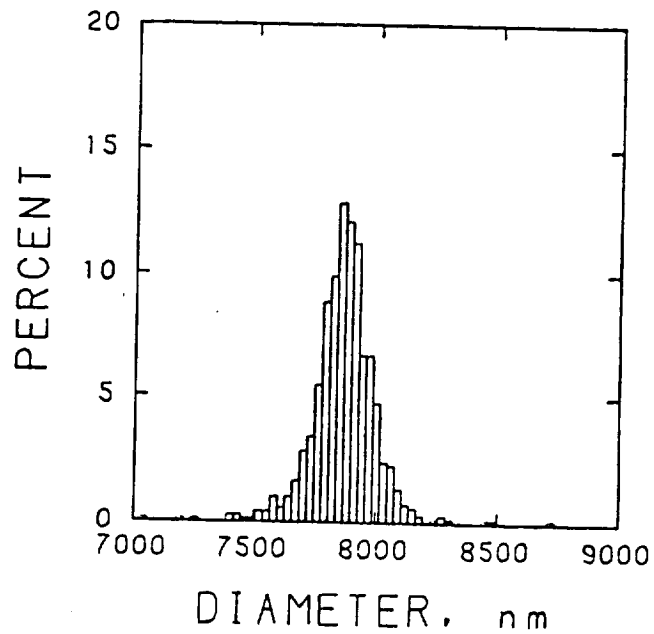
Figure 5-35.   Particle size distribution of STS-6 ground latex #9.

SAMPLE FLIGHT 11

D_n = 9963.4   PDI   = 1.000
D_w = 9967.4 D_{min} = 9100.0
N   = 1102 D_{max} =10960.0
D_v = 9964.7 D_a = 9964.1
S_d = 115.3   STEP =   30.0
D_q = 9968.7 D_s = 9966.1
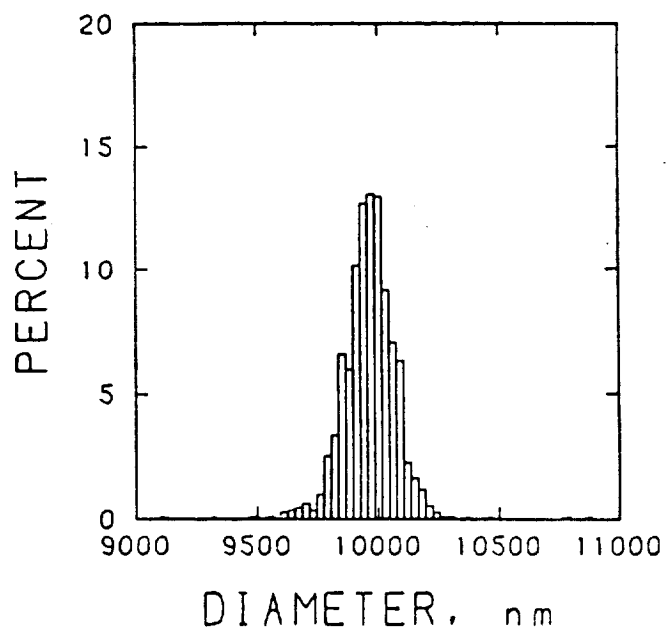
Figure 5-36.   Particle size distribution of STS-6
flight latex #11.

SAMPLE GROUND 11

D_n =10040.8   PDI = 1.002

D_w =10063.3 D_{min} = 9040.0

N = 1059 D_{max} =10960.0

D_v =10048.6 D_a =10044.8

S_d = 281.3   STEP = 30.0

D_q =10070.0 D_s =10056.2
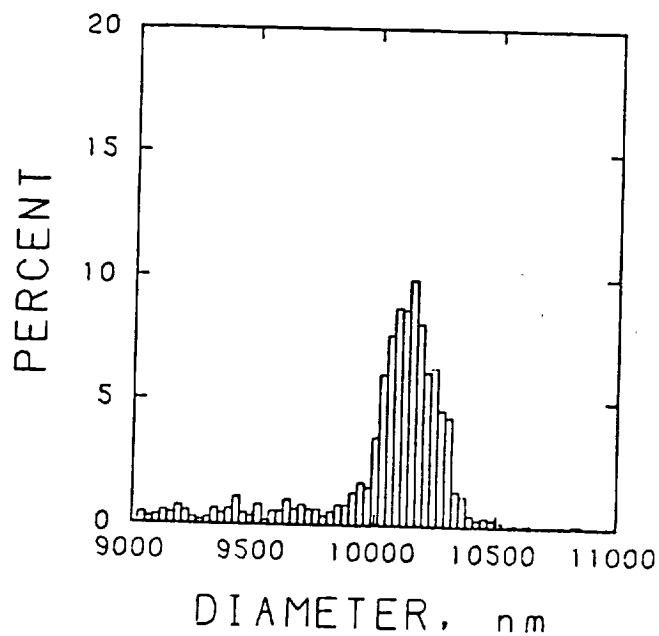
Figure 5-37. Particle size distribution of STS-6 ground latex #11.

Table 5-9.   Results of STS-6 Particle Size Analysis

Sample	$\bar{D}_n$, μm	σ, μm	n	$\sigma/\bar{D}_n$, %	Relative No. of Particles Deformed	Relative No. of Particles Over-size
Seed #6010C	5.63	0.073	328	1.30	0	1/168
Flight #9	7.94	0.122	829	1.53	1/63	1/267
Ground #9	7.86	0.137	675	1.74	0	1/220
Flight #11	9.96	0.115	1102	1.16	1/62	1/106
Ground #11	10.04	0.281	1059	2.80	1/1410	1/93
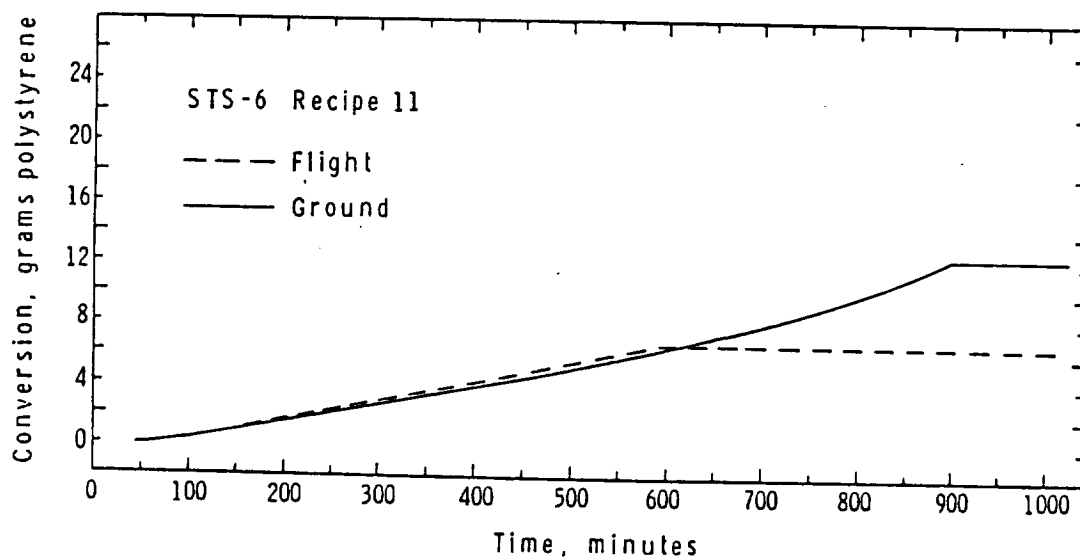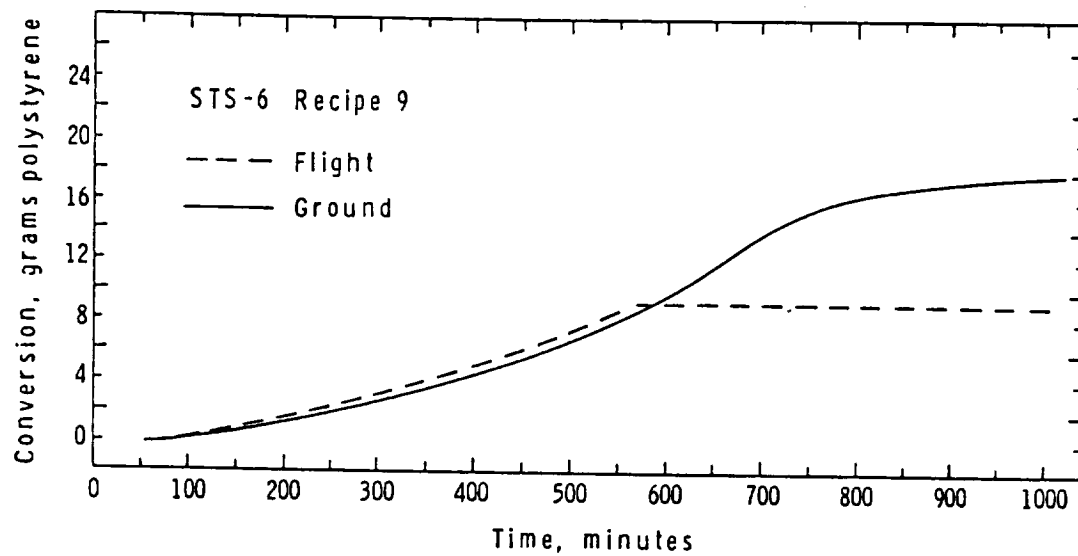
Figure 5-38. Conversion-time curves for the STS-6 flight and ground polymerizations.

5.2.4 STS-7

Four large-particle-size seeded polymerizations were conducted on STS-7 flight. Three recipes used the 10.3 μm crosslinked (0.015% DVB) seed latex #6027-3C and the fourth used the 7.9 μm flight latex #9 produced on the STS-6 mission. Unlike the other flight seed latexes, the 7.9 μm seed was used without further cleaning. Modifications were made on the flight reactors, to provide continuous oscillatory agitation in the "preprocess" mode. Two reactors also used two separate agitation speeds for the "preprocess" and the "process". The various combinations used for STS-7 are listed in Table 5-10. The recipes are given in Table 5-11. Recipe #15 and #16 were identical except for the different agitation rates.

All four reactors functioned properly for both the flight and ground-based experiments. Varying amounts of coagulum were formed in the samples, as given in Table 5-12. The solids contents and isooctane extraction results are also included.

Table 5-10. Recipe and Agitation Conditions for STS-7

Recipe #	Seed diameter (μm)	M/P	Oscillatory agitation rpm Preprocess	Process
13	7.9 *	6/1	13	13
14	10.3	4/1	13	13
15	10.3	6/1	13	6
16	10.3	6/1	6	3

* Flight latex #9 from STS-6

Flight latexes #13 and #14 had slightly lower yields than their

222

Table 5-11.   STS-7 Flight Recipes

| Recipe # | M/P | Initiator | Inhibitors | | Surfactants | | | Crosslinker |
		AMBN (%M)	HQ (%aq)	BQ (%aq)	AMA (%aq)	KX-3 (%aq)	PVP (%aq)	DVB (%M)
13	6/1	0.128	0.034	0.0004	0.031	0.013	0.135	0.015
14	4/1	0.106	0.034	0.0004	0.007	0.018	0.177	0.015
15 & 16	6/1	0.128	0.034	0.0004	0.005	0.016	0.166	0.015

Table 5-12.   Solids Contents, Isooctane Extraction Results and Estimated Coagulum of STS-7 Flight and Ground Latexes

| Sample | % Solids | gm styrene/100gm latex | | % Coagulum |
		exp.	design	
Flight #13	17.3	17.0	25.8	17 *
Ground #13	21.8	20.7		15
Flight #14	17.1	20.8	24.0	34 *
Ground #14	24.1	22.5		20
Flight #15	20.5	20.8	25.8	5 *
Ground #15	12.9	17.7		43
Flight #16	19.8	23.6	25.8	10 *
Ground #16	3.4	19.9		87

* estimated from the amount separated from the latex and recovered from the reactor; all others estimated from predicted versus measured product solids

ground-based counterparts, while the flight latexes #15 and #16 had much higher yields than obtained on the ground. The latter were attributed to the ineffective agitation which led to sedimentation and coalescence of the particles on the ground. The lower yields in flight latexes #13 and #14 are not so easily explained. One possibility was that the three days of preprocess agitation before the

launch, which was not experienced by the ground-based latexes, could have destabilized some of the particles.

The particle size analysis of the STS-7 latexes was accomplished by measuring individual particle diameters from SEM micrographs instead of TEM micrographs because of the high magnification distortion in the TEM at low magnification settings (see Chapter 6). Representative micrographs and particle size distributions of the seed, flight, and ground latexes are presented in Figure 5-39 to 5-56. The results are summarized in Table 5-13. The relative numbers of over-size particles and deformed particles, estimated by optical microscopy, are also included in the table.

The main distributions of all of the flight latexes were quite narrow. The coefficients of variation $(\sigma/\bar{D}_n)$ for these flight latexes were 1.1-1.2%, even smaller than those obtained for the STS-3 (1.5-1.9%) and STS-6 flight latexes (1.2-1.5%), probably because of the smaller contribution of magnification distortion to the measurement uncertainty in the SEM than in the TEM. ground latexes #13 $(\sigma/\bar{D}_n = 2.7\%)$ and #14 $(\sigma/\bar{D}_n = 2.3\%)$ had broader main distributions and larger small-particle-size tails in their distribution curves than the flight counterparts. Massive coagulum was formed in the ground #15 and #16 experiments; the latex particles remaining comprised broad distributions.

The relative numbers of over-size particles increased slightly with increasing particle size for the flight samples and more so for the ground analogues. The particle size distributions for ground latexes #15 and #16 were so broad that over-size particles were not

obvious. Deformed particles were also found in the flight samples, as was the case for the STS-6 experiments. Significant quantities were not found in the ground samples except for #13, which was prepared from the 7.9 μm flight seed, which itself contained some deformed particles.

The conversion-time curves for the STS-7 experiments are presented in Figures 5-57 and 5-58. Comparison of the flight and ground kinetics was difficult because of the difference in temperature-time profiles and the creaming, sedimentation, and coalescence of the particles in the ground experiments, due to insufficient agitation.

In summary, Figures 5-59 to 5-61 combine the particle size distributions of seeds, flight, and ground latexes for the STS-3, STS-6 and STS-7 flights on semilog plots. These distributions were normalized so that the area under each curve was approximately the same. The results indicated that distributions of all flight latexes were very narrow. The ground latexes, except #1, all had broader main distributions and larger small-particle-size tails than their flight counterparts. The particle size distributions of the ground latexes #15 and #16 were so broad that they could no longer be called "monodisperse". Off-size larger particles found in the flight and ground latexes ranged from 1/360 to 1/50 relative to the main distribution, generally increasing in number with increasing swelling ratio. Deformed particles, often barrel-shaped, were also found in the flight latexes of particle sizes >7 μm; however, they were virtually absent from the ground latexes. The post-process agitation, which was used
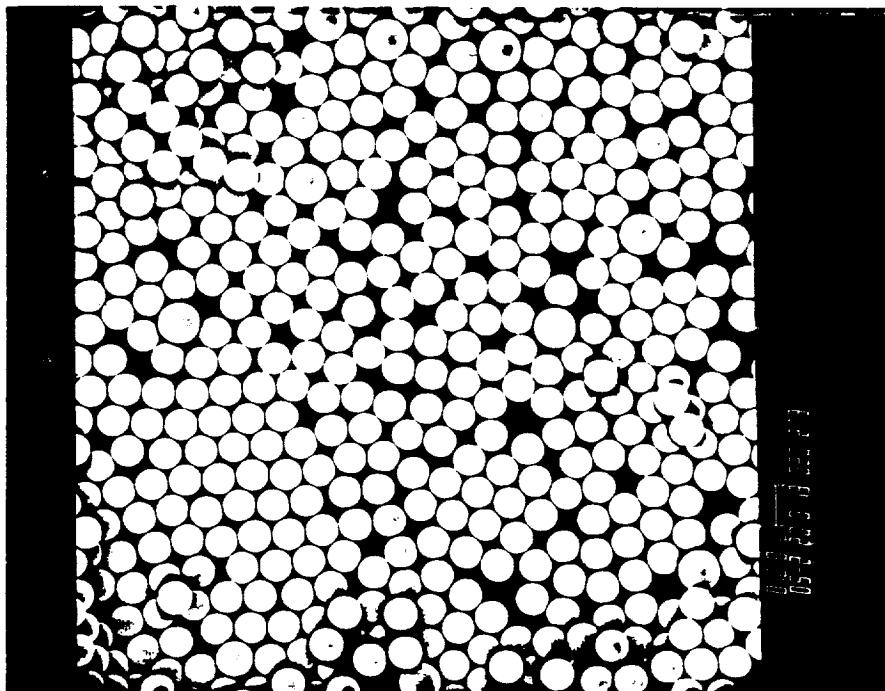
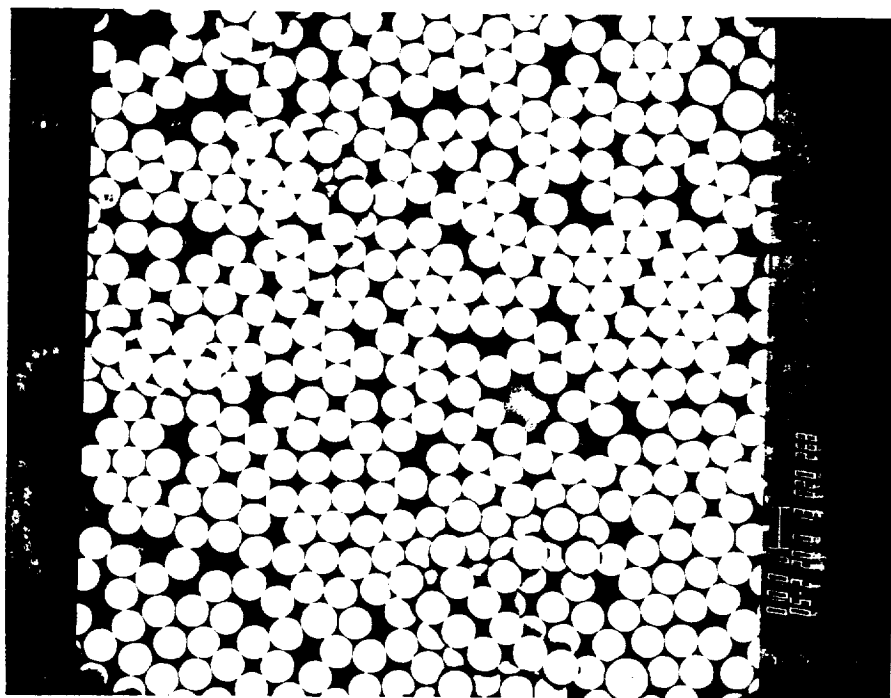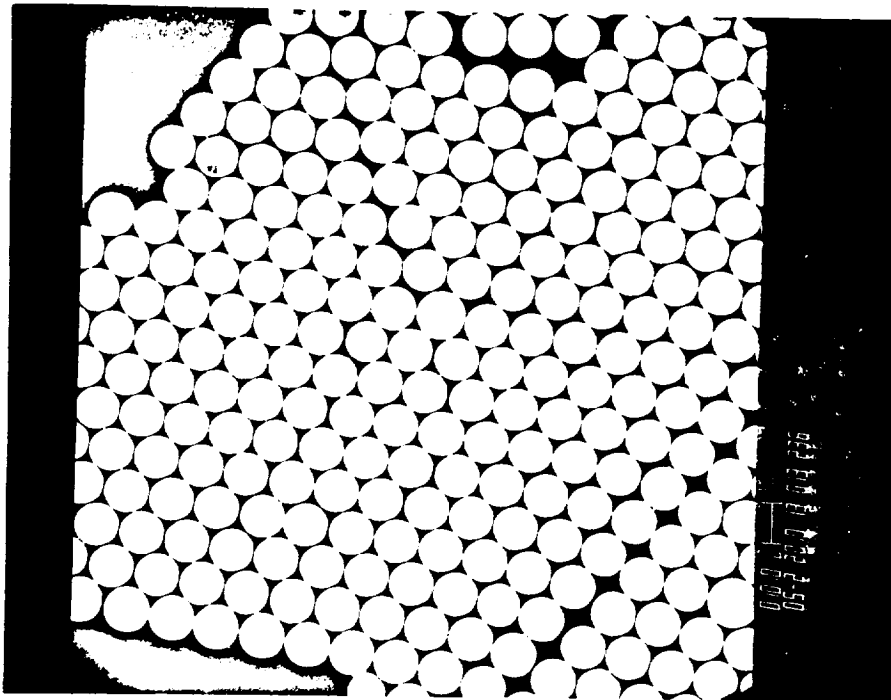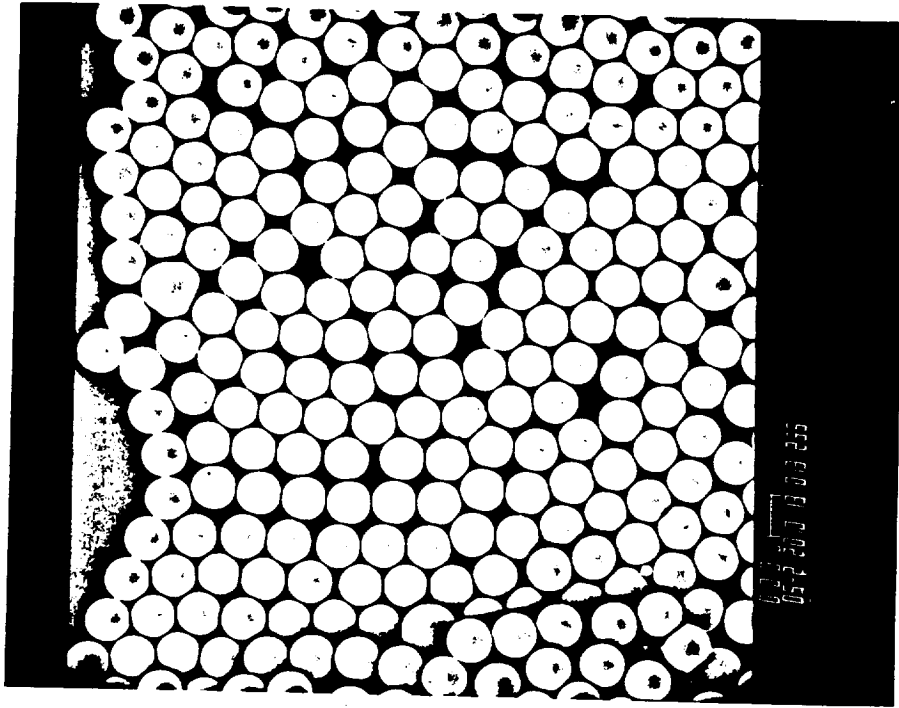Figure 5-39.   SEM micrographs of STS-7 flight seed #6027-3C.

Figure 5-40. SEM micrographs of STS-7 flight latex #13.

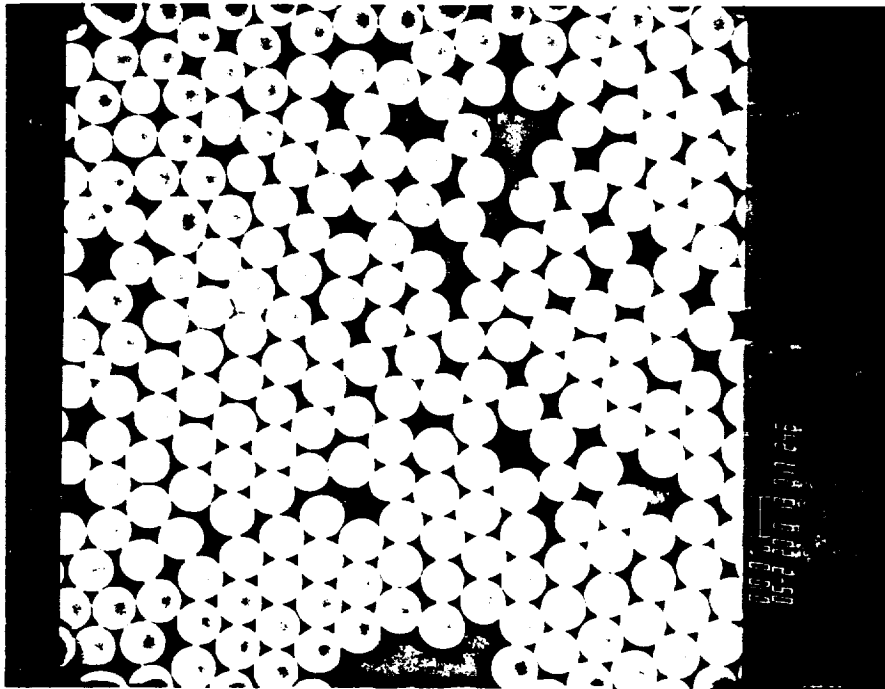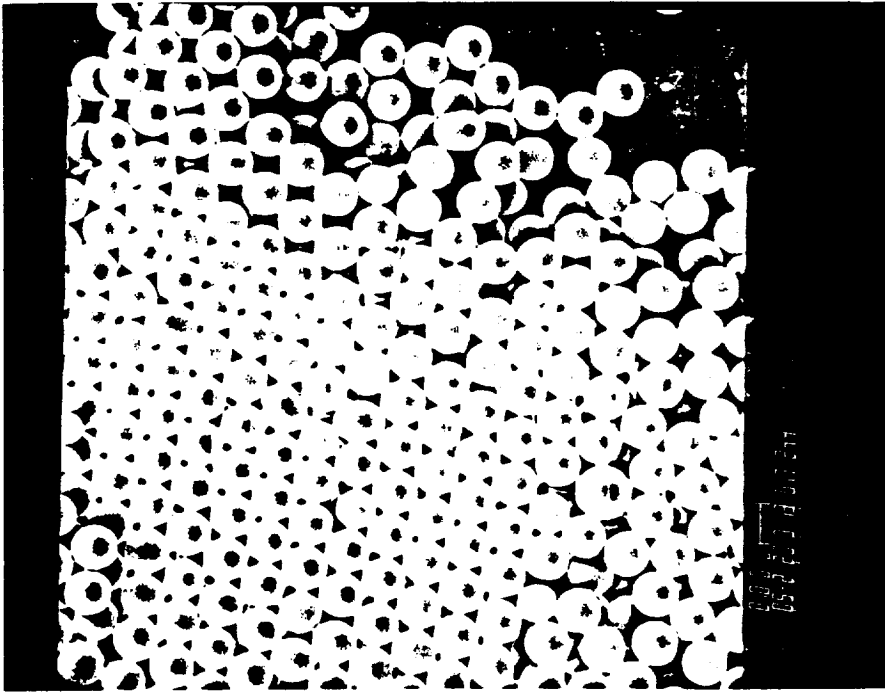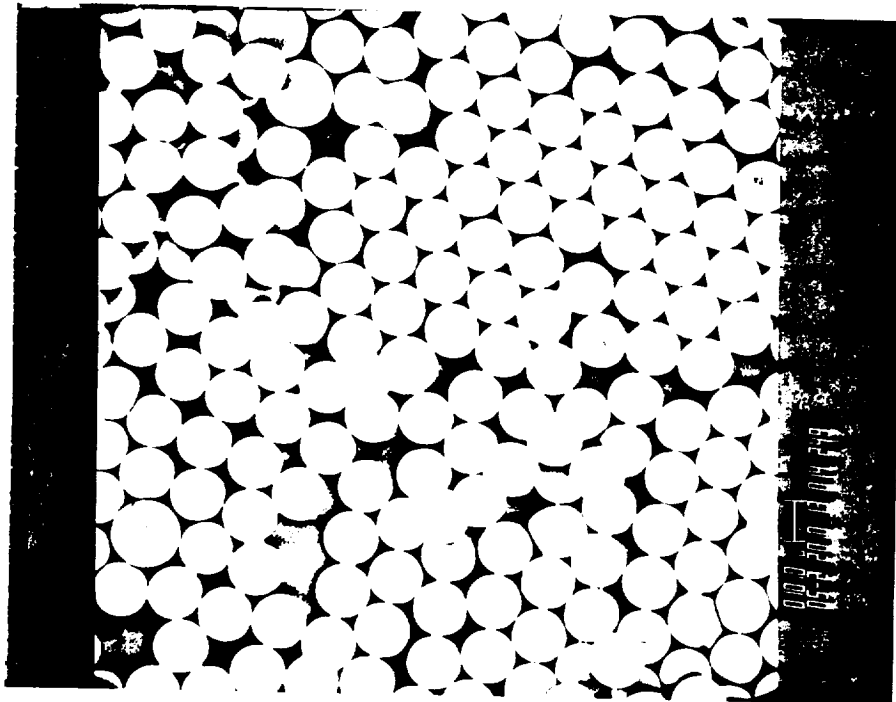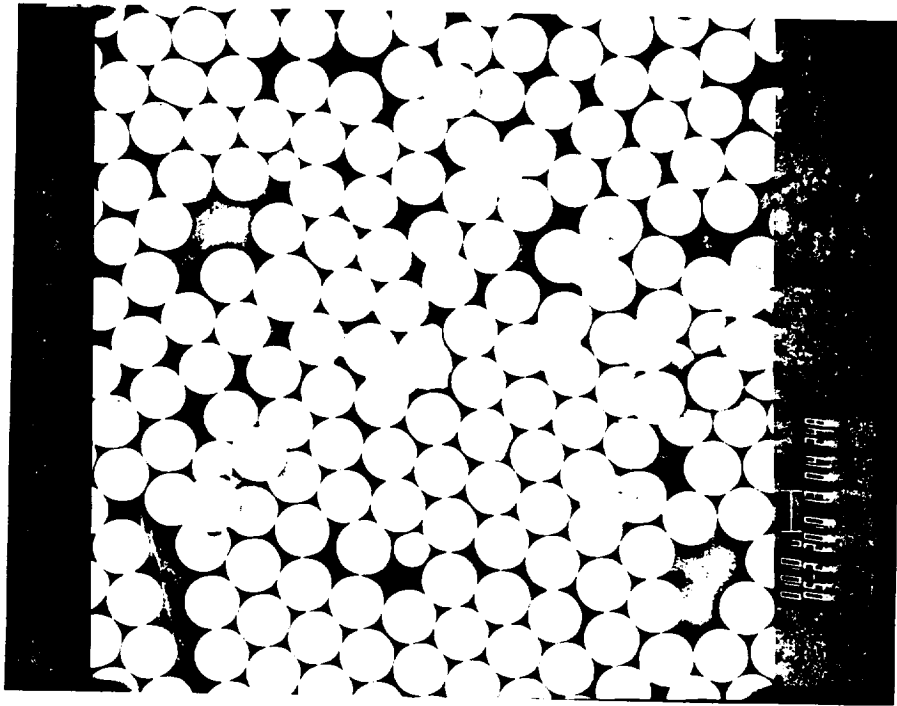Figure 5-41. SEM micrographs of STS-7 ground latex #13.

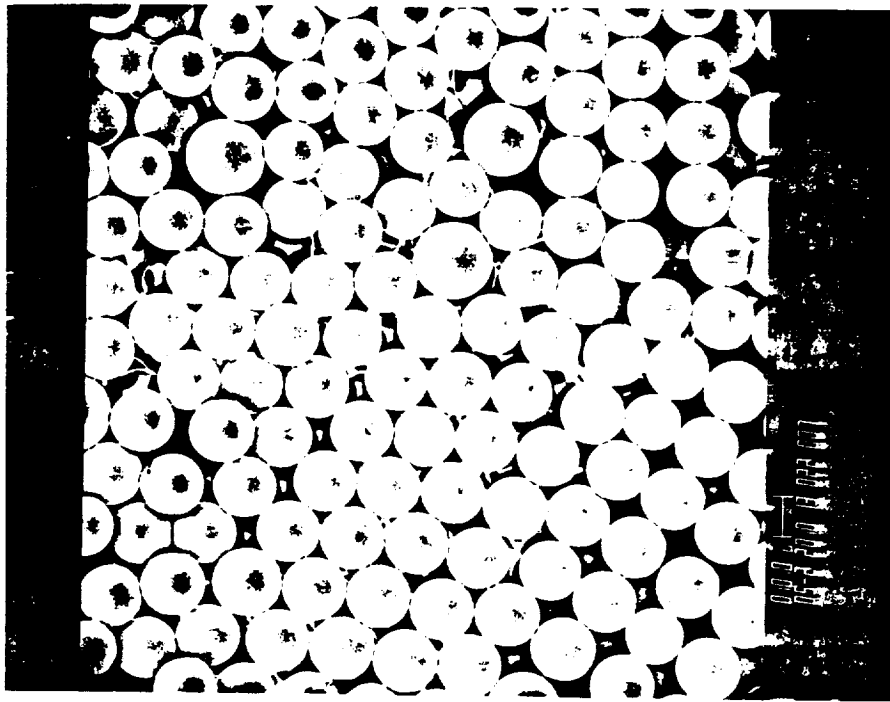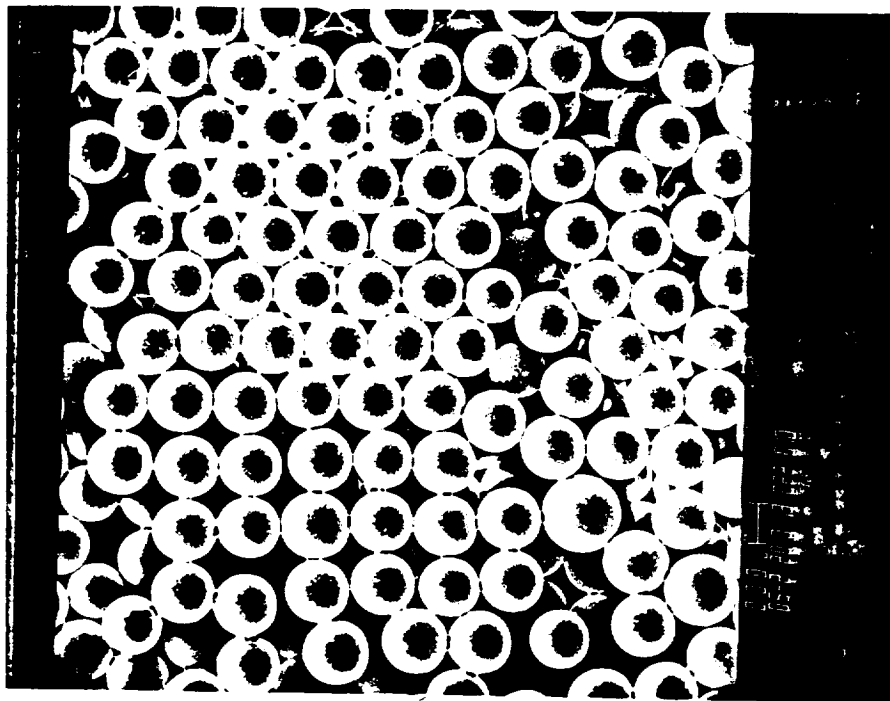Figure 5-42.   SEM micrographs of STS-7 flight latex #14.

229

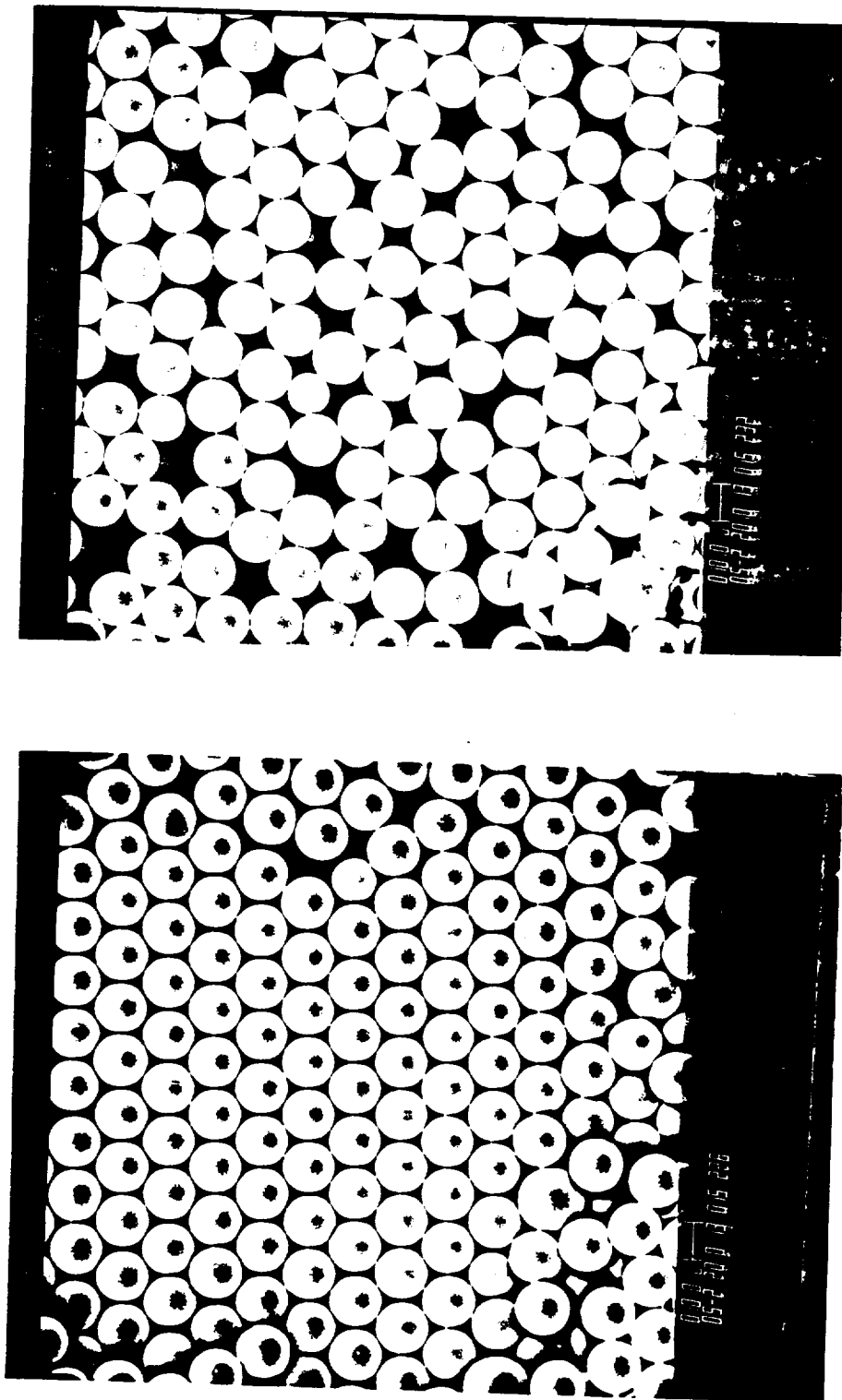Figure 5-43.   SEM micrographs of STS-7 ground latex #14.

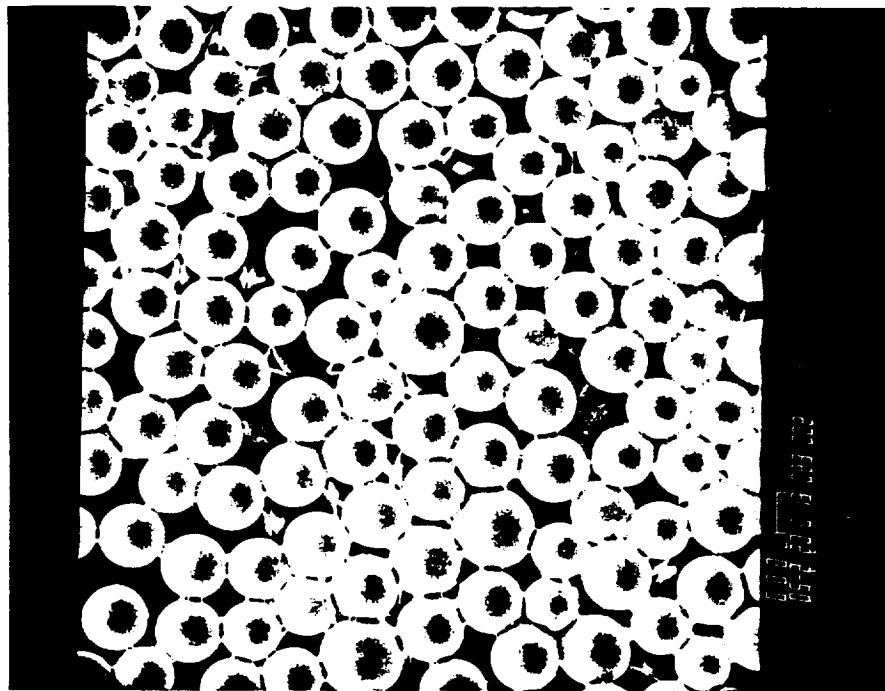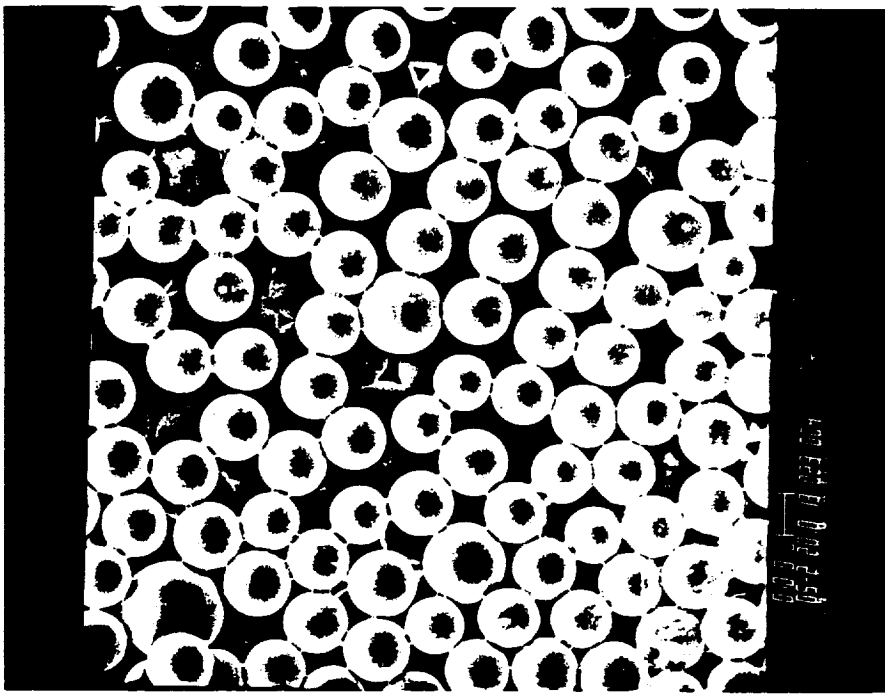Figure 5-44. SEM micrographs of STS-7 flight latex #15.

231

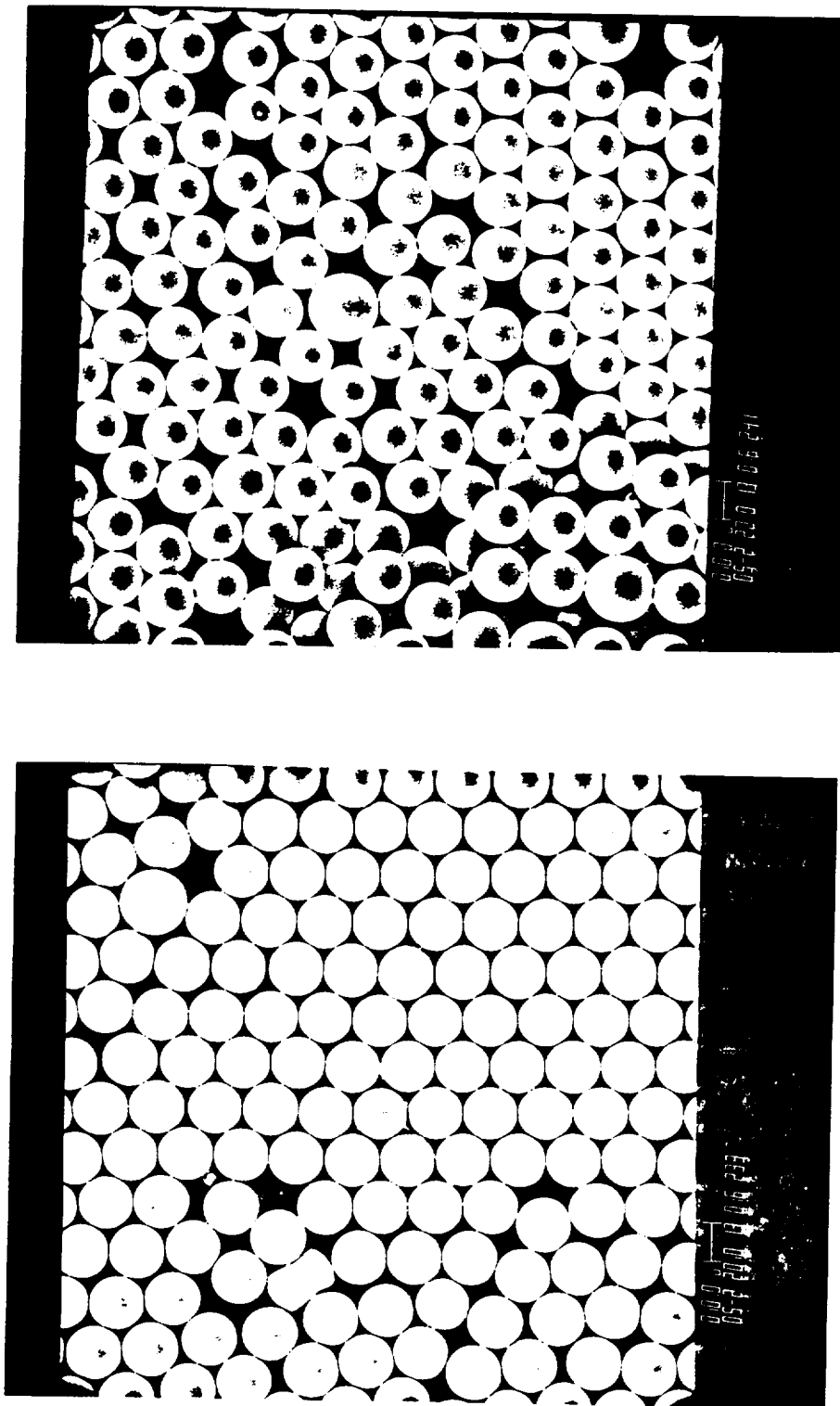Figure 5-45.   SEM micrographs of STS-7 ground latex #15.

Figure 5-46.   SEM micrographs of STS-7 flight latex #16.
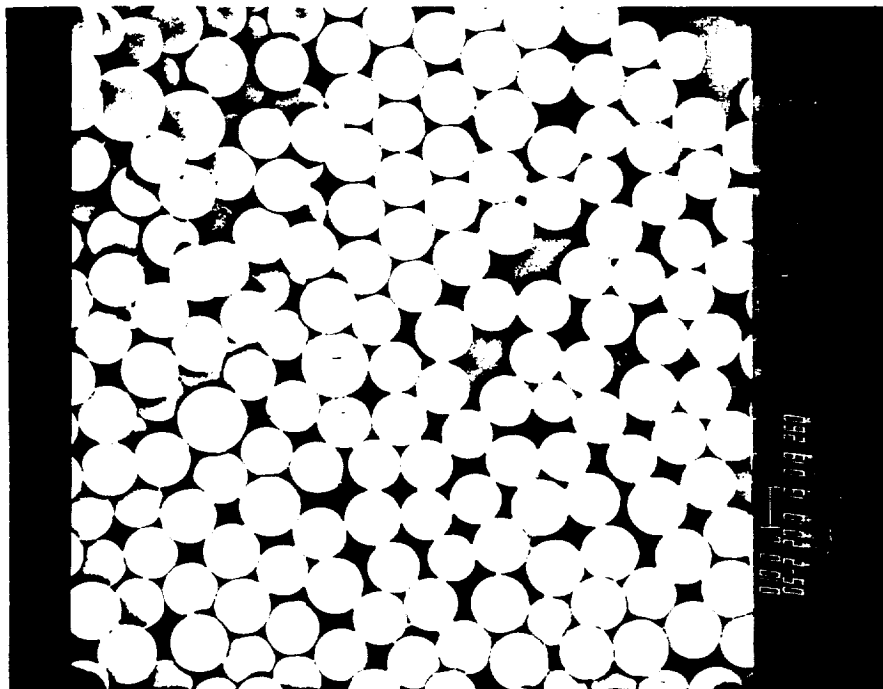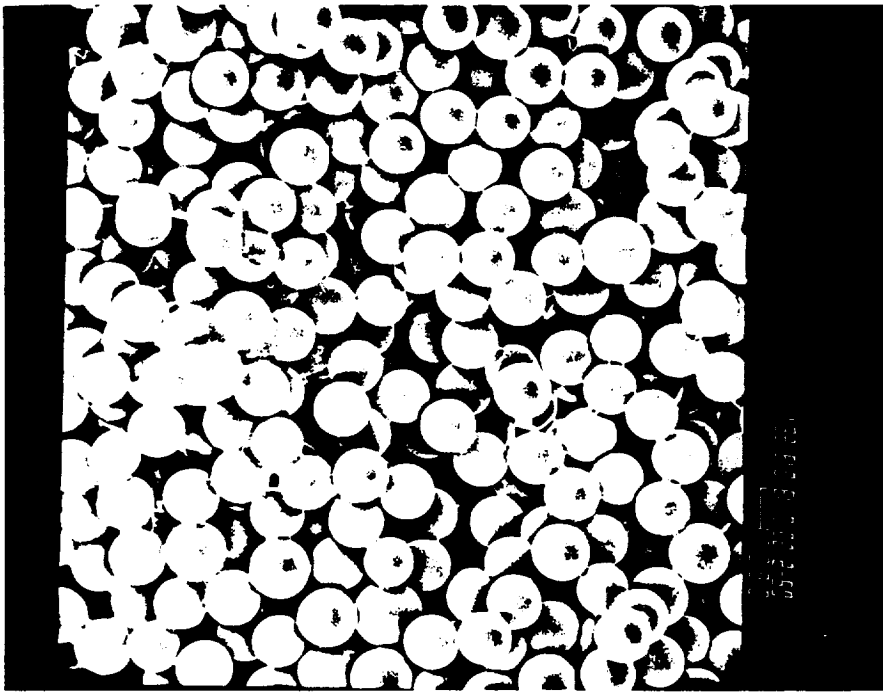
Figure 5-47. SEM micrographs of STS-7 ground latex #16.

234

SAMPLE SEED STS7

D_n =10295.8	PDI = 1.001
D_w =10301.1	D_{min} = 9930.0
N = 300	D_{max} =10650.0
D_v =10297.6	D_a =10296.7
S_d = 134.5	STEP = 60.0
D_q =10302.8	D_s =10299.3
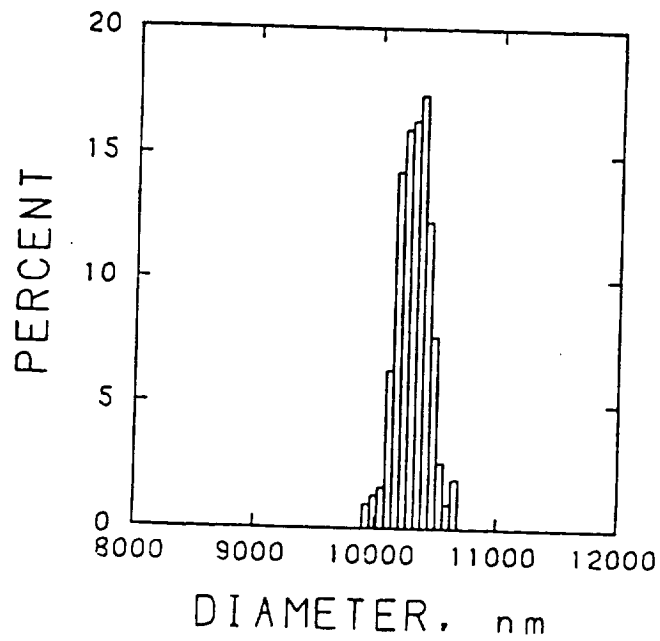
Figure 5-48. Particle size distribution of STS-7 flight seed #6027-3C.

SAMPLE FLIGHT 13

D_n =13120.6   PDI = 1.000
D_w =13125.7 D_{min} =12630.0
N   =   327 D_{max} =13590.0
D_v =13122.3 D_a =13121.5
S_d = 148.8   STEP =   60.0
D_q =13127.4 D_s =13124.0

Figure 5-49.   Particle size distribution of STS-7
flight latex #13.

SAMPLE GROUND 13

D_n =13892.1   PDI = 1.002
D_w =13920.7 D_{min} =12570.0
N   =   308 D_{max} =14610.0
D_v =13901.9 D_a =13897.1
S_d = 370.8   STEP =   60.0
D_q =13929.5 D_s =13911.5
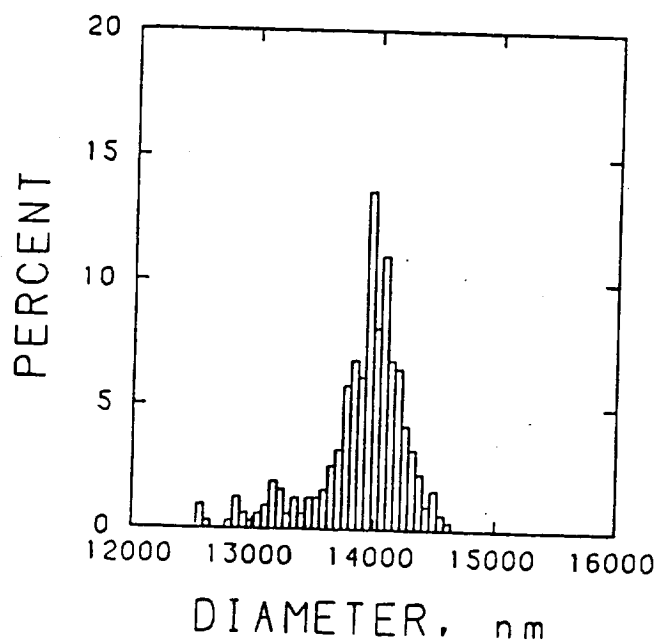
Figure 5-50.   Particle size distribution of STS-7
ground latex #13.

SAMPLE FLIGHT 14

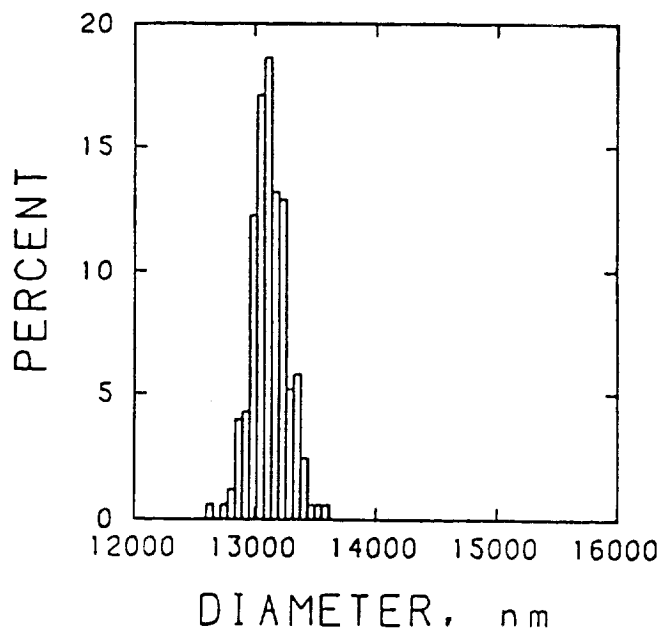|			
D_n =16635.4		PDI = 1.000
D_w =16642.7		D_{min} =16180.0
N = 322		D_{max} =17200.0
D_v =16637.8		D_a =16636.6
S_d = 200.5		STEP = 60.0
D_q =16645.1		D_s =16640.2
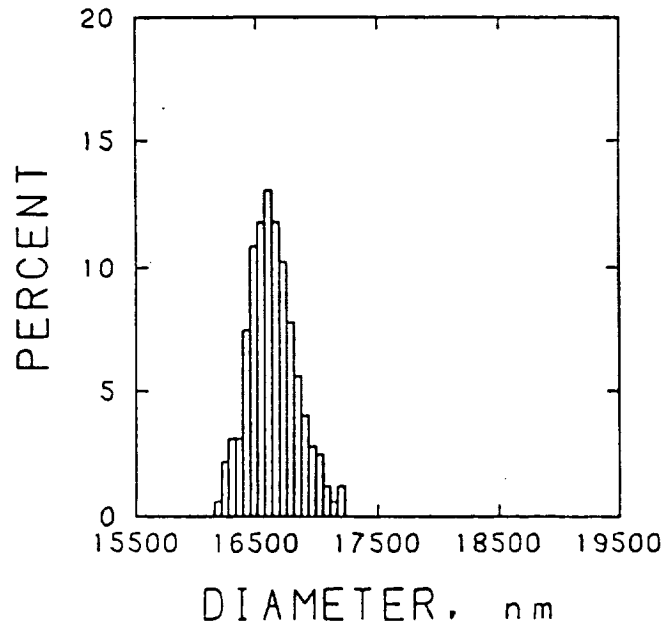
Figure 5-51. Particle size distribution of STS-7 flight latex #14.

SAMPLE GROUND 14

D_n =17170.6   PDI = 1.002
D_w =17196.7 D_{min} =15680.0
N =   326 D_{max} =17960.0
D_v =17179.5 D_a =17175.1
S_d = 393.5   STEP =   60.0
D_q =17204.8 D_s =17188.3
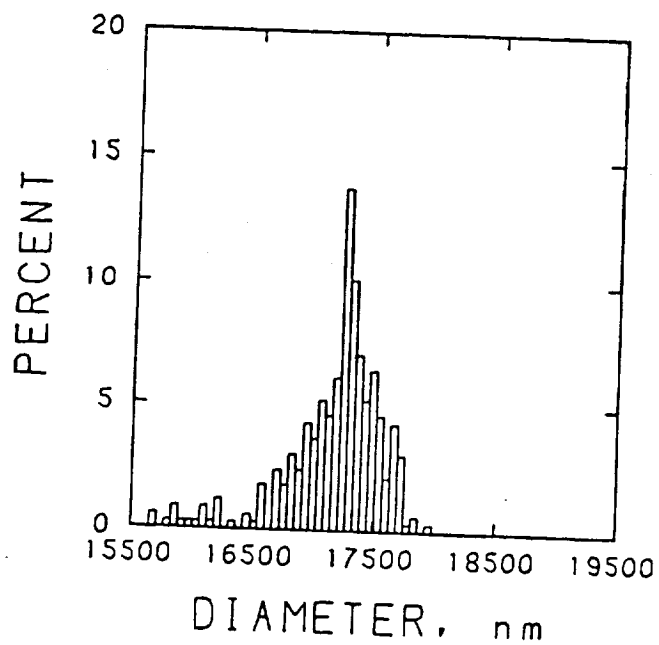
Figure 5-52.   Particle size distribution of STS-7
ground latex #14.

SAMPLE FLIGHT 15

D_n =17812.4		PDI = 1.000
D_w =17819.9		D_{min} =17030.0
N = 321		D_{max} =18950.0
D_v =17814.9		D_a =17813.7
S_d = 210.4		STEP = 60.0
D_q =17822.5		D_s =17817.4

Figure 5-53.   Particle size distribution of STS-7 flight latex #15.

SAMPLE GROUND 15

D_n =17682.5   PDI = 1.008

D_w =17829.1 D_{min} =15540.0

N =   275 D_{max} =19440.0

D_v =17732.6 D_a =17707.9

S_d = 949.2   STEP =   60.0

D_q =17873.4 D_s =17782.2
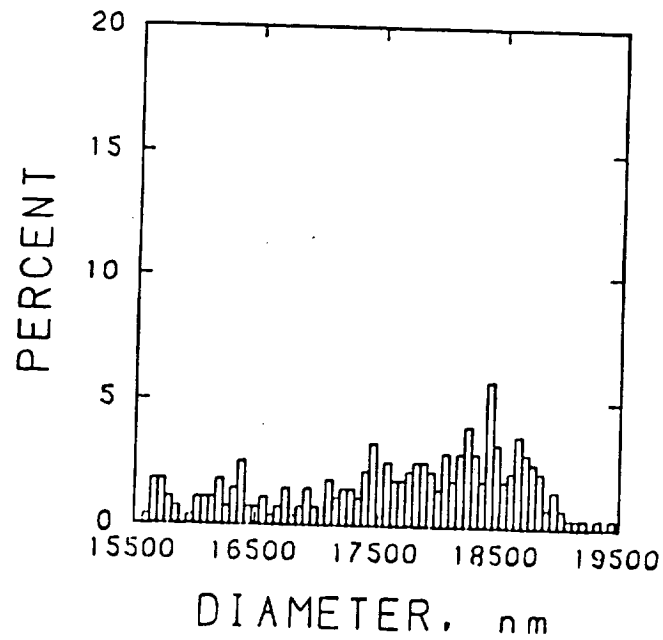
Figure 5-54.   Particle size distribution of STS-7
ground latex #15.

241

SAMPLE FLIGHT 16

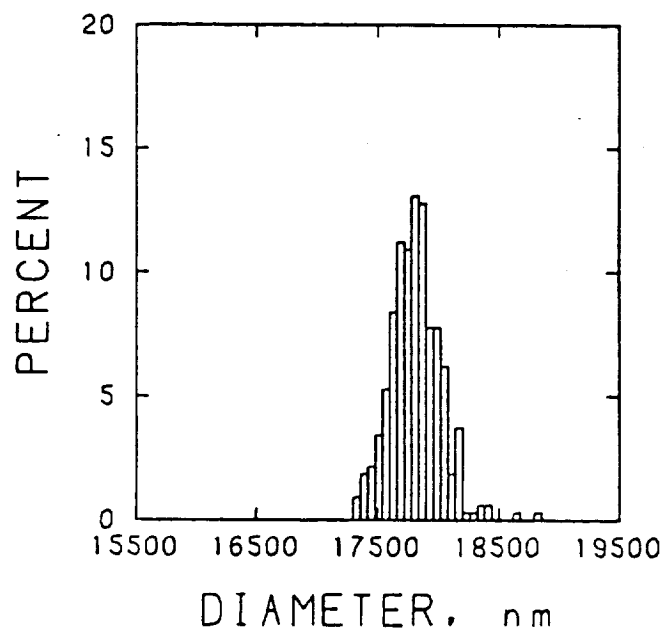|			
D_n =18184.6		PDI	= 1.000
D_w =18191.1		D_{min} =17030.0
N = 321		D_{max} =18770.0
D_v =18186.8		D_a =18185.7
S_d = 200.0		STEP = 60.0
D_q =18193.2		D_s =18188.9
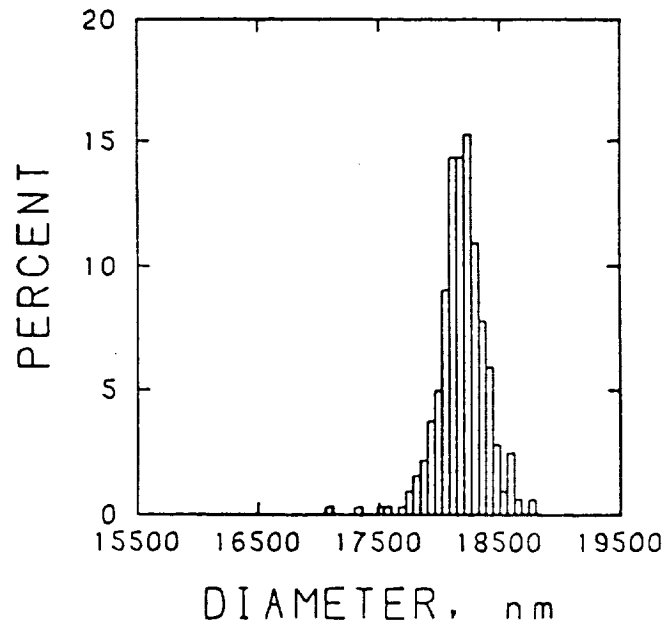
Figure 5-55. Particle size distribution of STS-7 flight latex #16.

SAMPLE GROUND 16

D_n =16968.0   PDI = 1.006
D_w =17076.7 D_{min} =15540.0
N =   361 D_{max} =19440.0
D_v =17003.8 D_a =16985.8
S_d = 777.6   STEP =   60.0
D_q =17114.6 D_s =17039.8
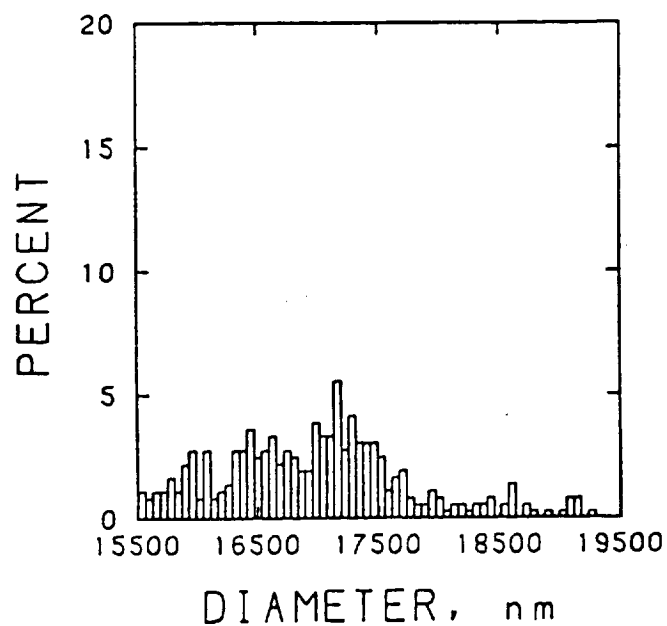
Figure 5-56.   Particle size distribution of STS-7
ground latex #16.

Table 5-13.   Results of STS-7 Particle Size Analysis

Sample	$\bar{D}_n$, μm	σ, μm	n	$\sigma/\bar{D}_n$, %	Relative No. of Particles Deformed	Relative No. of Particles Over-size
Seed #6027-3C (for #14,15,16)	10.30	0.135	300	1.31	negligible	1/130
Flight #13	13.12	0.149	327	1.13	1/220	1/360
Ground #13	13.89	0.371	308	2.67	1/60	1/120
Flight #14	16.64	0.201	322	1.21	1/110	1/90
Ground #14	17.17	0.394	326	2.29	negligible	1/50
Flight #15	17.81	0.210	321	1.18	1/770	1/70
Ground #15	17.68	0.949	275	5.37	negligible	>1/50
Flight #16	18.18	0.200	321	1.10	1/100	1/110
Ground #16	16.97	0.778	361	4.58	--	--
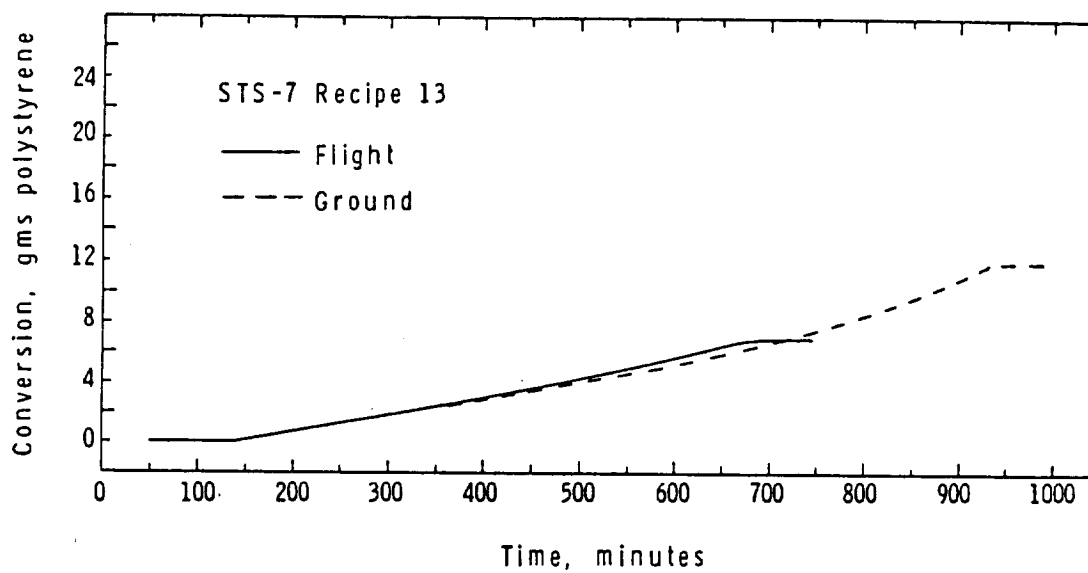
Figure 5-57. Conversion-time curves for STS-7
flight and ground latexes #13 and #14.

Figure 5-58. Conversion-time curves for STS-7
flight and ground latexes #15 and #16.

Figure 5-59. Combined particle size distributions of STS-3 seed, flight, and ground latexes.
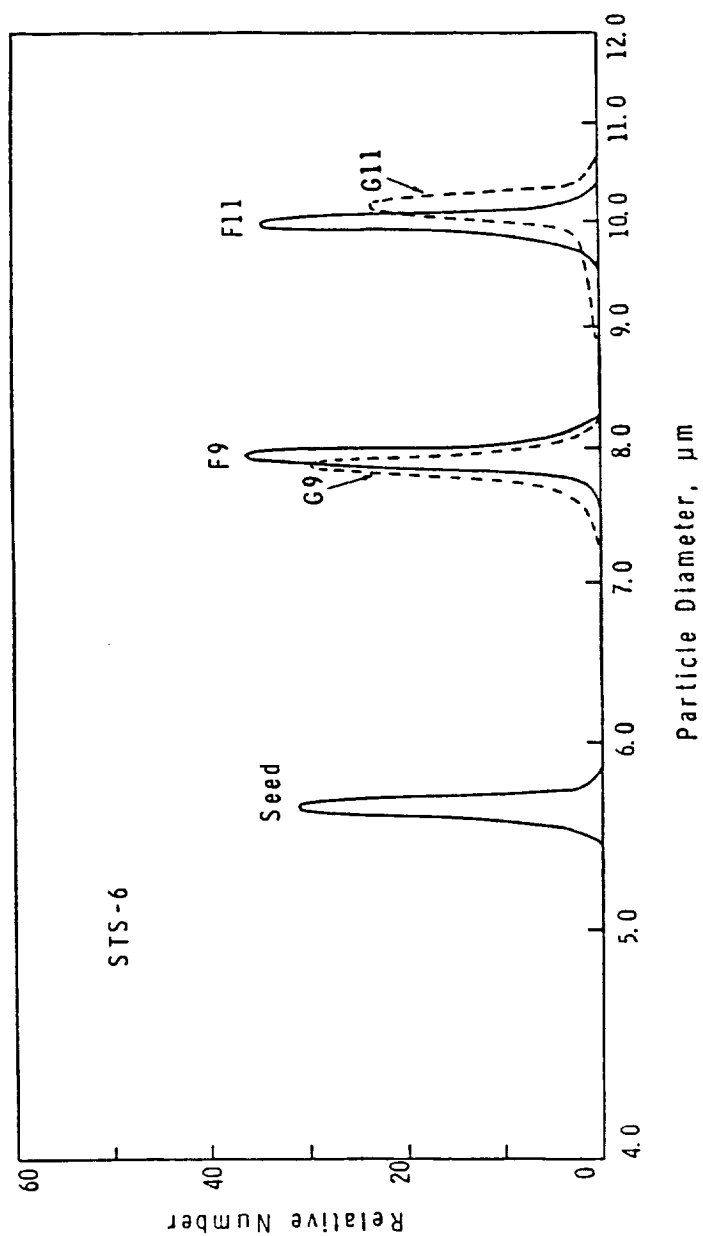
Figure 5-60. Combined particle size distributions of STS-6 seed, flight, and ground latexes.
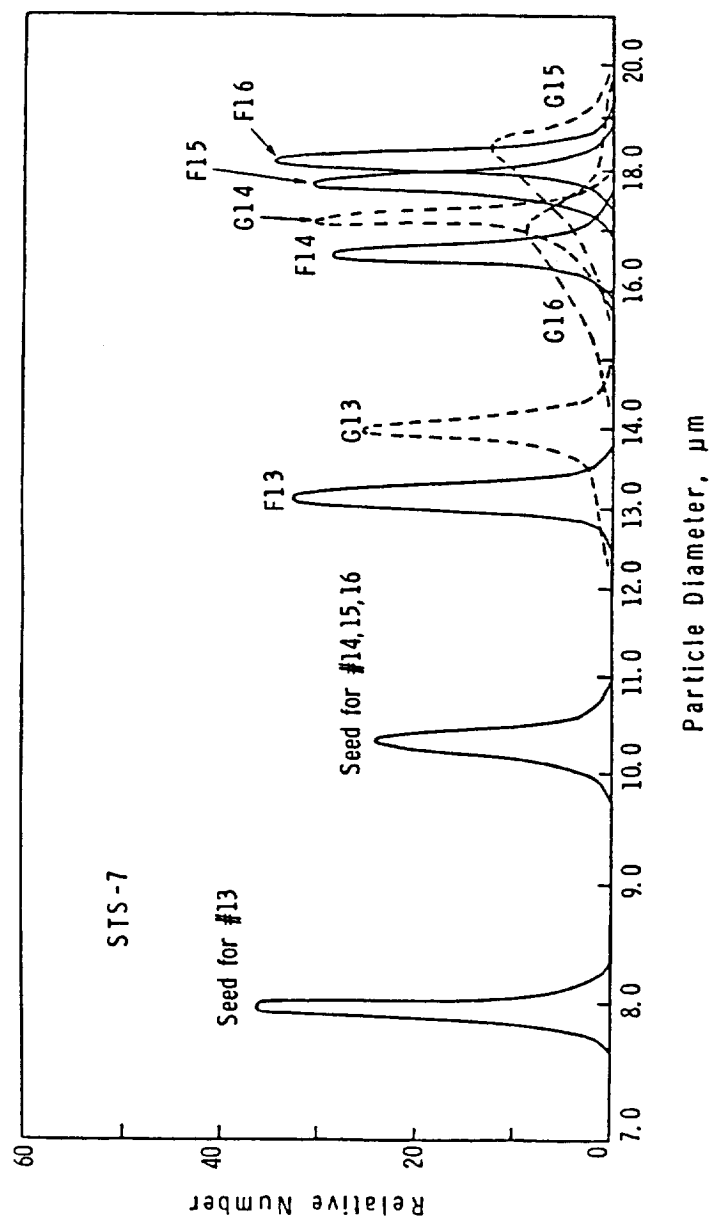
Figure 5-61. Combined particle size distributions of STS-7 seed, flight, and ground latexes.

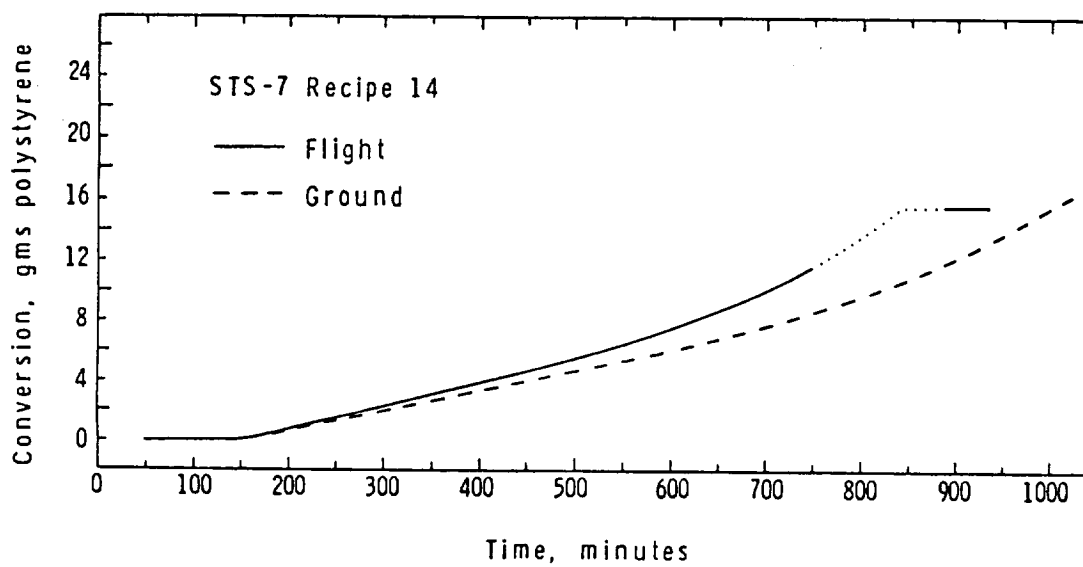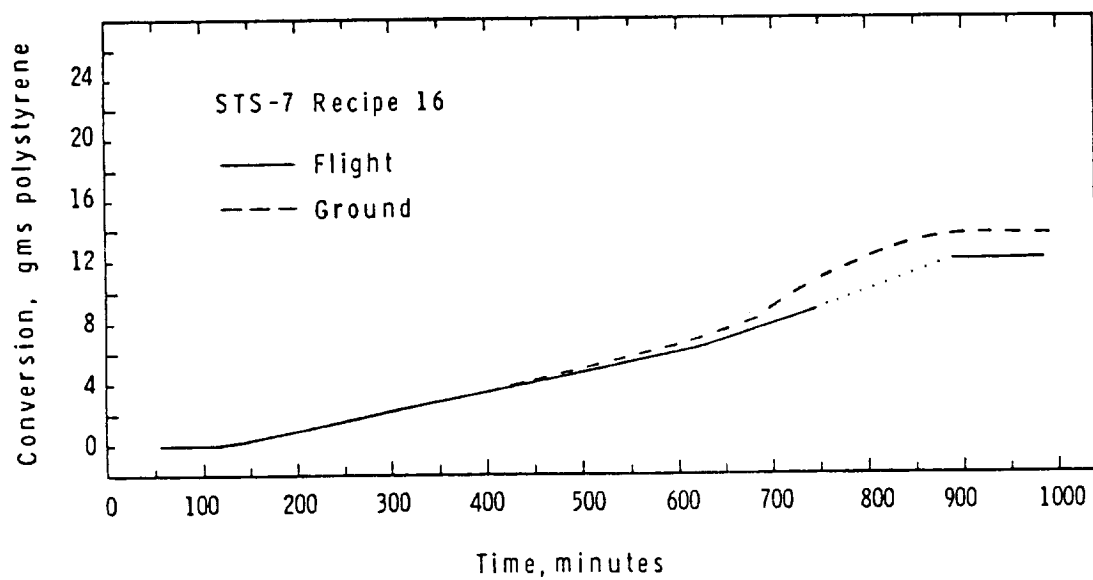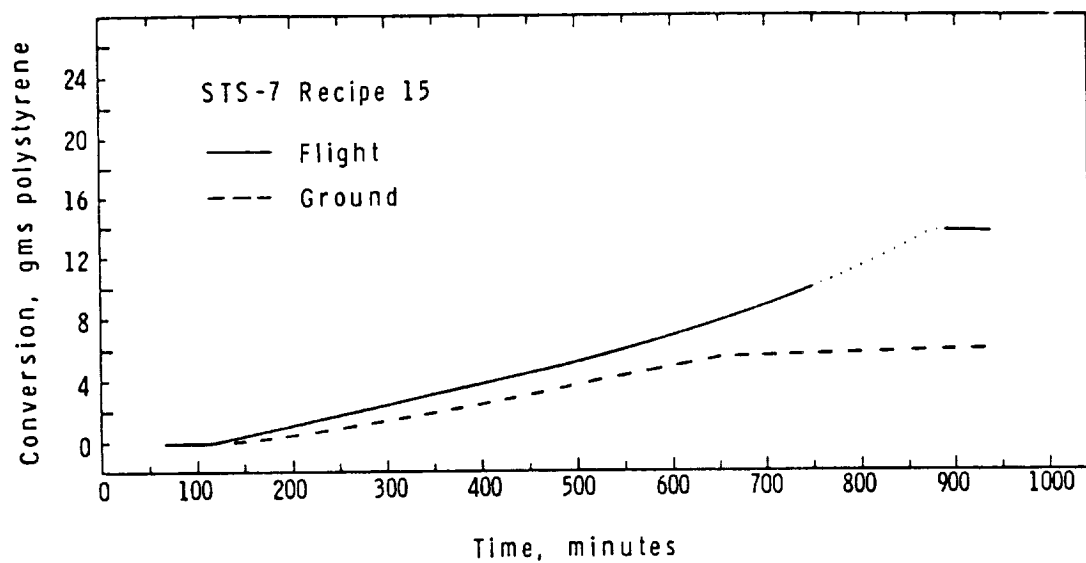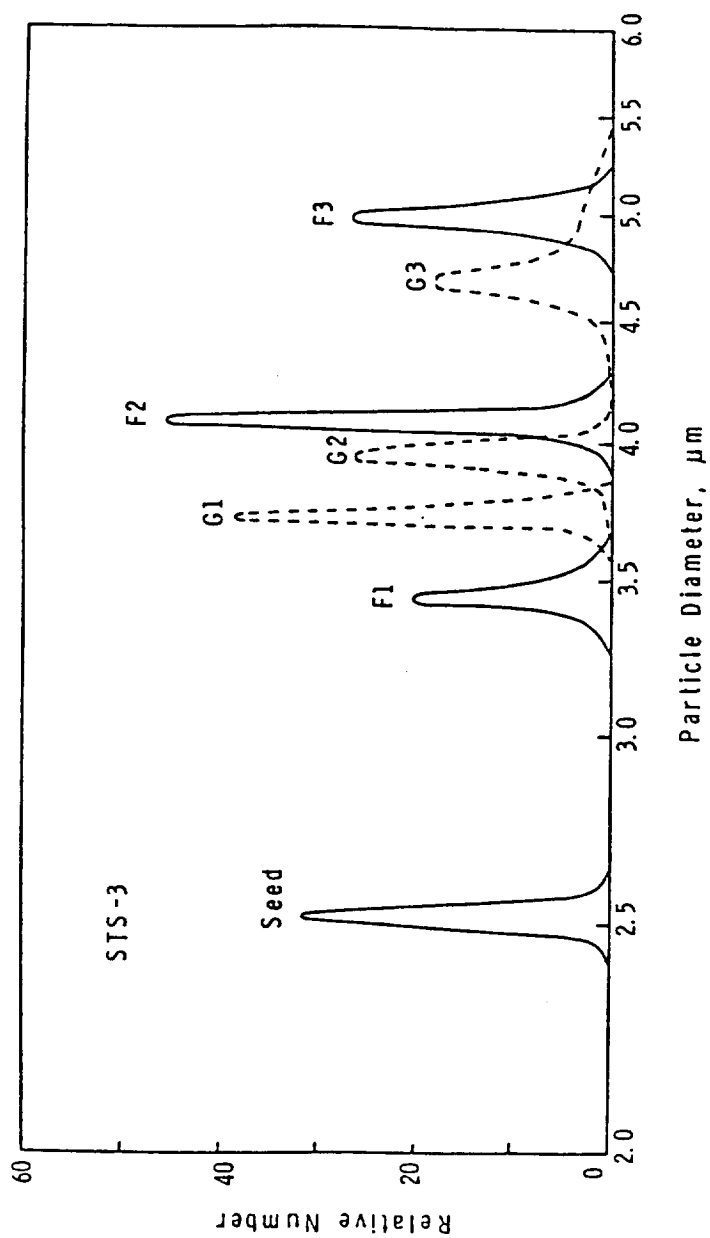for the flight experiments, but not for the ground-based analogues, could be responsible for the phenomenon. The barrel-shaped particles could be reformed into spheres by heating to a high temperature. Small particle generation was not quantitatively evaluated, but generally increased with particle size and swelling ratio. These could be removed by repeated sedimentation/separation.

5.3 Ground-Based Seeded Polymerization Sequences

During the time period between the STS-4 and STS-6 flights, several seeded polymerization sequences were conducted, to determine the upper limit of particle size to which that monodisperse latexes could be grown with the current initiator/inhibitor/stabilizer system. The first sequence started with the 0.40 μm seed (LS-1103-A) and finished in the sixth step at 11 μm. The recipes are given in Table 5-14. Water-soluble persulfate initiator was used in the first step, while oil-soluble AMBN initiator was used inthe other steps. The monomer-swollen latexes were polymerized by two methods, in capped bottles and in the laboratory prototype reactor LUMLR, at the same time. The bottle polymerizations were carried out in 12-oz bottles in a 70°C water bath (see Appendix A). Details of the design and operation of the prototype reactor LUMLR can be found elsewhere [71]. Figure 5-62 presents the conversion-time curves of the polymerizations conducted in the LUMLR. A much faster polymerization rate was obtained in the persulfate-initiated polymerization (step 1) than in the AMBN-initiated polymerizations. With the same AMBN concentration, steps 2 to 6 gave almost the same polymerization rate despite their

significant differences in particle size. SEM micrographs of the latexes from the first five steps in the LUMLR are presented in Figure 5-63. The sequence was not continued beyond step 6 because of the generation of significant number of new small particles.

Slight modifications were made for the second polymerization sequence. AMBN initiator was used in all of the steps. The surfactant levels were lowered. The recipes are given in Table 5-15. Figure 5-64 illustrates the concentrations of three surfactants used in various steps. This sequence was conducted with bottle polymerizations. The product yields and estimated particle diameters from each step are given in Table 5-16.

SEM micrographs of the product latexes are presented in Figures 5-65 to 5-68. The particle size distributions of the latexes were narrow up to step 6. Significant numbers of over-size particles and deformed particles were found in the latexes of the last two steps. Nevertheless, small fractions of narrow particle size distribution could still be recovered from these two products by the sedimentation /separation method. Figures 5-69 to 5-71 present SEM micrographs of the "upgraded" products of step 3 to step 8. These were cleaned by sedimentation and serum replacement (see Chapter 6). Although the removal of particles significantly larger or smaller than the normal particles was easy, it was much more difficult to remove completely the particles only slightly larger (twice in volume) than the normal particles.

In summary, monodisperse latex particles were successfully grown to 11 µm diameter with bottle polymerizations, and less successfully

Table 5-14. Recipes of the First Seeded Polymerization Sequence

Step #	Latex #	M/P	Initiators		Inhibitors		Surfactants			Crosslinker
			Persulfate (%aq)	AMBN (%M)	HQ (%aq)	BQ (%aq)	AMA (%aq)	KX-3 (%aq)	PVP (%aq)	DVB (%M)
1	5122	4	0.1	-	-	-	0.14	-	-	-
2	5123	4	-	0.12	0.03	-	0.14	-	-	-
3	5124	4	-	0.12	0.03	0.005	-	0.0175	0.175	0.015
4	5125	5	-	0.12	0.03	0.005	0.007	0.0175	0.175	0.015
5	5126	5	-	0.12	0.03	0.005	0.007	0.0175	0.175	0.015
6	5127	5	-	0.12	0.03	0.005	0.007	0.0175	0.175	0.015
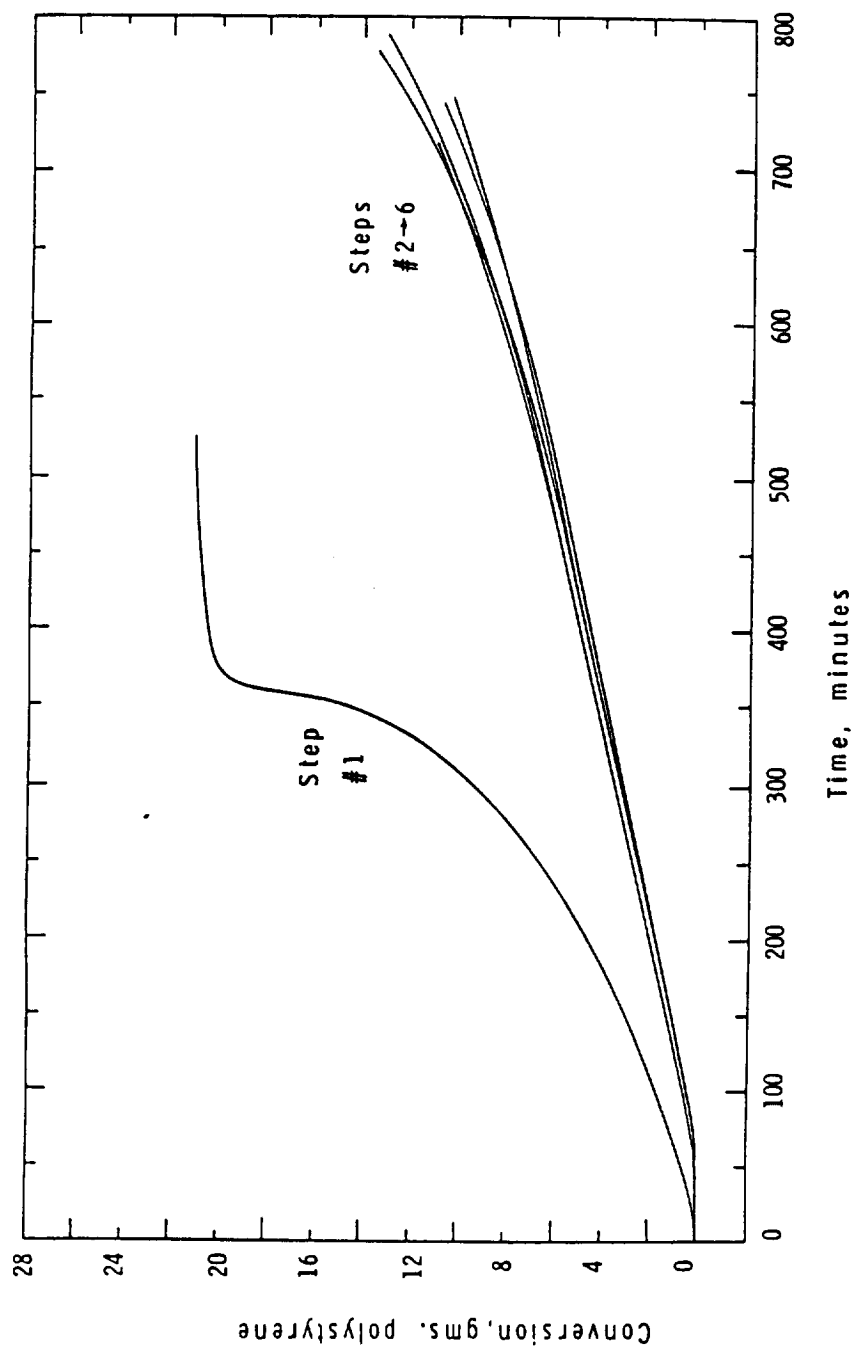
Figure 5-62. Conversion-time curves of the first seeded polymerization sequence in the LUMLR.

SSMLR 14
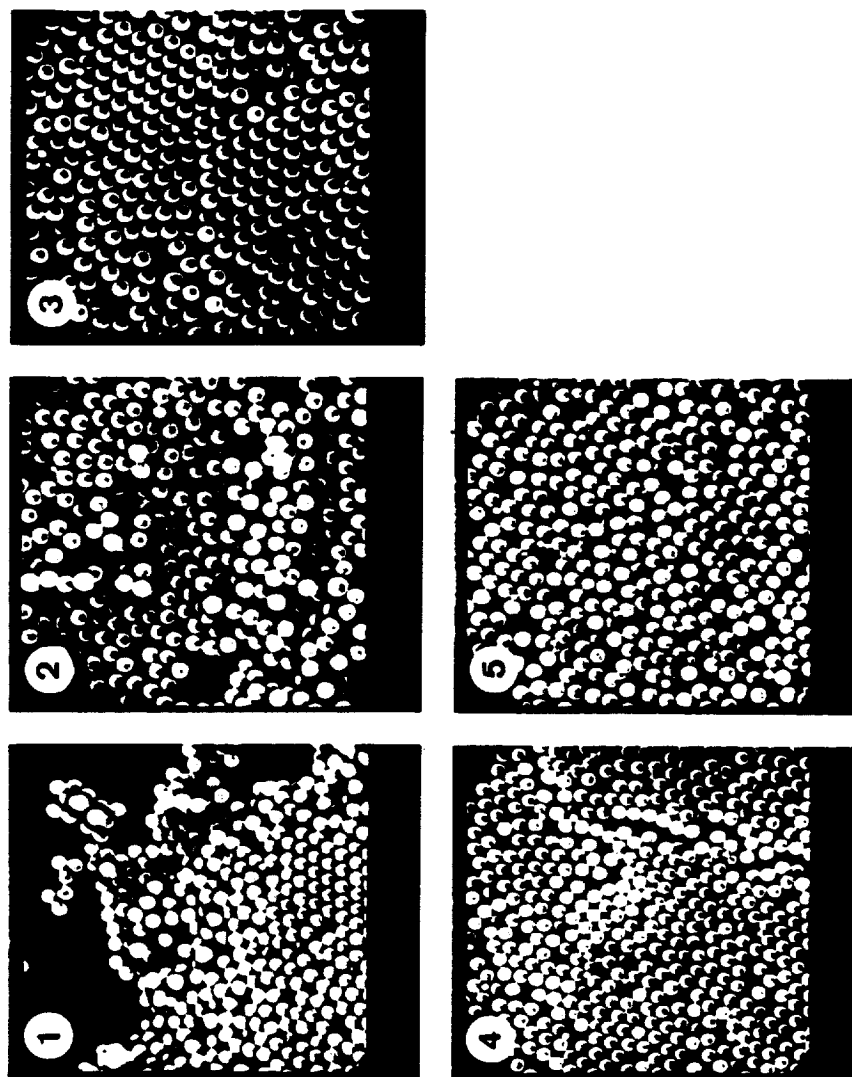
Figure 5-63. SEM micrographs of the latexes from the first seeded polymerization sequence in the LUMLR.

Table 5-15. Recipes of the Second Seeded Polymerization Sequence

Step #	Latex #	M/P	Initiator	Inhibitors		Surfactants			Crosslinker
			AMBN (%M)	HQ (%aq)	BQ (%aq)	AMA (%aq)	KX-3 (%aq)	PVP (%aq)	DVB (%M)
1	5130	4	0.12	0.03	0.005	0.14	-	-	-
2	5131	4	0.12	0.03	0.005	0.07	-	-	-
3	5132	4	0.12	0.03	0.005	-	0.010	0.10	0.015
4	5133	5	0.12	0.03	0.005	-	0.015	0.15	0.015
5	5136	5	0.12	0.03	0.005	0.004	0.015	0.15	0.015
6	5137	5	0.12	0.03	0.005	0.004	0.015	0.15	0.015
7	5138	5	0.12	0.03	0.005	0.004	0.015	0.15	0.015
8	5139	5	0.12	0.03	0.005	0.004	0.015	0.15	0.015

Table 5-16.   Product Yields and Estimated Particle
Diameters from Each Step of the Second Seeded Poly-
merization Sequence

Step #	Latex #	% Yield *	Estimated diameter, μm
1	5130	95	0.68
2	5131	95	1.2
3	5132	96	2.0
4	5133	95	3.4
5	5136	90	6.2
6	5137	81	11.0
7	5138	83	18.0
8	5139	74	35.0

* estimated from the predicted and measured product solids

to 18 μm and 35 μm.   The limit could probably be shifted to a larger

particle size by further improvements in recipe and reactor design.
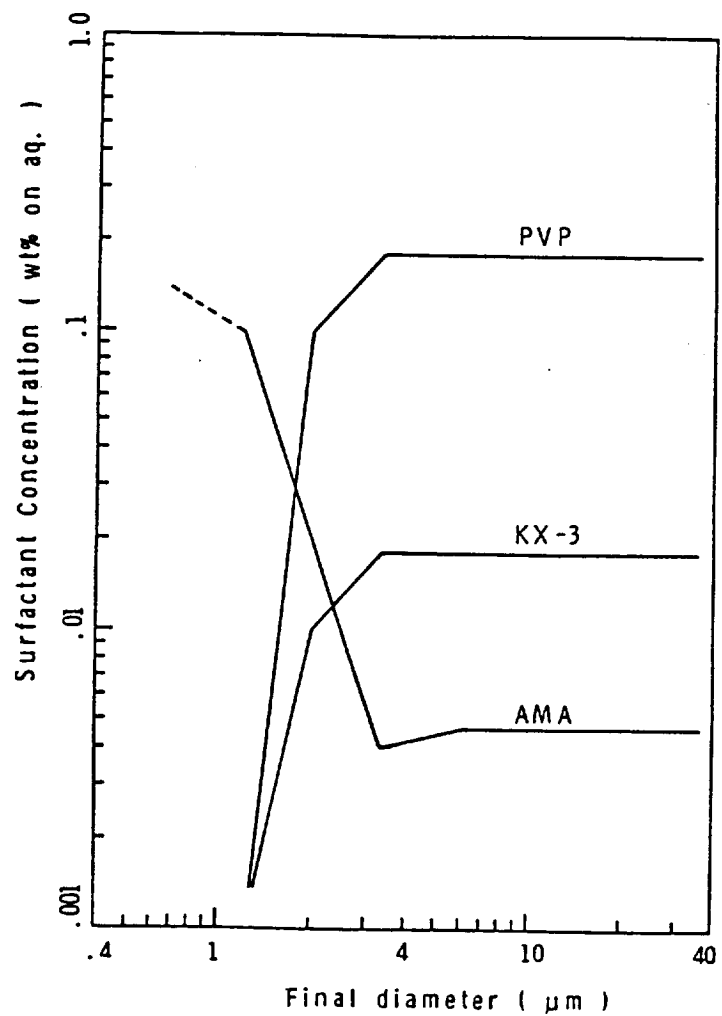
Figure 5-64.   Surfactant concentrations in the
various steps of the second seeded polymerization
sequence.
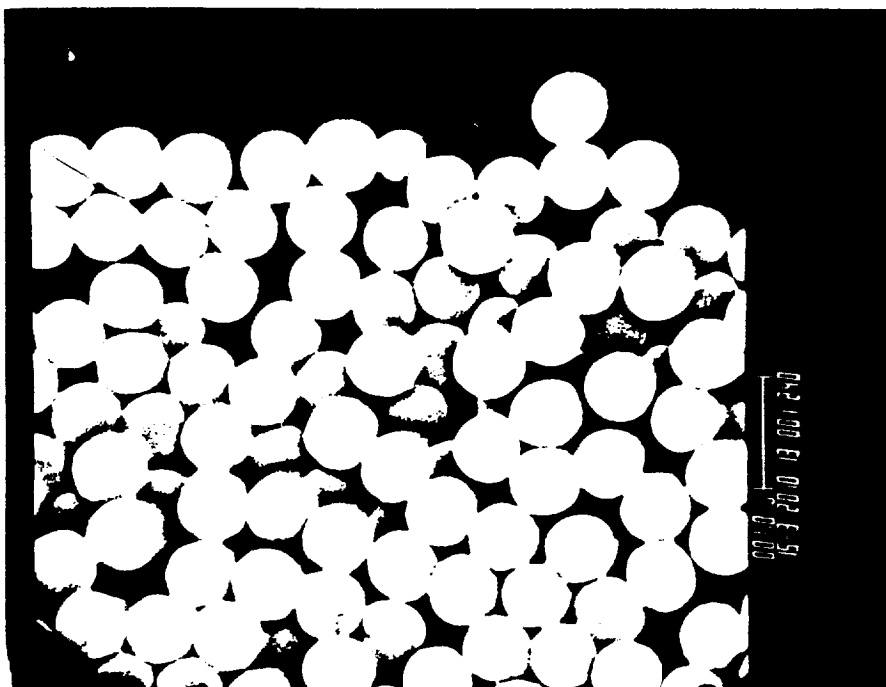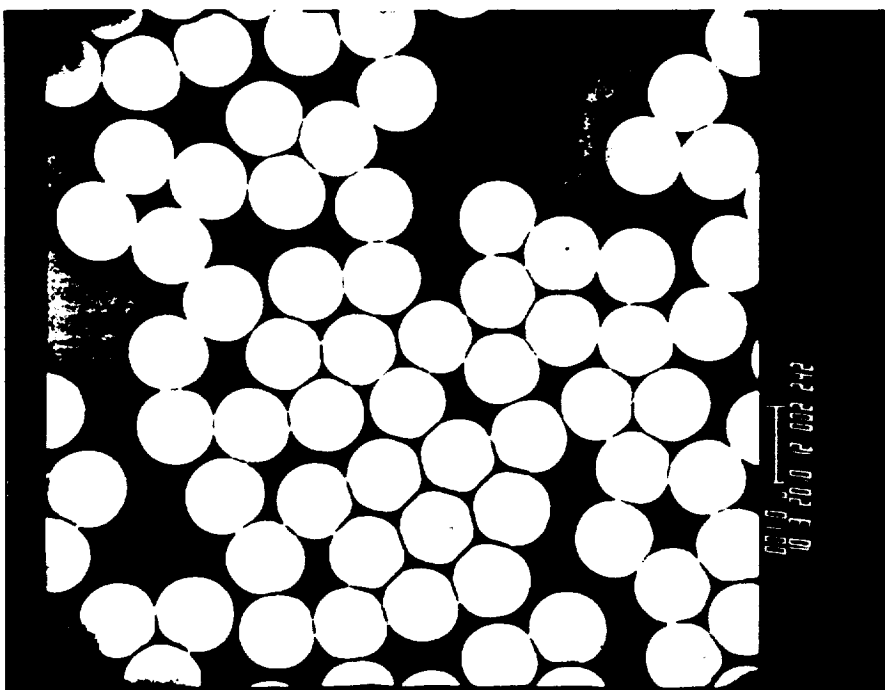
Figure 5-65.   SEM micrographs of latexes #5130 (left) and #5131 (right).
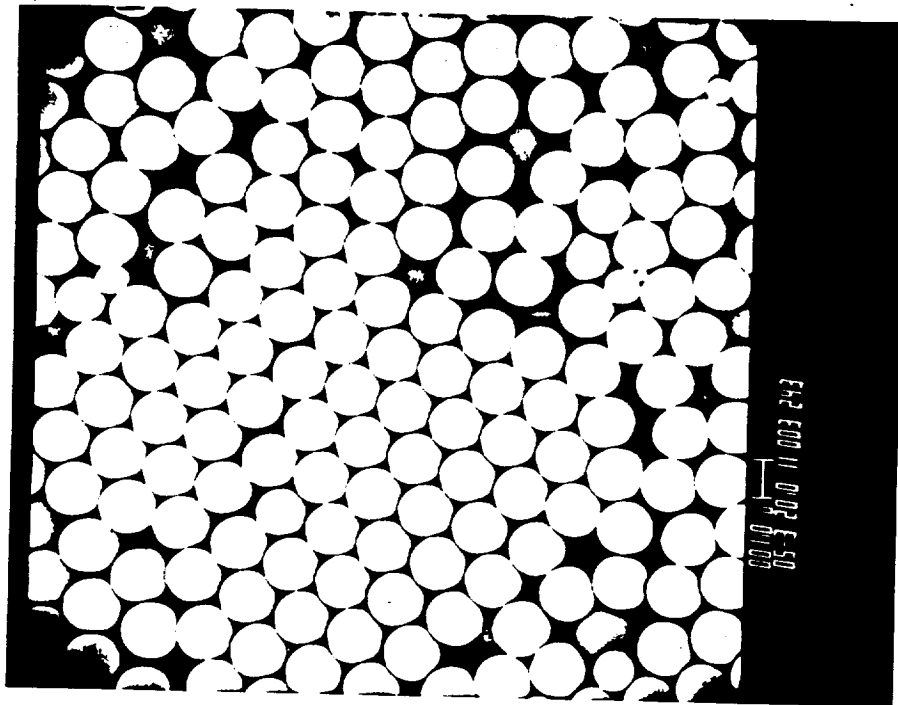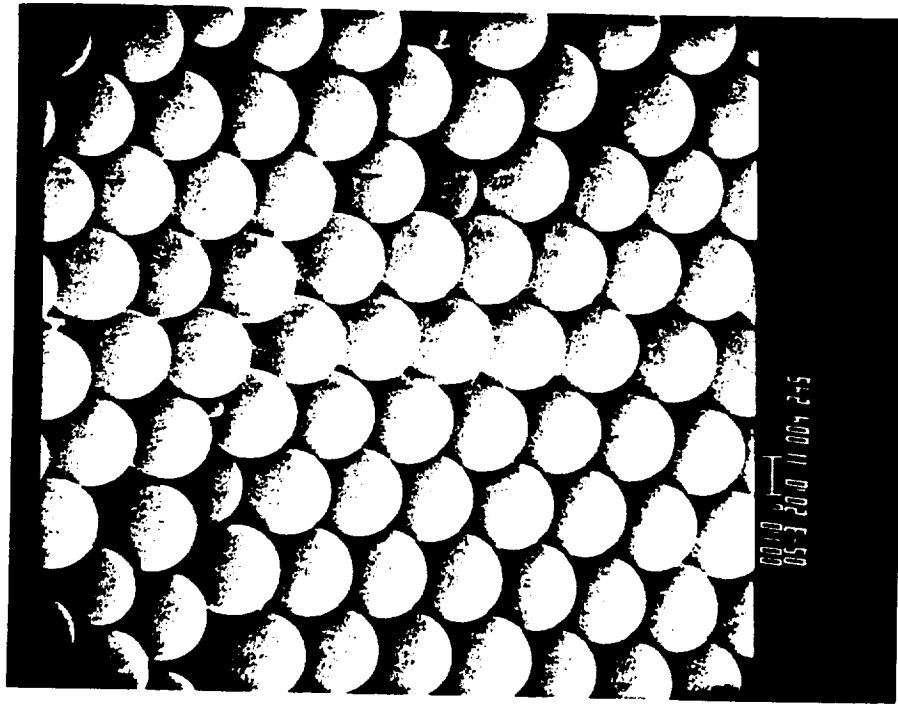
Figure 5-66. SEM micrographs of latexes #5132 (left) and #5133 (right).
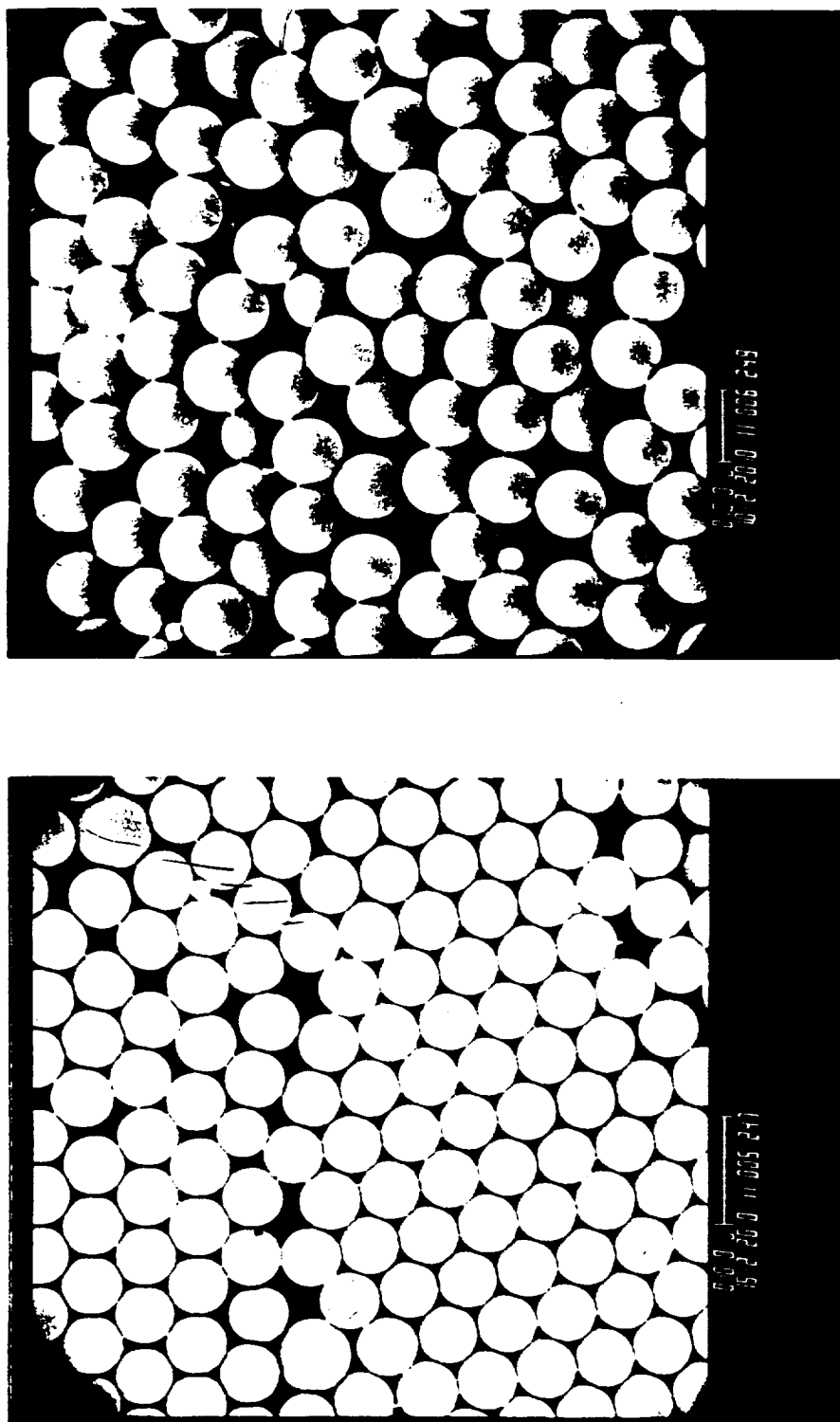
Figure 5-67. SEM micrographs of latexes #5136 (left) and #5137 (right).
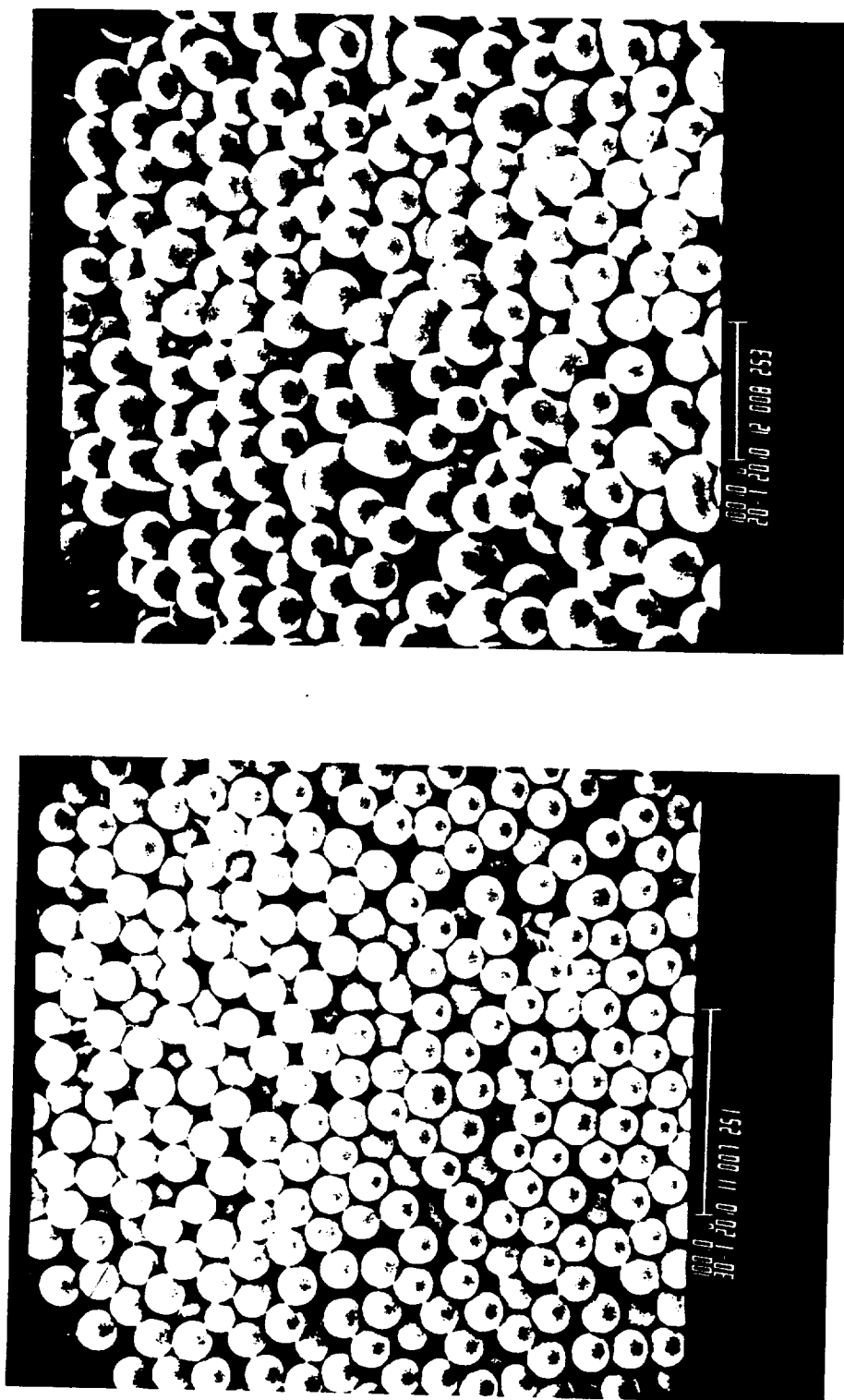
Figure 5-68. SEM micrographs of latexes #5138 (left) and #5139 (right).
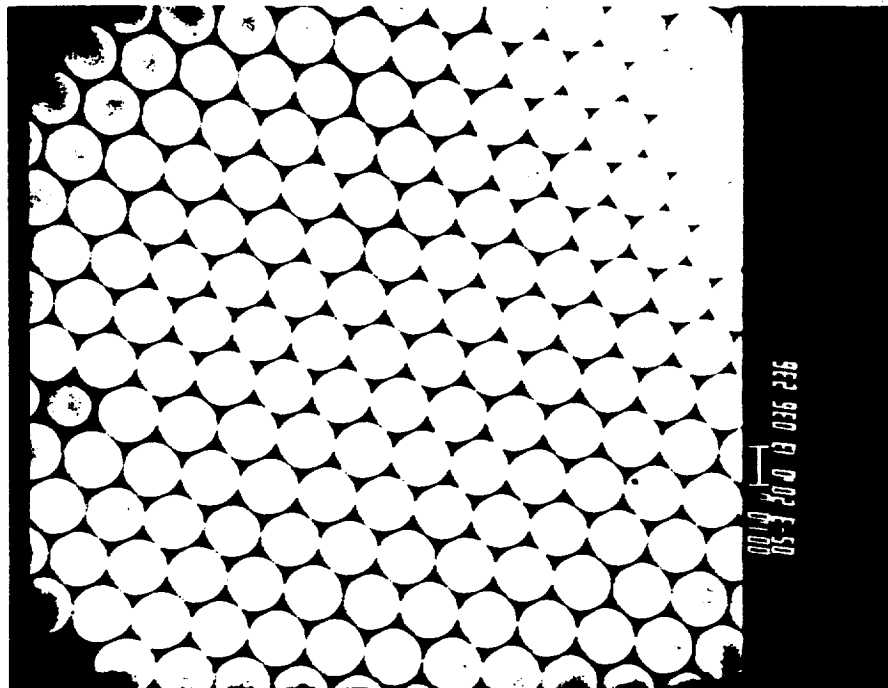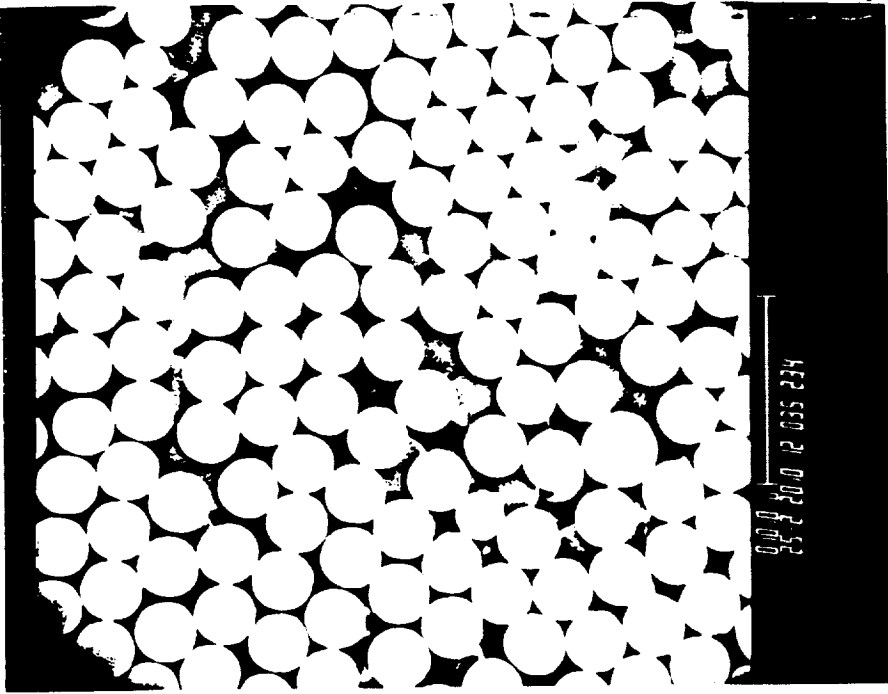
Figure 5-69. SEM micrographs of latex #5132C (left) cleaned by serum replacement and latex #5133C (right) cleaned by sedimentation and serum replacement.
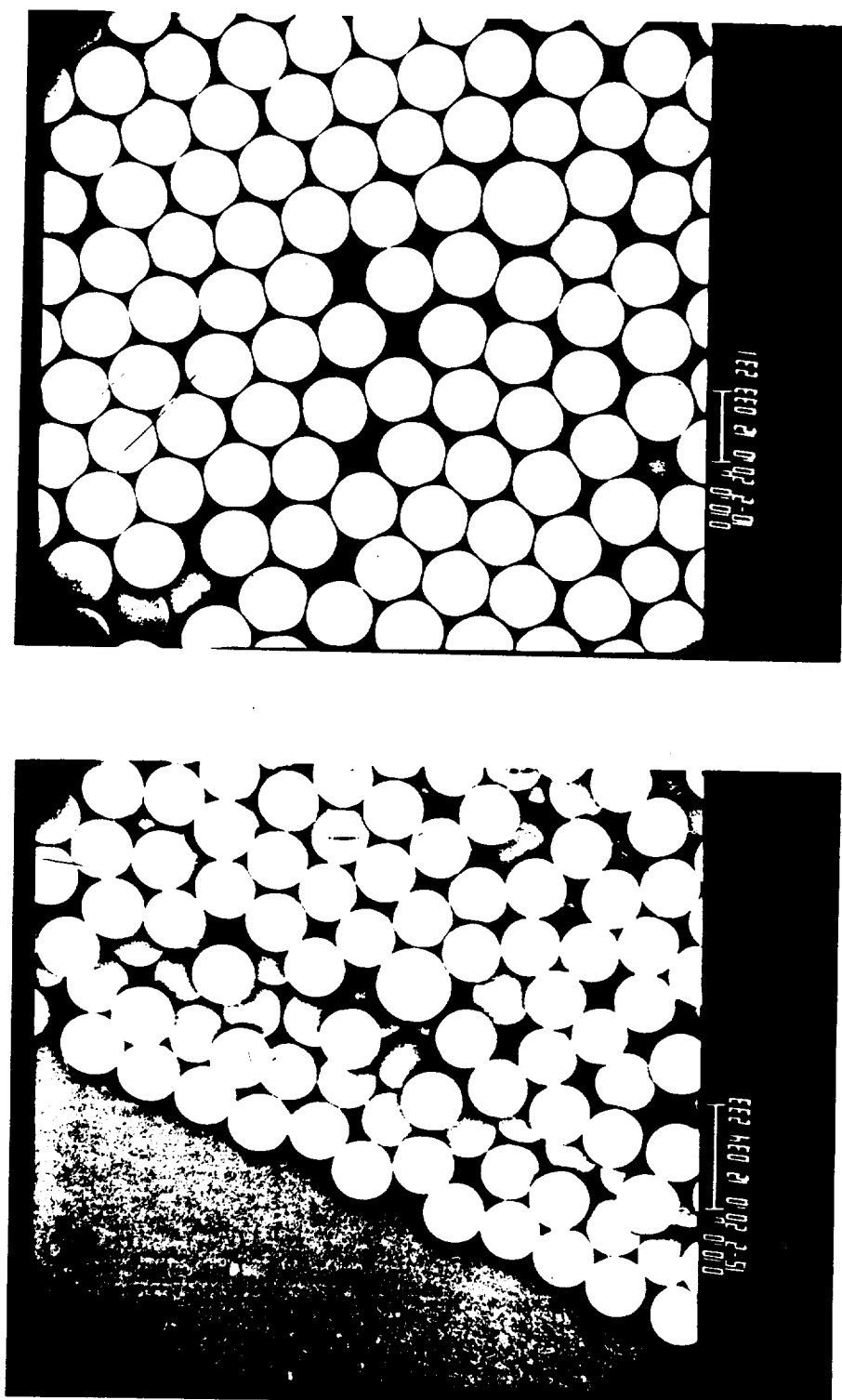
Figure 5-70. SEM micrographs of latex #5136C (left) cleaned by sedimentation and serum replacement and latex #5137C (right) cleaned by sedimentation.
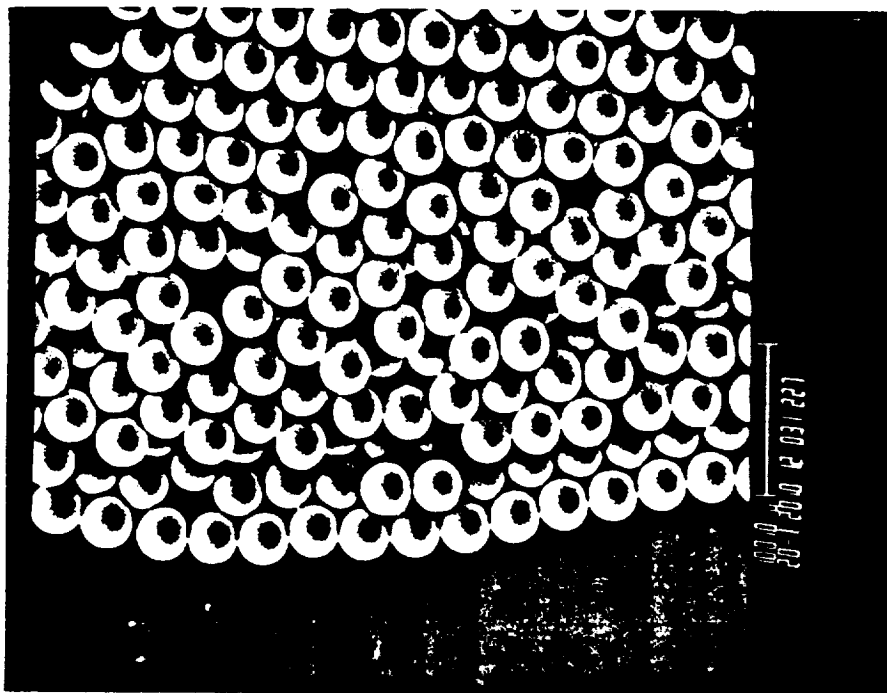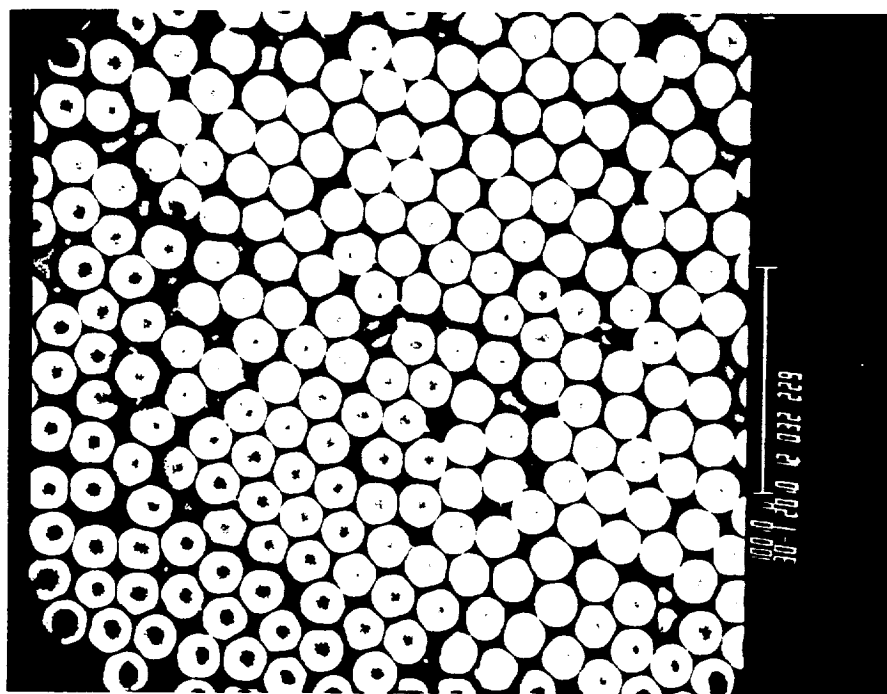
Figure 5-71. SEM micrographs of latex #5138C (left) and #5139C (right) cleaned by sedimentation.

CHAPTER 6

UPGRADING AND CHARACTERIZATION METHODS

It is desired to prepare monodisperse latexes that can be used without further treatment. However, a perfect product is difficult to obtain, especially for the larger particle sizes. Even with a carefully developed recipe, larger or smaller off-size particles are often formed in the polymerization products in the ratio of one out of hundreds. In some critical applications, the removal of surfactants and other ingredients in the product is also desired. Three complementary methods for removing off-size particles and surfactants, centrifugation, sedimentation and serum replacement, will be described in the first section of this chapter.

The second section deals with the measurement of particle size and particle size distribution. Optical microscopy, electron microscopy, and light scattering methods will be discussed.

Electrokinetic studies of colloid particles is important in understanding colloid stability, adsorption of charged species, and interaction of particles. The electrophoretic mobilities of some large-particle-size latexes prepared in this work have been determined using the automated electrokinetic analyzer Pen Kem System 3000. This will be the subject of the third section.

As discussed in Chapter 2, the molecular weight distribution of the polymer is important in determining the swellability of the latex particle. The operation of the GPC, its calibration, and the molecular weight calculation from the chromatogram is the subject of

the fourth section. Two types of columns were used in this study: the μ-Styragel column system with THF as mobile phase was used for determining the molecular weight distribution of the polystyrene samples; the TSK-GEL-PW aqueous column set was used for the polymeric surfactants.

6.1 Upgrading of Latex Products

Sedimentation is the simplest way to remove most of the off-size particles and surfactants in a large-particle-size polymerization product. The sedimentation vessel used in this study was a clear plastic cylindrical container, 14 cm high with a 2-liter volume. Two holes were drilled and valves were installed in the wall of the container; the first at 7 cm (half way), and the second at 2 cm from the bottom. The latex was first diluted to <10% and allowed to settle in the tank. As soon as the suspension level passed the first valve, the supernatant layer, which contained a large fraction of the small particles and surfactants, was drained out. The suspension was collected from the second valve. The sediment, which contained about half of the normal particles and a large fraction of over-size particles was then redispersed for another sedimentation. By repeating the sedimentation several times, most of the off-size particles and surfactants could be removed from the suspension. A sedimentation cycle took several hours to several days, depending on the particle size. For latexes of particle size larger than 10 um, a taller sedimentation tank, 18 cm high with a 2.5-liter volume, was used instead of the shorter tank.

For a very dilute suspension, the sedimentation rate follows the Stokes law:

$$U_s = (\rho_d - \rho_c)gd^2/18\mu_c \qquad (6\text{-}1)$$

where ρ_d is the particle density, ρ_c is the fluid density, g is the gravitational acceleration, d is the particle diameter, and μ_c is the fluid viscosity.

For a concentrated suspension, the relationship is quite complicated. Barnea and Mizrahi [116] have developed a general correlation:

$$C_{d\phi} = (0.63 + 4.8/\sqrt{Re_\phi})^2 \qquad (6\text{-}2)$$

where

$$C_{d\phi} = [4d(\rho_d - \rho_c)g/(3\rho_c U_\phi^2)][(1-\phi)/(1+\phi^{1/3})] \qquad (6\text{-}3)$$

and

$$\sqrt{Re_\phi} = \{U_\phi d \rho_c/\mu_c \, \exp[5\phi/3(1-\phi)]\}^{1/2} \qquad (6\text{-}4)$$

where Re_ϕ is the Reynolds number, ϕ is the volume fraction of solids, $C_{d\phi}$ is the drag coefficient, and U_ϕ is the settling velocity.

Zigrang and Sylvester [117] combined the equations to obtain an explicit equation for the settling velocity:

$$U_\phi = c - \sqrt{c^2 - a^2} \qquad (6\text{-}5)$$

where

$$c = (2a+b^2)/2 \qquad (6\text{-}6)$$

and

$$a = [2/(0.63\sqrt{3})] \{(\rho_d - \rho_c)gd(1-\phi)/[\rho_c(1+\phi^{1/3})]\}^{1/2} \qquad (6\text{-}7)$$

$$b = (4.8/0.63) \{\mu_c \, \exp[5\phi/3(1-\phi)]/(\rho_c d)\}^{1/2} \qquad (6\text{-}8)$$

Table 6-1 compares the settling velocity calculated from Stokes law and Zigrang-Sylvester equation for a polystyrene latex of 5.0 μm diameter. The following parameters were used in the calculation: ρ_d=1.05 g/cm^3, ρ_c=1.00 g/cm^3, μ_c=1.0 g/cm.sec, g=980 cm/sec^2.

Table 6-1. Settling Velocity of 5.0 μm Polystyrene Particles Calculated from Stokes Law and Zigrang-Sylvester Equation

U_s	$U_{\phi=0}$	$U_{\phi=0.05}$	$U_{\phi=0.10}$
0.24 cm/hr	0.25 cm/hr	0.16 cm/hr	0.13 cm/hr

Thus it takes at least 28 hours for the 5.0 μm particles to settle 7 cm and finish one cycle of sedimentation in the short tank. A latex with diameter smaller than 5.0 μm takes a longer time to finish one cycle of sedimentation. Therefore, it is more economical in time to clean latexes of smaller particle size using centrifugation.

The centrifugation was carried out in this study with a 3/4 HP centrifuge (International Centrifuge, Size 2). The latex was diluted and distributed in four 250 ml polypropylene bottles and subjected to centrifugation. With a proper selection of rotating speed and time, most of over-size particles along with part of the normal particles could be sedimented to the bottom of the bottle. For example, to clean a 2.5 μm latex, a rotating speed of 1400 rpm for 10 min. was used. After centrifugation, the sediment was recycled for collecting more normal particles. The decanted suspension was subjected to a

higher centrifugation force to concentrate the normal particles and to separate the small particles and surfactants.

To ensure that most of the off-size small particles and surfactants were removed, the latexes after centrifugation or sedimentation were subjected to a modified serum replacement method. The serum replacement method was originally developed in this laboratory for separating surfactants from latexes of submicron sizes and to study their adsorption isotherms [87]. The method uses a continuously stirred cell and a polycarbonate membrane with pore size slightly smaller than the latex particle diameter. Serum replacement of large-particle-size latexes, especially at higher concentrations, resulted in clogging of the membrane and formation of a cake of particles.

To use the serum replacement cell for cleaning large-particle-size latexes efficiently, several modifications were made. As shown in Figure 6-1, an additional hole was drilled in the exit port and an adapter was attached to serve as a bypass water inlet. The cell was positioned horizontally with a magnetic stirrer sitting sideways next to the exit port. By careful control of the flow rate difference between the two water inlets, a minimum pressure drop could be maintained across the membrane. With the modifications, a latex of high concentration (>10%) could be cleaned with reasonably high flow rate, without causing cake formation and membrane clogging.

The uniform pore-size polycarbonate membranes (Nuclepore Corp.) are available in pore sizes from 0.015 μm up to 12 μm. In this study, the serum replacement method has been used successfully to clean
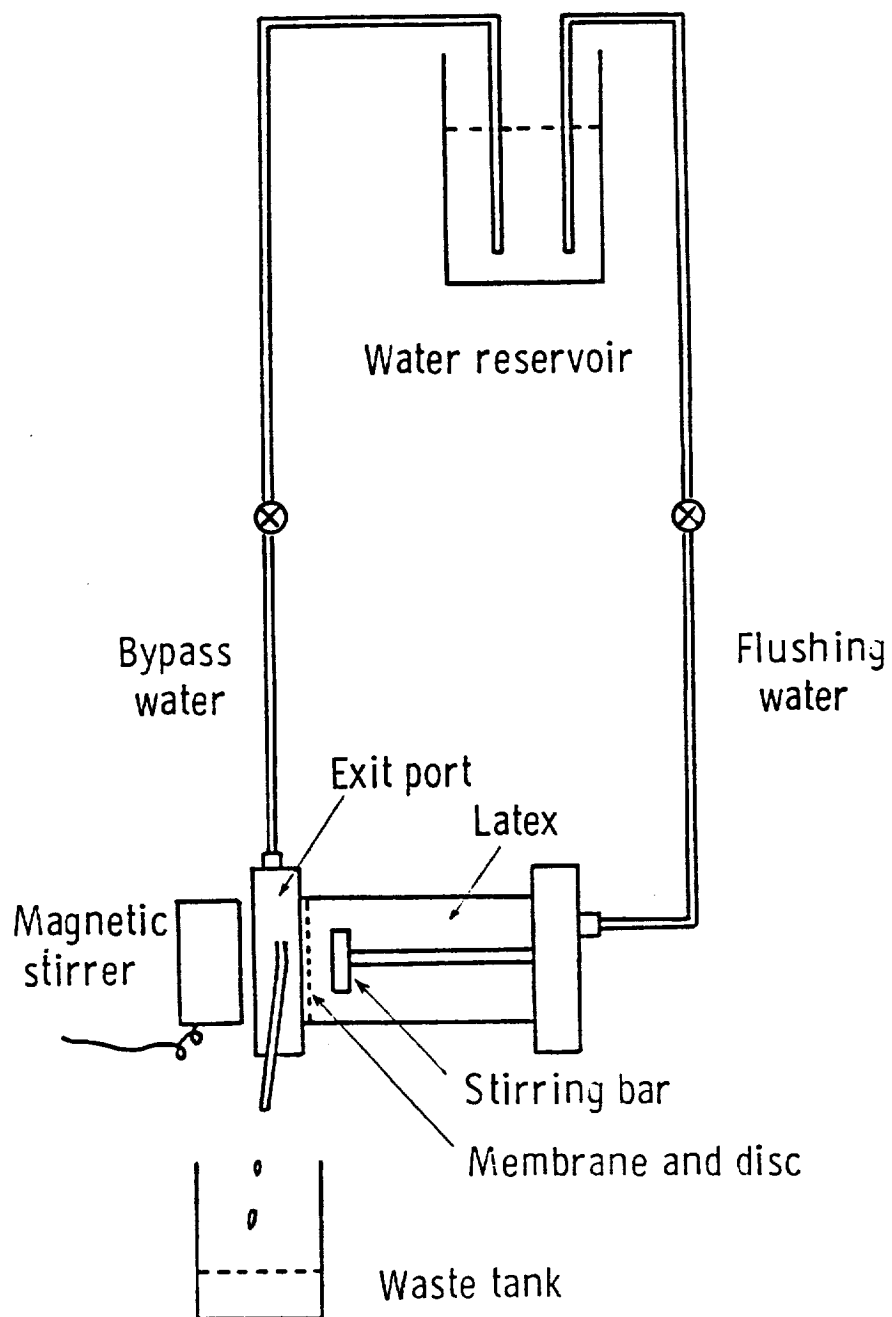
Figure 6-1.   Modified serum replacement cell for cleaning large-particle-size latexes.
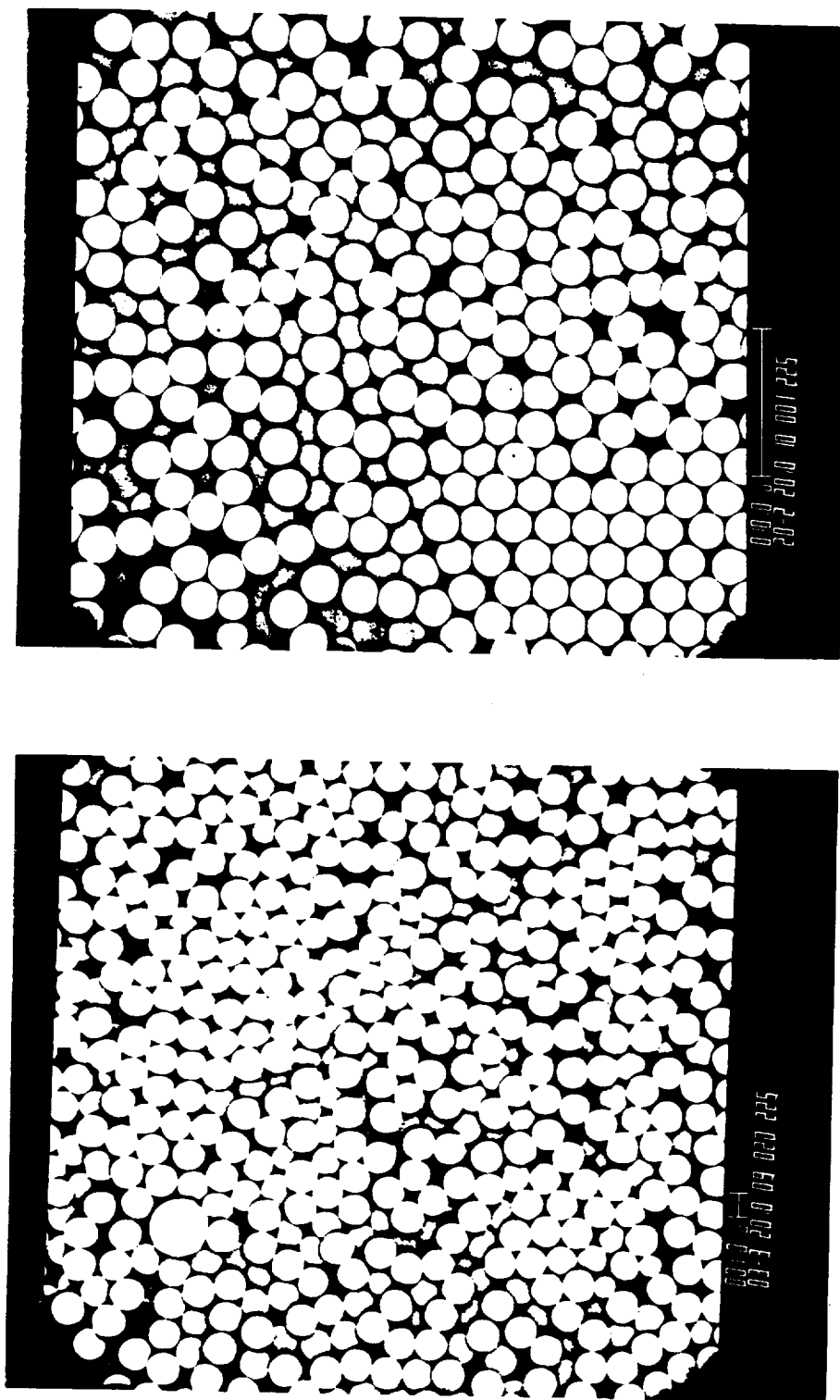
Figure 6-2. SEM micrographs of latex #4131-2 before (left) and after (right) cleaning by centrifugation plus serum replacement.

latexes of diameter up to 6 µm. Latexes larger than this size do not need the serum replacement method, because the sedimentation method is relatively efficient at those sizes. Figure 6-2 compares the SEM micrographs of the 2.5 µm latex #4131-2, before and after centrifugation plus serum replacement (with 2.0 µm membrane). The cleaned latex was used as seed in the STS-3 flight experiments. More examples of latexes cleaned by centrifugation, sedimentation, and serum replacement can be found in Chapter 5.

6.2 Determination of Particle Size

6.2.1 Microscopy

6.2.1.1 Optical Microscopy

Microscopy is the only method of obtaining particle size and size distribution by direct measurement of individual particles. Optical microscopy has been used for particle measurement for over 300 years. It is still the cheapest and fastest way for examining latex particles >2 µm. The microscope used in this laboratory was a Bausch & Lamb CL25. A 21X objective and a 17X eyepiece was usually used. The microscope was used mainly to estimate the average particle size and to count the number of over-size particles. To photograph the particles, a Nikon camera body was attached to the microscope with a T-mount. Tri-X film and Polycontrast print paper (both from Kodak) were used. The numbers of over-size and deformed particles were estimated by checking thousands of particles from the prints. The number-average particle sizes of the samples were also calculated from

the hexagonally packed arrays of the particles. Figure 6-3 shows the hexagonal packing of flight latex #11 from the STS-6 experiment. The line-to-line distance of the recticle was calibrated to be 28.6 μm. The average particle size obtained from this array was 9.9 μm, which is in excellent agreement with the value 9.96 μm obtained by TEM (Philips EM400).

6.2.1.2 Transmission Electron Microscopy

Because of its greater resolution, electron microscopy is very useful in determining latex particle size distributions. Other parameters such as particle shape and surface roughness can also be examined by electron microscopy.

Two transmission electron microscopes were available: the Philips EM300 and EM400. The EM300 was used in the routine check of research products because of its easy access; however, it was found that the EM400 gave more reliable results. In the analysis of flight samples from STS-3 and STS-6 experiments, the EM400 was used.

In this laboratory, latex samples of submicron size were usually examined on coated stainless steel grids of 200-300 mesh. For latexes of large particle size, grids of greater opening were preferred. Several types of grids purchased from Ernest F. Fullam, Inc. were tested; the Nickel 75 mesh Hexagonal was found to be the easiest to handle. A Formvar support film was first put on the grid and coated with a thin layer of carbon. A drop of diluted latex was then put on the coated grid. To reduce the segregation of off-size particles during drying of the sample, a small sample size was used; a syringe
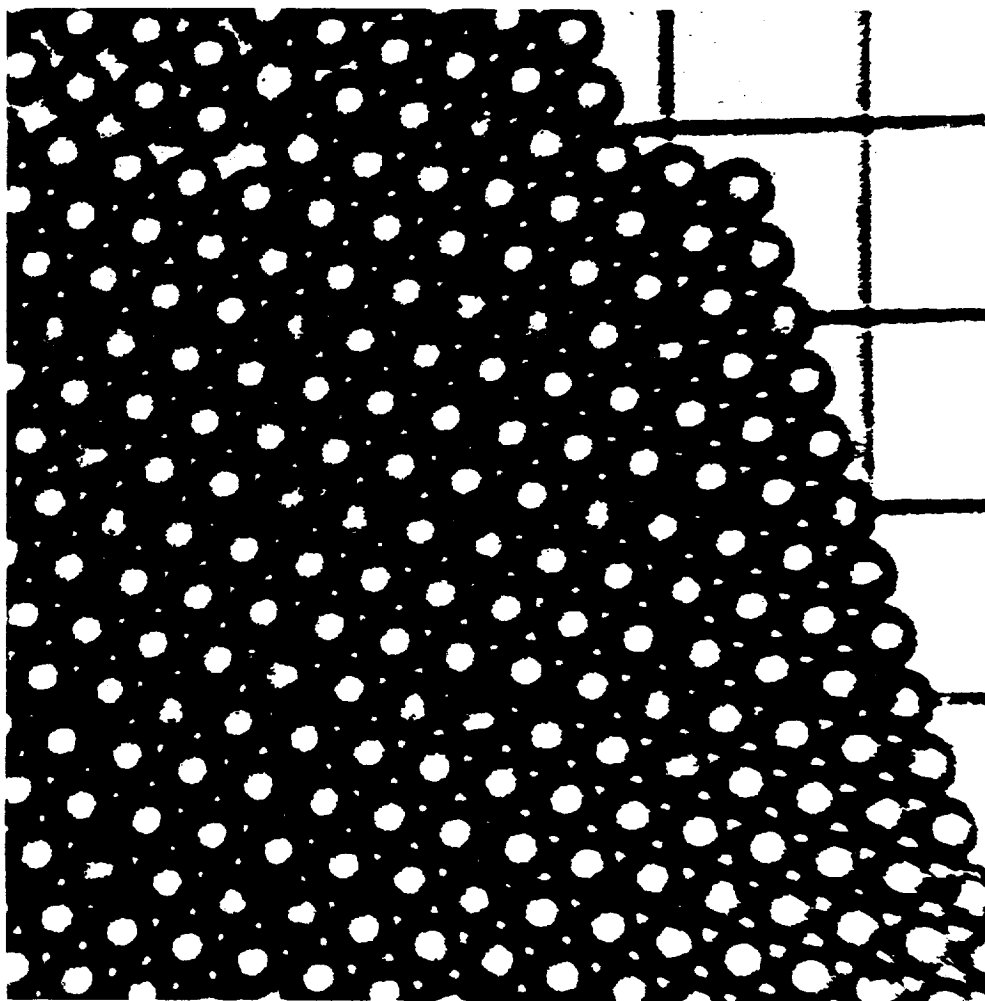
Figure 6-3.   Optical micrograph of hexagonal array
of flight latex #11.

with a fine needle was used to place a very small drop on the specimen substrate.

For soft latexes such as those containing telomers (Chapter 2), the cold-stage TEM was used. The cooling chamber of the microscope was filled with liquid nitrogen. A drop of latex was placed on a coated grid, and most of the drop was removed by touching the edge of the grid with a filter paper, leaving only a thin film of the latex. This specimen was then loaded into the microscope, frozen, and examined while still frozen.

The method usually used in this laboratory to calibrate the TEM magnification setting was to photograph a calibration grid, which comprised a silicon monooxide replica of an 1134 line/mm (or 2160 line/mm) diffraction grating, at the same magnification as used in photographing latex samples. The true magnification of a printed micrograph was calculated from the average line-to-line distance of the grating on a similar print. During the analysis of the STS-3 ground latexes with the EM300, it was found that magnification might have changed from specimen to specimen, or even from exposure to exposure. Therefore, a more reliable calibration method was pursued.

In the later analysis of flight latexes with the EM400, an internal calibration method was adopted. A tiny drop of aqueous suspension which contained fragments of the 2160 line/mm silicon monooxide grating replica (Ernest F. Fullam, Inc.), was placed on a coated grid and dried before the latex sample was applied. Thus the fragments of grating replica appeared on some of the micrographs along with the latex particles (Figure 6-4). The line-to-line distances of

the grating were measured in different prints to check the variance of magnification from exposure to exposure. The EM400 results from the analysis of the STS-6 flight latexes were very satisfactory. No significant change in magnification from exposure to exposure was noticed.

To obtain a representative particle size distribution, at least 300 particles were measured from the TEM prints. The measurements were carried out with a Zeiss Digital Image Analyzer Model MOP-3. The error from this instrument was estimated by measuring a single particle 20 times to be equivalent to a coefficient of variation of 0.5-0.7%.

Some degree of magnification distortion was observed in most of the micrographs of large-particle-size latexes. The diameter appeared to be larger in one direction than in other directions, especially for the particles away from the center of the micrograph. This phenomenon was also observed by investigators at the National Bureau of Standard (NBS) [115]. They found that distortion was significantly less in the tangent direction than the radial direction (1.4% vs 4.0%) and was fairly constant for a fixed radius about the center of the micrograph. They made use of this property by locating the position of each particle within one of four concentered zones. The diameter of each particle was then corrected for the average magnification distortion in each zone. In our analysis, the distortion was not always found to be in the radial direction. Therefore, the correction method developed by NBS was not applied. However, care was taken to measure all particles in the same direction, i.e., parallel to the long side
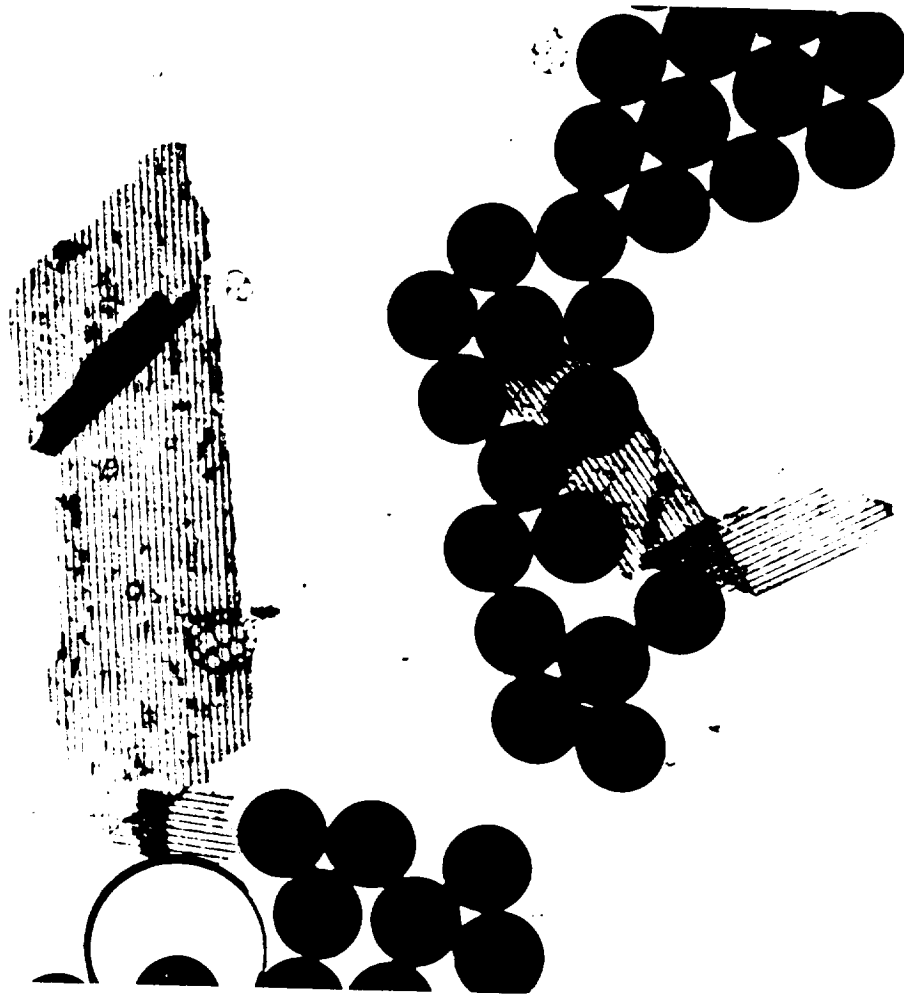
Figure 6-4.   TEM micrograph of latex #6010C with fragments of the 2160 lines/mm grating replica.

of the film. The distortion seemed to be smaller in this direction and it was hoped that this would minimize the error from magnification distortion.

A computer program named PSD, developed in this laboratory [118], was used to treat the data from the TEM measurements and to generate particle size averages and standard deviation, as well as the distribution curve. The results for all of the flight and ground latexes are presented in Chapter 5. The reported standard deviations were not corrected for any measurement uncertainty. For statistically independent quantities, the variances are additive, so that the measured standard deviation of the size distribution, σ_m, can be related to the true σ and the uncertainty in the measurement, U_i, by the following equation [115]:

$$\sigma_m = \sqrt{\sigma^2 + U_i^2} \tag{6-9}$$

By proper estimation of all types of measurement uncertainty, a more accurate standard deviation of the size distribution can be obtained.

Several polymethyl methacrylate latexes were used in the swelling study (Chapter 2). Their average diameters were estimated by light scattering and by TEM. Because these particles fused readily under electron beam, a negative staining method was used with these latexes. A 2% phosphotungstic acid (PTA) solution was prepared and stored under refrigeration. One drop of dilute latex (10-20%) was added to 1 ml of the PTA solution. The stained latex was then examined using the cold-stage procedure. Figure 6-5 shows micrographs of PTA-stained latex

PMMA I. The average particle diameter obtained, 0.40 μm, agreed well with the value from light scattering. The same staining method was also applied successfully to several polyethyl acrylate and polybutyl acrylate latexes.

6.2.1.3 Scanning Electron Microscopy

The scanning electron microscope (SEM) is one of the most versatile instruments available for the examination and analysis of the microstructural characteristics of solid objects [119]. The primary reason for the SEM's usefulness is the high resolution which can be obtained when bulk objects are examined; values of the order of 5 nm (0.005 μm) are usually quoted for commercial instruments. Another important feature of the SEM is the three-dimensional appearance of the specimen image, which is a direct result of the large depth of field. The greater depth of field of the SEM provides much more information about the specimen. The SEM is also capable of examining objects at very low magnification.

SEM was widely used in this study to get a qualitative estimation of the monodispersity and relative number of off-size particles in a latex sample. A tiny drop of latex was applied on a small piece of plastic coverslip, which was glued onto a SEM mounting stub. A thin layer of Au-Pd was coated on the specimen with a Polaron E5100 Sputter Coater. The specimen was then examined under an ETEC Autoscan electron microscope and photographed with Polaroid type 55 films. To make sure that particles of all sizes were included, usually two micrographs were taken for each specimen, one close to the edge and
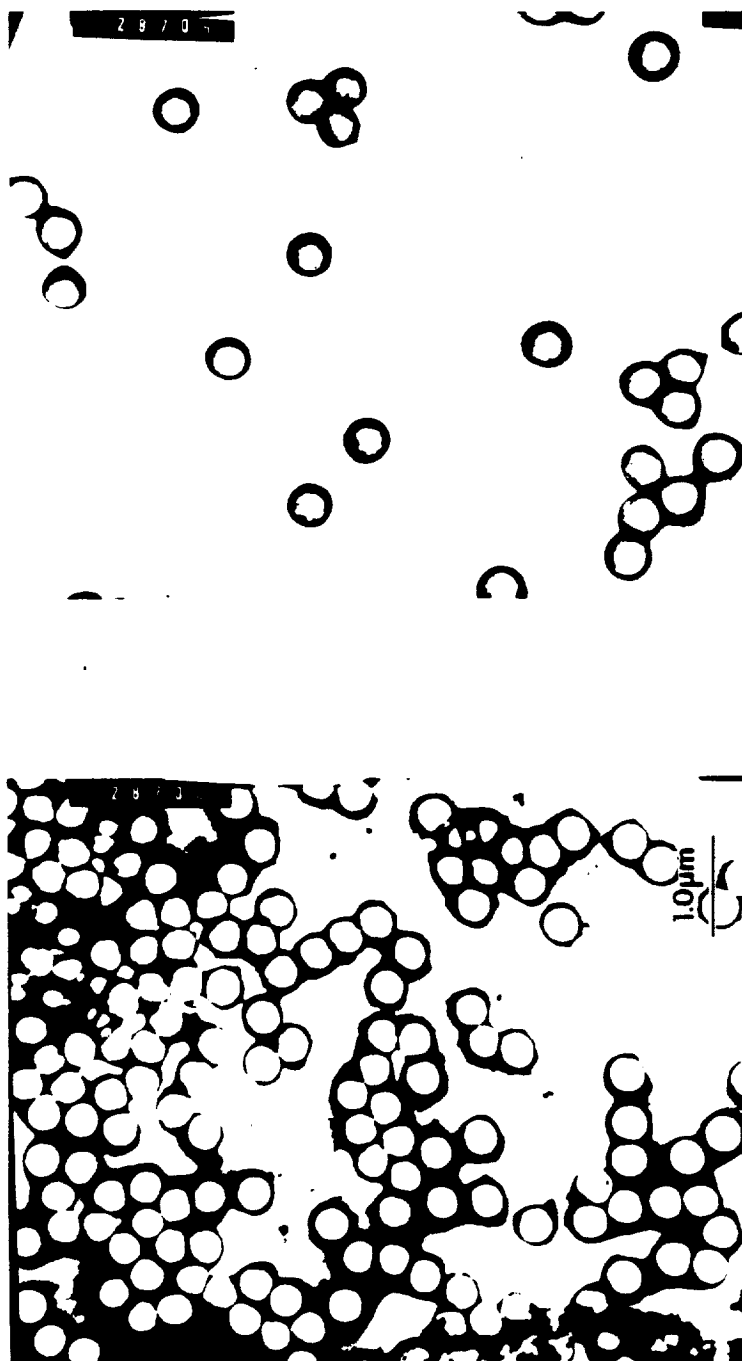
Figure 6-5.   TEM micrographs of latex PMMA 1 stained with phospho-
tungstic acid.

the other close to the center.

Because of the significant magnification distortion in the TEM at lower magnifications, the SEM was used for the determination of particle size distribution in latexes of particle size >10 μm. All of the STS-7 flight and ground latexes were determined in this way. The magnification was set at 500X and calibrated with an external standard, a Pelco 100x0.01mm copper disc, and an internal standard, a diffraction grating replica suspension. After the diluted latex was placed on a specimen stub and dried, a drop of the 1134 line/mm grating suspension was placed on top of the dried latex. The specimen was then dried, coated, and examined at zero-degree tilt. The particles were photographed and measured similarly to the TEM measurement. Figure 6-6 shows a micrograph with fragments of the grating replica.

The degree of magnification distortion in the SEM was checked with the 100x0.01mm copper disc standard (Figure 6-7). The standard was aligned horizontally and vertically, and photographed at different locations. Figure 6-8 gives the average line-to-line distance measured in nine different zones of the film plane. The results indicate that the vertical measurements are in general slightly larger than the horizontal measurements (about 1%) and the variation in either direction is relatively small.

6.2.2 Light Scattering - Forward Angle Ratio Method

Several methods have been developed for determining particle size using light scattering [120]. Of these, "dissymmetry" is a simple and

281
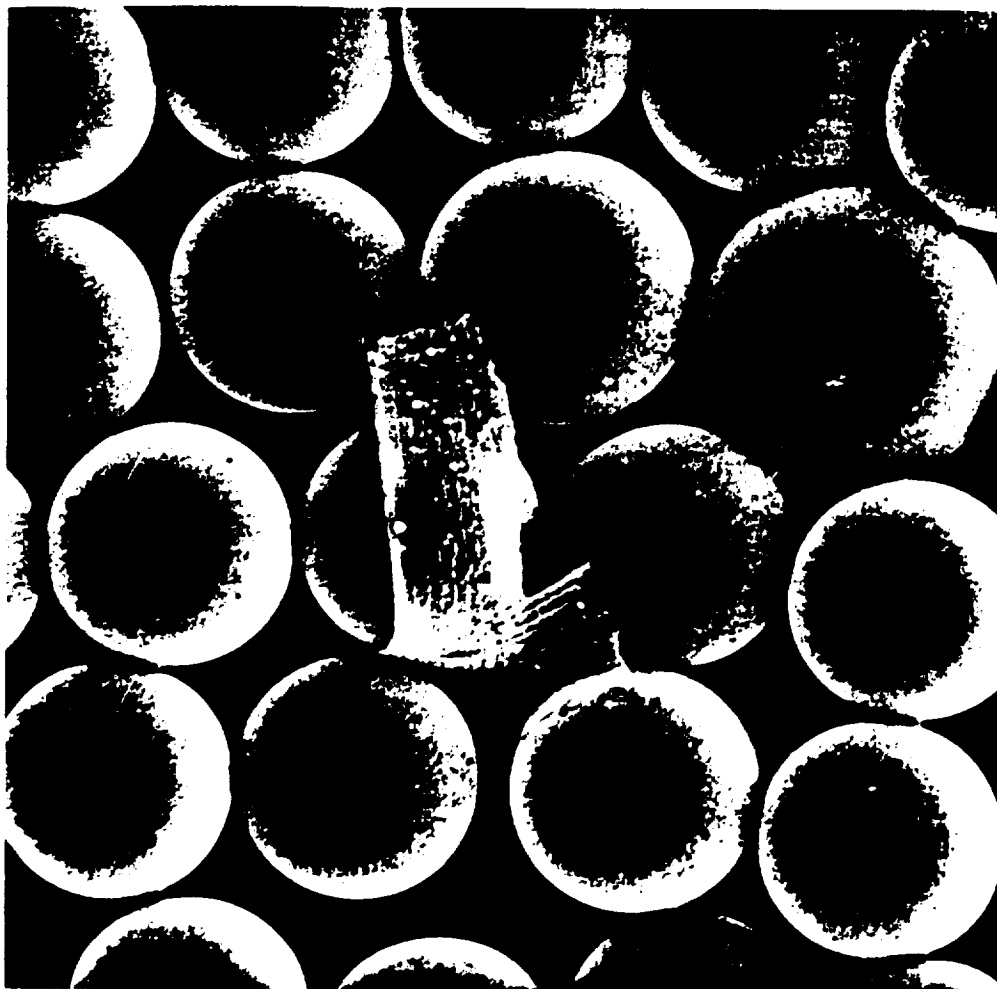
Figure 6-6.   SEM micrograph of ground latex #14
with fragments of the 1134 lines/mm grating replica.
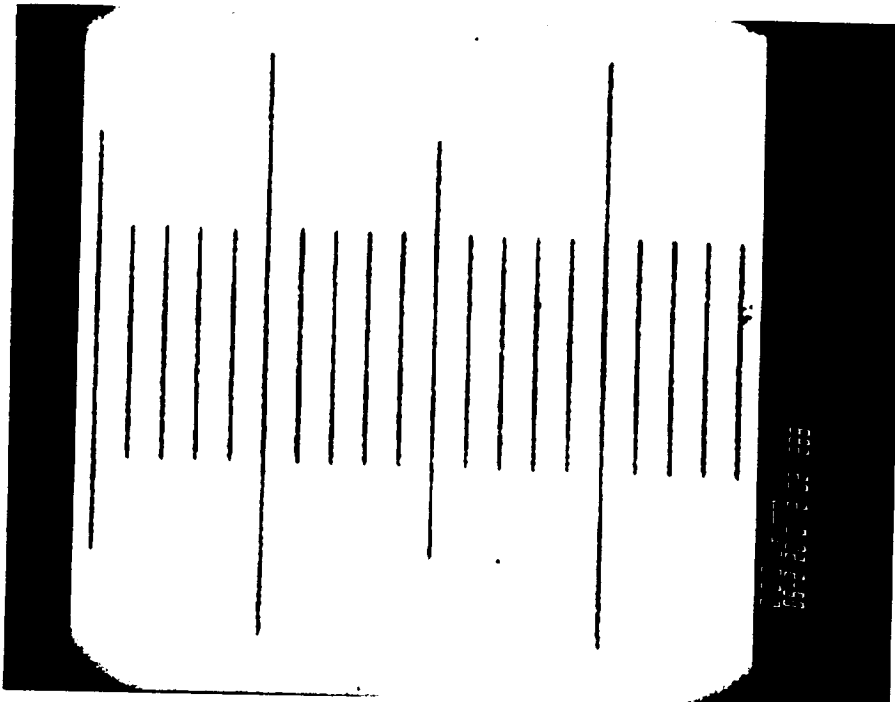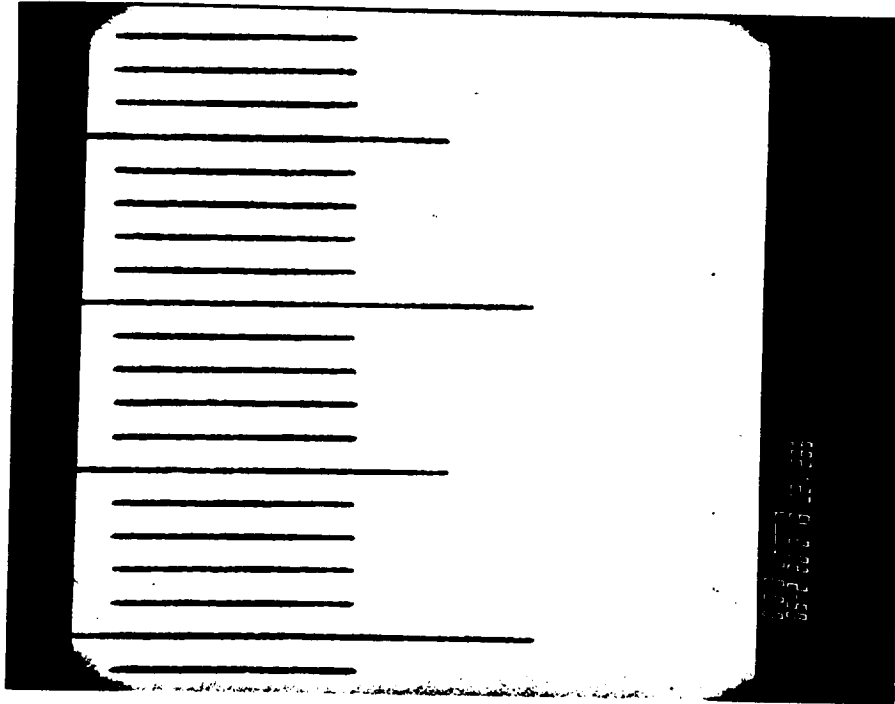
Figure 6-7. SEM micrographs of the Pelco 100x0.01 mm copper disc calibration standard.

Figure 6-8.   Spacing of the 100x0.01mm copper disc
standard measured in different zones of a film plane,
at 500x magnification setting.

attractive method; however, it is limited in application to D/λ_m values $<$ 0.60 for monodisperse systems [121], where D is the diameter of the scattering particles and λ_m the wave length of the light in the dispersion medium. With the Forward Angle Ratio method (FAR), the Mie theory shows that particle diameter up to D/λ_m = 2.0 or higher can be measured for monodisperse systems, and the results are practically independent of the refractive index ratio (m) between 1.1 and 1.2.

The following is a summary of the procedures commonly used in the FAR method [120, 121]:

1. Measure the intensity of scattered light at 10-degree intervals as a function of particle concentration.

2. Plot the intensity ratio $I_{\theta+10}/I_\theta$ for a chosen θ as a function of concentration and extrapolate to get the value at zero concentration $(X'_t)_o$.

3. The theoretical intensity values, i_θ and $i_{\theta+10}$, are available from Mie Table as a function of D/λ_m for a given m. Multiplying $i_{\theta+10}/i_\theta$ by $Sin(\theta)/Sin(\theta+10)$, the viewed angle correction, one obtains the theoretical intensity ratio X'_t as a function of D/λ_m.

4. Consult a graph of X'_t versus D/λ_m for the appropriate m value and obtain D from the experimentally determined intensity ratio $(X'_t)_o$.

In this study, simple equations relating D/λ_m and X'_t were derived based on tabulated values from the Mie theory. The equations were calibrated with monodisperse polystyrene latex standards and used

to calculate the particle sizes of unknown samples. Several polymethyl methacrylate latexes and telomerized polystyrene latexes of sizes up to 0.90 um were measured by this method.

A Brice-Pheonix model 2000 photometer with a cylindrical cell was used in this study. Monochromatic light filters with wavelengths in water λ_m of 489nm (red), 410nm (green) and 327nm (blue) were available. The FAR method was evaluated at two angular settings: $45°/35°$ and $30°/20°$. Dow monodisperse polystyrene latexes with the following sizes were used as calibration standards: 0.19 μm, 0.23 μm, 0.36 μm, 0.40 um, 0.60 μm and 0.79 μm.

Figure 6-9 shows the variation of measured intensity ratio with particle concentration for three polystyrene standards at the angular setting $45°/35°$. The theoretical intensity ratios from the Mie table are plotted versus D/λ_m in Figure 6-10 for $45°/35°$ and $30°/20°$ with m = 1.1 and 1.2.

As mentioned earlier, X'_t is not a strong function of m. An attempt was made to construct a master curve and derive a simple equation which could be used to calculate the particle diameter from $(X'_t)_o$ directly without knowing the exact value of m. Figure 6-11 is a result of the effort for $45°/35°$. The circles and squares are theoretical values from the Mie table for m=1.1 and m=1.2, respectively. The straight line is the least squares fit of all of these points. From the linear relationship on a log-log plot, an equation was obtained which is applicable to particles with m between 1.1 and 1.2, and $D/\lambda_m < 1.6$:

$$D/\lambda_m = 1.855 \ (0.728 - X'_t)^{0.5078} \tag{6-10}$$

A similar treatment was applied to the $30^{\circ}/20^{\circ}$ method; however, a straight line was not enough to cover the whole particle size range for this case (Figure 6-12). Therefore, a third-degree polynominal fit was used to obtain the following equation from the X'_t versus D/λ_m plot:

$$D/\lambda_m = 2.507 - 5.674X'_t + 10.291X'^2_t - 10.912X'^3_t \qquad (6-11)$$

Figure 6-13 compares the diameters of the monodisperse polystyrene standards measured by TEM and those calculated from equations (6-10) and (6-11), respectively. A straight line with slope of 1.07 indicates that an instrumental correction factor of 1.07 is required for the $45^{\circ}/35^{\circ}$ method, while no correction is needed for the $30^{\circ}/20^{\circ}$ method.

Figure 6-14 shows the measured intensity ratio versus particle concentration curves for three polymethyl methacrylate latexes at $45^{\circ}/35^{\circ}$. By using equation (6-10) and the correction factor, the following average particle diameters were obtained: 0.409 um for PMMA 1, 0.317 µm for PMMA II, and 0.194 um for PMMA III. These particle sizes agreed well with the TEM results.

Figure 6-15 shows the measured intensity ratio versus particle concentration curves for three telomerized polystyrene latexes at $30^{\circ}/20^{\circ}$. By using equation (6-11), the following average particle diameters were obtained: 0.60 µm for #2137-1, 0.71 µm for #3078-3, and 0.87 µm for #2054-4.

In summary, simplified equations for FAR $45^{\circ}/35^{\circ}$ and $30^{\circ}/20^{\circ}$ methods have been developed. The equations can be used to calculate
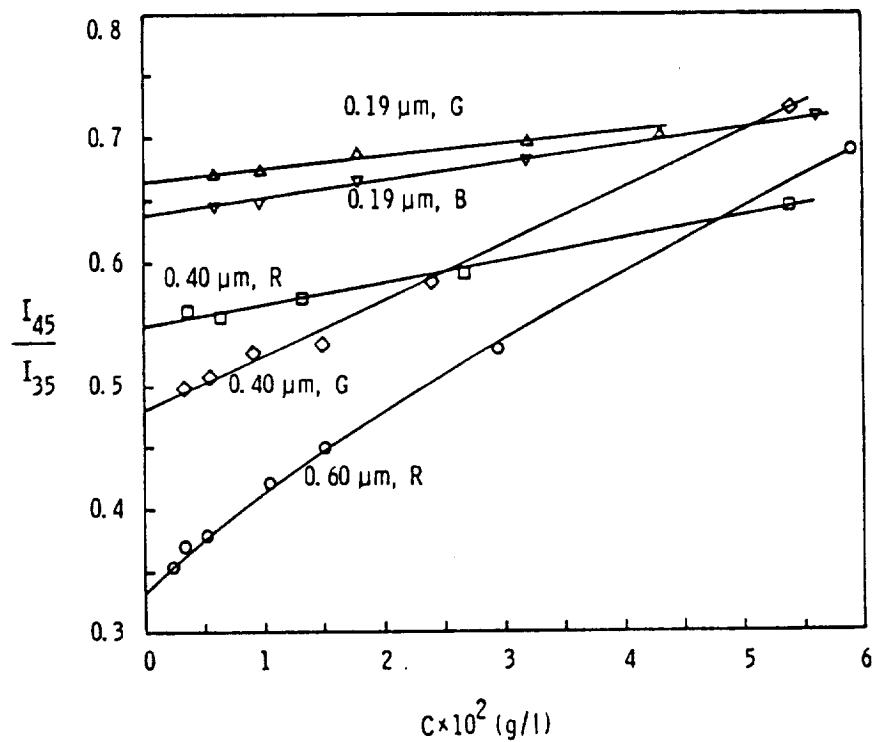
Figure 6-9.   Intensity ratio vs. concentration
plots for monodisperse polystyrene latex particles at
$45^\circ/35^\circ$; R = red light, λ_m = 489nm; G = green, 410nm;
B = blue, 327nm.
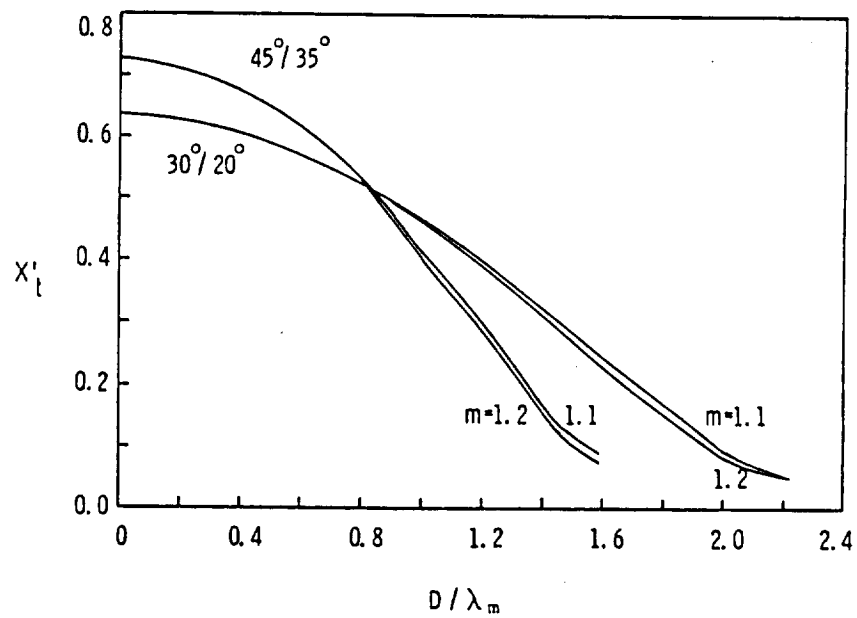
Figure 6-10.   Corrected Mie theory plot for m = 1.1
and 1.2 at 45°/35° and 30°/20°.
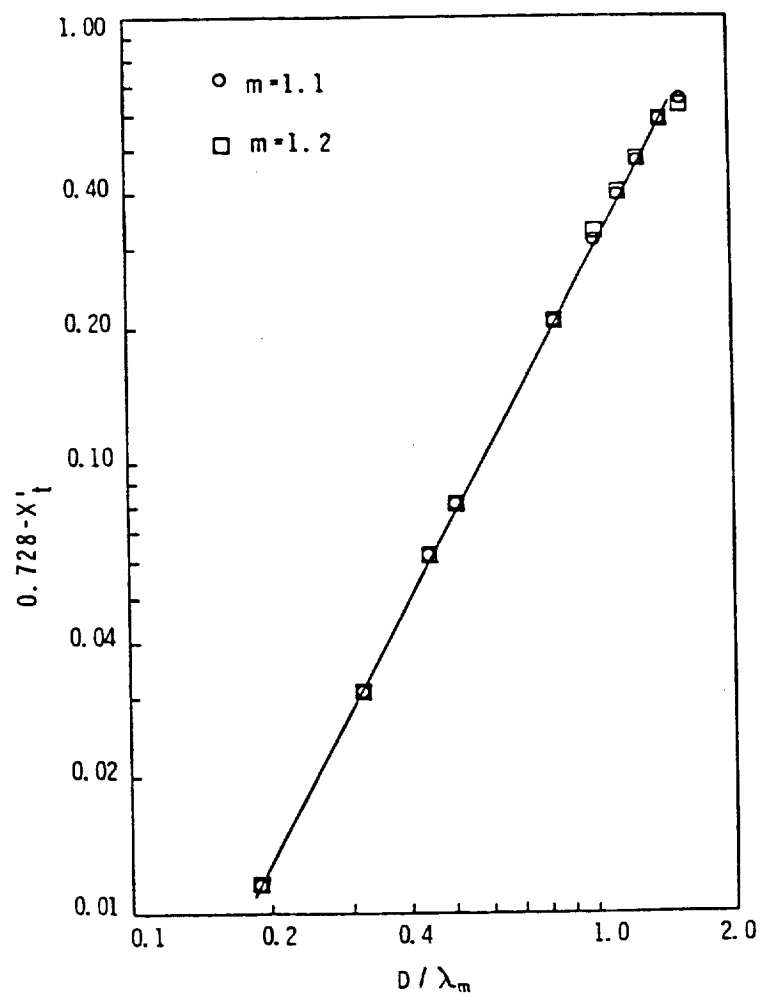
Figure 6-11.   Master curve of the intensity ratio at
45°/35° from the Mie table.
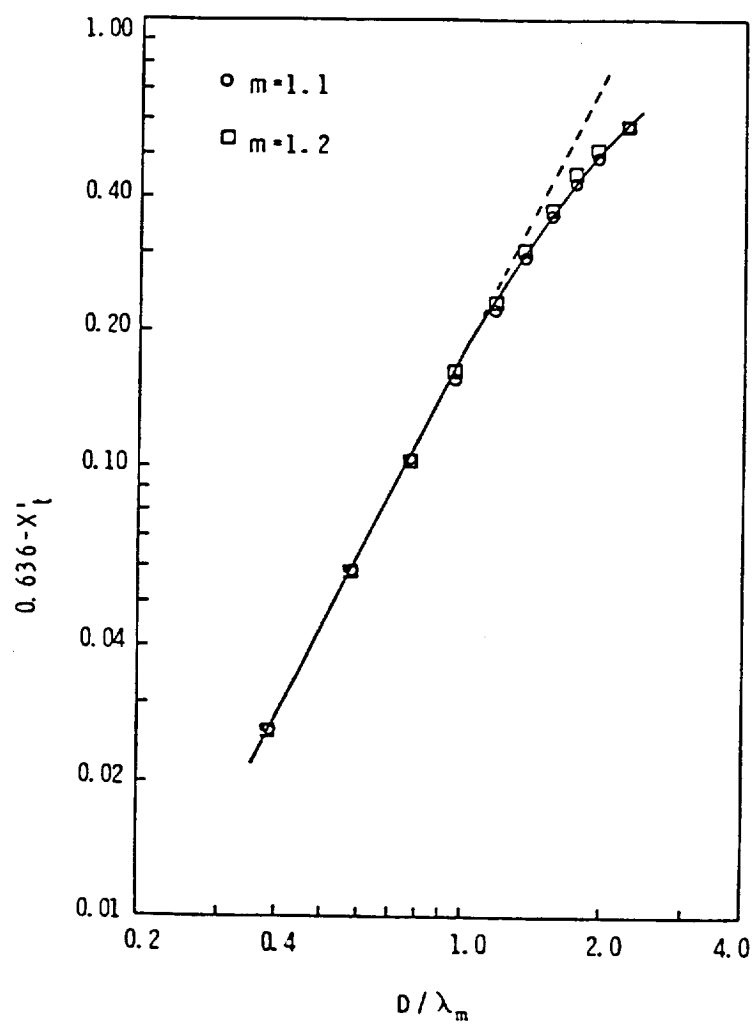
Figure 6-12.   Master curve of the intensity ratio at
$30^{\circ}/20^{\circ}$ from the Mie table.

291
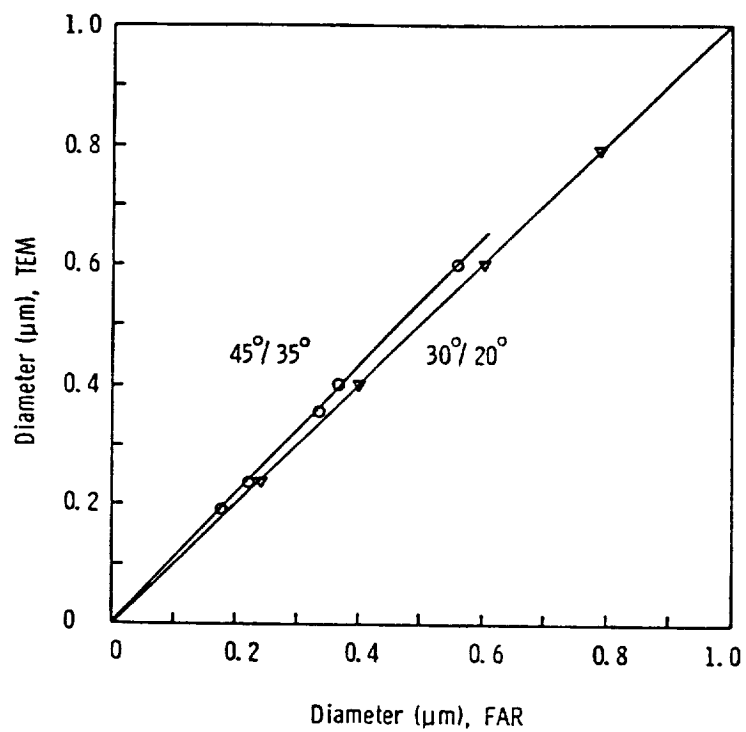
Figure 6-13. Comparison of latex particle diameters
as determined by Transmission Electron Microscopy and
the Forward Angle Ratio method from $45°/35°$ and
$30°/20°$ intensity ratios.
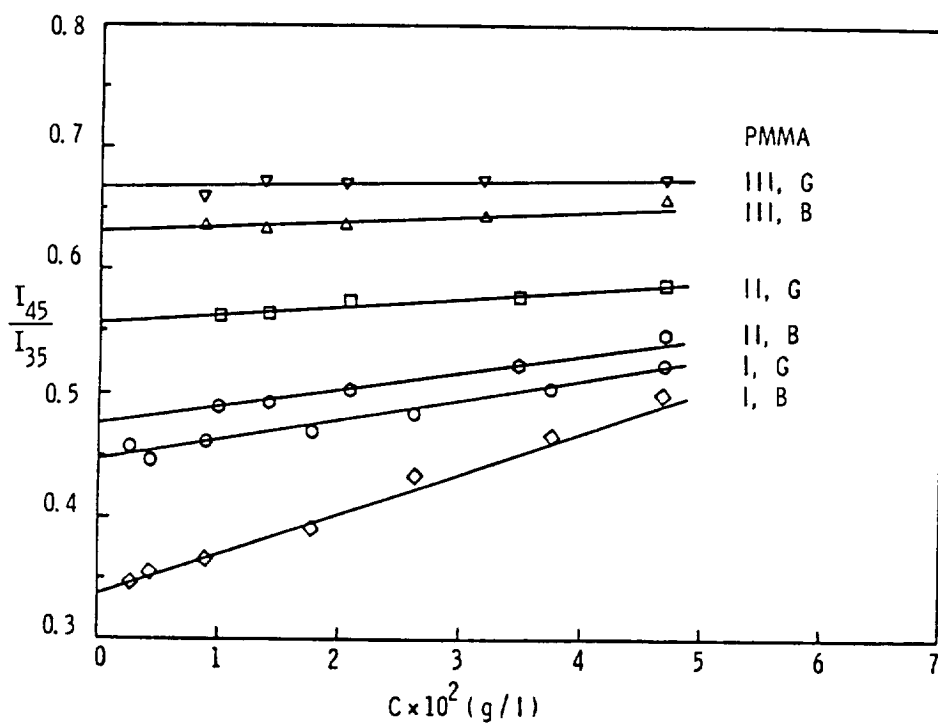
Figure 6-14.   Intensity ratio vs. concentration plots for polymethyl methacrylate latex particles at $45°/35°$; R = red light, λ_m = 489nm; G = green, 410nm; B = blue, 327nm.
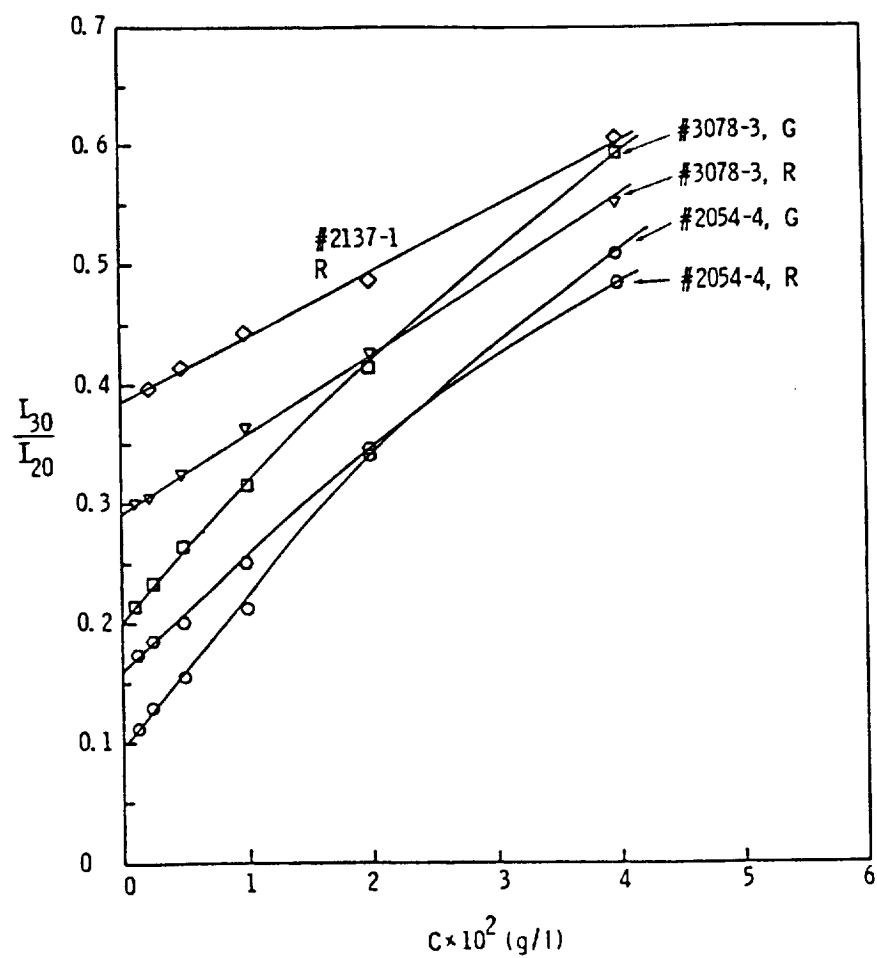
Figure 6-15. Intensity ratio vs. concentration plots for telomerized polystyrene latex particles at $30^\circ/20^\circ$; R = red light, λ_m = 489nm; G = green, 410nm; B = blue, 327nm.

particle diameter directly from the measured intensity ratio at zero concentration without knowing the exact m value, as long as m is between 1.1 and 1.2. An instrumental correction factor may be required for a certain angular setting.

6.3 Electrophoretic Mobility of Latex Particles

Electrophoretic mobility of several polystyrene latexes prepared in this study, in the size range of 2 - 11 μm, were measured in distilled-deionized water using the Pen Kem 3000 at 50 volts/cm. Latexes of diameter greater than 11 μm could not be easily measured by this instrument due to their high sedimentation rate in the electrophoresis cell. The results are summarized in Table 6-2. For comparison, a Dow monodisperse standard of 1.1 μm diameter was also measured under the same conditions. Figure 6-16 is an example of the mobility distribution curve obtained from Pen Kem 3000. All of the samples showed very narrow distributions of electrophoretic mobility. Since these latexes were prepared with an oil-soluble initiator which does not impart charged surface groups, the surface charge density of the latexes should be extremely low according to Sudol's study [71]. It is surprising to see that all these particles have significant and similar electrophoretic mobility values. Moreover, the values (-3.1 to -3.6 μm-cm/V-sec) agree with the values for polystyrene and poly-vinyltoluene latexes of different sizes and different surface charge density within experimental error.

For comparison, Table 6-3 lists the electrophoretic mobility of other latexes measured in water or a surfactant solution of very low

Table 6-2.   Electrophoretic Mobility of Large-
Particle-Size Monodisperse Latexes

Latex No.	Electrophoretic Mobility (μm-cm/V-sec)
#5132C (2.0 μm)	-3.1
#5133C (3.4 μm)	-3.5
#5136C (6.2 μm)	-3.3
#5137C (11 μm)	-3.1
Dow 1.1 μm PS	-3.3
#4131-2C (2.5 μm)	-3.2
#5053C (5.5 μm)	-3.6
#5084C (5.5 μm)	-3.2

concentration in our laboratory during the past few years. Even the
latexes without titratable charged surface groups, i.e., latexes with
only surface hydroxyl groups, showed the same electrophoretic mobility
value as latexes with higher surface charge density. A conclusion can
be drawn from these observations: polystyrene latexes with relatively
low surface charge density and in the size range of 0.35 to 10 μm,
probably including latexes of similar chemical structure such as poly-
vinyltoluene, tend to have electrophoretic mobilities of -3.3±0.3 μm-
cm/V-sec in water independent of differences in particle size and
surface charge density.

To further understand the relationship between electrophoretic
mobility and surface charge as well as material property, four
"charge-free" latexes, two polystyrene and two polymethyl
methacrylate, in the size range of 0.2-0.5 μm, were prepared with AIBN
initiator and Aerosol MA emulsifier. These latexes along with two
persulfate-initiated polymethyl methacrylate latexes were measured by
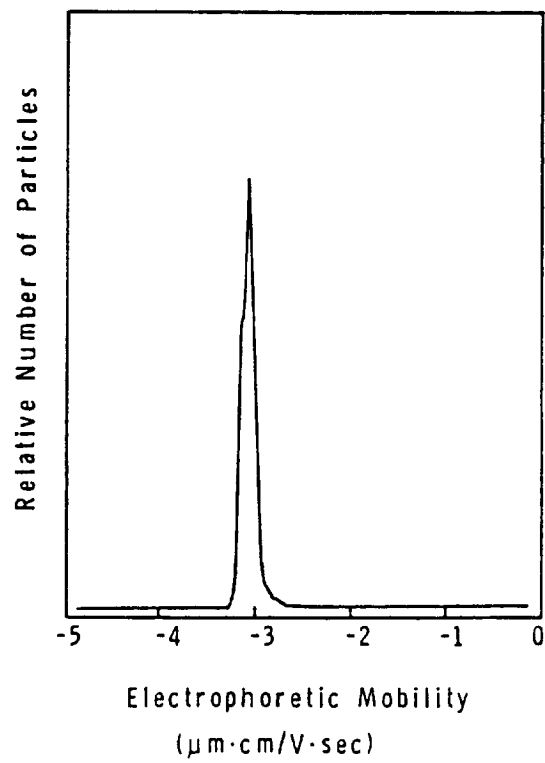
Figure 6-16. Electrophoretic mobility distribution of polystyrene latex #5137C particles.

Table 6-3. Electrophoretic Mobility of Polystyrene and Polyvinyl-toluene Latexes Measured in This Laboratory

Latex	Medium	Instrument	Mobility $(\mu m\text{-}cm/V\text{-}sec)$	Reference
Dow 0.357 μm PS	10^{-4}M SLS	Pen Kem 3000	-3.3	[122]
Dow 0.357 μm PS	10^{-4}M SLS	Pen Kem 500	-3.3	
Dow 0.357 μm PS	10^{-4}M SLS	Rank	-3.3	
Dow 1.1 μm PS	10^{-4}M SLS	Pen Kem 3000	-3.5	
Dow 1.1 μm PS	10^{-4}M SLS	Pen Kem 500	-3.6	
Dow 1.1 μm PS	10^{-4}M SLS	Rank	-3.5	
Dow 2.02 μm PVT	10^{-4}M SLS	Pen Kem 3000	-3.7	
Dow 2.02 μm PVT	10^{-4}M SLS	Pen Kem 500	-3.7	
Dow 2.02 μm PVT	10^{-4}M SLS	Rank	-3.8	
Dow 0.357 μm PS	Water	Pen Kem 3000	-3.2	[123]
Dow 0.357 μm PS	Water	Pen Kem 500	-3.0	
Dow 0.357 μm PS (Sulfate Form)	Water	Rank	-3.2	[124, 125]
(Hydroxyl Form)	Water	Rank	-3.1	
520' PS(0.53 μm) (Sulfate Form)	Water	Rank	-3.3	[126, 127, 128]
(Hydroxyl Form)	Water	Rank	-3.2	
(Carboxyl Form)	Water	Rank	-3.1	

Table 6-4.   Electrophoretic Mobility of AIBN-
initiated and Persulfate-Initiated Latexes

Latex No.	Initiator	Electrophoretic Mobility (μm-cm/V-sec)
PS #1 (0.2-0.5 μm)	AIBN	-3.0
PS #2 (0.2-0.5 μm)	AIBN	-3.1
PMMA #6 (0.2-0.5 μm)	AIBN	-1.9
PMMA #7 (0.2-0.5 μm)	AIBN	-1.6
PMMA 1 (0.409 μm)	Persulfate	-3.7
PMMA 11 (0.317 μm)	Persulfate	-3.9

the Pen Kem 3000 under the same conditions. Table 6-4 compares the
measured mobility results. Again, the two polystyrene latexes showed
mobilities in the same range as the other polystyrene latexes. The
two "charge-free" polymethyl methacrylate latexes had mobilities about
half the value of the polystyrene latexes. The two persulfate-
initiated polymethyl methacrylate latexes had mobility much higher
than the other two polymethyl methacrylate latexes owing to the
presence of additional charged surface groups. It appeared that
surface charge had more significant effect on the electrophoretic
mobility of polymethyl methacrylate latexes than of polystyrene
latexes.

6.4 Molecular Weight Distribution by GPC

6.4.1 Nonaqueous GPC System

All the molecular weight measurements in this study were carried
out with a Waters Associates ALC/GPC 201 Liquid Chromatograph. The
unit comprised a solvent delivery system Model 6000A, an universal

299

injector Model U6K, and a differential refractometer Model 401. Five μ-Styragel columns, 10^6Å, 10^5Å, 10^4Å, 10^3Å and 500Å, were used in determining the molecular weight distribution of nonaqueous polymers. All separations were done with a sample size of 0.05-0.3 ml of 0.5% polymer and with THF solvent at a flow rate of 2 ml/min. The column set was calibrated with polystyrene standards of molecular weight 840, 2,350, 3,600, 17,500, 35,000, 110,000, 200,000, 470,000, 650,000, 1,400,000, and 2,700,000. The standard of molecular weight 840 was purchased from Polysciences, Inc. The others were from Waters Associates.

There have been numerous studies dealing with the correction of instrumental spreading in GPC. One of the pioneer work is Tung's axial dispersion equation [129]. The equation corrects for Gaussian axial dispersion which occurs when a finite pulse is injected into the solvent stream which flows through the packed column of the GPC. Several attempts have been made to solve for the corrected chromatogram numerically. Hamielec and Ray [130] have found an analytical solution for the ratio of corrected to uncorrected molecular weight averages in terms of GPC parameters D_2 and h:

$$M_n(h)/M_n(\infty) = \exp\{(D_2)^2/4h\} \qquad (6\text{-}12)$$
$$M_w(h)/M_w(\infty) = \exp\{-(D_2)^2/4h\} \qquad (6\text{-}13)$$

where $M_n(h)$ and $M_n(\infty)$ are the dispersion corrected and uncorrected number average molecular weights and $M_w(h)$ and $M_w(\infty)$ are the corrected and uncorrected weight average molecular weights, D_2 is the slope of the logarithmic calibration curve $[M(V_e)=D_1\exp(-D_2V_e)]$, and h is a parameter describing the width of the spreading and is

300

$c - 9$

related to the standard deviation σ of the Gaussian distribution by $h=1/2\sigma^2$.

Most of molecular weight standards are prepared from anionic polymerization, by which the Poisson distribution is approached. Therefore, the shapes of the chromatograms for the standard samples are usually skewed and non-Gaussian. To overcome the difficulty of fitting a Gaussian distribution to non-Gaussian curves, Tung and Runyon [131] proposed to use only the leading halves of the chromatograms. The instrumental spreading characteristics determined by this method were found to depend on the elution volume but not on the nature of the polymer.

In this study, Hamielec's analytical solution and Tung's leading half technique were applied to correct the instrumental spreading. The spreading parameter, h, was determined from the leading half of the chromatogram of each standard (Figure 6-17). Table 6-5 and Figure 6-18 show an example of the calibration data thus obtained.

After the chromatogram of an unknown sample was obtained, the peak heights at every 0.5 ml elution volume were taken from the chromatogram. The chromatographic data along with the calibration data were input to use a computer program for calculating molecular weight averages and plotting the distribution curve. The program, named MWD [132], used a fourth-degree polynominal fit to obtain a log M vs. V_e function, and a third-degree polynominal fit to obtain a function of h vs. V_e from the calibration data. By using the calibration functions, the elution volumes in the sample data were converted to molecular weights. The molecular weight averages were then calculated by
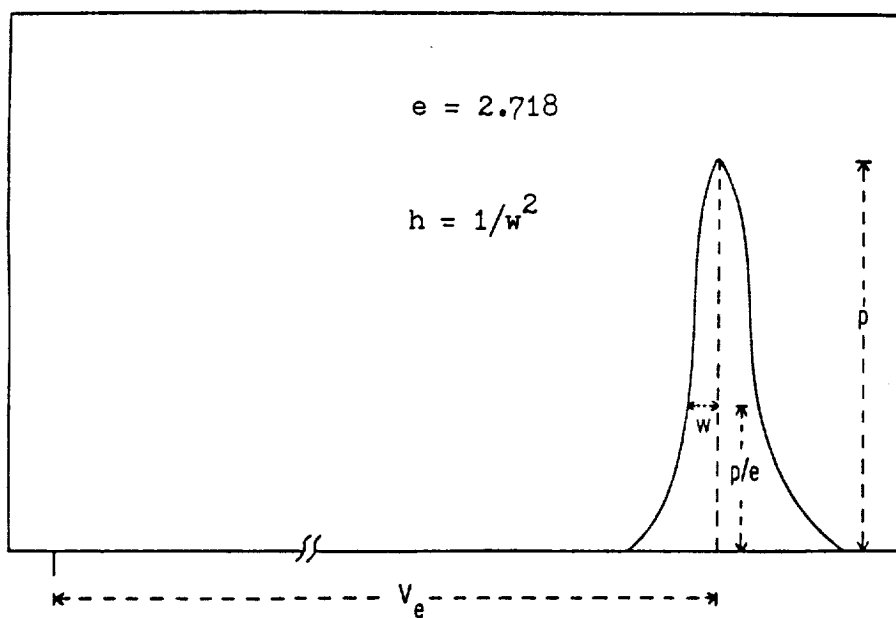
Figure 6-17. Determination of the spreading
parameter, h, from the chromatogram of a molecular
weight standard.

Table 6-5.   Calibration Data Obtained from the
Polystyrene Standards with the u-Styragel Column Set

M	$V_e(ml)$	h
1.04×10^2 +	50.9	-
8.40×10^2	44.7	0.37
2.35×10^3	40.7	0.42
3.60×10^3	40.1	0.59
1.75×10^4	36.1	0.59
3.50×10^4	34.3	0.83
1.10×10^5	31.6	0.91
2.00×10^5	30.5	1.00
4.70×10^5	28.8	1.00
6.50×10^5	27.7	0.91
1.44×10^6	26.3	0.76
2.70×10^6	25.6	0.69

+ Styrene
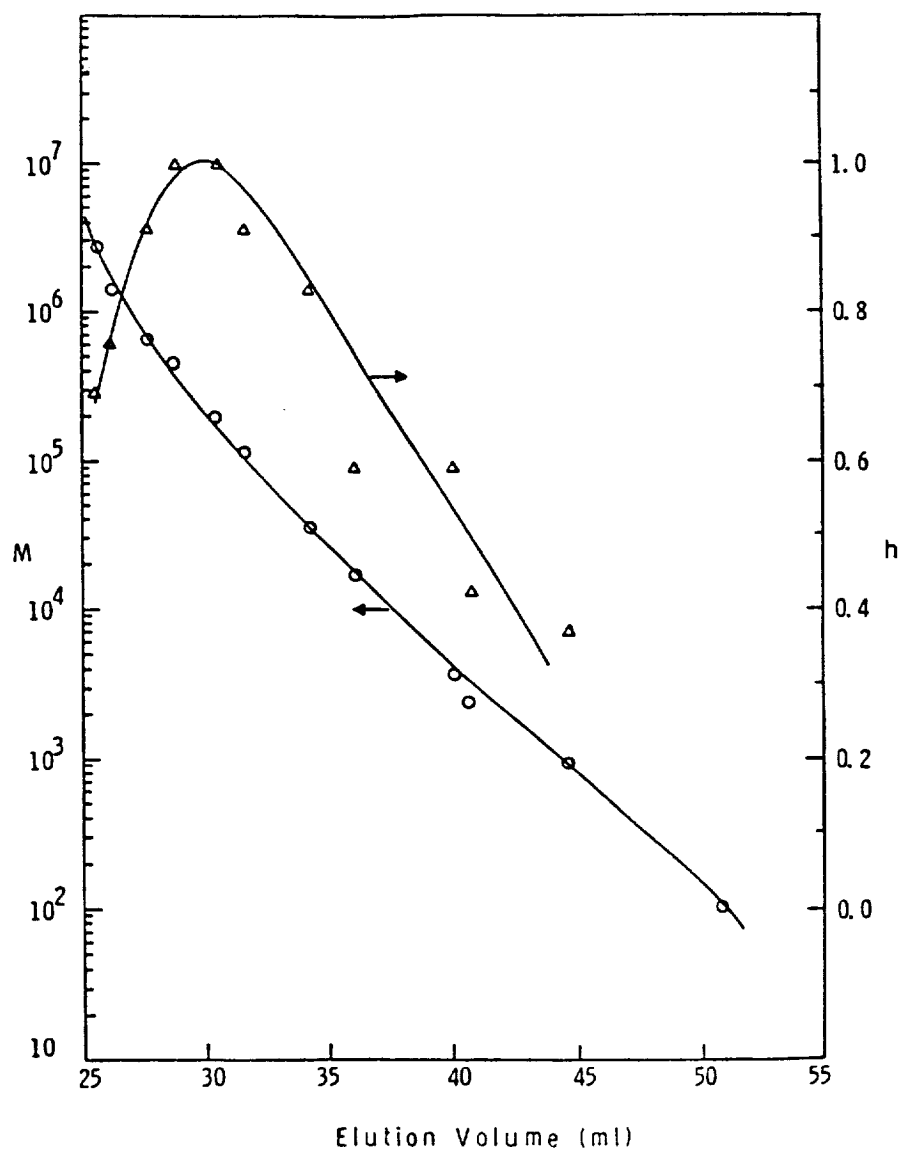
Figure 6-18. Calibration curves of the μ-Styragel column set.

304

integrating through the entire molecular weight range and correcting with the spreading function. An example of the distribution curve and molecular weight averages is presented in Figure 6-19. Two sets of molecular weight averages were reported: one was corrected with the spreading function, the other was not.

For samples other than polystyrene, the absolute molecular weight averages and distributions can also be calculated with the computer program by using the universal calibration method. It has been shown [133, 134] for many polymers that a single calibration curve will satisfy its GPC elution volume - molecular size relationship when the hydrodynamic volume of the polymer, as represented by the product of the intrinsic viscosity and molecular weight ($[\eta]M$), is plotted against the elution volume. Hence, for any elution volume, the following relationship holds for the sample polymer(2) and the calibration standard polymer(1):

$$[\eta]_1 M_1 = [\eta]_2 M_2 \qquad (6\text{-}14)$$

By using the Mark-Houwink equations, the molecular weight of the sample polymer eluting at volume V_e is related to the molecular weight of a polystyrene standard sample eluting at the same volume by the expression:

$$M_2 = (K_1/K_2)^{1/(a_2+1)} M_1^{(a_1+1)/(a_2+1)} \qquad (6\text{-}15)$$

The method has been shown to have wide applicability [135]. The procedure does, however, require very accurate values of the Mark-Houwink constants, K and a, for both the sample and the polymer standard in the same solvent. Literature values of the constants for

APPARENT MOLECULAR WEIGHT AVERAGES

NUMBER AVERAGE MWT =   .11E+06
WEIGHT AVERAGE MWT =   .53E+06
DISPERSITY,D   =   4.95

CORRECTED MOLECULAR WEIGHT AVERAGES

NUMBER AVERAGE MWT =   .12E+06
WEIGHT AVERAGE MWT =   .50E+06
DISPERSITY,D   =   4.12
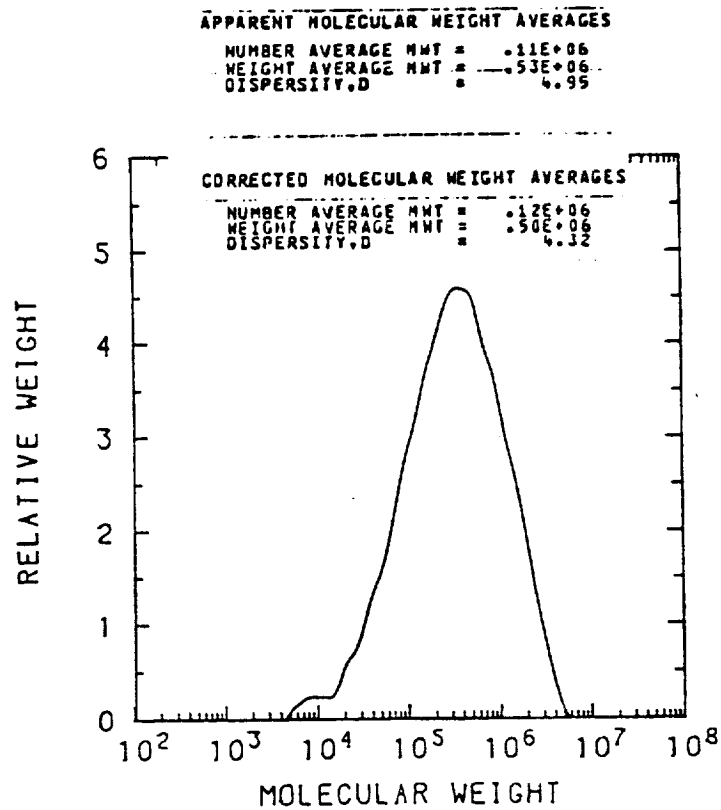
Figure 6-19.   A molecular weight distribution curve
and molecular weight averages generated by the
computer program MWD.

several polymer-solvent-temperature systems can be found in Mandik's review [136].

6.4.2 Aqueous GPC system

GPC of water-soluble polymers is a rapidly growing area, especially with the introduction of high-performance columns. However, the calibration of aqueous GPC columns is more difficult than the nonaqueous systems. Except for proteins, only a few well-characterized water-soluble standards are commercially available [137]. The universal calibration method has been tried in some studies dealing with water-soluble polymers [138, 139]. Also, Hamielec has used a broad molecular weight polyacrylamide standard to establish an universal calibration curve [140].

Hashimoto et al. [141] first applied TSK-GE1 PW type columns (Toyo Soda Co., Ltd., Japan) to investigate water-soluble polymers. Dextran, polyethylene glycol, polyacrylamide, polyvinyl alcohol, and polyvinylpyrrolidone were separated according to molecular size with no evidence of adsorption. This type of column was later confirmed by other investigators as one of the most suitable for synthetic water-soluble polymers [142]. To test the applicability of the universal calibration method on this type of column, the author analyzed some of Hashimoto's results. The peak elution volume from their chromatograms, the molecular weight, and the calculated hydrodynamic volume are presented in Table 6-7. Table 6-6 lists the Mark-Houwink constants used in calculating the hydrodynamic volume ($[\eta]M = KM^{a+1}$) of the polymers from the given molecular weight. By plotting

logarithm of the hydrodynamic volume against the elution volume, a

smooth calibration curve was obtained (Figure 6-20).

Table 6-6.   Mark-Houwink Constants for Water-
Soluble Polymers in Water

Polymer	K	a	Reference
Dextran	4.93×10^{-4}	0.60	[143]
Polyacrylamide	4.54×10^{-4}	0.66	[144]
Polyvinylpyrrolidone	6.76×10^{-4}	0.55	[145]

In our own study, three TSK-GEL PW type columns were used:

G6000PW, G5000PW and G3000PW, each of 0.75 cm ID. and 30 cm long.

Four dextran samples from Pharmacia Fine Chemicals and three poly-

acrylamide samples from Polysciences, Inc. were used for calibration.

The dextran samples came with a molecular weight distribution curve of

each, the polyacrylamide samples came with only an average molecular

weight of each.   These samples were run on the column set with

distilled-deionized water at 1.0 ml/min.   The chromatograms are

presented in Figure 6-21.   Resolution of the column set was so good

that some of the samples separated into two peaks.   Thus it was

impractical to use the peak elution volume for constructing a

calibration curve.

Since molecular weight distributions were available for all of

the dextran samples, the whole distribution curves or parts of the

distribution curves could be used to construct a calibration curve.

Figure 6-22 shows the differential molecular weight distribution and

cumulative molecular weight distribution (CMWD) for Dextran T10 given

Table 6-7.   Treated Chromatographic Data for
Hashimoto's TSK-GEL PW Column Set (Data from [141])

Sample	M	Peak V_e(ml)	$[\eta]$M
Dextran +			
T500	3.2×10^5	44.2	3.2×10^5
T250	1.8×10^5	45.5	1.3×10^5
T150	1.3×10^5	46.5	7.5×10^4
T 70	5.5×10^4	49.2	1.9×10^4
T 40	3.4×10^4	51.2	8.8×10^3
T 20	1.8×10^4	53.0	3.2×10^3
T 10	8.0×10^3	55.5	8.7×10^2
Polyvinylpyrrolidone *			
K-90	3.6×10^5	43.0	2.8×10^5
K-30	4.0×10^4	53.0	9.2×10^3
Polyacrylamide **			
K-5	3.64×10^6	32.2	3.5×10^7
Y-2	7.95×10^5	38.1	2.8×10^6
T-2	2.95×10^5	44.1	5.5×10^5
T-4	1.22×10^4	46.3	1.3×10^5

+ M = Peak molecular weight = $(\overline{M}_w \cdot \overline{M}_n)^{1/2}$

* M = "Average molecular weight"

** M = $\overline{M}_w$

309
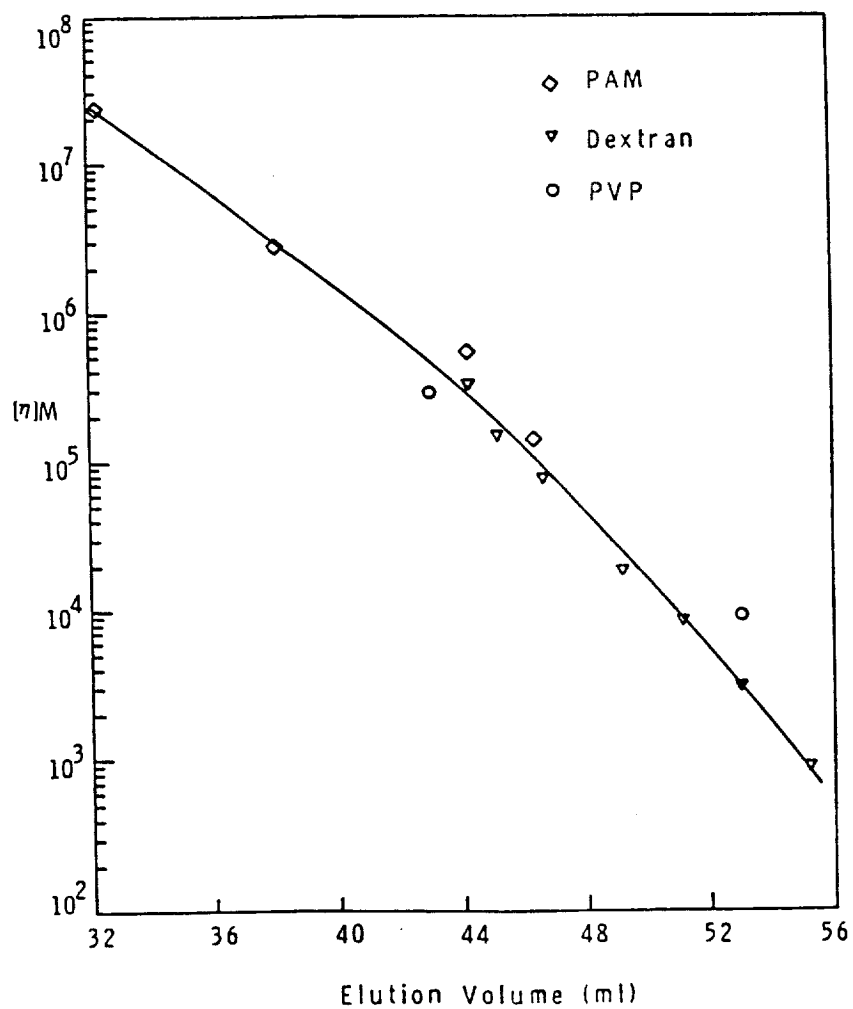
Figure 6-20.   Universal calibration curve for
Hashimoto's TSK-GEL PW column set (data from ⌊141⌋).

by the manufacturer. Three points were taken from the cumulative molecular weight distribution (CMWD) curve, namely the molecular weights at 10%, 50% and 90% CMWD. On the other hand, elution volume for the equivalent cumulative chromatographic distribution (CCD) were taken from the chromatogram. The calibration data thus obtained from the dextran samples are given in Table 6-8. In a similar way, the elution volumes of the polyacrylamide samples at 50% CCD were taken to match the average molecular weight. Figure 6-23 shows the calibration curve based on these data.

Computer calculation of molecular weight averages in the aqueous system was done similarly to the nonaqueous system, except that the spreading correction was not applied due to the lack of narrow molecular weight standards. A cubic spline data smoother was used in the program, designated AQMWD [146], to generate an universal calibration function based on the input calibration data. With this calibration function, the sample elution volume could be converted to the hydrodynamic volume and consequently to the molecular weight.

Several nonionic polymeric surfactants were analyzed with the TSK-GEL PW column set. Figure 6-24 gives molecular weight distribution of a polyacrylamide sample, PAM 50, generated from the computer program. More molecular weight distributions can be found in Chapter 4.
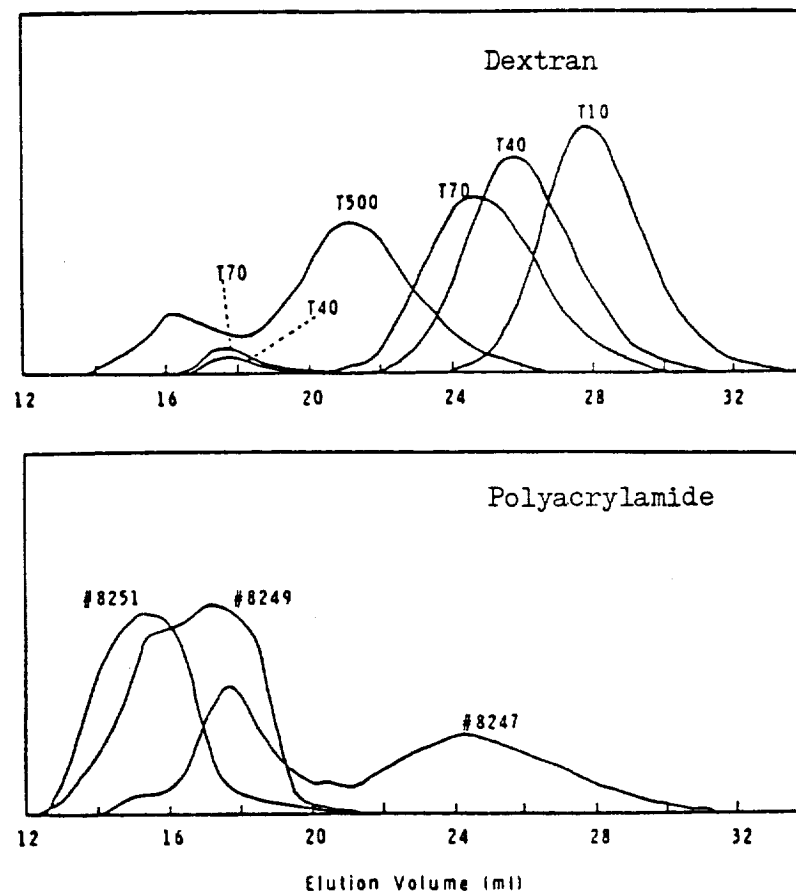
Figure 6-21. Chromatograms of Dextran T series and polyacrylamide samples on the TSK-GEL PW column set.

DEXTRAN T10

$\bar{M}_w = 9,700$ $\bar{M}_n = 6,000$ $|\eta| = 0.10$ lot 12728
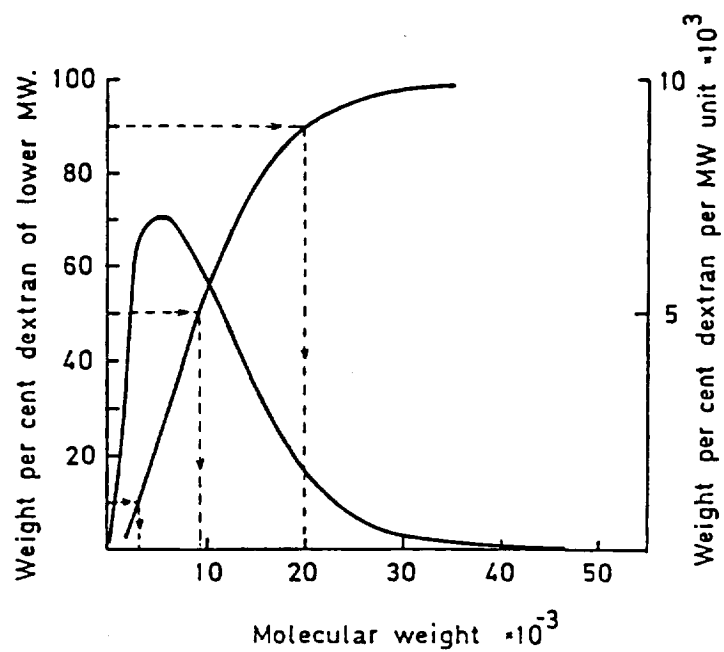
Molecular weight distribution by gelfiltration.

Figure 6-22.   Molecular weight distribution of Dextran T10 given by Pharmacia Fine Chemicals.

Table 6-8. Calibration Data Based on Cumulative Distributions from the TSK-GEL PW Column Set

Sample	% Cumulative Distribution	M	V_e(ml)	$[\eta]M$
Dextran				
T500	10	1.0×10^5	24.2	4.9×10^4
	50	2.7×10^5	22.0	2.4×10^5
	90	1.1×10^6	16.6	2.2×10^6
T 70	10	2.6×10^4	27.0	5.7×10^3
	50	6.0×10^4	24.9	2.2×10^4
	90	1.4×10^5	22.7	8.1×10^4
T 40	10	1.6×10^4	28.2	2.6×10^3
	50	3.6×10^4	26.0	9.6×10^3
	90	7.2×10^4	24.0	2.9×10^4
T 10	10	3.0×10^3	30.0	1.8×10^2
	50	9.0×10^3	28.1	1.1×10^3
	90	2.0×10^4	26.3	3.8×10^3
Polyacrylamide				
#8251	50	2.0×10^6	15.4	1.3×10^7
#8249	50	5.0×10^5	16.9	1.3×10^6
#8247	50	7.4×10^4	22.1	5.5×10^4
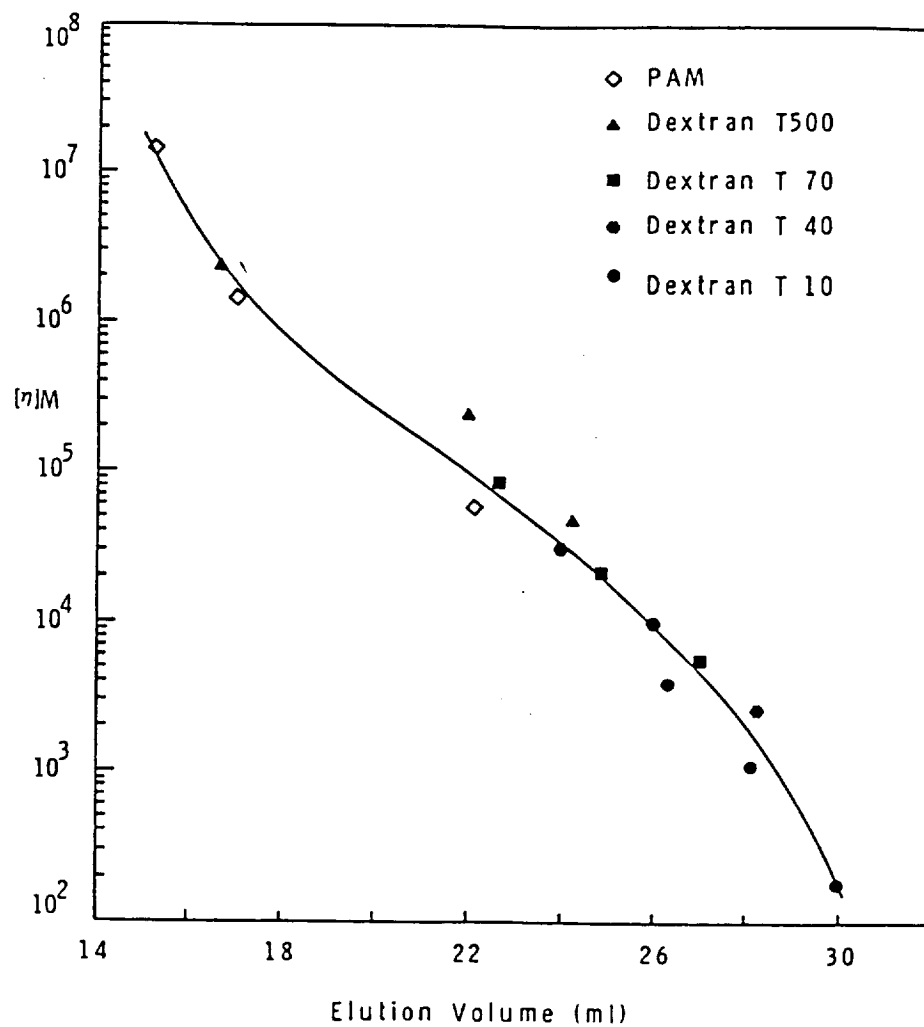
Figure 6-23. Universal calibration curve for the TSK-GEL PW column set, data based on the cumulative distributions of the standards.

PAM 50

NUMBER AVERAGE MWT = .76E+06
WEIGHT AVERAGE MWT = .13E+07
DISPERSITY,D = 1.65
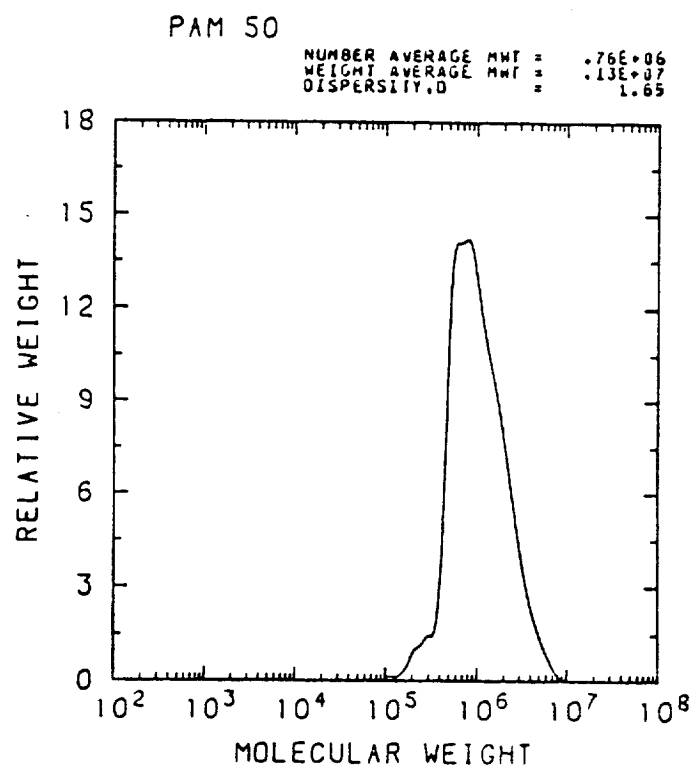
Figure 6-24.   Molecular weight distribution of poly-
acrylamide PAM 50.

CHAPTER 7

CONCLUSIONS AND SUGGESTIONS FOR FUTURE WORK

7.1 Conclusions

The conclusions from the present investigation may be summarized as follows:

(1) The equilibrium swelling of latex particles with monomer has been studied experimentally and theoretically. The thermodynamic model, Model I, which is based on the theory of Morton et al., has been used successfully to fit the experimental data and to obtain semi-empirical equations for the swelling of polystyrene and polymethyl methacrylate latexes. The semi-empirical equations provide a quick way to estimate the swelling ratios from the original particle size and the interfacial tension. In addition, a more generalized model, Model II, which takes into account the effect of water dissolved in the swollen particles and in the monomer phase, has been developed. The Model II might prove to be more suitable for describing the swelling phenomena of relatively hydrophilic systems.

(2) A "seeded-telomerization" swelling method using mercaptans as telogens has been developed. The method allows the growth of latex particles with a volume increase of >60 in one cycle. With two consecutive "seeded-telomerization" swelling cycles, an overall volume increase >5000 can be achieved.

(3) Comparison of various initiators in seeded polymerization indicates that an initiator with a lower water solubility has a lesser tendency to generate new small particles. Peroxy initiators are not

suitable for seeded polymerization in large-particle-size range because of the extremely low polymerization rate. Azo initiators, especially 2,2'-azobis-(2-methylbutyronitrile) (AMBN), are the best type of initiator for growing large-particle-size latex particles without generating new particles.

(4) A glass dilatometer has been developed to follow the kinetics of seeded emulsion polymerizations. The dilatometer works well with polymerization recipes containing no inhibitor. With an inhibitor-containing recipe, the kinetic measurements may be affected by the gas bubbles from the interaction of initiator and inhibitor.

(5) The dilatometer has been used to study the effect of inhibitors on the induction period and polymerization rate of a seeded polymerization system using an oil-soluble initiator. It was found that the inhibitors retards or slightly accelerates the polymerization, depending on the nature of the inhibitor. Unlike polymerizations in bulk or solution systems, a well-defined induction period was not observed owing to the complicated distribution of the initiator and the inhibitor between the aqueous and monomer-polymer phases. The inhibition time at ambient temperature could not be predicted from the observed induction period at a higher temperature.

(6) Many polymerization inhibitors and shortstoppers have been evaluated as "new particle inhibitors" in seeded polymerization. Many inhibitors are effective in preventing small particle generation; however, some severely retard the polymerization rate and some diminish the latex stability to electrolyte. An ideal "new particle inhibitor" which fulfills all of the requirements was not found and

318

indeed may not exist. A compromise must be made, with first consideration given to latex stability and monodispersity. Quinoid-type inhibitors, especially hydroquinone, which inhibit new particle generation without affecting colloid stability and monodispersity, are the best choice for this purpose.

(7) Although it is an excellent surfactant for preparation of submicron-size monodisperse latexes, Aerosol MA is ineffective in stabilizing latex particles >2 μm for swelling and subsequent polymerization. Several types of surfactants, including anionic, nonionic, copolymerizable, oligomeric, and polymeric, have been evaluated for stabilizing large particles without generating new small particles. It was found that the best results were obtained with a combination of three types of surfactants: anionic (e.g., Aerosol MA); oligomeric (e.g., Polywet KX-3) or copolymerizable (e.g., Cops I); and polymeric (e.g., polyvinylpyrrolidone).

(8) As particle size of the seeded polymerization increases, the formation of over-size particles in the product latex becomes more pronounced. These over-size particles may result from the coalescence of two or three normal particles during polymerization. The coalescence can be reduced by incorporating a crosslinking agent to harden the seed particles. However, a high degree of crosslinking may cause formation of deformed (pear-shaped) particles because of the uneven swelling and growth of the highly crosslinked core. It was found that 0.015-0.030% divinylbenzene based on monomer was most suitable.

(9) The method of successive seeded emulsion polymerization for

319

preparing monodisperse latexes has been extended beyond the 2.C-2.5 μm particle size limit. Latex particles with satisfactory uniformity have been grown successfully up to 11 μm diameter in bottle polymerizations, and less successfully to 18 μm and 35 μm.

(10) Four sets of microgravity experiments have been carried out in the STS-3, STS-4, STS-6, and STS-7 missions. In the STS-4 mission, the recipes were only partly converted because of flight hardware malfunction. Monodisperse latexes up to 18 μm in diameter have been prepared in microgravity. The coefficients of variation of the flight latexes are all in the range of 1-2%. The standard deviations express not only the width of particle size distributions, but also the errors in measuring the particle diameter in micrographs and the errors from magnification distortion. The actual standard deviations of the particle size distributions may be significantly smaller than the reported values.

(11) The flight and ground-based control experiments were carried out with very low agitation rates (6 and 3 rpm for recipes #15 and #16, 13 rpm for the rest). Significantly different results were obtained from polymerizations on ground and in microgravity, especially for the recipes with large seed sizes and high monomer/polymer ratios. The two largest particle size recipes with the lowest agitation rates, recipes #15 and #16, yielded stable latexes when polymerized in microgravity, while the ground-based polymerizations gave massive coagulum. All of the ground latexes, except #1, had broader main particle size distributions and much larger tails than their flight counterparts. The results indicated that much

better mixing was achieved in microgravity than on ground with the same agitator design. This supports the rationale given for preparing large-particle-size monodisperse latexes in space via seeded emulsion polymerization, i.e., minimum agitation can be used to give good mixing for growing large-particle-size latex particles uniformly in microgravity, without forming excess coagulum due to creaming, sedimentation, or excess shear in mixing.

(12) Off-size larger particles were found in flight and ground latexes to range from 1/360 to 1/50 relative to the main distribution, generally increasing in number with increasing swelling ratio. Deformed particles, often barrel-shaped, were also found in flight latexes of larger sizes (>7 μm), but were virtually absent from the ground latexes. Post-process agitation, which was used for the flight experiments, but not for the ground experiments, could be responsible for this phenomenon. The barrel-shaped particles could be reformed into spheres by heating to a high temperature. In future flight experiments, the procedure should be modified to eliminate the cause of formation of those deformed particles.

(13) Three complementary methods, centrifugation, sedimentation, and serum replacement, have been developed to upgrade imperfect batches of large-particle-size latexes by removing off-size larger and smaller particles.

(14) Electron microscopy has been the most reliable method to measure the particle size distributions of monodisperse latexes. Magnification distortion in the TEM is significant at low magnification settings. It is suggested that the SEM be used for

large-particle-size latexes instead of the TEM.

7.2 Suggestions for Future Work

The following suggestions might be considered for future study:

(1) Refining and scale-up of the ground-based seeded polymerization sequence.

(2) Further cleaning and characterization of the large-particle-size monodisperse latexes.

(3) Study of the stabilization mechanism of the three-surfactant combination.

(4) Systematic study of the role of inhibitors in emulsion polymerization.

(5) Study of the effects of other parameters, such as reaction temperature, type of monomer, and composition of dispersion medium, on the preparation of large-particle-size monodisperse latexes.

APPENDIX A

BOTTLE POLYMERIZATION

Seeded polymerizations in this study were usually carried out in 1-oz, 2-oz, 4-oz, or 12-oz capped bottles. The bottles were placed in safety baskets, which in turn were placed in a rotor and rotated end-over-end at about 30rpm in a constant-temperature bath. Occasionally a 32-oz bottle was used to prepare a large batch of seed latex. In this case, the bottle was placed on the rotor and rotated side-over-side instead of end-over-end. The bottles used were narrow-mouth glass bottles fitted with plastic screw caps. Two procedures were used, one for recipes using water-soluble initiators, and another for recipes using oil-soluble initiators.

In the first procedure, used for polymerizations with water-soluble initiators, three small holes were drilled in the middle of the cap. For each reactor bottle, a home-made rubber gasket was prepared. The gasket consisted of a circle of W-9 hard rubber and a smaller circle of W-7 soft rubber. The circles were tailor-cut such that, after they were glued together, the hard rubber circle would just fit inside of the cap while the smaller soft rubber circle would cover the holes in the cap. All the ingredients except initiator were charged into the bottle. The bottle was capped and tumbled to swell the particles. After swelling, the initiator solution was injected through the gasket with a hypodermic syringe and a needle. At the same time, the bottle was purged with zero-grade nitrogen for 5 min. using two needles, one for entry and the other for exit. The bottle

323

was then placed on the rotor and heated at 70°C for 20-24 hours. This procedure allowed direct contact of the reactants with the rubber gasket. Therefore, contamination was inevitable, as indicated by the yellowing of the monomer phase after tumbling.

In the second procedure, used for polymerizations with oil-soluble initiators, no holes were drilled in the cap. The gasket was made of a circle of hard rubber only. An aluminum foil was glued to the gasket with double-stick tape. Direct contact of the reactants with the rubber was thus avoided. All the ingredients were added at the beginning. The bottle was purged with nitrogen and then capped. After swelling, by tumbling at room temperature for at least 12 hours, the bottle was placed in the rotor and heated at 70°C for 20-24 hours.

APPENDIX B

PREDICTION OF WATER-MONOMER INTERFACIAL TENSION

FROM MUTUAL SOLUBILITIES

An empirical relationship was developed by Donahue and Bartell [147] for the solubilities of the mutually saturated organic liquid and water phases and the interfacial tension between these two phases in contact with one another. The interfacial tensions were found to be a linear function of the logarithm of the "degree of miscibility". The "degree of miscibility" was defined as $N_1 + N_2$, where N_1 is the mole fraction of the water in the organic phase and N_2 is the mole fraction of the organic liquid in the aqueous phase. The following equation can be derived from the data reported by Donahue and Bartell:

$$\gamma = -15.52 \log(N_1 + N_2) - 2.76 \tag{B-1}$$

The relationship can be used to predict interfacial tensions between water and monomers from their mutual solubilities. Conversely, the accuracy of the solubility data can be checked by comparing the predicted interfacial tensions with the measured interfacial tensions. Table B-1 presents the solubilities and interfacial tensions predicted by equation B-1 for some vinyl monomers. Experimental interfacial tensions, measured by the drop volume method, for three monomers are also listed in the table. The predicted and experimental interfacial tensions agreed quite well for the styrene and methyl methacrylate systems. The result for vinyl acetate supported the author's suspicion that the water in vinyl

Table B-1. Water-Monomer Mutual Solubilities and Predicted and
Measured Interfacial Tensions

Monomer	Solubility, g/100g		Mole fraction		$\log(N_1+N_2)$	γ, dyne/cm	
	Monomer/water	Water/monomer	N_2	N_1		Predicted	Measured
Styrene	0.032	0.070	0.000056	0.0040	-2.39	34.3	35.2
Methyl acrylate	5.0	2.5	0.0108	0.0998	-0.956	12.1	-
Methyl methacrylate	1.59	1.15	0.00285	0.0600	-1.20	15.9	13.2
Ethyl acrylate	1.5	1.5	0.00269	0.0769	-1.099	14.3	-
Butyl acrylate	0.2	0.7	0.00028	0.0474	-1.32	17.7	-
Vinyl acetate	2.5	0.1 *	0.0052	0.0048	-2.00	28.3	12.5
Vinyl acetate (corrected)	2.5	2.1	0.0052	0.0912	-1.02	13.1	12.5

* suspected to be a misprint of 2.1

acetate solubility, 0.1 g/100g, was a misprint of 2.1 g/100g.

APPENDIX C

CALCULATION OF INTERFACIAL TENSION FROM THE DROP VOLUME METHOD

Figure C-1 shows the device for measuring interfacial tension by drop volume. The inner wall of the tip was ground and polished to reduce the wall thickness. The tip was then sanded to give a smooth end. The tip radius was calibrated to be 0.0636 cm, by measuring the interfacial tension of the water-toluene and water-benzene systems, and comparing the measured values with the literature values.

Harkins and Brown [148] derived the following equation to correlate the surface tension, γ, with the drop weight, W (W=mg), and the tip radius, r:

$$\gamma = (mg/r) \, F \qquad\qquad (C-1)$$

The correction function, F, was related to V/r^3, where V is the drop volume. Experimental values for the correction function can be found in reference 149 . Figure C-2 shows F values for V/r^3 between 1 and 1000 on a semilog plot. For interfacial tension measurement, $V\Delta\rho g$ should be used instead of mg, where $\Delta\rho$ is the density difference between the two phases. A sample calculation is given below:

An average drop volume, $V = 0.911$ cm^3, was obtained for water-toluene system, with tip radius r = 0.0636 cm.

$$\Delta\rho = 0.133$$

$$V/r^3 = 354$$

from Figure C-1 $F = 0.195$

Therefore $\gamma = (V\Delta\rho g/r) \, F$

$$\gamma = (0.0911 \times 0.133 \times 980/0.0636) \times 0.195$$

$$= 36.4 \text{ dyne/cm}$$

2ml Microsyringe

Aqueous solution or
latex dispersion

No. 17 Cannula

Drop of aqueous solution
or latex dispersion

Monomer
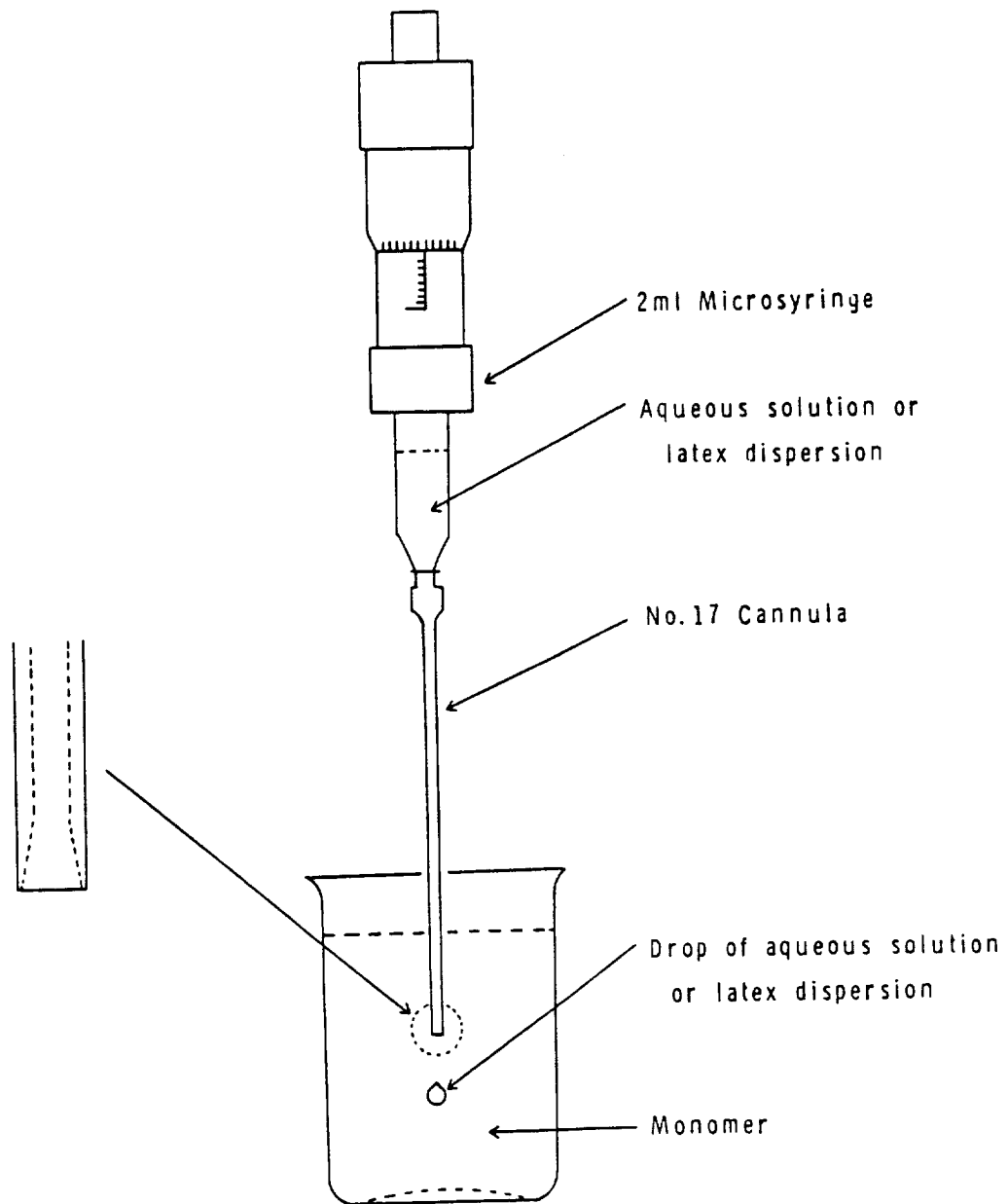
Figure C-1.   Device for the drop volume method.
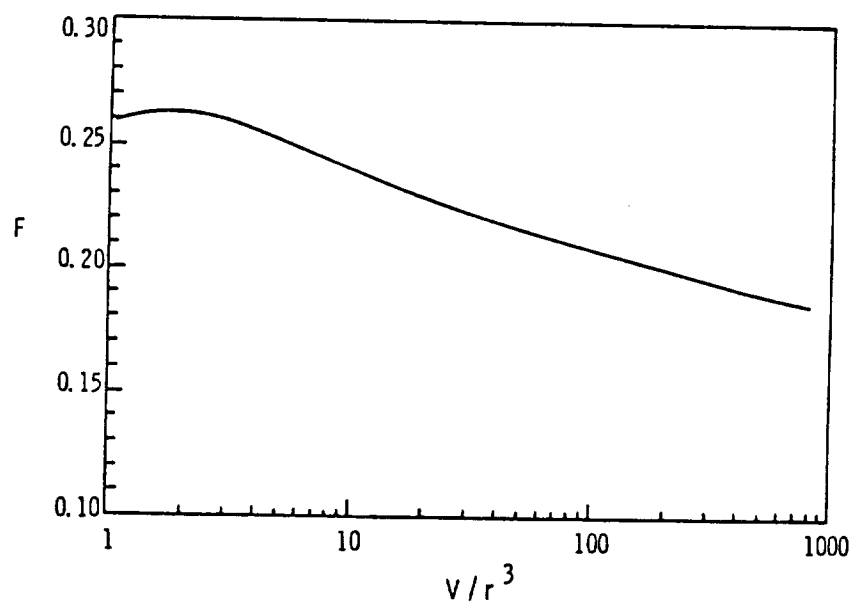
Figure C-2. Correction function for calculating interfacial tension from the drop volume.

APPENDIX D

DISTRIBUTION OF AN EMULSIFIER BETWEEN THE

PARTICLE SURFACE AND THE AQUEOUS PHASE

For Langmuir-type adsorption,

$$1/n = 1/N + 1/(C_A Nb) \tag{D-1}$$

where n is the number of molecules adsorbed per unit area, $N = 1/a_s$ is the value of n at saturation, C_A is the concentration in the surrounding media, and b is a constant.

Ahmed [87] studied the adsorption of Aerosol MA, Aerosol OT, and sodium dodecyl sulfate on the surface of polystyrene latex particles using the serum replacement method. The following data were obtained from the Langmuir plot of the Aerosol MA system: $a_s = 45 \times 10^{-16}$ cm^2/molecule, $b = 3.90 \times 10^2$ 1/mole.

Equation (D-1) can be rearranged to:

$$C_A = n/N \; / \; [b(1 - n/N)] \tag{D-2}$$

n/N by definition is the fractional surface coverage (FSC). Therefore:

$$C_A = FSC \; / \; [b(1 - FSC)] \tag{D-3}$$

The following example illustrates the calculation of the amounts of Aerosol MA on the particle surface and in the aqueous phase for a 20% solid polystyrene latex of diameter 1.0 μm with a surface coverage of 50%.

Particle diameter $d = 1.0 \times 10^{-4}$ cm

Solids content   SD = 0.20

Fractional surface coverage

$$FSC = 0.50$$

Particle number per unit volume of latex

$$N_p = 6 \, SD/(\pi d^3)$$

$$= 6 \times 0.20/[3.14 \times (1.0 \times 10^{-4})^3]$$

$$= 3.82 \times 10^{11} \text{ particles/cm}^3$$

$$= 3.82 \times 10^{14} \text{ particles/l}$$

Particle surface per unit volume of latex

$$A = \pi d^2 \, N_p$$

$$= 3.14 \times (1.0 \times 10^{-4})^2 (3.82 \times 10^{14})$$

$$= 1.2 \times 10^7 \text{ cm}^2/l$$

Emulsifier adsorbed per unit volume of latex

$$[E]_{ads} = FSC \, A/(a_s \, N_A)$$

$$= 0.50 \times 1.2 \times 10^7/(45 \times 10^{-16} \times 6.02 \times 10^{23})$$

$$= 2.2 \times 10^{-3} \text{ moles/l}$$

Emulsifier in the aqueous phase per unit volume of latex

$$[E]_{aq} = (1-SD) \, c_A$$

$$= (1-SD) \, FSC \, / \, [b(1 - FSC)]$$

$$= (1-0.20) \times 0.50/[3.90 \times 10^{-2}(1-0.50)]$$

$$= 2.1 \times 10^{-3} \text{ moles/l}$$

Total emulsifier $\quad [E]_{total} = [E]_{ads} + [E]_{aq}$

$$= 4.3 \times 10^{-3} \text{ moles/l}$$

REFERENCES

1. R. C. Backus and R. C. Williams, *J. Appl. Phys.*, 1948, <u>19</u>, 1186.

2. R. C. Backus and R. C. Williams, *J. Appl. Phys.*, 1949, <u>20</u>, 224.

3. C. H. Gerould, *J.Appl. Phys.*, 1950, <u>21</u>, 183.

4. W. V. Smith, *J. Am. Chem. Soc.*, 1948, <u>70</u>, 3695.

5. T. Alfrey, Jr., E. B. Bradford, J. W. Vanderhoff, and G. Oster, *J. Opt. Soc. Am.*, 1954, <u>44</u>, 603.

6. E. B. Bradford and J. W. Vanderhoff, *J. Appl. Phys.*, 1955, <u>26</u>, 864.

7. E. B. Bradford and J. W. Vanderhoff, *J. Colloid Sci.*, 1956, <u>11</u>, 135.

8. J. W. Vanderhoff, J. F. Vitkuske, E. B. Bradford, and T. Alfrey, Jr., *J. Polymer Sci.*, 1956, <u>20</u>, 225.

9. J. W. Vanderhoff, *Preprints, ACS Division Org. Coatings Plastics Chem.*, 1964, <u>24</u>, 223.

10. J. W. Vanderhoff and E. B. Bradford, *TAPPI*, 1956, <u>39</u>, 650.

11. J. W. Vanderhoff, F. J. Micale, and M. S. El-Aasser, "Production of Large-Particle-Size Monodisperse Latexes", proposal submitted in response to NASA A. O. No. OA-77-3, "Space Processing Investigation for STS Missions", April 1977.

12. T. Matsumoto and A. Ochi, *Kobunshi-Kagaku*, 1965, <u>22</u>, 481.

13. A. Kotera, K. Furusawa, and Y. Takeda, *Kolloid-Z. u. Z. Polymere*, 1970, <u>239</u>, 677.

14. A. Kotera, K. Furusawa, and K. Kudo, *Kolloid-Z. u. Z. Polymere*, 1970, <u>240</u>, 837.

15. R. H. Ottewill and J. N. Shaw, *Kolloid-Z. u. Z. Polymere*, 1967, <u>218</u>, 34.

16. J. W. Goodwin, J. Hearn, C. C. Ho, and R. H. Ottewill, *Br. Polymer J.*, 1973, <u>5</u>, 347.

17. J. W. Goodwin, J. Hearn, C. C. Ho, and R. H. Ottewill, *Colloid Polymer Sci.*, 1974, <u>252</u>, 464.

18. Y. Chung-li, J. W. Goodwin, and R. H. Ottewill, Prog. Colloid Polymer Sci., 1976, 60, 163.

19. E. Trommsdorff and C. E. Schildknecht, in "Polymer Processes", C. E. Schildknecht, ed., Interscience, New York, 1956, ch. III.

20. F. H. Winslow and W. Matreyek, Ind. Eng. Chem., 1951, 43, 1108.

21. E. Vanzo, J. Appl. Polymer Sci., 1972, 16, 1867.

22. Y. Almog and M. Levy, J. Polymer Sci., Polymer Chem. Ed., 1980, 18, 1.

23. Y. Almog and M. Levy, J. Polymer Sci., Polymer Chem. Ed., 1981, 19, 115.

24. Y. Almog and M. Levy, J. Polymer Sci., Polymer Chem. Ed., 1982, 20, 417.

25. Y. Almog and M. levy, Ind. Eng. Chem. Pro. Res. Dev., 1982, 21, 163.

26. J. Ugelstad, Makromol. Chem., 1978, 179, 815.

27. J. Ugelstad, K. H. Kaggerud, F. K. Hansen, and A. Berge, Makromol. Chem., 1979, 180, 737.

28. J. Ugelstad, P.C. Mørk, K. H. Kaggerud, T. Ellingsen, and A. Berge, Adv. Coll. Int. Sci., 1980, 13, 101.

29. J. Ugelstad, K. H. Kaggerud, and R. M. Fitch, in "Polymer Colloids II", R. M. Fitch, ed., Plenum Press, New York, 1980, p. 83.

30. "Dow Uniform Latex Particles", Dow Diagnostics technical bulletin, 1977.

31. J. W. Vanderhoff, Dow Chemical Co., 1959-63, unpublished research.

32. J. Th. G. Overbeek, Adv. Coll & Int. Sci., 1982, 15, 251.

33. I. M. Krieger and F. M. O'Neill, J. Am. Chem. Soc., 1968, 90, 3114.

34. J. W. Vanderhoff, H. J. van den Hul, R. J. M. Tausk, and J. Th. G. Overbeek, in "Clean Surfaces: Their Preparation and Characterization for Interfacial Studies", G. Goldfinger, ed., Marcel Dekker, New York, 1970, p. 15.

35. S. Hachisu, Y. Kobayashi, and A. Kose, J. Colloid Interface

Sci., 1973, <u>42</u>, 342.

36. S. Hachisu and Y. Kobayashi, <u>J</u>. <u>Colloid Interface Sci</u>., 1974,
   <u>46</u>, 470.

37. H. Fujita and K. Ametani, <u>Jap</u>. <u>J</u>. <u>Appl</u>. <u>Phys</u>., 1977, <u>16</u>, 1091.

38. K. Takano and S. Hachisu, <u>J</u>. <u>Colloid Interface Sci</u>., 1978, <u>66</u>,
   66.

39. P. R. Krumrine and J. V. Vanderhoff, in "Polymer Colloids II",
   R. M. Fitch, ed., Plenum Press, New York, 1980, p. 289.

40. T. Ohtsuki, A. Kishimoto, S. Mitaku, and K. Okano, <u>Jap</u>. <u>J</u>. <u>Appl</u>.
   <u>Phys</u>., 1981, <u>20</u>, 509.

41. J. A. Beunen and L. R. White, <u>Colloids</u> & <u>Surfaces</u>, 1981, <u>3</u>, 371.

42. M. Morton, S. Kaizerman, and M. W. Altier, <u>J</u>. <u>Colloid Sci</u>.,
   1954, <u>9</u>, 300.

43. E. Vanzo, R. H. Marchessault and V. Stannett, <u>J</u>. <u>Colloid Sci</u>.,
   1965, <u>20</u>, 62.

44. A. Klein and C. H. Kuist, <u>J</u>. <u>Polymer Sci</u>., 1973, <u>11</u>, 211.

45. J. L. Gardon, <u>J</u>. <u>Polymer Sci</u>., <u>Part A-1</u> , 1968, <u>6</u>, 2859.

46. J. L. Gardon, in "Interfacial Synthesis, Vol. 1", F. Millich and
   C. E. Carraher, Jr., eds., Marcel Dekker, New York, 1977, ch. 9.

47. G. Lohr, in "Polymer Colloids II", R. M. Fitch, ed., Plenum
   Press, New Yok, 1980, p. 71.

48. J. Guillot, <u>Makromol</u>. <u>Chem</u>., <u>Rapid Commun</u>., 1980, <u>1</u>, 697.

49. E. C. Leonard, <u>Vinyl and Diene Monomers</u>, <u>Part I-III</u>, John Wiley
   & Sons, New York, 1970-1971.

50. P. J. Flory, <u>Principles of Polymer Chemistry</u>, Cornell University
   Press, Ithaca, NY., 1953, p. 549.

51. R. A. Orwoll, <u>Rubber Chem</u>. <u>Tech</u>., 1977, <u>50</u>, 451.

52. H. Burrell, <u>Interchem</u>. <u>Rew</u>., 1955, <u>14</u>, 31.

53. J. W. Vanderhoff, E. B. Bradford, H. L. Tarkowski, and B. W.
   Wilkinson, <u>J</u>. <u>Polymer Sci</u>., 1961, <u>50</u>, 265.

54. R. F. Boyer, <u>J</u>. <u>Polymer Sci</u>., 1948, <u>3</u>, 97.

55. T. G. Fox, Polymer, 1961, 3, 111.

56. C. M. Starks, Free Radical Telomerization, Academic Press, New York, 1974.

57. L. J. Young, in "Polymer Handbook", J. Brandrup and E. H. Immergut, eds., Wiley(Interscience), New York, 1975, p. II-57.

58. F. Mayo, J. Am. Chem. Soc., 1943, 65, 2324.

59. G. Lichti, D. F. Sangster, B. C. Y. Whang, D. H. Napper, and R. G. Gilbert, J. Chem. Soc., Faraday Trans. 1, 1982, 78, 2129.

60. M. Nomura, Y. Minamino, K. Fujita, and M. Harada, J. Polymer Sci., Polymer Chem. Ed., 1982, 20, 1261.

61. D. C. Blackley, Emulsion Polymerization, Applied Science, London, 1975, p. 333-369.

62. D. C. Blackley, Emulsion Polymerization, Applied Science, London, 1975, p. 203-204.

63. J. W. Goodwin, R. H. Ottewill and R. Pelton, Colloid and Polymer Sci., 1979, 257, 61.

64. L.-J. Liu and I. M. Krieger, in "Emulsions, Latices and Dispersions", P. Becher and M. N. Yudenfreund, eds., Marcel Dekker, New York, 1978, p. 41.

65. B. M. E. van der Hoff, J. Polymer Sci., 1960, 48, 175.

66. B. M. E. van der Hoff, in "Solvent Properties of Surfactant Solutions", K. Shinoda, ed., Marcel Dekker, 1967, p. 328.

67. I. M. Kolthoff and I. K. Miller, J. Am. Chem. Soc., 1951, 73, 3055.

68. E. Trommosdorff, H. Köhle, and P. Lagally, Makromol. Chem., 1948, 1, 169.

69. T. Matsumoto, M. Okubo and T. Imai, Kobunshi Ronbunshu, 1974, 31, 576.

70. W. J. I. Bracke and E. Lanza (to Labofina S.A., Belgium), U.S. Patent 4,247,668 (1981).

71. E. D. Sudol, PhD dissertation, Lehigh University, 1983.

72. E. F. Kluchesky and L. B. Wakefield, Ind. Eng. Chem., 1949, 41, 1768.

73. D. C. Blackley, Emulsion Polymerization, Applied Science, London, 1975, p. 406-417.

74. L. B. Wakefield and R. L. Bebb, Ind. Eng. Chem., 1950, 42, 838.

75. G. J. Antlifinger and C. H. Lufter, Ind. Eng. Chem., 1953, 45, 182.

76. A. A. Koski and M. J. G. Davidson (to Polysar, Canada), U.S. Patent 4,242,477 (1980).

77. H. S. Smith, H. G. Werner, C. B. Westerhoff and L. H. Howland, Ind. Eng. Chem., 1951, 43, 212.

78. L. H. Howland, V. C. Neklutin, R. L. Provost and F. A. Mauger, Ind. Eng. Chem., 1953, 45, 1304.

79. D. H. Napper, in "Surface Chemistry and Colloids", M. Kerker, ed., Butterworths, London, 1972.

80. J. W. Vanderhoff, private communication.

81. N. Deželić, J. J. Petres, and G. J. Deželić, Kolloid-Z. u Z. Polymere, 1970, 242, 1142.

82. J. E. Vandegaer, J. Appl. Polymer Sci., 1965, 9, 2929.

83. J. W. Goodwin, R. H. Ottewill, R. Pelton, G. Vianello and D. E. Yates, Br. Polymer J., 1978, 10, 173.

84. J. R. Erickson and R. J. Seidewand, Preprints, ACS Div. Org. Coat. Plas. Chem., 1980, 43, 729.

85. J. R. Erickson and R. J. Seidewand, in "Emulsion Polymers and Emulsion Polymerization", D. R. Bassett and A. E. Hamielec, eds., American Chemical Society, Washington, D.C., 1981.

86. J. S. Dodge, M. E. Woods, and I. M. Krieger, J. Paint Tech., 1970, 42, 541.

87. S. M. Ahmed, PhD dissertation, Lehigh University, 1979.

88. B. W. Greene, D. P. Sheetz, and T. D. Filer, J. Colloid Interface Sci., 1970, 32, 90.

89. B. W. Greene and D. P. Sheetz, J. Colloid Interface Sci., 1970, 32, 96.

90. B. W. Greene and F. L. Saunders, J. Colloid Interface Sci., 1970, 33, 393.

91. M. S.-D. Juang and I. M. Krieger, *J. Polymer Sci., Polymer Chem. Ed.*, 1976, **14**, 2089.

92. R. L. Schild, M. S. El-Aasser, G. W. Poehlein, and J. W. Vanderhoff, in "Emulsions, Latices and Dispersions", P. Fecher and M. N. Yudenfreund, eds., Marcel Dekker, New York, 1978, p. 99.

93. M. Munzer and E. Trommsdorff, in "Polymerization Process", C. E. Schildknecht and I. Skeist, eds., Interscience, New York, 1977, ch. 5.

94. W. Starck and H. Freudenberger, Ger. 727,955 (I.G.); U.S. 2,227,163 (Gen. Aniline); Brit. 511,036 (I.G.); cf. U.S. 2,422,646 (A.P.C.).

95. J. M. G. Lankveld and J. Lyklema, *J. Colloid Interface Sci.*, 1972, **41**, 454.

96. S. Asakura and F. Oosawa, *J. Chem. Physics*, 1954, **22**, 1255.

97. S. Asakura and F. Oosawa, *J. Polymer Sci.*, 1958, **33**, 183.

98. P. R. Sperry, *J. Colloid Interface Sci.*, 1981, **82**, 62.

99. P. R. Sperry, *J. Colloid Interface Sci.*, 1982, **87**, 375.

100. L. Blecher, D. H. Lorenz, H. L. Lowd, A. S. Wood, and D. P. Wyman, in "Handbook of Water-Soluble Gums and Resins", R. L. Davison, ed., McGraw-Hill, Inc., 1980, ch. 21.

101. J. J. Kearney (to Diamond Alkali), U.S. Patent 2,857,367 (1958).

102. D. G. McNalty and R. I. Leininger (to Diamond Alkali), U.S. Patent 2,890,199 (1959).

103. S. Saito, *Kolloid-Z. u Z. Polymere*, 1967, **215**, 16.

104. M. L. Fishman and F. R. Eirich, *J. Polymer Sci.*, 1971, **75**, 3135.

105. M. L. Fishman and F. R. Eirich, *J. Polymer Sci.*, 1975, **79**, 2740.

106. M. M. Breuer and I. D. Robb, *Chemistry and Industry*, 1972, **1**, 530.

107. I. D. Robb, in "Anionic Surfactants - Physical Chemistry of Surfactant Action", Lucassen and Reynders, eds., Marcel Dekker, Inc., New York, 1981, ch. 3.

108. G. C. Kresheck and W. A. Hargraves, J. Colloid Interface Sci., 1981, 83, 1.

109. I. W. Kellaway and N. M. Najib, Int. J. Pharm., 1980, 6, 285.

110. R. Perkell and R. Ullman, J. Polymer Sci., 1961, 54, 127.

111. U.S. Patents 3,498,942; 3,498,943; 3,632,466; 3,772,382; 3,668,230; 3,776,874; 3,839,405.

112. "Polywet Oligomeric Surfactants", Uniroyal Technical Bulletin.

113. C. P. Roe, J. Colloid Interface Sci., 1971, 37, 93.

114. W. W. White and H. Jung, J. Polymer Sci., Symposium, 1974, 45, 197.

115. G. Mulholland, G. Hembree, and A. Hartman, "Sizing of Polystyrene Spheres Produced in Microgravity", report on work performed at National Bureau of Standards, November-December 1982.

116. E. Barnea and J. Mizrahi, Chem. Eng. J., 1973, 5, 171.

117. D. J. Zigrang and N. D. Sylvester, AIChEJ, 1981, 27, 1043.

118. N. Pramojaney, Permanent File on CYBER720, Lehigh University Computer Center.

119. J. I. Goldstein, D. E. Newbury, P. Echlin, D. C. Joy, C. Fiori, and E. Lifshin, Scanning Electron Microscopy and X-Ray Microanalysis, Plenum, New York, 1981, p. 2.

120. E. A. Collins, in "Advances in Emulsion Polymerization and Latex Technology", Lehigh University, 1983, Short Course Note.

121. S. H. Maron and P. E. Pierce, J. Polymer Sci., 1967, C27, 183.

122. R. V. Mann, F. J. Micale, and J. W. Vanderhoff, Graduate Research Progress Reports No. 16, p. 96, Emulsion Polymers Institute, Lehigh University, July 1981.

123. R. V. Mann, F. J. Micale, and J. W. Vanderhoff, Graduate Research Progress Reports No. 15, p. 81, Emulsion Polymers Institute, Lehigh University, January 1981.

124. C. M. Ma, F. J. Micale, M. S. El-Aasser, and J. W. Vanderhoff, Graduate Research Progress Reports No. 14, p. 54, Emulsion Polymers Institute, Lehigh University, July 1980.

125. C. M. Ma, F. J. Micale, M. S. El-Aasser, and J. W. Vanderhoff,

340

in "Emulsion Polymers and Emulsion Polymerization", D.
R. Bassett and A. E. Hamielec, eds., American Chemical Society,
Washington, D.C., 1981, p. 251.

126. A. Kamel, M. S. El-Aasser, and J. W. Vanderhoff, Graduate
Research Progress Reports No. 13, p. 54, Emulsion Polymers
Institute, Lehigh University, January 1980.

127. A. Kamel, M. S. El-Aasser, and J. W. Vanderhoff, Graduate
Research Progress Reports No. 14, p. 48, Emulsion Polymers
Institute, Lehigh University, July 1980.

128. A. Kamel, PhD dissertation, Lehigh University, 1981.

129. L. H. Tung, _J. Appl. Polymer Sci._, 1966, _10_, 375.

130. A. E. Hamielec and W. H. Ray, _J. Appl. Polymer Sci._, 1969, _13_,
1319.

131. L. H. Tung and J. R. Runyon, _J. Appl. Polymer Sci._, 1969, _13_,
2397.

132. C. M. Tseng, permanent file on CYBER720, Lehigh University
Computer Center.

133. Z. Grubisic, P. Remp, and H. Benoit, _J. Polymer Sci._, 1967, _B5_,
753.

134. M. J. R. Cantow, R. S. Porter, and J. F. Johnson, _J. Polymer
Sci._, _Part A-1_ , 1967, _5_, 987.

135. A. L. Spatoricio and B. Coulter, _J. Polymer Sci._, _Polymer Phys.
Ed._, 1973, _11_, 1139.

136. L. Mandik, _Prog. Org. Coatings_, 1977, _5_, 131.

137. A. R. Cooper and D. S. van Derveer, _J. Liq. Chromatogr._, 1978,
_1_, 693.

138. J. A. P. P. van Dijk, W. C. M. Henkens, and J. A. M. Smit, _J.
Polymer Sci._, _Polymer Phys. Ed._, 1976, _14_, 1485.

139. R. D. Hester and P. H. Mitchell, _J. Polymer Sci._, _Polymer Chem.
Ed._, 1980, _18_, 1727.

140. A. H. Abdel-Alim and A. E. Hamielec, _J. Appl. Polymer Sci._,
1974, _18_, 297.

141. T. Hashimoto, H. Sasaki, M. Aiura, and Y. Kato, _J. Polymer Sci._,
Polymer Phys. Ed., 1978, _16_, 1789.

142. P. L. Dubin and I. J. Levy, Polymer Preprints, 1981, 22, 132.

143. K. Gekko and H. Noguchi, Biopolymers, 1971, 10, 1513.

144. T. Ishige and A. E. Hamielec, J. Appl. Polymer Sci., 1973, 17, 1479.

145. G. B. Levy and H. P. Frank, J. Polymer Sci., 1953, 10, 371.

146. C. M. Tseng, permanent file on CYBER720, Lehigh University Computer Center.

147. D. J. Donahue and F. E. Bartell, J. Phys. Chem., 1952, 56, 480.

148. W. D. Harkins and F. E. Brown, J. Am. Chem. Soc., 1919, 41, 499.

149. W. D. Harkins and F. E. Brown, International Critical Tables, Vol. IV, McGraw-Hill, New York, 1928.

PART C

The Effect of Hydroquinone on the

Kinetics of the Seeded

Emulsion Polymerization of Styrene

Based on the M.S. Thesis

by

Anthony Silwanowicz

TABLE OF CONTENTS

ABSTRACT

Seeded polymerizations of polystyrene/styrene systems initiated by 0.5 m$\underline{M}$ potassium persulfate were carried out in a piston/cylinder prototype dilatometer (LUMLR). In long duration tests at room temperature in the absence of initiator, a thermal background polymerization rate was observed. This observation was confirmed by parallel tests run in a glass dilatometer. The rate of polymerization at room temperature in the absence of initiator was found to be 0.56% conversion/hour in the constant rate period. Hydroquinone was found to inhibit polymerization at room temperature for a length of time directly proportional to its initial concentration. The observed induction periods were only 1.8% of the length expected. It was postulated that this low inhibition efficiency was due to the slow oxidation of the non-inhibiting hydroquinone to benzoquinone which then caused the inhibition.

Studies of the solubility of hydroquinone in water and in styrene indicated that hydroquinone should partition primarily in the aqueous phase. This result was confirmed by measurement of the surface charge density for samples with and without hydroquinone, which showed that the hydroquinone neutralized free radicals

1

only in the aqueous phase. Molecular weight
determinations indicated that no copolymerization of
styrene and hydroquinone occurred as had been observed
for bulk polymerizations at high temperatures.
Although generally considered an inhibitor, hydro-
quinone was found to cause retardation of the polymeri-
zation rate in seeded emulsion polymerizations, and
this lower rate was also found to be reproducible.

I. INTRODUCTION

Perhaps the most studied emulsion polymerization
system to date has been one containing styrene monomer
and an aqueous phase initiator, potassium persulfate.
The reaction kinetics of this system have been well
documented and are frequently used to test the validity
of different theories of emulsion polymerization.
Indeed, since this system has been so extensively
studied, it has been referred to as a classical
emulsion polymerization. Despite all the attention
devoted to the emulsion polymerization of styrene, it
still retains some poorly understood aspects. One such
aspect is the mechanism by which certain additives
alter the polymerization rate. Depending on the magni-
tude of the change observed in the rate, these additi-
ves are characterized as either inhibitors or
retarders. An additive that completely prevents poly-
merization for a length of time and then allows the
reaction to proceed at the normal rate is termed an
inhibitor. An additive that lowers the polymerization
rate is termed a retarder. The inhibition and retar-
dation of the bulk polymerization of styrene have been
well studied[1]. However, considerably less attention
has been devoted to the effect of inhibitors or retar-
ders on the emulsion polymerization of styrene.

3

The behavior of bulk styrene and styrene emulsified in water are markedly different. This became apparent after analyzing the results of an emulsion polymerization experiment carried on board the third orbital mission of the Space Shuttle "Columbia". This experiment was a polystyrene/styrene seeded emulsion polymerization initiated by potassium persulfate which was intended to produce a monodisperse latex. This classical system was designed as a "control" experiment to compare the polymerization kinetics obtained in the microgravity of earth orbit to the kinetics obtained in an earth based experiment. Because of the time constraints dictated by the Shuttle preparation schedule, the prepared recipe was required to sit in a reactor on board the Space Shuttle for nearly four days prior to reaction. During this four day delay however, the recipe was polymerized to completion, thus eliminating its value as a control experiment. The occurrence of this unexpected polymerization without the heat-up to reaction temperature, prompted the search for an explanation of this result and the subsequent design of a new "control" experiment. This control experiment had to meet three criteria. First, the recipe had to be a classical emulsion polymerization system containing small (submicron) sized seed particles, styrene monomer, and potassium persulfate

4

initiator. Secondly, because of the four day delay prior to reaction, the system had to resist any room temperature polymerization prior to heat-up to the 70°C reaction temperature. Finally, the reaction had to yield reproducible kinetics. For these reasons, the addition of an inhibitor to the seeded emulsion system was deemed necessary.

Thus, the purpose of this study was twofold: to obtain information on the action of inhibitors in emulsion polymerization; and to use this information to develop a control experiment for a spaceflight experiment which satisfied the above criteria.

II. THEORETICAL BACKGROUND

Emulsion polymerization is generally subdivided into three intervals. Interval I covers the nucleation of polymer particles and in this interval monomer droplets, emulsifier ions, micelles, and monomer-swollen polymer particles coexist in the aqueous phase. In Interval II, the micelles no longer exist, there is no further nucleation of particles, and polymerization occurs in the monomer-swollen polymer particles. The monomer droplets still exist in the aqueous phase and act as a monomer-supplying resevoir for the poly-merizing particles. Interval III commences when monomer droplets no longer exist, and in this interval, polymerization continues in the monomer-swollen particles. A seeded polymerization is a technique often used to produce a monodisperse latex. In this method, a monodisperse seed latex is preswollen with monomer and then polymerized. This eliminates the par-ticle nucleation stage (Interval I) and the polymeriza-tion occurs only in the swollen particles. In this way the uniformity of the particle size is maintained.

The mechanistic view of emulsion polymerization given above was first proposed by Harkins[2] and was later quantified by Smith and Ewart[3]. Smith and Ewart were not able to obtain a general solution to the steady state equation they developed, but they were

able to solve it for three separate cases: the case

where the average number of radicals per particle ($\bar{n}$)

was much less than 1 (Case I), the case where $\bar{n}$ was

equal to ½ (Case II), and the case where $\bar{n}$ was much

greater than 1 (Case III). The value of $\bar{n}$ is deter-

mined by the rate of entry, the rate of desorption, and

the rate of termination of free radicals, and in the

case of styrene emulsion polymerization, is generally

equal to ½.

The rate of polymerization (Rp), in a seeded

emulsion polymerization is given by[4]

$$R_p = k_p [M_p] \bar{n} N_p / N_A \tag{1}$$

where k_p = propagation rate constant

$$= 2.2 \times 10^7 \exp(-7400/1.987 \ T)$$

liter/mole sec for styrene

$[M_p]$ = concentration of monomer in the

particles, moles/liter

N_p = number of particles, liter^{-1}

$\bar{n}$ = average number of radicals per

particle

N_A = Avogadro's number

The average number of radicals per particle, n, can

be expressed as[5]

$$\bar{n} = (0.25 + a/2)^{\frac{1}{2}} \tag{2}$$

7

$$a = R_{abs} V_p N_A^2 / N_p k_{tp} \qquad (3)$$

where R_{abs} = rate of radical absorption,

moles/liter sec obtained from

the initiator decomposition

rate

V_p = particle volume, liter

k_{tp} = termination rate constant within a

particle, liter/mole sec

In this study, the rate of polymerization for a polystyrene/styrene seeded system was measured via a dilatometer. From the rate data, values of $\bar{n}$ could be calculated by rearranging equation (1). These values for $\bar{n}$ could then be substituted into equation (2) and values of the termination rate constant could then be extracted.

The kinetic rate equation for an inhibitor-containing polymerization has been derived in the literature.[1,6] In this derivation, the reaction between a growing chain, $M\bullet_n$, and an inhibitor molecule, Z, is considered to occur with a rate constant k_z. Equation (4) shows this inhibition reaction.

$$M\bullet_n + Z \xrightarrow{k_z} M_n + Z\bullet \qquad (4)$$
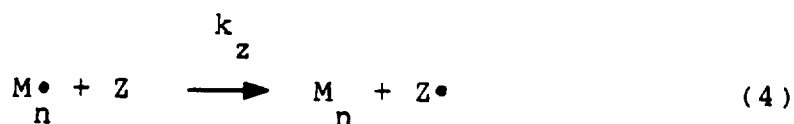
This inhibition reaction results in the termination of

8

the growing chain and the formation of an essentially
unreactive radical. The rate equation for an inhibited
polymerization is given by:

$$R_p = \frac{K_p [M] R_i}{k_z [Z]} \qquad (5)$$

where R_i = rate of initiation

[Z] = concentration of inhibitor

The inhibition constant z, is defined as the ratio of
the rate constants for inhibition and propagation:

$$z = \frac{k_z}{k_p} \qquad (6)$$

A substance which alters the polymerization rate can be
characterized as an inhibitor or a retarder depending
on the magnitude of the inhibition constant. Thus,
there is no sharply defined boundary separating inhibi-
tors from retarders, but rather a continuum over which
the effect on polymerization rate varies from no effect
at all, to a complete cessation of polymerization.

III. EXPERIMENTAL

A. Reactor Description

The study of emulsion polymerization kinetics requires a technique which allows one to determine the percent monomer converted to polymer as a function of time. From a plot of these conversion-time data one can then extract values for the polymerization rate, which is often the desired information in a kinetic study. Two of the more popular methods employed for the collection of conversion-time data in an emulsion polymerization are gravimetric analysis and dilatometry.

Gravimetric analysis is a simple, though crude technique which essentially involves the periodic sampling and weighing of small amounts of the reacting mixture. In this technique, a sample of the polymerizing mixture is removed from the reactor and weighed. To this sample then, is added a known amount of inhibitor, frequently hydroquinone, to shortstop the reaction and then this sample is dried in an oven to evaporate water and monomer to leave only a solid. From the amount of solid (polymer) formed, the initial weight of the sample, and a knowledge of the initial amount of monomer present, one can calculate the per-

10

cent conversion of monomer to polymer. Although this technique is straightforward and does not require any specialized equipment (other than a balance), it has some important limitations. First, due to the delay associated with sampling and weighing, the time at which a particular conversion occurs will be uncertain. This error in the determination of time becomes more important as the rate of reaction increases. Thus, the second limitation of gravimetric analysis is that for very rapid reactions, the method is simply not sensitive enough and will lead to a great deal of scatter in the data. Finally, if one tries to obtain more accurate results by sampling more often, this method becomes very tedious, especially for long reactions.

Dilatometry, although it offers greater accuracy than gravimetric analysis, also presents some experimental difficulties. It requires that one use a specialized piece of equipment, namely a dilatometer. A dilatometer is often simply a glass flask to which has been attached a glass capillary column. The reacting mixture is loaded into the glass flask and capillary assembly and then lowered into a constant temperature bath. As monomer polymerizes the density increases, and hence the total volume of the reactants decreases. This change in volume can be observed as a change in the height of liquid in the capillary. From a

knowledge of the intial recipe and the volume of the capillary, one can then convert the change in liquid height to actual percent conversion. When using a dilatometer, one must always be careful not to trap any bubbles of air in the flask or capillary, as these will distort any liquid contraction due to conversion.

The collection of conversion-time data in a weightless environment presents special problems. In the form described above, neither gravimetric analysis nor dilatometry can be used to determine the kinetics of an emulsion polymerization. For this reason a novel reactor had to be designed which could both contain the reactants and also record the data that would yield the reaction kinetics. Figure 1 shows a diagram of the prototype reactor designed for the spaceflight experiments. This reactor, called the Lehigh University Monodisperse Latex Reactor (LUMLR), was designed and built by General Electric and was used to collect most of the kinetic data in this report. The LUMLR is a stainless steel piston/cylinder-type dilatometer. In the following description, the numbers listed in parentheses refer to the numbered components in Figure 1. The reactants fill a 100 cc volume in the cylinder(10), and the piston(4) sits on the surface of the liquid. A compressed spring (3) in the piston forces the piston to remain on the surface of the liquid.
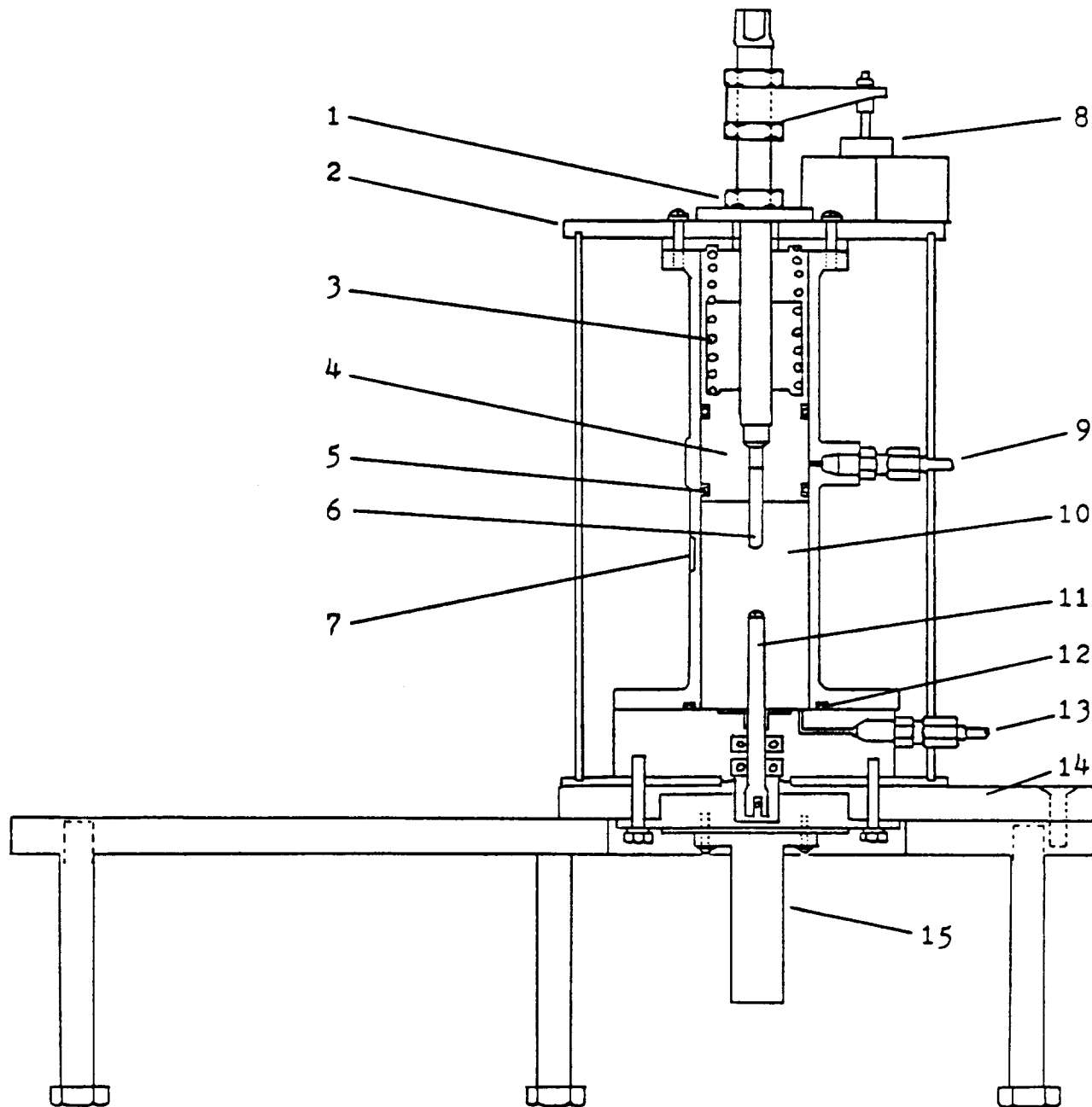
12

Figure 1. Diagram of the Lehigh University Monodisperse Latex Reactor(LUMLR). 1. bolt; 2. textalite housing cover; 3. spring; 4. piston; 5. o-ring; 6. fluid temperature probe; 7. cylinder temperature thermistor; 8. LVDT; 9. exit port; 10. reaction volume; 11. stirrer shaft; 12. o-ring; 13. filling port; 14. baseplate; 15. stirrer motor.

Thus, as the volume of the liquid decreases due to polymerization, the piston height also decreases. This change in position is translated into a voltage signal by a Linear Voltage Differential Transducer (LVDT) (8). By calibrating this device, one can easily convert the output voltage data into distance traveled by the piston and then into volume change. Temperature sensors (6,7) measure the temperature of the fluid and of the reactor wall, respectively. The latex was heated by means of electrical heating tape wrapped around the bottom half of the stainless steel cylinder. A temperature controller enabled the polymerizations to run at either 70°C or 90°C. The latex was prevented from leaking out of the cylinder by the use of two o-rings; one located on the piston (5), and the other in the base of the cylinder (12). During polymerization, the reactants were agitated by a stirrer located in the base of the reactor. The teflon stirrer blade was attached to a stirrer shaft (11) which was powered by a stirrer motor (15, TRW, Globe Motor Division) and could be operated in one of three modes: clockwise agitation, counterclockwise agitation, and oscillatory or "washing machine" agitation. In addition to this, the speed of the stirrer could be varied from about 5 - 25 rpm. In this work, all polymerizations were carried out using oscillatory stirring at a speed of 13 rpm.

The controls for the stirring and heating of the LUMLR, along with all of the other electronics, are housed in a metal container called the MLR controller . A diagram of the LUMLR, the controller, and the automatic data recording device (A.D. Data Minilogger, ML-10A) appears in Figure 2. The data recorder contains an internal clock, and can be set to scan and record up to ten input voltages at several regular time intervals. This permits data to be recorded regularly for long duration experiments. After a polymerization the time/temperature/volume data recorded on the cassette tape were reduced with the aid of a computer program and conversion-time curves generated along with plots of other useful kinetic data.

B. <u>Recipe Preparation</u>

In all cases, the polymerizations were carried out in the LUMLR, except where noted, on a seeded polystyrene/styrene system. The method of seeded emulsion polymerization of styrene was described earlier in this report. The polystyrene seed used in all experiments was a 0.19 μm diameter monodisperse latex obtained from the Dow Chemical Co. (LS 1102-A). The stock latex which was approximately 45 weight percent solids, was first filtered through glass wool and then diluted to approximately 6% solids by the addition of distilled, deionized water. The diluted latex was
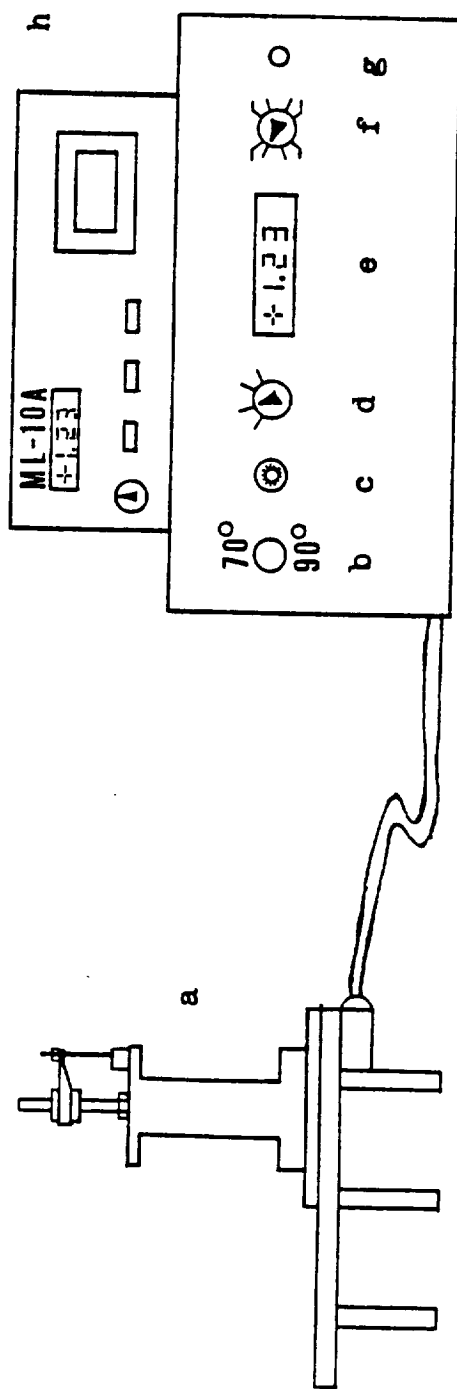
15

Figure 2. Apparatus for polymerization in LUMLR. a. LUMLR; b. reactor temperature selection switch; c. stirrer rpm selection switch; d. stirring mode selection switch; e. digital display panel meter; f. data display selection switch; g. power on/off button; h. data cassette recorder with timer.

poured into a one liter pyrex glass bottle and a clean magnetic stirring bar was added. The latex was then ion-exchanged by using approximately 10 grams of a mixed bed of anionic (Dowex 1) and cationic (Dowex 50) ion-exchange resin (Dow Chemical Co.). Both the anionic and the cationic ion-exchange resin had previously been carefully purified according to the procedure described by Vanderhoff, et al.[7] The mixed bed resin in the dilute latex was gently agitated by the magnetic stirrer for two hours after which the resin was removed by filtering the latex through glass wool. Fresh resin was added, and the procedure was repeated five times. This ion-exchange procedure was designed to remove any emulsifier or electrolyte (e.g. initiator or salts left over from the preparation of the stock latex) that may have been in the stock latex. The seed latex thus cleaned, was next concentrated to approximately 16 - 21% solids in a serum replacement cell. A membrane (Nuclepore Co.) with very uniform, 0.2 μm diameter pores was used in the cell to filter out water while containing the polystyrene particles. Clogging of the membrane by the particles was minimized by vigorously agitating the latex during the filtration.

The styrene monomer (Fisher Scientific Co., certified grade, inhibited) was washed several times with an equal volume of a 10% by weight aqueous sodium hydroxide solution

17

in a separatory funnel to remove the inhibitor. The monomer was then washed with distilled deionized water until litmus paper indicated the absence of base. To the washed monomer was then added approximately 100 grams/liter of anhydrous sodium sulfate to remove any water. After tumbling for several minutes, the washed monomer was stored in a refrigerator at -20°C. Prior to use, the styrene was doubly distilled with the second distillation occurring immediately prior to the mixing of the recipe. Both distillations were done under a blanket of very pure and dry nitrogen gas at a pressure of 10 mmHg in an all glass distillation rig with greaseless joints.

Potassium persulfate (Fisher Scientific Co., certified grade) was purified by recrystallizing it from distilled deionized water at a low temperature. The crystals were washed with acetone (Bioclinical Laboratories, technical grade) several times and then dried at room temperature in a vacuum oven. The dried crystals were stored under dry nitrogen gas in a refrigerator at -5°C.

Aerosol MA-80 emulsifier (sodium dioctyl sulphosuccinate, American Cyanamid, industrial grade) was used without purification, but was diluted to approximately 8 - 9% by weight in distilled deionized water before use. Sodium bicarbonate (Fisher

Scientific Co., certified grade), p-benzoquinone, and hydroquinone (both Fisher Scientific Co., purified grade), were all used as recieved, without further purification.

Using the above materials, the recipes were prepared as follows. Into a clean 8-ounce bottle was weighed the aqueous Aerosol MA-80 solution using a Sauter four-place analytical balance. The amount of emulsifier added was calculated to yield 8% coverage of the final particle surface; this amount being determined from the known adsorption isotherm of Aerosol MA on polystyrene. Next, the sodium bicarbonate buffer was added as a solid to the bottle. The amount of buffer added was in all cases equal to the amount (by weight) of initiator added. The buffer was added to prevent the latex from becoming acidic during the course of the polymerization. To the emulsifier and buffer was then added the cleaned 0.19 μm diameter polystyrene seed latex. The seed latex was added in an amount which would form a recipe with a 10 weight percent solids content. Thus, in the case of a 200 g recipe, seed latex containing 20 g of polystyrene particles was added. The inhibitor was added as an aqueous solution when the concentration was to be less than 6 parts per million (ppm) based on the total grams of recipe. This aqueous solution was added to the bottle prior to

the addition of the seed latex. When the inhibitor concentration was to be greater than 6 ppm however, the inhibitor was added as a solid after the seed latex had been added. Next, distilled deionized water was added to the bottle, with 5 grams being retained for later addition with the initiator. Finally, the doubly distilled styrene monomer was added to the bottle. The design monomer-to-polymer ratio in all cases was 2:1. Thus, in a 200 g recipe containing 20 g of polystyrene seed, 40 g of styrene monomer was added. The bottle containing the recipe was then sealed with a polyseal plastic cap to prevent leakage during the swelling procedure. The bottle was placed in a rubber drum (7.5 in. diameter, 8.25 in. height) lined with foam padding, and inclined at an angle of approximately 45° from the axis of the drum. The drum lid was secured by a plastic screw and the drum was placed with its axis horizontal on a lapidary tumbler. The tumbler rotated the drum at approximately 33 rpm. In this manner the seed particles were swelled by the monomer at room temperature, with the gentle agitation described, for 16 - 20 hours. At the completion of the 16 - 20 hour swelling period, the bottle was removed from the tumbler. The potassium persulfate initiator was weighed out and then added to the 5 g of distilled deionized water that was saved. After the initiator

20

had completely dissolved, the solution was added to the now swollen latex recipe. The bottle was then resealed and gently agitated by hand for several minutes to insure even distribution of the initiator throughout the swollen latex mixture. The amount of initiator used in the recipes, was 0.5m$\underline{M}$ based on the aqueous phase, unless otherwise noted.

At the completion of the swelling stage, there was invariably a slight amount of residual monomer present as a separate phase on the surface of the swollen latex. This incomplete swelling was probably caused by the interfacial tension between the seed latex and the monomer being too high due to the extremely low amount of emulsifier added. This idea is supported by the fact that when a latex containing a great deal more emulsifier (stock Dow LS1102-A uncleaned latex) was used as the seed, there was no residual monomer apparent and the swelling was 100% complete. The experimental determination of the amount of monomer present in the seed particles is discussed in another section of this report. In all cases, any residual monomer that did not swell the particles, and remained as a separate phase, was removed. This removal was accomplished by filtering the swollen latex through glass wool into a clean 500 ml round bottom flask. Any monomer layer that may have existed was trapped in the

21

glass wool upon filtering, and therefore, only the swollen latex was allowed to enter the flask. Once loaded with the swollen latex, the flask was fitted with a ground glass attachment to which could be connected a length of rubber vacuum tubing. By fitting the vacuum tubing to an aspirator, the pressure in the round bottom flask could be reduced enough to cause out-gassing, with consequent removal of dissolved oxygen. A diagram of the degassing operation appears in Figure 3. For all runs, the swollen latexes were degassed at a pressure of about 20 mmHg for 45 minutes. The pressure was regulated by means of a glass needle valve attached to the vacuum line by a plastic T-joint. By using this needle valve, the pressure was gradually reduced to 20 mmHg in order to avoid violent bubbling. After the 45 minute degassing period, the pressure was raised to atmospheric pressure and the swollen latex was then ready to be loaded into the LUMLR.

C. Loading of the LUMLR

The loading of the prototype dilatometer presents unique problems due to the unconventional design. As with conventional glass dilatometers, the presence of an air bubble in the prototype dilatometer is an undesirable situation which can result in inaccurate kinetics. The LUMLR presents an additional difficulty in that its stainless steel construction prevents the
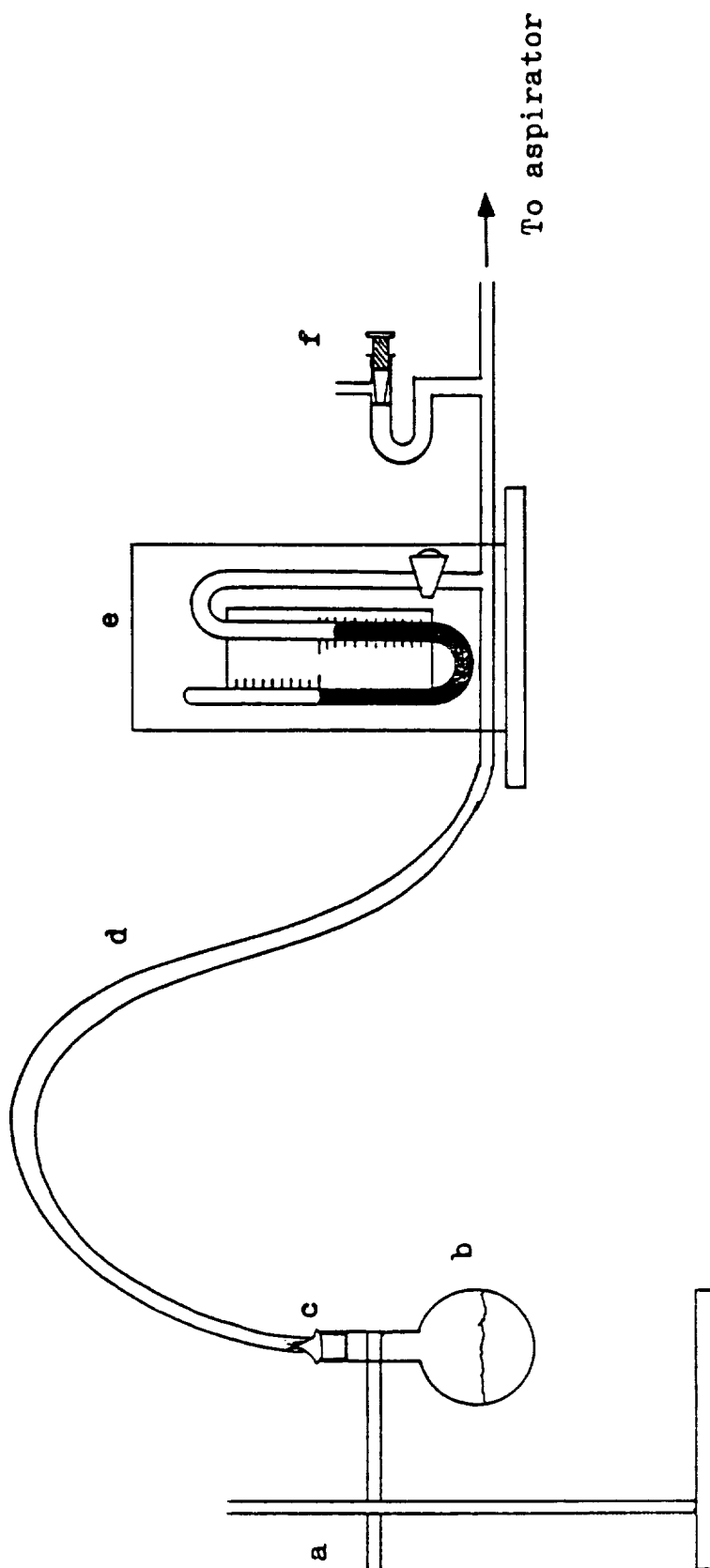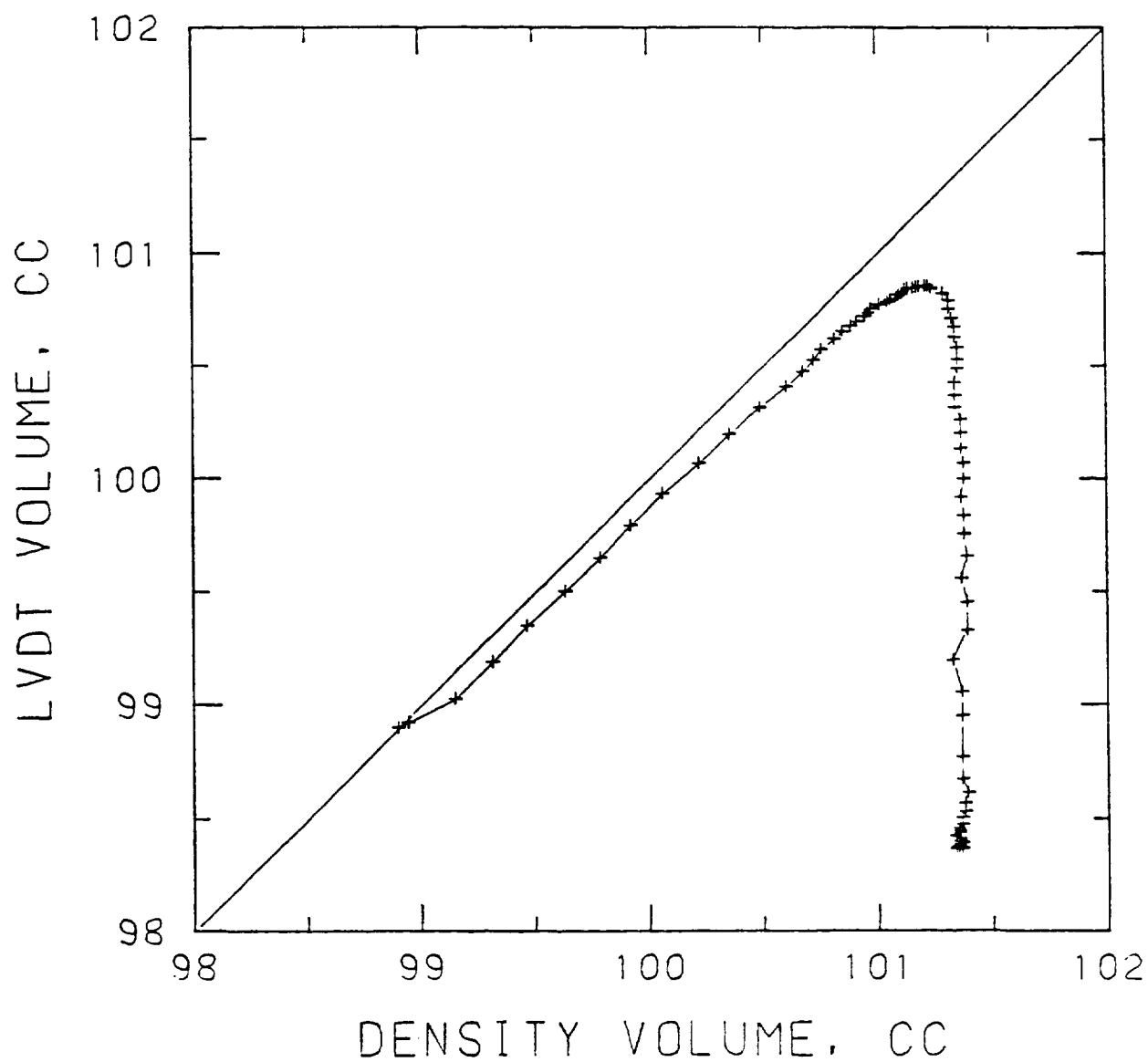
22

Figure 3. Degassing apparatus for swollen latex recipes. a. ringstand and clamp to support flask; b. latex-containing round bottom flask; c. ground glass adapter; d. rubber vacuum tubing; e. manometer; f. needle valve for pressure regulation.

To aspirator

detection of an entrapped air bubble by visual inspection. Thus, care must be exercised during the reactor loading procedure in order to insure that no air bubbles become entrapped in the LUMLR. If however, an air bubble does become caught in the reactor, it will become apparent when the volume change data is analyzed.

As the reactants are heated to reaction temperature, the volume of the reactants increases. From a knowledge of the amount and the density of each component in the reactor, and assuming that the density of the mixture is the sum of the component densities, the volume as a function of temperature for the swollen latex can be calculated. This calculated volume as a function of temperature can be compared to the volume measured by the LVDT during heat-up, and can be used to detect the presence of an air bubble. The presence of an air bubble in the reactor will cause the measured volume to differ from the predicted volume since the expansion will be offset by the compression of the bubble. Figure 4 shows the effect of an air bubble in the LUMLR on the expansion behavior of a swollen latex during heating. The volume measured by the LVDT, is plotted on the ordinate, while the predicted volume is plotted along the abcissa. The fact that the predicted volume is greater than the actual volume measured by

24

Figure 4.   Comparison of measured volume(LVDT) and predicted
            volume(DENSITY) for a swollen latex recipe in-
            dicating the presence of an air bubble in the
            reactor.

the LVDT, indicates that the latex expansion is being offset by the compression of the air bubble. As one proceeds from left to right along the diagonal, the latex is expanding, and when the curve begins a vertical decline, it is indicative of volume contraction due to polymerization. For this reason, expansion data that lie below the 45° line, as is the case in Figure 4, will be incorrectly interpreted to mean that conversion occurred during the heat-up period. In contrast, Figure 5 illustrates similar expansion data for a polymerization which shows no indication of the presence of an air bubble in the reactor. The data lie directly on the 45° line, indicating that the observed and the expected expansion are identical.

Since obtaining accurate kinetics is hindered by the presence of an air bubble in the dilatometer, effort was directed at preventing, or at least minimizing, this inclusion of air. To this end, a technique, developed in this laboratory by E.D. Sudol, was used to load the LUMLR which greatly improved the reliability of the observed kinetics. This technique involved the loading of the LUMLR under reduced pressure, with the idea that if a bubble were to become entrapped in the reactor, the force exerted by the piston on the reactor volume would cause the bubble to collapse and be reabsorbed by the latex. A complete
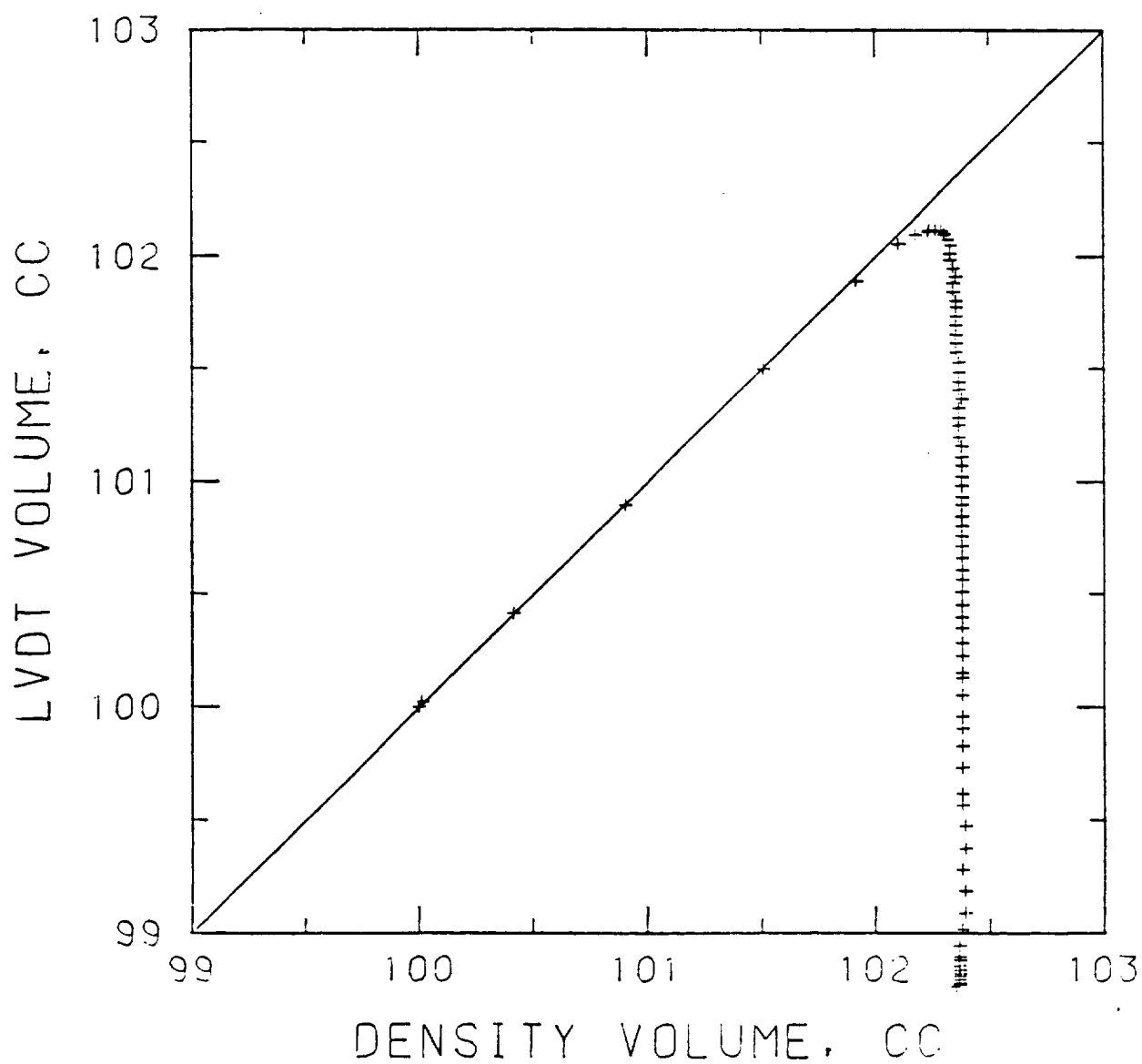
Figure 5. Comparison of measured volume(LVDT) and predicted volume(DENSITY) for a swollen latex recipe showing no indication of an air bubble in the reactor.

description of the low pressure LUMLR loading method follows below.

After a swollen latex was degassed and the pressure in the flask raised back to atmospheric pressure, the ground glass adapter and vacuum tubing were removed from the flask. A ground glass adapter, with a tube extending to just above the latex surface, and a short glass sidearm, was then placed in the round bottom flask. To the short glass sidearm was connected a 1 meter length of teflon tubing of 2 mm I.D. by using a small piece of Tygon tubing as an adapter. The other end of the teflon tubing also had a Tygon tubing adapter and was connected to one end of a stainless steel valve (Swagelok Co.). The other end of the valve was a male end of a quick-disconnect valve (Swagelok Co.). With the valve closed and the male end unconnected, the round bottom flask was carefully inverted. The flask was supported in the inverted position on a ringstand by using two clamps. Once the flask was firmly secured, the vacuum line was attached to the long glass adapter tube. The male end of the quick-disconnect valve was next connected to the filling port quick-disconnect piece on the LUMLR (13 in Figure 1). A 125 ml erlenmeyer flask was fitted with a rubber stopper through which two glass tubes protruded. One of the glass tubes was connected to the LUMLR exit

28

port (9 in Figure 1) by means of a Tygon tubing adapter, and the other tube was connected to the vacuum line. In this way, the erlenmeyer flask served as a trap for any latex that overflowed the LUMLR exit port during loading. Next, the piston position was checked to verify that it was at its maximum height (i.e. providing the maximum empty volume in the reactor) by making sure the bolt (1 in Figure 1) could not be turned clockwise any further. Finally, the LUMLR and its platform were inclined so that the exit port was at an angle of approximately 20° from the horizontal. A diagram of the loading equipment appears in Figure 6, and in the following description, the letters in parentheses refer to the letters labeling this figure. With the fill valve closed (f) and the vacuum cut-off valve open (h), the vacuum pump (or aspirator) was turned on and the needle valve was adjusted so that the entire system was under a pressure of approximately 35mmHg. When the pressure was stabilized, the fill valve was opened and latex began flowing through the teflon tubing into the reactor. In order to induce flow, the round bottom flask and ringstand were elevated, thus providing a hydrostatic head. After about 20 - 30 minutes the reactor would be filled and latex would begin to overflow into the erlenmeyer flask. After air bubbles were no longer visible in the
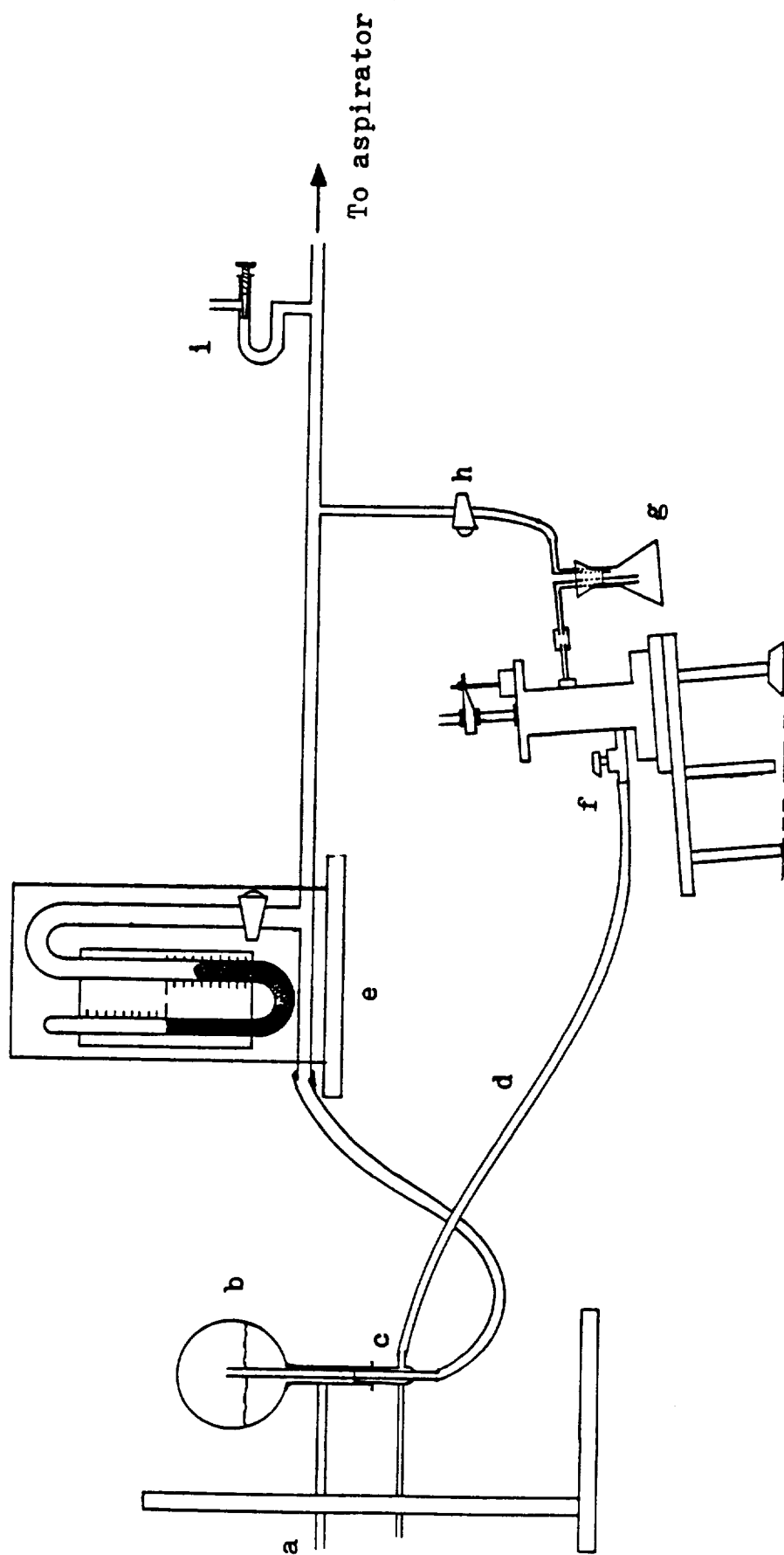
Figure 6. Apparatus configuration for low pressure loading of the LUMLR. a. ring-stand and clamps to support flask; b. inverted flask; c. glass adapter with sidearm; d. teflon tubing; e. manometer; f. fill valve with quick disconnect piece; g. overflow flask; h. vacuum cut-off valve; i. needle valve.

overflow tube, the fill valve was closed and the piston
was lowered until no more fluid was expelled from the
exit port, and the piston no longer moved. The vacuum
cut-off valve was closed and the fill valve was opened
so that the pressure of the piston forced latex back
into the round bottom flask as the piston was lowered
to the 100 cm^3 calibrated position. This accomplished,
the fill valve was then closed and removed from the
quick-disconnect piece on the LUMLR. After the
pressure was raised to atmospheric pressure, the erlen-
meyer flask and the vacuum tubing were disconnected and
the LUMLR, on its platform, was then electrically con-
nected to the LUMLR controller. The fill port and exit
port were cleaned and the insulation was wrapped around
the reactor. With this done, a polymerization could
now be run in the reactor.

D. Polymerization, Data Collection, and Reactor
    Unloading

Prior to heating the swollen latex to reaction tem-
perature, the volume of the reactants was monitored by
means of the LVDT signal for approximately ¼ hour to
determine if there was a leak in the system. This was
done by releasing the piston (by loosening the bolt)
and recording the LVDT voltage on a chart recorder. If
there was no leakage apparent, the stirrer was then

31

switched into the oscillatory mode and the volume once again monitored for a ½ hour period. At the end of this period, the automatic data recording device was switched on and the initial data recorded on a cassette tape. The data recorded were the LVDT voltage, the fluid temperature, the cylinder temperature, the heater voltage, and the time. At time zero, the heater was turned on. For the first 35 to 40 minutes data were recorded every minute, while after this initial heat-up period, data were recorded every 5 or 10 minutes depending on the rate of reaction (the higher the rate, the more often data were recorded). The reaction was considered complete when the chart recorder trace of the LVDT voltage appeared essentially level. At this point the recording of data was stopped, and the heater and stirrer were turned off. The quick-disconnect piece was removed from the fill port with the piston position fixed by the bolt. The fill port was cleaned to remove any unreacted latex trapped there and to prevent this contaminant from entering the reactor during piston removal. The quick-disconnect was then reconnected to the fill port and the piston was raised to its highest elevation by using the bolt. The piston support (i.e. the textalite housing cover, 2 in Figure 1) was then unfastened from the cylinder, and the piston and housing cover were removed from the

32

cylinder. The latex was then decanted into a 4 ounce
bottle using a clean glass funnel, the bottle capped
and immediately quenched under cold running water.
During the cooling of the product latex the reactor was
thoroughly cleaned with water, acetone, and toluene.
The o-ring at the base of the stirrer shaft was
replaced, while the other o-rings were simply cleaned
and re-used. The fill valve was disassembled and care-
fully cleaned to remove all trapped latex. After the
reactor was completely cleaned it was rinsed with ace-
tone and covered to prevent the settling of dust on any
internal surface.

E. <u>Analysis of Product Latexes</u>

Although the polymerization kinetics were of pri-
mary importance in this investigation, the additional
characterization of the product latexes frequently led
to a greater understanding of the actual polymerization
process. Thus, the product latexes were analyzed gra-
vimetrically to determine the final solids content and
to compare the measured solids content to the design
value of 30%. Either scanning electron microscopy
(SEM) or transmission electron miscroscopy (TEM) was
used to determine final particle size and to evaluate
the monodispersity of the sample. Gel Permeation
Chromotography (GPC) was used to measure the polymer
molecular weight, and conductometric titration was used

33

to determine the surface charge density of the polymer particles. The amount of residual styrene in the latex was determined by extraction with isooctane and subsequent absorbance of UV radiation by the isooctane. This technique was also used to determine the amount of monomer imbibed by the polystyrene seed particles in the swollen latex. This isooctane extraction technique along with some of the product characterization techniques, will now be reviewed here in some detail.

1. Isooctane Extraction Procedure

The procedure for the isooctane extraction of a swollen latex and a product latex was essentially the same, with the only difference being the amount of latex sample initially taken, and the amount of isooctane used for the dilution of the extractant. For the analysis of a swollen latex, approximately 0.2 ml (0.5 ml for a product latex) of the latex was carefully weighed into a 1-ounce bottle containing a known weight of isooctane (ca. 20 g). This bottle containing the swollen latex sample in isooctane was then tumbled end-over-end in a lapidary tumbler for 48 hours. At the end of this tumbling period, six drops of the extractant from the swollen latex (10 drops for a product latex) was carefully weighed into a known weight of isooctane (about 20 g for a swollen latex; 10 g for a product latex). This isooctane solution contained

34

about 5 -10 x 10^{-6} g styrene per g solution. The exact concentration of styrene was determined by measuring the absorbance of the styrene/isooctane solution using a UV absorbance monitor with a flow-through cell (Instrument Specialty Co., Model 1840). The styrene/isooctane solution was pumped through the UV absorbance monitor using a constant flow rate syringe pump (Harvard Apparats, Model 940). The absorbance was measured at a wavelength of 245 nm on a chart recorder and using the calibration curve shown in Figure 7, the actual concentration of styrene was determined. Using this concentration, along with the weight of latex and isooctane taken, the concentration of styrene in the latex was then used to calculate a corrected recipe which accounted for incomplete swelling of the polystyrene particles. A sample calculation appears in Appendix A. This corrected recipe for the swollen latex was used in the analysis of the kinetics. The amount of residual styrene in the product latex was determined and this information, in conjunction with the initial styrene concentration, was used to calculate the final conversion as a check for the conversion determined by the volume contraction data.

2. Molecular Weight Determination

Molecular weight distributions were determined
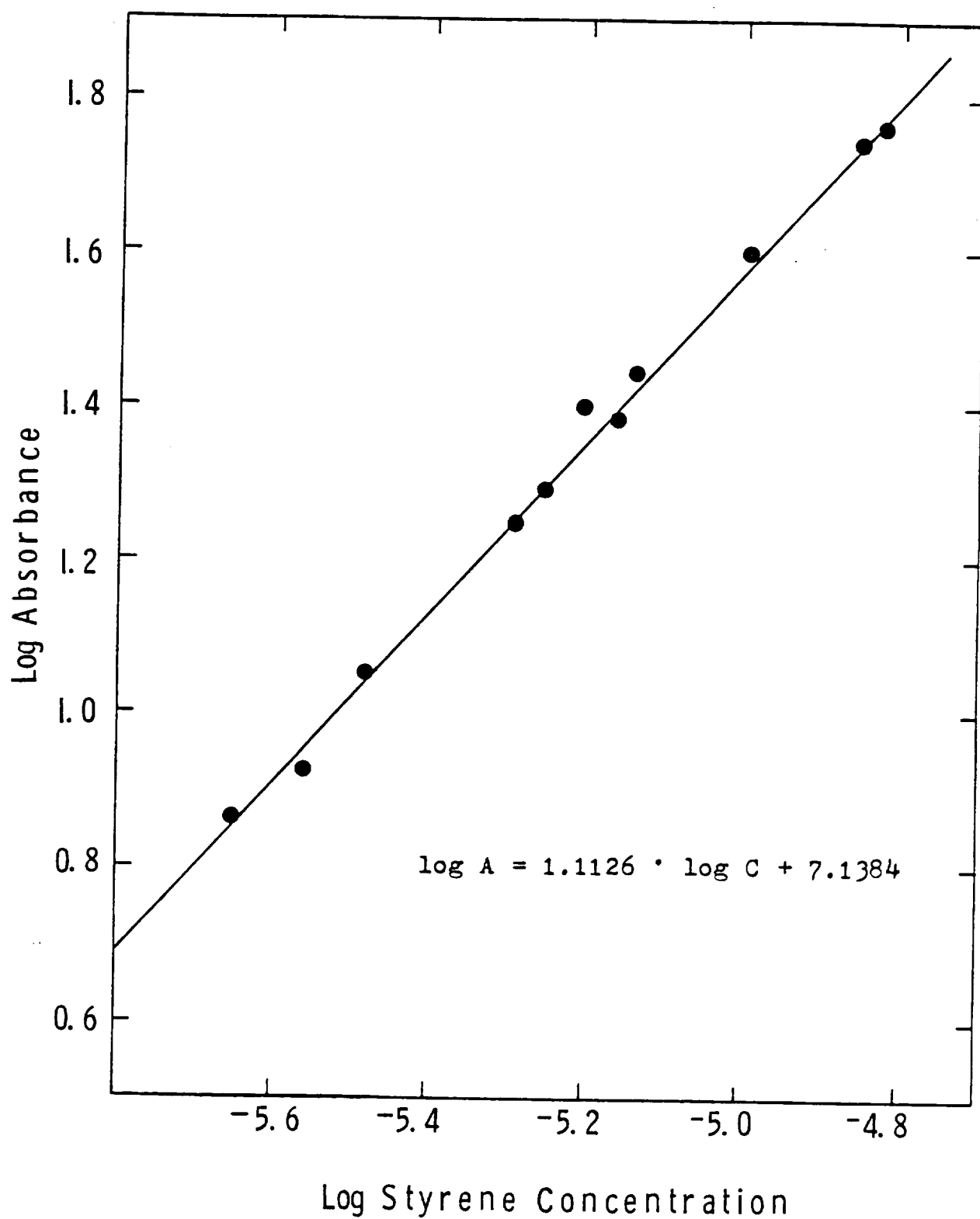
log A = 1.1126 · log C + 7.1384

Figure 7. Calibration curve for isooctane extractions.

using a GPC unit (Waters Associates, Model 201) which
was outfitted with six columns and one pre column (μ -
Styragel, Toyo Soda, Japan). Dried polystyrene,
obtained by heating latex to 70°C in an oven for gravi-
metric determination of solids content, was dissolved
in tetrahydrofuran (THF) to form solutions of 0.5
weight % polymer. These solutions were agitated until
completely dissolved, filtered using a Millipore pre-
filter and a Millipore filter with a 0.5 μm diameter
pore size. Using a solvent flow rate of 2.0 ml/min, the
samples were injected into the GPC and a differential
refractometer was used to detect the polymer exiting
the columns. The varying refractive index of the solu-
tion was recorded on a chart recorder and these data
were used as input, along with calibration data, to a
computer program which calculated the weight and number
average molecular weights and also plotted the molecu-
lar weight distributions.

3. Conductometric Titrations

To determine the surface charge density on latex
particles due to sulfate ions from the potassium per-
sulfate initiator, the technique of conductometric
titration was employed. Before the analysis, several
grams of latex was diluted to approximately 5 weight %
polymer. This latex was then ion-exchanged (as
described earlier) to remove all unbound ionic species.

37

Using at least 1 gram of polymer, the cleaned latex was further diluted with distilled deionized water in a clean 250 ml beaker. This solution was next bubbled with dry nitrogen gas for ½ hour. With the solution being stirred with a magnetic stirrer, sodium hydroxide solution (0.02N, Fisher Scientific Co.) was added with a constant flow rate burette. The conductance of the solution was monitored as a function of the added base, with two platinum electrodes and recorded on a chart recorder. From this information the surface charge density was then calculated. A sample calculation appears in Appendix B.

4. Particle Size Analysis

The diameters of the polymer particles were measured electronically from TEM photographs using the Zeiss MOP-3 analyzing system (Carl Zeiss, Inc.).

III. RESULTS AND DISCUSSION

A. The Existence of a Background Polymerization Rate in Emulsion

As mentioned in the introduction, the failure of the "control" experiment on the first flight of the MLR experiment on the Space Shuttle, provided the impetus for this study of the submicron particle seeded emulsion polymerization of styrene. Figure 8 shows a conversion-time curve for the Shuttle (STS-3) control experiment. What this figure illustrates is that not only did the sample begin polymerizing before it was heated to the 70°C reaction temperature, but also that the conversion for this recipe was essentially 100% prior to the 70°C period. This horizontal conversion-time curve indicates that there was no volume contraction due to polymerization. These results were quite unexpected since the decomposition rate of potassium persulfate at room temperature ($k_d = 6.6 \times 10^{-9}$ sec^{-1}) was considered too low to initiate polymerization. Since the possibility existed that the reactors had experienced a relatively high (35°C) ambient temperature while in the orbiter prior to launch, work was begun to determine the cause for the premature polymerization.
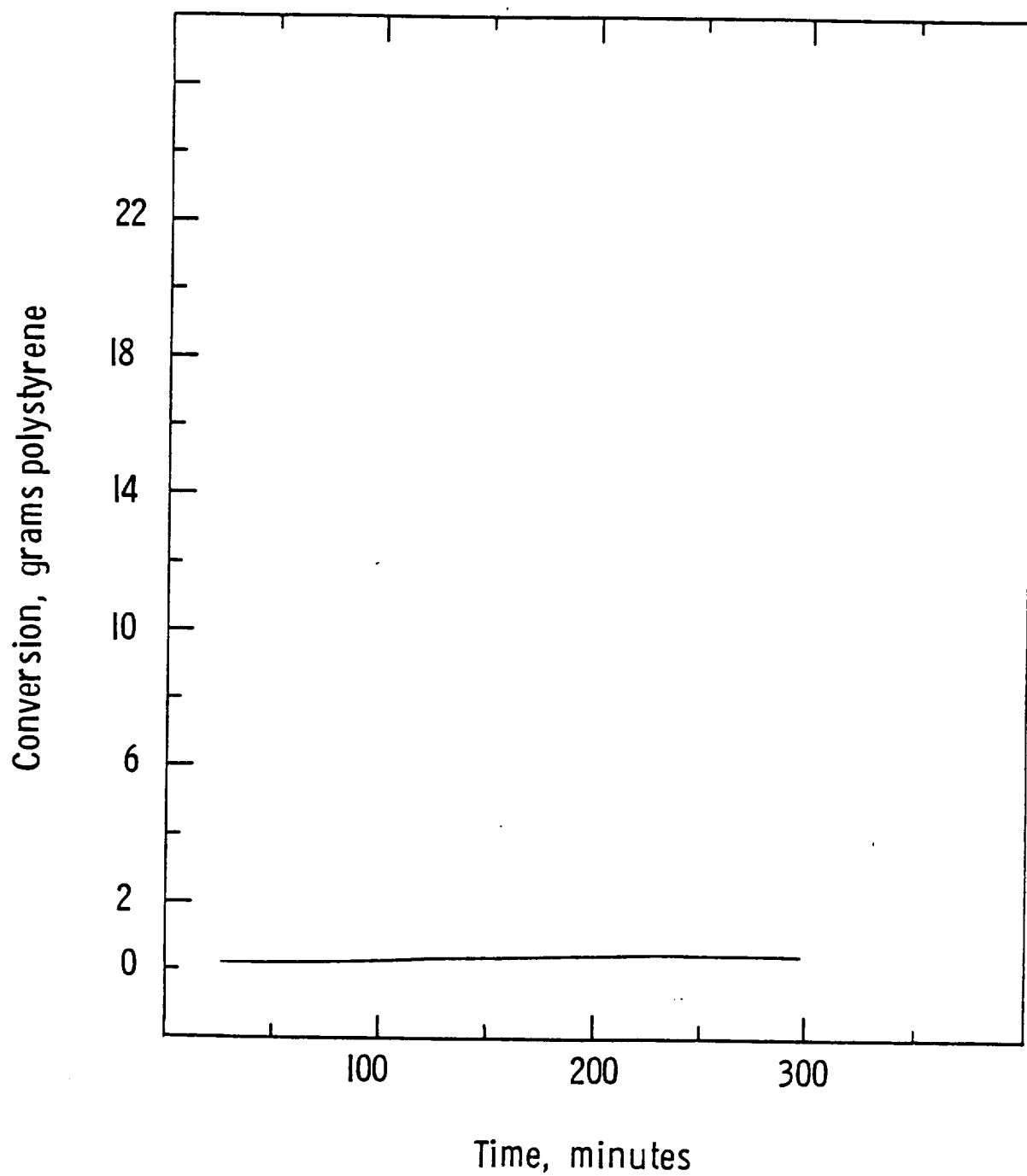
Figure 8. Conversion versus time curve for the 70°C poly-
merization of the STS-3 control experiment.

In order to examine the role the initiator played in the polymerization of the control recipe prior to heat-up, a similar recipe was devised which differed only in that it contained neither initiator nor buffer. Table I lists the weight fractions of the recipe components for the flight control recipe (STS-3 Control) and the recipe containing no initiator or buffer (CON-1). The CON-1 recipe was mixed and then loaded in the LUMLR according to the procedure described in sections III B and III C. The loaded reactor was then allowed to sit with no stirring at an average room temperature of 21°C. The data were recorded automatically on a data cassette tape. Figure 9 shows the conversion time history for the room temperature polymerization of styrene-swollen polystyrene latex in the absence of initiator. These data reveal that even at the relatively low temperature of 21°C, polymerization begins after only 5 hours. The rate of polymerization can be calculated from conversion-time data by measuring the slope of the line passing through the data. By calculating the slope of the conversion-time curve in the constant rate period (i.e. the straight line portion of the curve), a value of 0.56% conversion/hour was obtained for the rate of reaction. It was conjectured that this observed polymerization was due strictly to the thermal polymerization of styrene in the polymer

41

TABLE I

COMPARISON OF STS-3 CONTROL RECIPE AND RECIPE

CONTAINING NO INITIATOR

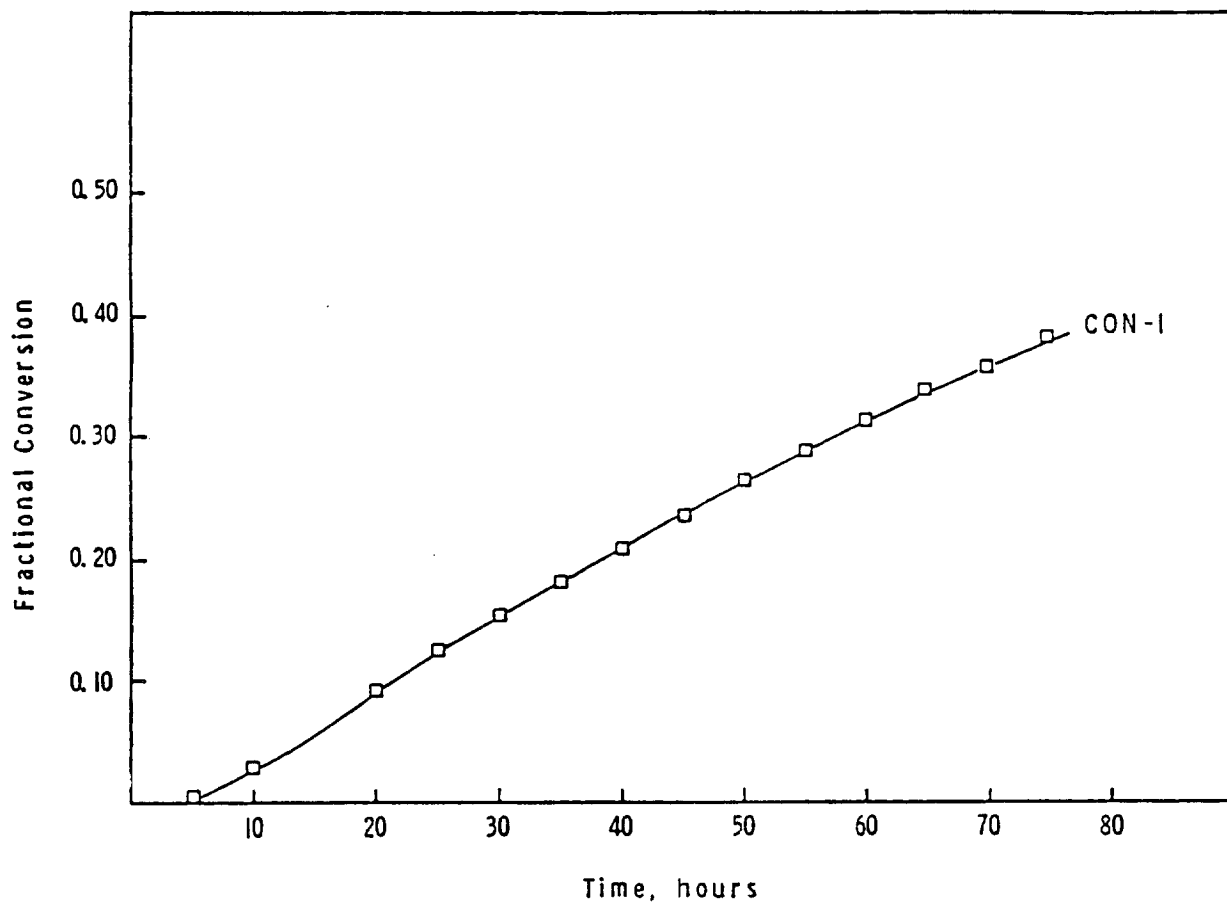|	STS-3 Control	CON-1
0.19μm PS seed	0.100 wt. fraction	0.100 wt. fraction
Styrene monomer	0.200	0.200
Water	0.699	0.699
Aerosol MA-80 Emulsifier	0.00062	0.00062
Potassium Persulfate Initiator	0.000189	-------
Sodium Bicarbonate Buffer	0.000189	-------

Figure 9. Conversion-time history for the seeded emulsion polymerization of styrene at 21°C in the absence of initiator.

particles. However, the value for the rate of bulk polymerization of styrene at 20°C as reported in the literature, is only 0.20% conversion/hour.[6] Because the experimentally measured polymerization rate differed greatly from the bulk polymerization rate of styrene cited in the literature, it was thought that perhaps the stainless steel of the reactor either catalyzed the production of, or otherwise provided, the free radicals which initiated the polymerization. Therefore, an identical recipe was formulated and loaded into a conventional glass dilatometer, in order to determine the effect of stainless steel on the observed polymerization rate. A diagram of the glass dilatometer is shown in Figure 10. For the first trial of the glass dilatometer, no stirring was used since none was used for the polymerization in the LUMLR. The dilatometer was loaded with approximately 60 grams of swollen latex while taking care not to include any air bubbles in the glass bulb for the reason described earlier (see section III-A). A blanket of nitrogen gas was introduced into the capillary and the height of the liquid in the capillary was recorded as a function of time. Since this was to be a room temperature polymerization, no constant temperature bath was employed. The conversion-time data for the room temperature seeded emulsion polymerization of styrene in a glass

44

To nitrogen cylinder

2 mm I.D. capillary with 50 cm scale
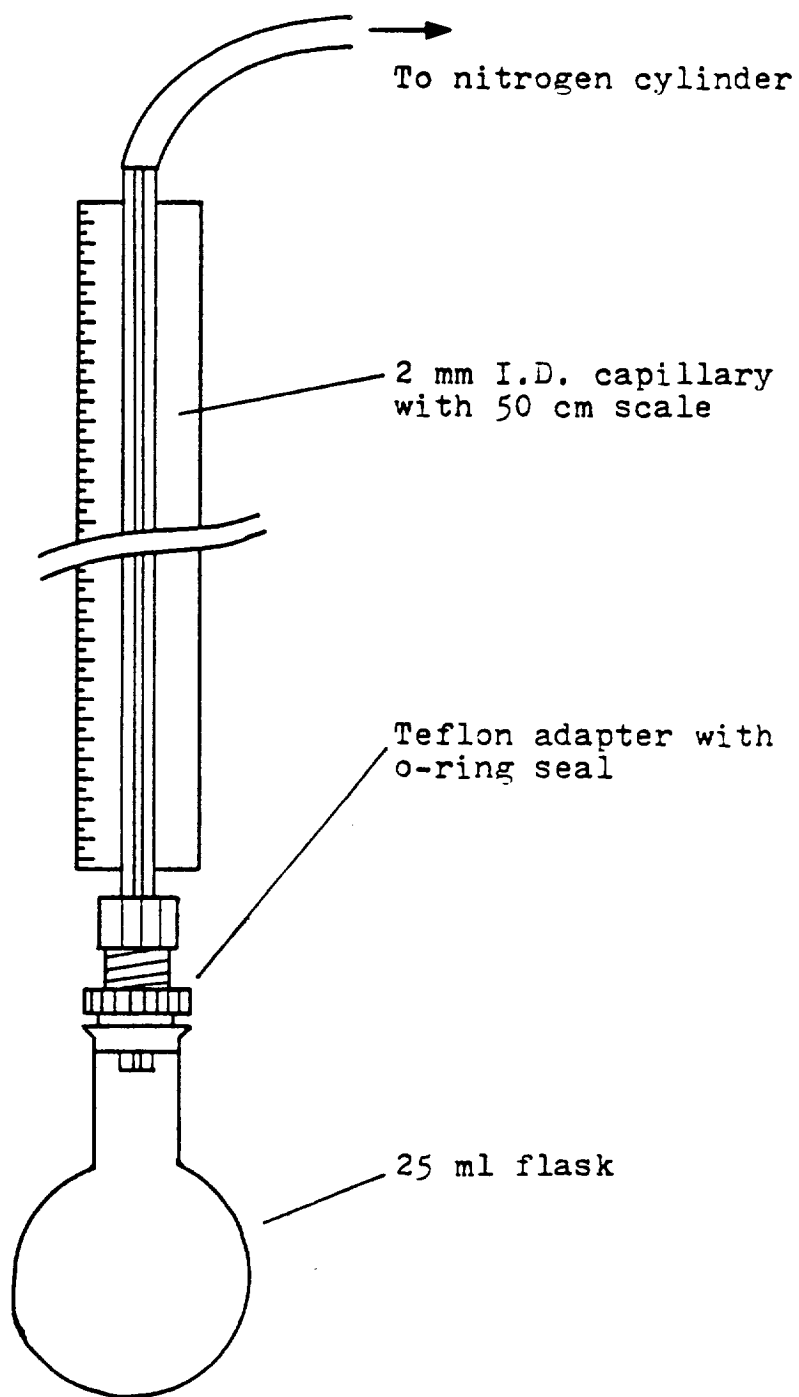
Teflon adapter with o-ring seal

25 ml flask

Figure 10. Diagram of a conventional glass dilatometer.

dilatometer appear in Figure 11. These data (CON-1D) are plotted along with the data obtained in the LUMLR. The presence of a 25 hour induction period for the polymerization run in the glass dilatometer may have resulted from an incomplete nitrogen purge of the capillary, thus allowing oxygen gas to inhibit the reaction. Indeed, it was the existence of this induction period which caused the final conversions of the two latexes to differ somewhat. However, the shapes of the curves are similar and, in fact, in the constant rate period the calculated rate is 0.55% conversion/hour for the polymerization in the glass dilatometer. That the rates seem to be nearly identical in both the LUMLR and in the conventional glass dilatometer, seems to indicate that the observed polymerization in the absence of initiator in the LUMLR is not due to some effect associated with the stainless steel. Since the polymerization is not due to some external factor such as reactor material, and it occurs even in the absence of initiator, what is actually being observed is the "background" thermal polymerization of styrene in the swollen polymer particles.

In order to ascertain whether this background polymerization rate could be eliminated, a recipe identical to CON-1 was prepared and to this recipe was added 0.0480 g of hydroquinone (240 ppm based on total
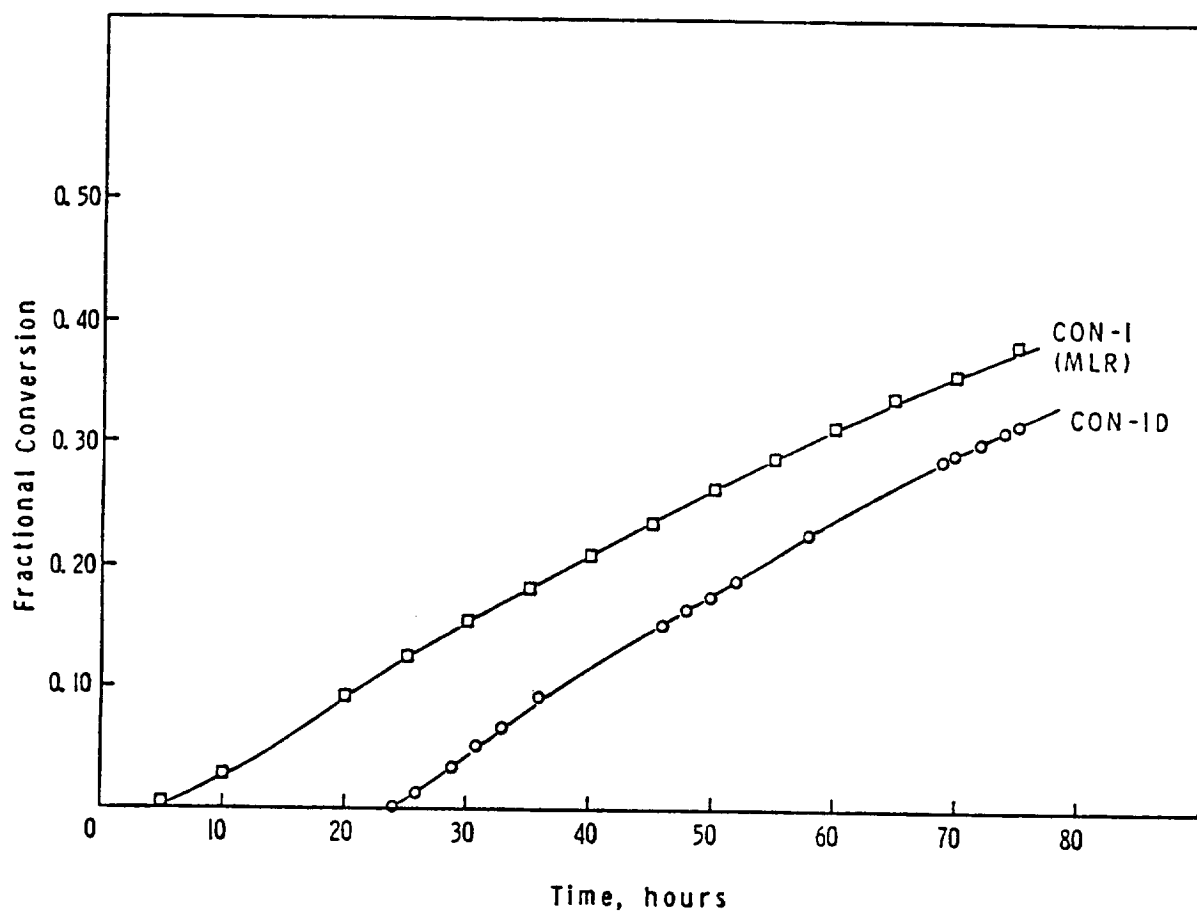
Figure 11. Conversion due to thermal polymerization at room temperature in the absence of initiator of a recipe loaded in the LUMLR(□) and in a glass dilatometer(o).

recipe). Hydroquinone is often used to shortstop or prevent polymerization for both bulk and emulsion systems. The volume of the reactants as a function of time was monitored in the LUMLR. After 96 hours at room temperature (21°C) there was no conversion of monomer to polymer. This was confirmed by a parallel experiment run in the glass dilatometer. After the four day period at room temperature, the reactor was heated to 70°C and the volume again monitored as a function of time. The conversion-time history for this recipe is shown in Figure 12. The existence of a 1200 minute induction period at 70°C indicates that the hydroquinone was effective in neutralizing any free radicals that may have been generated. However, after the 1200 minute period during which no polymerization occurred, the reaction then proceeded at a rate of 1.36% conversion/hour in the constant rate period. Figure 13 shows a semi-logarithmic plot of the polymerization rate in moles polymer formed/second as a function of the weight fraction of polymer present based on the oil phase. This plot illustrates the initial constant rate period and the subsequent decrease in the polymerization rate at higher conversion. The fact that the polymerization rate at 70°C was more than twice the rate observed at 21°C, proves that the background polymerization in emulsion is due to some thermal, free
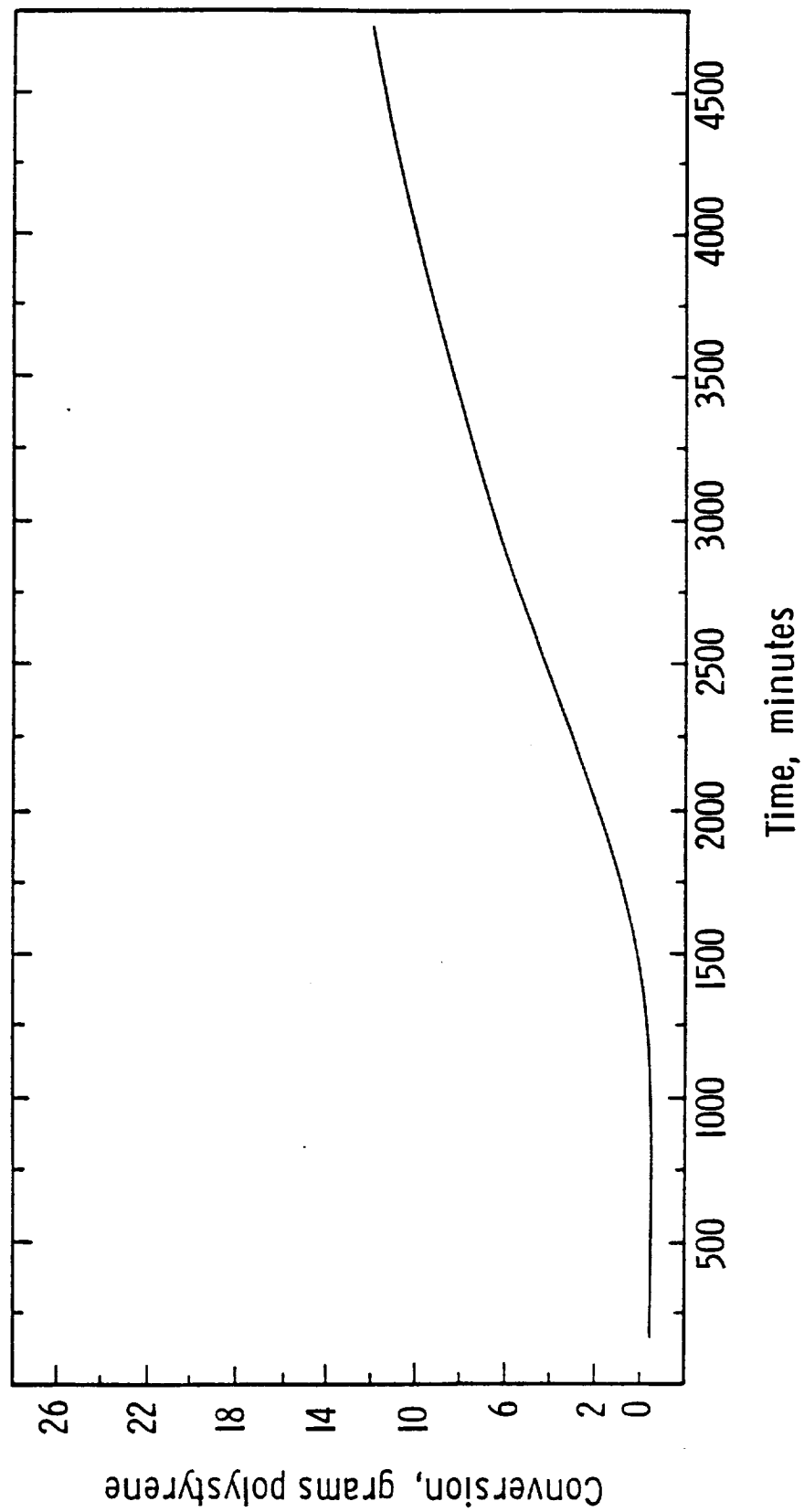
48

Figure 12. The conversion-time history for a recipe containing no initiator and 240 ppm of hydroquinone polymerized at 70°C in the LUMLR.
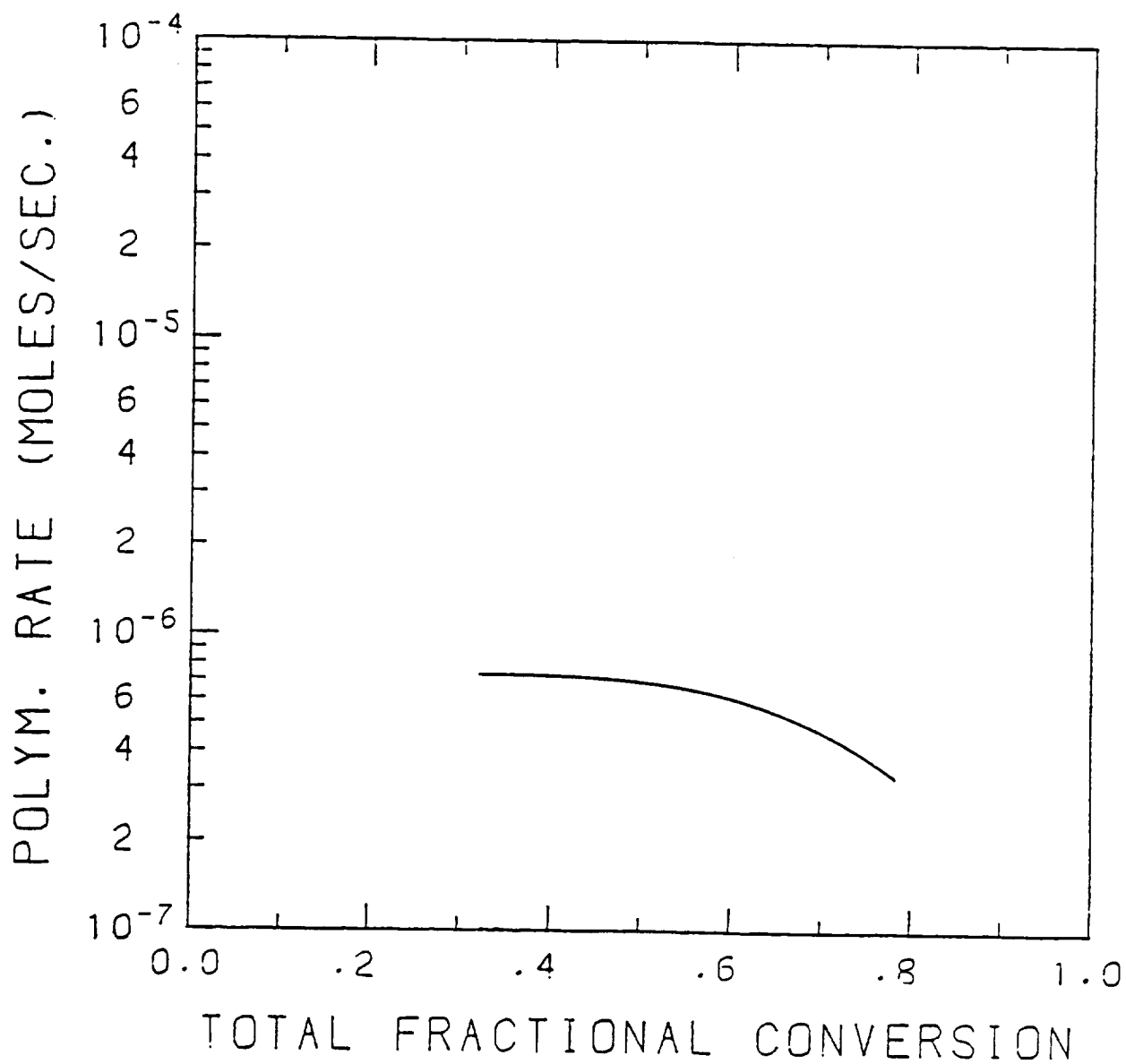
Figure 13. The polymerization rate at 70°C as a function of the weight fraction of polymer for a recipe containing no initiator and 240 ppm hydroquinone.

radical generating mechanism. Since the rate of poly-
merization in emulsion is much greater than the rate
observed for the bulk polymerization of styrene at the
same temperature, it appears that the two phenomena are
the result of two different mechanisms. The results
imply that the observed rate in emulsion is due to the
thermal generation of radicals in the aqueous phase,
the degree of subdivision (or compartmentalization) of
the system, or a combination of the two factors.

With a knowledge of the rate of polymerization,
equation (1) can be rearranged and solved for $\bar{n}$ the
average number of free radicals per particle. As
discussed previously (section II), styrene is
generallly assumed to follow Smith-Ewart case 2 kine-
tics. For this case, $\bar{n}$, is assumed to equal $\frac{1}{2}$; that
is, on the average, the particles are polymerizing half
of the time during a particular time interval. As
larger particle size is reached, frequently $\bar{n}$ will be
greater than $\frac{1}{2}$, since the bimolecular termination reac-
tion is no longer instantaneous and each particle can
accomodate more than one free radical at a particular
instant in time. One would expect to observe a steady
state value of $\bar{n} < \frac{1}{2}$ only when particle size is very
small and initiator concentration is low. It was
therefore surprising to find that the room temperature
seeded emulsion polymerization of styrene in the

51

absence of initiator yielded a steady state value of $\bar{n}$ = 0.21 (i.e. case I kinetics). Figure 14 shows a plot of $\bar{n}$ versus time. The scatter in the data is a numerical artifact of differentiating the conversion-time curve to obtain values for the instantaneous rate of polymerization. By fitting a straight line to the data however, a horizontal line, corresponding to a value for $\bar{n}$ equal to 0.21, is obtained. This steady state value for $\bar{n}$, indicates that there is significant free radical desorption occurring. This can occur by the transfer of free radical activity to a monomer molecule (and thereby terminating a growing chain), with subsequent desorption of the monomeric free radical into the aqueous phase[4,8,9]. Other workers have also reported a steady state value of $\bar{n} < \frac{1}{2}$ in the emulsion polymerization of styrene[10,11]. Thus, the initiator-free seeded emulsion polymerization of styrene using 0.19 μm diameter seed particles can be said to follow Smith-Ewart case I kinetics in which a steady state rate of polymerization is obtained at both room temperature and 70°C. The observed polymerization seems to be the emulsion polymerization equivalent of the thermally induced bulk polymerization of styrene. This background polymerization can be inhibited for at least four days at room temperature by the addition of 240 ppm of hydroquinone. As is the case with initiator-
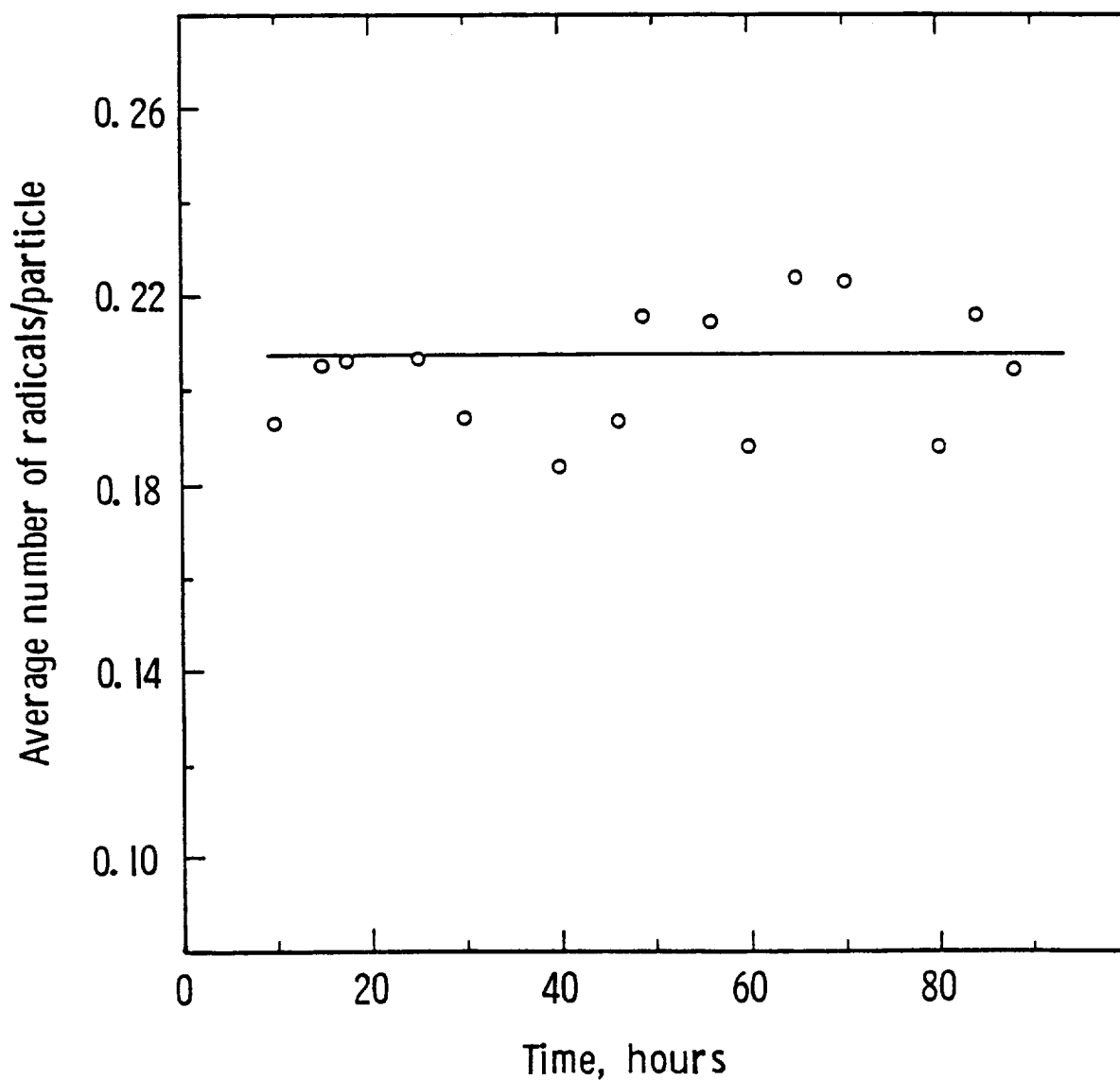
Figure 14.   Plot of average number of free radicals per
             particle(n̄) as a function of time for the room
             temperature seeded emulsion polymerization of
             styrene in the absence of initiator showing
             Smith-Ewart case 1 behavior.

53   C-9

containing polymerizations, the background polymerization rate is a function of the temperature, indicating that the production of free radicals during the background polymerization is a thermally induced process.

B. The Effect of Variation of Hydroquinone Concentration on Polymerization Rate

The results of recipes CON-1 and CON-2 indicated that not only would polymerization occur in a seeded emulsion system in the absence of initiator, but that this thermal polymerization could be inhibited for several days with the addition of hydroquinone. Thus, the kinetics of hydroquinone-containing polymerizations were studied in order to gain some understanding of how the inhibitor affected the polymerization, and also to determine whether a hydroquinone-containing recipe could satisfy the criteria for a control experiment aboard the Space Shuttle.

The ability of hydroquinone to inhibit or shortstop polymerizations has been well documented in the literature[6,9,12,13], and for this reason it was chosen for these experiments. Recipes were formulated containing varying amounts of hydroquinone and the recipes were evaluated in terms of the length of the observed induction period at room temperature, and the measured poly-

merization rate at 70°C relative to a recipe containing no inhibitor. The amount of styrene inbibed by the polystyrene seed was determined by the isooctane extraction technique described earlier. Table II lists the different concentrations of hydroquinone used in these experiments and also lists the weight fraction of polystyrene and styrene in each recipe as determined by extraction with isooctane. All of the recipes contained 0.5 mM of potassium persulfate initiator, based on the aqueous phase, and also contained enough Aerosol MA-80 to cover 8% of the fully converted particle surface.

The initial hydroquinone concentration used in recipe CON-3, 6 ppm, was designed to yield a two hour induction period at 70°C. This hydroquinone concentration was calculated based on the known decomposition rate of potassium persulfate at 70°C and with the assumption that each hydroquinone molecule could neutralize two sulfate ion radicals produced by the decomposition of initiator. After degassing, the recipe was polymerized in the LUMLR at 70°C. Figure 15 shows the conversion-time history for the inhibitor-containing recipe (CON-3) plotted on the same axis as another persulfate-initiated polymerization (SS5-1). Recipe SS5-1 differed from CON-3 in that it contained 50% less emulsifier and also contained no inhibitor.

55

TABLE II

RECIPE VARIABLES FOR INHIBITOR-CONTAINING FORMULATIONS

Recipe Designation	Initial Hydroquinone Concentration (ppm)	Weight Fraction Polystyrene	Weight Fraction Styrene
CON-3	6.0	.100	.193
CON-4	6.0	.101	.190
CON-5	0.0	.100	.199
CON-6	0.51	.100	.200
CON-7	2.3	.100	.200
CON-8	3.5	.100	.200
CON-10	25.0	.102	.181
CON-11	25.0	.101	.187
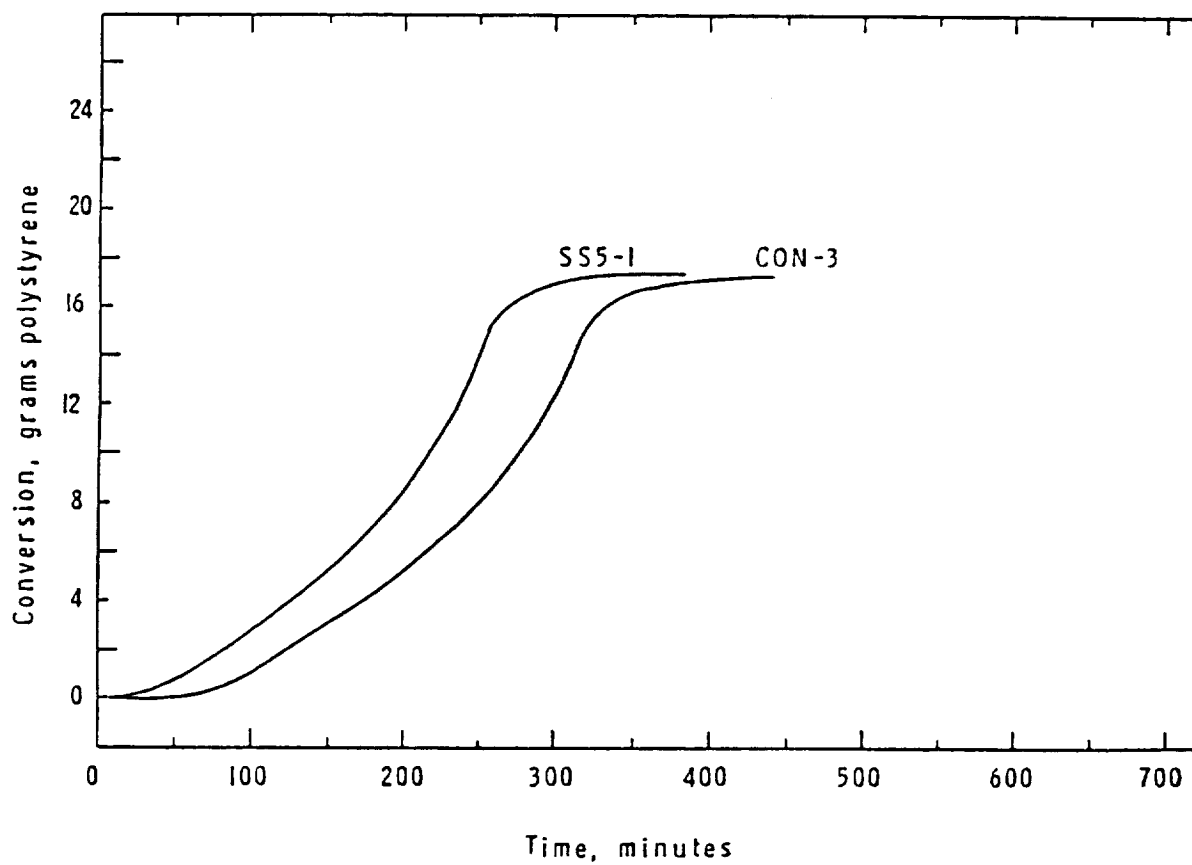
Figure 15. Conversion-time histories for a recipe containing no inhibitor(SS5-1) and one containing 6 ppm hydroquinone(CON-3).

The conversion-time curves for the two recipes appear to be nearly identical in shape, with the only difference being the existence of an induction period for the recipe containing hydroquinone. From these results it appeared that hydroquinone would not cause any retardation of the polymerization rate.

Although the recipe was designed to yield a two hour induction period at 70°C, the observed length of the induction period was only 70 minutes. This was characteristic of all polymerizations containing hydroquinone. The observed induction period was always shorter than the expected induction period, even at low temperatures. For this reason, a recipe identical to CON-3 was tested to determine whether it could prevent polymerization for four days at room temperature. Once it was confirmed that 6 ppm of hydroquinone could indeed prevent polymerization at room temperature for nearly five days, this recipe (CON-4) was then heated to the 70°C reaction temperature and the obtained kinetics were then compared to the results obtained when a delay at room temperature was not incorporated into the test (CON-3). These results are presented in Figure 16. The observed induction period for CON-4 was shorter than that observed with CON-3 because more hydroquinone was neutralized, or "used up", during the five day delay at room temperature. Another difference
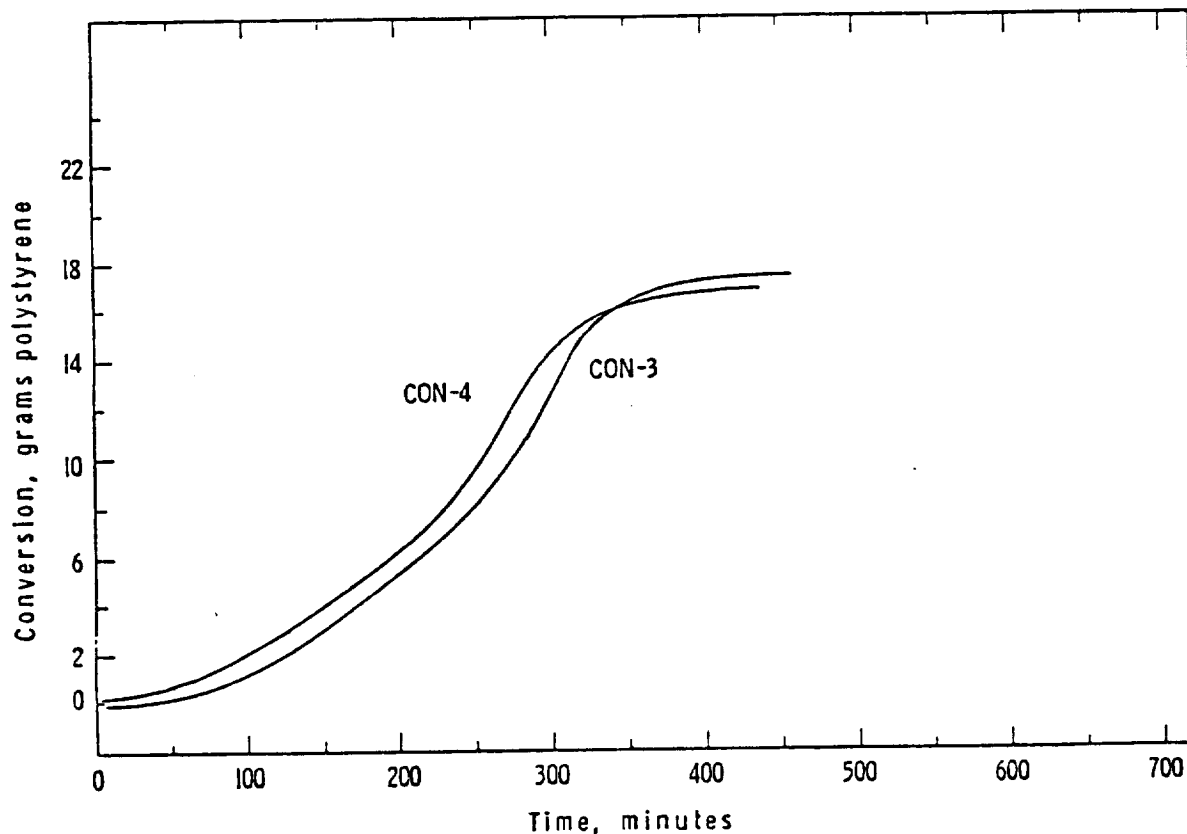
Figure 16. Conversion-time histories for a polystyrene/styrene seeded emulsion polymerization recipe initiated by potassium persulfate and containing 6 ppm hydroquinone. CON-3 was polymerized at 70°C, while CON-4 was run at 21°C for 5 days and then heated to 70°C.

apparent in the two conversion-time histories is the slight retardation of the initial polymerization rate exhibited by CON-4. This retardation was attributed to the presence of a large excess of hydroquinone at the start of the 70°C period. A series of room temperature polymerizations were run in order to minimize the amount of excess hydroquinone present at the end of a four day period at room temperature. In addition, a recipe (CON-5) which contained no inhibitor but was otherwise identical to the inhibitor-containing recipes, was run in order to serve as a qualitative measure of the amount of retardation of polymerization rate caused by hydroquinone. Figure 17 shows conversion-time histories for a 70°C polymerization of a recipe containing 6ppm hydroquinone (CON-4), and an identical recipe containing no inhibitor (CON-5). Although the two curves are similar, the polymerization rates for the two recipes are different, albeit difficult to compare on a conversion-time plot. Figure 18 better illustrates the differences in polymerization rate for CON-4 and CON-5 at various conversions. The log of the polymerization rate is plotted as a function of the weight fraction of polymer based on the oil phase. It is apparent that the recipe containing hydroquinone has both a lower initial and final polymerization rate when compared to the rate of polymerization for a recipe
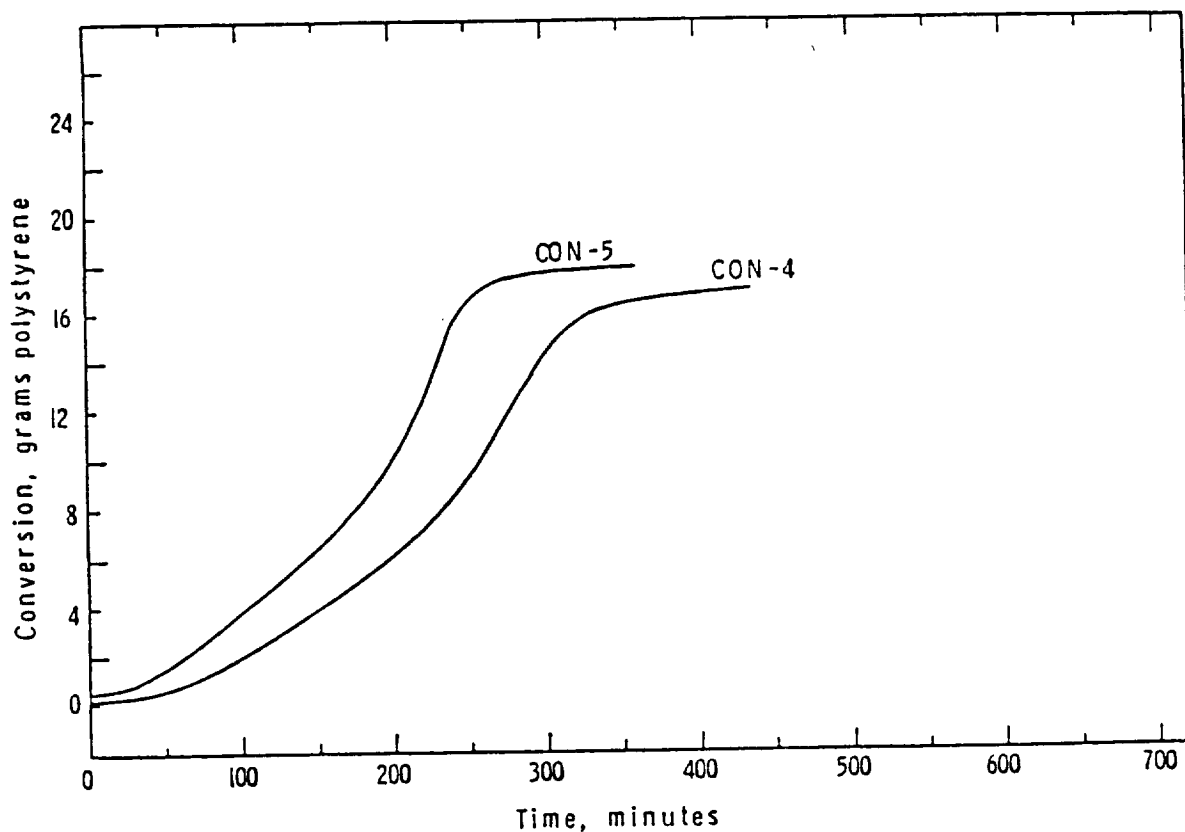
60

Figure 17. Conversion-time histories for a recipe containing 6 ppm hydroquinone(CON-4) and an identical recipe containing no inhibitor(CON-5) in a polystyrene/-styrene seeded system initiated by potassium persulfate at 70°C.
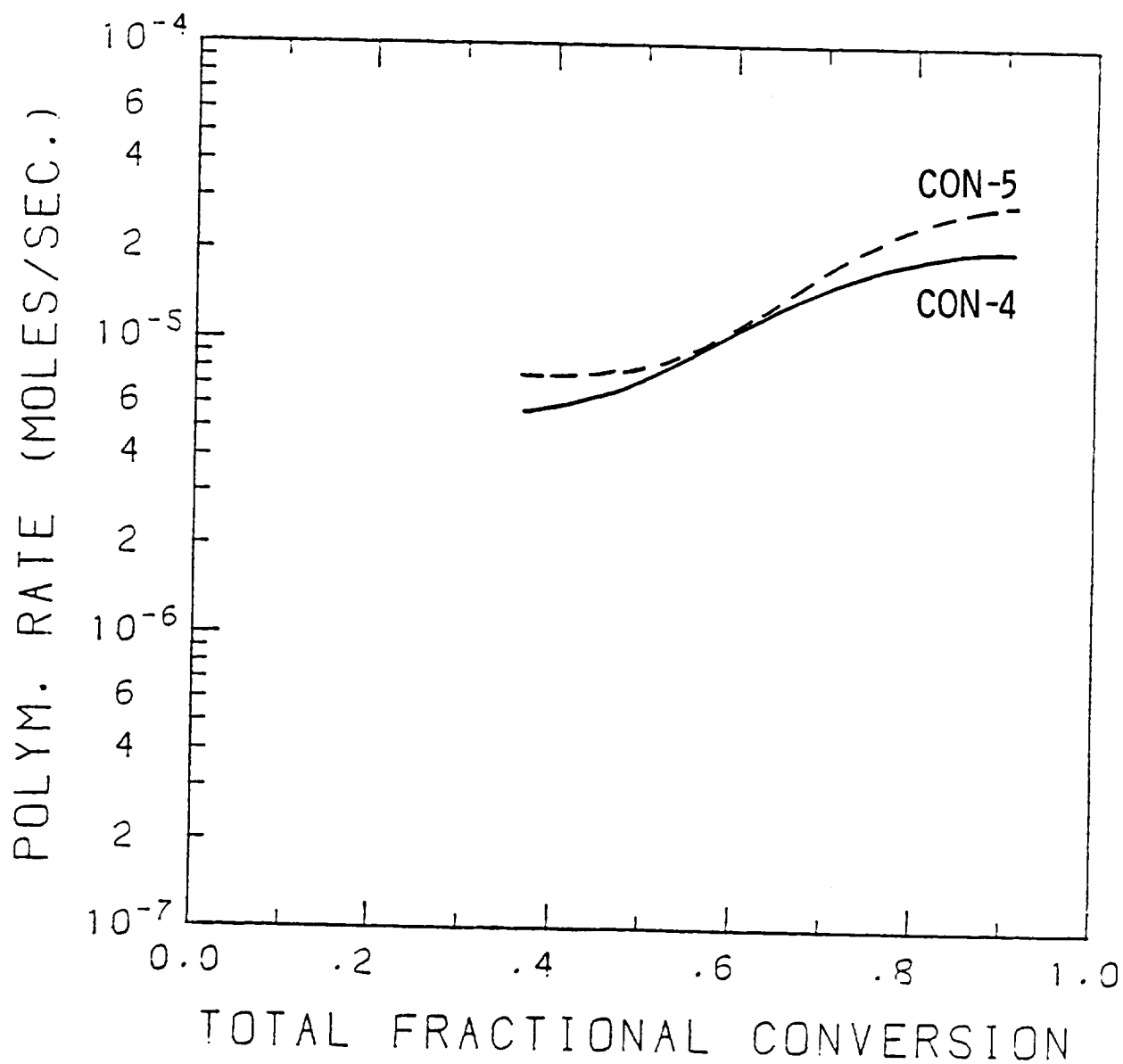
61

Figure 18. The variation in polymerization rate at 70°C for a recipe containing 6 ppm hydroquinone(CON-4) and an identical recipe containing no inhibitor (CON-5).

with no inhibitor. Thus, although hydroquinone is considered an inhibitor, there is evidence that it behaves more like a retarder than an inhibitor. Confirmation of the retardation of polymerization by hydroquinone was obtained in room temperature polymerizations of recipes containing different initial amounts of hydroquinone. Conversion-time data were obtained for a recipe containing 0.5 ppm hydroquinone (CON-6) and one containing 2.3 ppm hydroquinone (CON-7), in the LUMLR at room temperature. The polymerization rate as a function of the total fractional conversion was calculated and the initial rates plotted in Figure 19. The plot of log polymerization rate versus total fractional conversion shows that the initial rate of reaction at 21°C is dependent on the initial hydroquinone concentration. The recipe containing 2.3 ppm of hydroquinone has a lower initial polymerization rate than the recipe containing 0.5 ppm of hydroquinone. This fact indicates that not only does hydroquinone cause retardation of the polymerization rate, but that the degree of retardation is dependent on the initial concentration of hydroquinone in the recipe.

The duration of the observed induction period at 21°C was studied as a function of initial hydroquinone concentration. Table III lists the initial hydroquinone concentration and the observed length of the
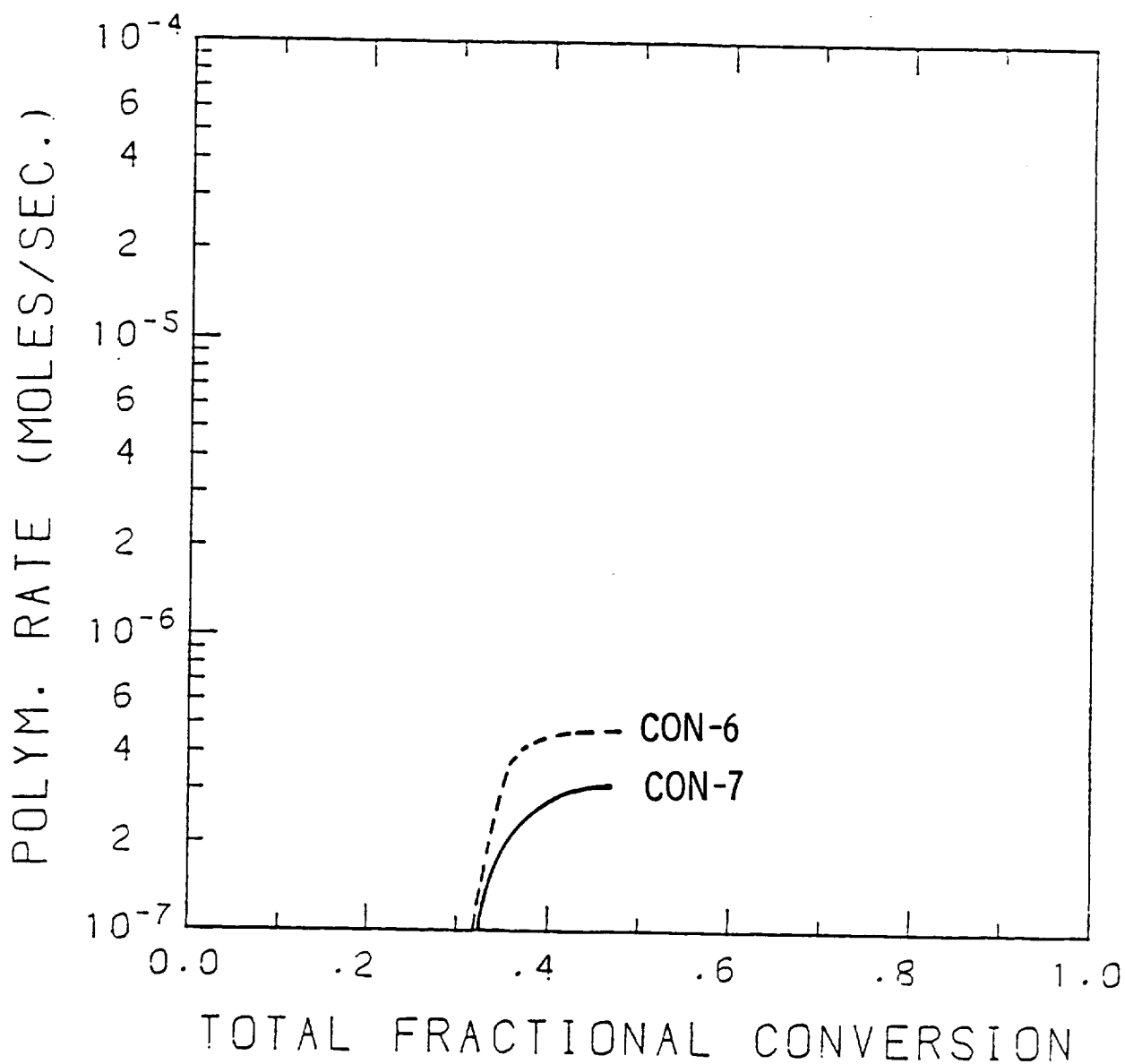
Figure 19. The effect of initial hydroquinone concentration
on the initial rate of a room temperature
polystyrene/styrene seeded emulsion polymerization.

TABLE III

INITIAL HYDROQUINONE CONCENTRATIONS AND MEASURED LENGTH

OF INDUCTION PERIODS AT 21°C

Recipe Designation	Initial Hydroquinone Concentration (ppm)	Initial Initiator Concentration (m$\underline{M}$)	Observed Induction Period (hours)
CON-1	0.0	0.0	8.3
CON-3	6.0	0.5	120.0
CON-6	0.51	0.5	35.0
CON-7	2.3	0.5	70.8
CON-8	3.5	0.5	98.0
GR-4	0.0	1.0	24.0
LUMLR-4A	0.0	1.0	24.0
LUMLR-4B	0.0	1.0	25.0

induction period for several recipes. Three recipes
(GR-4, LUMLR-4A, LUMLR-4B) contained no inhibitor but
1.0 mM potassium persulfate. These three recipes
yielded induction periods lasting about 24 hours at
room temperature. This is illustrated in Figure 20.
The LVDT voltage, which is proportional to conversion,
is plotted on the ordinate and time in hours is plotted
on the abscissa. These experiments show that in the
absence of inhibitor, an induction period lasting
approximately 24 hours is nevertheless observed. This
result was attributed to the presence of residual oxy-
gen in the recipe which was not removed by the
degassing procedure. The inhibiting power of oxygen
has been cited in the literature[6,10,14]. To estimate
the amount of oxygen gas remaining in a recipe after
degassing at 20 mmHg, a Henry's Law calculation was
made which gave an approximate value for the solubility
of oxygen gas in water at room temperatue and 20 mmHg
pressure. This calculation appears in Appendix C. The
estimated amount of oxygen gas in the latex after
degassing is 4.4×10^{-6} moles O_2/175 g recipe which is
a small amount but on the same order as the hydro-
quinone concentrations used (ca. $1 - 5 \times 10^{-6}$ moles/175 g recipe). Thus, the assumption that
the observed 24 hour induction period in a room tem-
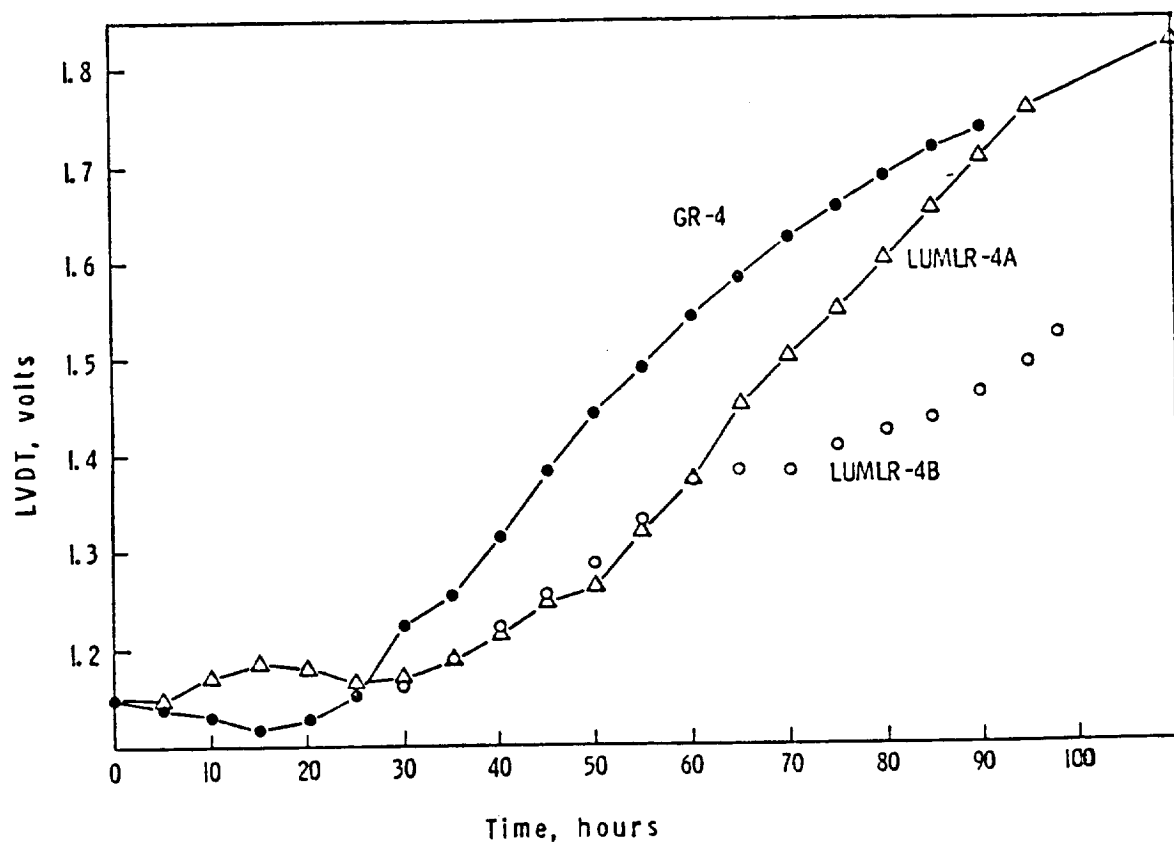perature polymerization is due to residual oxygen

66

Figure 20. Conversion-time curves for the persulfate-initiated polystyrene/styrene seeded emulsion polymerization system without inhibitor showing a 25 hour induction period at room temperature.

appears to be a valid one.

The observed induction period was plotted as a
function of the initial hydroquinone concentration and
appears in Figure 21. The data are fitted well by a
straight line, indicating that the observed induction
period is linearly dependent on the initial hydro-
quinone concentration. Initially, this linear depen-
dence of induction period on hydroquinone concentration
was surprising. However, an examination of the litera-
ture revealed that Tudos[15] had derived a theoretical
expression for the variation of induction period with
inhibitor concentration for the bulk polymerization of
styrene. Tudos used several assumptions to simplify
the equation to the following form:

$$t_i = \frac{2z_o}{k_i m_o^2}$$

where t_i = length of induction period

z_o = initial inhibitor concentration

k_i = rate constant for radical production

m_o = initial monomer concentration

This equation predicted a linear dependence of induc-
tion period on initial inhibitor concentration for the
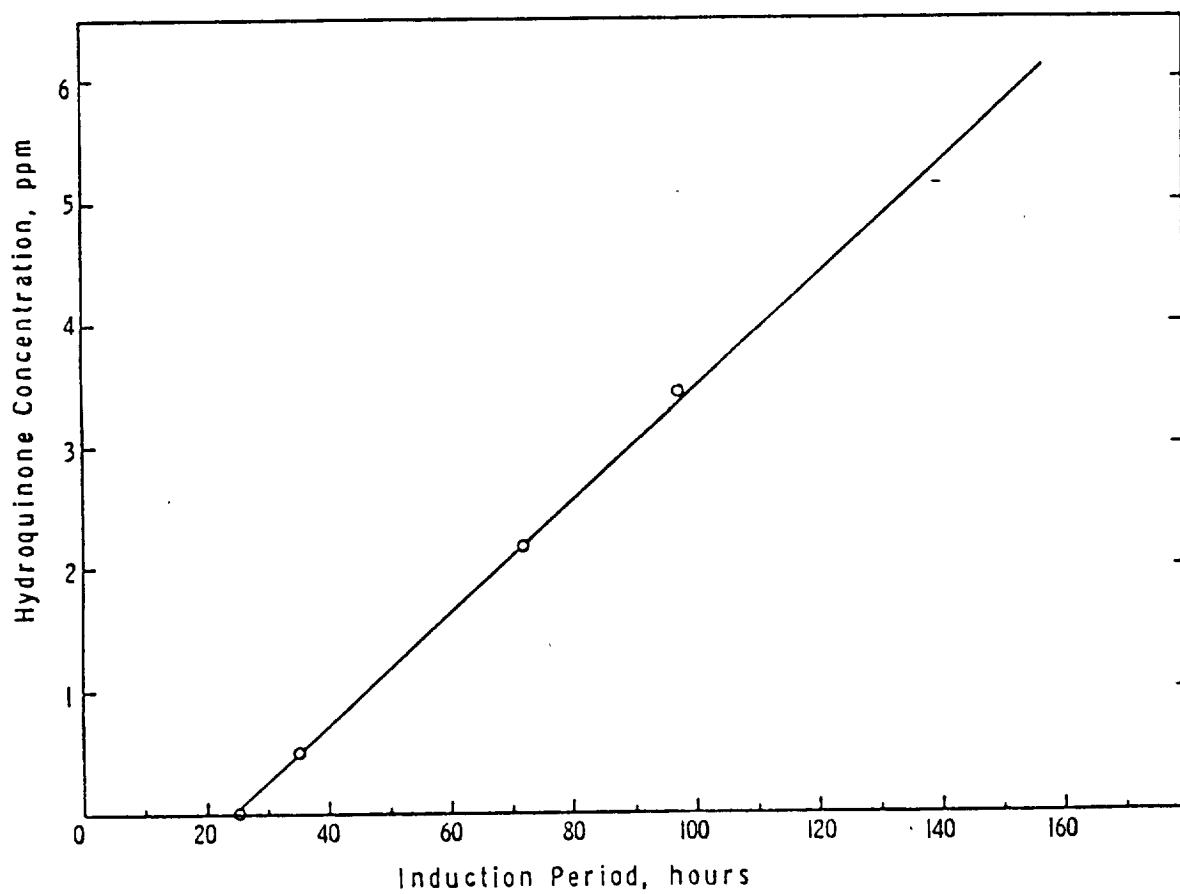low temperature bulk polymerization of styrene.

68

Figure 21. Plot of inhibitor concentration versus observed
induction period at room temperature.

Furthermore, he reasoned that this linear relationship indicated that there were no side reactions (e.g. copolymerization of the styrene and inhibitor) occurring at low temperatures. Foord[16] found that the benzoquinone-inhibited thermal (i.e. no initiator) bulk polymerization of styrene at higher temperatures also yielded a linear dependence of induction period on initial benzoquinone concentration. Melville and Watson[17] however, found a slower increase in induction period than predicted by Foord, and this was attributed to copolymerization of the inhibitor with the styrene. Figure 22 shows a comparison of the expected and observed induction periods at room temperature for various concentrations of hydroquinone and a constant initiator concentration of 0.5 m$\underline{M}$. The expected induction period was calculated based on the known decomposition rate of initiator at room temperature, and on the assumption that each inhibitor molecule neutralized two sulfate ion radicals. The observed induction periods were extracted from rate data acquired during room temperature polymerizations. There is a marked difference between the expected and the observed results. By comparing the slopes of the two curves, the observed efficiency of inhibition was calculated to be only 1.8%. This exceedingly low effectiveness of the hydroquinone, coupled with the observation that the length of the
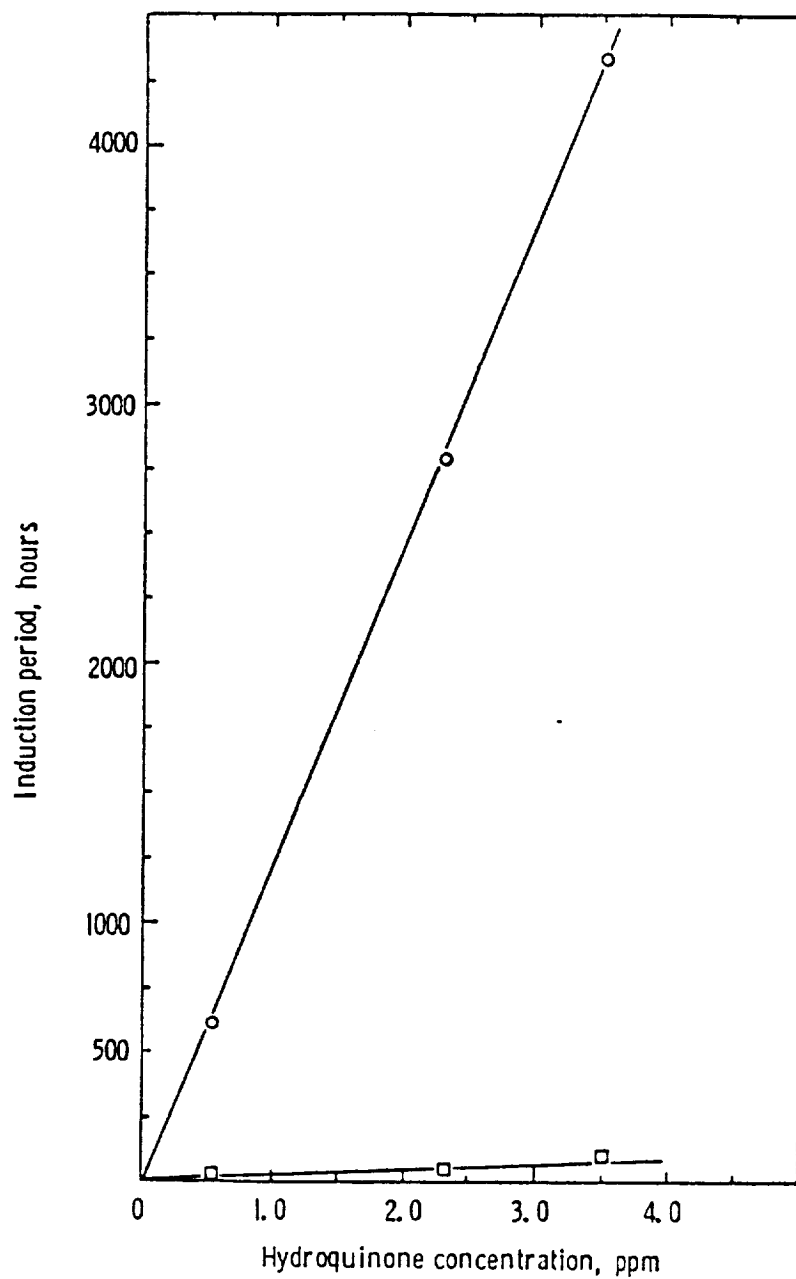
70

Figure 22. Comparison of expected(o) and observed(□) induction periods at room temperature.

induction period was zero-order with respect to initial concentration of hydroquinone, suggested that the inhibition observed was caused by an impurity (such as benzoquinone) in the hyroquinone sample, and that the hydroquinone itself was inactive. Blackley[9] and Odian[6] both found hyroquinone was an inhibitor only in the presence of oxygen, and that the inhibition observed was due to the oxidation of hydroquinone to benzoquinone. Thus, the hydroquinone sample was tested for the presence of an impurity which was believed to be present in amount of 1.8% based upon weight. The hydroquinone was analyzed using IR spectroscopy, UV absorbance, and proton NMR. The IR spectrogram was inconclusive, but the UV absorbance did not show the presence of any benzoquinone. As a more sensitive test, the hydroquinone was next analyzed using proton NMR. The sample was dissolved in deuterated DMSO, placed in a sample tube, and then analyzed. The resulting spectrum is shown in Figure 23. The only peaks detected were due to the hydroquinone, the hydroxyl groups on the hydroquinone, water due to atmospheric moisture, and the DMSO solvent. As a comparison, benzoquinone was also analyzed after dissolving it in d-DMSO. The resulting spectrum, shown in Figure 24, exhibits only a single main peak which implies that no impurities exist in the benzoquinone
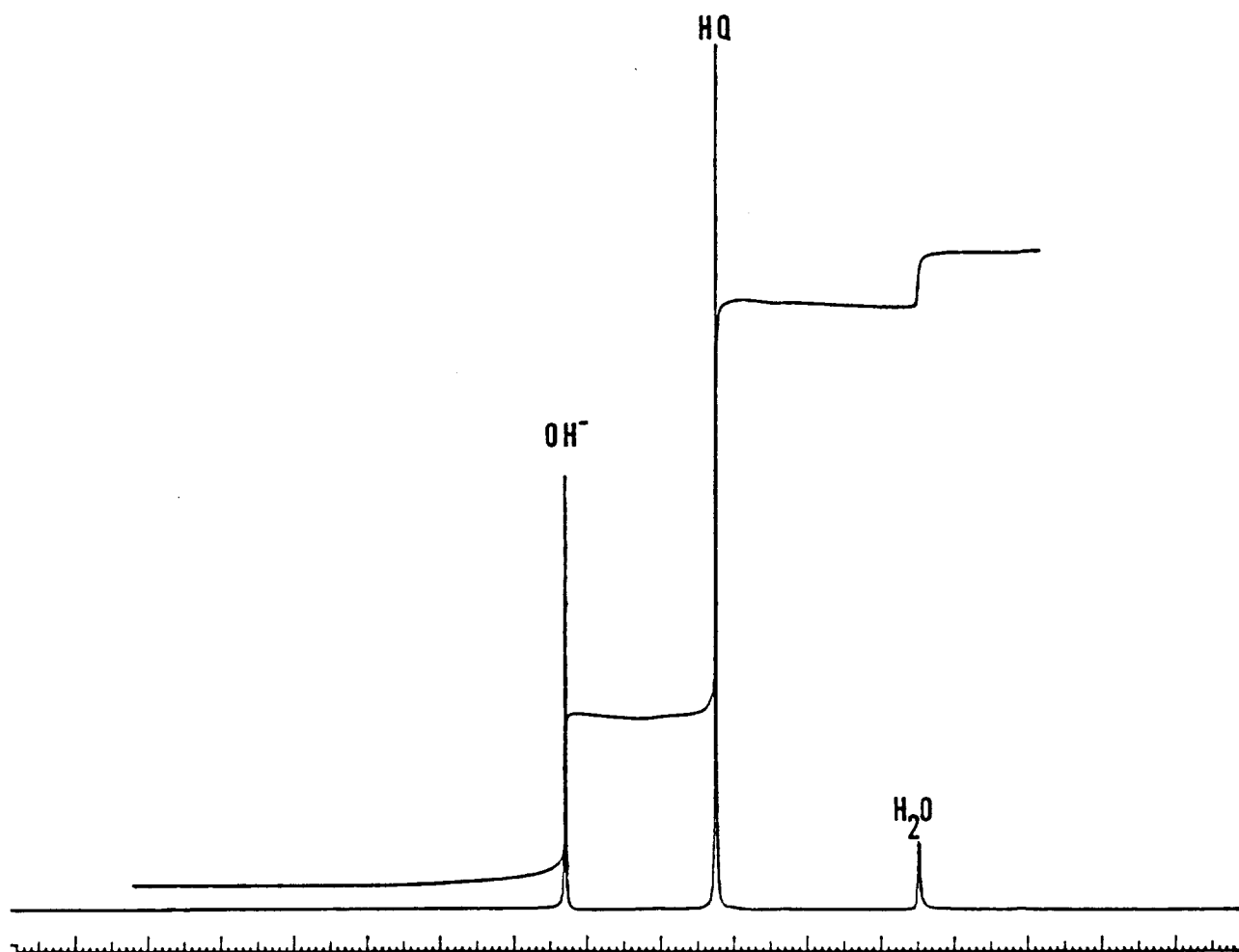
72

Figure 23. Proton NMR spectrum of a hydroquinone sample dissolved in d-DMSO showing the resonance peaks due to hydroquinone(HQ), hydroxyl ions(OH⁻), and water(H_2O).
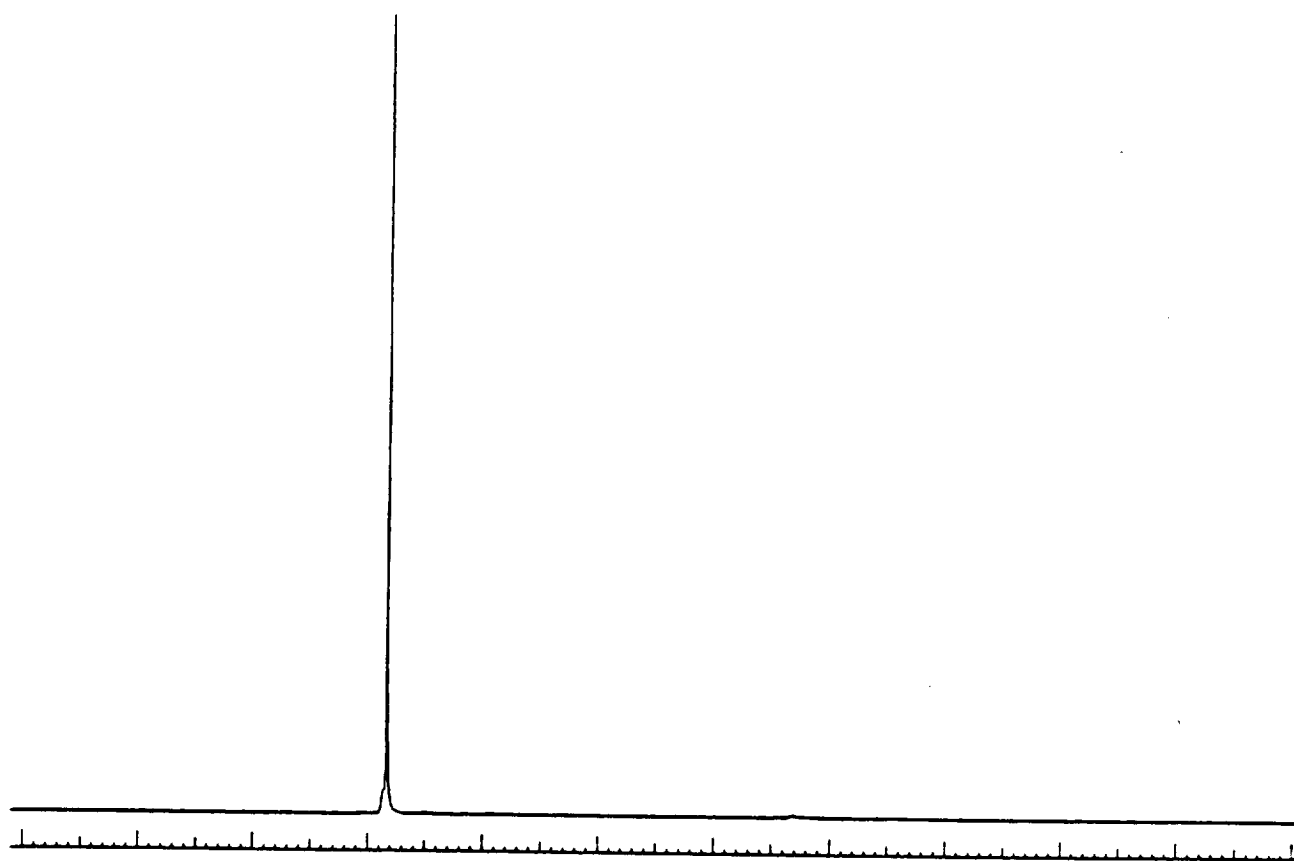
73

Figure 24. Proton NMR spectrum of benzoquinone dissolved in
d-DMSO showing the single peak characteristic of
a pure sample.

sample. Thus, the observed low efficiency of inhibition exhibited by hydroquinone was not due to the presence of any impurity in the sample.

Another possible reason for the low efficiency of hydroquinone, and the observed retardation of the polymerization rate after the end of the induction period, is that perhaps the hydroquinone partitions partially in the oil phase and partially in the aqueous phase. Klein and Barabas[18] have presented evidence that in some cases, hydroquinone can partition completely in the oil phase. However, experimentally determined solubility data does not confirm this. The solubility of hydroquinone was determined by measuring the solids content of a saturated solution of hydroquinone in water and in styrene. The solubility was 8.1% in water at room temperature and less than 0.03% in styrene at room temperature, which seemed to indicate that very little hydroquinone should partition in the oil phase. Partitioning of hydroquinone in the oil phase was also not detected when added to a mixture of styrene and water. The hydroquinone slowly oxidizes in water to form a brown solution. Since no brown color was observed in the styrene phase, while the aqueous phase was brown, it appeared that essentially no hydroquinone existed in the oil phase.

As mentioned earlier, several researchers have

found that hydroquinone only acts as an inhibitor when oxygen is present and can oxidize the hydroquinone to benzoquinone. The possibility therefore existed, that the observed low inhibition efficiency of hydroquinone was due to a rate-determining oxidation reaction to benzoquinone. To test this hypothesis, the induction period due to oxidation (ca. 25 hours) was subtracted from the observed induction periods to give induction periods due strictly to the added inhibitor. These values were compared to the expected induction periods, and an average efficiency was calculated. By inserting this value into a zero-order kinetic rate equation, a value for the rate constant for the oxidation of hydro-quinone was extracted. This calculation appears in Appendix D. The value of the rate constant for the oxidation of hydroquinone obtained by this analysis was $k = 3.9 \times 10^{-13}$ moles hydroquinone/sec. Thus, the data do not exclude the possibility that inhibition is limited by the rate of hydroquinone oxidation. In order to determine whether the formation of ben-zoquinone caused the observed induction periods, a recipe containing 3.5 ppm of benzoquinone was run at room temperature in the LUMLR. The induction period for this reaction lasted for only 60 hours compared to a 98 hour induction period obtained with the same con-centration of hydroquinone. This difference could be

explained by the fact that benzoquinone is known to decompose to form complex degradation products in an alkaline medium[13] and that the recipes used in this work had a pH of approximately 8 when prepared. Perhaps unless the benzoquinone reacts immediately with free radicals, it oxidizes to form these complex degradation products which have no inhibiting power. In the case of hydroquinone, the low rate of benzoquinone production does not allow much benzoquinone to remain in excess in the solution and therefore the further oxidation of benzoquinone to ineffective degradation products does not occur.

Since there has been speculation in the literature that hydroquinone can copolymerize with styrene the molecular weight of the polymer produced was measured using Gel Permeation Chromatography. The calculated values of molecular weight appear in Table IV. These values indicate no trend toward lower molecular weight with increasing hydroquinone concentration as would be expected if copolymerization occurred. This evidence seems to show that there was no copolymerization of hydroquinone and styrene in the styrene/polystyrene seeded system studied.

To test if the hydroquinone terminated free radicals in the styrene-swollen polystyrene particles, the surface charge density of the product polymer was

TABLE IV

CALCULATED NUMBER AVERAGE (Mn) AND WEIGHT AVERAGE (Mw)

MOLECULAR WEIGHTS OF POLYSTYRENE PRODUCTS

Recipe Designation	Initial Hydroquinone Concentration (ppm)	Mn	Mw
CON-3	6.0	1.9×10^5	7.5×10^5
CON-4	6.0	1.9×10^5	9.5×10^5
CON-5	0.0	1.7×10^5	9.5×10^5
CON-6	0.51	1.3×10^5	9.6×10^5
CON-8	3.5	1.8×10^5	7.9×10^5
CON-9	3.5	1.9×10^5	8.7×10^5

calculated from conductometric titration results. If termination of the growing chains occurred due to hydroquinone, the surface charge density would be expected to be higher than for a similar recipe containing no hydroquinone. However, the values obtained for the surface charge density were 15.2 micro equivalents/gm and 14.7 micro equivalents/gm for a sample containing no hydroquinone and 3.5 ppm hydroquinone, respectively. Since these values differed by only 3%, and the sample containing no inhibitor had the higher surface charge density, the conclusion was that the inhibitor terminated radicals in the aqueous phase only and not in the polymer particles.

C. Flight Experiment Results

Since the flight reactors were loaded approximately four days prior to the start of the polymerization, and the temperature-time history for the reactors during this four day delay could not be predicted, a recipe had to be designed which would be able to withstand both the time delay and possible high ambient temperature (e.g. 30°C) without polymerization. For this reason a recipe containing a relatively high amount of hydroquinone (25 ppm) was tested for its ability to satisfy the two criteria above. This recipe was exposed to a 30°C environment for four days and then polymerized at 70°C (CON-11). This recipe was repeated

and polymerized at 70°C with no delay at a lower temperature (CON-10). The conversion-time histories for the two polymerizations are compared in Figure 25. Although the two runs both exhibit a retardation in polymerization rate when compared to an identical recipe containing no hydroquinone, the conversion-time curves are essentially identical for the two hydroquinone-containing recipes. Except for the presence of a shorter induction period for the recipe exposed to the 30°C environment, the curves are otherwise identical in shape. Since this recipe yielded reproducible kinetics, and allowed an adequate margin for time and temperature variations, it was chosen as the control recipe for a spaceflight experiment.

The control experiment was run on STS-7, the maiden voyage of the Space Shuttle Challenger which left Kennedy Space Center on April 4, 1983. When the flight reactors were unloaded after the return of the Challenger, a styrene monomer odor was detected in the reactor containing the control recipe. This indicated that the polymerization did not go to completion during the 17 hour period at 70°C. It was thought that perhaps there had been a hardware malfunction and the reactor had not heated to the 70°C reaction temperature. However, an examination of the recorded temperature-time data revealed that the heating to
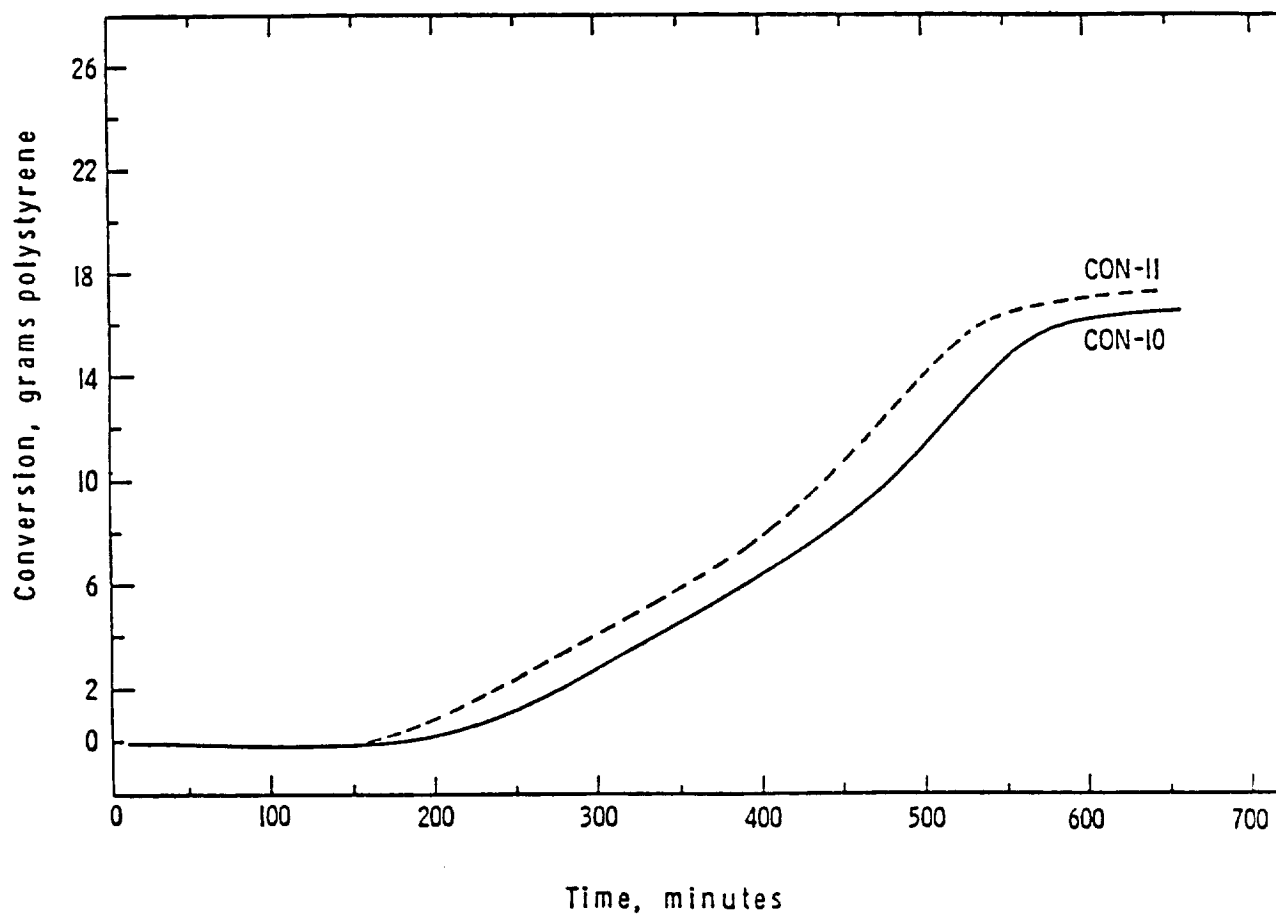
80

Figure 25. Comparison of the conversion-time histories for a
recipe polymerized at 70°C immediately after
loading(CON-10), and a recipe exposed to a 30°C
environment for 4 days prior to polymerization at
70°C(CON-11).

reaction temperature had proceeded normally. The possibility remained that there was an impurity in the reactor or the recipe which caused the polymerization to be severely retarded. The flight recipe was therefore re-run in the same reactor during a ground based test. Again, the conversion was not complete. Figure 26 shows the conversion-time histories for the flight (F-12) and ground (G-12) experiments. When compared to the conversion-time curves for the same recipe obtained in the LUMLR, the flight and ground experiment kinetics were very different. Not only were the conversions low (about 70% and 80% for the flight and ground experiments, respectively), but the polymerization rates were much lower for the flight and ground experiments. To test whether the recipes were somehow contaminated by a retarder, the leftover swollen latexes from the flight and ground experiments were loaded, undegassed, into glass dilatometers and heated to 70°C. The conversion-time curves for the recipe run in the LUMLR, the ground experiment, and the recipe run in the glass dilatometer appear in Figure 27. What is immediately obvious is that the ground experiment results are very different from the results of the two other polymerizations. The difference between the kinetics obtained in the LUMLR and in the glass dilatometer was attributed to the slight retardation caused
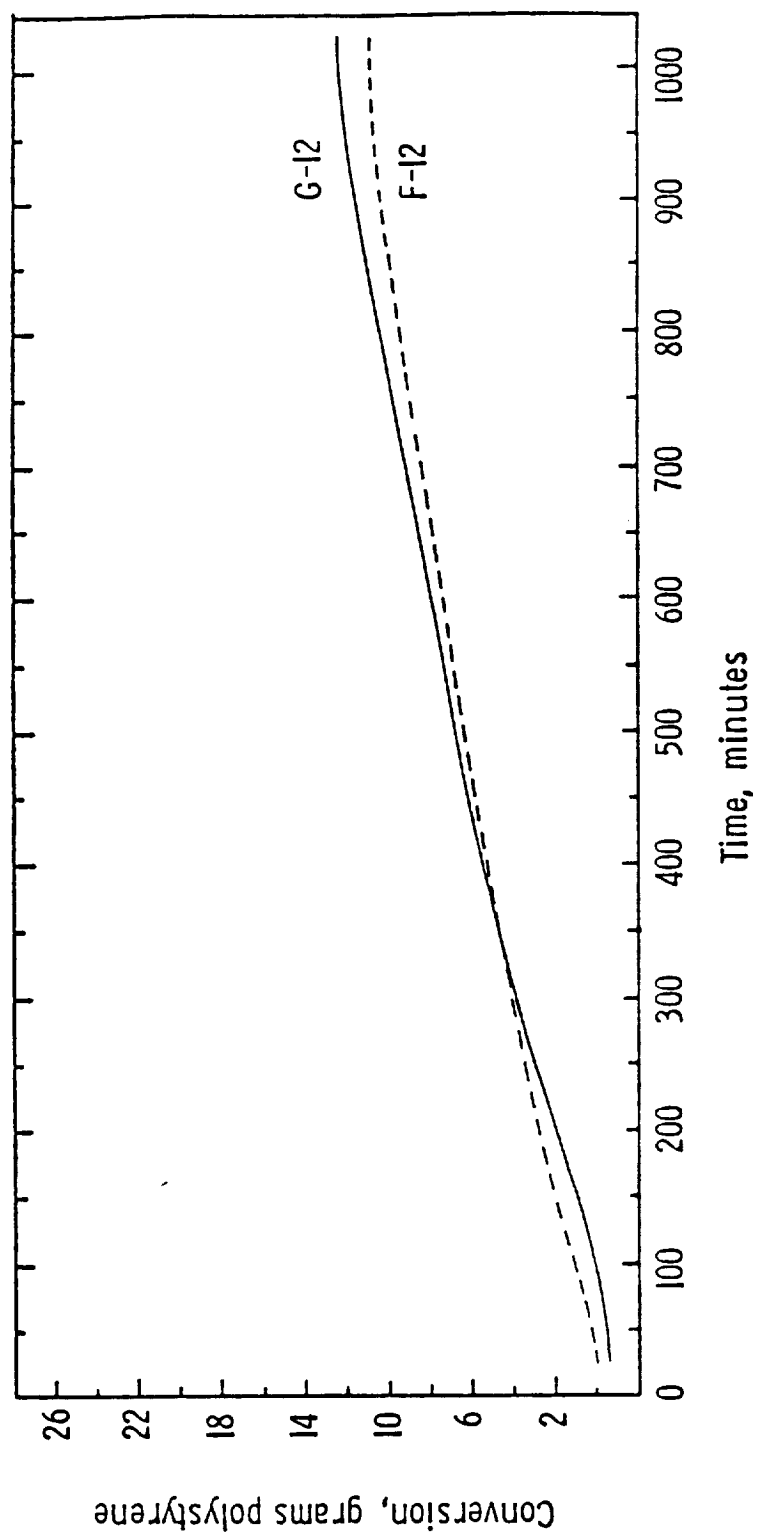
Figure 26. Conversion-time histories for the flight experiment (F-12) and the ground run experiment (G-12).
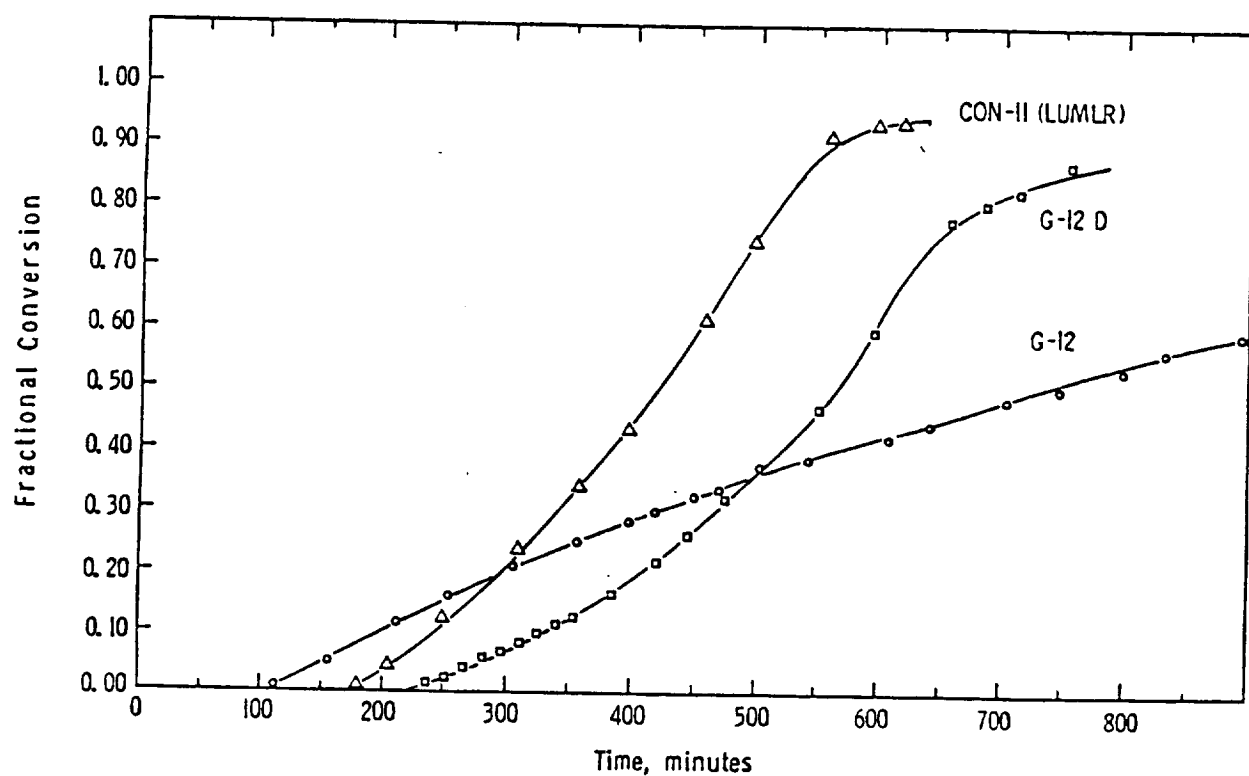
83

Figure 27. Conversion-time curves for identical recipes run in the LUMLR (CON-11), in a glass dilatometer (G-12D), and in the flight reactor during the ground run (G-12).

84

by the oxygen not removed by degassing prior to the loading of the glass dilatometer. Since the leftover swollen recipes yielded similar kinetics when polymerized at 70°C, it was concluded that the flight and ground experiment recipes were contaminated by a substance which was not removed from the reactors during cleaning. This impurity was thus able to severely retard the polymerization rate and also limit the final conversion of each recipe.

The product latexes from the flight and ground experiments were also characterized in terms of their particle size distributions. The particle size distribution histograms for the flight and ground experiments appear in Figure 28 and Figure 29 respectively. These histograms reveal that the two samples have nearly identical particle size distributions, with an average particle diameter of 246 nm. The samples were fairly monodisperse with the flight sample having a standard deviation of 3.6% and the ground sample having a 3.8% standard deviation. Thus, it appears that the impurity did not drastically broaden the final particle size distributions and it also seems that the effect of gravity on submicron seeded emulsion polymerization is essentially nil.

SAMPLE FLIGHT 12

D_n = 246.4   PDI   = 1.004

D_w = 247.4 D_{min} = 152.5

N   =   670 D_{max} = 347.5

D_v = 246.8 D_a = 246.6

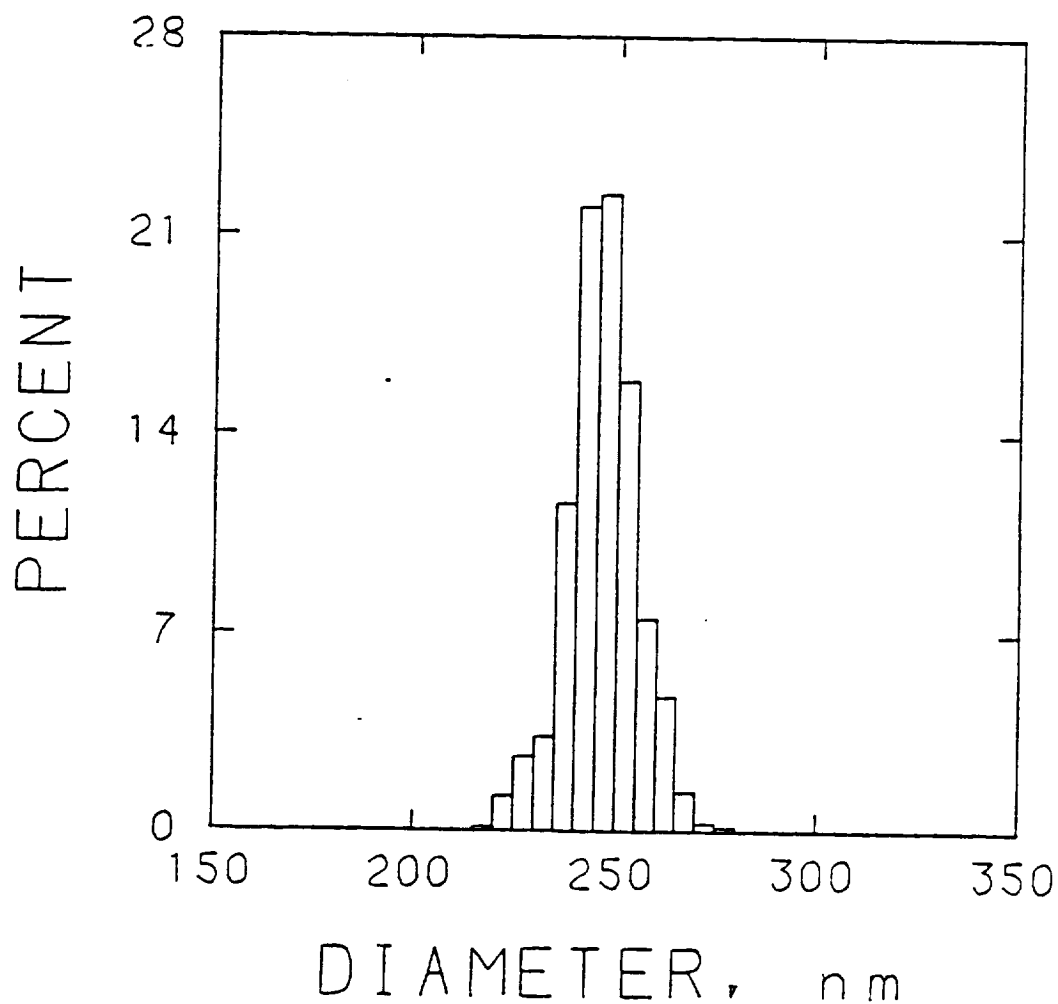S_d =   8.9   STEP =   5.0

D_q = 247.7 D_s = 247.1

Figure 28. Particle size distribution histogram for the flight sample.

SAMPLE GROUND 12

D_n = 246.2   PDI   = 1.004
D_w = 247.3 D_{min} = 152.5
N   =   1172 D_{max} = 347.5
D_v = 246.6 D_a = 246.4
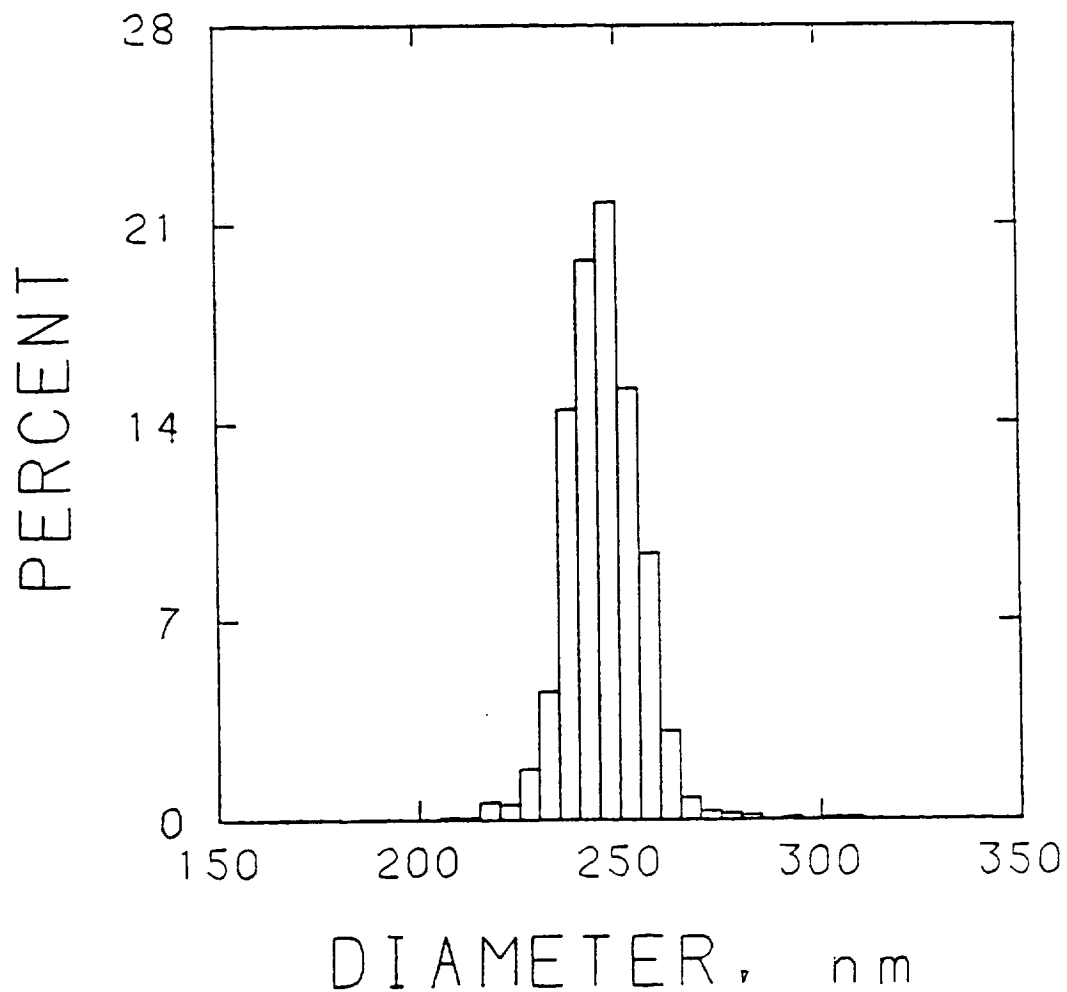S_d =   9.5   STEP =   5.0
D_q = 247.7 D_s = 246.9

Figure 29. Particle size distribution histogram for
the ground run sample.

IV. CONCLUSIONS

1. There is a thermally induced "background" polymerization rate in a seeded emulsion system which is much higher than the thermal bulk polymerization rate of styrene. This suggests that free radicals are thermally generated in the aqueous phase.

2. Hydroquinone yields induction periods at room temperature of only 1.8% of the length predicted by the decomposition rate data for potassium persulfate initiator. The rate of hydroquinone disappearance is zero order with respect to initial hydroquinone concentration.

3. The linear dependence of induction period on initial hydroquinone concentration, along with the molecular weight measurements, indicate that no copolymerization of hydroquinone with styrene occurs.

4. Conductometric titrations indicate that hydroquinone reacts with free radicals in the aqueous phase and not in the oil phase.

5. Hydroquinone is not an ideal inhibitor, and when added to a seeded emulsion polymerization recipe, causes a retardation of the polymerization rate.

6. The hydroquinone and benzoquinone samples used were found by NMR to be essentially pure and the low efficiency of inhibition observed was probably due to slow oxidation of the substances in water.

7. Both the flight and ground run experiments exhibited severe retardation of polymerization rate and low final conversion due to contaminants in the reactor.

8. The measured particle size distributions showed that the contaminants had little or no effect on the quality of the final latex in terms of monodispersity.

REFERENCES

1. P.J. Flory, "Principles of Polymer Chemistry," Chap. 4, Cornell University Press, Ithaca, N.Y., 1953.

2. W.D. Harkins, J. Am.Chem. Soc., 69, 1428(1947).

3. W.V. Smith and R.H. Ewart, J. Chem. Phys., 16, 592(1948).

4. J. Ugelstad and F. K. Hansen, Rubber Chemistry and Tech., 49, 3(1976).

5. J. Ugelstad and P. C. Mørk, Brit. Polym. J., 2, 31(1970).

6. G. Odian, in "Principles of Polymerization", 2nd ed., McGraw-Hill, New York (1970).

7. J.W. Vanderhoff, H.J. van den Hul, R.J.M. Tausk, and J.Th.G. Overbeek, in "Clean Surfaces: Their Preparation and Characterization for Interfacial Studies" (G. Goldfingfer, ed.), Marcel Dekker, New York (1970).

8. J.W. Vanderhoff, in "Vinyl Polymerization Vol. I, Part II", Ham G.E., ed., Marcel Dekker, New York, 1969, Chap. 1.

9. D. Blackley, "Emulsion Polymerization", Applied Science Publishers, (1975).

10. B.S. Hawkett, D.H. Napper, R.G. Gilbert, J. Chem. Soc. Faraday Trans. I, 76, 1323(1980).

11. B.S. Hawkett, D.H. Napper, R.G. Gilbert, J. Chem. Soc. Faraday Trans. I, 77, 2395(1981).

12. E.F. Kluchesky and L.B. Wakefield, Industrial and Eng. Chem., 41, No.8, 1768(1949).

13. F.A. Bovey and I.M. Kolthoff, J. Poly. Sci., 5, No.5, 569(1950).

14. B.W. Brooks and Makanjuola, J.C.S. Faraday Trans. I, 77, (1981).

15. F.Tudos, J. Poly. Sci., 30, 343(1958).

16. S.G. Foord, J. Chem. Soc., 48(1940).

17. H.W. Melville and W.F. Watson, Trans. Faraday Soc., $\underline{44}$, 886(1948).

18. A. Klein and E. S. Barabas, Preprints of Proceedings of ACS Meeting, Honolulu, 1979.

APPENDICIES

Appendix A: Calculation of Styrene Content of Swollen Latex

From the measured Absorbance and the calibration curve in Figure 7, calculate the concentration of styrene in the 2nd dilution(c).

Ex: $c = 5.947 \times 10^{-6}$ g styrene/g solution

19.28 g = weight isooctane

.2288 g = weight swollen latex added to above isooctane

.0527 g = weight of above mixture added to additional isooctane

28.8793 g = weight of solution formed by addition of .0527 g mixture to additional isooctane

$(5.947 \times 10^{-6}$ g styrene/g solution$) \cdot (20.8793$ g$)$
$= 1.24 \times 10^{-4}$ g styrene

$(1.24 \times 10^{-4}$ g styrene$) \cdot (.0527$ g$)$
$= 2.36 \times 10^{-3}$ g styrene

$(2.36 \times 10^{-3}$ g styrene$) \cdot (19.28$ g$)$
$= 4.54 \times 10^{-2}$ g styrene

$(4.54 \times 10^{-2}$ g styrene$)/(.2288$ g latex$) = .199 \dfrac{\text{g styrene}}{\text{g latex}}$

design swelling ratio $= 0.20 \dfrac{\text{g styrene}}{\text{g latex}}$
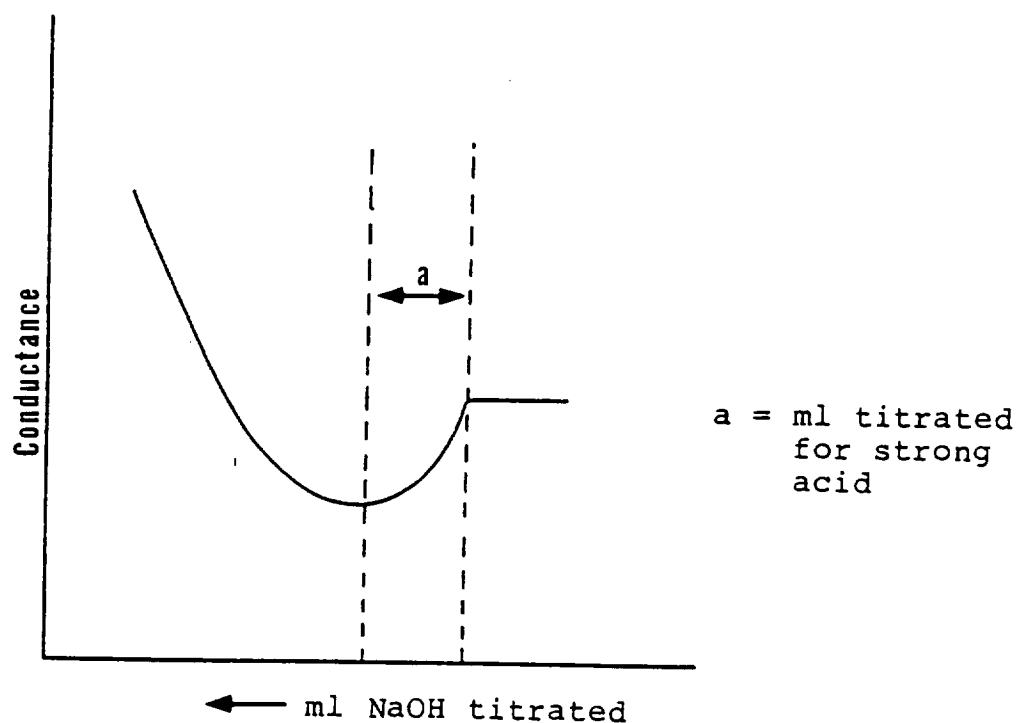
Appendix B: Determination of Surface Charge
              Density from Conductometric Titration
              Data

Data Required:

1. grams polymer titrated

2. particle size
    → area/particle → wt./particle → particles/gram

    → area/gm → gm/area

3. ml of NaOH titrated and normality of NaOH

Calculate:

I.   equivalents/gm polymer = $\dfrac{N_{NaOH} \times ml_{NaOH}}{wt.\ polymer \times 1000}$

a = ml titrated
    for strong
    acid

ml NaOH titrated

CON-5: particle diameter = 0.24 μm = .24 x 10^{-4} cm

57.33 g latex x .04575 $\underline{\text{g PS}}$ = 2.62 g PS
g latex

area = $D^2/4$ = 4.524 x 10^{-10} cm^2/particle

wt./particle = (5.43 x 10^{-15} cm^3/particle)·(1.05g/cm^3)

= 5.70 x 10^{-15} g/particle

particles/g = $\dfrac{1}{5.70 \times 10^{-15} \text{ g/particle}}$ =

1.754 x 10^{14} particles/g

1.754 x 10^{14} $\dfrac{\text{particles}}{\text{g}}$ x 4.52 x 10^{-10} cm^2/particle

=79,367 cm^2/g

2.0 N x $\dfrac{(0.1 \text{ cm} \times 0.2 \text{ ml/cm})}{2.62 \text{ g} \times 1000}$ = 1.52 x 10^{-5} equivalents/g PS

or

15.2 μ-equivalents/g

95

T°C	20	25	
H	4.01	4.38	$\times 10^4$

X_A = mole fraction in liquid phase

P_A = partial pressure in atmospheres

@ 21°C $H = 4.084 \times 10^4$

$$X_A = \frac{P_A}{H_A}$$

$$X_A = \frac{1}{4.084 \times 10^4} = 2.449 \times 10^{-5} \frac{\text{moles } O_2}{\text{mole } H_2O}$$

@ 1 atm

$$X_A = \frac{20/760}{4.084 \times 10^4} = 6.444 \times 10^{-7} \frac{\text{moles } O_2}{\text{mole } H_2O}$$

@ 20 mmHg

$$122.359 \text{ g } H_2O \text{ in recipe} \cdot \frac{1 \text{mole } H_2O}{18 \text{ g } H_2O}$$

$$= 6.798 \text{ moles } H_2O \cdot 6.44 \times 10^{-7} \frac{\text{mole } O_2}{\text{mole } H_2O}$$

$$= 4.38 \times 10^{-6} \frac{\text{moles } O_2}{\text{recipe}}$$

Appendix D: Calculation of Rate Constant
              for the Oxidation of Hydroquinone
              in Emulsion at Room Temperature

Efficiency of Hydroquinone based on induction period:

CON-6: $\dfrac{10hr}{563.2hr}$ = 0.01776

CON-7: $\dfrac{45.83}{2557}$ = 0.01792

CON-8: $\dfrac{73.00}{3.975 \times 10^3}$ = 0.0183

Average Efficiency = 0.0183 (or 1.8%)

$$BQ = 0.018015\ [HQ]_o$$

$$k = \frac{[HQ]_o - [HQ]}{\Delta t}$$

$$\frac{[HQ]_o - [HQ]}{[HQ]_o} = 0.0185 = \frac{kt_{induction}}{[HQ]_o}$$

$$k = \frac{[HQ]_o \cdot 0.018}{t_{induction}}$$

CON-6: $k = 4.09 \times 10^{-13}$ moles/sec

CON-7: $k = 3.96 \times 10^{-13}$ moles/sec

CON-8: $k = 3.80 \times 10^{-13}$ moles/sec

Average $k = 3.9 \times 10^{-13}$ $\dfrac{\text{moles hydroquinone}}{\text{sec}}$